Publishing House ASV

begell house, inc. publishers

PAACH

Scientific coordination is carried out by the Russian Academy of Architecture and Construction Sciences (RAACS)

Volume 21 • Issue 4 • 2025

ISSN 2588-0195 (Online)
ISSN 2587-9618 (Print) Continues ISSN 1524-5845

International Journal for

Computational Civil and Structural Engineering

Международный журнал по расчету гражданских и строительных конструкций

https://ijccse.iasv.ru/

DOI: 10.22337/2587-9618
GICID: 71.0000.1500.2830

EXECUTIVE EDITOR

Vladimir I. Travush,
Full Member of RAACS, Professor, Dr.Sc.,
Vice-President of the Russian Academy
of Architecture and Construction Sciences;
Urban Planning Institute
of Residential and Public Buildings;
24, Ulitsa Bolshaya Dmitrovka, 107031, Moscow, Russia

EDITOR-IN-CHIEF

Vladimir N. Sidorov,
Full Member of RAACS, Professor, Dr.Sc., National Research Moscow State University of Civil Engineering; Russian University of Transport (RUT – MIIT); Moscow Institute of Architecture (State Academy); Perm National Research Polytechnic University; 26, Yaroslavskoe Shosse, 129337, Moscow, Russia

EDITORIAL DIRECTOR

Valery I. Telichenko,
Full Member of RAACS, Professor, Dr.Sc.,
The First Vice-President of the Russian Academy
of Architecture and Construction Sciences;
Honorary President of National Research
Moscow State University of Civil Engineering;
24, Ulitsa Bolshaya Dmitrovka, 107031, Moscow, Russia

MANAGING EDITOR

Nadezhda S. Nikitina,
Professor, Ph.D.,
Director of ASV Publishing House;
National Research Moscow State University
of Civil Engineering;
26, Yaroslavskoe Shosse, 129337, Moscow, Russia

ASSOCIATE EDITORS

Pavel A. Akimov,
Full Member of RAACS, Professor, Dr.Sc.,
Acting Rector of National Research
Moscow State University of Civil Engineering;
Vice-President of the Russian Academy
of Architecture and Construction Sciences;
Tomsk State University of Architecture and Building;
Russian University of Friendship of Peoples;
26, Yaroslavskoe Shosse, 129337, Moscow, Russia

Alexander M. Belostotsky,
Full Member of RAACS, Professor, Dr.Sc.,
Research & Development Center "STADYO";
National Research Moscow State University of Civil Engineering; Russian University of Transport (RUT – MIIT); Russian University of Friendship of Peoples;
Perm National Research Polytechnic University;
Tomsk State University of Architecture and Building;
Irkutsk National Research Technical University;
8th Floor, 18, ul. Tretya Yamskogo Polya,
125040, Moscow, Russia

Mikhail Belyi, Professor, Dr.Sc.,
Dassault Systèmes Simulia;
1301 Atwood Ave Suite 101W
02919 Johnston, RI, United States

Vitaly Bulgakov, Professor, Dr.Sc.,
Micro Focus;
Newbury, United Kingdom

Nikolai P. Osmolovskii, Professor, Dr.Sc.,
Systems Research Institute, Polish Academy of Sciences;
Kazimierz Pulaski University
of Technology and Humanities in Radom;
29, ul. Malczewskiego, 26-600, Radom, Poland

Gregory P. Panasenko, Professor, Dr.Sc.,
Equipe d'Analise Numerique; NMR CNRS 5585
University Gean Mehnet;
23 rue. P.Michelon 42023, St.Etienne, France

Scientific coordination is carried out by the Russian Academy of Architecture and Construction Sciences (RAACS)

PUBLISHER

ASV Publishing House
(ООО «Издательство АСВ»)
19/1,12, Yaroslavskoe Shosse, 120338, Moscow, Russia
Tel. +7(925)084-74-24; E-mail: iasv@iasv.ru; Интернет-сайт: http://iasv.ru/

ADVISORY EDITORIAL BOARD

Mojtaba Aslami, Ph.D,
Fasa University; Daneshjou blvd,
Fasa, Fars Province, Iran

Klaus-Jurgen Bathe, Professor
Massachusetts Institute
of Technology;
Cambridge, MA 02139, USA

Alexander T. Bekker,
Academician of RAACS,
Professor, Dr.Sc.,
Far Eastern Federal University;
Russian Academy of Architecture
and Construction Sciences;
8, Sukhanova Street, Vladivostok,
690950, Russia

Tomas Bock, Professor, Dr.-Ing.,
Technical University of Munich,
Arcisstrasse 21, D-80333
Munich, Germany

Jan Buynak, Professor, Ph.D.,
University of Žilina;
1, Univerzitná, Žilina, 010 26,
Slovakia

Vladimir T. Erofeev,
Full Member of RAACS,
Professor, Dr.Sc.,
Ogarev Mordovia State University;
68, Bolshevistskaya Str., Saransk
430005, Republic of Mordovia,
Russia

Victor S. Fedorov,
Full Member of RAACS,
Professor, Dr.Sc.,
Russian University of Transport
(RUT – MIIT);
9b9 Obrazcova Street, Moscow,
127994, Russia

Sergey V. Fedosov,
Full Member of RAACS,
Professor, Dr.Sc.,
Russian Academy of Architecture
and Construction Sciences;
24, Ul. Bolshaya Dmitrovka, 107031,
Moscow, Russia

Sergiy Yu. Fialko,
Professor, Dr.Sc.,
Cracow University of Technology;
24, Warszawska Street, Kraków,
31-155, Poland

Vladimir G. Gagarin,
Corresponding Member
of RAACS, Professor, Dr.Sc.,
Research Institute of Building
Physics of Russian Academy
of Architecture and Construction
Sciences;
21, Lokomotivny Proezd,
Moscow, 127238, Russia

Vyatcheslav A. Ilyichev,
Full Member of RAACS,
Professor, Dr.Sc.,
Russian Academy of Architecture
and Construction Sciences;
Podzemproekt Ltd.;
24, Ulitsa Bolshaya Dmitrovka,
Moscow, 107031, Russia

Marek Iwański,
Professor, Dr.Sc.,
Kielce University of Technology;
7, al. Tysiąclecia Państwa Polskiego
Kielce, 25 – 314, Poland

Sergey Yu. Kalashnikov,
Corresponding Member of RAACS,
Professor, Dr.Sc.,
Volgograd State Technical
University; 28, Lenin avenue,
Volgograd, 400005, Russia

Semen S. Kaprielov,
Academician of RAACS,
Professor, Dr.Sc.,
Research Center of Construction;
6, 2nd Institutskaya St., Moscow,
109428, Russia

Nikolay I. Karpenko,
Full Member of RAACS,
Professor, Dr.Sc.,
Research Institute of Building
Physics of Russian Academy
of Architecture and Construction
Sciences; Russian Academy of
Architecture and Construction
Sciences; 21, Lokomotivny Proezd,
Moscow, 127238, Russia

Vladimir V. Karpov,
Professor, Dr.Sc., Saint Petersburg
State University of Architecture and
Civil Engineering;
4, 2-nd Krasnoarmeiskaya Steet,
Saint Petersburg, 190005, Russia

Galina G. Kashevarova,
Corresponding Member
of RAACS, Professor, Dr.Sc.,
Perm National Research
Polytechnic University;
29 Komsomolsky pros., Perm,
Perm Krai, 614990, Russia

John T. Katsikadelis,
Professor, Dr.Eng, PhD, Dr.h.c.,
National Technical University of
Athens; Zografou Campus
9, Iroon Polytechniou str
15780 Zografou, Greece

Vitaly I. Kolchunov,
Full Member of RAACS,
Professor, Dr.Sc., Southwest State
University; Russian Academy of
Architecture and Construction
Sciences; 94, 50 let Oktyabrya,
Kursk, 305040, Russia

Dmitry V. Kozlov, Corresponding
Member of RAACS
Dr. Sc. Engineering, Professor, Head
of the Department of Hydraulics and
Hydrotechnical Construction, NRU
MGSU, 26, Yaroslavskoe Shosse.,
129337, Moscow, Russia

Markus König, Professor
Ruhr-Universität Bochum;
150, Universitätsstraße, Bochum,
44801, Germany

Sergey B. Kositsin,
Advisor of RAACS,
Professor, Dr.Sc.,
Russian University of Transport
(RUT – MIIT); 9b9 Obrazcova
Street, Moscow, 127994, Russia

Sergey B. Krylov,
Full Member of RAACS,
Professor, Dr.Sc.,
Research Center of Construction;
6, 2nd Institutskaya St., Moscow,
109428, Russia

Sergey A. Kudryavtsev,
Corresponding Member of of
RAACS, Professor, Dr.Sc., Far
Eastern State Transport University;
47, Serysheva St., 680021,
Khabarovsk, Russia

Sergey V. Kuznetsov,
Professor, Dr.Sc.,
Ishlinsky Institute for Problems in Mechanics of the Russian Academy of Sciences;
101-1, Prosp. Vernadskogo,
Moscow, 119526, Russia

Vladimir V. Lalin,
Professor, Dr.Sc.,
Peter the Great Saint-Petersburg Polytechnic University;
29, Ul. Politechnicheskaya,
Saint-Petersburg, 195251, Russia

Leonid S. Lyakhovich,
Full Member of RAACS,
Professor, Dr.Sc., Tomsk State University of Architecture and Building; 2, Solyanaya Sq., Tomsk, 634003, Russia

Rashid A. Mangushev,
Corresponding Member of RAACS, Professor, Dr.Sc.,
Saint Petersburg State University of Architecture and Civil Engineering;
4, 2-nd Krasnoarmeiskaya Steet,
Saint Petersburg, 190005, Russia

Ilizar T. Mirsayapov,
Corresponding Member of RAACS, Professor, Dr.Sc., Kazan State University of Architecture and Engineering; 1, Zelenaya Street, Kazan, 420043, Republic of Tatarstan, Russia

Vladimir L. Mondrus,
Corresponding Member of RAACS, Professor, Dr.Sc.,
National Research Moscow State University of Civil Engineering;
Yaroslavskoe Shosse 26,
Moscow, 129337, Russia

Valery I. Morozov,
Corresponding Member of RAACS, Professor, Dr.Sc.,
Saint Petersburg State University of Architecture and Civil Engineering;
4, 2-nd Krasnoarmeiskaya Steet,
Saint Petersburg, 190005, Russia

Igor G. Ovchinnikov, Professor, Dr.Sc., Tyumen Industrial University; 38, Volodarsky St., 625000, Tyumen, Russia

Anatoly V. Perelmuter,
Foreign Member of RAACS,
Professor, Dr.Sc., SCAD Soft;
Office 1,2, 3a Osvity street,
Kiev, 03037, Ukraine

Alexey N. Petrov,
Advisor of RAACS, Professor, Dr.Sc., Petrozavodsk State University; 33, Lenina Prospect, Petrozavodsk, 185910, Republic of Karelia, Russia

Vladilen V. Petrov,
Full Member of RAACS,
Professor, Dr.Sc.,
Yuri Gagarin State Technical University of Saratov;
77 Politechnicheskaya Street,
Saratov, 410054, Russia

Jerzy Z. Piotrowski,
Professor, Dr.Sc.,
Kielce University of Technology;
al. Tysiąclecia Państwa Polskiego 7,
Kielce, 25 – 314, Poland

Chengzhi Qi, Professor, Dr.Sc.,
Beijing University of Civil Engineering and Architecture;
1, Zhanlanlu, Xicheng District,
Beijing, China

Vladimir P. Selyaev,
Full Member of RAACS,
Professor, Dr.Sc., Ogarev Mordovia State University;
68, Bolshevistskaya Str., Saransk 430005, Republic of Mordovia, Russia

Eun Chul Shin,
Professor, Ph.D.,
Incheon National University;
(Songdo-dong)119 Academy-ro,
Yeonsu-gu, Incheon, Korea

D.V. Singh,
Professor, Ph.D,
University of Roorkee;
Roorkee, India, 247667

Wacław Szcześniak,
Foreign Member of RAACS,
Professor, Dr.Sc.,
Lublin University of Technology;
Ul. Nadbystrzycka 40,
20-618 Lublin, Poland

Tadatsugu Tanaka,
Professor, Dr.Sc.,
Tokyo University; 7-3-1 Hongo,
Bunkyo, Tokyo, 113-8654, Japan

Josef Vican,
Professor, Ph.D,
University of Žilina;
1, Univerzitná, Žilina, 010 26,
Slovakia

Zbigniew Wojcicki,
Professor, Dr.Sc.,
Wroclaw University of Technology;
11 Grunwaldzki Sq., 50-377,
Wrocław, Poland

Artur Zbiciak, Professor, Dr.Sc.,
Warsaw University of Technology;
Pl. Politechniki 1, 00-661 Warsaw,
Poland

Segrey I. Zhavoronok, Ph.D.,
Institute of Applied Mechanics of Russian Academy of Sciences;
Moscow Aviation Institute (National Research University);
7, Leningradsky Prt.,
Moscow, 125040, Russia

Askar Zhussupbekov,
Professor, Dr.Sc.,
Eurasian National University;
5, Munaitpassov street, Astana,
010000, Kazakhstan

TECHNICAL EDITOR

Taymuraz B. Kaytukov,
Advisor of RAACS,
Associate Professor, Ph.D.,
Vice-Rector of National Research Moscow State University of Civil Engineering;
Yaroslavskoe Shosse 26,
Moscow, 129337, Russia

EDITORIAL TEAM

Vadim K. Akhmetov, Professor, Dr.Sc., National Research Moscow State University of Civil Engineering; 26, Yaroslavskoe Shosse, 129337 Moscow, Russia

Pavel A. Akimov, Full Member of RAACS, Professor, Dr.Sc., Acting Rector of National Research Moscow State University of Civil Engineering; Vice-President of the Russian Academy of Architecture and Construction Sciences; Tomsk State University of Architecture and Building; Russian University of Friendship of Peoples; 26, Yaroslavskoe Shosse, 129337, Moscow, Russia

Alexander M. Belostotsky, Full Member of RAACS, Professor, Dr.Sc., Research & Development Center "STADYO"; National Research Moscow State University of Civil Engineering; Russian University of Transport (RUT – MIIT); Russian University of Friendship of Peoples; Perm National Research Polytechnic University; Tomsk State University of Architecture and Building; Irkutsk National Research Technical University; 8th Floor, 18, ul. Tretya Yamskogo Polya, 125040, Moscow, Russia

Mikhail Belyi, Professor, Dr.Sc., Dassault Systèmes Simulia; 1301 Atwood Ave Suite 101W 02919 Johnston, RI, United States

Vitaly Bulgakov, Professor, Dr.Sc., Micro Focus; Newbury, United Kingdom

Charles El Nouty, Professor, Dr.Sc., LAGA Paris-13 Sorbonne Paris Cite; 99 avenue J.B. Clément, 93430 Villetaneuse, France

Natalya N. Fedorova, Professor, Dr.Sc., Novosibirsk State University of Architecture and Civil Engineering (SIBSTRIN); 113 Leningradskaya Street, Novosibirsk, 630008, Russia

Darya Filatova, Professor, Dr.Sc., Probability, Assessment, Reasoning and Inference Studies Research Group, EPHE Laboratoire CHART (PARIS) 4-14, rue Ferrus, 75014 Paris

Vladimir Ya. Gecha, Professor, Dr.Sc., Research and Production Enterprise All-Russia Scientific-Research Institute of Electromechanics with Plant Named after A.G. Iosiphyan; 30, Volnaya Street, Moscow, 105187, Russia

Taymuraz B. Kaytukov, Advisor of RAACS, Associate Professor, Ph.D, Vice-Rector of National Research Moscow State University of Civil Engineering; 26, Yaroslavskoe Shosse, 129337, Moscow, Russia

Marina L. Mozgaleva, Professor, Dr.Sc., National Research Moscow State University of Civil Engineering; 26, Yaroslavskoe Shosse, 129337 Moscow, Russia

Nadezhda S. Nikitina, Professor, Ph.D., Director of ASV Publishing House; National Research Moscow State University of Civil Engineering; 26, Yaroslavskoe Shosse, 129337 Moscow, Russia

Nikolai P. Osmolovskii, Professor, Dr.Sc., Systems Research Institute Polish Academy of Sciences; Kazimierz Pulaski University of Technology and Humanities in Radom; 29, ul. Malczewskiego, 26-600, Radom, Poland

Gregory P. Panasenko, Professor, Dr.Sc., Equipe d'Analise Numerique NMR CNRS 5585 University Gean Mehnet; 23 rue. P.Michelon 42023, St.Etienne, France

Andreas Rauh, Prof. Dr.-Ing. habil. Carl von Ossietzky Universität Oldenburg, Germany School II - Department of Computing Science Group Distributed Control in Interconnected Systems D-26111 Oldenburg, Germany

Zhan Shi, Professor LPSM, Université Paris VI 4 place Jussieu, F-75252 Paris Cedex 05, France

Marina V. Shitikova, National Research Moscow State University of Civil Engineering, Advisor of RAACS, Professor, Dr.Sc., Voronezh State Technical University; 14, Moscow Avenue, Voronezh, 394026, Russia

Igor L. Shubin, Corresponding Member of RAACS, Professor, Dr.Sc., Research Institute of Building Physics of Russian Academy of Architecture and Construction Sciences; 21, Lokomotivny Proezd, Moscow, 127238, Russia

Vladimir N. Sidorov, Full Member of RAACS, Professor, Dr.Sc., National Research Moscow State University of Civil Engineering; Russian University of Transport (RUT – MIIT); Moscow Institute of Architecture (State Academy); Perm National Research Polytechnic University; 26, Yaroslavskoe Shosse, 129337, Moscow, Russia

Valery I. Telichenko, Full Member of RAACS, Professor, Dr.Sc., The First Vice-President of the Russian Academy of Architecture and Construction Sciences; National Research Moscow State University of Civil Engineering; 24, Ulitsa Bolshaya Dmitrovka, 107031, Moscow, Russia

Vladimir I. Travush, Full Member of RAACS, Professor, Dr.Sc., Vice-President of the Russian Academy of Architecture and Construction Sciences; Urban Planning Institute of Residential and Public Buildings; 24, Ulitsa Bolshaya Dmitrovka, 107031, Moscow, Russia

INVITED REVIEWERS

Akimbek A. Abdikalikov, Professor, Dr.Sc.,
Kyrgyz State University of Construction, Transport and Architecture n.a. N. Isanov;
34 Maldybayeva Str., Bishkek, 720020, Biskek, Kyrgyzstan

Vladimir N. Alekhin, Advisor of RAACS, Professor, Dr.Sc.,
Ural Federal University named after the first President of Russia B.N. Yeltsin;
19 Mira Street, Ekaterinburg, 620002, Russia

Irina N. Afanasyeva, Ph.D., University of Florida; Gainesville, FL 32611, USA

Ján Čelko, Professor, PhD, Ing., University of Žilina; Univerzitná 1, 010 26, Žilina, Slovakia

Tatyana L. Dmitrieva, Professor, Dr.Sc.,
Irkutsk National Research Technical University; 83, Lermontov street, Irkutsk, 664074, Russia

Petr P. Gaidzhurov, Advisor of RAACS, Professor, Dr.Sc.,
Don State Technical University; 1, Gagarina Square, Rostov-on-Don, 344000, Russia

Jacek Grosel, Associate Professor, Dr inz.
Wroclaw University of Technology; 11 Grunwaldzki Sq., 50-377, Wrocław, Poland

Stanislaw Jemioło, Professor, Dr.Sc.,
Warsaw University of Technology; 1, Pl. Politechniki, 00-661, Warsaw, Poland

Konstantin I. Khenokh, M.Ing., M.Sc.,
General Dynamics C4 Systems; 8201 E McDowell Rd, Scottsdale, AZ 85257, USA

Christian Koch, Dr.-Ing., Ruhr-Universität Bochum;
Lehrstuhl für Informatik im Bauwesen, Gebäude IA, 44780, Bochum, Germany

Gaik A. Manuylov, Professor, Ph.D.,
Moscow State University of Railway Engineering; 9, Obraztsova Street, Moscow, 127994, Russia

Alexander S. Noskov, Professor, Dr.Sc.,
Ural Federal University named after the first President of Russia B.N. Yeltsin;
19 Mira Street, Ekaterinburg, 620002, Russia

Ilya I. Ovchinnikov, Professor, Dr.Sc., Tyumen Industrial University; 38, Volodarsky St., 625000, Tyumen, Russia

Grzegorz Świt, Professor, Dr.hab. Inż.,
Kielce University of Technology; 7, al. Tysiąclecia Państwa Polskiego, Kielce, 25 – 314, Poland

AIMS AND SCOPE

The aim of the Journal is to advance the research and practice in structural engineering through the application of computational methods. The Journal will publish original papers and educational articles of general value to the field that will bridge the gap between high-performance construction materials, large-scale engineering systems and advanced methods of analysis.

The scope of the Journal includes papers on computer methods in the areas of structural engineering, civil engineering materials and problems concerned with multiple physical processes interacting at multiple spatial and temporal scales. The Journal is intended to be of interest and use to researches and practitioners in academic, governmental and industrial communities.

ОБЩАЯ ИНФОРМАЦИЯ О ЖУРНАЛЕ

International Journal for Computational Civil and Structural Engineering

(Международный журнал по расчету гражданских и строительных конструкций)

Международный научный журнал "International Journal for Computational Civil and Structural Engineering (Международный журнал по расчету гражданских и строительных конструкций)" (IJCCSE) является ведущим научным периодическим изданием по направлению «Инженерные и технические науки», издаваемым, начиная с 1999 года (ISSN 2588-0195 (Online); ISSN 2587-9618 (Print) Continues ISSN 1524-5845). В журнале на высоком научно-техническом уровне рассматриваются проблемы численного и компьютерного моделирования в строительстве, актуальные вопросы разработки, исследования, развития, верификации, апробации и приложений численных, численно-аналитических методов, программно-алгоритмического обеспечения и выполнения автоматизированного проектирования, мониторинга и комплексного наукоемкого расчетно-теоретического и экспериментального обоснования напряженно-деформированного (и иного) состояния, прочности, устойчивости, надежности и безопасности ответственных объектов гражданского и промышленного строительства, энергетики, машиностроения, транспорта, биотехнологий и других высокотехнологичных отраслей.

В редакционный совет журнала входят известные российские и зарубежные деятели науки и техники (в том числе академики, члены-корреспонденты, иностранные члены, почетные члены и советники Российской академии архитектуры и строительных наук). Основной критерий отбора статей для публикации в журнале − их высокий научный уровень, соответствие которому определяется в ходе высококвалифицированного рецензирования и объективной экспертизы, поступающих в редакцию материалов.

Журнал входит в Перечень ВАК РФ ведущих рецензируемых научных изданий, в которых должны быть опубликованы основные научные результаты диссертаций на соискание ученой степени кандидата наук, на соискание ученой степени доктора наук по научным специальностям и соответствующим им отраслям науки:

- 1.1.8 – Механика деформируемого твердого тела (технические науки),
- 1.2.2 – Математическое моделирование численные методы и комплексы программ (технические науки),
- 2.1.1 – Строительные конструкции, здания и сооружения (технические науки),
- 2.1.2 – Основания и фундаменты, подземные сооружения (технические науки),
- 2.1.5 – Строительные материалы и изделия (технические науки),
- 05.23.07 – Гидротехническое строительство (технические науки),
- 2.1.9 – Строительная механика (технические науки)

В Российской Федерации журнал индексируется Российским индексом научного цитирования (РИНЦ).

Журнал входит в базу данных Russian Science Citation Index (RSCI), полностью интегрированную с платформой Web of Science. Журнал имеет международный статус и высылается в ведущие библиотеки и научные организации мира.

Издатели журнала – *Издательство Ассоциации строительных высших учебных заведений /АСВ/* (Россия, г. Москва) и до 2017 года *Издательский дом Begell House Inc*. (США, г. Нью-Йорк). Официальными партнерами издания является *Российская академия архитектуры и строительных наук* (РААСН), осуществляющая научное курирование издания, и *Научно-исследовательский центр СтаДиО* (ЗАО НИЦ СтаДиО).

Цели журнала – демонстрировать в публикациях российскому и международному профессиональному сообществу новейшие достижения науки в области вычислительных методов решения фундаментальных и прикладных технических задач, прежде всего в области строительства.

Задачи журнала:

• предоставление российским и зарубежным ученым и специалистам возможности публиковать результаты своих исследований;

• привлечение внимания к наиболее актуальным, перспективным, прорывным и интересным направлениям развития и приложений численных и численно-аналитических методов решения фундаментальных и прикладных технических задач, совершенствования технологий математического, компьютерного моделирования, разработки и верификации реализующего программно-алгоритмического обеспечения;

• обеспечение обмена мнениями между исследователями из разных регионов и государств.

Тематика журнала. К рассмотрению и публикации в журнале принимаются аналитические материалы, научные статьи, обзоры, рецензии и отзывы на научные публикации по фундаментальным и прикладным вопросам технических наук, прежде всего в области строительства. В журнале также публикуются информационные материалы, освещающие научные мероприятия и передовые достижения Российской академии архитектуры и строительных наук, научно-образовательных и проектно-конструкторских организаций.

Тематика статей, принимаемых к публикации в журнале, соответствует его названию и охватывает направления научных исследований в области разработки, исследования и приложений численных и численно-аналитических методов, программного обеспечения, технологий компьютерного моделирования в решении прикладных задач в области строительства, а также соответствующие профильные специальности, представленные в диссертационных советах профильных образовательных организациях высшего образования.

Редакционная политика. Политика редакционной коллегии журнала базируется на современных юридических требованиях в отношении авторского права, законности, плагиата и клеветы, изложенных в законодательстве Российской Федерации, и этических принципах, поддерживаемых сообществом ведущих издателей научной периодики.

За публикацию статей плата с авторов не взымается. Публикация статей в журнале бесплатная. На платной основе в журнале могут быть опубликованы материалы рекламного характера, имеющие прямое отношение к тематике журнала.

Журнал предоставляет непосредственный открытый доступ к своему контенту, исходя из следующего принципа: свободный открытый доступ к результатам исследований способствует увеличению глобального обмена знаниями.

Индексирование. Публикации в журнале входят в системы расчетов индексов цитирования авторов и журналов. «Индекс цитирования» – числовой показатель, характеризующий значимость данной статьи и вычисляющийся на основе последующих публикаций, ссылающихся на данную работу.

Авторам. Прежде чем направить статью в редакцию журнала, авторам следует ознакомиться со всеми материалами, размещенными в разделах сайта журнала (интернет-сайт Российской академии архитектуры и строительных наук (http://raasn.ru); подраздел «Издания РААСН» или интернет-сайт Издательства АСВ (http://iasv.ru); подраздел «Журнал IJCCSE»): с основной информацией о журнале, его целями и задачами, составом редакционной коллегии и редакционного совета, редакционной политикой, порядком рецензирования направляемых в журнал статей, сведениями о соблюдении редакционной этики, о политике авторского права и лицензирования, о представлении журнала в информационных системах (индексировании), информацией о подписке на журнал, контактными данными и пр. Журнал работает по лицензии Creative Commons типа cc by-nc-sa (Attribution Non-Commercial Share Alike) – Лицензия «С указанием авторства – Некоммерческая – Копилефт».

Рецензирование. Все научные статьи, поступившие в редакцию журнала, проходят обязательное двойное слепое рецензирование (рецензент не знает авторов рукописи, авторы рукописи не знают рецензентов).

Заимствования и плагиат. Редакционная коллегия журнала при рассмотрении статьи проводит проверку материала с помощью системы «Антиплагиат». В случае обнаружения многочисленных заимствований редакция действует в соответствии с правилами COPE.

Подписка. Журнал зарегистрирован в Федеральном агентстве по средствам массовой информации и охраны культурного наследия Российской Федерации. Индекс в общероссийском каталоге РОСПЕЧАТЬ − 18076.

По вопросам подписки на международный научный журнал “International Journal for Computational Civil and Structural Engineering (Международный журнал по расчету гражданских и строительных конструкций)” обращайтесь в Агентство «Роспечать» (Официальный сайт в сети Интернет: http://www.rosp.ru/) или в издательство Ассоциации строительных вузов (АСВ) в соответствии со следующими контактными данными:

ООО «Издательство АСВ»

Юридический адрес: 129337, Россия, г. Москва, Ярославское ш., д. 26, офис 705;

Фактический адрес: 129337, Россия, г. Москва, Ярославское ш., д. 19, корп. 1, 5 этаж, офис 12 (ТЦ Соле Молл);

Телефоны: +7 (925) 084-74-24;

Интернет-сайт: www.iasv.ru. Адрес электронной почты: iasv@iasv.ru.

Контактная информация. По всем вопросам работы редакции, рецензирования, согласования правки текстов и публикации статей следует обращаться к главному редактору журнала академику РААСН *Сидорову Владимиру Николаевичу* (адреса электронной почты: sidorov.vladimir@gmail.com, sidorov@iasv.ru, iasv@iasv.ru, sidorov@raasn.ru) или к техническому редактору журнала советнику РААСН *Кайтукову Таймуразу Батразовичу* (адреса электронной почты: tkaytukov@gmail.com; kaytukov@raasn.ru). Кроме того, по указанным вопросам, а также по вопросам размещения в журнале рекламных материалов можно обращаться к генеральному директору ООО «Издательство АСВ» *Никитиной Надежде Сергеевне* (адреса электронной почты: iasv@iasv.ru, nsnikitina@mail.ru, ijccse@iasv.ru).

Журнал становится технологичнее. Издательство АСВ с сентября 2016 года является членом Международной ассоциации издателей научной литературы (Publishers International Linking Association (PILA)), осуществляющей свою деятельность на платформе CrossRef. Оригинальным статьям, публикуемым в журнале, будут присваиваться уникальные номера (индексы DOI – Digital Object Identifier), что значительно облегчит поиск метаданных и местонахождение полнотекстового произведения. DOI – это система определения научного контента в сети Интернет.

С октября 2016 года стал возможен прием статей на рассмотрение и рецензирование через онлайн систему приема статей Open Journal Systems на сайте журнала (электронная редакция): https://ijccse.iasv.ru.

Автор имеет возможность следить за продвижением статьи в редакции журнала в личном кабинете Open Journal Systems и получать соответствующие уведомления по электронной почте.

В феврале 2018 года журнал был зарегистрирован в Directory of open access journals (DOAJ) (это один из самых известных поисковых сервисов в мире, который предоставляет открытый доступ к материалам и индексирует не только заголовки журналов, но и научные статьи), в сентябре 2018 года включен в продукты EBSCO Publishing.

В ноябре 2020 года журнал начал индексироваться в международной базе Scopus.

Журнал International Journal for Computational Civil and Structural Engineering входит в первый уровень Единого государственного перечня научных изданий – «Белого списка» – Министерства Науки и высшего образования Российской Федерации (ЕГПНИ)

International Journal for
Computational Civil and Structural Engineering
(Международный журнал по расчету гражданских и строительных конструкций)
Volume 21, Issue 4 ***2025***

Scientific coordination is carried out by the Russian Academy of Architecture and Construction Sciences (RAACS)

CONTENTS

The Advisability of Application of a Unified Environmental Assessment to Building Operations Throughout All Life Cycle Stages **14**
Dmitriy Yu. Zheldakov, Vladimir T. Erofeev, Yury L. Skolubovich, Sergey I. Pakhomov, Valery P. Meshalkin, Irina V. Stepina

Deformation of Reinforced High-Strength Lightweight Concrete Elements Under Combined Eccentric Compression and Torsion **27**
Margarita A. Amelina, Natalia V. Fedorova, Nikita M. Selyutin, Elena Y. Yolkina

Efficient Algorithm of The Buckling Lengths Method in Analysis of Spatial Frame Systems for Stability **41**
Eugene I. Britvin, Moshe Eisenbeger

Dynamic Model of High-Frequency Vibration Dampers for Power Line Conductors **56**
Alexander N. Danilin, Andrey P. Zakharov, Alexander E. Fedorov, Valery A. Feldstein

An Experimental Investigation of the Thermomechanical Performance of Wood Structures Assembled with Densified Wooden Dowels Under Fire Exposure **73**
T.T. Tran, M. Khelifa, M. Khelifa, M. Oudjene, M. Debal, Y. Rogaume

Concretes with Additives Produced by Sol-Gel Method **83**
Larisa A. Urkhanova, Solbon A. Lkhasaranov, Andrey A. Ivanov, Dmitry V. Dobrynin, Imad Jamal Moslemani

Some Aspects of Testing Fibre-Reinforced Polymer Bars Under Sustained and Dynamic Loads and Various Exposures **94**
Evgeny Yu. Yurin, Sergey K. Khlebnikov, Ulyana V. Kudyakova, Konstantin L. Kudyakov, Andrey V. Buchkin

New Alternative Approach for the Algerian Seismic Design Code (RPA) of RC Building with Soft First Story **102**
Hamou Kada, Kheir Eddine Ramdane, Mabrouk Hamane

Prediction of Ground Subsidence by Modeling Tunnel Boring Machine Technology **114**
Armen Z. Ter-Martirosyan, Ilya O. Isaev, Evgenii N. Kriuchkov, Maksim N. Shlapak

Numerical Modeling of Cast-In-Place Reinforced Concrete Bubble Deck Floor Slabs Utilized in Earthquake-Prone Regions. Part Two 130
Alexander M. Belostotsky, Alexander I. Nagibovich, Sergey V. Scherbina, Tatiana N. Vasileva

Probabilistic Dynamic Analysis of a Single-Mass Vibration Isolation System 146
Vladimir A. Smirnov, Marina V. Shitikova

Stress-Strain State of Slip-Critical Connections in Metal Structures, with Regard to the Specifics of Bolt Tension Control 162
Andrey A.Vasilkin, Georgiy V. Zubkov

Drawing the Nomogram for Overhumidification of the Building Envelope 177
Kirill P. Zubarev, Yulia A. Sapronova, Vladimir D. Fedoseev

Numerical Modelling of Wind Loads. Verification and Validation for the Kemerovo Museum, Theatre and Education Complex 185
Alexander M. Belostotsky, Oleg S. Goryachevsky, Sergey G. Saiyan, Alexandra M. Efimova

Kinetics of Solid-Phase Interaction Between Dissimilar Crystalline Materials Under an Applied Load in a Wide Temperature Range 205
Valery V. Abramov, Yulia G. Zheglova, Vera V. Dolgusheva

About Development of Computational Schemes of Group Targeted Kinematic Devices for Some Elastic Systems 215
Leonid S. Lyakhovich, Pavel A. Akimov, Zaur R. Galyautdinov, Andrey S. Plyaskin

Title Emergency Calculation of the Industrial Building Structure 229
Valeriy I. Telichenko, Vladimir I. Rimshin, Ekaterina S. Ketsko

About Development of Computational Schemes of Additional Device on a Structure, that Allows for Targeted Changes of Natural Frequencies to Preset Values 240
Leonid S. Lyakhovich, Pavel A. Akimov, Zaur R. Galyautdinov, Andrey S. Plyaskin

International Journal for
Computational Civil and Structural Engineering
(Международный журнал по расчету гражданских и строительных конструкций)
Volume 21, Issue 4 ***2025***

Scientific coordination is carried out by the Russian Academy of Architecture and Construction Sciences (RAACS)

СОДЕРЖАНИЕ

Применение единой оценки экологичности строительства на всех этапах жизненного цикла **14**
Д.Ю. Желдаков, В.Т. Ерофеев, Ю.Л. Сколубович, С.И. Пахомов, В.П. Мешалкин, И.В. Степина

Деформирование армированных элементов из легкого бетона повышенной прочности при внецентренном сжатии с кручением **27**
М.А. Амелина, Н.В. Федорова, Н.М. Селютин, Е.Ю. Ёлкина

Эффективный алгоритм метода расчетных длин при анализе устойчивости пространственных рамных систем **41**
Е.И.Бритвин, М.Эйсебергер

Динамическая модель гасителей высокочастотных вибраций проводов линий электропередачи **56**
А.Н. Данилин, А.П. Захаров, А.Е. Фёдоров, В.А. Фельдштейн

Экспериментальное исследование термо-механических свойств деревянных конструкций, собранных на уплотненных деревянных нагелях, при огневом воздействии **73**
Т.Т. Тран, М. Хелифа, М. Уджене, М. Дебал, Ю. Рогаум

Бетоны с добавками, полученными золь-гель методом **83**
Л.А. Урханова, С.А. Лхасаранов, А.А. Иванов, Д.В. Добрынин, Имад Жамаль Мослемани

Некоторые аспекты испытаний арматуры композитной полимерной при длительной и динамической нагрузках и различных воздействиях **94**
Е.Ю. Юрин, С.К. Хлебников, У.В. Кудякова, К.Л. Кудяков, А.В. Бучкин

Новый альтернативный подход к алжирскому сейсмическому проектировочному кодексу (RPA) для железобетонных зданий с мягким первым этажом **102**
Хаму Када, .Хейр Эддин Рамдан, Мабрук Хаман

Прогноз осадки земной поверхности при моделировании технологии проходки тоннеля механизированным комплексомс металлическими каркасами **114**
А.З. Тер-Мартиросян, И.О. Исаев, Е.Н. Крючков, М.Н. Шлапак

Численное моделирование монолитных железобетонных перекрытий с пустотообразователями, применяемых в сейсмически активных районах. Часть 2 **130**
А.М. Белостоцкий, А.И. Нагибович, С.В. Щербина, Т.Н. Васильева

Вероятностный расчёт одномассовой виброзащитной системы **146**
В.А. Смирнов, М.В. Шитикова

Напряженно-деформированное состояние фрикционных соединений металлических конструкций с учетом особенностей контроля натяжения болтов **162**
А.А. Василькин, Г.В. Зубков

Построение номограммы переувлажнения ограждающей конструкции здания **177**
К.П. Зубарев, Ю.А. Сапронова, В.Д. Федосеев

Верификация и валидация численного моделирования ветровых нагрузок на примере музейного и театрально-образовательного комплекса в г. Кемерово **185**
А.М. Белостоцкий, О.С. Горячевский, С.Г. Саиян, А.М. Ефимова

Кинетика твердофазного взаимодействия между разнородными кристаллическими материалами под действием приложенной нагрузки в широком диапазоне температур **205**
В.В. Абрамов, Ю.Г. Жеглова, В.В. Долгушева

О формировании расчетных схем групповых прицельных кинематических устройств для некоторых упругих систем **215**
Л.С. Ляхович, П.А. Акимов, З.Р. Галяутдинов, А.С. Пляскин

Расчёт аварийной ситуации конструкции производственного здания **229**
В.И. Теличенко, В.И. Римшин, Е.С. Кецко

О формировании расчетной схемы дополнительного устройства на сооружении, позволяющего прицельно изменять до заданных значений частоты собственных колебаний **240**
Л.С. Ляхович, П.А. Акимов, З.Р. Галяутдинов, А.С. Пляскин

DOI:10.22337/2587-9618-2025-21-4-14-26

THE ADVISABILITY OF APPLICATION OF A UNIFIED ENVIRONMENTAL ASSESSMENT TO BUILDING OPERATIONS THROUGHOUT ALL LIFE CYCLE STAGES

Dmitriy Yu. Zheldakov [1], Vladimir T. Erofeev[2], Yury L. Skolubovich [3], Sergey I. Pakhomov [4], Valery P. Meshalkin [5], Irina V. Stepina [2]

[1] Research Institute of Building Physics of the Russian Academy of Architecture and Building Sciences, Moscow, RUSSIA
[2] National Research Moscow State University of Civil Engineering, Moscow, RUSSIA
[3] Novosibirsk State University of Architecture and Civil Engineering (Sibstrin), Novosibirsk, RUSSIA
[4] Russian Academy of SciencesMoscow, RUSSIA
[5] D.I. Mendeleev Russian University of Chemical Technology, Moscow, RUSSIA

Abstract: This paper proposes a method for calculating the environmental impact of constructional materials used in buildings and structures. The method is based on a broader - as compared to the currently accepted assessment pertaining solely to greenhouse gas emissions - approach to environmental impact assessment of building operations and erected structures. As a functional unit, the proposed method employs the maximum single-exposure permissible concentration (MPC) of carbon dioxide in the air of the work zone. This approach enables the assessment of a building's environmental impact with account to all harmful gas emissions into the atmosphere, expressed in CO_2 equivalents. The assessment encompasses all stages of the life cycle. The paper presents the results of surveys of enterprises engaged in manufacture of constructional materials along with a methodology for converting gas emissions into equivalent to CO_2 quantities. The analysis of emission calculations reveals that prioritizing CO_2 emissions in the latter provides a distorted picture of the manufacture's burden on the environment. The paper also describes a technology for purifying manufacture emissions from harmful gases as a result of using the methodology to identify the most environmentally damaging areas of manufacture.

Keywords: harmful gas emissions, carbon footprint, constructional material manufacture, calculation method, survey methodology

ПРИМЕНЕНИЕ ЕДИНОЙ ОЦЕНКИ ЭКОЛОГИЧНОСТИ СТРОИТЕЛЬСТВА НА ВСЕХ ЭТАПАХ ЖИЗНЕННОГО ЦИКЛА

Д.Ю. Желдаков [1], В.Т. Ерофеев [2], Ю.Л. Сколубович [3], С.И. Пахомов [4], В.П. Мешалкин [5], И.В. Степина [2]

[1] Научно-исследовательский институт строительной физики Российской Академии Архитектуры и Строительных наук, г. Москва, РОССИЯ
[2] Национальный исследовательский Московский государственный строительный университет, г. Москва, РОССИЯ
[3] Новосибирский государственный архитектурно-строительный университет (Сибстрин), г. Новосибирск, РОССИЯ
[4] Российская академия наук, г. Москва, РОССИЯ
[5] Российский химико-технологический университет имени Д.И. Менделеева, г. Москва, РОССИЯ

Аннотация: В работе предлагается метод расчета экологичности строительных материалов зданий и сооружений. В основу метода положен более широкий, по сравнению с общепринятой в последнее время оценкой производства только по выбросам газов, создающих парниковый эффект, подход к оценке воздействия на окружающую среду строительства и эксплуатации зданий. При этом в качестве функциональной единицы предложено считать значение максимально разовой в воздухе рабочей зоны ПДК диоксида углерода. Такой подход дает возможность оценивать воздействие здания на окружающую среду по всем выбросам вредных газов в атмосферу в объемах, эквивалентных выбросам углекислого газа. Оценка

производится на всех стадиях жизненного цикла. В работе приводятся результаты обследования предприятий по выпуску строительных материалов, методика пересчета выбросов в эквивалентное CO_2 количество газов. Проводится анализ расчета выбросов, делается вывод о том, что расчет по выбросу CO_2 в атмосферу дает искаженную картину нагрузки производства на окружающую среду. Приводится технология очистки выбросов производства от вредных газов, как результат использования методики с целью определения наиболее вредных участков производства.

Ключевые слова: выбросы вредных газов, углеродный след, производство строительных материалов, методика расчета, методика обследования

TITLE

The life cycle of any building or structure consists of the following stages: raw material extraction, transportation to factories, preparation and manufacture of constructional materials; delivery of materials to the construction site, building operations, operation of a capital facility; demolition and waste processing (disposal) of a capital facility [1, 2].

There is a significant number of methodologies assessing the environmental impact of each stage of a life cycle [3, 4, 5]. However, the main problem is that, to date, there is no methodology that makes it possible to compare each of these stages using a unified set of characteristics.

A second, equally important problem is that when assessing pollution, it is not taken into account that any manufacture, generation of heat and power (electricity), operation of vehicles, release a significant amount of gases into the atmosphere. The impact of these gases on the human body is much more significant than the impact of CO_2. These gases include the well-known nitrogen and sulfur oxides, carbon monoxide, saturated and unsaturated hydrocarbons, ammonia, and others. The danger of these gases to humans is defined in the Sanitary Rules and Norms SanPiN 1.2.3685-21 «Hygienic standards and requirements for ensuring the safety and (or) harmlessness of environmental factors for humans» [6], which specifies over 2300 substances for which permissible concentration limits (PCLs) of pollutants in the air of the work zone are defined. A significant amount of harmful gases, posing a danger to humans that in some cases exceeds the danger of CO_2 by millions of times [7, 8], is released into the atmosphere during the manufacture of constructional materials and the population breathes them in.

Meanwhile, the GOST standards, which are identical to the ISO 14000 series, only consider carbon dioxide emissions, neglecting other harmful gases [9, 10]. This, in turn, disincentivizes factories from adopting manufacture technologies that would reduce the quantity of these emissions [11-13].

Quantifying carbon dioxide emissions during the production of various wall structures is essential for accounting for anthropogenic greenhouse gas emissions. Research [14] has shown that timber and wood-frame buildings sequester more carbon compared to the energy consumed in their production, making these types of building structures the most environmentally friendly. The combination of a traditional renewable material—wood—and modern insulation materials provides the required energy efficiency of buildings, as mandated by European legislation. In North America and Scandinavia, a set of measures has been developed to promote the use of wood in construction. Traditionally, brick buildings are widely common in Hungary and Russia, indicating a significant additional potential for carbon sequestration. The recent trend of increasing the share of wooden housing construction could be further enhanced through specific state support measures [14].

It’s important to note that our reliance on foreign standards focused on reducing the so-called “carbon footprint” is often inappropriate in many cases. A telling example of issuing non-operational documents is the standard. The authors of this standard write that it was copied not even from foreign standards, but

from the documents of Western public organizations such as BREEAM, LEED, Code for Sustainable Homes, Living Building Challenge, Home Quality Mark, and Green Globes. This article proposes a unified methodology developed to enable comparative analysis of the environmental performance of any buildings and structures throughout all stages of its life cycle. Furthermore, the methodology allows for the assessment of environmental impact not only from gases defined as greenhouse gases, but also considering all harmful emissions into the atmosphere. As a specific outcome of the calculation, the environmental performance of a single stage can be determined, or an assessment can be made focusing only on specific gases. For example, assessing the environmental performance of the constructional material manufacturing stage will allow for evaluating the environmental impact of each material used in the construction, while calculations of CO_2, CH_4, and N_2O content let assess the greenhouse effect.

The results obtained from calculating the environmental performance of a construction project will incentivize the formulation of measures and proposals as well as their implementation in order to reduce environmental impact during the building operations.

This work was conducted in accordance with the Development Strategy of the Construction Industry and Housing and Communal Services of the Russian Federation for the period up to 2030, with a forecast until 2035, approved by the Resolution of the Government of the Russian Federation No. 3268-r dated October 31, 2022.

ASSESSMENT METHODOLOGY

1.1 Key Indicators

The main goal of the developed assessment method is to justify the need for modernization of the manufacture of materials, products, and structures in order to improve the environmental performance of manufacture processes throughout all stages of the building's life cycle. It also aims to conduct a comparative environmental analysis of technological measures implemented at the enterprise.

In the developed methodology, it is proposed to introduce a functional unit for assessing environmental impact, equal to the value of the maximum permissible single-exposure concentration (MPC) of carbon dioxide in the air of the work zone. The value of the maximum permissible single-exposure concentration in the air of the work zone was set on condition that there is no assessment of the maximum permissible concentration of CO_2 under other exposure conditions (e.g., average daily or average per work shift) using SanPiN [5].

Table 1 presents the results of the analysis of MPCs using SanPiN as per [5, Table 2.1]. It can be seen that the harmful effect of all gases on humans is much more significant than that of carbon dioxide, and for some, such as benzo(a)pyrene, this difference is 180 million times greater.

Table 1. Harmful emissions and conversion factors with account to the functional unit for assessing environmental impact

№	Gas	Maximum Permissible Single Exposure Concentration (MPC) in the Air of the Work Zone, mg/m^3	Position in table 2.1 [5]	Conversion Factor to Equivalent CO2 Quantity
1	Carbon Dioxide, CO_2	27000	2124	1,0
2	Carbon Monoxide, CO	20	2122	1350
3	Nitrogen Dioxide, NO_2	2	4	13500
4	Nitric Oxide, NO	5	5	5400
5	Ammonia, NH_3	20	178	1350
	Nitric Acid, HNO_3	2	7	13500
6	Sulfur Dioxide, SO_2	10	1837	2700

7	Inorganic Dust: 70-20% SiO_2			
8	Benzo(a)pyrene, $C_{20}H_{12}$	0,00015*	253	$1,8 \cdot 10^8$
9	Mixture of Saturated Hydrocarbons, CnHm	900	2120	30
10	Formaldehyde	0,05	2172	$5,4 \cdot 10^5$
11	Phenol	0,1	2171	$2,7 \cdot 10^5$

* average daily MPC per work shift

It is proposed that the carbon dioxide-equivalent amount of gas entering the atmosphere, considering the concept of the functional unit, be calculated by multiplying the mass of the emitted gas by the ratio of the MPC of CO_2 against the MPC of the emitted gas. The calculations use maximum permissible single-exposure concentrations in the air of the work zone, as this is the only mention of carbon dioxide in [5].

It should be noted that the indicator of the carbon dioxide-equivalent amount of gas differs significantly from the indicator defined in the normative documents for the carbon footprint as per ISO 14001:2004 11, where the carbon dioxide-equivalent amount of gas is determined by emissivity.

A carbon load factor (CLF) is introduced, equal to the ratio of pollutants (by mass) entering the atmosphere in the amount equivalent in hazard to the amount (by mass) of carbon dioxide at the stages of raw material extraction and transportation, construction materials manufacture, building operation and its disposal to the mass of the building materials [kg/kg]. Also, a building environmental performance indicator (BEPI) is introduced, defined against the amount of CO_2 equivalent the total mass of the materials used in construction to the volume of the building.

1.2 Calculation of Key Indicators and Values

The mass of pollutants entering the atmosphere in the amount equivalent in hazard to the carbon dioxide amount during the raw material extraction and transportation stage is calculated considering the electrical and thermal energy consumed by machinery and equipment during loading and transport of the raw materials to the manufacturing facility.

The mass of pollutants entering the atmosphere during the constructional materials manufacture stage in the amount equivalent in hazard to the amount of the carbon dioxide is calculated based on emissions of pollutants into the atmosphere during manufacture, as well as the electrical and thermal energy consumed when manufacturing the materials [15, 7].

The mass of pollutants entering the atmosphere during the building operations in the amount equivalent in hazard to the amount of CO_2 is calculated based on the electrical and thermal energy consumed directly on the construction site by machinery, equipment, and transport vehicles, including the transportation of constructional materials to the site and for everyday needs.

The mass of pollutants entering the atmosphere during the operational stage in the amount equivalent in hazard to the amount of CO2 is estimated based on the electrical and thermal energy consumed by building's dwellers over its entire operational period (design life), excluding urbanistic loads. In this case, the total heat loss of the building during the heating period, kWh/year, should be determined according to Appendix G SR 50.13330.

The mass of pollutants entering the atmosphere during the demolition and disposal stage in the amount equivalent in hazard to the amount of carbon dioxide is calculated considering the electrical and thermal energy consumed directly during demolition and disposal by machinery, equipment and transport vehicles, including the transportation of dismantled constructional materials for recycling and disposal.

Therefore, the impact on atmosphere at all stages of the life cycle can be expressed through fuel consumption, making the calculation universal. During the constructional materials manufacture, the environmental load determined by manufacture emissions is additionally assessed.

1.3 Calculation of emissions from the generation of thermal and electrical energy

When an enterprise consumes thermal and electrical energy, the emissions of pollutants are converted to the emissions from the combustion of natural gas at combined heat and power (CHP) plants and enterprise's boiler facilities. The specific heat of natural gas combustion is taken to be equal 8000 kCal/m3 (9.3 kW/m3, 33.5 MJ/m3) [16, 17]. The composition of natural gas is assumed to be 75% CH_4 and 25% H_2, with fuel combustion occurring at α = 1.05. The calculation is performed according to the methodology presented in [18]. These characteristics of natural gas are provided as being the most common to the majority of natural gas fuel consumed by CHP plants, but they can be modified and recalculated using the presented methodology.

The amount of natural gas consumed to generate electricity and heat at the enterprise is then calculated.

$$Vg = Q/8000 \text{ kCal}, \text{ m}^3 \quad (1)$$

The volume of combustion products is equal to:

$$V_{cmb.pr} = Vco_2+V_{O2excess}+V_{H2O}+V_{N2}, \text{ m}^3 \quad (2)$$

where Vco_2 is the volume of carbon dioxide entering the atmosphere with the combustion products $Vco_2 = 0.75Vg$, m^3 (3)

Then the mass of CO_2 with the exit gases is:

$$Mco_2 = Vco_2*44/22.4, \text{ kg} \quad (4)$$

V_{H2O} - the volume of water vapor entering the atmosphere with the combustion products:

From hydrogen combustion:

$$V_{H2O} = 0.25*Vg, \text{ m}^3 \quad (5)$$

From methane combustion:

$$V_{H2O} = 0.75*2*Vg, \text{ m}^3 \quad (6)$$

V_{N2} - the amount of nitrogen in the combustion products is derived from the volume of oxygen required for the combustion of methane and hydrogen:

$$V_{N2} = 2*0.75*Vg+0.25*Vg, \text{ m}^3 \quad (7)$$

$V_{O2excess}$ – the volume of excess oxygen in the combustion products. At α = 1.05, the following holds:

$$V_{O2excess} = Vo_2*(\alpha - 1), \text{ m}^3 \quad (8)$$

$$V_{N2} = Vo_2*79 / 21, \text{ m}^3 \quad (9)$$

Since the concentration of pollutants is determined in dry combustion products, we determine their volume, Vdg, considering (2), (5), and (6):

$$Vdg = Vco_2+Vo_{2excess}+V_{N2}, \text{ m}^3 \quad (10)$$

1.4 Calculation of Emissions for Diesel Engines

The calculation of emissions for diesel engines is based on the chemical composition of diesel fuel, which is assumed to be as follows: carbon 86,2%, hydrogen 12,8%, oxygen 1,0%. Fuel combustion occurs with an excess air coefficient of α = 1,10. The theoretical (stoichiometric) amount of air required for complete combustion of 1 kg of fuel is calculated according to [18].

1. The theoretical (stoichiometric) amount of air required for complete combustion of 1 kg of fuel is calculated using the formula:

$$Vo = Vmolar/0.21(C/12+H/2–O/32) =$$
$$= (22.4/0.21)*(0.862/12+0.128/2 – 0.01/32) =$$
$$=12.1 \text{ m}^3/\text{kg} \quad (11)$$

2. The volume of carbon dioxide in the combustion products is calculated as:

$$Vco_2 =22.4*C/12 = 22.4*0.862/12 = 1.61 \text{ m}^3/\text{kg} \quad (12)$$

Then, the mass of CO_2 emissions is:

$$Mco_2 = Vco_2 * 44 / 22.4 = 3.16 \text{ kg/kg} \quad (13)$$

3. The volume of oxygen and nitrogen in the combustion products is calculated as:

$$Vo_2 = 0.21*(\alpha - 1)*Vo = 0.21*(1.1 - 1)*12.1 = 0.254 \text{ m}^3/\text{kg} \quad (14)$$

$$V_{N2} = 0.79 *\alpha*Vo = 0.79 * 1.1 * 12.1 = 10.51 \text{ m}^3/\text{kg} \quad (15)$$

4. The volume of dry combustion products is:

$$Vdg = Vco_2+Vo_2+V_{N2}=1.61+0.254+10.51 = 12.374 \text{ m}^3/\text{kg} \quad (16)$$

The amount of emissions is calculated as the volume of dry gases multiplied by the concentration of the pollutant.

The concentration of pollutants in the combustion products of diesel fuel [19] and natural gas [20, 21] are taken from Table 2.

Table 2. Concentration of Pollutants in Combustion Products

№	Pollutant	Emission Concentration, mg/m³	
		From Diesel Fuel Combustion	From Natural Gas Combustion
1	Carbon Monoxide, CO	1250	300
2	Nitrogen Oxides on conversion to NO_2	200	125
3	Sulfur Dioxide, SO_2	28,6	--
4	Formaldehyde	13,4	--
5	Unsaturated hydrocarbons	67	--
7	Benzo(a)pyrene	0,0005	$2 \cdot 10^{-6}$
8	Carbon Dioxide (CO_2)	As per calculation	As per calculation

RESULTS AND DISCUSSION

The authors have conducted a survey calculating the environmental load for several enterprises using the developed methodology. This article presents an analysis of the survey results from the Rockwool mineral wool production plant in Zheleznodorozhny, Moscow Oblast. The first two stages of the life cycle are examined in detail: raw material extraction, transportation, and the manufacture stage itself. The production volume is 1,390,000 m³ or 98,000 tons of mineral wool per year. The plant has 42 emission sources. Electricity consumption is 126,777,532 kWh (2022-year data). On-site transportation is provided by 7 diesel-powered forklifts.

During the manufacture, a survey encompassed all 42 emission sources. At each sampling point, the diameter of the process pipeline, the gas velocity, and the gas temperature were recorded. When selecting a gas analyzer for analyzing harmful emissions in industrial gas samples and hydrocarbon fuel combustion products, it is important to consider their potential concentrations. For example, the concentration of carbon dioxide in combustion products is approximately 10%, while in process gases, it is often equal to the concentration in air, that is, 0,03% by volume. The concentration of NO_2 also varies from 150 – 350 mg/m³ in combustion products to 0,1 – 1 mg/m³ in urban air. A «Polar-7» portable multi-component gas analyzer (manufactured by Promekopribor LLC) was used to measure high concentrations, and a «Signal – 44» gas analyzer (manufactured by Gasoanalit LLC) to deal with low concentrations.

A summary of the survey and calculated emissions of harmful gases released into the environment during manufacture are shown in Table 3.

Diesel fuel consumption at the enterprise is 18,772 l or 14,435.7 kg, and electricity consumption is 126,777,532 kWh, which is equivalent to 13,631,993 m³ of natural gas.

The calculation of harmful substance emissions, converted to the equivalent hazard-weighted emission, is performed using equations (1) – (10) for natural gas and (11) – (16) for diesel fuel. The concentration of harmful gases in the emissions is taken from Table 2. The results of calculating harmful substance emissions from the operation of diesel transport and electricity

consumption at the manufacturing stage are shown in Table 4.

Table 3. Manufacturing emissions

№	Emission substances	Total emission in tons per year	% of general emission	Conversion factor	Amount of Gas Equivalent to Carbon Dioxide, tons/year	% of total emission
1	**2**	**3**		**4**	**5**	**6**
1	Nitrogen Dioxide	39,639	0,20	13500	535 126,5	15,3
2	Nitric Oxide	8,175	0,04	5400	44 145,0	1,26
3	Ammonia	53,837	0,27	1350	72 680,0	2,07
4	Sulfur Dioxide	7,078		2700	19 110,6	0,55
5	Inorganic Dust: 70-20% SiO_2	177,368	0,90	2700 (in SO_2 with account of 50%)	239 446,8	6,85
6	Carbon Monoxide	157,973	0,80	1350	213 263,6	6,10
7	Benzo[a]pyrene	$4,18*10^{-7}$		$1,8*10^{8}$	75,2	0,002
8	Mixture of Saturated Hydrocarbons	2,101		30	63,0	0,002
9	Formaldehyde	3,959	0,02	$5,4*10^{5}$	2 137 860,0	61,15
10	Phenol	0,795		$2,7*10^{5}$	214 650,0	6,14
11	Carbon Dioxide	19671,9	97,76	1	19 671,9	0,56
	Total				3 496 092,6	

Table 4. Calculation results concerning harmful substance emissions from diesel transport operation and electricity consumption during manufacture

№	Pollutant	Pollutant Emissions					
		Diesel vehicle operation			Electricity from CHP (Combined Heat and Power Plant)		
		Concentration, mg/m^3	Emission, tons	Equivalent emission, tons	Concentration, mg/m^3	Emission, tons	Equivalent emission, tons
1	Carbon Monoxide, CO	1250	0,22	297	300	30,35	40 972,5
2	Nitrogen Oxides, as NO_2	200	0,036	482,3	125	12,65	170 775,0
3	Sulfur Dioxide, SO_2	28,6	$5,1*10-3$	13,79	--		
4	Formaldehyde	13,4	$2,4*10^{-3}$	1296,0	--		
5	Unsaturated hydrocarbons	67	0,012	0,36	--		
7	Benzo[a]pyrene	0,0005	$0,09*10^{-6}$	16,1	$2\cdot10^{-6}$	$2,02*10^{-7}$	36,4
8	Carbon Dioxide CO_2	As per calculation 3,16 kg/kg of fuel	45,6	45,6	As per calculation 1,47 kg/m^3 of natural gas	20 039,0	20 039,0
	Total			2 151,15			231 822,9

During the raw material extraction and transportation stage for mineral wool production, according to the survey results, the plant receives per year up to 125000 tons of dolomite, bauxite, tuff, and blast furnace slag as raw materials, with an average transportation distance of 400 km.

The excavator's work rate is 20 m^3/h, and its fuel consumption is 30,0 L/h. The density of bauxite and dolomite can be assumed to be 3000 kg/m^3. The excavator loads 60 tons per hour onto transport vehicles; therefore, extracting and loading 125000 tons (calculated for bauxite and dolomite) will require 2083.3 hours of operation. The fuel consumption will be 62,500 L, or 48062,5 kg of diesel fuel.

Transportation is carried out by rail. The specific electricity consumption depends on the track profile, type of rolling stock, speed, weather conditions, etc. In freight traffic on flat terrain, it is 10–12 W-h/(ton-km), and on mountainous sections, it is 25–32 W-h/(ton-km). We will assume 15 W-h/(ton-km). Then, the electricity consumption for transporting 125 000 tons of raw materials to the distance of 400 km will be:

15 W-h/(ton-km) * 125000 t * 400 km = 750 000 kW-h, which corresponds to a calorific value of 80 645,2 m^3 of natural gas.

The calculation of pollutants' emissions, converted to the equivalent hazard-weighted emission, is performed using equations (1) – (10) for natural gas and (11) – (16) for diesel fuel. The concentration of harmful gases in the emissions is taken from Table 2. The results of calculating harmful substance emissions during the extraction and transportation stage, in the volume required for manufacture, are presented in Table 5.

Table 5. Calculation results for pollutants during the extraction and transportation stage

№	Pollutant	Pollutant emissions					
		Raw material extraction			Raw material transportation		
		Concentration, mg/m^3	Emission, tons	Equivalent emission, tons	Concentration, mg/m^3	Emission, tons	Equivalent emission, tons
1	Carbon Monoxide, CO	1250	0,74	1004,6	300	0,18	243,0
2	Nitrogen Oxides, as NO_2	200	0,12	1606,5	125	0,075	1009,94
3	Sulfur Dioxide, SO_2	28,6	0,017	45,9	--		
4	Formaldehyde	13,4	$8,0*10^{-3}$	4305,4	--		
5	Unsaturated hydrocarbons	67	0,04	1,20	--		
7	Benzo[a]pyrene	0,0005	$0,3*10^{-6}$	54,0	$2 \cdot 10^{-6}$	$1,61*10^{-8}$	0,22
8	Carbon Dioxide CO_2	As per calculation 3,16 kg/kg of fuel	151,88	151,88	As per calculation 1,47 kg/m^3 of natural gas	118,55	118,55
	Total			7 169,48			1 371,71

The total emission of pollutants during the extraction, transportation, and manufacture stage is presented in Table 6.

Table 6. Total emission of pollutants during the extraction, transportation, and manufacture stages

№	Source of emission	Equivalent emission, tons/year
1	**Extraction and transportation stage** (Table 5)	8 541,19
1.1	Extraction	7 169,48
1.2	Transportation	1 371,71
2	**Manufacture stage**	
1	Release of toxic gases from manufacturing process (Table 3)	3 496 092,6
2	Harmful gas emissions from enterprise's vehicles (Table 4)	2 151,15
3	Harmful gas emissions from electricity/power generation (Section 4)	231 822,9
	Total	3 730 066,65

Considering the production volume of 1 390 000 m³/year or 98.0 tons/year, the Carbon Footprint Coefficient (CFC) will be 3 730 066.65 / 98 000 = 38,06.

The analysis of the survey results and the proposed calculation methods allows us to draw several important conclusions:

1. If the enterprise's emissions are assessed solely by the mass of harmful gases released into the atmosphere, carbon dioxide emissions significantly outweigh the emissions of other gases. For example, according to Table 3, which assesses the technological emissions from mineral wool production, carbon dioxide emissions account for 97,76% by mass. However, when considering the same production process against the amount of gas equivalent in hazard to the amount of carbon dioxide the carbon dioxide emission only accounts for 0,56%. In this case, the highest value, equal to 61,15%, belongs to formaldehyde emissions – an aliphatic aldehyde of methanol and formic acid, which is a colorless gas with a pungent odor. This approach, defined by the developed calculation method, leads to the conclusion that, to reduce atmospheric pollution, it is primarily necessary to reduce the formaldehyde content in the enterprise's emissions. In [22], it was shown that a technological solution could be the afterburning of formaldehyde by directing it to the burners of the production boiler plant.
2. The developed method provides the opportunity to assess the environmental burden on the atmosphere at each stage of the life cycle, as well as for different functional production processes within a single stage. Table 6 shows that the extraction and transportation of raw materials contributes only 0,23% of the pollution released into the atmosphere across the two stages: extraction - transportation, and the production of mineral wool. Within the production stage, according to Table 6, it can be estimated that the enterprise's diesel motor transport emits only 0,06% of the total hazard-equivalent mass of emissions, while the generation of electricity/power sourced externally by the enterprise accounts for 6,6%.
3. The method allows, if necessary, for the estimation of greenhouse gas emissions alone. Furthermore, a comparison of the results for carbon dioxide emissions, according to the developed methodology and that one approved by Order No. 15-r issued by the Ministry of Natural Resources and Ecology of the Russian Federation dated April 16, 2015 [20], shows complete correlation. However, the developed methodology provides an opportunity to assess carbon dioxide emissions more accurately, taking into account the chemical composition of the fuel consumed.
4. Calculation of the Carbon Footprint Coefficient (CFC) using the developed methodology allows to determine the environmental performance of constructional materials and life cycle stages as objectively as possible.

CONCLUSION

The proposed methodology gives a more accurate account of the environmental burden throughout all stages of the buildings and structures' life cycle due to calculation of emissions of all harmful gases released into the atmosphere. The method is based on the introduction of a functional unit for assessing environmental impact, equal to the maximum permissible concentration (MPC) of carbon dioxide in the air of the work zone at a single exposure. This makes it possible to compare emission quantities at each stage, as well as to identify the most environmentally sensitive areas at each stage of manufacture. Of great importance in the presented methodology is its simplicity and illustrative nature.

ACKNOWLEDGEMENTS

The research was funded by the National Research Moscow State University of Civil Engineering (grant for fundamental scientific research, project No. 05-661/130).

REFERENCES

1. **Tetior A.N.** (2006). Gorodskaya ekologiya [Urban Ecology]. Moscow: Academy, 336 pp.
2. **Temikeev K**. (2024) Life cycle of buildings and structures. Life cycle stages. *BIO Web of Conferences*. EDP Sciences, Vol. 107. pp. 06007. https://doi.org/10.1051/bioconf/202410706007
3. **Kudryavceva O.V., Ledashheva T.N., Pinaev V.E.** (2023). Metodika i praktika ocenki vozdejstviya na okruzhayushhuyu sredu. Proektnaya dokumentaciya [Methodology and Practice of Environmental Impact Assessment. Project Documentation]. M. : MGU M. V. Lomonosova,. 172 pp.
4. **Vasilenko T.A., Sverguzova S.V.** (2019). Ocenka vozdejstviya na okruzhayushhuyu sredu i e`kologicheskaya e`kspertiza inzhenerny`x proektov [Environmental impact assessment and ecological expertise of engineering projects]. M.: Infra-Inzheneriya. 264 pp.
5. **Glinyanova I. Yu., Erofeev V. T., Afonin V.V.** (2023). E`kologicheskij monitoring territorij uslovno chisty`x zon Volgogradskoj aglomeracii [Environmental monitoring of the territories of conditionally clean zones of the Volgograd agglomeration]. Vestnik MGSU. Vol. 18. No. 4. pp. 584–594.
6. **Eremina N.A.** (2021). O novy`x gigienicheskix normativax i trebovaniyax k obespeche-niyu bezopasnosti faktorov okruzha-yushhej sredy`. Sostoyanie i perspekti-vy` razvitiya e`lektro-i teplotexnologii (XXI Benardosovskie chteniya) [On new hygienic standards and requirements for ensuring the safety of environmental factors // The state and prospects of development of electrical and thermal technology (XXI Benardos Readings)]. pp. 167-171.
7. **Mehra, S., Singh, M., Sharma, G., Kumar, S., Navishi, & Chadha, P.** (2022). Impact of construction material on environment. Ecological and Health Effects of Building Materials, 427-442. https://doi.org/10.1007/978-3-030-76073-1_22
8. **Pacheco-Torgal F., Jalali S., Fucic A**. (ed.). Toxicity of building materials. – Elsevier, 2012.
9. **Kashina I.V., Levenko A.D., Samojlo-va A.Yu.** (2017). Problemma e`kologichnosti stroitel`ny`x materialov. Analiz zhiznennogo cikla zdanij i sooruzhe-nij. Stroitel`stvo i texnogennaya bezopasnost` [Kashina I.V., Levenko A.D., Samoilova A.Yu. The problem of environmental friendliness of building materials. Analysis of the life cycle of buildings and structures. Construction and technogenic safety]. № 8. Pp. 7-13.
10. **Meshalkin V.P., Bobkov V.I., Kani-shhev O.A.** (2021). Komp`yuternaya polumarkovskaya model` upravleniya e`kspluatacionnoj nadezhnost`yu slozhnoj gazoanaliticheskoj sistemy` kontrolya ximicheskix zagryaznenij. Doklady` Rossijskoj akademii nauk. Ximiya, nauki o materialax [Computer semi-Markov model of operational reliability control of complex gas analytical system for chemical pollution monitoring. Reports of the Russian Academy of Sciences. Chemistry, Materials Science]. Vol. 497. No 1, pp. 14-21 DOI: 10.31857/S2686953521020060.
11. **Erofeev V.T., Al Dulaimi Salman Dawood Salman, Dergunova A.V.** (2021). The improving the durability and environmental friendliness of buildings and structures in the textile industry through the use of materials modified with microbiological additives. Proceedings of higher education institutions. Textile Industry Technology. No 3 (393). pp. 141–146.
12. **Erofeev, V.T., Smirnov, V.F., Svetlov, D.A., Vasil`ev, O.D., Vil`dyaeva, M.V., Goik, V.G.** (2019). Stroitel`-stvo, rekonstrukciya i e`kspluataciya zdanij i sooruzhenij s uchetom e`kolo-gicheskix i medicinskix aspektov. In Vestnik Privolzhskogo territorial`-nogo otdeleniya Rossijskoj akademii arxitektury` i stroitel`ny`x nauk [Construction, reconstruction and op-

eration of buildings and structures taking into account environmental and medical aspects. Bulletin of the Volga Territorial Branch of the Russian Academy of Architecture and Construction Sciences]. pp. 219-232.

13. **Svetlov D.A., Boriskin A.S., Dergunova A.V., Vildaiva M.V., Erofeev V.T.** (2022). Disinfection and sterilization of air and internal surfaces of industrial premises. Lecture Notes in Civil Engineering. Vol. 189. pp. 38–43.
14. **Pastori Z., Borchok Z., Gorbacheva G.A.** (2015). Balans CO_2 razlichny`x vidov stenovy`x konstrukcij. Stroitel`ny`e materialy`[CO_2 balance of different types of wall structures. Building materials]. No 12. pp. 76-77.
15. **Mikulčić, H., Klemeš, J.J., Vujanović, M., Urbaniec, K., & Duić, N.** (2016). Reducing greenhouse gasses emissions by fostering the deployment of alternative raw materials and energy sources in the cleaner cement manufacturing process. Journal of cleaner production. Vol. 136. pp. 119-132. https://doi.org/10.1016/j.jclepro.2016.04.145
16. **Meshalkin V.P., Dovì V.G., Bobkov V.I., Belyakov A.V., Butusov O.B., Garabadzhiu A.V., Burukhina T.F., Khodchenko S.M.** (2021). State of the art and research development prospects of energy and resource-efficient environmentally safe chemical process systems engineering. Mendeleev Communications. Vol. 31. pp. 593–604. DOI: 10.1016/j.mencom.2021.09.003
17. Normativy` udel`ny`x vy`brosov zagryaznyayushhix veshhestv v atmosferu ot kotel`ny`x ustanovok TE`S. M. : Minobrnauki Rossii [Standards for specific emissions of pollutants into the atmosphere from thermal power plant boiler units. Moscow: Ministry of Education and Science of Russia]. 2013.
18. **Ravich M.B.** (1977). E`ffektivnost` ispol`zovaniya topliva [Efficiency of fuel use]. M. – Nedra. — 344 S.
19. **Pepina L.A., Sozontova A.N.** 2017. Zagryaznenie atmosfernogo vozduxa avtomobil`no-dorozhny`m transportom [Air pollution from road transport]. Alfabild, 1(1). pp. 99-110.
20. **Podlipenskaya L.E., Topalova S.V., Alferova M.A.** (2012). Dinamika intensivnosti dvizheniya gorodskogo avtomobil`nogo transporta i zagryazne-niya atmosfernogo vozduxa ego vy`bro-sami [Dynamics of the intensity of urban motor transport and air pollution by its emissions. Russian Medical and Biological Bulletin named after Academician I.P. Pavlov]. Rossijskij mediko-biologicheskij vestnik im. Akademika I.P. Pavlova. No 4. pp. 58–62.
21. **Vasil`eva M.A., Dubczov S.N., Zhoxova N.V., Palej A.A., Pisanko Yu.V., Tolpy`gin L.I.** (2016). Ocenka urovnya koncentracii ae`rozol`ny`x chasticz u avtomobil`noj dorogi i LE`P v srav-nenii s fonovy`mi pokazatelyami sub-mikronny`x chasticz estestvennoj atmo-sfery` [Estimation of the level of concentration of aerosol particles near a road and power transmission line in comparison with background indicators of submicron particles of the natural atmosphere. Proceedings of the Main Geophysical Observatory named after A.I. Voeikov]. Trudy` glavnoj geofizicheskoj observatorii im A.I. Voejkova. No 580. pp. 99–109.
22. **Zheldakov D.Yu.** (2024). Metod opredeleniya e`kologichnosti stroitel`ny`x materialov [Method for determining the environmental friendliness of building materials. Biosphere compatibility: man, region, technology]. Biosfernaya sovmesti-most`: chelovek, region, texnologii. No 1(45). pp. 73–82.

СПИСОК ЛИТЕРАТУРЫ

1. **Тетиор, А.Н.** (2006). Городская экология. М.: Академия Изд. центр. 336 с.
2. **Temikeev K.** (2024). Life cycle of buildings and structures. Life cycle stages. BIO

Web of Conferences. EDP Sciences. Vol. 107. pp. 06007. https://doi.org/10.1051/bioconf/202410706007

3. **Кудрявцева О.В., Ледащева Т.Н., Пинаев В.Е.** Методика и практика оценки воздействия на окружающую среду. Проектная документация. – М. : МГУ им. М. В. Ломоносова, 2023. – 172 с.
4. **Василенко Т.А., Свергузова С.В.** Оценка воздействия на окружающую среду и экологическая экспертиза инженерных проектов. – М.: Инфра-Инженерия, 2019. – 264 с.
5. **Глинянова И.Ю., Ерофеев В.Т., Афонин В.В.** (2023). Экологический мониторинг территорий условно чистых зон Волгоградской агломерации. Вестник МГСУ. Т. 18. №. 4. С. 584-594.
6. **Еремина Н.А**. (2021). О новых гигиенических нормативах и требованиях к обеспечению безопасности факторов окружающей среды. Состояние и перспективы развития электро-и теплотехнологии (XXI Бенардосовские чтения). С. 167-171.
7. **Mehra, S., Singh, M., Sharma, G., Kumar, S., Navishi, & Chadha, P. (**2022). Impact of construction material on environment. Ecological and Health Effects of Building Materials, 427-442. https://doi.org/10.1007/978-3-030-76073-1_22
8. **Pacheco-Torgal F., Jalali S., Fucic A.** (ed.). (2012). Toxicity of building materials. Elsevier.
9. **Кашина И.В., Левенко А.Д., Самойлова А.Ю.** (2017). Проблемма экологичности строительных материалов. Анализ жизненного цикла зданий и сооружений. Строительство и техногенная безопасность. № 8. С. 7-13.
10. **Мешалкин В.П., Бобков В.И., Канищев О.А.** (2021). Компьютерная полумарковская модель управления эксплуатационной надежностью сложной газоаналитической системы контроля химических загрязнений. Доклады Российской академии наук. Химия, науки о материалах. Т. 497. № 1, С. 14-21 DOI: 10.31857/S2686953521020060.
11. **Erofeev V.T., Al Dulaimi Salman Dawood Salman, Dergunova A.V.** (2021). The improving the durability and environmental friendliness of buildings and structures in the textile industry through the use of materials modified with microbiological additives. Proceedings of higher education institutions. Textile Industry Technology. No 3 (393). pp. 141–146.
12. **Ерофеев, В.Т., Смирнов, В.Ф., Светлов, Д.А., Васильев, О.Д., Вильдяева, М.В., Гоик, В.Г.** (2019). Строительство, реконструкция и эксплуатация зданий и сооружений с учетом экологических и медицинских аспектов. Вестник Приволжского территориального отделения Российской академии архитектуры и строительных наук, С. 219-232.
13. **Svetlov D.A., Boriskin A.S., Dergunova A.V., Vildaiva M.V., Erofeev V.T**. (2022). Disinfection and sterilization of air and internal surfaces of industrial premises. Lecture Notes in Civil Engineering. Vol. 189. pp. 38–43.
14. **Пастори З., Борчок З., Горбачева Г.А.** (2015). Баланс CO_2 различных видов стеновых конструкций. Строительные материалы. №. 12. С. 76-77.
15. **Mikulčić, H., Klemeš, J.J., Vujanović, M., Urbaniec, K., & Duić, N.** (2016). Reducing greenhouse gasses emissions by fostering the deployment of alternative raw materials and energy sources in the cleaner cement manufacturing process. Journal of cleaner production. Vol. 136. pp. 119-132. https://doi.org/10.1016/j.jclepro.2016.04.145
16. **Meshalkin V.P., Dovì V.G., Bobkov V.I., Belyakov A.V., Butusov O.B., Garabadzhiu A.V., Burukhina T.F., Khodchenko S.M.** (2021). State of the art and research development prospects of energy and resource-efficient environmentally safe chemical process systems engineering. Mendeleev Communications. Vol. 31. pp. 593–604. DOI: 10.1016/j.mencom.2021.09.003

17. Нормативы удельных выбросов загрязняющих веществ в атмосферу от котельных установок ТЭС. М. : Минобрнауки России. 2013.
18. **Равич М.Б.** (1977). Эффективность использования топлива. М. – Недра. — 344 С.
19. **Пепина Л.А., Созонтова А.Н.** 2017. Загрязнение атмосферного воздуха автомобильно-дорожным транспортом. Alfabild, 1(1). С. 99-110.
20. **Подлипенская Л.Е., Топалова С.В., Алферова М.А.** (2012). Динамика интенсивности движения городского автомобильного транспорта и загрязнения атмосферного воздуха его выбросами. Российский медико-биологический вестник им. Академика И.П. Павлова. № 4. С. 58–62.
21. **Васильева М.А., Дубцов С.Н., Жохова Н.В., Палей А.А., Писанко Ю.В., Толпыгин Л.И**. (2016). Оценка уровня концентрации аэрозольных частиц у автомобильной дороги и ЛЭП в сравнении с фоновыми показателями субмикронных частиц естественной атмосферы. Труды главной геофизической обсерватории им А.И. Воейкова. № 580. С. 99–109.
22. **Желдаков Д.Ю.** (2024). Метод определения экологичности строительных материалов. Биосферная совместимость: человек, регион, технологии. № 1(45). С. 73–82.

Zheldakov Dmitry Yuryevich - PhD in Engineering, Leading Researcher, Lab. #12, NIISF RAASN, Lokomotivny proezd, 21. Moscow, Russia. djeld@mail.ru

Erofeev Vladimir Trofimovich - Doctor of Engineering, Professor, Professor of the Department of Construction Materials Science, National Research Moscow State University of Civil Engineering, 129337, Yaroslavskoe sh., 26, Moscow, Russia. erofeevvt@bk.ru

Skolubovich Yury Leonidovich - Doctor of Engineering, Professor, Rector of NGASU (Sibstrin), Leningradskaya str., 113, Novosibirsk, Russia. rector@sibstrin.ru

Pakhomov Sergey Ivanovich - Doctor of Chemical Sciences, Professor. Head of the Department for Support of the Organization of State Scientific Certification of the Russian Academy of Sciences, 119334, Leninsky Prospekt, 32A, Moscow, Russia. Sipakhomov@pran.ru

Meshalkin Valery Pavlovich - Doctor of Technical Sciences, Academician of the Russian Academy of Sciences, Director of the International Institute of Resource-Saving Logistics and Technological Innovation (REC), D.I. Mendeleyev University of Chemical Technology of Russia. 125047, Miusskaya Square, 9, Moscow, Russia. vpmeshalkin@gmail.com

Stepina Irina Vasilievna - Candidate of Technical Sciences, Associate Professor, Associate Professor of the Department of Construction Materials Science of the National Research Moscow State University of Civil Engineering, 129337, Yaroslavskoe Highway, 26, Moscow, Russia. sudeykina@mail.ru

Желдаков Дмитрий Юрьевич - кандидат технических наук, ведущий научный сотрудник лаб. #12 НИИСФ РААСН, Локомотивный проезд, д.21. Москва, Россия. djeld@mail.ru

Ерофеев Владимир Трофимович – доктор технических наук, профессор, профессор кафедры строительного материаловедения Национального исследовательского Московского государственного строительного университета, 129337, Ярославское ш., 26, Москва, Россия. erofeevvt@bk.ru

Сколубович Юрий Леонидович - доктор технических наук, профессор, ректор НГАСУ (Сибстрин), ул. Ленинградская, 113, г. Новосибирск, Россия. rector@sibstrin.ru

Пахомов Сергей Иванович - доктор химических наук, проф. начальник управления сопровождения организации государственной научной аттестации РАН, 119334, Ленинский пр., д 32А, Москва, Россия. Sipakhomov@pran.ru

Мешалкин Валерий Павлович - доктор технических наук, академик РАН, директор международного института логистики ресурсосбережения и технологической инноватики (НОЦ), Российский химико-технологический университет имени Д.И. Менделеева. 125047, Миусская площадь д. 9, г. Москва, Россия. vpmeshalkin@gmail.com

Степина Ирина Васильевна – кандидат технических наук, доцент, доцент кафедры строительного материаловедения Национального исследовательского Московского государственного строительного университета, 129337, Ярославское ш., 26, Москва, Россия. sudeykina@mail.ru

DOI:10.22337/2587-9618-2025-21-4-27-40

DEFORMATION OF REINFORCED HIGH-STRENGTH LIGHTWEIGHT CONCRETE ELEMENTS UNDER COMBINED ECCENTRIC COMPRESSION AND TORSION

Margarita A. Amelina [1], Natalia V. Fedorova [1], Nikita M. Selyutin [2], Elena Y. Yolkina [3]

[1] National Research Moscow State University of Civil Engineering (NRU MGSU), Moscow, RUSSIA
[2] A.A. Gvozdev Research Institute of Concrete and Reinforced Concrete, JSC «Research Center «Construction», Moscow, RUSSIA
[3] MonArch LLC, Moscow, RUSSIA

Abstract: This paper presents the results of an experimental study on the deformation and failure of reinforced high-strength lightweight concrete elements under combined eccentric compression and torsion. The physical patterns and characteristics of deformation for such elements under the specified stress state have been established. The investigated parameters include concrete and reinforcement strains, crack patterns and crack widths, as well as deflections and angles of twist for the elements under consideration. The study demonstrates that crack formation in high-strength lightweight reinforced concrete structures has its own specificities: under loading with an eccentrically applied compressive force and a torque, one or several spatial cracks develop. As the load increases, one dominant crack emerges, leading to failure along this crack. A further characteristic of the deformation behavior is that after crack initiation, the deformation stage range leading to failure is more than two times shorter compared to structures made of conventional normal-weight concrete. A comparison of the obtained experimental data with the results of calculations based on the proposed analytical model confirms its reliability and potential for practical application.

Keywords: High-strength lightweight concrete, complex stress state, torsion, eccentric compression, experimental studies

ДЕФОРМИРОВАНИЕ АРМИРОВАННЫХ ЭЛЕМЕНТОВ ИЗ ЛЕГКОГО БЕТОНА ПОВЫШЕННОЙ ПРОЧНОСТИ ПРИ ВНЕЦЕНТРЕННОМ СЖАТИИ С КРУЧЕНИЕМ

М.А. Амелина [1], Н.В. Федорова [1], Н.М. Селютин [2], Е.Ю. Ёлкина [3]

[1] Национальный исследовательский Московский государственный строительный университет (НИУ МГСУ) г. Москва, РОССИЯ
[2] Научно-исследовательский институт бетона и железобетона им. А.А. Гвоздева АО «НИЦ «Строительство», г. Москва, РОССИЯ
[3] ООО «МонАрх», г. Москва, РОССИЯ

Аннотация: Приведены результаты экспериментальных исследований деформирования и разрушения железобетонных элементов из легкого высокопрочного бетона при внецентренном сжатии с кручением. Установлены физические закономерности и особенности деформирования таких элементов при рассматриваемом напряженном состоянии, определены деформации бетона и арматура, картины и ширина раскрытия трещин, а также прогибы и углы закручивания для рассматриваемых элементов. Показано, что трещинообразование в конструкциях из легкого высокопрочного железобетона имеют свою специфику: при нагружении к элементу внецентренно приложенной сжимающей силы и крутящего момента в нём образуются одна или несколько пространственных трещин из которых, по мере нагружения выделяется одна и по ней происходит разрушение. Особенностью деформирования является и то, что после образования трещин в рассматриваемом элементе диапазон стадии деформирования до

разрушения более чем в два раза меньший, чем в конструкциях из обычного тяжелого бетона. Сопоставлением полученных опытных данных с результатами расчета по предложенной аналитической модели подтверждена ее достоверность и возможность практического использования.

Ключевые слова: легкий бетон повышенной прочности, сложное напряженное состояние, кручение, внецентренное сжатие, экспериментальные исследования

INTRODUCTION

Currently, both domestically and internationally, intensive research is being conducted aimed at the development and application of high-strength structural lightweight concrete. In current Russian [11] and foreign codes for the design of reinforced concrete structures [12, 13], the class of structural lightweight concretes is limited. Consequently, these documents lack the physico-mechanical characteristics of high-strength lightweight concrete. At the same time, in Russia, an experimental self-compacting high-strength lightweight concrete with density grades below D2000 and strength classes B50-B65 [1-3] has been developed, which appears to be a highly promising material for lightweight load-bearing walls, columns, and floors of high-rise buildings [2,7]. This direction, associated with the use of a new generation of lightweight concretes in the construction industry aimed at reducing building mass, is gaining new relevance, especially for construction in seismically active regions and for the design of buildings and structures considering special impacts [2,5,6,14]. However, due to the low initial modulus of elasticity of lightweight concretes and other physico-mechanical peculiarities of the material, a problem arises in ensuring the stiffness of floors and other flexural and eccentrically loaded compression members.

An analysis of Russian [1-6] and foreign [8-10] publications on lightweight concrete research shows that lightweight concrete as a material in reinforced concrete structures can possess good performance characteristics in construction due to its expectedly lower contribution to the structure's self-weight. However, as noted in the publications, despite some experience in using such concrete for load-bearing elements of buildings, existing research on this material in Russia and abroad is limited to the study of mixes [2] and some physico-mechanical properties. Recently completed studies on the strength and deformation characteristics of self-compacting high-strength expanded clay concrete of classes B50–B65 [1-3], as well as the long-term deformation of such concretes with different structures [4], can be noted here.

Foreign research is increasingly focusing on the study of the physico-mechanical properties of lightweight concrete with various types of fiber reinforcement. For example, study [8] experimentally investigated the mechanical properties and the complete stress-strain diagram of lightweight concrete reinforced with steel and carbon fibers. The research was conducted on cylindrical specimens with strength classes from LC40 to LC60 and a fiber volume fraction from 0% to 0.9%. The results of these tests showed that steel fiber can significantly increase flexural strength and split tensile strength.

Publication [9] presents a series of tests on cylinders made of steel fiber-reinforced lightweight aggregate concrete (SFRLWAC) aimed at developing a physical deformation model for this material (SFRLWAC) under monotonic compressive loading. Experiments established that adding steel fiber to lightweight concrete has an insignificant effect on the ascending branch of the stress-strain curve but has a noticeable effect on the descending (post-peak) branch of deformation. The publication also includes some analysis results for beam structures (1200mm span, 200×150 mm cross-section) made of steel fiber-reinforced

lightweight concrete. It is shown that adding steel fiber changes the pattern of crack propagation in the structures. In conventional lightweight concrete, cracks propagate parallel to the load direction (normal cracks), whereas in steel fiber-reinforced lightweight concrete structures, the direction of crack development under load changes, and the cracks gradually incline and become perpendicular to the load direction.

Research on the physico-mechanical properties of lightweight concrete with a strength of 50-70 MPa, reinforced with carbon and polypropylene fibers both individually and in hybrid form, is presented in publication [10]. As a result, these studies obtained parameters such as slump cone flow, density, segregation resistance, compressive strength, split tensile strength, flexural strength, compressive stress-strain diagrams, and other characteristics of the fiber-reinforced lightweight concrete.

Research works on the stress-strain behavior of structures made from the new generation of high-strength lightweight concretes are practically absent in open sources. Apart from the mentioned publication [9], which studied beam structures made of high-strength lightweight concrete and steel fiber-reinforced lightweight concrete under a complex stress state—bending from a concentrated force—a few other publications dedicated to studying the stress-strain state of beam structures made of high-strength lightweight concretes under simple stress states are known, such as works [15-18]. Separate recent studies conducted for structures made of high-strength normal-weight concrete under various stress states [19-21] have shown a number of specific features of their deformation, cracking, and failure compared to structures made of normal-strength concrete.

In this regard, the goal of this research was to conduct experimental studies of the deformation and failure of reinforced concrete elements made of high-strength lightweight concrete under eccentric compression with torsion, and to establish the features, physical nature, and parameters of their load-bearing capacity in comparison with calculated values obtained using a developed analytical model [22].

METHODS

To achieve the goal and objectives of the research, a program of experimental studies was developed accordingly. This program included the design and fabrication of test specimens, a methodology for measuring test parameters, and methods and equipment for loading the test specimens. Three series of test specimens were designed and manufactured (Figure 1):

Series 1K-1 (1K-1.1, 1K-1.2, 1K-1.3) — Reinforced concrete columns, 3 units, each 2000 mm long with a cross-section of 100x50 mm. Longitudinal reinforcement: 8 mm diameter (4 bars) and 6 mm diameter (2 bars). Transverse reinforcement: 2 mm diameter with a spacing *of s=120 mm* (Figure 1a).

Series 1K-2 (1K-2.1, 1K-2.2, 1K-2.3) — Reinforced concrete columns, 3 units, each 2000 mm long with a cross-section of 100x50 mm. Longitudinal reinforcement: 8 mm diameter (4 bars). Transverse reinforcement: 2 mm diameter with a spacing of *s=120 mm* (Figure 1b).

Series 1K-3 (1K-3.1, 1K-3.2, 1K-3.3) — Reinforced concrete columns, 3 units, each 2000 mm long with a cross-section of 100x50 mm. Longitudinal reinforcement: 6 mm diameter (4 bars). Transverse reinforcement: 2 mm diameter with a spacing of *s=120 mm* (Figure 1c).

Materials used for manufacturing the test specimens: High-strength lightweight concrete B40. The structural reinforcement was of class A500C, and the transverse reinforcement was made from wire with characteristics equivalent to class A240 reinforcement.

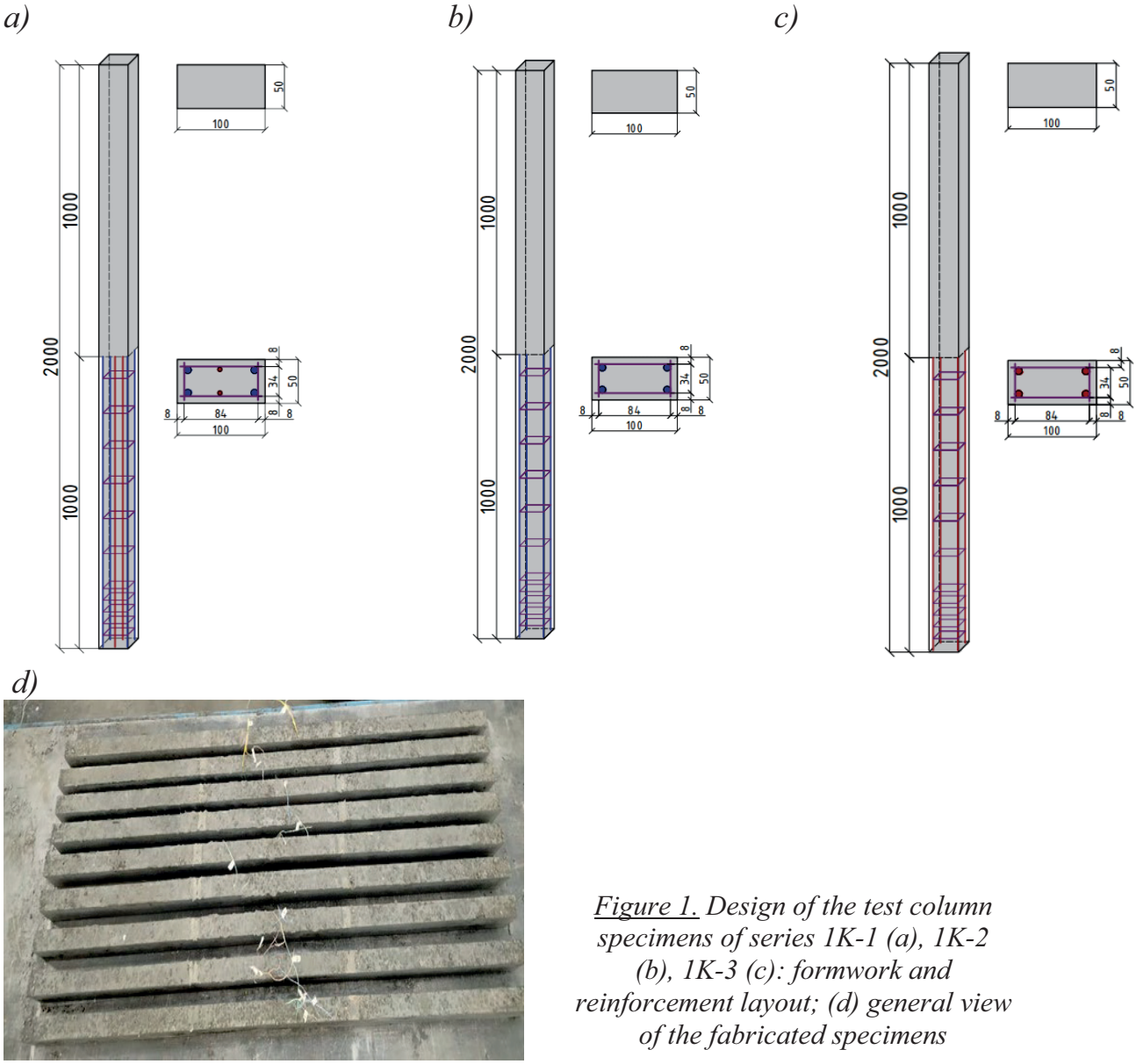
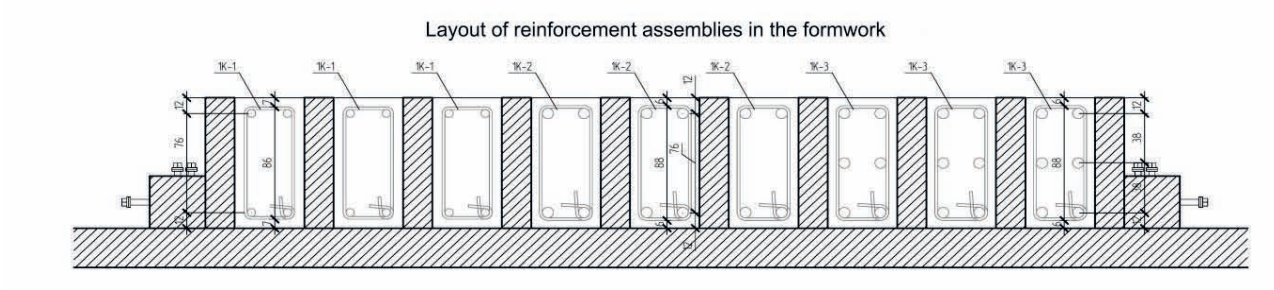


Figure 1. Design of the test column specimens of series 1K-1 (a), 1K-2 (b), 1K-3 (c): formwork and reinforcement layout; (d) general view of the fabricated specimens

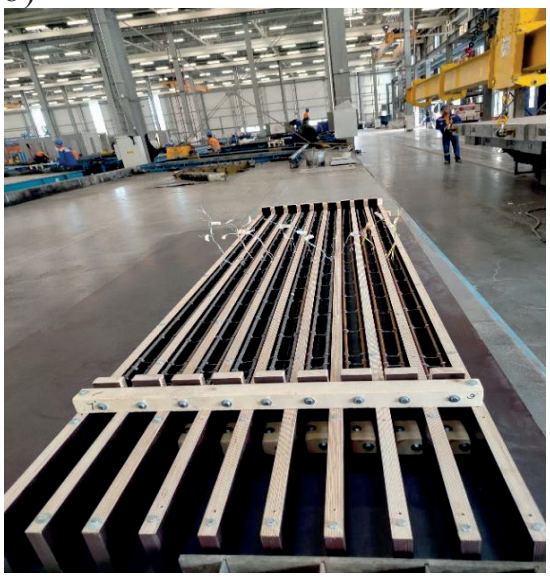
Manufacturing of the test specimens for all series was carried out in specially designed and manufactured formwork made of waterproof plywood (Figure 2a). The concreting of the test specimens was performed at the "MonArkh Group of Companies" construction materials plant (Figures 2b, 2c). The experimental research was conducted in the laboratory of the Mytishchi branch of the National Research Moscow State University of Civil Engineering (MGSU).

Concurrently with the main structural specimens, auxiliary prism and cube specimens were fabricated and tested using concrete from the same batch as that used for the main test specimens. The characteristics of the tested cubes and prisms are presented in Table 1.

a)



b)



c)

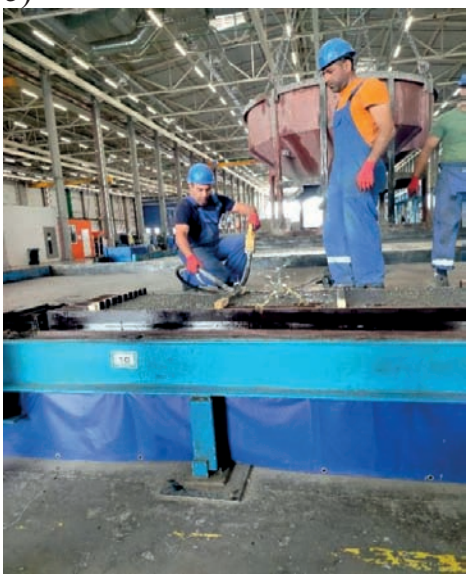


Figure 2. Formwork layout with installed rebar cages (a, b) and a general view of the test structures during concreting (c)

Table 1. Key Properties of Cube and Prism Specimens

Series / Specimen ID	Dimensions, mm	Mass, g	Average Mass, g	Density, kg/m³	Avg. Density, kg/m³	Failure Load, kN	Avg. Failure Load, kN
Series 1K / Cube 1	104x100x99	1815	**1826,6**	1762,62	**1762,05**	375	**381,6**
Series 1K / Cube 2	104x100x100	1860		1788,46		420	
Series 1K / Cube 3	101x100x103	1805		1735,07		350	

№	Specimen Series*	Failure Load (kN)*	Modulus of Elasticity (MPa)*	Poisson's Ratio*	R, MPa	R_b, MPa
1	1K-1	200	$22 \cdot 10^3$	0,24	40	30,77

2	1K-2	200	$21{,}7 \cdot 10^3$	0,28	40	30,77
3	1K-3	200	$20 \cdot 10^3$	0,29	40	30,77
	Average 1K	**200**	$21{,}3 \cdot 10^3$	**0,27**	40	30,77

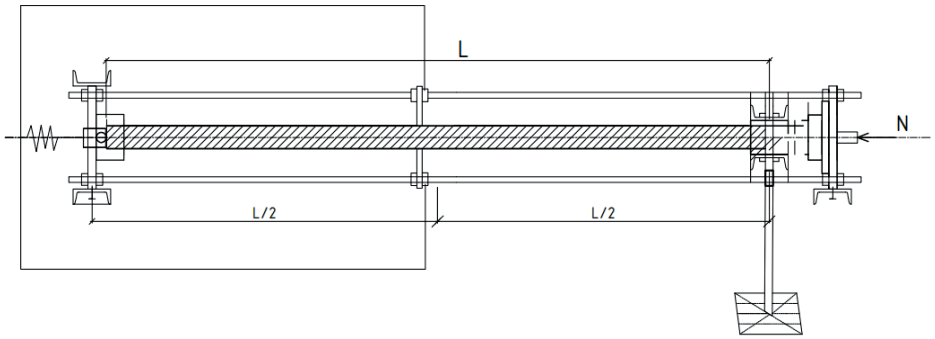
* Average Value for Each Specimen Series

RESULTS AND DISCUSSION

To test the experimental specimens, special non-standard equipment was designed and manufactured in the form of a rigid frame with tie rods, fixed support, and rotational devices (Figure 3). One end of the test specimen was rigidly fixed in the crosshead. A compressive force with a specified eccentricity was applied to the other end using a jack. Simultaneously, a torque was applied to the specimen via a lever rigidly connected to it through a roller assembly.

The applied compressive force and the torque acting on the specimen were measured. During the experiment, mechanical instruments were used to measure deflections in two planes of the specimen and at several sections along its length, as well as the angles of twist due to the torque, longitudinal strains, and shear strains. A digital video camera was used to record the crack formation pattern and measure the crack width at different stages of loading the structure.

a)



b)



Figure 3. Experimental test setup: (a) schematic diagram; (b) general view

Based on the experimentally measured strains in the investigated sections of the columns, "load-strain" dependencies were constructed for the test columns 1K-1, 1K-2, and 1K-3. The experimental values of the cracking load for the test specimens were determined from the principal strain values. For specimen 1K-1 made of B40 concrete, the cracking load $(Ne)_{crc}+T_{crc}$ was 0.544 kN·m. For specimen 1K-2, it was 0.429 kN·m, and for specimen 1K-3, it was 0.413 kN·m.

Comparing the experimental values of the principal concrete strains (curves 2, 3) with the calculated ones (curves 1, 4) obtained from the strain data of strain gauges oriented at 0°, 45°, and 90° to the longitudinal axis of the specimen (see Figure 3), it can be observed that the proposed computational model satisfactorily describes the deformation in complexly stressed sections of the structures at different loading levels. A similar conclusion can be drawn from the analysis of the tensile reinforcement strains. The obtained strain graphs (Figure 5) show that after crack formation in the reinforcement, a sharp increase in strain occurs, and yielding is reached relatively quickly.

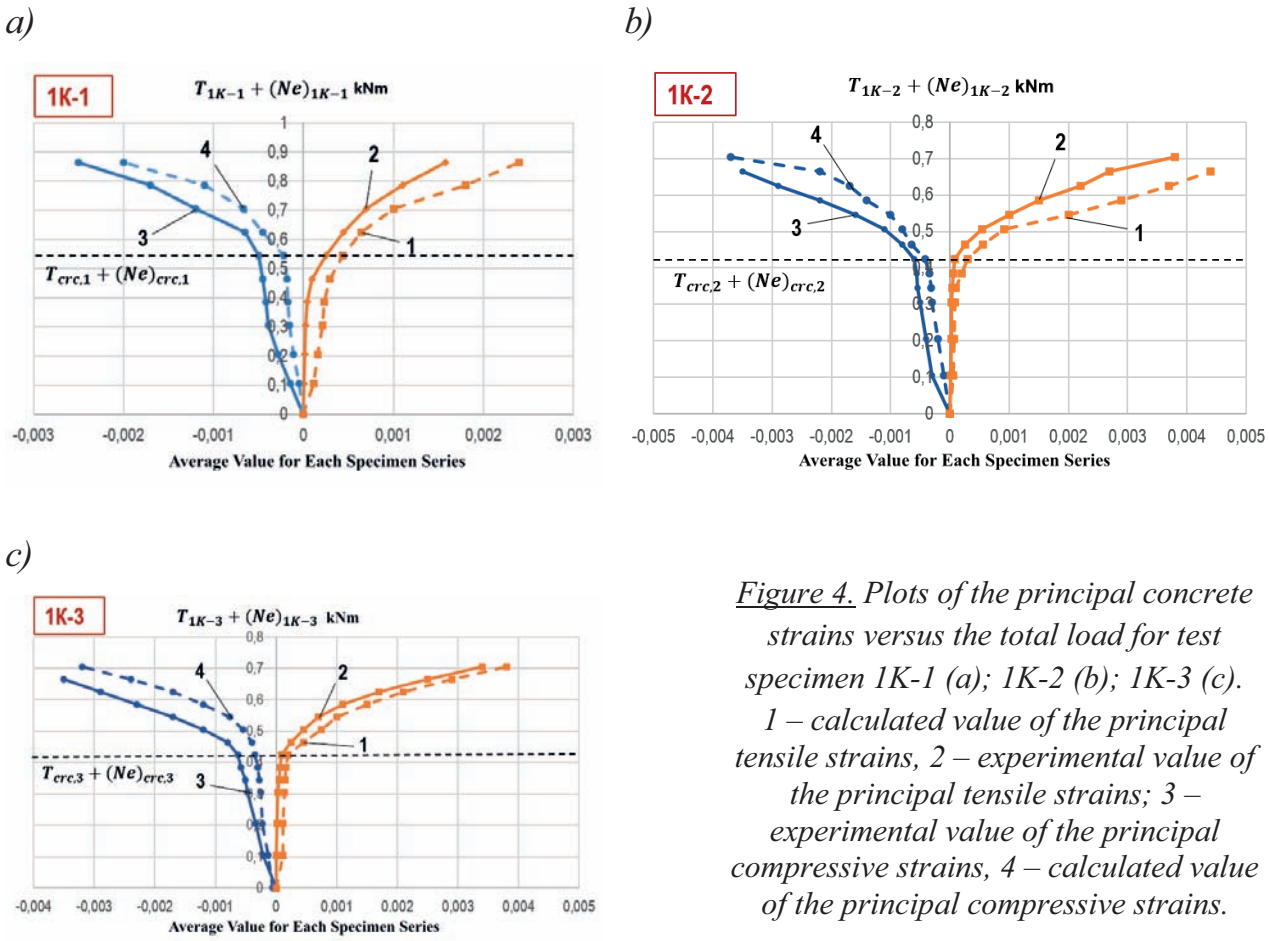


Figure 4. Plots of the principal concrete strains versus the total load for test specimen 1K-1 (a); 1K-2 (b); 1K-3 (c). 1 – calculated value of the principal tensile strains, 2 – experimental value of the principal tensile strains; 3 – experimental value of the principal compressive strains, 4 – calculated value of the principal compressive strains.

For lightweight expanded clay concrete, within the load range (up to 40-50% of the ultimate load), the relationship between stresses and strains, both compressive and tensile, can be considered with sufficient accuracy as close to linear. An increase in load causes a non-linear growth of deformations in both compressed and tensile concrete.

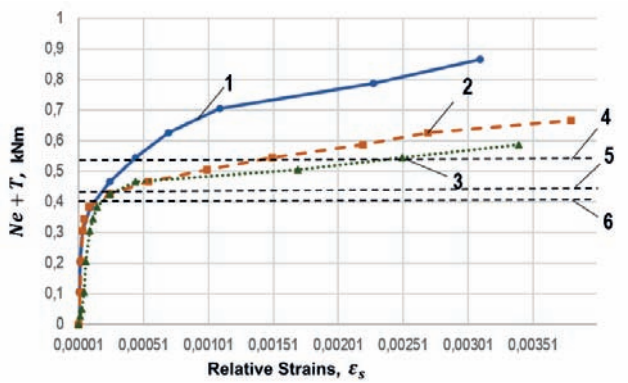


Figure 5. Plots of tensile reinforcement strain versus load: 1 – strain values for 1K-1, 2 – for 1K-2, 3 – for 1K-3, 4 – crack formation load $(Ne)_{crc}+T_{crc}$ for specimen 1K-1, 5 – same for specimen 1K-2, 6 – same for specimen 1K-3

Analyzing the experimental "load-deflection" and "load-angle of twist" graphs (Figures 6, 7), the following can be noted. The deformation range of the structures, from the moment a spatial crack forms until the failure of the test specimen, constitutes 15–20%. It is pertinent to note that for high-strength heavyweight concrete, the formation of the first crack also occurs at a relatively high load level, typically in the range of 70-90% of the failure load [23,24]. This indicates significant differences in the physical phenomena governing the resistance of such structures compared to structures made of conventional concrete.

The crack pattern (Figure 8a) obtained for specimen 1K-1 appeared at load stage VIII under a load of 0.544 kN·m. Subsequently, with a slight increase in load, a brittle failure of the test specimen occurred along the section of one of the initially formed spatial cracks and through the compressed concrete.

A similar process of crack formation was observed for the test specimens of series 1K-2 (Figure 8b) and 1K-3. Cracks appeared at load stage IX under a load of 0.429 kN·m and at load stage VII under a load of 0.413 kN·m, respectively.

A similar crack pattern was also obtained during the testing of structures made of high-strength heavyweight concrete [23, 24].

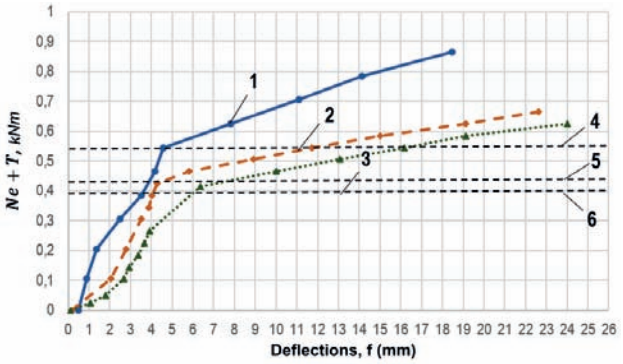


Figure 6. Load-deflection curves for the specimens: 1 – 1K-1, 2 – 1K-2, 3 – 1K-3; 4 – crack formation $(Ne)_{crc}+T_{crc}$ for specimen 1K-1, 5 – same for specimen 1K-2, 6 – same for specimen 1K-3

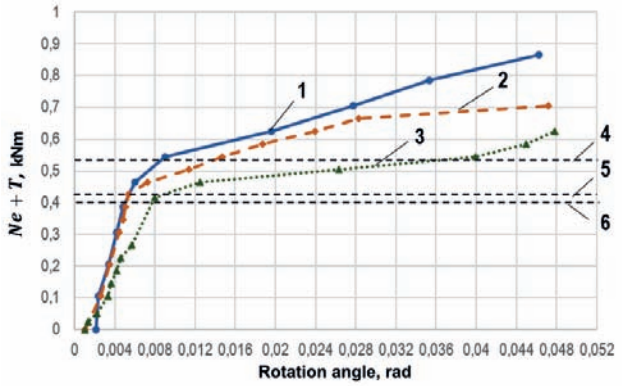
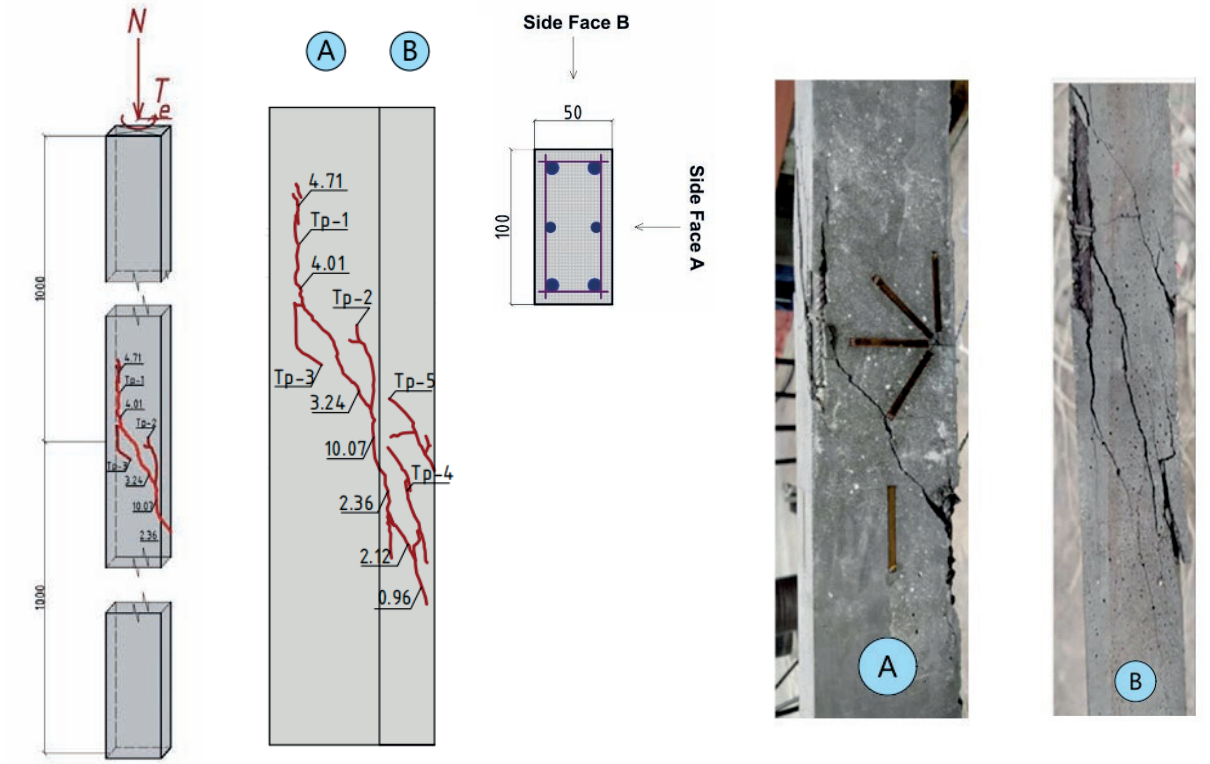


Figure 7. Load-rotation angle curves for the specimens: 1 – 1K-1, 2 – 1K-2, 3 – 1K-3; 4 – crack formation $(Ne)_{crc}+T_{crc}$ for specimen 1K-1, 5 – same for specimen 1K-2, 6 – same for specimen 1K-3

a)



b)

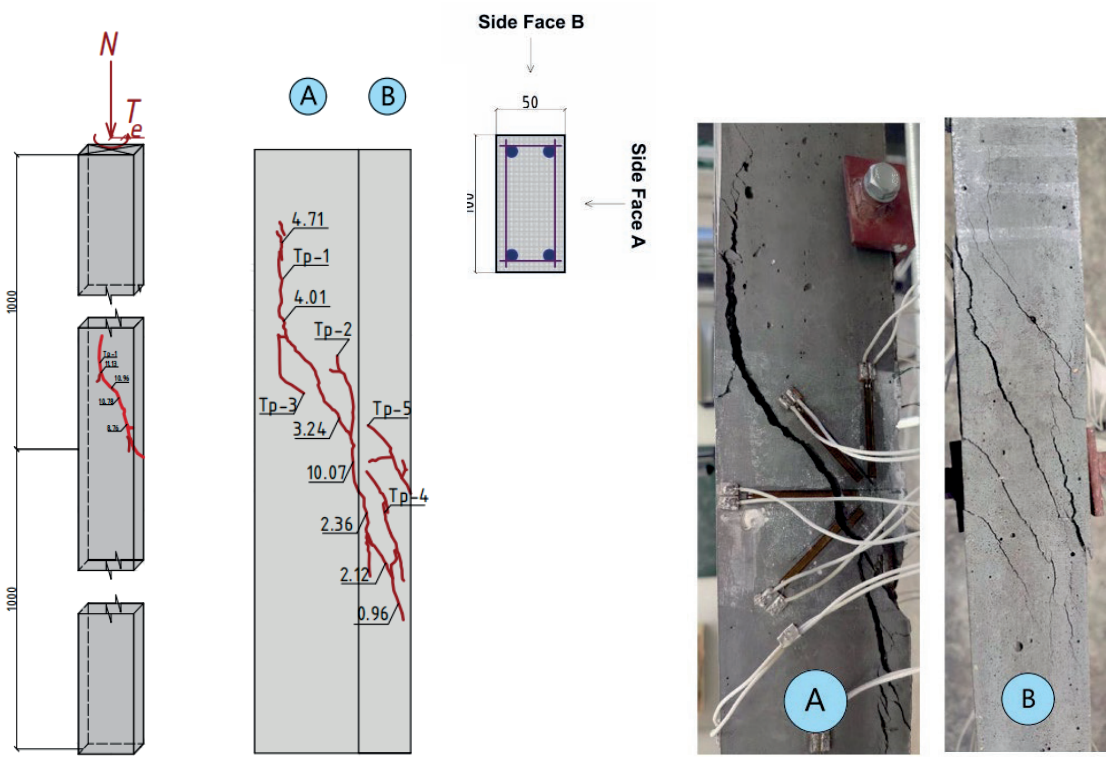


Figure 8. Experimental crack pattern for specimen 1K-1 (a) and specimen 1K-2 (b)

CONCLUSION

1. Experimental studies of three series of test column specimens made of high-strength lightweight concrete B40 under eccentric compression with torsion revealed the specific characteristics of their load-bearing resistance at all loading levels, including up to the point of ultimate capacity exhaustion.
2. It was established that under the considered complex stress state—eccentric compression with torsion—several spatial cracks form in the reinforced concrete structures made of high-strength lightweight concrete. The width of one of these cracks increases intensively as the load increases, and the ultimate load-bearing capacity is exhausted along a spatial section passing through this crack and the compressed concrete.
3. The obtained experimental data on the deformation of concrete and reinforcement, deflections, and rotation angles for the test specimens, both before and after crack formation, made it possible to identify the physical specifics of the load-bearing resistance of structures made from high-strength lightweight reinforced concrete. Crack formation in such structures occurs at a relatively high load level, constituting 80-85% of the failure load. After crack formation, the relative range of their deformation until failure constitutes 15-20% of the structure's load-bearing capacity. This indicates significant differences in the physical phenomena governing the resistance of such structures compared to structures made of conventional concrete.

ACKNOWLEDGEMENTS

The research was funded by the Russian Science Foundation (RSF), grant number 24-49-10010, https://rscf.ru/project/24-49-10010/.

REFERENCES

1. **Kaprielov, S.S., Sheynfeld, A.V., Karpenko, N.I., Selyutin, N.M., Moiseenko, G.A., Bezgodov, I.M.** (2025) Strength and deformation characteristics of high-strength self-compacting lightweight concretes on artificial and natural porous aggregates. *Concrete and Reinforced Concrete*, no. 3 (628), pp. 52–68. https://doi.org/10.37538/0005-9889-2025-3(628)-52-68
2. **Kaprielov, S.S., Sheynfeld, A.V., Selyutin, N.M.** (2023) Self-compacting high-strength expanded clay concrete of classes B50–B65 – a new generation of lightweight concretes for high-rise building structures. *Stroitel'nye Materialy [Construction Materials]*, no. 4, pp. 42–50. https://doi.org/10.31659/0585-430X-2023-812-4-42-50
3. **Kaprielov, S.S., Sheynfeld, A.V., Travush, V.I., Karpenko, N.I., Krylov, S.B.** (2023) Assessment of the strength and deformation characteristics of high-strength concretes in structures and the dynamics of their change over time. *Stroitel'nye Materialy [Construction Materials]*, no. 11, pp. 28–38.
4. **Kaprielov, S.S., Sheynfeld, A.V., Dondyukov, V.G.** (2017) Cements and additives for the production of high-strength concretes. *Stroitel'nye Materialy [Construction Materials]*, no. 11, pp. 4–10.
5. **Shorin, V.M.** (2010) Application of expanded clay concrete in construction – the way to energy and resource efficiency, safety of buildings and structures. *Stroitel'nye Materialy [Construction Materials]*, no. 8, pp. 8–10.
6. **Nesvetaeev, G.V., Belyaev, A.V.** (2016) Deformation properties of self-compacting expanded clay concrete. *Internet-zhurnal "NAUKOVEDENIE" [Online Journal "Science Studies"]*, vol. 8, no. 2. Available at: http://naukovedenie.ru/PDF/06TVN216.

pdf (accessed: dd.mm.yyyy). doi: 10.15862/06TVN216

7. **Kaprielov, S.S., Sheynfeld, A.V., Al-Omais, D., Zaytsev, A.S.** (2018) Experience in production and quality control of high-strength concretes in the construction of the high-rise complex "OKO" in the MIBC "Moscow-City". *Promyshlennoe i Grazhdanskoe Stroitel'stvo [Industrial and Civil Engineering]*, no. 1, pp. 18–24.
8. **Liu, X., Wu, T., Liu, Y.** (2019) Stress-strain relationship for plain and fibre-reinforced lightweight aggregate concrete. *Construction and Building Materials*, vol. 225, pp. 256–272. https://doi.org/10.1016/j.conbuildmat.2019.07.173
9. **Dabbagh, H., Amoorezae, K.** (2019) Stress-strain Relationship for Steel Fiber-reinforced Lightweight Aggregate Concrete under Uniaxial Compression. *Journal of Stress Analysis*, vol. 4, no. 1, pp. [indicate pages].
10. **Wei, H., Wu, T., Yang, X.** (2020) Properties of Lightweight Aggregate Concrete Reinforced with Carbon and/or Polypropylene Fibers. *Materials*, vol. 13, no. 3, p. 640. https://doi.org/10.3390/ma13030640
11. **SP 63.13330.2018 (2018)** Betonnye i zhelezobetonnye konstruktsii. Osnovnye polozheniya. Aktualizirovannaya redaktsiya SNiP 52-01-2003 [Concrete and reinforced concrete structures. Main provisions. Updated version of SNiP 52-01-2003]. [Online]. Moscow. Available at: http://docs.cntd.ru/document/556156861 (accessed: dd.mm.yyyy).
12. **ACI 318-19 (2019)** *Building Code Requirements for Structural Concrete and Commentary*. American Concrete Institute.
13. **SP 5.03.01-2020 (2020)** Stroitel'nye konstruktsii i osnovaniya. Konstruktsii betonnye i zhelezobetonnye. Pravila proektirovaniya [Building structures and foundations. Concrete and reinforced concrete structures. Design rules]. [Online]. Minsk. Available at: [indicate URL] (accessed: dd.mm.yyyy).
14. **Kolchunov, V.I., Fedorova, N.V**. (2018) Some problems of the survivability of reinforced concrete structural systems under emergency impacts. *Vestnik NITs "Stroitel'stvo" [Bulletin of the Scientific Research Center "Construction"]*, no. 1, pp. 115–119.
15. **Rubin, O.D., Lisichkin, S.E., Kuznetsov, S.Yu., Balagurov, V.B., Baklykov, I.V.** (2021) Experimental studies of reinforced concrete structures made of lightweight high-strength concrete (as applied to the caisson gate structure of a dry dock). *Prirodoobustroistvo [Environmental Engineering]*, no. 4, pp. 58–66. doi: 10.26897/1997-6011-2021-4-58-66
16. **Shafigh, P., Kobraei, M., Razavi Tosee, S.V. (2011)** An investigation of the flexural behaviour of reinforced lightweight concrete. *International Journal of the Physical Sciences*, vol. 6, no. 10, pp. 2414–2421.
17. **Fang, Y., Xu, Y., Gu, R.** (2022) Experiment and Analysis of Mechanical Properties of Lightweight Concrete Prefabricated Building Structure Beams. *International Journal of Concrete Structures and Materials*, vol. 16, Article 5. https://doi.org/10.1186/s40069-021-00496-3
18. **Jahami, A., Dayaa, L., Assaad, J.J., Baalbaki, O., Khatib, J.** (2024) Flexural Strength of Structural Beams Cast Using Combined Normal-Weight and Lightweight Concrete Mixtures. *Buildings*, vol. 14, no. 12, p. 3787. https://doi.org/10.3390/buildings14123787
19. **Kolchunov, V.I., Demyanov, A.I., Pechenev, I.V.** (2020) Results of experimental studies of square cross-section structures under torsion with bending. *Stroitel'stvo i Rekonstruktsiya [Construction and Reconstruction]*, no. 5 (91), pp. 3–12.

20. **Travush, V.I., Karpenko, N.I., Kolchunov, Vl.I., Kaprielov, S.S., Demyanov, A.I., Bulkin, S.A., Moskovtseva, V.S.** (2020) Results of experimental studies of complexly stressed beams of circular cross-section made of high-strength fiber-reinforced concrete. *Stroitel'naya Mekhanika Inzhenernykh Konstruktsii i Sooruzhenii [Structural Mechanics of Engineering Constructions and Buildings]*, no. 4, pp. 290–297.
21. **Kolchunov, Vl.I., Fedorova, N.V., Savin, S.Y., Moskovtseva, V.S**. (2025) Analytical Model of Crack Opening in Reinforced Concrete Structures Based on DCE. *Buildings*, vol. 15, no. 12, p. 2096. https://doi.org/10.3390/buildings15122096
22. **Kolchunov, V.I., Amelina, M.A.** (2025) Deformation of an eccentrically compressed and torsion-loaded reinforced concrete element. *Nauchnyy Vestnik VGASU. Stroitel'stvo i Arkhitektura [Scientific Bulletin of VGASU. Construction and Architecture]*, iss. 2 (78), pp. 11–25.
23. **Travush, V.I., Karpenko, N.I., Kolchunov, V.I., Kaprielov, S.S., Demyanov, A.I., Konorev, A.V. (2018)** Results of experimental studies of square and box sections made of high-strength concrete under torsion with bending. *Stroitel'stvo i Rekonstruktsiya [Construction and Reconstruction]*, no. 6, pp. 32–43.
24. **Travush, V.I., Karpenko, N.I., Kolchunov, Vl.I., Kaprielov, S.S., Demyanov, A.I., Konorev, A.V. (2019)** Main results of experimental studies of reinforced concrete structures made of high-strength concrete B100 of circular and annular sections under torsion with bending. *Stroitel'naya Mekhanika Inzhenernykh Konstruktsii i Sooruzhenii [Structural Mechanics of Engineering Constructions and Buildings]*, vol. 15, no. 1, pp. 51–61. doi: 10.22363/1815-5235-2019-15-1-51-61

СПИСОК ЛИТЕРАТУРЫ

1. **Каприелов С.С., Шейнфельд А.В., Карпенко Н.И., Селютин Н.М., Моисеенко Г.А., Безгодов И.М.** Прочностные и деформационные характеристики высокопрочных самоуплотняющихся легких бетонов на искусственных и природных пористых заполнителях // *Бетон и железобетон. 2025.* № 3 (628). С. 52–68. https://doi.org/10.37538/0005-9889-2025-3(628)-52-68
2. **Каприелов С.С., Шейнфельд А.В., Селютин Н.М.** Самоуплотняющийся высокопрочный керамзитобетон классов В50–В65 – новое поколение легких бетонов для конструкций высотных зданий // *Строительные материалы. 2023.* № 4. С. 42–50. DOI: https://doi.org/10.31659/0585-430X-2023-812-4-42-50
3. **Каприелов С.С., Шейнфельд А.В., Травуш В.И., Карпенко Н.И., Крылов С.Б.** Оценка прочностных и деформационных характеристик высокопрочных бетонов в конструкциях и динамики их изменения во времени // *Строительные материалы. 2023.* № 11. С. 28–38.
4. **Каприелов С.С., Шейнфельд А.В., Дондуков В.Г.** Цементы и добавки для производства высокопрочных бетонов // *Строительные материалы. 2017*. № 11. С. 4–10.
5. **Шорин В.М.** Применение керамзитобетона в строительстве – путь к энерго- и ресурсоэффективности, безопасности зданий и сооружений // *Строительные материалы. 2010.* № 8. С. 8–10.
6. **Несветаев Г.В., Беляев А.В.** Деформационные свойства

самоуплотняющегося керамзитобетона // *Интернет-журнал «НАУКОВЕДЕНИЕ». 2016.* Т. 8. № 2. Режим доступа: http://naukovedenie.ru/PDF/06TVN216.pdf (дата обращения: дд.мм.гггг). DOI: 10.15862/06TVN216

7. **Каприелов С.С., Шейнфельд А.В., Аль-Омаис Д., Зайцев А.С.** Опыт производства и контроля качества высокопрочных бетонов на строительстве высотного комплекса "ОКО" в ММДЦ "Москва-Сити" // *Промышленное и гражданское строительство. 2018*. № 1. С. 18–24.
8. **Liu X., Wu T., Liu Y.** Stress-strain relationship for plain and fibre-reinforced lightweight aggregate concrete // *Construction and Building Materials. 2019*. Vol. 225. P. 256–272. https://doi.org/10.1016/j.conbuildmat.2019.07.173
9. **Dabbagh H., Amoorezae K**. Stress-strain Relationship for Steel Fiber-reinforced Lightweight Aggregate Concrete under Uniaxial Compression // *Journal of Stress Analysis. 2019.* Vol. 4. No. 1. P. [указать страницы].
10. **Wei H., Wu T., Yang X**. Properties of Lightweight Aggregate Concrete Reinforced with Carbon and/or Polypropylene Fibers // *Materials. 2020.* Vol. 13. No. 3. P. 640. https://doi.org/10.3390/ma13030640
11. **СП 63.13330.2018** Бетонные и железобетонные конструкции. Основные положения. Актуализированная редакция СНиП 52-01-2003 [Электронный ресурс]. – М., 2018. – Режим доступа: http://docs.cntd.ru/document/556156861 (дата обращения: дд.мм.гггг).
12. **ACI 318-19:** Building Code Requirements for Structural Concrete and Commentary. – American Concrete Institute, 2019.
13. **СП 5.03.01-2020** Строительные конструкции и основания. Конструкции бетонные и железобетонные. Правила проектирования [Электронный ресурс]. – Минск, 2020. – Режим доступа: (дата обращения: дд.мм.гггг).
14. **Колчунов В.И., Федорова Н.В.** Некоторые проблемы живучести железобетонных конструктивных систем при аварийных воздействиях // *Вестник НИЦ «Строительство». 2018.* № 1. С. 115–119.
15. **Рубин О.Д., Лисичкин С.Е., Кузнецов С.Ю., Балагуров В.Б., Баклыков И.В.** Экспериментальные исследования железобетонных конструкций из легкого высокопрочного бетона (применительно к конструкции батопорта сухого дока) // *Природообустройство. 2021.* № 4. С. 58–66. DOI: 10.26897/1997-6011-2021-4-58-66
16. **Shafigh P., Kobraei M., Razavi Tosee S.V.** An investigation of the flexural behaviour of reinforced lightweight concrete // *International Journal of the Physical Sciences. 2011*. Vol. 6. No. 10. P. 2414–2421.
17. **Fang Y., Xu Y., Gu R**. Experiment and Analysis of Mechanical Properties of Lightweight Concrete Prefabricated Building Structure Beams // *International Journal of Concrete Structures and Materials. 2022*. Vol. 16. Article 5. https://doi.org/10.1186/s40069-021-00496-3
18. **Jahami A., Dayaa L., Assaad J.J., Baalbaki O., Khatib J.** Flexural Strength of Structural Beams Cast Using Combined Normal-Weight and Lightweight Concrete Mixtures // *Buildings. 2024*. Vol. 14. No. 12. P. 3787. https://doi.org/10.3390/buildings14123787
19. **Колчунов В.И., Демьянов А.И., Печенев И.В.** Результаты экспериментальных исследований конструкций квадратного сечения при кручении с изгибом // *Строительство и реконструкция. 2020*. № 5 (91). С. 3–12.
20. **Травуш В.И., Карпенко Н.И., Колчунов Вл.И., Каприелов С.С., Демьянов А.И., Булкин С.А.,**

Московцева В.С. Результаты экспериментальных исследований сложнонапряженных балок круглого поперечного сечения из высокопрочного фиброжелезобетона // *Строительная механика инженерных конструкций и сооружений. 2020*. № 4. С. 290–297.

21. **Kolchunov Vl.I., Fedorova N.V., Savin S.Y., Moskovtseva V.S.** Analytical Model of Crack Opening in Reinforced Concrete Structures Based on DCE // *Buildings. 2025.* Vol. 15. No. 12. P. 2096. https://doi.org/10.3390/buildings15122096
22. **Колчунов В.И., Амелина М.А.** Деформирование внецентренно сжатого и испытывающего кручение железобетонного элемента // *Научный вестник ВГАСУ. Строительство и архитектура. 2025.* Вып. 2 (78). С. 11–25.
23. **Травуш В.И., Карпенко Н.И., Колчунов В.И., Каприелов С.С., Демьянов А.И., Конорев А.В.** Результаты экспериментальных исследований конструкций квадратного и коробчатого сечений из высокопрочного бетона при кручении с изгибом // *Строительство и реконструкция. 2018;*(6):32-43.
24. **Травуш В.И., Карпенко Н.И., Колчунов Вл.И., Каприелов С.С., Демьянов А.И., Конорев А.В.** Основные результаты экспериментальных исследований железобетонных конструкций из высокопрочного бетона В100 круглого и кольцевого сечений при кручении с изгибом // *Строительная механика инженерных конструкций и сооружений. 2019.* Т. 15. № 1. С. 51-61. DOI: 10.22363/1815-5235-2019-15-1-51-61

Amelina Margarita Andreevna – Postgraduate Student, Department of Reinforced Concrete and Masonry Structures, Federal State Budgetary Educational Institution of Higher Education «National Research Moscow State University of Civil Engineering» (NRU MGSU), 26 Yaroslavskoe Shosse, Moscow, 129337, Russia. margo.dremova@mail.ru

Амелина Маргарита Андреевна – аспирант кафедры Железобетонных и каменных конструкций Федерального государственного бюджетного образовательного учреждения высшего образования «Национальный исследовательский Московский государственный строительный университет» (НИУ МГСУ), 129337, Россия, г. Москва, Ярославское шоссе, д. 26. margo.dremova@mail.ru

Fedorova Natalia Vitalievna – Doctor of Technical Sciences, Professor, Director of the Branch of NRU MGSU, Federal State Budgetary Educational Institution of Higher Education «National Research Moscow State University of Civil Engineering» (NRU MGSU), 26 Yaroslavskoe Shosse, Moscow, 129337, Russia. FedorovaNV@gic.mgsu.ru

Федорова Наталия Витальевна – доктор технических наук, профессор, директор Филиала «НИУ МГСУ», Федеральное государственное бюджетное образовательное учреждение высшего образования «Национальный исследовательский Московский государственный строительный университет» (НИУ МГСУ), д. 26, Ярославское шоссе, г. Москва, 129337, Россия, FedorovaNV@gic.mgsu.ru

Selyutin Nikita Mikhailovich – Engineer, Research Fellow, Laboratory of Chemical Admixtures and Modified Concretes (No. 16), A.A. Gvozdev Research Institute of Concrete and Reinforced Concrete (NIIZhB), JSC «Research Center «Construction», 6, building 5, 2-ya Institutskaya St., Moscow, 109428, Russia. selyutin@masterbeton-mb.ru

Селютин Никит Михайлович - инженер, научный сотрудник лаборатории химических добавок и модифицированных бетонов (№ 16), НИИЖБ им. А.А. Гвоздева АО «НИЦ «Строительство», Россия, 109428, г. Москва, 2-я Институтская ул., д. 6, корп. 5. selyutin@masterbeton-mb.ru

Yolkina Elena Yurievna – Employee, MonArch LLC, 31a, building 1, Leningradsky Prospect, Moscow, 125284, Russia. e.elkina@mon-arch.ru

Ёлкина Елена Юрьевна – сотрудник ООО «МонАрх», Россия, 125284, город Москва, Ленинградский пр-кт, д.31а строение 1.e.elkina@mon-arch.ru

International Journal for Computational Civil and Structural Engineering, 21(4) 41–55 (2025)

DOI:10.22337/2587-9618-2025-21-4-41-55

EFFICIENT ALGORITHM OF THE BUCKLING LENGTHS METHOD IN ANALYSIS OF SPATIAL FRAME SYSTEMS FOR STABILITY

Eugene I. Britvin [1], Moshe Eisenbeger [2]

[1] DANRAZ Ltd. Haifa, ISRAEL
[2] Israel Institute of Technology, Haifa, ISRAEL

Abstract: An effective computational algorithm has been developed that allows finding the buckling lengths of the rod elements of frame structures. A matrix of unit reaction from the side the rest of the structure is formed for each element and eigenvalues problem of longitudinal bending equation of the rod is solved. When searching for eigenvalues, the stress state in all elements of the system except the tested rod is fixed. The algorithm takes into account the interaction of each studied element with all other elements of the structure. The constructed algorithm allows, in a limited time, commensurate with the expenditure of a conventional static calculation, to find an exact solution to the problem of eigenvalues for each rod and to determine the buckling lengths of all rod elements included in the structure.

Keywords: buckling, buckling of the rod systems, buckling length, effective length, check local buckling

ЭФФЕКТИВНЫЙ АЛГОРИТМ МЕТОДА РАСЧЕТНЫХ ДЛИН ПРИ АНАЛИЗЕ УСТОЙЧИВОСТИ ПРОСТРАНСТВЕННЫХ РАМНЫХ СИСТЕМ

Е.И. Бритвин [1], М. Эйсебергер [2]

[1] DANRAZ Ltd. Хайфа, ИЗРАИЛЬ
[2] Israel Institute of Technology, Хайфа, ИЗРАИЛЬ

Аннотация: Построен эффективный вычислительный алгоритм, позволяющий находить расчетные длины стержневых элементов рамных конструкций. Для каждого элемента формируется матрица единичных реакций со стороны остальной конструкции и, с учетом этих реакций, решается задача о собственных значениях уравнения продольного изгиба стержня. При поиске собственных значений напряженное состояние во всех элементах системы, кроме тестируемого стержня, фиксируется. Алгоритм учитывает взаимодействие каждого исследуемого элемента со всеми остальными элементами конструкции. Построенный алгоритм позволяет за ограниченное время, соизмеримое с затратами на обычный статический расчет, найти точное решение задачи о собственных значениях для каждого стержня и определить расчетные длины всех стержневых элементов входящих в конструкцию.

Ключевые слова: устойчивость, устойчивость стержневых систем, расчетная длина, свободная длина, проверка локальной устойчивости

1. INTRODUCTION

Checking the local stability of rod elements is one of the most important checks necessary to ensure reliable operation of building structures. A significant contribution to the development of methods for calculating the local stability of rod elements was made by both foreign and domestic authors. Here, first of all, it is necessary to note the works of G.I. Belyj [1], A.V. Alexandrov [2,3], I.D. Grudev [4], G.A. Manuilov1 [5], A.M. Belostotsky [6,7], A.V. Perelmuter, V.I. Slivker [8] and many other authors. In foreign publications, the modern concept of the method

for checking the local stability of rod elements, based on the concept of the calculated length, is presented in the work of Y. Duan and W.F. Chen [9].Currently, two methods have been established for checking the local stability of frame structures - the direct analysis method [10,11,12] (a number of standards allow the direct setting of the initial irregularities of the rod elements within the framework of the P-Delta analysis [13,14]) and a method based on the specifying of the effective lengths of rod elements. The value of the effective length method is that it provides a simple approach to assessing the stability of frame members. It is based on solving the problem of longitudinal bending of a hinged rod with a sinusoidal shape of the initial roughness. As a result, the so-called buckling factor φ for central compression is found, which makes it possible to calculate the longitudinal force at which a stress equal to the design resistance R_y arises in one of the fibers of the rod (in European standards this coefficient is called "reduction" factor for the relevant buckling mode" and is indicated by the letter χ). The canonical form defining the coefficient φ has the form

$$\varphi = \frac{1}{\phi + \sqrt{\phi^2 - \bar{\lambda}^2}}, \qquad (1)$$

where $\bar{\lambda} = \frac{\lambda}{\pi}\sqrt{\frac{R_y}{E}}$ is the reduced slenderness of the rod, $\lambda = \frac{l}{i}$ is the slenderness of the rod, E is the elastic modulus of the material, and the parameter ϕ is calculated by the formula: $\phi = \frac{1}{2}(1 + \bar{e} + \bar{\lambda}^2)$, where $\bar{e} = \frac{Af_0}{W}$ is the reduced eccentricity of the roughness normalized in a certain way (here A and W are the area and modulus of section). Domestic standards СП 16.13330.2017 [15] use the same formula with some ritual changes. When moving to the case of arbitrary restrictions of the ends of the rod, it is proposed to substitute in the formula for calculating the slenderness λ, instead of the physical length of the rod l, the effective length of the rod l_p – the distance between the inflection points on the buckling shape curve. This substitution is justified by the fact that in this way an arbitrary rod with arbitrary boundary conditions is, as it were, reduced to a hingedly supported one. In [16] it was shown that, indeed, if we take the form of the initial irregularity proportional to the form of buckling of the rod under the appropriate boundary conditions, then formula (1) remains valid, and the role of the physical length of the rod is transferred to the effective length. This proof can be considered some justification for the method of checking the local stability of rods based on the concept of the "effective length" of the rod, although the approach itself requires additional research.

But, whatever it was, the key problem in the methodology for checking the local stability of rods is the determination of these same effective lengths. Many works are devoted to this problem. Since in the general case it is not possible to determine the boundary conditions for each individual rod (the boundary conditions for an individual rod are determined by the system of pushback reactions from all other elements of the structure), a certain fragment of the structure adjacent to the tested rod is identified and, introducing some simplifying assumptions, solve for the selected rod the problem of bucklnug [17-28]. Based on the found eigenvalues, the required effective length is determined. In this regard, it is worth mentioning the important work of R.H. Wood [17], which established the theoretical basis for the calculation of buckling in the European BS EN 1993 [13], as well as in the American standards AISC/AISC 360-16 [14]. For a more accurate analysis of buckling, F. Cheong-Siat-Moi [18] drew attention to the need to take into account the influence on the behavior of an individual member, both the elements surrounding it, and the influence of the entire system. J. Heldesland and R. Bjørhovde [20] showed the importance of fully accounting for the contribution of adjacent elements to the rotational stiffness of the ends of the element. R.K. Bridge and D.J. Fraser drew attention to the fact that if a significant longitudinal force acts in the elements adjacent the member, this can

weaken its rigidity and reduce the critical force [19]. To solve the problem of lightly loaded members, A.V. Perelmuter and V.I. Slivker [8] applied the method of "additional loading of passive elements". The "additional loading" method was implemented in the industrial software package SCAD [33]. Many other authors contributed to the solution of the problem of local stability of rods based on the effective length method [21-29]. And this list of works is far from exhaustive. A good overview of works in this direction can be found, for example, in [29]. The disadvantage of this approach is that, firstly, the selected fragment of the structure does not always reliably provide real boundary conditions for the element under study. Secondly, the critical load of an individual rod inside a frame structure cannot be obtained without taking into account the forces in the remaining elements of the structure, since the stress state in the remaining elements of the structure affects the stiffness of the end reactions of the selected element and changes its effective length. And thirdly, since each element requires an individual approach when choosing a calculation fragment, this approach does not allow us to formalize the problem of determining effective lengths. This complicates its implementation within computer systems. Thus, following this path, the engineer is forced to either make difficult arithmetic calculations in advance, or use various reference books [13-15,30], which, as a rule, makes the analysis even more inaccurate.

In an effort to avoid complex mathematical calculations, engineers very often use the results of a structural buckling analysis to assign effective lengths to structural members. The calculation for overall stability involves a proportional increase in the forces in the elements to the level at which the structure loses stability, and the resulting values of the critical forces in the elements are used to determine the effective lengths. This approach could be considered valid if the actual internal forces were equal to the critical ones. In fact, the actual distribution of forces is always much less than the critical one. An overestimation of the axial forces leads to a softening of the boundary conditions for each individual rod. As a result, with this approach, the effective length of all rod elements always turns out to be overestimated.

This paper presents a universal algorithm that allows you to determine the effective lengths of all rod elements that make up a structure, regardless of its complexity and taking into account the real stress state in the structural elements, allowing you to fully automate this procedure.

2. ANALYSIS

Consider the structure depicted in Figure 1*a*. Let us want to find the effective length of the rod attached to nodes r and s. To do this, it is necessary to construct a matrix of unit reactions of the system reduced to nodes r and s (Fig. 1*b*). Let's denote this matrix $\boldsymbol{S_{rs}}$. Next, we exclude from this matrix the unit reactions of the element $r - s$ itself, and instead of them we add the reactions of the same element as a function of the critical parameter $\alpha = l\sqrt{N/EI}$, where l – rod length, E – modulus of elasticity of the material, I is the moment of inertia of the cross section of the rod, and N – the value of the axial force in the element. Let us denote the own matrix of unit reactions of the tested rod $\boldsymbol{S_M}(\alpha)$.

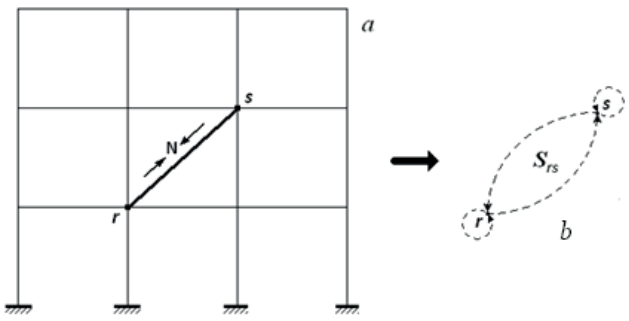


Figure 1. a – design model of the structure; b – design model reduced to the attachment points of the tested element – all superimposed restrictions of the main system, except those superimposed on nodes r and s, are reset (dotted lines with arrows conventionally depict the mutual influence of the nodes)

Thus, the task of determining the effective length of the element $r - s$ reduces to solving the equation

$$det\,[\,\boldsymbol{S}_{rs} - \boldsymbol{S}_M(\alpha_0) + \boldsymbol{S}_M(\alpha)] = 0 \qquad (2)$$

relative to the parameter α (here $\boldsymbol{S}_M(\alpha_0)$ – the matrix of unit reactions of the element $r - s$ at the current value of the longitudinal force N_0). For example, for a rigidly clamped rod (plane problem) in the local coordinate system of the rod, the matrix $\boldsymbol{S}_M(\alpha)$ has the form [31]

$$\boldsymbol{S}_M(\alpha) = \begin{pmatrix} \frac{EA}{l} & 0 & 0 & -\frac{EA}{l} & 0 & 0 \\ 0 & \frac{12EI}{l^3}\eta_1 & \frac{6EI}{l^2}\eta_2 & 0 & -\frac{12EI}{l^3}\eta_1 & \frac{6EI}{l^2}\eta_2 \\ 0 & \frac{6EI}{l^2}\eta_2 & \frac{4EI}{l}\eta_3 & 0 & -\frac{6EI}{l^2}\eta_2 & \frac{2EI}{l}\eta_4 \\ -\frac{EA}{l} & 0 & 0 & \frac{EA}{l} & 0 & 0 \\ 0 & -\frac{12EI}{l^3}\eta_1 & -\frac{6EI}{l^2}\eta_2 & 0 & \frac{12EI}{l^3}\eta_1 & -\frac{6EI}{l^2}\eta_2 \\ 0 & \frac{6EI}{l^2}\eta_2 & \frac{2EI}{l}\eta_4 & 0 & -\frac{6EI}{l^2}\eta_2 & \frac{4EI}{l}\eta_3 \end{pmatrix} \qquad (3)$$

where

$$\eta_1 = \frac{\left(\frac{\alpha}{2}\right)^3}{3\left(\mathrm{tg}\frac{\alpha}{2} - \frac{\alpha}{2}\right)}, \quad \eta_2 = \frac{\left(\frac{\alpha}{2}\right)^2 \mathrm{tg}\frac{\alpha}{2}}{3\left(\mathrm{tg}\frac{\alpha}{2} - \frac{\alpha}{2}\right)},$$
$$\eta_3 = \frac{1 - \frac{\alpha}{\mathrm{tg}\alpha}}{\frac{8}{\alpha}\left(\mathrm{tg}\frac{\alpha}{2} - \frac{\alpha}{2}\right)}, \quad \eta_4 = \frac{\frac{\alpha}{\sin\alpha} - 1}{\frac{4}{\alpha}\left(\mathrm{tg}\frac{\alpha}{2} - \frac{\alpha}{2}\right)}. \qquad (4)$$

And, of course, before including the matrices $\boldsymbol{S}_M(\alpha_0)$ and $\boldsymbol{S}_M(\alpha)$ in equation (2), they must be converted to the global coordinate system. After the solution to equation (2) has been found, the value of the effective length coefficient is calculated according to the formula $\mu = \pi/\alpha$ (effective length coefficient – the ratio of the effective length of the rod to the physical length). The main difficulty of the described procedure is the construction of a stiffness matrix reduced to the attachment points of the tested rod (matrix $\boldsymbol{S}_{rs}$) . If, for example, we use the Gaussian elimination procedure for this, we will need to place the rows corresponding to the nodes of the tested rod at the end of the system stiffness matrix and process them with all the overlying rows. That is, in fact, it is necessary to perform a direct sweep along the entire matrix of the system. And this procedure will need to be performed for each rod. It is clear that if our structure consists of hundreds or thousands of rods, such a procedure becomes impossible.

3. FORMATION OF THE SYSTEM STIFFNESS MATRIX REDUCED TO NODES r AND s.

Let's assume that we somehow managed to construct a matrix inverse to the original stiffness matrix of the system – the flexibility matrix. Let's denote this matrix by the letter ***F.*** Note that the physical meaning of the coefficients in this matrix f_{ij} is movement in direction of the *i-th* degree of freedom from a unit force applied in the direction of *j-th* degree of freedom. The flexibility matrix has one remarkable property – if you select in it the blocks corresponding to the deformations of individual nodes, form a common (truncated) matrix from these blocks and calculate its inverse matrix, then the matrix thus obtained is nothing more than the stiffness matrix of the entire system reduced to the selected nodes.

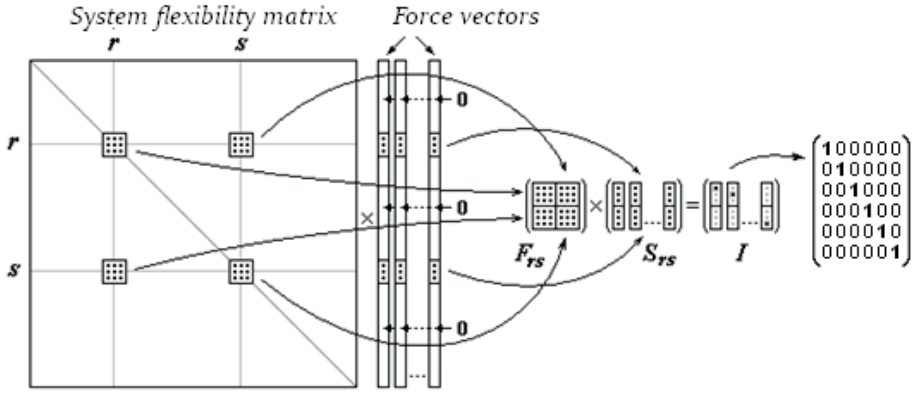


Figure 2. Formation of a truncated flexibility matrix and its transformation into a stiffness matrix of the entire system, reduced to the selected nodes

Indeed, let us introduce a vector of forces whose components for all degrees of freedom, except those corresponding to the selected nodes, are equal to zero (Fig. 2, first column of force vectors). We select the components corresponding to the selected degrees of freedom (in the figure – degrees of freedom related to nodes r and s) in such a way that, when multiplied by the flexibility matrix for the first degree of freedom, related to the selected group of nodes, we obtain a value of generalized displacement equal to 1, and for all others – 0 (Fig. 2, first column of matrix $\boldsymbol{I}$). Obviously, the force vector selected in this way is nothing other than the reactions in the restrictions imposed on the nodes r and s from a single displacement of the first of these reactions, provided that all other nodes, except for those actually fixed, are free (the force vector is defined in such a way that the reactions in these reactions are zero).

Continuing this procedure for all other restrictions of the truncated system, we arrive at the obvious equality:

$$\boldsymbol{F}_{rs} \cdot \boldsymbol{S}_{rs} = \boldsymbol{I}\,, \tag{5}$$

where $\boldsymbol{F}_{rs}$ is a truncated flexibility matrix formed from cells of the general flexibility matrix related to selected nodes, $\boldsymbol{S}_{rs}$ – stiffness matrix of the entire system reduced to selected pair of nodes, $\boldsymbol{I}$ unit matrix. Hence, the required stiffness matrix of the system reduced to the selected nodes is determined by the equality

$$\boldsymbol{S}_{rs} = \boldsymbol{F}_{rs}^{-1} \tag{6}$$

Thus, in the presence of flexibility matrix for the entire system, it is possible to select in it the blocks associated with a specific element and form a stiffness matrix reduced to the selected nodes. The next step is to subtract the unit reactions of the tested element $\boldsymbol{S}_M(\alpha_0)$ from the given stiffness matrix $\boldsymbol{S}_{rs}$ and substituting instead the matrix of the same element $\boldsymbol{S}_M(\alpha)$, but depending on the parameter α – eigenvalue of the boundary value problem. But here everything is being hampered to the very matrix of flexibility of the entire system $\boldsymbol{S}$. Firstly, the system's flexibility matrix is completely filled, which causes problems with storing the matrix, and secondly, even taking into account the symmetry of the flexibility matrix, the costs of its formation may turn out to be incommensurate with the capabilities of modern household computers. However, the peculiarities of the problem allow us to solve this problem with very little computational effort.

4. FORMATION OF THE FLEXIBILITY MATRIX OF THE ENTIRE STRUCTURE

First, we note that, despite the fact that the flexibility matrix is completely filled, all the matrix blocks of interest to us will be located within the same band structure as the original stiffness matrix. Secondly, since the flexibility

matrix (like the stiffness matrix) is symmetrical, it is sufficient to form, for example, only the elements lying below or above the main diagonal. Formally, the procedure for constructing a flexibility matrix is reduced to solving a system of equations

$$\boldsymbol{S} \cdot \boldsymbol{F} = \boldsymbol{I}, \qquad (7)$$

where $\boldsymbol{S}$ and $\boldsymbol{F}$ are the stiffness and flexibility matrices of the entire system, $\boldsymbol{I}$ is the identity matrix. To calculate the flexibility matrix $\boldsymbol{F}$, we will consider equation (7) as a system of n equations with n columns of right-hand sides. The i *-th* column of the right-hand sides contains a unit in the i*-th* position. All other elements of the i*-th* column initially contain zeros. Let us divide the procedure for solving equation (7) into 3 stages: the first is the reduction of the stiffness matrix $\boldsymbol{S}$ to a triangular view using the Gauss method; the second is a forward Gaussian sweep on the matrix $\boldsymbol{I}$; third – Gaussian inverse sweep on matrix $\boldsymbol{I}$. Figure 3 on the left shows the stiffness matrix of the system, reduced to a triangular form by a forward Gaussian sweep. On the right is the process of converting the identity matrix into a flexibility matrix.

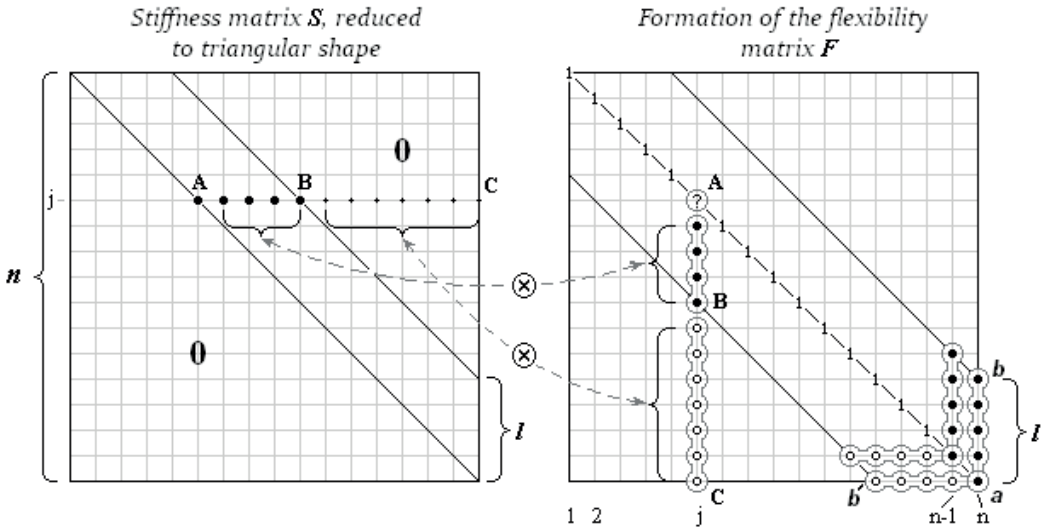


Figure 3. The process of forming the system flexibility matrix

As a result of a direct sweep on the matrix $\boldsymbol{I}$ the entire triangle below the main diagonal will be filled, and the zeros above the main diagonal and the ones on the main diagonal will remain in their original state. Let's consider the reverse sweep procedure using the example of the j*-th* column of the formed flexibility matrix (Fig. 3). Let, as a result of the backward procedure, all elements of the j*-th* column lying below the main diagonal were calculated. To find the diagonal element (indicated by the sign '**?**'), you need to multiply the previously calculated elements of the j*-th* column (**A,C**] of the generated flexibility matrix by the elements of the j*-th* row (**A,C**] of the stiffness matrix. Then subtract the resulting amount from unity (element **A** matrix located on the right) and divide the result by the diagonal element of the stiffness matrix (element **A** matrix located on the left). Obviously, the values of the previously calculated elements of the j*-th* column lying below point **B**, located on boundary of the band structure of the flexibility matrix, will not affect the value of the diagonal element **A** of the flexibility matrices, since all of them will be multiplied by the zeros of the j*-th* row of the stiffness matrix, located above the width of the band. Similarly, when forming all elements of the j*-th* columns located above the main diagonal, elements located below element **B**, will also not affect their values in any way for the

same reason. Thus, the procedure for reverse sweep by the *j-th* column of matrices ***I*** can be written as follows:

$$f_{i,j}=\begin{cases}\dfrac{1}{s_{i,i}}\left(1-\sum\limits_{k=1}^{l_i-1}s_{i,i+k}f_{i+k,i}\right), & i=j,\\ -\dfrac{1}{s_{i,i}}\sum\limits_{k=1}^{l_i-1}s_{i,i+k}f_{i+k,j}, & i=j-1,j-2,...,1\end{cases} \tag{8}$$

where l_i – bandwidth of the *i-th* row. This means that there is no need to either calculate or store flexibility matrix elements located outside the bandwidth. Thus, if there is a way to calculate the elements of the *j-th* columns of the flexibility matrix located within the width of the band below the diagonal element, without preliminary calculation of the elements located outside the band, then the problem of forming a flexibility matrix will be solved.

The following algorithm solves this problem. We perform the first step of the algorithm – reducing the matrix ***S*** to triangular form using the Gaussian procedure**.** The second step is a direct sweep through the matrix ***I.*** But, since the last column of matrix ***I*** remains unchanged after the forward sweep (recall that the last *n-th* column of matrix ***I*** contains the only non-zero element – one in cell $[n,n]$), then by omitting the forward sweep, you can immediately perform a reverse sweep along this column. And, since the elements of matrix ***F*** outside the width of the band are of no interest to us, the reverse sweep can be made not to the entire height of the matrix, but only within the width of the band – section $[\boldsymbol{ab}]$ (see Fig. 3). Since the flexibility matrix is symmetric, we reflect the elements of the $[\boldsymbol{ab}]$ column onto the $[\boldsymbol{ab'}]$ row. Let's move on to the (n-1)*-th* column of matrix ***F.*** Since the subdiagonal element in this column is already known, we immediately perform the reverse sweep, starting with the diagonal element and also within the width of the band. We reflect the calculated elements of the (n-1)*-th* column onto the (n-1)*-th* row. Continuing this procedure, we successively fill in the band structure of the matrix ***F.*** The algorithm can be constructed in such a way that it will not be necessary to fill the subdiagonal part of the matrix ***F.*** Therefore, the required external memory for storing the required data of matrix ***F*** no more than what is needed to store the band structure of the system's stiffness matrix.

To avoid reloading the rows of the factorized triangular matrix ***S***, the elements of the matrix ***F*** should be calculated in the sequence shown in Figure 4.

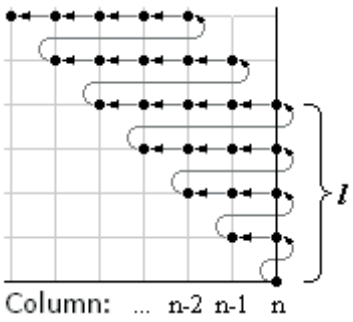


Figure 4. Sequence of formation of elements of the flexibility matrix

The coefficients of the matrix ***F*** are found using recurrent formulas.

$$\begin{cases} f_{i,i+m}=-\dfrac{1}{s_{i,i}}\left(\sum\limits_{k=1}^{m}s_{i,i+k}f_{i+k,i+m}+\sum\limits_{k=m+1}^{l_i-1}s_{i,i+k}f_{i+m,i+k}\right), & m>0,\\ f_{i,i}=\dfrac{1}{s_{i,i}}\left(1-\sum\limits_{k=1}^{l_i-1}s_{i,i+k}f_{i,i+k}\right), & m=0.\end{cases} \tag{9}$$

Index i is go over through the sequence $i=n,n-1,\dots,1$, and for each value of index i index m runs through values $m=l_i-1,l_i-2,\dots,0$. Table 1 shows the number of operations required to reduce a matrix of order n and bandwidth l to triangular form, and the number of operations required to form the band structure of the inverse matrix

Table 1. Number of operations

Operation	Direct Gaussian move	Forming the tape inverse matrix
Division	$nl-\frac{l(l-1)}{2}$	$nl-\frac{l(l-1)}{2}$
Multiplication	$\frac{nl(l-1)}{2}-\frac{l(l-1)(2l-1)}{6}$	$nl(l-1)-\frac{l(l-1)(2l-1)}{3}$
Subtraction	$\frac{nl(l-1)}{2}-\frac{l(l-1)(2l-1)}{6}$	$nl(l-1)-\frac{l(l-1)(2l-1)}{3}$

As you can see, the number of operations for forming a band of the inverse matrix is approximately 2 times greater than the number of operations for the Gaussian elimination procedure, which is much more efficient than forming a system stiffness matrix and processing it according to Gaussian for each element separately.

After the "band" of the system's flexibility matrix $\boldsymbol{F}$ is formed follow the procedure described above. For each rod, we "pull out" from the flexibility matrix the cells corresponding to the attachment points of the rod and form a truncated flexibility matrix of the rod attachments $\boldsymbol{F}_{sk}$. This is a relatively small matrix – in the case of a spatial system, it is a 12×12 matrix. We calculate its inverse matrix – the stiffness matrix of the system reduced to the nodes of the tested rod $\boldsymbol{S}_{sk}$. Since the initial matrix of the system is formed taking into account the single reactions of the tested rod, we subtract the rod's own stiffness matrix $\boldsymbol{S}_M(\alpha_0)$ from the given matrix. We add to the given stiffness matrix the rod's own stiffness matrix as a function of the parameter α – $\boldsymbol{S}_M(\alpha)$. We find the eigenvalues of the parameter α. For each value of α we construct a mode of buckling. Based on the mode, we determine relative to which principal axis of the section the bending occurs according to this mode. We continue the search for eigenvalues until we find the smallest eigenvalue for each principal axis of the section. Using the formula $\mu = \pi/\alpha$ we determine the coefficient of the effective length of the rod relative to both principal axes of the section.

5. EXAMPLE

The algorithm described above was successfully implemented on the SELENA computing complex [32]. As an example, consider the flat frame shown in Figure 5. I-section columns HE 320C ($\mathbf{A} = 2.3695\cdot10^{-2}$ m^2, $\mathbf{I} = 4.8711\cdot10^{-4}$ m^4) . Crossbars – box section RVS 300×300×15 ($\mathbf{A} = 1.6521\cdot10^{-2}$ m^2, $\mathbf{I} = 2.1959\cdot10^{-4}$ m^4). The elastic modulus is taken equal to $\mathbf{E} = 2.0594\cdot10^{11}$ N/m^2.

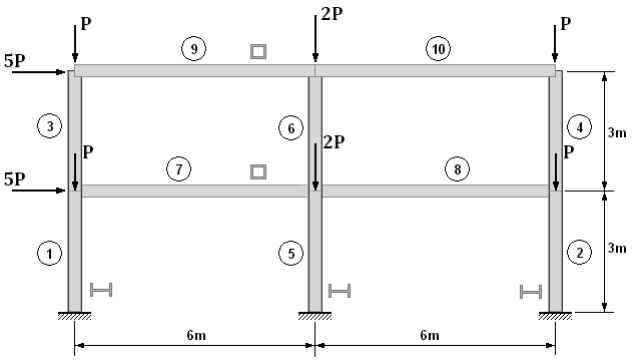


Figure 5. Example of a flat frame

This flat frame structure loses stability at a force value P equal to $1.005\cdot10^7$ N. Figure 6 shows the curves of changes in the values of the effective length coefficient μ depending on the load intensity P for six columns calculated in accordance with the described algorithm.

Let's perform "manual" testing of the algorithm using column No.5 as an example (in Figure 7*a* this element is designated **AB**). For simplicity, we will assume that there is no external load.

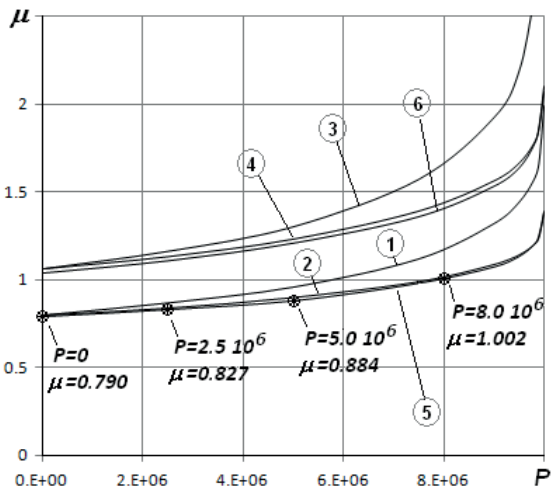


Figure 6. Graphs of the dependence of the coefficient of the effective length μ of columns on the load level P

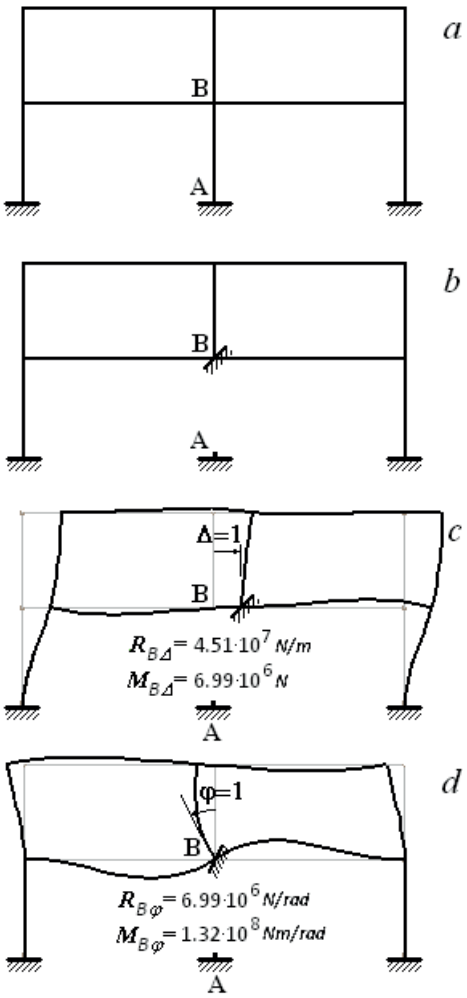


Figure 7. Example of "manual" check for element No.5.

Element No.5 is excluded from the design diagram and constraint is added at node **B** (node **A** is initially fixed, Fig. 7*b*). We give node **B** a unit horizontal displacement $\Delta = 1$ and determine the reactions $R_{B\Delta}$ and $M_{B\Delta}$ (Fig. 7*c*). We rotate node **B** by an angle $\varphi = 1$ and determine the reactions $R_{B\varphi}$ and $M_{B\varphi}$ (Fig. 7*d*□ □□□We add our own unit reactions of rod No.5 as a function of the parameter α (see formulas (3,4)).As a result, the system stiffness matrix reduced to nodes **A** and **B** will have the form

$$\boldsymbol{S} = \begin{pmatrix} R_{B\Delta} + \frac{12EI}{l^3}\frac{\left(\frac{\alpha}{2}\right)^3}{3\left(\mathrm{tg}\frac{\alpha}{2} - \frac{\alpha}{2}\right)} & R_{B\varphi} + \frac{6EI}{l^2}\frac{\left(\frac{\alpha}{2}\right)^2 \mathrm{tg}\frac{\alpha}{2}}{3\left(\mathrm{tg}\frac{\alpha}{2} - \frac{\alpha}{2}\right)} \\ M_{B\Delta} + \frac{6EI}{l^2}\frac{\left(\frac{\alpha}{2}\right)^2 \mathrm{tg}\frac{\alpha}{2}}{3\left(\mathrm{tg}\frac{\alpha}{2} - \frac{\alpha}{2}\right)} & M_{B\varphi} + \frac{4EI}{l}\frac{\frac{\alpha}{2}\left(1 - \frac{\alpha}{\mathrm{tg}\alpha}\right)}{4\left(\mathrm{tg}\frac{\alpha}{2} - \frac{\alpha}{2}\right)} \end{pmatrix} . \quad (10)$$

For element No.5 we have: $\frac{12EI}{l^3} = \frac{12 \cdot 2.0594\ 10^{11} \cdot 4.8711\ 10^{-4}}{3^3} = 0.4458\ 10^8 N/m.$

$\frac{6EI}{l^2} = \frac{12 \cdot 2.0594\ 10^{11} \cdot 4.8711\ 10^{-4}}{3^2} = 0.6688\ 10^8 N.$

$\frac{4EI}{l} = \frac{12 \cdot 2.0594\ 10^{11} \cdot 4.8711\ 10^{-4}}{3} = 1.3375\ 10^8 Nm.$

Now it remains to find a parameter value α that satisfies the requirement $\det(\boldsymbol{S}(\alpha)) = 0$. The zero value of the determinant is reached at $\alpha = 3.977$, which exactly corresponds to the value $\mu = \frac{\pi}{\alpha} = 0.790$ found by the program at zero load (see Fig. 6, point $P = 0$).

Figure 8 shows graphs of changes in the function $\det(\boldsymbol{S}) = f(\alpha)$ at different load levels P. The results are summarized in Table 2. Based on the found values of zero points of function $f(\alpha)$ (Fig. 8) the coefficient μ values corresponding to four load levels were determined and superimposed on the graph $\mu = \mu(P)$ for element No.5 (Fig. 6). As you can see, all the shown marks fall exactly on the curve calculated in accordance with the algorithm.

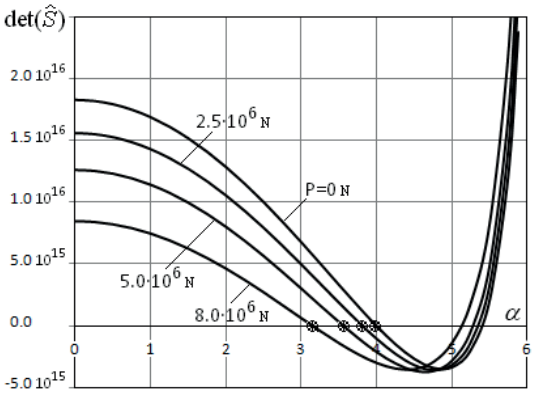


*Figure 8. Graph of the function $det(S) = f(\alpha)$ for rod **AB** at various levels of external load*

Table 2. Coefficient α at 4 levels of external load

P (*N*)	$R_{B\Delta}$ (*N/m*)	$M_{B\Delta}$ $R_{B\varphi}$ (*N*)	$M_{B\varphi}$ (*Nm/rad*)	α	μ
0	$4.507 \cdot 10^7$	$6.993 \cdot 10^6$	$1.316 \cdot 10^8$	3,977	0.790
$2.5 \cdot 10^6$	$3.982 \cdot 10^7$	$7.231 \cdot 10^6$	$1.161 \cdot 10^8$	3.799	0.827
$5.0 \cdot 10^6$	$3.386 \cdot 10^7$	$7.166 \cdot 10^6$	$0.973 \cdot 10^8$	3,554	0.884
$8.0 \cdot 10^6$	$2.473 \cdot 10^7$	$5.278 \cdot 10^6$	$0.636 \cdot 10^8$	3.137	1.002

Fig. 9 shows the design model of a 4-story 4-span frame. All rods are of the same cross-section. The floors and the ceiling are loaded with the same distributed load.

The graphs in Fig. 10 show the curves of the buckling length coefficient μ dependence on the load level for columns (A, B, C), calculated programmatically based on the algorithm described above. The load level in relation to the critical state is plotted on the abscissa scale. The numbers indicate the floor numbers.

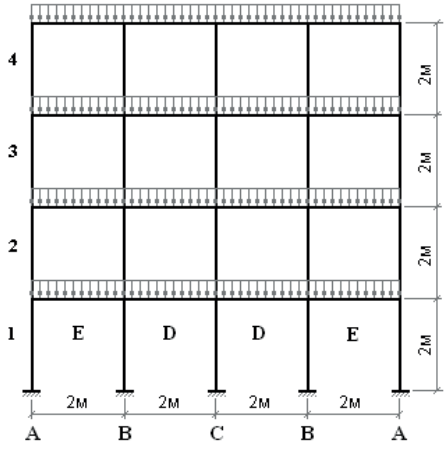


Figure 9. Design model of a 4-storey 4-span frame

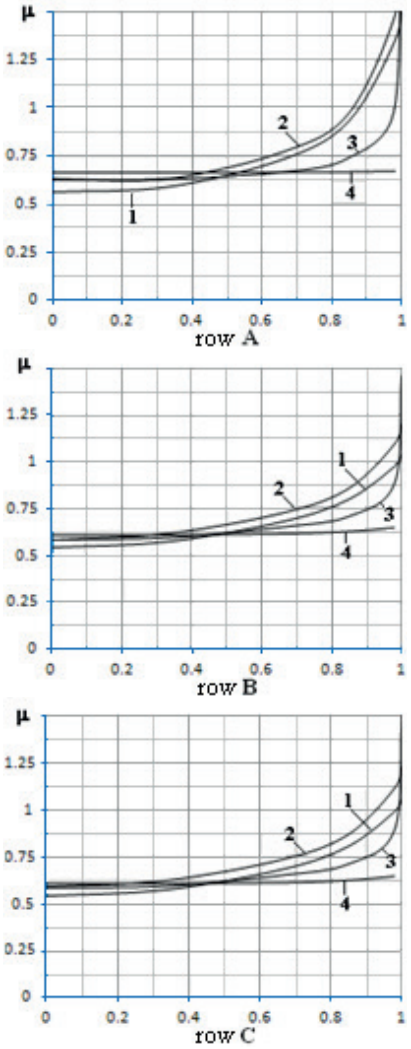


Figure 10. Graphs of the dependence of the coefficient μ on the load level

Table 3 shows the limit values of the coefficient μ corresponding to the critical state of the structure. Note that these limit values correspond to the "standard" calculation scheme of analysis of overall stability, when searching for a critical state, the load increase in all elements of the system proportional to the same parameter.

Table 3. Values of the coefficient μ when the load reaches a critical value

Floor	**A**	**B**	**C**
4	3.141	2.055	2.131
3	2.192	1.464	1.501
2	1.785	1.197	1.225
1	1.545	1.037	1.064

It is somewhat more difficult to check the algorithm works if the acting load does not reach the critical value. To do this, it is necessary to find a way to fix the stress state of the structure at a certain level (below the critical value), and vary the force in one tested rod, bringing it to a loss of stability. Of the programs known to us, only the SCAD software package can provide such an possibility [33]. We are talking about the method of "additional loading of passive elements", described in the work [8]. The program allows, having formed a calculated combination of loadings for performing the overall buckling analysis, to fix individual loadings, and to carry out "additional loading" on the remaining loadings.

In order to test the algorithm operation, the following scheme was implemented - a design combination was created consisting of two loadings. The first loading included a distributed load, as shown in Figure 9. This loading was included in the design combination with a combination factor of 0.9 and was fixed. The second loading consisted of two unit forces applied to the ends of the tested rod and directed towards each other, thus simulating its compression. Variation was allowed only for the second loading. Based on the found critical force, the coefficient of the buckling length of the rod was calculated using the formula $\mu_{test} = \frac{\pi}{l}\sqrt{\frac{EI_{test}}{N_{1,test}+N_{2.test}}}$, where $N_{1,test} -$ is the force in the tested rod from the first loading, and $N_{2,test} -$ is the critical force in the same rod from the second loading. All column elements in rows A, B and C were tested. Table 4 shows the results of the experiment.

Table 4. Values of the coefficient μ when the load reaches 0.9 of the critical value

Floor	A	B	C
4	0.668 0.668	0.636 0.635	0.632 0.631
3	0.784 0.784	0.748 0.747	0.749 0.747
2	1.082 1.083	0.930 0.929	0.935 0.934
1	1.039 1.039	0.859 0.857	0.867 0.865

The numerator of each fraction contains the value of the coefficient μ obtained by the SCAD program, and the denominator contains the value obtained by the described algorithm implemented in the SELENA program. As can be seen, the results are almost identical.

6. CONCLUSION

The speed of the algorithm described above is ensured by the fact that, as has been shown, the boundary conditions at both ends of a particular element can be obtained by inverting a very small fragment of the overall flexibility matrix of the structure. In turn, it is shown that to solve the problem, not the entire flexibility matrix is needed, but only that part of it that lies within the band structure of the system's stiffness matrix. An effective method for forming the required flexibility matrix band is proposed. Experiments show that the time required to calculate the effective lengths of all structural elements is comparable to the time required for one static calculation per one load. And the fact that only the band structure of the flexibility matrix is used does not impose excessive demands on the use of external memory.

Some notes on using the algorithm. Since the stiffness of a structure depends not only on the geometric characteristics of the elements, but also on their stress state, when preparing the initial stiffness matrix, the unit reactions of the elements must be included taking into account the longitudinal forces acting in them. To ensure a certain safety factor of structural strength, it can be recommended to increase the values of forces from the design combination of loads by 15-20%. A more strong option – perform a preliminary search for the most unfavorable combinations of loads and for each element set the largest value of longitudinal force over the entire sample of possible load combinations. This seems all the more appropriate since calculators, as a rule, do not recalculate the effective lengths of bars for various combinations of load cases. And some overestimation of longitudinal forces in

individual rods only affects the boundary conditions of neighboring rods, which will contribute to a certain robustness of stability. In this case, it is necessary to ensure that the given combination of forces does not take the structure beyond the limits of loss of overall stability. Considering that in reality, in the vast majority of cases, structures have a significantly larger robustness of overall stability, such a cautious approach would provide a guaranteed robustness of strength without excessive waste of material.
The algorithm, in the form in which it is presented in this work, cannot be applied to compound rods and rods with intermediate nodes. With a little modification this shortcoming can be eliminated. The authors hope that they will have the opportunity to continue work in this direction.

7. ACKNOWLEDGEMENTS

The authors express their gratitude to Anatoly Viktorovich Perelmuter and Mikhail Anatolyevich Perelmuter for their help in preparing the work for publication. Special thanks to the Reviewer of the work for constructive comments, which definitely made the work better.

REFERENCES

1. **Belyj G.I.** O raschete uprugikh sterzhney po deformirovannoy skheme pri deystvii aktivnykh i parametricheskikh nagruzok [On the calculation of elastic rods according to a deformed scheme under the action of active and parametric loads] // Mekhanika sterzhnevykh sistem i sploshnykh sred. 1980. S. 41–48.
2. **Aleksandrov A.V.** Rol' otdel'nykh elementov sterzhnevoy sistemy pri potere ustoychivosti [The role of individual elements of the rod system during loss of stability]. Vestnik MIITa. Nauchno-tekhnicheskiy zhurnal. Vypusk 5. - M.: 2001, s. 46.
3. **Aleksandrov A.V., Travush V.I., Matveyev A.V.** O raschete sterzhnevykh konstruktsiy na ustoychivost' [On the calculation of rod structures for stability]. PGS Promyshlennoye i grazhdanskoye stroitel'stvo. - 2002. - № 3. - S. 16-19.
4. **Grudev I.D., Artomov A.A.** Pryamoy metod raschota szhatykh elementov stal'nykh konstruktsiy v sostave sooruzheniya [Direct method for calculating compressed elements of steel structures as part of a building] // Promyshlennoye i grazhdanskoye stroitel'stvo. 2003. - №6. - s. 34-36.
5. **Manuylov, G.A., Kositsyn S.B.** O chuvstvitel'nosti kriticheskikh nagruzok dlya dvuparametricheskikh uprugikh sistem k nachal'nym nesovershestvam [On the sensitivity of critical loads for two-parameter elastic systems to initial imperfections] // Stroitel'naya mekhanika i raschet sooruzheniy. - 2008. - № 5. - S. 12-18.
6. **Belostotskiy A.M., Pavlov A.S.** Raschet konstruktsiy bol'sheproletnykh zdaniy s uchetom fizicheskoy, geometricheskoy i konstruktivnoy nelineynostey [Calculation of structures of large-span buildings taking into account physical, geometric and structural nonlinearities] // International Journal for Computational Civil and Structural Engineering. - 2010. - T. 6, № 1-2. - S. 80-86.
7. **Belostotskiy A.M., Akimov P.A., Pavlov A.S., Kaytukov T.B., Afanas'yeva I.N.** O razrabotke, issledovanii i verifikatsii korrektnykh chislennykh metodov resheniya nelineynykh zadach deformirovaniya, ustoychivosti i zakriticheskogo povedeniya tonkostennykh obolochechno-sterzhnevykh konstruktsiy [On the development, study and verification of correct numerical methods for solving nonlinear problems of deformation, stability and postcritical behavior of thin-walled shell-rod structures] // Stroitel'naya

mekhanika i raschet sooruzheniy. 2014. № 5 (256). C. 7—13.
8. **Perelmuter A.V., Slivker V.I.** Ustoychivost' ravnovesiya i rodstvennyye problem [Stability of equilibrium and related problems]. Tom III. – M.: Izdatel'stvo SKAD SOFT, 2011.
9. **I. Duan, W.F. Chen.** "Effective Length Factors of Compression Members", Structural Engineering Handbook, Ed. Chen Wai-Fah, CRC Press LLC, Boca Raton,1999.
10. **Britvin E.I., Tarnopolskyi A.A.,** K voprosu o proverne ustoychyvosty sterzhnevykh konstruktsiy [To the question of checking the stability of rod structures], zh. Budivnyts′tvo Ukrainy, №1, 2006h. s.22-27.
11. **D.W. White, A. Surovek,** and **S.C. Kim**, Direct Analysis and Design Using Amplified First-Order Analysis Part 1: Combined Braced and Gravity Framing Systems, Engineering Journal, 305-322, 2007.
12. **D.W. White, A. Surovek,** and **S.C. Kim**, Direct Analysis and Design Using Amplified First-Order Analysis Part 2: Moment Frames and General Framing Systems, Engineering Journal, 323-340, 2007.
13. EN 1993-1-1 (2005) Eurocode 3: Design of steel structures – Part 1-1: General rules and rules for buildings. The European Union Per Regulation 305/2011.
14. AISC/AISC 360-16. Specification for Structural Steel Buildings. An American National Standard. July 7, 2016.
15. SP 16.13330.2017, Stal'nyye konstruktsii [Steel structures], SNiP II-23-81*, Moskva, 2017.
16. **Britvin E.I.** K voprosu ob opredelenii raschetnykh dlin sterzhnevykh elementov ramnykh prostranstvennykh system [On the issue of determining the calculated lengths of rod elements of frame spatial systems], Stroitel'naya mekhanika i raschet sooruzheniy, 2019. № 3. S. 31-38.
17. **R.H. Wood**, Effective length of columns in multi-story buildings, The Struct. Eng., Vol. 52, pp. 351-364, 1974.
18. **F. Cheong-Siat-Moy**, K-factor paradox, J. Struct. Eng., Vol. 112(8), pp. 1747–1760, 1986.
19. **R.Q. Bridge, D.J. Fraser**, Improved G-factor method for evaluating effective lengths of columns, J. Struct. Eng., Vol. 113(6), pp. 1341–1356, 1997.
20. **J. Hellesland, R. Bjorhovde**, Improved frame stability analysis with effective lengths, J. Struct. Eng., Vol. 122(11), pp. 1275–1283, 1996.
21. **M. Horne**, An Approximate Method for Calculating the Elastic Critical Loads of Multi-Story Plane Frames, 1975.
22. **L. Duan, W.F. Chen**, Effective length factor for columns in braced frames, J. Struct. Eng., Vol. 114(10), pp. 2357–2370, 1988.
23. **N. Kishi, W. Chen, Y. Goto**, Effective length factor of columns in semirigid and unbraced frames, J. Struct. Eng., Vol. 123(3), pp. 313–320, 1997.
24. **D.W. White, J.F. Hajjar**, Buckling models and stability design of steel frames: a unified approach, J. Constr. Steel Res., Vol. 42(3), pp. 171–207, 1997.
25. **Oppe M., Muller C.,Iles C**., NCC: buckling length of columns; rigorous approach, London, Accsess Steel, 2005.
26. **J. Hellesland**, Mechanics and effective lengths of columns with positive and negative end restraints, Eng. Struct., Vol. 29(12), pp. 3464–3474, 2007.
27. **Webber A., Orr J.J., Shepherd P., Crothers K**., The effective length of columns in multi-storey frames, Engineering Structures, Vol. 102, pp. 132-143, 2015.
28. **M. Farajian, P. Sharafi, K. Kildashti**, The influence of inter-module connections on the effective length of columns in multi-story modular steel frames, J. Constr. Steel Res., Vol. 177, pp. 1–26, 2021.
29. **N.-I. Kim, D.-H. Choi**, System buckling analysis for multi-story frames subjected to nonconservative forces, Int. J. Steel Struct., Vol. 15(2), pp. 285–297, 2015.

30. **Leytes S.D.** Spravochnik po opredeleniyu svobodnykh dlin elementov stal'nykh konstruktsiy [Handbook for determining free lengths of steel structure elements], M.: Proyektstal'konstruktsiya, 1967.
31. Прочность, устойчивость, колебания. Справочник в трех томах. Под редакцией И.А.Биргера и Я.Г.Пановко, изд. “Машиностроение”, М. 1968.
32. Prochnost', ustoychivost', kolebaniya. Universal'nyy programmnyy kompleks dlya rascheta konstruktsiy na prochnost' SELENA [Universal software package for calculating the strength of structures SELENA]. Sayt: selenasys.com, 580 S.
33. SCAD Office.V.23.System SCAD++ / V.S.Karpilovskyy, E.Z.Kryksunov, A.A Maliarenko, A.V.Perelmuter, M.A.Perelmuter, S.Y. Fialko. — Publishing House SCAD SOFT, 2024. — 992 p.

СПИСОК ЛИТЕРАТУРЫ

1. **Белый Г.И.** О расчете упругих стержней по деформированной схеме при действии активных и параметрических нагрузок // Механика стержневых систем и сплошных сред. 1980. С. 41–48.
2. **Александров А.В.** Роль отдельных элементов стержневой системы при потере устойчивости. Вестник МИИТа. Научно-технический журнал. Выпуск 5. - М.: 2001, с. 46.
3. **Александров А.В., Травуш В.И., Матвеев А.В.** О расчете стержневых конструкций на устойчивость. ПГС Промышленное и гражданское строительство. - 2002. - № 3. - С. 16-19.
4. **Грудев И.Д., Артёмов А.А.** Прямой метод расчёта сжатых элементов стальных конструкций в составе сооружения // Промышленное и гражданское строительство. 2003. - №6. - с. 34-36.
5. **Мануйлов, Г.А., Косицын С.Б.** О чувствительности критических нагрузок для двупараметрических упругих систем к начальным несовершествам // Строительная механика и расчет сооружений. - 2008. - № 5. - С. 12-18.
6. **Белостоцкий А.М., Павлов А.С.** Расчет конструкций большепролетных зданий с учетом физической, геометрической и конструктивной нелинейностей // International Journal for Computational Civil and Structural Engineering. - 2010. - Т. 6, № 1-2. - С. 80-86.
7. **Белостоцкий А.М., Акимов П.А., Павлов А.С., Кайтуков Т.Б., Афанасьева И.Н.** О разработке, исследовании и верификации корректных численных методов решения нелинейных задач деформирования, устойчивости и закритического поведения тонкостенных оболочечно-стержневых конструкций // Строительная механика и расчет сооружений. 2014. № 5 (256). С. 7—13.
8. **Перельмутер А.В., Сливкер В.И.** Устойчивость равновесия и родственные проблемы. Том III. – М.: Издательство СКАД СОФТ, 2011.
9. **I. Duan, W.F. Chen.** “Effective Length Factors of Compression Members”, Structural Engineering Handbook, Ed. Chen Wai-Fah, CRC Press LLC, Boca Raton,1999.
10. **Бритвин Е.И., Тарнопольский А.А.**, К вопросу о проверке устойчивости стержневих конструкцій, ж.Будівництво Україні, №1, 2006г. с.22-27.
11. **D.W. White, A. Surovek,** and **S.C. Kim**, Direct Analysis and Design Using Amplified First-Order Analysis Part 1: Combined Braced and Gravity Framing Systems, Engineering Journal, 305-322, 2007.
12. **D.W. White, A. Surovek,** and **S.C. Kim**, Direct Analysis and Design Using Amplified First-Order Analysis Part 2: Moment Frames and General Framing Systems, Engineering Journal, 323-340, 2007.
13. EN 1993-1-1 (2005) Eurocode 3: Design of steel structures – Part 1-1: General rules and

rules for buildings. The European Union Per Regulation 305/2011.
14. AISC/AISC 360-16. Specification for Structural Steel Buildings. An American National Standard. July 7, 2016.
15. СП 16.13330.2017, Стальные конструкции, СНиП II-23-81*, Москва, 2017.
16. **Бритвин Е.И**. К вопросу об определении расчетных длин стержневых элементов рамных пространственных систем, Строительная механика и расчет сооружений, 2019. № 3. С. 31-38.
17. **R.H. Wood**, Effective length of columns in multi-story buildings, The Struct. Eng., Vol. 52, pp. 351-364, 1974.
18. **F. Cheong-Siat-Moy**, K-factor paradox, J. Struct. Eng., Vol. 112(8), pp. 1747–1760, 1986.
19. **R.Q. Bridge, D.J. Fraser**, Improved G-factor method for evaluating effective lengths of columns, J. Struct. Eng., Vol. 113(6), pp. 1341–1356, 1997.
20. **J. Hellesland, R. Bjorhovde**, Improved frame stability analysis with effective lengths, J. Struct. Eng., Vol. 122(11), pp. 1275–1283, 1996.
21. **M. Horne**, An Approximate Method for Calculating the Elastic Critical Loads of Multi-Story Plane Frames, 1975.
22. **L. Duan, W.F. Chen**, Effective length factor for columns in braced frames, J. Struct. Eng., Vol. 114(10), pp. 2357–2370, 1988.
23. **N. Kishi, W. Chen, Y. Goto**, Effective length factor of columns in semirigid and unbraced frames, J. Struct. Eng., Vol. 123(3), pp. 313–320, 1997.
24. **D.W. White, J.F. Hajjar**, Buckling models and stability design of steel frames: a unified approach, J. Constr. Steel Res., Vol. 42(3), pp. 171–207, 1997.
25. **Oppe M., Muller C.,Iles C**., NCC: buckling length of columns; rigorous approach, London, Accsess Steel, 2005.
26. **J. Hellesland**, Mechanics and effective lengths of columns with positive and negative end restraints, Eng. Struct., Vol. 29(12), pp. 3464–3474, 2007.
27. **Webber A., Orr J.J., Shepherd P., Crothers K**., The effective length of columns in multi-storey frames, Engineering Structures, Vol. 102, pp. 132-143, 2015.
28. **M. Farajian, P. Sharafi, K. Kildashti**, The influence of inter-module connections on the effective length of columns in multi-story modular steel frames, J. Constr. Steel Res., Vol. 177, pp. 1–26, 2021.
29. **N.-I. Kim, D.-H. Choi**, System buckling analysis for multi-story frames subjected to nonconservative forces, Int. J. Steel Struct., Vol. 15(2), pp. 285–297, 2015.
30. **Лейтес С.Д.** Справочник по определению свободных длин элементов стальных конструкций, М.: Проектстальконструкция, 1967.
31. Прочность, устойчивость, колебания. Справочник в трех томах. Под редакцией И.А.Биргера и Я.Г.Пановко, изд. “Машиностроение”, М. 1968.
32. Прочность, устойчивость, колебания. Универсальный программный комплекс для расчета конструкций на прочность SELENA. Сайт: selenasys.com, 580 С.
33. SCAD Office.Версия 23.Вычислительный комплекс SCAD++ / В.С. Карпиловский, Э.З. Криксунов, А.А. Маляренко, А.В. Перельмутер, М.А. Перельмутер, С.Ю. Фиалко. — Издательство «СКАД СОФТ» , 2024.— 992 стр.

Eugene I. Britvin, Ph.D, DANRZ Ltd.; 6 Trufa St., Tirat Carmel, Israel; E-Mail: evgbritvin@gmail.com.

Moshe Eisenberger, Ph.D, Professor, Faculty of Civil and Environmental Engineering, Technion, Haifa, Israel; E-mail: cvrmosh@technion.ac.il.

Евгений Исаакович Бритвин, кандидат физико-математических наук; DANRZ Ltd.; 6 Trufa St., Tirat Carmel, Israel, E-Mail: evgbritvin@gmail.com.

Моше Эйсенбергер, Ph.D, Профессор, Факультет гражданского строительства и экологии, Технион, Haifa, Israel; E-mail: cvrmosh@technion.ac.il.

DOI:10.22337/2587-9618-2025-21-4-56-72

DYNAMIC MODEL OF HIGH-FREQUENCY VIBRATION DAMPERS FOR POWER LINE CONDUCTORS

Alexander N. Danilin [1], Andrey P. Zakharov [2], Alexander E. Fedorov [1], Valery A. Feldstein [1,2]

[1] Institute of Applied Mechanics of the Russian Academy of Sciences, Moscow, RUSSIA
[2] Moscow Institute of Physics and Technology, Moscow, RUSSIA

Abstract: A dynamic model of an aeolian vibration damper for overhead power transmission line conductors has been developed, taking into account energy dissipation in the material structure. Based on the model, a dynamic stiffness matrix of the damper has been obtained, intended for use in a combined dynamic model of "conductor – damper". The damper's cable consoles are considered as beams made of a material with internal friction, to which the concept of microplastic deformations is applied. It is believed that the damper design is symmetrical relative to the vertical plane of the conductor sag, and during oscillations, it moves in this plane. The equations of oscillations are obtained in Lagrange form in matrix notations. The influence of the damping coefficient on energy dissipation power and oscillation amplitudes in resonance modes has been studied. The coefficients of amplitude and phase distribution (shape factor) of translational and rotational oscillations of loads have been determined depending on the radius of inertia and load eccentricity. Dimensionless nomograms of the damper arm's natural frequencies have been constructed in relevant parameter change ranges. The dependence of dimensionless dissipation power on frequency has been investigated.

Keywords: overhead power line, aeolian vibration, Stockbridge dampers, energy dissipation, dynamic model, dynamic stiffness matrix, parametric analysis, amplitude-frequency characteristics

ДИНАМИЧЕСКАЯ МОДЕЛЬ ГАСИТЕЛЕЙ ВЫСОКОЧАСТОТНЫХ ВИБРАЦИЙ ПРОВОДОВ ЛИНИЙ ЭЛЕКТРОПЕРЕДАЧИ

А.Н. Данилин [1], А.П. Захаров [2], А.Е. Фёдоров [1], В.А. Фельдштейн [1,2]

[1] Институт прикладной механики Российской академии наук, г. Москва, РОССИЯ
[2] Московский физико-технический институт, г. Москва, РОССИЯ

Аннотация: Разработана динамическая модель гасителя эоловой вибрации проводов воздушных линий электропередачи с учётом энергорассеяния в структуре материала. На основе модели получена матрица динамической жёсткости гасителя, предназначенная для использования в объединенной динамической модели «провод – гаситель». Тросовые консоли гасителя рассматриваются как балки из материала, обладающего внутренним трением, к которому применяется концепция микропластических деформаций. Считается, что конструкция гасителя симметрична относительно вертикальной плоскости провисания провода и при колебаниях она совершает движение в этой плоскости. Уравнения колебаний получены в форме Лагранжа в матричном виде. Исследовано влияние коэффициента демпфирования на мощность диссипации энергии и амплитуды колебаний в резонансных режимах. Определены коэффициенты распределения амплитуд и фаз-(коэффициент формы) поступательных и вращательных колебаний грузов в зависимости от радиуса инерции и эксцентриситета грузов. Построены безразмерные номограммы собственных частот плеча гасителя в актуальных диапазонах изменения параметров. Исследована зависимость безразмерной мощности диссипации от частоты.

Ключевые слова: воздушная линия электропередачи, эолова вибрация, гасители Стокбриджа, диссипация энергии, динамическая модель, матрица динамической жесткости, параметрический анализ, амплитудно-частотные характеристики

1. INTRODUCTION

The paper examines dynamic models of Stockbridge dampers utilized on overhead power lines (OHL) for the mitigation of aeolian vibrations, which arise from the intermittent release of Karman vortices from the conductor in wind flow [1]. Figure 1 depicts a frequently employed damper along with a schematic representation of its installation on a conductor [2].

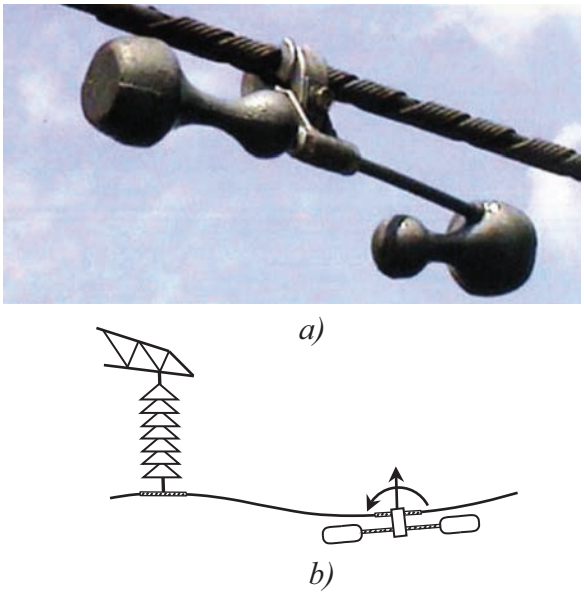


Figure 1. Vibration damper (a) and its installation diagram on the OHL conductor (b)

Mechanically, the damper consists of a pair of double arms (oscillators), with the inertial elements constructed as massive weights and the elastic elements designed according to traditional principles using elastic console cables. These cables also serve as dampers due to friction among the spiral wires that comprise them. In the presence of aeolian vibrations, a stationary transverse wave is established within the span, leading to kinematic excitation of the damper connected to the conductor. This excitation results in translational movement primarily in the vertical direction and rotation around an axis perpendicular to the plane of the conductor's sagging. Typically, the damper designs exhibit symmetry concerning the vertical plane of the conductor's sagging, and during oscillations, they perform planar motion within this plane.

The Stockbridge damper was developed in 1925 by George H. Stockbridge following several instances of damage to power transmission lines attributed to aeolian vibration [3]. Subsequently, the Stockbridge damper entered an extended phase of development and enhancement [3-7]. In 1932, R. Monroe and R. Templin proposed a two-degree-of-freedom damper.

Modern designs were developed as a result of extensive research conducted in the late 1960s and 1970s [6]. In 1968, R. Claren and G. Diana developed a variant of an asymmetric damper with various weights and arms of cable elements. A damper with two attachment points to a conductor, known as the Haro damper, was developed by L. Haro and T. Seppa in 1970. The Dogbone variant is another modern damper design that resembles a dog bone in shape. The damper was proposed by the Australian engineer and inventor Philip W. Dulhunty around 1976. The weights of the damper are slightly shifted to the side to create a third torsional degree of freedom, which allows the cable not only to bend vertically, but also to twist.

Despite the successful development of aeolian vibration dampers, practically no rules for designing dampers, analyzing their effectiveness and use were published at that time. Since the early 1970s, the first mathematical models of vibrations of Stockbridge dampers and similar variants began to appear [8-16]. H. Wagner et al. (1973) investigated the dynamic response of a symmetrical Stockbridge damper, which was modeled as a massless cable with weights attached to its ends [9]. P. Hagedorn (1980) proposed the concept of optimal the mechanical impedance of the damper, using a simple computational model [13]. The correctness of P. Hagedorn's approximate calculations was subsequently confirmed by B. Schaefer (1981) [15]. Based on these works, new design concepts for dampers with increased efficiency were considered [14].

In 1995, M. Markiewicz published a method and computational model for estimating the op-

timal dynamic characteristics of Stockbridge dampers designed for installation near anchor supports [16]. It is shown that the efficiency of a standard damper used in such spans can be increased due to its correct location on the conductor.

The bibliography of further research is extensive and covers various aspects of the vibrations of dampers themselves and the "conductor – dampers" systems. Significant results have been published, for example, in works [17-29].

In this paper, a dynamic vibration model of the damper is constructed, focused on further use in the combined dynamic model "conductor – damper". Such a combination is easily carried out if the dynamic stiffness matrix of the damper is known, which relates the amplitudes of the generalized forces applied to the clamp to the amplitudes of the generalized displacements caused by them. This article describes a dynamic model of the damper and a method for constructing the mentioned dynamic stiffness matrix, analyzes the spectrum of natural vibrations of the damper depending on the dimensionless values of the radius of inertia, the eccentricity of the weights and the damping coefficient. The dissipation in the elastic console is taken into account based on the model of internal friction, according to which the modulus of elasticity of the material is considered a complex quantity, the imaginary part of which characterizes the dissipation of vibration energy.

2. PHYSICAL MODEL AND VIBRATION EQUATIONS

The main function of a vibration damper is to dissipate mechanical energy due to friction and to change the shape of the conductor in the edge zone of the span in order to reduce bending deformations. In traditional Stockbridge type dampers with a console made of a cable, friction is provided by internal friction when the spiral wires that make up the cable slip. This allows consoles to be considered as beams made of a material with internal friction, to which the concept of microplastic deformations is applied [30, 31]. According to this model, the modulus of material elasticity is assumed to be complex: $E_K = E\left(1+i\eta\right)$, where η is the damping coefficient, which has the order of the logarithmic decrement of vibrations. Usually, due to the smallness of the internal friction, it is assumed that $\eta^2 << 1$. However, in this case, the damping is not assumed to be small. A refined version of relation is also known [31], which is used further:

$$E_K = E\left(a+ib\right),$$
$$a = \frac{1-\eta^2/4}{1+\eta^2/4}, \quad b = \frac{\eta}{1+\eta^2/4}. \tag{1}$$

Since $a^2+b^2=1$, then $a^2+b^2=1$, where $\psi = \operatorname{arctg}\left(b/a\right)$ and $E_\kappa = Ee^{i\psi}$. Therefore, taking into account the designation $D = EI$, the flexural rigidity of the console –

$$D_\kappa = E_\kappa I = EIe^{i\psi} = De^{i\psi}. \tag{2}$$

The primary mass of the damper is concentrated in the weights and the clamp; therefore, the inertia of the console is not taken into account.

The inertial elements of the damper – the clamp (along with the segment of conductor it encompasses) and the weights – are considered as rigid bodies characterized by their masses m_i, moments of inertia in the vertical plane $J_i = m_i r_i^2$ relative to their centers of mass C_i, and the distances (eccentricities) $\left|d_i\right| = P_i C_i$ between the centers of mass and the point designated as the pole. The indices $i = 0,1,2$ refer to the clamp, the left arm, and the right arm, as illustrated in figure 2.

Depending on the configuration of the weight, its center of mass C_i can be located on different sides of the attachment point P_i to the console. This option is used, for example, in VORTX™ vibration dampers by the well-known company

PLP (Preformed Line Products). This circumstance is taken into account by the sign of the eccentricity: $d_1 < 0$, $d_2 > 0$. Both possible attachment options for the weights are schematically shown in figure 1.2.

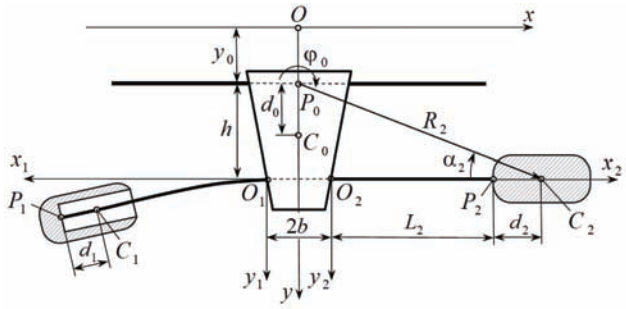


Figure 2. On deriving the vibration equations of the damper

It is assumed that the inertial characteristics of the loads, the lengths of the consoles L_i and the eccentricities d_i in the arms of the damper are different. This difference expands the frequency range of the damper and is used in practice.

The oscillations of the damper are considered with respect to a stationary right coordinate system $Oxyz$, the origin of which is located on the axis of the stationary conductor that is in equilibrium, and the longitudinal axis x is directed along the tangent. When aeolian vibration occurs, the clamp, along with the conductor, performs vertical and rotational oscillations relative to the axis Oz. Horizontal movements of the clamp can be neglected, as the longitudinal stiffness of the conductor is significantly greater than the transverse stiffness. The position of the clamp is determined by the vertical displacement y_0 of the point P_0 and the angle of rotation φ_0 relative to the stationary coordinate system. In addition to the stationary coordinate system, movable systems $O_i x_i y_i z_i \, (i = 1, 2)$ are introduced for each arm, which are associated with the clamp and therefore convenient for determining the deformations of the consoles.

As generalized coordinates for the clamp, the absolute coordinate y_0 and the angle of rotation φ_0 are chosen. It is advisable to choose the other generalized coordinates in such a way that the potential energy can be expressed as simply as possible in terms of the deflections and angles of rotation of the extreme sections of the console. This is convenient for further development of the model towards a more accurate account of the mechanical characteristics of the console, for example, to account for the dependence of the bending stiffness of the cables on their deflection [32]. For this purpose, movable coordinate systems $O_i x_i y_i z_i$ are used, relative to which the position of the weights is defined by the vertical displacements $y_{1,2}$ of the points $P_{1,2}$ and the angles of rotation $\varphi_{1,2}$. Then, the potential energy of the elastic deformations of the console takes the simplest form:

$$\Pi_i = \frac{1}{2}\left(g_i^{11} y_i^2 + 2 g_i^{12} y_i \varphi_i + g_i^{22} \varphi_i^2\right),$$

where y_i, φ_i are deflection and angle of rotation at the extreme section of the console, and g_i^{mn} – elements of the stiffness matrix of the i-th console:

$$\boldsymbol{G}_i = \begin{pmatrix} 12 D_к / L_i^3 & -6 D_к / L_i^2 \\ -6 D_к / L_i^2 & 4 D_к / L_i \end{pmatrix}.$$

In the case under consideration

$$\Pi = \frac{1}{2}\sum_{i=1}^{2}\left(g_i^{11} y_i^2 + 2 g_i^{12} y_i \varphi_i + g_i^{22} \varphi_i^2\right). \quad (3)$$

The total potential energy consists of the energy of elastic deformations of the console Π and the energy of the change in the center of gravity of the weights U. Let's evaluate these components. The inertia force of the weight, deforming the console, is of the order of $F = mA\omega^2$, where A – the amplitude of oscillations with frequency ω, and creates an average bending moment $M \approx mA\omega^2 L$ in the console, which corresponds

to the deformation energy Π: $M^2 L/D_K$. The gravitational part of the potential energy $U = mgA$. Comparing these values, we find: Π/U: $mA\omega^4 L^3/(D_K g)$. Even in the low-frequency range of aeolian vibration, at the amplitude $A \approx 0.01$м and typical parameters of the dampers [33], the elastic energy exceeds the gravitational energy by 1-2 orders of magnitude. It follows that the "pendulum" effect is insignificant for the operation of the system as an oscillation damper.

Kinetic energy of the damper:

$$K = \frac{m_0}{2}\left(V_0^2 + r_0^2\dot{\varphi}_0^2\right) + \frac{m_1}{2}\left[V_1^2 + r_1^2\left(\dot{\varphi}_0 - \dot{\varphi}_1\right)^2\right] + \\ + \frac{m_2}{2}\left[V_2^2 + r_2^2\left(\dot{\varphi}_0 + \dot{\varphi}_2\right)^2\right],$$

where V_i^2 are the squares of the absolute velocities of the centers of mass of the clamp $(i = 0)$ and weights $(i = 1,2)$, expressed in terms of their vertical and horizontal components:

$$V_0^2 = \dot{y}_0^2 + d_0^2\dot{\varphi}_0^2,$$
$$V_1^2 = \left(\dot{y}_0 + \dot{y}_1 + d_1\dot{\varphi}_1 - R_1\dot{\varphi}_0\cos\alpha_1\right)^2 + \\ + R_1^2\dot{\varphi}_0^2\sin^2\alpha_1,$$
$$V_2^2 = \left(\dot{y}_0 + \dot{y}_2 + d_2\dot{\varphi}_2 + R_2\dot{\varphi}_0\cos\alpha_2\right)^2 + \\ + R_2^2\dot{\varphi}_0^2\sin^2\alpha_2.$$

It is indicated here: $R_{1,2}^2 = \left(L_{1,2} + d_{1,2} + b\right)^2 + h^2$, and further it is taken into account that $R_{1,2}\cos\alpha_{1,2} = L_{1,2} + d_{1,2} + b = l_{1,2}$ (see figure 2).

The elementary work of the external forces applied to the clamp from the conductor side is equal to: $\delta A_y = F_C\delta y_0$, $\delta A_\varphi = M_C\delta\varphi_0$.

The equations of vibrations in the Lagrangian form [34, 35] can be presented in matrix notations. We will introduce a column vector of generalized coordinates and generalized external forces:

$$\boldsymbol{q} = \left(y_0\ \varphi_0\ y_1\ \varphi_1\ y_2\ \varphi_2\right)^T = \left(\boldsymbol{q}_0\ \boldsymbol{q}_1\ \boldsymbol{q}_2\right)^T, \\ \boldsymbol{Q} = \left(F_C\ M_C\ 0\ 0\ 0\ 0\right)^T, \tag{4}$$

as well as the inertia and stiffness matrices, which can be conveniently represented in block form:

$$\boldsymbol{M} = \begin{pmatrix} \boldsymbol{M}_{11} & \boldsymbol{M}_{12} & \boldsymbol{M}_{13} \\ \boldsymbol{M}_{12}^T & \boldsymbol{M}_{22} & \boldsymbol{0} \\ \boldsymbol{M}_{13}^T & \boldsymbol{0} & \boldsymbol{M}_{33} \end{pmatrix}, \\ \boldsymbol{C} = D_k\begin{pmatrix} \boldsymbol{0} & \boldsymbol{0} & \boldsymbol{0} \\ \boldsymbol{0} & \boldsymbol{C}_{22} & \boldsymbol{0} \\ \boldsymbol{0} & \boldsymbol{0} & \boldsymbol{C}_{33} \end{pmatrix}; \\ \boldsymbol{M}_{11} = \begin{pmatrix} m_\Sigma & \lambda_2 - \lambda_1 \\ \lambda_2 - \lambda_1 & \theta_\Sigma \end{pmatrix}, \\ \boldsymbol{M}_{22} = \begin{pmatrix} m_1 & \zeta_1 \\ \zeta_1 & \theta_1 \end{pmatrix},\ \boldsymbol{M}_{33} = \begin{pmatrix} m_2 & \zeta_2 \\ \zeta_2 & \theta_2 \end{pmatrix}, \\ \boldsymbol{M}_{12} = \begin{pmatrix} m_1 & \zeta_1 \\ -\lambda_1 & -\mu_1 \end{pmatrix},\ \boldsymbol{M}_{13} = \begin{pmatrix} m_2 & \zeta_2 \\ \lambda_2 & \mu_2 \end{pmatrix}, \tag{5}$$

where:

$$m_\Sigma = m_0 + m_1 + m_2,$$
$$\theta_\Sigma = m_0(r_0^2 + d_0^2) + m_1(R_1^2 + r_1^2) + m_2(R_2^2 + r_2^2)$$

– mass and moment of inertia of the entire damper relative to the pole O; $\theta_i = m_i(r_i^2 + d_i^2)$ – moments of inertia of weights relative to the poles P_i; $\zeta_i = m_i d_i$, $\lambda_i = m_i l_i$, $\mu_i = m_i(r_i^2 + d_i l_i)$ $(i = 1,2)$; $\boldsymbol{C}_{22} = \boldsymbol{G}_1$, $\boldsymbol{C}_{33} = \boldsymbol{G}_2$; $\boldsymbol{0}$ – zero 2×2-matrix.

Then the equations of vibrations will be written in the form:

$$\boldsymbol{M}\ddot{\boldsymbol{q}} + \boldsymbol{C}\boldsymbol{q} = \boldsymbol{Q}. \tag{6}$$

The forced vibrations of the damper installed on the vibrating conductor in the OHL span (span mode) [36] are excited by the action of periodic force and moment from the conductor, so that

the vector of generalized forces in the right part of (6) has the form

$$\boldsymbol{Q} = \left(F_C e^{i\omega t} \;\; M_C e^{i\omega t} \;\; 0 \;\; 0 \;\; 0 \;\; 0 \right)^T . \qquad (7)$$

This mode is further considered when determining the dynamic stiffness matrix used in constructing the combined "conductor – damper" model.

Important characteristics of vibration dampers include natural frequencies, amplitude-frequency characteristics (AFC), and the power of mechanical energy dissipation performed by the damping element of the damper. Current regulatory documents, for example [36], provide for its experimental determination through tests on a vibration stand that implements harmonic oscillations of the platform with an amplitude that changes according to the law $A(\omega)$.

In this case, the damper clamp is fixed immovably on the stand platform, while the weights perform a complex motion: a translational motion together with the stand platform and a relative motion with respect to the platform (stand mode). Then the loads are affected by the inertia of the portable motion, which reduces to a force and a moment with amplitudes $m_i A\omega^2$ and $d_i m_i A\omega^2$, as follows from (5), at $y_0 = Ae^{i\omega t}$, $\varphi_0 = 0$.

Therefore, in relation to this mode, in the general equation (6), the vector $\boldsymbol{q}$ defines the relative motion, and the vector $\boldsymbol{Q}$ defines the portable inertia forces. When testing the dampers, the frequency amplitude is scanned in such a way that the set amplitude of the platform speed is maintained $A\omega = V = (0.05 - 0.2)\,\text{m/s}$, so that

$$\boldsymbol{Q} = \left(0 \;\; 0 \;\; m_1\omega V \;\; d_1 m_1 \omega V \;\; m_2 \omega V \;\; d_2 m_2 \omega V \right)^T .$$

In the experiments, the damper arms oscillate practically independently; the weak mutual influence due to the elasticity of the clamp should be attributed to nonlinear effects that are insignificant in this case and is not taken into account. Such independent – partial oscillations of individual arms are also of interest and are described by equation (6), if instead of the general matrices $\boldsymbol{A}$, $\boldsymbol{C}$, we use their blocks A_{22}, C_{22}, or , A_{33}, C_{33}:

$$\begin{aligned} \left(C_{22} - \omega^2 M_{22} \right) \boldsymbol{q}_1 &= \boldsymbol{Q}_1 , \\ \left(C_{33} - \omega^2 M_{33} \right) \boldsymbol{q}_2 &= \boldsymbol{Q}_2 . \end{aligned} \qquad (8)$$

2. DYNAMIC CHARACTERISTICS OF THE DAMPER

In the following, we will focus on the design parameters that are typical for practically used vibration dampers (see table 1).

Table 1. Parameters of a typical vibration damper

Weight		
Mass m, kg	Radius of inertia r, mm	Eccentricity d, mm
1	40	15
Console		
Bending stiffness D, $\text{N}\cdot\text{m}^2$	Length L, mm	
1–6	100	
Clamp		
Mass m_0, kg	Moment of inertia J_0, $\text{kg}\cdot\text{m}^2$	
0.3	0.0003	

Setting the bending stiffness in the form of a range is due to the fact that this parameter for a console made of a spiral cable depends on the amplitude of the weight vibrations. At low amplitudes, the individual wires are pressed against each other and the console deforms like a solid section beam; in this case, the stiffness has the maximum value $D \approx 6\ \text{Н}\cdot\text{м}^2$. At high amplitudes, the wires slip each other in the console, as a result of which each of them bends independently; as a result, the stiffness of the console decreases and reaches a minimum value

$D \approx 1\ \text{Н}\cdot\text{м}^2$. This means that the elastic element in the form of a spiral cable, generally speaking, has a non-linearity.

Partial oscillations realized in the stand mode are described by equations (8). Due to the identity of the equations, the subscripts will be omitted when considering a single equation. Let us write down the system of equations with respect to the oscillation amplitudes in an expanded form, assuming: $y = Ye^{i\omega t}$, $\varphi = \Phi e^{i\omega t}$:

$$\begin{pmatrix} g^{11} - m\omega^2 & g^{12} - \varsigma\omega^2 \\ g^{12} - \varsigma\omega^2 & g^{22} - \theta\omega^2 \end{pmatrix} \begin{pmatrix} Y \\ \Phi \end{pmatrix} = \omega V \begin{pmatrix} m \\ \varsigma \end{pmatrix}. \quad (9)$$

In the following, the notation is used:

$$\rho = r/L,\ \delta = d/L,\ f = Y/L,$$
$$p = \omega\sqrt{mL^3/3D} = \omega/\omega_0,$$

where ω_0 is the lowest natural frequency of the console with bending stiffness and point mass m at the free end of the console. Turning to these variables, we transform the system (9) to the form

$$\begin{pmatrix} 4e^{i\psi} - p^2 & -2e^{i\psi} - \delta p^2 \\ -2e^{i\psi} - \delta p^2 & 4e^{i\psi}/3 - (\delta^2 + \rho^2)p^2 \end{pmatrix} \begin{pmatrix} f \\ \Phi \end{pmatrix} = \frac{Vp}{L\omega_0} \begin{pmatrix} 1 \\ \delta \end{pmatrix}. \quad (10)$$

Considering (1), (2), the solution of these equations is written as:

$$f = \frac{V}{L\omega_0}\frac{p}{\Delta}\left[2e^{i\psi}\left(\frac{2}{3} + \delta\right) - \rho^2 p^2\right] = \frac{V}{L\omega_0} f_\%,$$
$$\Phi = \frac{V}{L\omega_0}\frac{p}{\Delta} 2e^{i\psi}\left(1 + 2\delta\right) = \frac{V}{L\omega_0}\Phi_\%. \quad (11)$$

Here:

$$\Delta(p) = \rho^2 p^4 - 4p^2 e^{i\psi} c + 4e^{2i\psi}/3 = \Delta_R + i\Delta_I$$

is the determinant of the system (10); dimensionless variables:

$$\Delta_R = \rho^2 p^4 - 4p^2 ca + 4\left(a^2 - b^2\right)/3,$$
$$\Delta_I = 4b\left(2a - p^2 c\right);$$
$$f_\% = \frac{p}{\Delta_R^2 + \Delta_I^2}(f_R + if_I)(\Delta_R - i\Delta_I), \quad (12)$$
$$\Phi_\% = \frac{p}{\Delta_R^2 + \Delta_I^2} 2(1 + 2\delta)(a + ib)(\Delta_R - i\Delta_I),$$

with coefficients:

$$c = 1/3 + \rho^2 + \delta(\delta + 1),$$
$$f_R = 2a(2/3 + \delta) - \rho^2 p^4,\ f_I = 2b(2/3 + \delta). \quad (13)$$

The ratio of amplitudes during frequency scanning varies according to the law:

$$\beta = \frac{\Phi_\%}{f_\%} = \frac{2\left(1 + 2\delta\right)}{f_R^2 + f_I^2}(\beta_R + i\beta_I), \quad (14)$$

where are the real and imaginary parts:

$$\beta_R = af_R + bf_I,\ \beta_I = bf_R - af_I. \quad (15)$$

Let's first consider the characteristics of the damper without taking into account damping. The equation $\text{Re}\left[\Delta(p)\right] = 0$ defines the natural frequencies of free harmonic oscillations of a conservative system. In the expanded form –

$$\left(3\rho^2/4\right)p^4 - 3cp^2 + 1 = 0 \quad (16)$$

with discriminant $\vartheta(\delta, \rho) = 9c^2 - 3\rho^2 \geq 0$.

It is fundamentally important that the natural frequencies of the damper are located in the current frequency range characteristic of aeolian vibration. As can be seen, the dimensionless partial frequencies of the damper are determined by two parameters δ and ρ, moreover, a pair of values $\delta = -1/2$, $\rho = 1/\sqrt{12} = 0,289$ (solu-

tion of the system of equations $\partial\vartheta/\partial\delta = 0$, $\partial\vartheta/\partial\rho = 0$) plays a special role: for these values, the discriminant of equation (16) is zero and its roots are multiples. In dimensional variables, this means that when $d = -\sqrt{3}\,r$ both frequencies coincide: $\omega_1 = \omega_2 = \sqrt{12D/mL^3}$.

Figure 3 shows the dependences of the dimensionless frequencies $p_{1,2}$ on the eccentricity of the load (parameter δ) at different values of the radius of inertia (parameter ρ).

The curves corresponding to $\delta = -1/2$, $\rho = 1/\sqrt{12} \approx 0.289$ are limiting: at $\delta \to -1/2$, the frequencies approach each other: the lower frequency p_1 reaches its maximum, and the upper frequency p_2 reaches its minimum, and $p_1(-1/2) = p_2(-1/2) = 2$.

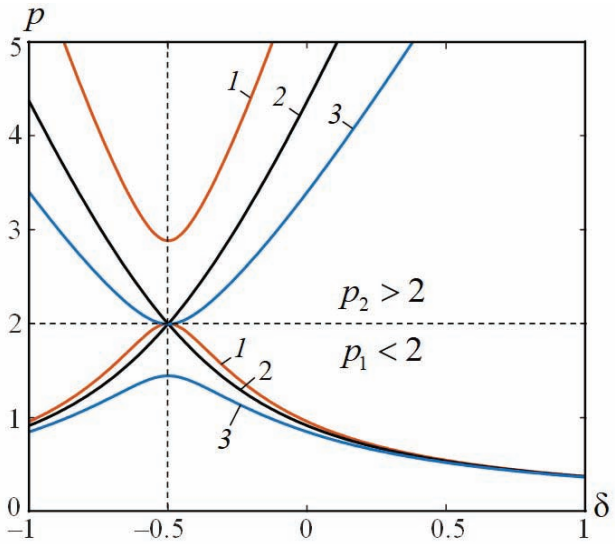


Figure 3. Dependencies $p_{1,2}(\delta)$ for different parameter values $\rho = 0.2,\ 0.289,\ 0.4$ (curves 1, 2, 3, respectively)

The symmetry of the curves relative to the vertical $\delta = -1/2$ shows that from the point of view of controlling the natural frequencies by choosing the geometry of the damper, the schemes at $|\delta| > 1/2$ are irrational. For designing a low-frequency damper for damping vibration, for example, in the band ≈ 5 Hz and below, a scheme in which both frequencies lie in a narrow low-frequency region may be rational. The proximity of the frequencies is achieved by purely geometric means: negative eccentricity and mass distribution, and the "smallness" of the frequencies is achieved by choosing the parameters that determine the scale frequency $\omega_0 = \sqrt{3D/mL^3}$.

From the point of view of practical properties of the damper, designs with multiple frequencies should be considered irrational for the following reasons. Firstly, instead of two frequencies at which the damping effect is manifested, there remains one, which narrows the operating frequency range of the device. Secondly, transverse and torsional vibrations are realized independently, i.e. there is no connection between them, which leads to a decrease in the damping efficiency. In this regard, it is possible not to consider variants with a strong negative eccentricity, when $\delta < -1/2$. The proximity of $\delta \approx -1/2$ is also inappropriate, since in this case the amplitude distribution coefficients (shape factor) and phase relationships of translational and torsional vibrations of loads, determined from the first equation (10) at $\psi = 0$, reveal a strong dependence on the geometric parameters δ and ρ:

$$\gamma_{1,2} = \frac{\Phi_{1,2}}{f_{1,2}} = \frac{4 - p_{1,2}^2(\delta,\rho)}{2 + \delta \cdot p_{1,2}^2(\delta,\rho)}. \qquad (17)$$

Note the difference between relations (14) and (17). The first relates to forced oscillations and is a function of the excitation frequency; the second relates to free oscillations at natural frequencies. Of course, at natural frequencies in the absence of damping they coincide: $\gamma_{1,2} = \beta_{1,2}$.

The signs of the quantities $\gamma_{1,2}$ determine the relationship of the oscillation phases. With a positive eccentricity $(\delta > 0)$, the denominator is positive and the sign of the coefficients $\gamma_{1,2}$ depends only on the frequency. As follows

from the graphs in figure 3 $p_1 < 2$, $p_2 > 2$. Therefore, at the first natural frequency, the generalized coordinates change in phase, and at the second, they are in antiphase, regardless of the parameters δ, ρ and, therefore, the geometry of the weights. However, with a negative eccentricity $(\delta < 0)$, the signs and values of the shape factors depend in a complex way on the relationship of the geometric parameters δ, ρ, as evidenced by the curves in figure 4. In practical terms, such a strong dependence can manifest itself in instability of the oscillation modes.

Taking into account the above, nomograms of the natural frequencies of the damper arm in the current ranges of change of the eccentricity (ρ) and the radius of gyration of the load (δ) are calculated (figure 5). The given dependencies can be used for rational "tuning" of the damper to the required frequency range.

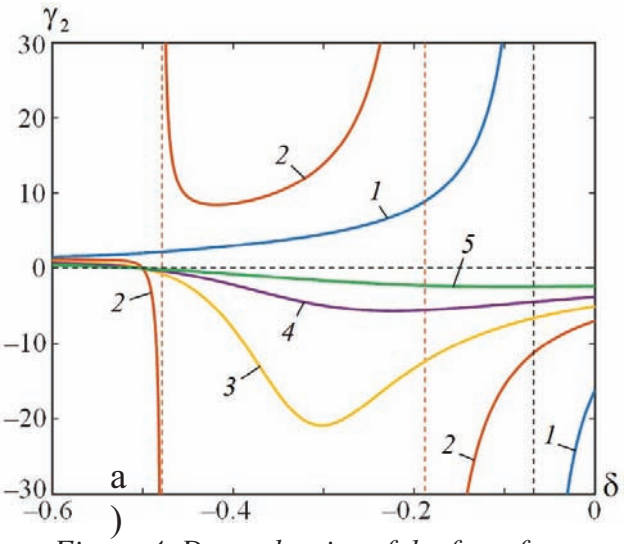


Figure 4. Dependencies of the form factor $\gamma_2(\delta)$ *for different values of the parameter* $\rho = 0.2, 0.3, 0.35, 0.4, 0.5$ *(curves 1–5)*

With small damping, the natural frequencies practically coincide with the resonant frequencies of the real system. However, in the case of a damper, the function of which is to dampen oscillations, it is advisable to make the attenuation sufficiently large, which can lead to a divergence of the natural and resonant frequencies.

The latter are revealed in the amplitude-frequency characteristics, determined experimentally during tests on a vibration stand or theoretically from the solution of non-homogeneous equations. Since the conditions for excitation of forced oscillations can be different, the AFC also differ. Of practical importance are the conditions of the stand and the conditions of the flight, that is, excitation from the side of the wire on which the damper is installed.

Let us consider a variant of an equal-shoulder damper under stand conditions, returning to equations (10) and their solution (11). In accordance with formulas (12), expressions for modules of functions $\left|f(p)\right|$, $\left|\Phi(p)\right|$ have the form:

$$\left|f(p)\right| = p\sqrt{\frac{f_R^2 + f_I^2}{\Delta_R^2 + \Delta_I^2}}, \qquad \left|\Phi(p)\right| = p\frac{2(1+2\delta)}{\sqrt{\Delta_R^2 + \Delta_I^2}}. \tag{18}$$

Formulas (18) represent the AFC of the damper under stand conditions. They are graphically shown in figure 6 a) and b). The calculations were performed using the values of the parameters: $\eta = 0.1...0.5$, $\rho = 0.4$, $\delta = 0.15$.

The graphs of the functions $\left|f(p)\right|$, $\left|\Phi(p)\right|$ show that in this case damping plays a significant role only at resonances; at intermediate frequencies, the calculation results with and without internal friction are almost identical. The resonant frequencies of the damped and conservative systems (the latter are equal in this case $p_1 = 0.72$, $p_2 = 4.02$) also practically coincide.

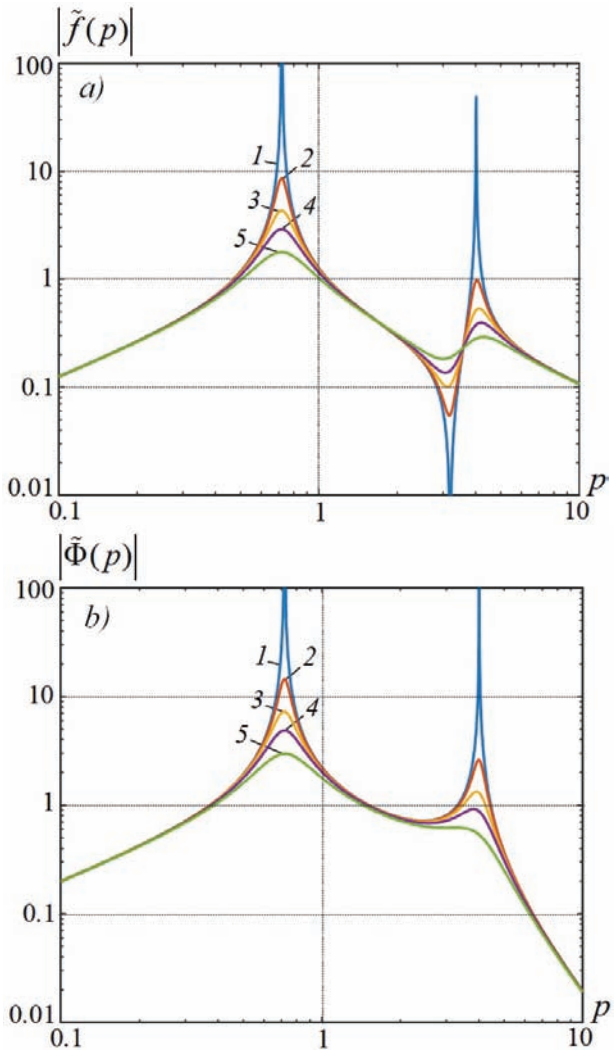


Figure 6. AFC of the damper at different values of the damping coefficient (curves 1–5)

Note that, as follows from (11), at $p \approx \sqrt{4/3+2\delta}/\rho$, the amplitude of vertical vibrations of the load drops sharply (in the absence of friction, it turns to zero). This is a manifestation of the Den Hartog effect [37], when, during forced oscillations of a system with two degrees of freedom at a certain frequency, one of the generalized coordinates "freezes", which is used to dampen vibrations. This effect is clearly manifested in the absence of friction (the first curve in figure 6 a), however, in relation to the damper, it is rather a negative factor. Note also that the dimensionless AFC $|\tilde{f}(p)|$, $|\tilde{\Phi}(p)|$ do not depend on the frequency scanning mode, which appears only when returning to the dimensional values according to (11).

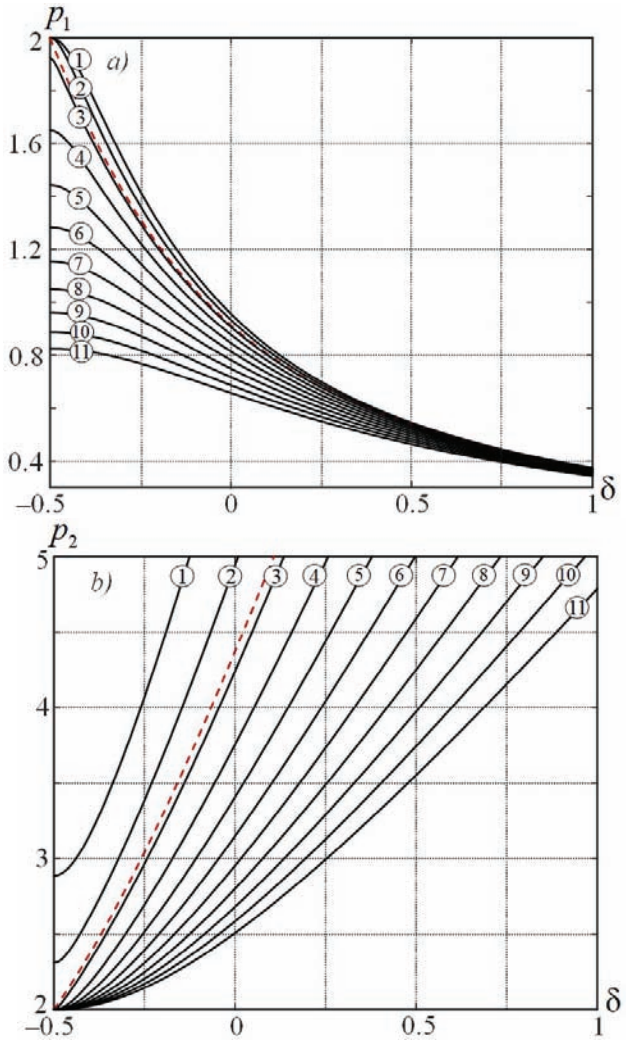


Figure 5. Dependences of the dimensionless natural frequencies of the damper arm $p_{1,2}(\delta)$ at $\rho = 0.2 - 1.2$ (curves 1–11 in increments 0.1); the dotted line shows the dependences at the "boundary" value $\rho = 0.289$

Next, we consider the frequency dependence of dissipation on the frequency of forced oscillations. The power dissipation of mechanical energy due to internal friction in each arm of the damper, as follows from (3), is equal to the imaginary part of the amplitude value of the potential energy divided by a quarter of the oscillation period:

$$W = \frac{12D\omega}{\pi L}\left| f^2 - f\Phi + \frac{1}{3}\Phi^2 \right| \sin\psi \,.$$

Considering (11) and the relation (14) between the amplitudes of translational and rotational oscillations, we find:

$$W = mV^2\omega_0\Theta\left(\delta,\rho,\psi,p\right),$$

where

$$\Theta\left(\delta,\rho,\psi,p\right) = \frac{4}{\pi}p\left|f^2\right|\left|1-\beta+\frac{1}{3}\beta^2\right|\sin\psi \quad (19)$$

is a dimensionless function of only the dimensionless geometric parameters of the damper, the damping coefficient in the form (2) and the frequency. Using (12)-(15), it is not difficult to obtain expressions for modules:

$$\left|f^2\right| = p^2\frac{f_{\mathrm{R}}^2 + f_{\mathrm{I}}^2}{\Delta_{\mathrm{R}}^2 + \Delta_{\mathrm{I}}^2},$$

$$\left|1-\beta+\frac{1}{3}\beta^2\right| = \frac{1}{f_{\mathrm{R}}^2 + f_{\mathrm{I}}^2}\sqrt{\Theta_{\mathrm{R}}^2 + \Theta_{\mathrm{I}}^2},$$

where

$$\Theta_{\mathrm{R}} = f_{\mathrm{R}}^2 + f_{\mathrm{I}}^2 -$$

$$-2(1+2\delta)\left[\beta_{\mathrm{R}} - \frac{2}{3}\frac{1+2\delta}{f_{\mathrm{R}}^2 + f_{\mathrm{I}}^2}\left(\beta_{\mathrm{R}}^2 - \beta_{\mathrm{I}}^2\right)\right],$$

$$\Theta_{\mathrm{I}} = -2(1+2\delta)\beta_{\mathrm{I}}\left[1 - \frac{4}{3}\frac{1+2\delta}{f_{\mathrm{R}}^2 + f_{\mathrm{I}}^2}\beta_{\mathrm{R}}\right].$$

Then, instead of (19), we will have the formula:

$$\Theta\left(\delta,\rho,\psi,p\right) = \\ = \frac{4}{\pi}\frac{p^3}{\Delta_{\mathrm{R}}^2 + \Delta_{\mathrm{I}}^2}\sqrt{\Theta_{\mathrm{R}}^2 + \Theta_{\mathrm{I}}^2}\sin\psi\,. \quad (20)$$

Figure 7 shows the dependences of the dimensionless dissipation power (20) on the frequency p at values $\eta = 0.1,\ 0.5$.

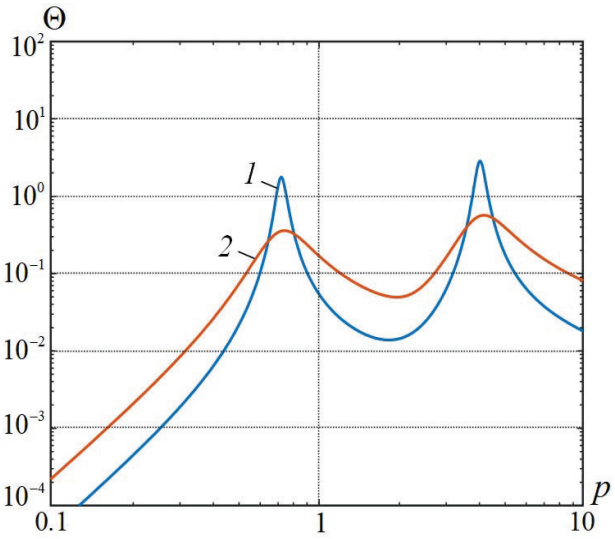


Figure 7. Dependence of the dimensionless dissipation power on the frequency at values $\eta = 0.1,\ 0.5$ *(curves 1, 2);* $\rho = 0.4,\ \delta = 0.15$

Note that as the damping coefficient increases, the dissipation power at the resonances decreases, while away from the resonances, on the contrary, it increases. At first glance, this strange phenomenon is explained by the fact that as η increases, the resonant amplitude of oscillations a decreases For example, for a single-degree oscillator with internal friction, excited by a vibration stand with a table amplitude A, it is inversely proportional to η: $a \sim A/\eta$. At the same time, the power of dissipation $w \sim a^2\eta$. It follows that $w \sim A^2/\eta$. A similar result holds for an oscillator with viscous Rayleigh friction. In the practice of designing and testing dampers, it is known that the dissipation power is reduced by artificially increasing damping by increasing interwire friction, which led to the "locking" of the cable console.

In a system with two degrees of freedom, the situation is different. Figure 8 shows the dependences of the dissipation power at the damper resonances on the damping coefficient (solid curves).

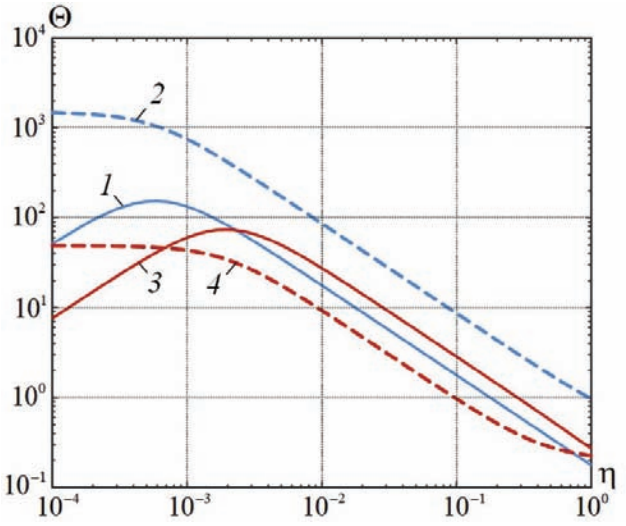


Figure 8. The influence of the damping coefficient on the dimensionless dissipation power (solid curves 1, 3) and the amplitude of vertical oscillations (dashed curves 2, 4) in resonant modes at $p_r = 0.719$ *(curves 1, 2) and* $p_r = 4.02$ *(curves 3, 4);* $\rho = 0.4,\ \delta = 0.15$

Similar dependences for the amplitudes of vertical oscillations are also shown here. As can be seen, for each resonance frequency there is a value at which the dissipation reaches a maximum. However, these maxima are achieved at the cost of too large amplitudes, which are unacceptable in practice for reasons of strength.

Note that the damping coefficient in this case is considered constant, whereas it can depend on the amplitude of oscillations, especially in cable-type consoles, in which the interwire friction obviously depends on the manufacturing technology. It follows that the choice of the design parameters of the damper should be based on an experimental study of its damping characteristics. The same applies to the amplitude dependence of the bending stiffness.

3. DYNAMIC STIFFNESS MATRIX OF THE DAMPER

When combining a conductor in the overhead line span with a vibration damper, it is convenient to characterize the latter with a dynamic stiffness matrix calculated at the attachment point to the clamp. Dynamic stiffness has the same meaning as static stiffness, but differs from it in that it does not relate force to displacement, but rather their amplitudes during forced vibrations, and thus depends on frequency [38].

We will proceed from equations (6), taking into account the internal damping, which now plays a significant role. We will represent the vector of amplitudes of the generalized forces acting on the clamp from the wire side in accordance with formulas (7) in the form: $\boldsymbol{Q} = \boldsymbol{Q}^0 e^{i\omega t}$. We will use a similar form for the desired solution: $\boldsymbol{q} = \boldsymbol{q}^0 e^{i\omega t}$, where $\boldsymbol{q}^0$ is the complex amplitude of the oscillations.

Let us introduce the following notation by analogy with (1.4): $\boldsymbol{Q}_0^0 = (F_C\ M_C)^T$, $\boldsymbol{0} = (0\ \ 0)^T$, $\boldsymbol{q}_i^0 = (Y_i^0\ \ \Phi_i^0)^T$, which allow us to rewrite the system (6) in expanded form:

$$
\begin{aligned}
&-\omega^2\left(\boldsymbol{M}_{11}\boldsymbol{q}_0^0 + \boldsymbol{M}_{12}\boldsymbol{q}_1^0 + \boldsymbol{M}_{13}\boldsymbol{q}_2^0\right) = \boldsymbol{Q}_0^0,\\
&-\omega^2\boldsymbol{M}_{12}^T\boldsymbol{q}_0^0 + \left(\boldsymbol{G}_1 - \omega^2\boldsymbol{M}_{22}\right)\boldsymbol{q}_1^0 = \boldsymbol{0},\\
&-\omega^2\boldsymbol{M}_{13}^T\boldsymbol{q}_0^0 + \left(\boldsymbol{G}_2 - \omega^2\boldsymbol{M}_{33}\right)\boldsymbol{q}_2^0 = \boldsymbol{0}.
\end{aligned}
$$

From the last two equations we express the vectors $\boldsymbol{q}_{1,2}^0$ through the vector $\boldsymbol{q}_0^0$:

$$
\begin{aligned}
\boldsymbol{q}_1^0 &= \omega^2\left(\boldsymbol{G}_1 - \omega^2\boldsymbol{M}_{22}\right)^{-1}\boldsymbol{M}_{12}^T\boldsymbol{q}_0^0,\\
\boldsymbol{q}_2^0 &= \omega^2\left(\boldsymbol{G}_2 - \omega^2\boldsymbol{M}_{33}\right)^{-1}\boldsymbol{M}_{13}^T\boldsymbol{q}_0^0.
\end{aligned}
$$

Then from the first equation we have: $\boldsymbol{C}^*\boldsymbol{q}_0^0 = \boldsymbol{Q}_0^0$, where

$$
\begin{aligned}
\boldsymbol{C}^* = -\omega^2\Big\{\boldsymbol{M}_{11} + \omega^2\Big[&\boldsymbol{M}_{12}\left(\boldsymbol{G}_1 - \omega^2\boldsymbol{M}_{22}\right)^{-1}\boldsymbol{M}_{12}^T +\\
&+ \boldsymbol{M}_{13}\left(\boldsymbol{G}_2 - \omega^2\boldsymbol{M}_{33}\right)^{-1}\boldsymbol{M}_{13}^T\Big]\Big\}
\end{aligned}
$$

is the desired matrix of the dynamic stiffness of the damper. Note that the elements of the matrix

are complex quantities. Therefore, for example, the modulus of the displacement determined using the rigidity matrix determines its amplitude, and the argument is the phase shift of the displacement relative to the harmonic force causing it.

The obtained stiffness matrix allows to easily include the damper in the dynamic model of the span, since it can be considered as a set of concentrated "springs" characterized by dynamic stiffnesses and connected to the conductor.

CONCLUSION

The developed dynamic model covers the main properties of Stockbridge vibration dampers, widely used to reduce the amplitudes of aeolian vibration of overhead power transmission line conductors. The model and the results obtained on its basis can be used for design calculations of damper natural frequencies. The obtained dynamic stiffness can be used to include the damper in the dynamic span model, which is necessary to assess the effectiveness of the damper and determine the best position of the damper in the span.

Taking into account the nonlinearity of the elastic characteristics of the console is the subject of further development of this model.

ACKNOWLEDGEMENT

This study was carried out in accordance with the state assignment of the Institute of Applied Mechanics of the Russian Academy of Sciences.

REFERENCES

1. EPRI: Transmission Line Reference Book. Wind-Induced Conductor Motion. Electric Power Research Institute, Palo Alto, California, 1979.
2. Guidelines for standard protection against vibration and sub-vibrations of wires and lightning cables of overhead power transmission lines with a voltage of 35-750 kV. RD 34.20.182-90. Service of Excellence, ORGRES, Moscow, 1991, 70 p. (in Russian).
3. **Stockbridge G.H.** 1928. Vibration damper, U.S. Patent No. 1.675.391.
4. SALVI Research Department Paper 2. Dampers efficiency evaluation. 1968, Milan: Salvi Sp. A.
5. SALVI Research Department Paper 3. SALVI 4D damper. 1968, Milan: Salvi Sp. A.
6. **Chan J.** EPRI transmission line reference book: Wind induced-induced conductor motion. Palo Alto, California: Electric Power Research Institute, 2006.
7. **Havard D.** Assessment of the Cowal JCT x Longwood TS for vibration control. Toronto, Ontario, 2008.
8. **Claren R., Diana G.** Mathematical analysis of transmission line vibration // IEEE Transactions on Power Apparatus and Systems. 1969, PAS-88(12), pp. 1741-1771.
9. **Wagner H., Ramamurti V., Sastry R.V.R., Hartman K.** Dynamics of Stockbridge dampers // Journal of Sound and Vibration, 1973, Vol. 30(2), pp. 207-220.
10. **Allnut J.G., Rowbottom M.D.** Damping of Aeolian vibration on overhead lines by vibration dampers // Proceedings of the Institute of Electrical and Electronic Engineers, 1974, Vol. 121, pp. 1175-1178.
11. **Dhotarad M.S., Ganesan N., Rao B.V.A.** Transmission line vibration // Journal of Sound and Vibration, 1978, Vol. 60, pp. 217-227.
12. **Dhotarad M.S., Ganesan N., Rao B.V.A.** Transmission line vibration with 4R dampers // Journal of Sound and Vibration, 1978, Vol. 60, pp. 604-608.
13. **Hagedorn P**. Ein einfaches Rechenmodell zur Berechnung winderregter Schwingungen an Hochspannugsleitungen mit Dämpfern // Ingenieur Archiv, 1980, Vol. 49, ss. 161-177.

14. **Hagedorn P.** On the optimal design of Stockbridge dampers // Proceedings of CIGRE Symposium, Stockholm, 1981, S 22-81, paper 112-10.
15. **Schäfer B.** The energy method and the exact solution for conductor oscillations, a comparison // Proceedings of CIGRE Symposium, Stockholm, 1981, S 22-81, paper 112-11.
16. **Markiewicz M.** Optimum dynamic characteristics of Stockbridge dampers for dead-end spans // Journal of Sound and Vibration, 1995, Vol. 188(2), pp. 243-256.
17. **Sauter D., Hagedorn P.** On the hysteresis of wire cables in Stockbridge dampers // International Journal of Non-linear Mechanics, 2002, Vol. 37, pp. 1435-1459.
18. **Lu M.L., Chan J.K.** An efficient algorithm for Aeolian vibration of single conductor with multiple dampers // IEEE Transactions on Power Delivery, 2007, Vol. 22(3), pp. 1822-1829.
19. **Barbieri N., Barbieri R.** Dynamic analysis of Stockbridge damper // Advances in Acoustics and Vibration, 2012, Article ID 659398, 8 p.
20. **Li L., Cao H., Jiang Y., Chen Y.,** Experimental study on mitigation devices of Aeolian vibration of bundled conductors // Journal of Vibration and Control, 2013, Vol. 22, pp. 1217-1227.
21. **Langlois S., Legeron F.** Prediction of Aeolian vibration of transmission line conductors using a nonlinear time history model – Part I: Damper model // IEEE Transactions of Power Delivery, 2014, Vol. 29, Iss. 3, pp. 1168-1175.
22. **Langlois S., Legeron F.** Prediction of Aeolian vibration of transmission line conductors using a nonlinear time history model – Part II: Conductor and damper model // IEEE Transactions of Power Delivery, 2014, Vol. 29, Iss. 3, pp. 1176-1183.
23. **Barry O., Zu J.W., Oguamanam D.C.D.** Nonlinear dynamics of Stockbridge dampers // Journal of Dynamic Systems. Measurement and Control, 2015, Vol. 137, pp. 1-7.
24. **Barbieri N., Barbieri R., Silva R.A., Mannala M.J., Barbieri L.S.** Nonlinear dynamic analysis of wire-rope isolator and Stockbridge damper // Nonlinear Dynamics, 2016, Vol. 86, pp. 501-512.
25. **Havard D.** Interaction of vibration dampers with surge arresters CIGRÉ B2 TF 007. Convenor CIGRE Science & Engineering, 2016, Vol. 6, pp. 32-45.
26. **Vaja N., Barry O., Tanbour E.** On the modeling and analysis of a vibration absorber for overhead powerlines with multiple resonant frequencies // Engineering Structures, 2018, Vol. 175, pp. 711-720.
27. **Foti F., Martinelli L.** Hysteretic behavior of Stockbridge dampers: modelling and parameter identification // Mathematical Problems in Engineering, 2018, Vol. 2018, Article ID 8925121, 17 p.
28. **Luo X., Wang L., Zhang Y.** Nonlinear numerical model with contact for Stockbridge vibration damper and experimental validation // Journal of Vibration and Control, 2016, Vol. 22(5), pp. 1217-1227.
29. **Luo X.Y., Zhang Y.S., Zheng Y.P.** Nonlinear revision of the linear model for Stockbridge vibration damper and experiment validation // Applied Mechanics and Materials, 2013, Vol. 328, pp. 504-508.
30. **Panovko Ya.G.** Internal friction during vibrations of elastic systems. Moscow, Fizmatgiz, 1960, 193 p. (in Russian).
31. **Sorokin E.S.** On the theory of internal friction during vibrations of elastic systems. Moscow, Gosstroizdat, 1960, 131 p. (in Russian).
32. **Papailiou K.O.** On the bending stiffness of transmission line conductors // IEEE Transactions on Power Delivery, 1997, Vol. 12(4), pp. 1576-1588.
33. Recommendations for the use of multi-frequency vibration dampers of GWP and unified vibration dampers of GWP on overhead transmission lines with a voltage of 35-750 kV. FROM 34.20.264-2005. Mos-

cow: Center for industrial and technical information of energy enterprises and technical training ORGRES. 2008. 20 p. (in Russian).
34. **Filippov A.P.** Vibrations of elastic systems. Kiev, Ed. Academy of Sciences of the Ukrainian SSR, 1956, 322 p. (in Russian).
35. **Loitsyansky L.G., Lurie A.I.** Course of theoretical mechanics. Vol. II, Moscow, Nauka, 1983, 640 p. (in Russian).
36. GOST R 51155-2017. Linear fittings. Acceptance rules and test methods, Moscow, Standartinform, 2017, 42 p. (in Russian).
37. **Den Hartog J.P.** Mechanical vibrations. Dover Publications, Inc., N.Y., 1985, 449 p.
38. **Panovko Ya.G., Gubanova I.I.** Stability and oscillations of elastic systems. Moscow, Nauka, 1964, 336 p. (in Russian).

СПИСОК ЛИТЕРАТУРЫ

1. EPRI: Transmission Line Reference Book. Wind-Induced Conductor Motion. Electric Power Research Institute, Palo Alto, California, 1979.
2. Методические указания по типовой защите от вибрации и субколебаний проводов и грозотросов воздушных линий электропередачи напряжением 35-750 кВ. РД 34.20.182-90. Служба передового опыта, ОРГРЭС: М., 1991, 70 с.
3. **Stockbridge G.H.** 1928. Vibration damper, U.S. Patent No. 1.675.391.
4. SALVI Research Department Paper 2. Dampers efficiency evaluation. 1968, Milan: Salvi Sp. A.
5. SALVI Research Department Paper 3. SALVI 4D damper. 1968, Milan: Salvi Sp. A.
6. **Chan J.** EPRI transmission line reference book: Wind induced-induced conductor motion. Palo Alto, California: Electric Power Research Institute, 2006.
7. **Havard D.** Assessment of the Cowal JCT x Longwood TS for vibration control. Toronto, Ontario, 2008.
8. **Claren R., Diana G.** Mathematical analysis of transmission line vibration // IEEE Transactions on Power Apparatus and Systems. 1969, PAS-88(12), pp. 1741-1771.
9. **Wagner H., Ramamurti V., Sastry R.V.R., Hartman K.** Dynamics of Stockbridge dampers // Journal of Sound and Vibration, 1973, Vol. 30(2), pp. 207-220.
10. **Allnut J.G., Rowbottom M.D.** Damping of Aeolian vibration on overhead lines by vibration dampers // Proceedings of the Institute of Electrical and Electronic Engineers, 1974, Vol. 121, pp. 1175-1178.
11. **Dhotarad M.S., Ganesan N., Rao B.V.A.** Transmission line vibration // Journal of Sound and Vibration, 1978, Vol. 60, pp. 217-227.
12. **Dhotarad M.S., Ganesan N., Rao B.V.A.** Transmission line vibration with 4R dampers // Journal of Sound and Vibration, 1978, Vol. 60, pp. 604-608.
13. **Hagedorn P**. Ein einfaches Rechenmodell zur Berechnung winderregter Schwingungen an Hochspannugsleitungen mit Dämpfern // Ingenieur Archiv, 1980, Vol. 49, ss. 161-177.
14. **Hagedorn P.** On the optimal design of Stockbridge dampers // Proceedings of CIGRE Symposium, Stockholm, 1981, S 22-81, paper 112-10.
15. **Schäfer B.** The energy method and the exact solution for conductor oscillations, a comparison // Proceedings of CIGRE Symposium, Stockholm, 1981, S 22-81, paper 112-11.
16. **Markiewicz M.** Optimum dynamic characteristics of Stockbridge dampers for dead-end spans // Journal of Sound and Vibration, 1995, Vol. 188(2), pp. 243-256.
17. **Sauter D., Hagedorn P.** On the hysteresis of wire cables in Stockbridge dampers // International Journal of Non-linear Mechanics, 2002, Vol. 37, pp. 1435-1459.
18. **Lu M.L., Chan J.K.** An efficient algorithm for Aeolian vibration of single conductor with multiple dampers // IEEE Transactions

on Power Delivery, 2007, Vol. 22(3), pp. 1822-1829.
19. **Barbieri N., Barbieri R.** Dynamic analysis of Stockbridge damper // Advances in Acoustics and Vibration, 2012, Article ID 659398, 8 p.
20. **Li L., Cao H., Jiang Y., Chen Y.,** Experimental study on mitigation devices of Aeolian vibration of bundled conductors // Journal of Vibration and Control, 2013, Vol. 22, pp. 1217-1227.
21. **Langlois S., Legeron F.** Prediction of Aeolian vibration of transmission line conductors using a nonlinear time history model – Part I: Damper model // IEEE Transactions of Power Delivery, 2014, Vol. 29, Iss. 3, pp. 1168-1175.
22. **Langlois S., Legeron F.** Prediction of Aeolian vibration of transmission line conductors using a nonlinear time history model – Part II: Conductor and damper model // IEEE Transactions of Power Delivery, 2014, Vol. 29, Iss. 3, pp. 1176-1183.
23. **Barry O., Zu J.W., Oguamanam D.C.D.** Nonlinear dynamics of Stockbridge dampers // Journal of Dynamic Systems. Measurement and Control, 2015, Vol. 137, pp. 1-7.
24. **Barbieri N., Barbieri R., Silva R.A., Mannala M.J., Barbieri L.S.** Nonlinear dynamic analysis of wire-rope isolator and Stockbridge damper // Nonlinear Dynamics, 2016, Vol. 86, pp. 501-512.
25. **Havard D.** Interaction of vibration dampers with surge arresters CIGRÉ B2 TF 007. Convenor CIGRE Science & Engineering, 2016, Vol. 6, pp. 32-45.
26. **Vaja N., Barry O., Tanbour E.** On the modeling and analysis of a vibration absorber for overhead powerlines with multiple resonant frequencies // Engineering Structures, 2018, Vol. 175, pp. 711-720.
27. **Foti F., Martinelli L.** Hysteretic behavior of Stockbridge dampers: modelling and parameter identification // Mathematical Problems in Engineering, 2018, Vol. 2018, Article ID 8925121, 17 p.
28. **Luo X., Wang L., Zhang Y.** Nonlinear numerical model with contact for Stockbridge vibration damper and experimental validation // Journal of Vibration and Control, 2016, Vol. 22(5), pp. 1217-1227.
29. **Luo X.Y., Zhang Y.S., Zheng Y.P.** Nonlinear revision of the linear model for Stockbridge vibration damper and experiment validation // Applied Mechanics and Materials, 2013, Vol. 328, pp. 504-508.
30. **Пановко Я.Г.** Внутреннее трение при колебаниях упругих систем. М.: Физматгиз. 1960. 193 с.
31. **Сорокин Е.С.** К теории внутреннего трения при колебаниях упругих систем. М.: Госстройиздат. 1960. 131 с.
32. **Papailiou K.O.** On the bending stiffness of transmission line conductors // IEEE Transactions on Power Delivery, 1997, Vol. 12(4), pp. 1576-1588.
33. Рекомендации по применению многочастотных гасителей вибрации ГВП и унифицированных гасителей вибрации ГВУ на воздушных линиях электропередачи напряжением 35-750 кВ. СО 34.20.264-2005. М.: Центр производственно-технической информации энергопредприятий и технического обучения ОРГРЭС. 2008. 20 с.
34. **Филиппов А.П.** Колебания упругих систем. Киев: Изд. АН УССР, 1956. 322 с.
35. **Лойцянский Л.Г., Лурье А.И.** Курс теоретической механики. Т. II. М.: Наука. 1983. 640 с.
36. ГОСТ Р 51155-2017. Арматура линейная. Правила приемки и методы испытаний. М., Стандартинформ, 2017. 42 с.
37. **Ден-Гартог Д.П.** Механические колебания. М., Физматгиз, 1960, 580 с.
38. **Пановко Я.Г., Губанова И.И.** Устойчивость и колебаний упругих систем. М., Наука, 1964, 336 с.

Alexander Nikolaevich Danilin, Doctor of Physical and Mathematical Sciences, Chief Researcher, Institute of Applied Mechanics of the Russian Academy of Sciences (IAM RAS); Department of Mechanics of Adaptive Composite Materials and Systems; 7, building 1, Leningradsky Prospekt, Moscow, 125040, Russia; andanilin@yandex.ru;

Andrey Petrovich Zakharov, postgraduate student, IAM RAS; Department of Mechanics of Adaptive Composite Materials and Systems; 7, building 1, Leningradsky Prospekt, Moscow, 125040, Russia; andreyzakharoff@yandex.ru

Alexander Evgenievich Fedorov, postgraduate student, IAM RAS; Department of Mechanics of Adaptive Composite Materials and Systems; 7, building 1, Leningradsky Prospekt, Moscow, 125040, Russia; iam@iam.ras.ru

Valery Adolfovich Feldstein, Doctor of Technical Sciences, Leading Researcher, IAM RAS; Department of Mechanics of Adaptive Composite Materials and Systems; 7, building 1, Leningradsky Prospekt, Moscow, 125040, Russia; dinpro@mail.ru

Александр Николаевич Данилин, доктор физико-математических наук, главный научный сотрудник ФГБУН Института прикладной механики Российской академии наук (ИПРИМ РАН); Отдел механики адаптивных композиционных материалов и систем; д.7, стр.1, Ленинградский просп., Москва, 125040, Россия; andanilin@yandex.ru;

Андрей Петрович Захаров, аспирант ИПРИМ РАН; Отдел механики адаптивных композиционных материалов и систем; д.7, стр.1, Ленинградский просп., Москва, 125040, Россия; andreyzakharoff@yandex.ru

Александр Евгеньевич Фёдоров, аспирант ИПРИМ РАН; Отдел механики адаптивных композиционных материалов и систем; д.7, стр.1, Ленинградский просп., Москва, 125040, Россия; iam@iam.ras.ru

Валерий Адольфович Фельдштейн, доктор технических наук, ведущий научный сотрудник ИПРИМ РАН; Отдел механики адаптивных композиционных материалов и систем; д.7, стр.1, Ленинградский просп., Москва, 125040, Россия; dinpro@mail.ru

DOI:10.22337/2587-9618-2025-21-4-73-82

AN EXPERIMENTAL INVESTIGATION OF THE THERMOMECHANICAL PERFORMANCE OF WOOD STRUCTURES ASSEMBLED WITH DENSIFIED WOODEN DOWELS UNDER FIRE EXPOSURE

T.T. Tran [1], M. Khelifa [2], M. Oudjene [3], M. Debal [2], Y. Rogaume [2]

[1] Hanoi Architectural University, Hanoi, VIETNAM
[2] University of Lorraine, Epinal, FRANCE
[3] Department of Civil and Water Engineering, University of Laval, Québec, CANADA

Abstract: This study presents an experimental investigation into the thermomechanical behavior of wood structures assembled with densified wooden dowels under fire exposure. The research focuses on Adhesive-Free Engineered Wood Products (AFEWPs), particularly adhesive-free cross-laminated timber (AFCLT) panels, and timber connections incorporating either thermo-mechanically compressed wooden dowels or conventional steel dowels. A series of thermal and thermomechanical tests were conducted to evaluate internal temperature distribution, charring behavior, and structural displacement at elevated temperatures. The fire performance of dowel-type connections was assessed by comparing the thermal response and deformation of joints using wooden and steel dowels. The results indicate that timber connections incorporating densified wooden dowels exhibited better thermal insulation and lower charring rates compared to those with steel dowels, thereby improving the overall fire resistance of the jointed assemblies. This study highlights the potential of densified wood dowel as a sustainable and fire-resilient alternative to metallic fasteners in engineered wood. structures.

Keywords: Thermomechanical behavior, Densified wooden dowels, Adhesive-Free Engineered Wood Products (AFEWPs), Adhesive-Free Cross-Laminated Timber (AFCLT), Timber connection, Sustainable fasteners, Engineered wood structures

ЭКСПЕРИМЕНТАЛЬНОЕ ИССЛЕДОВАНИЕ ТЕРМОМЕХАНИЧЕСКИХ ХАРАКТЕРИСТИК ДЕРЕВЯННЫХ КОНСТРУКЦИЙ, СОБРАННЫХ С ПОМОЩЬЮ УПЛОТНЕННЫХ ДЕРЕВЯННЫХ НАГЕЛЕЙ, ПРИ ОГНЕВЫХ ВОЗДЕЙСТВИЯХ

Т.Т. Тран [1], М. Хелифа [2], М. Уджене [3], М. Дебал [2], Ю. Рогаум [2]

[1] Ханойский архитектурный университет, г. Ханой, ВЬЕТНАМ
[2] Университет Лотарингии, ЛЕРМАБ, г. Эпинал, ФРАНЦИЯ
[3] Факультет гражданского и водного строительства, Университет Лаваля, г. Квебек, КАНАДА

Аннотация: В данном исследовании представлены результаты экспериментального изучения термомеханического поведения деревянных конструкций, соединенных с помощью уплотненных деревянных нагелей, при огневом воздействии. В исследовании рассматриваются безклеевые соединения деревянных элементов (AFEWP), в частности, панелей из перекрестно-ламинированной древесины (AFCLT) и деревянных соединений, в которых используются термомеханически спрессованные деревянные нагели или обычные стальные нагели. Была проведена серия термических и термомеханических испытаний для оценки внутреннего распределения температуры, поведения при обугливании и деформации конструкции при повышенных температурах. Пожаростойкость соединений с использованием нагелей оценивалась путем сравнения теплового сопротивления и деформации соединений с использованием деревянных и стальных нагелей. Результаты показывают, что деревянные соединения с использованием уплотненных деревянных нагелей демонстрировали лучшую теплоизоляцию и более низкие показатели обугливания по сравнению с соединениями со стальными

нагелями. Это улучшало общую пожаростойкость соединенных конструкций. Данное исследование подчеркивает потенциал уплотненных деревянных нагелей как экологичной и огнестойкой альтернативы металлическим крепежным элементам в конструкциях из древесины.

Ключевые слова: термомеханическое поведение, уплотненные деревянные нагели, деревянные элементы с безклеевым соединением (AFEWP), поперечно-ламинированная древесина без клея (AFCLT), соединение элементов из древесины, экологичные крепежные элементы, конструкции из дерева

INTRODUCTION

The environmental impact of the construction industry is substantial, with buildings accounting for approximately 40% of global energy consumption and up to 33% of greenhouse gas (GHG) emissions worldwide. In response, recent initiatives have promoted the use of renewable and low-carbon materials, particularly engineered wood products (EWPs) such as glued laminated timber (glulam) and cross-laminated timber (CLT). These materials store carbon and are derived from renewable resources, making them attractive for sustainable construction. However, their widespread use is constrained by the reliance on petrochemical-based adhesives, which pose challenges in terms of recyclability, environmental compatibility, and long-term durability.

To address these limitations, the North-West-European Interreg research initiative “Towards Free Adhesive Buildings (AFTB)” has introduced a new class of Adhesive-Free Engineered Wood Products (AFEWPs), which utilize thermo-mechanically densified wood dowels as mechanical connectors in place of traditional adhesives. These dowels exhibit a shape-memory effect—commonly referred to as “strain recovery”—that allows them to swell in pre-drilled holes and form tight, durable joints under varying humidity conditions [1]. This connection concept not only eliminates synthetic adhesives but also supports the development of scalable, fully wooden structural systems aligned with sustainability goals.

While the mechanical performance of densified wood dowel joints has been studied to some extent [2-14], their behavior under elevated temperatures remains underexplored. Given the inherent combustibility of timber, understanding the thermal and thermomechanical response of these adhesive-free connections is essential for assessing their viability in fire-exposed environments. Recent research has begun addressing this gap through both experimental and numerical investigations [15], highlighting the need to evaluate fire-induced thermal degradation, heat transfer, and structural deformation in dowel-connected wood assemblies.

To further this understanding, the present study conducts an experimental program focusing on both adhesive-free cross-laminated timber (AFCLT) panels and dowel-type timber connections. The AFCLT panels were exposed to radiant heat fluxes of 49 and 60 kW/m², with the primary objective of assessing charring depth as an indicator of fire-induced degradation. These panel-scale tests are designed to complement prior cone calorimeter experiments conducted on natural and densified wood [15], providing additional insight into heat penetration and material loss under realistic fire exposure.

In parallel, timber connections assembled with either densified wooden dowels or conventional steel dowels were subjected to the same heat flux levels. For these connections, detailed measurements were performed to capture temperature profiles, char layer evolution, and thermally induced displacements. Instrumentation included embedded thermocouples and displacement sensors to monitor the coupled thermal–mechanical response of each joint configuration, while a 3D laser scanning technique was employed to

quantify the charring profile on exposed surfaces. This two-part experimental approach enables direct comparison between panel-level and connection-level behavior, offering a comprehensive understanding of the influence of connector type on fire performance. Overall, the findings aim to validate the use of densified wood dowels as a viable, fire-resilient, and sustainable alternative to metallic fasteners in engineered wood structures.

EXPERIMENTAL SETUP

Fire testing of CLT panels asembled with densified wooden dowels

Fire resistance tests were conducted on adhesive-free cross-laminated timber (CLT) panels to evaluate the thermal performance of densified wooden dowels used as mechanical connectors. Each CLT specimen consisted of three orthogonally laminated layers, with each layer composed of three oak panels measuring 150 × 450 mm and 25 mm in thickness. The detailed panel dimensions are provided in Figure 1. The layers were connected using densified spruce dowels with a diameter of 16 mm. Both the oak panels and dowels had a uniform moisture content of 10%.

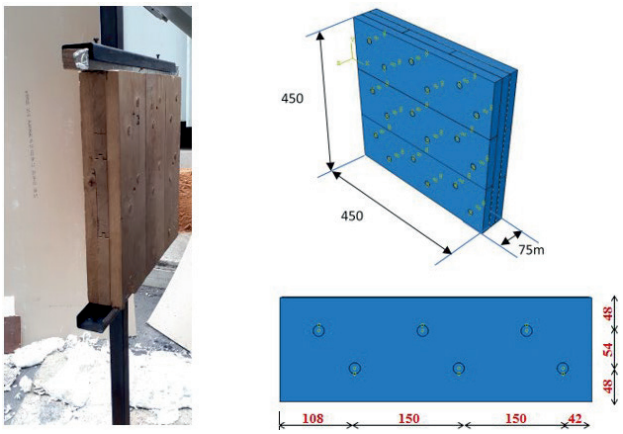


Figure 1. Adhesive-free CLT panel geometry and specimen dimensions

The experimental setup for the fire test of Adhesive-free CLT panels is illustrated in Figure 1. A dedicated test furnace was developed for this purpose, employing four radiant panels as the heat source. Each panel delivered a nominal heat flux of 100 kW/m² and could reach surface temperatures up to approximately 2000 °C. The CLT specimens were horizontally exposed to constant external heat fluxes. Depending on the desired intensity, the distance between the panels and the specimen surface was set at either 20 cm for 60 kW/m² or 30 cm for 49 kW/m². Two replicate tests were conducted for each heat flux level.

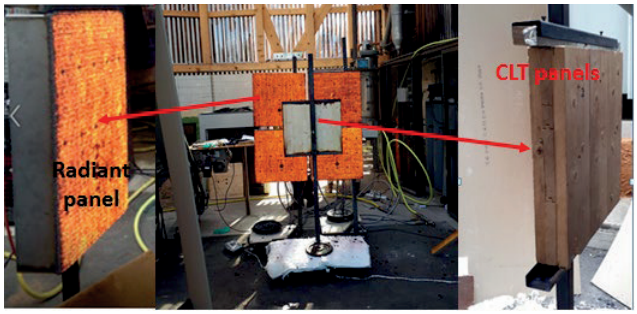


Figure 2. Testing diagram of fire test of Adhesive-free CLT panels

Thermo-mechanical testing of L-shaped connection assembled with densified wood dowels

To evaluate the structural performance of densified wooden dowels, fire tests were conducted on L-shaped timber connections composed of a column and a beam. Each specimen incorporated four dowels with a diameter of 16 mm, joining three-layer laminates with 32 mm thickness per layer. The CLT panels were made from the same material described previously. The experimental results were used to compare the performance of densified dowels with conventional steel dowels. Geometrical details of the connection and the finite element model are provided in Figure 3. Oak wood was used for the laminates in both tests, with an average measured moisture content of 10%. The fire tests were conducted for two types of dowel materials: conventional steel and densified spruce. This comparison enables an evaluation of the effectiveness of using compressed wooden dowels as an alternative to traditional steel connectors.

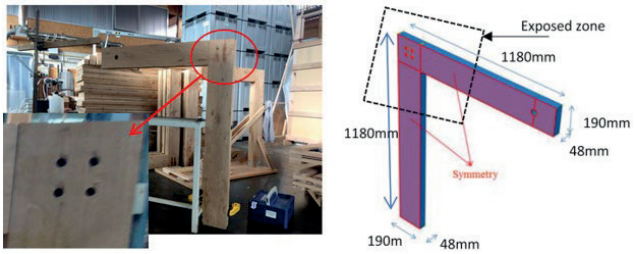


Figure 3. Detailed structure of L-shaped connection

Figure 4 illustrates the fire testing setup for L-shaped timber connections. Radiant panels, each rated at 100 kW/m² and capable of reaching 2000 °C, provided controlled heat exposure. To limit edge effects, gypsum plasterboards were used as thermal shields. Specimens were exposed horizontally to constant heat fluxes of 49 and 60 kW/m², achieved by adjusting the heater distance to 30 cm and 20 cm, respectively. The heating regime was calibrated to match the ISO 834 [16] standard, ensuring consistency with Eurocode 5 [17] assumptions.

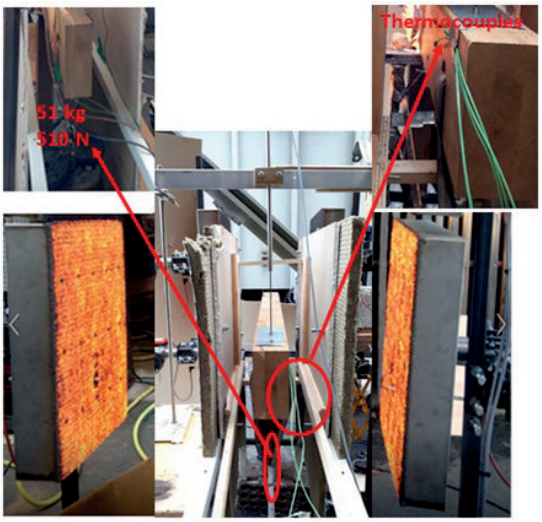


Figure 4. Experimental setup for thermo-mechanical testing of connections

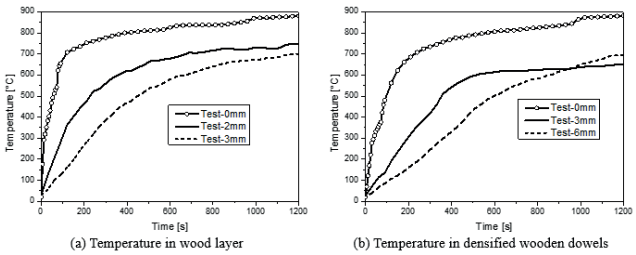
Surface temperatures were monitored using a multispectral infrared camera, while internal temperatures were recorded every second via a USB TC-08 PICO system. Type K thermocouples (1 mm diameter) were embedded at multiple depths in both timber layers and dowels. Deflections were tracked using LVDTs at the free end of each specimen. Two repeated tests were conducted for each dowel type and heat flux condition.

RESULTS AND DISCUSSION

Time–temperature profiles in reinforced L-joints

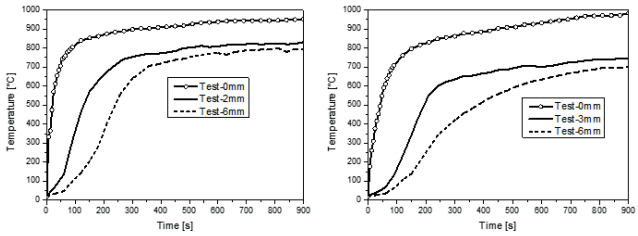
Figures 5–8 present time–temperature profiles recorded in an L-joint specimen reinforced with either densified wooden dowels (Figs. 5 and 6) or steel dowels (Figs. 7 and 8) under radiant heat fluxes of 49 kW/m² and 60 kW/m². Each plot shows temperature traces at the joint surface (0 mm) and at increasing depths (2 mm, 3 mm, up to 6 mm), thereby capturing the thermal response of both the wood layer and the dowel material. By juxtaposing these data, one can directly assess how heat-flux intensity, dowel thermal conductivity, and sensor depth govern the rate of temperature rise, peak temperatures achieved, and overall thermal gradient across the connection. The following discussion elaborates on these interactions and their implications for fire performance.

Under a 60 kW/m² heat flux, the L-joint heats up significantly faster than under 49 kW/m². For example, the surface sensor (Test–0 mm) reaches 400 °C in about 350 s at 60 kW/m², compared to roughly 500 s at 49 kW/m². Likewise, the temperature difference between shallow and deeper sensors grows larger at the higher flux, indicating a steeper thermal gradient through the joint.



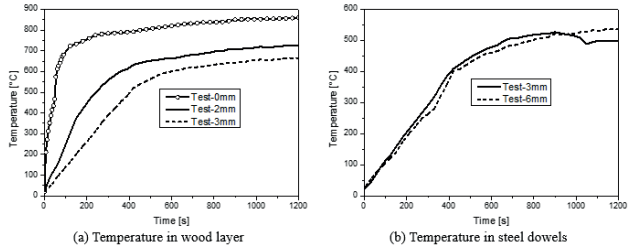
(a) Temperature in wood layer (b) Temperature in densified wooden dowels

Figure 5. Temperature evolution in an L-joint reinforced with densified wooden dowels under a 49 kW/m² heat flux



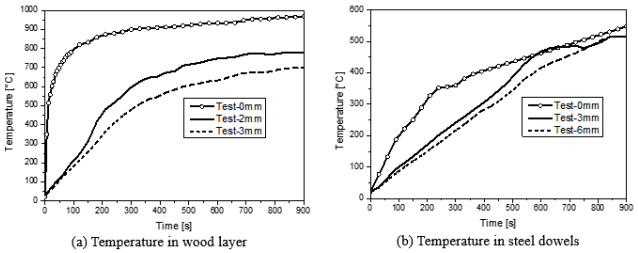
(a) Temperature in wood layer (b) Temperature in densified wooden dowels

Figure 6. Temperature evolution in an L-joint reinforced with densified wooden dowels under a 60 kW/m² heat flux



(a) Temperature in wood layer (b) Temperature in steel dowels

Figure 7. Temperature evolution in an L-joint reinforced with steel dowels under a 49 kW/m² heat flux



(a) Temperature in wood layer (b) Temperature in steel dowels

Figure 8. Temperature evolution in an L-joint reinforced with steel dowels under a 60 kW/m² heat flux

When reinforced with densified wooden dowels, the joint exhibits a much slower heat-up rate than with steel dowels. After 1 200 s at 49 kW/m², the wooden dowel surface remains below 700 °C, whereas with steel dowels it approaches 900 °C in only ~1 000 s. The low thermal conductivity of the wooden dowels provides additional insulation, while the high conductivity of steel creates a pronounced thermal bridge that accelerates heat transfer into the wood substrate.

Sensor depth further highlights these differences. In wooden-dowel joints, Test–2 mm and Test–3 mm lag the surface by 100–150 °C at equivalent times, demonstrating effective heat resistance. In contrast, steel-dowel joints show only a 20–30 s delay between the surface and a 6 mm depth, reflecting rapid conduction through the metal dowel even at greater depths.

Overall, densified wooden dowels markedly extend the time to critical temperatures and improve fire performance of L-joints, making them preferable where fire resistance is paramount. Steel dowels, while mechanically robust, accelerate heat ingress and risk earlier structural compromise. These effects intensify at higher heat fluxes. For fire-sensitive connections, designers should favor wooden dowels or incorporate thermal insulation when steel dowels are unavoidable.

Post-fire residual cross-section measurement

Figure 9 illustrates the laser-scanning arrangement used to capture the post-fire geometry of the CLT panel and L-joint specimens.



Figure 9. Laser-scanning setup for post-fire residual cross-section measurement

After carefully removing the charred surface layer, a high-resolution terrestrial laser scanner was mounted on a fixed tripod at a known distance and orientation relative to each joint. The scanner emitted a dense grid of laser pulses across the exposed cross-section, generating a 3D point cloud with sub-millimetre accuracy in less than two minutes per specimen. Custom software then interpolated these points to reconstruct the true residual timber profile, enabling precise measurement of section loss

and deformation. Compared with conventional caliper or ruler methods, this non-contact approach greatly accelerates data collection, minimizes human error, and delivers a comprehensive, high-fidelity record of the remaining cross-section.

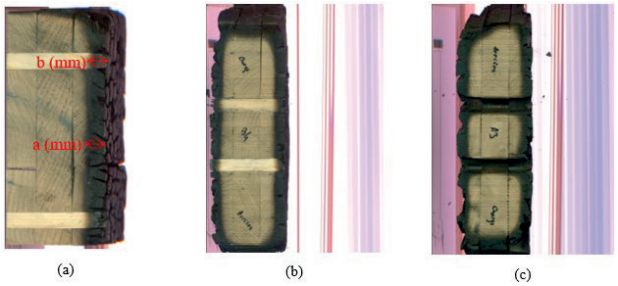


Figure 10. Residual cross-sections after fire exposure: (a) CLT panel; (b) L-joint reinforced with densified wooden dowels; (c) L-joint reinforced with steel dowels

Figure 10 displays the residual char across three specimens: in the unreinforced CLT panel (a), the char layer forms uniformly across the cross-section, indicating surface-controlled heat transfer; similarly, the L-joint reinforced with densified wooden dowels (b) maintains a generally even char depth, with only slight deepening adjacent to each dowel, demonstrating their insulating effect; by contrast, the steel-dowel joint (c) exhibits pronounced, irregular charring along and around each metal connector, evidencing thermal bridging that accelerates interior wood degradation.

Tables 1–3 summarize char depths measured in CLT panels and L-joints reinforced with densified wooden or steel dowels after exposures to 49 kW/m² or 60 kW/m² for 15 min or 20 min.

Table 1. Charring depth in CLT panels after fire exposure

Speciment	Heat flux (kW/m²)	Time (min)	a (mm)	b (mm)
Panel 1	49	15	13	10,5
Panel 2	49	15	15	11
Panel 3	60	15	15	11,5

Table 2. Charring depth in L-joint reinforced with densified wooden dowels after fire exposure

Speciment	Heat flux (kW/m²)	Time (min)	a (mm)	b (mm)
Connection 1	49	20	15	12
Connection 2	49	20	14,5	10
Connection 3	60	15	16	11
Connection 4	60	15	16.5	11

Table 3. Charring depth in L-joint reinforced with steel dowels after fire exposure

Speciment	Heat flux (kW/m²)	Time (min)	a (mm)	b (mm)
Connection 1	49	20	17	-
Connection 3	60	15	17	-
Connection 4	60	15	17	-

Quantitatively, CLT panels exhibited a = 13 mm and b = 10.5 mm at 49 kW/m² for 15 min, and a = 15 mm and b = 11.5 mm at 60 kW/m² for 15 min. In comparison, wooden-dowel L-joints showed slightly greater surface char, a = 14.5 mm (Δ +1.5 mm) and b = 10 mm (Δ –0.5 mm) at 49 kW/m²/15 min, and increased further to a = 15 mm and b = 12 mm at 49 kW/m²/20 min, indicating that longer exposure narrows the a–b gap from 4.5 mm to 3 mm. Under the higher flux of 60 kW/m²/15 min, wooden-dowel joints reached a = 16.5 mm and b = 11 mm, versus a = 16 mm and b = 11 mm at 60 kW/m²/20 min, demonstrating aggressive surface charring but relatively stable dowel charring. Steel-dowel joints, by contrast, consistently reached a = 17 mm under both 49 kW/m²/20 min and 60 kW/m²/15 min, exceeding wooden configurations by approximately 0.5–2.5 mm. These results confirm that densified wooden dowels moderate heat penetration, maintaining 20–30% lower char depths in the dowel zone, while steel dowels create a pronounced thermal bridge that accelerates surface charring. Increased heat flux and longer durations uniformly deepen char layers across all specimens, but the effect is most pronounced with steel dowels.

Deflection at the free end

Progressive perimeter charring under radiant heating steadily erodes the joint's effective cross-section and flexural rigidity, driving a monotonic increase in free-end deflection. A potentiometer mounted on the top plate continuously tracked this displacement while each L-joint carried a constant vertical load of 51 kg. Figures 11 and 12 document the resulting time-dependent deflection histories for specimens exposed to uniform heat fluxes of 49 kW m^{-2} and 60 kW m^{-2}, respectively. By presenting duplicate tests for both densified-wood and steel dowel configurations, the plots provide a clear basis for assessing how connector material alters the onset, rate, and ultimate magnitude of thermally induced deformation.

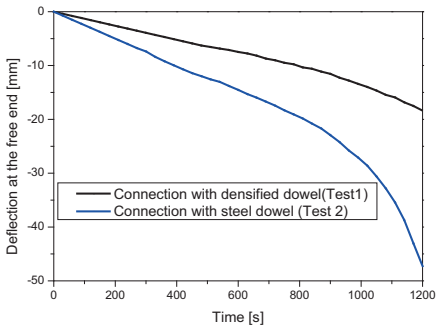


Figure 11. Deflection of the specimen under 49 kW/m² heat flux

Figure 11 records the deflection history of two connections, one assembled with densified-wood dowels and the other with steel dowels, while they are exposed to an external heat flux of 49 kW m-². Both specimens gradually lose stiffness as charring progresses, but the rate differs markedly: the steel-dowel assembly deflects almost –45 mm after 1,200 s, whereas the densified-dowel counterpart reaches only about –25 mm. The near-linear trajectories in this plot suggest a steady decline in bending stiffness, yet the steeper slope of the steel-dowel curve points to earlier thermal weakening or local slip at the steel-to-wood interface.

Figure 12 reveals that elevating the radiant heat flux to 60 kW m^{-2} magnifies the performance gap between connector types: densified-wood dowel joints level off at roughly –20 to –30 mm of free-end deflection after 900 s, whereas steel-dowel joints plunge far deeper, terminating near –55 mm in Test 1 and almost –100 mm in Test 2—roughly two- to four-times the residual displacement of their wooden counterparts. The divergence emerges within the first 200 s, when both steel-dowel curves steepen sharply, but it is this final displacement gap of up to 70 mm that most clearly underscores the connectors' contrasting fire behaviour: densified dowels appear to stabilise once peripheral charring reaches them, while steel dowels act as thermal bridges that accelerate internal charring and trigger runaway stiffness loss, producing both larger and more scattered ultimate deformations.

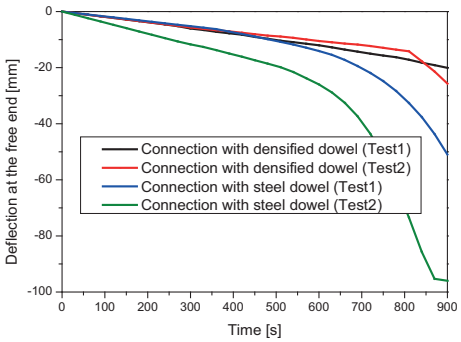


Figure 12. Deflection of the specimen under 60 kW/m² heat flux

Under identical thermal exposures, joints reinforced with thermo-densified wooden dowels consistently outperform those assembled with steel fasteners. At both 49 and 60 kW m^{-2} the wooden-dowel specimens retain flexural stiffness for longer and limit peak free-end deflection to substantially lower values. The contrast is most striking at 60 kW m^{-2}: densified-wood dowels keep the connection in the elastic , whereas steel-dowel joints have already entered inelastic deformation and experience rapid stiffness loss. Replicate tests with wooden dowels also follow nearly identical trajectories, while the steel-dowel tests diverge more noticeably—evidence of the greater predictability and repeatability achieved when metallic heat sinks are eliminated.

From a design perspective, substituting steel dowels with densified wooden dowels can meaningfully delay critical deformation, thereby extending the window for evacuation or active fire-fighting intervention. By avoiding the thermal-bridge effect inherent to steel, wooden dowels reduce peak deflections and enhance the fire resilience and sustainability of mass-timber connections.

CONCLUSION

The experimental programme confirms that replacing conventional steel dowels with thermo-densified wooden dowels markedly enhances the fire performance of engineered-wood connections and CLT panels. At both 49 kW m^{-2} and 60 kW m^{-2} incident heat fluxes, wooden-dowel joints (i) delay the attainment of critical temperatures, (ii) reduce char penetration in the dowel zone by 20–30 %, and (iii) limit free-end deflection to roughly 20–30 mm, compared with 55–100 mm for comparable steel-dowel joints. The advantage is most pronounced at the higher flux: densified-wood dowel joints stay in the elastic while their steel-reinforced counterparts have already entered inelastic deformation and begun to shed stiffness, while the duplicate wooden-dowel tests align far more closely—evidence of tighter repeatability.

Char-pattern analyses reinforce these findings. Unreinforced CLT panels and wooden-dowel joints develop relatively uniform char layers, whereas steel-dowel joints exhibit deep, irregular charring around each connector, evidencing a pronounced thermal-bridge effect that accelerates interior degradation. Measured residual char depths corroborate this behaviour, showing only 0.5–2.5 mm additional char adjacent to densified dowels but substantially deeper local charring around steel fasteners.

From a design perspective, substituting steel dowels with densified wooden dowels can postpone excessive deformation and lengthen the evacuation or intervention window during a fire without introducing metallic heat-sink effects. The results therefore position densified wooden dowels as a sustainable, fire-resilient alternative to metallic fasteners in mass-timber structures. Future work should evaluate long-term durability under hygro-thermal cycling, explore hybrid fastening strategies, and translate these laboratory insights into performance-based design guidelines for adhesive-free engineered-wood construction.

REFERENCES

1. **Fang C.H., Cloutier A., Blanchet P., Koubaa A., Mariotti N.,** Densification of Wood Veneers Combined with Oil-Heat Treatment. Part 1: Dimensional Stability, BioRessources 6 (1), p. 373-385.
2. **Sotayo A., Bradley D., Bather M., Sareh P., Oudjene M., El-Houjeyri I., Harte A.M., Mehra S., O'Ceallaigh C., Haller P., Namari S., Makradi A., Belouettar S., Bouhala L., Deneufbourg F., and Guan Z.** (2020) Review of state of the art of dowel laminated timber members and densified wood materials as sustainable engineered wood products for construction and building applications, Devel. Built Envir. 1, https://doi.org/10.1016/j.dibe.2019.100004.
3. **Anshari B., Guan Z., Kitamori A., Jung K., Hassel I., Komatsu K.,** Mechanical and moisture-dependent swelling properties of compressed Japanese cedar, Construction and Building Materials 25 (2011), p. 1718-1725.
4. **Jung K., Kitamori A., Komatsu K.,** Evaluation on structural performance of compressed wood as shear dowel, Holzforschung 62 (2008), p. 461-467.
5. **Jung K., Kitamori A., Komatsu K.,** Development of a joint system using a compressed wooden fastener I: evaluation of pull-out and rotation performance for a column-sill joint, Journal of Wood Science 55 (2009), p. 273-282.
6. **Jung K., Kitamori A., Komatsu K.,** Development of a joint system using a compressed wooden fastener II: evaluation

of rotation performance for a column-beam joint, Journal of Wood Science 56 (2010a.), p. 118-126.
7. **Jung K., Murakami S., Kitamori A., Chang W.S., Komatsu K.,** Improvement of glued-in-rod joint system using compressed wooden dowel, Holzforschung 64 (2010b), p. 799-804.
8. **Li L., Gong M., Chui Y., Schneider M., Li D.,** Measurement of the elastic parameters of densified balsamfir wood in the radial-tangential plane using a digital image correlation (DIC) method, Journal of Materials Science 48 (2013), p. 7728-7735.
9. **Yoshihara H., Tsunematsu S.,** Bending and shear properties of compressed Sitka spruce, Wood Science and Technology 41 (2007), p. 117-131.
10. **Navi P., Heger F.,** Combined densification and thermo-hydro-mechanical processing of wood, MRS Bull 29 (2004), p. 332-336.
11. **Inoue M., Norimoto M., Tanahashi M., Rowell R.M.,** Steam or heat fixation of compressed wood, Wood and Fiber Science 25 (1993a), p. 224-235.
12. **Song J., Chen C., Zhu S., Zhu M., Dai J., Ray U., Li Y., Kuang Y., Li Y., Quispe N.**, Processing bulk natural wood into a high-performance structural material, Nature 554 (2018) 224.
13. **Bui T.-A, Oudjene M., Khelifa M., Rogaume Y.,** Towards experimental and numerical assessment of the vibrational serviceability comfort of adhesive free laminated timber beams and CLT panels assembled using compressed wood dowels, Eng. Struct. 213C (2020), 110586.
14. **El-Houjeyri I., Thi V.D., Oudjene M., Khelifa M., Sotato A,Guan Z.**, Experimental investigations on adhesive free laminated oak timber beams and timber-to-timber joints assembled using thermo mechanically compressed wood dowels, Constr. Build. Mater. 222 (2019), p. 288–299.
15. **Tran T.T., Thi V.D., Oudjene M., Khelifa M., Girods P., Debal M., Rogaume Y.,** Fire structural performance of thermo-mechanically compressed spruce timber by means experiments and a three-step multi-reactions pyrolysis 3D-finite element modelling, Constr. Build. Mater. 320 (2022).
16. ISO 834-1, Fire resistance tests-Elements of building construction-Part 1: General requirements, International Organization for Standardization, 1999.
17. EN 1995-1-1:2004, Eurocode 5: design of timber structures – part 1. 1: general rules and rules for buildings, European Committee for Standardization, Brussels, Belgium, (E).

СПИСОК ЛИТЕРАТУРЫ

1. **Fang C.H., Cloutier A., Blanchet P., Koubaa A., Mariotti N.** Densification of Wood Veneers Combined with Oil-Heat Treatment. Part 1: Dimensional Stability, BioRessources 6 (1), p. 373-385.
2. **Sotayo A., Bradley D., Bather M., Sareh P., Oudjene M., El-Houjeyri I., Harte A.M., Mehra S., O'Ceallaigh C., Haller P., Namari S., Makradi A., Belouettar S., Bouhala L., Deneufbourg F., and Guan Z.** (2020) Review of state of the art of dowel laminated timber members and densified wood materials as sustainable engineered wood products for construction and building applications, Devel. Built Envir. 1, https://doi.org/10.1016/j.dibe.2019.100004.
3. **Anshari B., Guan Z., Kitamori A., Jung K., Hassel I., Komatsu K**. Mechanical and moisture-dependent swelling properties of compressed Japanese cedar, Construction and Building Materials 25 (2011), p. 1718-1725.
4. **Jung K., Kitamori A., Komatsu K**., Evaluation on structural performance of compressed wood as shear dowel, Holzforschung 62 (2008), p. 461-467.
5. **Jung K., Kitamori A., Komatsu K.,** Development of a joint system using a compressed wooden fastener I: evaluation of pull-out and rotation performance for a column-sill joint, Journal of Wood Science 55 (2009), p. 273-282.

6. **Jung K., Kitamori A., Komatsu K.,** Development of a joint system using a compressed wooden fastener II: evaluation of rotation performance for a column-beam joint, Journal of Wood Science 56 (2010a.), p. 118-126.
7. **Jung K., Murakami S., Kitamori A., Chang W.S., Komatsu K.,** Improvement of glued-in-rod joint system using compressed wooden dowel, Holzforschung 64 (2010b), p. 799-804.
8. **Li L., Gong M., Chui Y., Schneider M., Li D.,** Measurement of the elastic parameters of densified balsamfir wood in the radial-tangential plane using a digital image correlation (DIC) method, Journal of Materials Science 48 (2013), p. 7728-7735.
9. **Yoshihara H., Tsunematsu S.,** Bending and shear properties of compressed Sitka spruce, Wood Science and Technology 41 (2007), p. 117-131.
10. **Navi P., Heger F.,** Combined densification and thermo-hydro-mechanical processing of wood, MRS Bull 29 (2004), p. 332-336.
11. **Inoue M., Norimoto M., Tanahashi M., Rowell R.M.,** Steam or heat fixation of compressed wood, Wood and Fiber Science 25 (1993a), p. 224-235.
12. **Song J., Chen C., Zhu S., Zhu M., Dai J., Ray U., Li Y., Kuang Y., Li Y., Quispe N.**, Processing bulk natural wood into a high-performance structural material, Nature 554 (2018) 224.
13. **Bui T.-A, Oudjene M., Khelifa M., Rogaume Y.,** Towards experimental and numerical assessment of the vibrational serviceability comfort of adhesive free laminated timber beams and CLT panels assembled using compressed wood dowels, Eng. Struct. 213C (2020), 110586.
14. **El-Houjeyri I., Thi V.D., Oudjene M., Khelifa M., Sotato A,Guan Z.**, Experimental investigations on adhesive free laminated oak timber beams and timber-to-timber joints assembled using thermo mechanically compressed wood dowels, Constr. Build. Mater. 222 (2019), p. 288–299.
15. **Tran T.T., Thi V.D., Oudjene M., Khelifa M., Girods P., Debal M., Rogaume Y.,** Fire structural performance of thermo-mechanically compressed spruce timber by means experiments and a three-step multi-reactions pyrolysis 3D-finite element modelling, Constr. Build. Mater. 320 (2022).
16. ISO 834-1, Fire resistance tests-Elements of building construction-Part 1: General requirements, International Organization for Standardization, 1999.
17. EN 1995-1-1:2004, Eurocode 5: design of timber structures – part 1. 1: general rules and rules for buildings, European Committee for Standardization, Brussels, Belgium, (E).

T.T. Tran – Hanoi Architectural University, Km 10, Nguyen Trai street, Thanh Xuan district, Hanoi city, VIETNAM , e-mail: tuantt@hau.edu.vn

M. Khelifa – University of Lorraine, Lermab, EA 4370, 27 rue Philippe Seguin, 88051 Epinal, France, e-mail: tuantt@hau.edu.vn

M. Oudjene – Department of Civil and Water Engineering, University of Laval, 1065 avenue de la Médecine, Québec, Canada, e-mail: tuantt@hau.edu.vn

M. Debal – University of Lorraine, Lermab, EA 4370, 27 rue Philippe Seguin, 88051 Epinal, France, e-mail: tuantt@hau.edu.vn

Y. Rogaume – University of Lorraine, Lermab, EA 4370, 27 rue Philippe SEGUIN, 88051 Epinal, France, e-mail: tuantt@hau.edu.vn

Т.Т. Тран – Ханойский архитектурный университет, 10, улица Нгуен Траи, район Тхань Суан, город Ханой, Вьетнам, e-mail: tuantt@hau.edu.vn

М. Хелифа – Университет Лотарингии, ЛЕРМАБ, ЕА 4370, 27 улица Филиппа Сегуина, 88051 Эпинал, ФРАНЦИЯ, e-mail: tuantt@hau.edu.vn

М. Уджене – Факультет гражданского и водного строительства, Университет Лаваля, 1065 проспект Медицины, Квебек, Канада, e-mail: tuantt@hau.edu.vn

М. Дебал – Университет Лотарингии, ЛЕРМАБ, ЕА 4370, 27 улица Филиппа Сегуина, 88051 Эпинал, Франция, e-mail: tuantt@hau.edu.vn

Ю. Рогаум – Университет Лотарингии, ЛЕРМАБ, ЕА 4370, 27 улица Филиппа Сегуина, 88051 Эпинал, Франция, e-mail: tuantt@hau.edu.vn

DOI:10.22337/2587-9618-2025-21-4-83-93

CONCRETES WITH ADDITIVES PRODUCED BY SOL-GEL METHOD

Larisa A. Urkhanova [1], Solbon A. Lkhasaranov [2], Andrey A. Ivanov [2], Dmitry V. Dobrynin [2], Imad Jamal Moslemani [3]

[1] National Research Moscow State University of Civil Engineering, Moscow, RUSSIA
[2] East Siberia State University of Technology and Management, Ulan-Ude, RUSSIA
[3] Moscow Automobile and Road Construction State Technical University (MADI), Moscow, RUSSIA

Abstract: Additives with various functional purposes are used to modify concrete. Ultra- and nanodispersed additives produced using sol-gel technologies show great promise. The article examines different methods for producing modifying additives of silicon dioxide sol and metal hydroxides to enhance the properties of concrete for unique structures, civil engineering projects, and road construction.

The research utilized aluminosilicate materials—perlite rocks with varying degrees of crystallinity—as active mineral additives. Ultra-dispersed additives were obtained through the hydrolysis of a strong base and weak acid salt—sodium silicofluoride (Na_2SiF_6), hydrolysis of Portland cement, and hydrolysis of inorganic salts such as $CaCl_2$, $Ca(NO_3)_2$, and $CaSO_4$. Another method for producing a colloidal additive to modify cement stone and concrete involved mixing liquid colloidal fungicidal sulfur with water.

Modification with sulfur sol increases concrete strength by 10–25% for constructing fuel storage buildings and hydraulic structures of nuclear power plants.

Concrete for hydraulic structures using a complex additive containing silicic acid sol and superplasticizer is characterized by high physical-mechanical, hydrophysical, and operational performance.

When using an ultra-dispersed additive obtained through Portland cement hydrolysis, the strength of heavy concrete increases by 24% at the design age.

It has been established that modifying concrete for road pavements with micro-dosages of colloidal solutions of inorganic salts ($CaCl_2$, $Ca(NO_3)_2$, $CaSO_4$) increases the compressive and flexural strength of the composite. Ultra-dispersed additives have the greatest impact on accelerating the gain of concrete strength within the first 7 days of curing.

Keywords: heavy concrete, Portland cement, ultrafine additives, sol-gel method, silicic acid sol, superplasticizer, vitreous perlite, crystallized perlite, compressive strength, flexural strength, dense concrete structure

БЕТОНЫ С ДОБАВКАМИ, ПОЛУЧЕННЫМИ ЗОЛЬ-ГЕЛЬ МЕТОДОМ

Л.А. Урханова [1], С.А. Лхасаранов [2], А.А. Иванов [2], Д.В. Добрынин [2], Имад Жамаль Мослемани [3]

[1] Национальный исследовательский Московский государственный строительный университет, г. Москва, РОССИЯ
[2] Восточно-Сибирский государственный университет технологий и управления, г. Улан-Удэ, РОССИЯ
[3] Московский автомобильно-дорожный государственный технический университет (МАДИ), г. Москва, РОССИЯ

Аннотация: Для модификации бетона используются добавки, обладающие различным функциональным назначением. Перспективными являются ультра- и нанодисперсные добавки, полученные по золь-гель технологиям. В статье рассмотрены различные способы получения модифицирующих добавок золя диоксида кремния и гидроксидов металлов для улучшения свойств бетонов для уникальных сооружений, объектов гражданского и дорожного строительства.

В исследованиях в качестве активных минеральных добавок были использованы алюмосиликатные материалы - перлитовые породы с разной степенью кристалличности. Ультрадисперсные добавки получали путем гидролиза соли сильного основания и слабой кислоты - кремнефтористого натрия

Na_2SiF_6, гидролиза портландцемента, гидролиза неорганических солей, таких как $CaCl_2$, $Ca(NO_3)_2$, CaSO4. Еще одним способом получения коллоидной добавки для модификации цементного камня и бетона являлся процесс перемешивания с водой жидкой коллоидной фунгицидной серы.
Модифицирование золем серы позволяет увеличить прочность бетона на 10-25% для строительства зданий хранилищ топлива и гидротехнических сооружений атомных электростанций.
Бетоны для гидротехнических сооружений с применением комплексной добавки, содержащей золь кремниевой кислоты и суперпластификатор, характеризуются высокими физико-механическими, гидрофизическими и эксплуатационными показателями.
При использовании ультрадисперсной добавки, полученной при гидролизе портландцемента, происходит увеличение прочности тяжелого бетона на 24% в проектном возрасте.
Установлено, что при модификации бетона для покрытий автомобильных дорог микродозировками коллоидных растворов неорганических солей $CaCl_2$, $Ca(NO_3)_2$, $CaSO_4$ происходит увеличение прочности при сжатии и изгибе композита. Наибольшее влияние ультрадисперсные добавки оказывают на ускорение набора прочности бетона в возрасте до 7 суток твердения.

Ключевые слова: тяжелый бетон, портландцемент, ультрадисперсные добавки, золь-гель метод, золь кремниевой кислоты, суперпластификатор, стекловидный перлит, закристаллизованный перлит, прочность при сжатии, прочность при изгибе, плотная структура бетона

INTRODUCTION

The use of concrete in modern construction is unimaginable without various functional additives: plasticizing agents with water-reducing effects or providing rheological properties of the concrete mix [1-3], active mineral additives that increase the strength and density of the cement system [4, 5], modifying additives that improve the deformation and special properties of cement material, for example, elastic properties or corrosion resistance [6, 7].

Among the wide variety of used additives, the modification of concrete with ultra- and nanodispersed additives, especially SiO_2 nanoparticles as a basis for the pozzolanic reaction, is considered one of the most promising methods for improving the physicomechanical properties of the composite and is gradually being introduced into domestic construction practice. However, the low rate of implementation is associated with the lack of available industrial technologies for synthesizing additives and, as a consequence, limited practical experience in using them to modify the structure and properties of concrete [1].

Among all known methods for producing ultra- and nanodispersed particles, the sol-gel technology is particularly popular due to its accessibility and low-cost raw materials [8]. At the same time, sol-gel technologies for synthesizing additives differ in the type of precursor used, the composition of catalysts, the structure of the solvent, and the type of stabilizer [9].

The effectiveness of controlling the shape and size of particles and the nature of their surface during synthesis can be ensured by changing external conditions: pH of the medium, precursor concentration, solvent, aging temperature and time, nature of the catalyst, etc. Varying these parameters affects the reaction rate, the mechanism of the sol-gel transition, the nature of the polymerized particles formed in the sol, and the volumetric nature of the gel [9, 10].

The type of precursor used and the concentration of the aqueous solution determine the composition, shape, and size of the ultra- and nanodispersed particles of the obtained additives, resistance to external influences, aggregative and sedimentation stability, reactivity in the environment of hydrating cement, and cost.

Taking into account modern physicochemical concepts and approaches to producing ultra- and nanodispersed particles, the research team conducted studies on modifying the structure and properties of cement concrete for unique structures, civil and road construction facilities using additives of various compositions obtained using sol-gel technology.

Ultra-dispersed additives of silicon dioxide and metal hydroxides in the form of sol will help reduce porosity and improve the microstructure of cement stone, enhancing the physicomechanical properties of concrete when used.

MATERIALS AND METHODS

To improve the properties and enhance the physical-mechanical and operational characteristics of concrete based on ultrafine additives, Portland cement CEM I 42.5 N (GOST 31108-2020) was used as a binder. The cement was supplied by Tmlyuicement LLC and Cementum Center LLC.

As active mineral additives (fillers) in the concrete mix composition, finely ground vitreous and crystallized perlite from the Mukhor-Tala deposit (Republic of Buryatia) were used, depending on the composition. The chemical compositions of vitreous and crystallized perlite are presented in Table 1.

Table 1-Chemical composition of glassy and crystallized perlite, mass.%

As surfactants (surface-active agents), superplasticizers based on modified polycarboxylates (from Poliplast-Siberia LLC) and naphthalene-formaldehyde superplasticizer S-3 were used. These were added to the mixing water in amounts of 0.2% and 0.7% of the cement mass, respectively.

The study proposed low-temperature, technologically simple, and accessible methods for producing ultrafine additives (UFA) through the hydrolysis of a salt of a strong base and a weak acid — sodium silicofluoride (Na_2SiF_6). The aim was to modify the properties of cement stone with colloidal particles of silicofluoride acid and hydrolysis salt products, as well as Portland cement (PC) [11, 12].

The multicomponent sol obtained during PC hydrolysis contains simultaneously silicic acid, aluminum hydroxide, iron hydroxide, and calcium hydroxide [12]. Additionally, UFA were obtained through the hydrolysis of inorganic salts such as $CaCl_2$, $Ca(NO_3)_2$, $CaSO_4$, and $CuSO_4$. As a result of the multistage salt hydrolysis process, hydroxide salts of the corresponding metals are formed [13,14].

Another method for producing a colloidal additive to modify cement stone and concrete was the process of mixing liquid colloidal fungicidal sulfur (LCFS) with water. LCFS was obtained through the processing of sulfur-containing industrial waste and contains 40% sulfur. When mixed with water, LCFS turns into a suspension due to the nanoscale size of sulfur particles — 15–35 nm [15].

The additive consumption, at mother liquor concentrations of 0.75% and 2.0%, ranged from 0.2–3.0% of the cement mass. This, when recalculated to dry matter, amounted to thousandths of a percent, depending on the type of additives and the water-cement ratio.

The concrete mix, with workability grade P1–P3 depending on the concrete application area, was prepared by mixing pre-dosed components in a laboratory concrete mixer for 1 minute. These components included Portland cement, finely dispersed perlite, sand with a fineness modulus M_f=2.1, crushed stone fractions of 5–10 and 10–20 mm, and water containing dosed additives obtained by sol-gel technology and superplasticizers.

From the concrete mix of equal mobility, cube samples measuring 100 × 100 × 100 mm were molded and tested using standard methods. For each type of test, samples were manufactured in accordance with the requirements of GOST 10181-2014 «Concrete mixtures. Testing methods», GOST 10180-2012 «Concretes. Methods for determining strength using control samples», GOST 12730.5-2018 «Concretes. Methods for determining water resistance», GOST 24452-2023 «Concretes. Methods for determining prismatic strength, elastic modulus, and Poisson's ratio».

RESULTS AND DISCUSSION

It is known that one of the main problems arising during the synthesis of additives using

the sol-gel method is the aggregative and sedimentation instability of their aqueous solutions, which subsequently transform into a gel. To stabilize the ultrafine additives (UFA), surfactants based on naphthalene-formaldehyde and polycarboxylates were added to the reaction solution. These surfactants tend to adsorb onto the hydrophilic surface of ultrafine particles, preventing their further aggregation and extending the storage life of the additives to 15–20 days without altering their properties.

All the studied additives, when used in rational quantities, ensure the improvement of the physical and mechanical properties of concrete for various functional purposes, accelerating the hardening process during the initial hardening period. The introduction of micro-dosages of sulfur sol allows for an increase in concrete strength by 10–25% for the construction of fuel storage buildings and hydraulic structures of nuclear power plants, or to reduce cement consumption when designing the composition of the concrete mix. Simultaneously, this accelerates the hardening processes and the achievement of design strength, while increasing the corrosion resistance of concrete, which leads to an extension of the service life of the structures (Table 2).

Table 1. Chemical composition of glassy and crystallized perlite, mass.%

Material	SiO_2	Al_2O_3	Fe_2O_3	FeO	CaO	MgO	TiO_2	SO_3	K_2O	Na_2O	R_2O	LOI
Vitreous perlite	68,40	13,75	0,50	0,06	0,50	0,30	0,15	0,10	3,91	3,37	-	5,97
Crystallized perlite	73,13	11,7	1,08	1,71	0,55	0,30	-	-	-	-	6,4	7,65

Table 2. The effect of the amount of liquid colloidal fungicidal sulfur additive on the rate of strength gain of concrete for nuclear power plant structures

A type of sulfur sol	Amount of additive, % of cement mass		Compressive strength, MPa, after hardening, days			Ratio of strength indicators, $R\tau$ / R_{28}	
	counting on the solution	based on dry weight	3	7	28	τ = 3 days	τ = 7 days
Liquid colloidal fungicidal sulfur	0.6	$4.8 \cdot 10^{-3}$	22	34	39	0.39	0.76
	1	$6.4 \cdot 10^{-3}$	21	35	40	0.56	0.87
	1.5	$8.0 \cdot 10^{-3}$	20	34	49	0.53	0.90
	2	$9.6 \cdot 10^{-3}$	19	31	46	0.52	0.87
	3	$14.4 \cdot 10^{-3}$	19	27	44	0.49	0.78
Concrete without additives	-	-	15	30	39	0.39	0.76

Taking into account the modern requirements of the construction industry, it is necessary to ensure an appropriate level of safety for massive concrete and reinforced concrete hydraulic structures, primarily those that have been in long-term operation and require repair or reinforcement.

One of the main problems of hydraulic concrete is dangerous cracking, which leads to the rapid decommissioning of hydraulic structures. Obtaining hydraulic concrete with enhanced operational properties can be achieved through multi-level regulation of the structure and properties of the binder using a complex additive containing silicic acid sol and superplasticizer, which interacts with cement hydration products at the nano-, meso- and macro-levels, and also affects the formation of the structure and properties of cement stone.

As research results have shown, concretes using a complex additive are characterized by high physical-mechanical, hydro physical and operational indicators, which confirms the creation of a dense material structure and the strengthening effect of the additive.

The use of vitreous perlite in concrete improves the technological properties of the concrete mix, reduces the content of Portland cement in the mix composition, and together with the complex additive leads to an improvement in the basic properties of hydraulic concrete with composite binder (Table 3).

One of the promising methods for producing multicomponent silicic acid sol is the hydrolysis of Portland cement. The process of Portland cement hydrolysis occurs in several stages, with the formation of hydroxide salts containing the corresponding metallic elements at one of the intermediate stages.

A heavy concrete was developed for modification for monolithic construction having the following composition: Portland cement — 420 kg, sand — 760 kg, crushed stone with a fraction of 5–20 mm — 930 kg, water — 215 liters. The consumption of the ultrafine additive in the form of a 2% solution amounted to 5% of the binder mass (Table 4).

Table 3. Effect of a complex additive containing silicic acid sol (sodium fluorosilicate hydrolysis) and surfactants on the properties of hydraulic concrete

Composition	Compressive strength, MPa		Flexural strength, MPa		Crack resistance index	Water absorption, %	Water resistance	Frost resistance, cycles, F_2	Corrosion resistance coefficient	Modulus of elasticity E_b, MPa×10^3	Prism strength, MPa	Poisson's ratio	Total porosity, cm^3/g
	3 days	28 days	7 days	28 days									
PC	24.6	38.7	4.1	7.1	0.18	4.90	W10	150	1.32	32.362	34.6	0.216	0.096
PC+20% perlite + superplasticizer	28.8	48.1	4.3	7.5	0.19	3.66	W12	200	1.62	35.680	40.2	0.202	0.090
PC+ complex additive	30.2	45.5	6.9	10.6	0.21	3.05	W14	300	1.79	34.493	39.6	0.191	0.089
PC+ 20% perlite + complex additive	35.2	53.4	7.8	10.9	0.22	2.43	W16	300	1.86	37.345	46.3	0.199	0.081

Table 4. Effect of ultrafine additive obtained by hydrolysis of Portland cement on the properties of heavy concrete

Properties	Indicators of concrete	
	control	with additives
Concrete mix mobility (slump), cm	13	12
Volume of entrained air, %	4.3	4,5
Average density of concrete, kg/m^3	2320	2335
Compressive strength, MPa, at age		
3 days	14.5	18.5
7 days	21.3	29.3
28 days	32.1	39.8

The introduction of a multicomponent sol in the form of an ultrafine additive provides a significant improvement in the strength characteristics of concrete: the compressive strength of concrete increases by 37% compared to the control composition at an age of up to 7 days of hardening and by 24% at the design age. This effect is achieved due to the active interaction of the ultrafine additive with the hydration products of Portland cement clinker minerals.

During the hydrolysis of Portland cement, active dissolution is observed not only of exchange ions, but also of hydrated forms of ions $Ca(OH)^{+}$ and $(H_2SiO_4)^{2-}$, which sequentially saturate the aqueous solution. After that, the formation of new crystalline phases occurs in the volume and on the surface of the particles (Fig. 1).

Concrete mix for road pavements must comply with the requirements and conditions of regulatory documents [16].

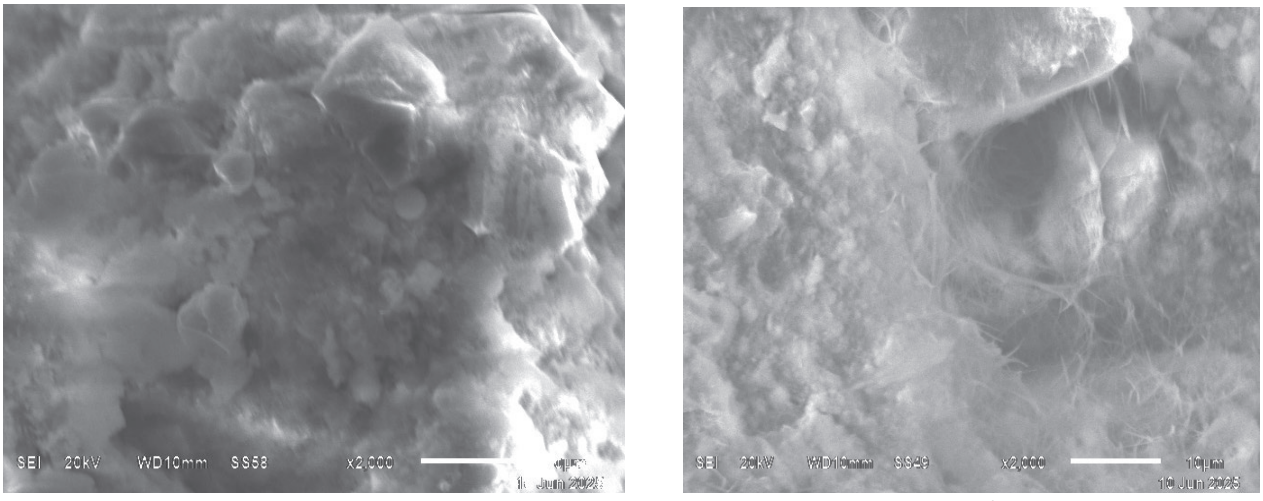
The production of high-quality concrete for road construction requires the use of quality components: cement, mineral additives, sand, crushed stone, chemical additives. It is also necessary to create optimal conditions for concrete hardening, which will increase the durability and reliability of cement-concrete structures by regulating the properties of the composite [16, 17].

When producing concrete mix, it is important to ensure uniformity, workability, and a rational water-cement ratio.

According to GOST R 59300, the concrete mix for road pavements constructed in sliding formwork must meet the P1 grade (cone slump from 1 to 4 cm) in terms of workability and the required volume of entrained air from 5% to 7%. This mobility class was adopted to ensure better placement and compaction of the concrete mix without surface defects, in combination with other properties of the concrete mix.

For research purposes, a concrete mix design calculation was carried out for road pavements of technical category I with a compressive strength class of B30. The dosage of additives in the form of a 2% solution in the concrete mix was 0.1–0.2% of the cement mass, calculated on dry salt.

The analysis of the results obtained showed that $CaCl_2$ and $CaSO_4$ additives increase the strength of concrete by an average of 22–42% during the design hardening time, effectively accelerating the concrete hardening process in the early stages of hardening and increasing its strength by 40–90% on the 3rd day of hardening (Fig. 2).



a *b*

Figure 1. Microstructure of cement stone modified with an ultrafine additive obtained by hydrolysis of Portland cement (x2000): a – control, b – with an ultrafine additive

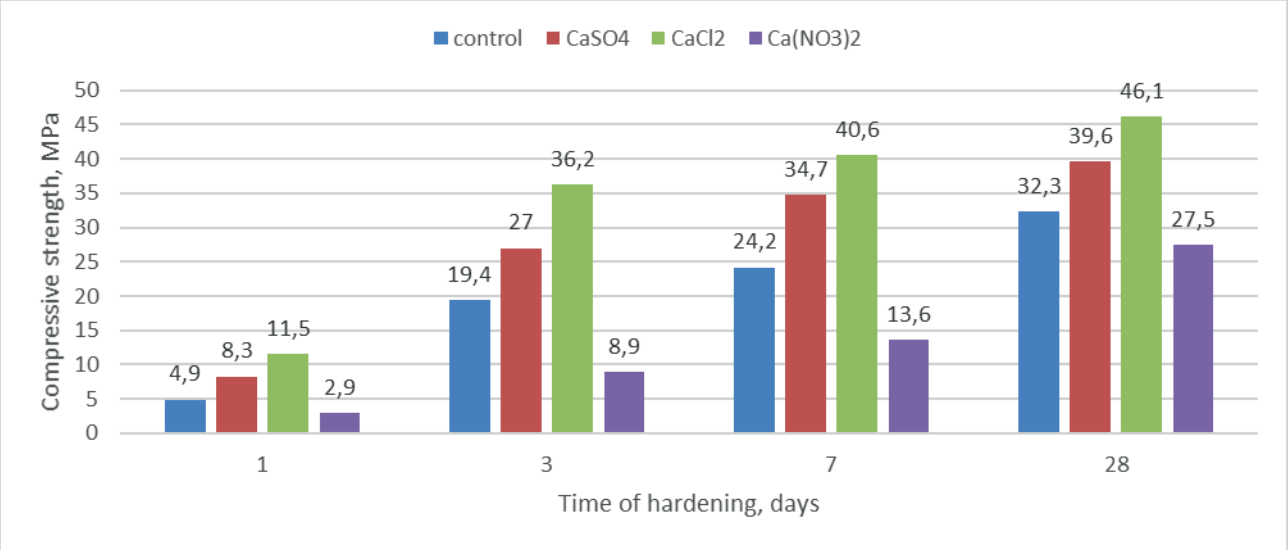


Figure 2. Kinetics of hardening of concrete for road surfaces with modifying additives obtained using sol-gel technology

The increase in strength of Portland cement and concrete with micro-dosages of additives is associated with changes in the porosity of the hydrate stone, its phase composition, and microstructure.

The tensile strength index in bending of concrete is important for ensuring the durability and safety of road surfaces. Road surfaces are constantly exposed to dynamic loads, including bending loads that occur under vehicle loads and temperature deformations.

Various methods are known to increase the tensile strength in bending of concretes for road pavements — mainly micro-reinforcement with fiber [18]. However, it is also possible to increase the strength characteristics of concrete by modifying the structure of the cement stone in concrete using chemical or electrophysical methods [18–21].

A study of the tensile strength in bending of concrete samples using micro-dosing of $CaCl_2$ salt (Table 4) showed that the use of an additive in the form of a 2% solution in an amount of 0.2%, calculated on dry salt from the mass of cement, increases the tensile strength in bending by 45% in 28 days of hardening.

Table 4. Results of tensile testing of cement concrete under bending

Composition	Flexural tensile strength of concrete, MPa, at age, days			
	1	3	7	28
PC	0.6	1.1	1.5	2.9
PC+$CaCl_2$	1.6	1.9	2.7	4.2

The hydroxides formed by multivalent metals in the form of colloidal solutions with varying time-dependent stability immobilize part of the water into the hydration shell. This leads to a decrease in the water-to-cement ratio while maintaining the rheological characteristics of the cement paste and the formation of a denser structure of the cement stone.

Such constrained conditions promote the growth of fibrous calcium hydrosilicates, thereby increasing the tensile strength in bending of concrete.

CONCLUSION

Here are the results of the authors' research on improving the physical-mechanical and operational properties of concrete for various functional purposes in civil, hydraulic, and road construction using modifying additives produced by sol-gel technologies.

The processes of producing additives using various precursors and their concentrations have been studied. It has been substantiated that the selection of stabilizers and optimization of production conditions allows for the targeted regulation of the synthesis of modifying additives with the required particle morphology and size, as well as physicochemical properties.

It has been proven that the use of additives accelerates the hardening processes and the rate of strength gain in concrete, which is associated with changes in the structure and phase composition of cement composites. The developed methods and approaches for producing modifying additives must meet the technical and economic criteria for the effective use of concrete for its intended purpose, taking into account the requirements of regulatory documents and design documentation.

ACKNOWLEDGEMENTS

The article was prepared under the grant "Young scientists of ESSUTM-2025".

REFERENCES

1. **Nelubova V.V., Kuzmin E.O., Strokova V.V.** Structure and properties of nanodispersed silica synthesized by sol-gel method // Construction Materials. 2022. No. 12. P. 38-44.
2. **Shuldyakov K.V., Trofimov B.Y., Kramar L.Y.** High-frost-resistant concrete without air entrainment // Construction Materials. 2020. No. 6. P. 18-26.
3. **Fedosov S.V., Ibragimov A.M., Redkina A.S., Nesterov S.A.** Determination of technological parameters of mechanomagnetic activation of aqueous systems with plasticizing additive // Construction Materials. 2010. No. 3. P. 49-51.
4. **Tkach E.V., Temirkanov R.I., Tkach S.A**. Comprehensive study of modified concrete based on activated microsilicon together with micro-reinforcing fiber to improve performance // Bulletin of the Tomsk Polytechnic University. Geo Assets Engineering. 2021. Vol. 332. No. 5. P. 215-226. DOI: 10.18799/24131830/2021/5/3204.
5. **Larsen O.A., Alexandrova O.V., Narut V.V., Polozov A.A., Bakhrakh A.M**. Study of properties of active mineral additives for use in hydraulic engineering construction // Bulletin of BSTU named after V.G. Shukhov. 2020. No. 8. P. 8-14. DOI: 10.34031/2071-7318-2020-5-8-8-17.
6. **Stepanova V.F., Rozental N.K., Chekhniy G.V., Baev S.M.** Determination of corrosion resistance of shotcrete as a protective coating for concrete and reinforced concrete structures // Construction Materials. 2018. No. 8. P. 69-72.
7. **Kasatkin S.P.** Highly efficient concrete modified with complex chemical additive containing nanodispersions of hydrodioxide of silicon: PhD thesis. Saint Petersburg, 2023. 138 p. URL: https://pstu.ru/files/2/file/Dissertaciya._Kasatkin_S.P._02.07.2023.pdf.
8. **Savelyeva M.A., Urkhanova L.A., Khardaev P.K.** Prospects of using

colloidal additives for modification of cement stone // Construction Materials. 2017. No. 11. P. 59-63.
9. **Strokova V.V., Nelubova V.V., Kuzmin E.O., Ryltsova I.G., Gubareva E.N., Baskakov P.S.** Technologies of sol-gel synthesis of nano-silica as a modifier of materials based on… DOI: 10.31659/0585-430X-2023-811-3-43-72.
10. **Julie Candra C.S., Shadiya M.A., Bipinbal P.K., Sunil K.** Narayanankutty. Effect of olivine nanosilica on the reinforcement of natural rubber nanosilica composites. Materials Today. Proceedings. 2019. Vol. 9, pp. 127-132. DOI: 10.1016/j.matpr.2019.02.047.
11. **Urkhanova L.A., Ivanov A.A., Lkhasaranov S.A.** Composite cement with dispersed perlite and colloidal additive for hydraulic concrete // Cement and its Application. 2024. No. 1. DOI: 10.61907/CIA.2024.87.76.001
12. **Urkhanova L.A., Lkhasaranov S.A., Danzanov D.V.** Synthesis of ultrafine additive obtained by hydrolysis of Portland cement for modification of cement stone // Cement and its application. – 2022. – No. 4. – P. 52-56.
13. **Urkhanova L.A., Berezovsky P.V., Arkhincheeva N.V.** Modification of cement stone with micro-additives of inorganic salts // Construction materials. – 2021. – No. 1-2. – P. 21-29.
14. **Urkhanova L.A., Dobrynin D.V., Lkhasaranov S.A., Berezovsky P.V.** Improving the physicomechanical properties of concrete with micro-additives of inorganic salts // Bulletin of ВСГУТУ. – 2025. – No. 2. – P.
15. **Urkhanova L.A., Moslemany I.Zh.** Improving the physicomechanical properties of cement stone using highly dispersed sulfur // Cement and its application. – 2025. – No. 2. – P. 67-70.
16. **Kaitukov B.A., Parusov A.A.** Improving the quality of concrete pavements in road construction // System technologies. – 2021. – No. 40. – P. 71-74.
17. **Mironenko M.A.** Regulating the properties of road concrete through chemical additives // Bulletin of Science. – 2024. – No. 6 (75). – Vol. 1. – P. 1823-1833. ISSN 2712-8849 // Electronic resource: https://www.вестник-науки.рф/article/15412.
18. **Kramar L.Ya., Kudyakov A.I., Trofimov B.Ya., Shuldyakov K.V.** Cement heavy concretes for the construction of high-speed roads // Bulletin of the Tomsk State University of Architecture and Construction. – 2017. – No. 4. – P. 147-157.
19. **Bazhenov Yu.M., Demyanova V.S., Kalashnikov V.I.** Modified high-quality concretes / Yu.M. Bazhenov, V.S. Demyanova, V.I. Kalashnikov. – Moscow: ASV Publishing House, 2006. – 368 p.
20. Improving the quality of cement stone through multifrequency ultrasonic activation of mixing water / A.I. Kudyakov, A.G. Petrov, G.G. Petrov, K.V. Ikonnikova // Bulletin of the Tomsk State University of Architecture and Construction. – 2012. – No. 3. – P. 143-152.
21. The effect of the additive «MK-polycarboxylate superplasticizer» on cement hydration, structure, and properties of cement stone / K.V. Shuldyakov, L.Ya. Kramar, B.Ya. Trofimov, N.A. Mamaev // Cement and its application. – 2013. – No. 2. – P. 114-118**.**

СПИОК ЛИТЕРАТУРЫ

1. **Nelubova V.V., Kuzmin E.O., Strokova V.V.** Structure and properties of nanodispersed silica synthesized by sol-gel method // Construction Materials. 2022. No. 12. P. 38-44.
2. **Shuldyakov K.V., Trofimov B.Y., Kramar L.Y.** High-frost-resistant concrete without air entrainment // Construction Materials. 2020. No. 6. P. 18-26.

3. **Fedosov S.V., Ibragimov A.M., Redkina A.S., Nesterov S.A.** Determination of technological parameters of mechanomagnetic activation of aqueous systems with plasticizing additive // Construction Materials. 2010. No. 3. P. 49-51.
4. **Tkach E.V., Temirkanov R.I., Tkach S.A**. Comprehensive study of modified concrete based on activated microsilicon together with micro-reinforcing fiber to improve performance // Bulletin of the Tomsk Polytechnic University. Geo Assets Engineering. 2021. Vol. 332. No. 5. P. 215-226. DOI: 10.18799/24131830/2021/5/3204.
5. **Larsen O.A., Alexandrova O.V., Narut V.V., Polozov A.A., Bakhrakh A.M**. Study of properties of active mineral additives for use in hydraulic engineering construction // Bulletin of BSTU named after V.G. Shukhov. 2020. No. 8. P. 8-14. DOI: 10.34031/2071-7318-2020-5-8-8-17.
6. **Stepanova V.F., Rozental N.K., Chekhniy G.V., Baev S.M.** Determination of corrosion resistance of shotcrete as a protective coating for concrete and reinforced concrete structures // Construction Materials. 2018. No. 8. P. 69-72.
7. **Kasatkin S.P.** Highly efficient concrete modified with complex chemical additive containing nanodispersions of hydrodioxide of silicon: PhD thesis. Saint Petersburg, 2023. 138 p. URL: https://pstu.ru/files/2/file/Dissertaciya._Kasatkin_S.P._02.07.2023.pdf.
8. **Savelyeva M.A., Urkhanova L.A., Khardaev P.K.** Prospects of using colloidal additives for modification of cement stone // Construction Materials. 2017. No. 11. P. 59-63.
9. **Strokova V.V., Nelubova V.V., Kuzmin E.O., Ryltsova I.G., Gubareva E.N., Baskakov P.S.** Technologies of sol-gel synthesis of nano-silica as a modifier of materials based on… DOI: 10.31659/0585-430X-2023-811-3-43-72.
10. **Julie Candra C.S., Shadiya M.A., Bipinbal P.K., Sunil K.** Narayanankutty. Effect of olivine nanosilica on the reinforcement of natural rubber nanosilica composites. Materials Today. Proceedings. 2019. Vol. 9, pp. 127-132. DOI: 10.1016/j.matpr.2019.02.047.
11. **Urkhanova L.A., Ivanov A.A., Lkhasaranov S.A.** Composite cement with dispersed perlite and colloidal additive for hydraulic concrete // Cement and its Application. 2024. No. 1. DOI: 10.61907/CIA.2024.87.76.001
12. **Urkhanova L.A., Lkhasaranov S.A., Danzanov D.V.** Synthesis of ultrafine additive obtained by hydrolysis of Portland cement for modification of cement stone // Cement and its application. – 2022. – No. 4. – P. 52-56.
13. **Urkhanova L.A., Berezovsky P.V., Arkhincheeva N.V.** Modification of cement stone with micro-additives of inorganic salts // Construction materials. – 2021. – No. 1-2. – P. 21-29.
14. **Urkhanova L.A., Dobrynin D.V., Lkhasaranov S.A., Berezovsky P.V.** Improving the physicomechanical properties of concrete with micro-additives of inorganic salts // Bulletin of ВСГУТУ. – 2025. – No. 2. – P.
15. **Urkhanova L.A., Moslemany I.Zh.** Improving the physicomechanical properties of cement stone using highly dispersed sulfur // Cement and its application. – 2025. – No. 2. – P. 67-70.
16. **Kaitukov B.A., Parusov A.A.** Improving the quality of concrete pavements in road construction // System technologies. – 2021. – No. 40. – P. 71-74.
17. **Mironenko M.A.** Regulating the properties of road concrete through chemical additives // Bulletin of Science. – 2024. – No. 6 (75). – Vol. 1. – P. 1823-1833. ISSN 2712-8849 // Electronic resource: https://www.вестник-науки.рф/article/15412.
18. **Kramar L.Ya., Kudyakov A.I., Trofimov B.Ya., Shuldyakov K.V.** Cement heavy concretes for the construction of high-speed

roads // Bulletin of the Tomsk State University of Architecture and Construction. – 2017. – No. 4. – P. 147-157.
19. **Bazhenov Yu.M., Demyanova V.S., Kalashnikov V.I.** Modified high-quality concretes / Yu.M. Bazhenov, V.S. Demyanova, V.I. Kalashnikov. – Moscow: ASV Publishing House, 2006. – 368 p.
20. Improving the quality of cement stone through multifrequency ultrasonic activation of mixing water / A.I. Kudyakov, A.G. Petrov, G.G. Petrov, K.V. Ikonnikova // Bulletin of the Tomsk State University of Architecture and Construction. – 2012. – No. 3. – P. 143-152.
21. The effect of the additive «MK-polycarboxylate superplasticizer» on cement hydration, structure, and properties of cement stone / K.V. Shuldyakov, L.Ya. Kramar, B.Ya. Trofimov, N.A. Mamaev // Cement and its application. – 2013. – No. 2. – P. 114-118**.**

Larisa Alekseevna Urkhanova, Doctor of Technical Sciences, Professor, Professor of the Department of Urban Planning, National Research Moscow State University of Civil Engineering, 26 Yaroslavskoe Highway, Moscow, 129337, Russia, urkhanova@mail.ru

Solbon Alexandrovich Lkhasaranov, Candidate of Technical Sciences, Associate Professor, Head of the Department of Construction Materials, Highways and Woodworking, East Siberian State University of Technology and Management, 40V Klyuchevskaya Street, Ulan-Ude, 670013, Russia, solbon230187@mail.ru

Andrey Andreevich Ivanov, Lecturer of the Department of Construction Materials, Highways and Woodworking, East Siberian State University of Technology and Management, 40V Klyuchevskaya Street, Ulan-Ude, 670013, Russia, vadim290607@gmail.com

Dmitry Vyacheslavovich Dobrynin, Postgraduate Student of the Department of Construction Materials, Highways and Woodworking, East Siberian State University of Technology and Management, 40V Klyuchevskaya Street, Ulan-Ude, 670013, Russia

Imad Jamal Moslemany, Postgraduate Student of the Department of Road Construction Materials and Chemical Technologies, Moscow Automobile and Road Construction State Technical University (MADI), 64 Leningradsky Prospekt, Moscow, 125319, Russia

Лариса Алексеевна Урханова, д-р техн. наук, профессор, профессор кафедры «Градостроительство», Национальный исследовательский Московский государственный строительный университет, дом 26, Ярославское шоссе, г. Москва, 129337, Россия, urkhanova@mail.ru

Солбон Александрович Лхасаранов, канд. техн. наук, доцент, зав. кафедрой «Строительные материалы, автомобильные дороги и деревообработка», Восточно-Сибирский государственный университет технологий и управления, дом 40В, ул. Ключевская, г. Улан-Удэ, 670013, Россия, solbon230187@mail.ru

Андрей Андреевич Иванов, преподаватель кафедры «Строительные материалы, автомобильные дороги и деревообработка», Восточно-Сибирский государственный университет технологий и управления, дом 40В, ул. Ключевская, г. Улан-Удэ, 670013, Россия, vadim290607@gmail.com

Дмитрий Вячеславович Добрынин, аспирант кафедры «Строительные материалы, автомобильные дороги и деревообработка», Восточно-Сибирский государственный университет технологий и управления, дом 40В, ул. Ключевская, г. Улан-Удэ, 670013, Россия

Имад Жамаль Мослемани, аспирант кафедры «Дорожно-строительные материалы и химические технологии» Московский автомобильно-дорожный государственный технический университет (МАДИ), дом 64, Ленинградский проспект, г. Москва, 125319, Россия

DOI:10.22337/2587-9618-2025-21-4-94-101

SOME ASPECTS OF TESTING FIBRE-REINFORCED POLYMER BARS UNDER SUSTAINED AND DYNAMIC LOADS AND VARIOUS EXPOSURES

Evgeny Yu. Yurin [1], Sergey K. Khlebnikov [1,2], Ulyana V. Kudyakova [1], Konstantin L. Kudyakov [1,2], Andrey V. Buchkin [1]

[1] Research Institute of Reinforced Concrete named after A.A. Gvozdev in JSC Research Center of Construction, Moscow, RUSSIA

[2] National Research Moscow State University of Civil Engineering, Moscow, RUSSIA

Abstract: The physical-mechanical and rheological properties of fibre-reinforced polymer bars (FRP bars) have been studied predominantly under short-term static loading. In real-world operation, reinforced concrete structures are subjected to a complex combination of various factors, including sustained loads, cyclic dynamic loads (including fully reversed), temperature effects, and exposure to aggressive environments. Russian regulatory documents for the design of reinforced concrete structures partially account for these factors using generalized reduction factors. Standard test methods for determining the combined influence of these factors on the properties of FRP bars are currently lacking.

The aim of this research is to identify a number of features in the preparation and implementation of tests to assess the combined influence of operational factors on the strength and deformation characteristics of FRP bars. The paper presents the prerequisites for developing a test program to study the behavior of reinforcement under long-term static loading under conditions of elevated temperature and alkaline environment of concrete, as well as under repeatedly applied dynamic load (including the fully reversed «compression-tension» mode) with varying cycle parameters. The goal is to derive analytical relationships and diagrams for the long-term strength and fatigue strength of FRP bars, which consider the influence of temperature, aggressive environment, and loading cycle parameters.

The obtained results form the basis for a comprehensive program of experimental research, the development of test methods, and the prediction of the behavior of FRP bars in real-world operating conditions as part of concrete structures. They enable a transition from using generalized coefficients to calculations that account for specific exposures. This is a key step towards improving the regulatory framework and designing reliable, durable, and safe reinforced concrete structures with FRP bars.

Keywords: fibre-reinforced polymer bars, strength, durability, sustained load, dynamic load, cyclic load, alkaline environment of concrete, temperature effect

НЕКОТОРЫЕ АСПЕКТЫ ИСПЫТАНИЙ АРМАТУРЫ КОМПОЗИТНОЙ ПОЛИМЕРНОЙ ПРИ ДЛИТЕЛЬНОЙ И ДИНАМИЧЕСКОЙ НАГРУЗКАХ И РАЗЛИЧНЫХ ВОЗДЕЙСТВИЯХ

Е.Ю. Юрин [1], С.К. Хлебников [1,2], У.В. Кудякова [1], К.Л. Кудяков [1,2], А.В. Бучкин [1]

[1] Научно-исследовательский, проектно-конструкторский и технологический институт бетона и железобетона им. А.А. Гвоздева АО «Национальный исследовательский центр «Строительство», г. Москва, РОССИЯ

[2] Национальный исследовательский Московский государственный строительный университет, г. Москва, РОССИЯ

Аннотация: Физико-механические и реологические свойства арматуры композитной полимерной (АКП) изучены преимущественно в условиях кратковременного статического нагружения. В реальной эксплуатации железобетонные конструкции подвергаются комплексному воздействию различных факторов, в т.ч. длительные нагрузки, циклические динамические (включая знакопеременные) нагрузки,

температурные воздействия, воздействия агрессивных сред. Нормативные документы РФ по проектированию армированных бетонных конструкций частично учитывают данные факторы при помощи обобщенных коэффициентов. Стандартные методы испытаний по определению комплексного влияния данных факторов на свойства АКП в настоящее время отсутствуют.
Целью данного исследования является определение ряда особенностей при подготовке и реализации испытаний для оценки комплексного влияния эксплуатационных факторов на прочностные и деформационные характеристики АКП. В работе приведены предпосылки для составления программы испытаний по изучению поведения арматуры при длительном статическом нагружении в условиях повышенной температуры и щелочной среды, а также при многократно повторяющейся динамической нагрузке (включая знакопеременный режим «сжатие-растяжение») с варьируемыми параметрами цикла, с выявлением аналитических зависимостей и диаграмм длительной и усталостной прочности АКП, которые учитывают влияние температуры, агрессивной среды и параметров цикла нагружения.
Полученные результаты являются основной для выполнения комплекса экспериментальных исследований, разработки методов испытаний и прогнозирования поведения АКП в реальных условиях эксплуатации в составе бетонных конструкций и позволяют перейти от использования обобщенных коэффициентов к расчету с учетом конкретных воздействий. Это является ключевым шагом для совершенствования нормативной базы и проектирования надежных, долговечных и безопасных железобетонных конструкций с АКП.

Ключевые слова: арматура композитная полимерная, прочность, долговечность, длительная нагрузка, динамическая нагрузка, циклическая нагрузка, щелочная среда бетона, температурное воздействие

INTRODUCTION

The characteristics of fibre-reinforced polymer bars (FRP bars) have been primarily studied under short-term static loads [1, 2, 3, 4, 5]. Meanwhile, during the standard operation of reinforced concrete structures of buildings and facilities, other loads and exposures arise that must be considered in design, among which the following can be highlighted:
- sustained load (dead weight of structures and materials, the sustained part of live load, prestressing of reinforcement) [6, 7, 8, 9];
- short-term dynamic and repeatedly applied cyclic load with different cycle parameters (including fully reversed «compression-tension»), seismic actio [5, 9, 10, 11, 12];
- temperature effects (including those approaching or exceeding the glass transition temperature of the polymers);
- exposure to the alkaline environment of concretea [3, 4, 6, 13];
- others.

Currently, in domestic and foreign codes for the design of reinforced concrete structures with FRP bars, the consideration of these loads and exposures (separately or in combination) is performed using generalized reduction factors or is not performed at all. However, in some cases, these parameters can have a critical impact on the mechanical safety and reliability of such structures. For example, with poorly manufactured FRP bars, the combined action of elevated temperature and an alkaline environment can lead to degradation of the interphase layer, disrupting the bond between concrete and reinforcement. The manifestation of fatigue or creep in polymers under long-term dynamic or static loading, depending on the load parameters and material, can significantly reduce the strength of FRP bars. The resistance of FRP bars to compressive loads, which arise in the sections of compressed and eccentrically compressed reinforced concrete elements under long-term static and fully reversed dynamic loads, is currently not accounted for in the Russian codes and has been insufficiently studied [14].

MATERIALS AND METHODS

Along with leading research organizations, the Research Institute of Reinforced Concrete named after A.A. Gvozdev in JSC Research Center of Construction is engaged in comprehensive research in these areas, considering both individual factors and their combined influence.

A test program is being implemented to evaluate the strength of FRP bars under the separate and combined action of elevated temperature, alkaline environment, and sustained load with variation of their parameters.

Sustained load tests are performed on a special test stand with a vertical arrangement of specimens (Figure 1). A constant tensile load is applied to the specimens through a system of levers and calibrated weights, without restricting their strain. The load is monitored by a load cell.

Testing is performed according to the methodology of GOST 32492-2024, considering the provisions of ASTM D7337/D7337M-12 (2019), ACI 440.3R-2012, CAN/CSA S806-12 (R2017), FIB Bulletin 40 [15, 16, 17, 18, 19].

In 2025, the automation of the test stand and its modernization for new types of tests are planned.



Figure 1. General view of long-term testing of FRP bar specimens (before test stand modernization)

The influence of an aggressive liquid environment is produced via additionally installed vessels in the form of tubes sealed at the ends. Local controlled heating of the specimens is achieved using a heating cable.

Monitoring of longitudinal strain is performed automatically using high-precision LVDT sensors (prior to modernization, using mechanical strain gauges with dial indicators). The exact time and nature of failure are recorded using video recording.

A research program is also being implemented to study the strength and deformability of FRP bars under repeatedly applied dynamic load with various cycle parameters (including fully reversed loads and assessment of fatigue strength). The test methodology is based on the provisions of GOST 32492-2024 [15].

Tests are performed on specially prepared specimens (Figure 2) in automatic servohydraulic testing systems (Instron 8802, etc.), which allow applying an axial cyclic load with specified amplitude-frequency characteristics.

Measurement of longitudinal strain is carried out using high-frequency measurement systems connected to strain gauges, clip-on extensometers, and COD (Crack Opening Displacement) sensors.

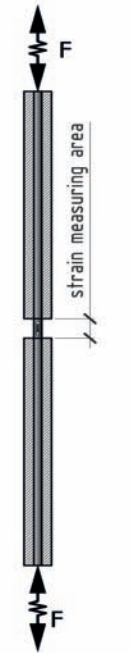


Figure 2. Schematic diagram of testing FRP bars under cyclic load with different values of the stress ratio (R)

It should be noted that this test scheme technically allows for the additional consideration of the influence of an aggressive environment and elevated temperatures, similar to the long-term tests.

It is also reasonable to investigate the possible influence of the specimen gauge length on the fatigue strength under axial fully reversed cyclic load according to the «compression-tension» mode.

RESULTS AND DISCUSSION

The described tests are aimed at obtaining analytical relationships and diagrams used for predicting the strength and strain of FRP bars in the design of reinforced concrete structures (Figures 3 and 4). These relationships and diagrams can be obtained based on GOST 32492-2024, taking into account the provisions of ASTM D7337/D7337M-12 (2019), ACI 440.3R-2012, CAN/CSA S806-12 (R2017) [15, 16, 17, 18].

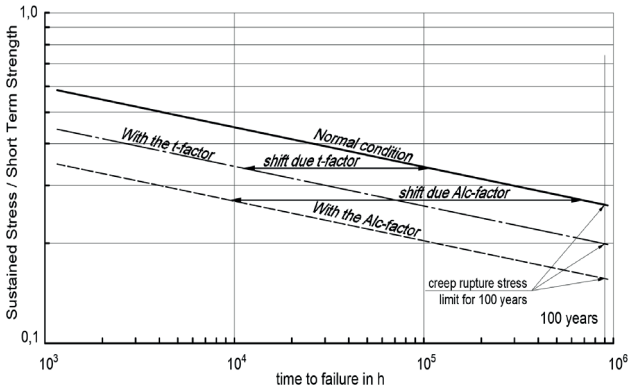


Figure 3. Characteristic predictive relationships and diagrams of the long-term strength of FRP bars under exposure to aggressive environments and elevated temperature

Figure 3 shows a characteristic predictive diagram of the long-term strength of FRP bars under normal operating conditions, as well as diagrams accounting for the influence of ambient temperature (t-factor) and exposure to aggressive environments (Alc-factor) under sustained tensile load (the diagrams are shown schematically and can be refined based on test results).

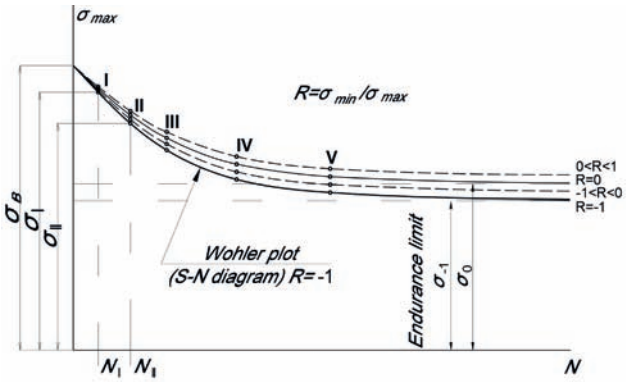


Figure 4. Characteristic predictive diagrams of the fatigue strength of FRP bars under cyclic repeatedly applied tensile load with different cycle asymmetry ratios (R)

Figure 4 shows characteristic predictive diagrams of the fatigue strength of FRP bars under cyclic repeatedly applied tensile load depending on the nature of the loading cycle. The Wohler plots (S-N diagrams) show the change in the strength of FRP bars (σ_i) after N_i loading cycles (the diagrams are shown schematically and can be refined based on test results).

The importance of validating the obtained results through additional studies of the stress-strain state of concrete structures reinforced with FRP bars under characteristic loadings and exposures should be noted.

CONCLUSION

1. The design of reliable and durable concrete structures reinforced with FRP bars requires accounting for multiple factors, including the influence of different types of loads and exposures on material characteristics. The insufficient number of studies is a barrier to the application of FRP bars.

2. The features of the tests on FRP bars under sustained and dynamic load, considering external exposures, being implemented at the Research Institute of Reinforced Concrete named after A.A. Gvozdev in JSC Research Center of Construction, are outlined.

3. Characteristic analytical graphs and relationships are proposed, which, considering the test results, can serve as a tool for designing concrete structures reinforced with FRP bars, accounting for the predicted degree of degradation of FRP bar properties under sustained loads and exposures.
4. The importance of validating the obtained results through additional studies of the stress-strain state of concrete structures reinforced with FRP bars under characteristic loadings and exposures should be emphasized.

ACKNOWLEDGEMENTS

The authors express their gratitude to Federal Autonomous Institution «Federal Center for Standardization» (FAU «FCC») and JSC Research Center of Construction for their support in conducting the research.

REFERENCES

1. **Plevkov V.S., Baldin I.V., Kudyakov K.L., Nevskii A.V.** Strength and deformability of polymer composites under tensile and compressive loads. Journal of Construction and Architecture. 2016; 5(58):91-101. (in Russian).
2. **Plevkov V.S., Tamrazyan A.G., Kudyakov K.L.** Strength and crack resistance of bent fiber-reinforced concrete elements with prestressed glass composite reinforcement under static and short-term dynamic loading. Tomsk, Publishing House of Tomsk State University of Architecture and Civil Engineering; 2021. (in Russian).
3. **Stepanova V.F., Stepanov A.Yu., Zhirkov E.P.** Composite polymer reinforcement. Moscow: ASV Publ.; 2013. (In Russian).
4. **Stepanova V.F., Buchkin A.V., Kudyakov K.L., Stepanov A.Yu.** Composite polymer fittings and composite poly mer products. Moscow, 2023. (in Russian).
5. **Mamin A.N., Khlebnikov S.K.** Use Fiber-Reinforced Polymer Bars in Concrete Structures Subject to Dynamic Loads. Reinforced Concrete Structures. 2025; 1(9):26-34. (In Russian).
6. **Yurin E.Yu., Buchkin A.V., Kudyakov K.L.** Effects of alkaline concrete media on glass composite reinforcement under prolonged load action // Results of scientific and dissertation research : Collection of abstracts of the reporting scientific and technical session, Moscow, October 01-31, 2024. Moscow: Science and Research Center of Construction, 2024, pp. 20-21. (In Russian).
7. **Rossini M., Saqan E., Nanni A.** Prediction of the creep rupture strength of GFRP bars // Construction and Building Materials, 227, 116620(1-11), 2019. DOI : 10.1016/j.conbuildmat.2019.08.001.
8. **Benmokrane B., Brown V., Khaled M., Nanni A., Rossini M., Shield C.** Creep-Rupture Limit for GFRP Bars Subjected to Sustained Loads // Journal of Composites for Construction, 2019. 23. 06019001. 10.1061/(ASCE)CC.1943-5614.0000971.
9. **Tanks J., Naito K., Ueda H.** Characterization of the Static, Creep, and Fatigue Tensile Behavior of Basalt Fiber Polypropylene Composite Rods for Passive Concrete Reinforcement // Polymers, 13, 3136, 2021. https://doi.org/10.3390/ polym13183136.
10. **Ray, B.C., Rathorea D. A** review on mechanical behavior of FRP composites at different loading speeds // Critical reviews in solid state and materials sciences. – 2015. – V. 40. – Pp. 119–135. DOI: 10.1080/10408436.2014.940443.
11. **Ocholaa R.O., Marcusa K., Nurickb G.N., Franzc T.** Mechanical behavior of glass and carbon fiber reinforced composites at varying strain rates // Composite Structures. – 2004. – V. 63. – Pp. 455–467.

12. **Tarek M.F.E.** Strength of prestressed bent beam elements reinforced with fiberglass reinforcement under the action of short-term dynamic loads [dissertation]. Moscow; 1992. (In Russian).
13. **Tu J., Hua X., Kui G.** Prediction of the Long-Term Performance and Durability of GFRP Bars under the Combined Effect of a Sustained Load and Severe Environments // Materials, 13, 2020. DOI: 10.3390/ma13102341.
14. **Kornev O., Kakusha V., Zhidkov Y., Lapshinov A., Mikhaldykin E.** Durability and structural evaluation of bridge girders prestressed with gfrp ties after 41 years of maintenance // 11th International Conference on Fiber-Reinforced Polymer (FRP) Composites in Civil Engineering (CICE 24-26 July 2023). https://doi.org/10.5281/zenodo.8161100.
15. GOST 32492-2024. Fibre-reinforced polymer bars for reinforcement of concrete structures. Methods for determining physical and mechanical characteristics, 2025 (In Russian).
16. ASTM D7337/D7337M-12. Standard Test Method for Tensile Creep Rupture of Fiber Reinforced Polymer Matrix Composite Bars, 2019.
17. ACI 440.3R. Guide Test Methods for Fiber-Reinforced Polymer (FRP) Composites for Reinforcing or Strengthening Concrete and Masonry Structures, 2012.
18. CAN/CSA S806-12 (R2017). Design and construction of building structures with fiber-reinforced polymers, 2017.
19. FIB Bulletin 40: FRP reinforcement in RC structures, 2007.

СПИСОК ЛИТЕРАТУРЫ

1. **Плевков В.С., Балдин И.В., Кудяков К.Л., Невский А.В.** Прочность и деформативность арматуры композитной полимерной при статическом и кратковременном динамическом растяжении, и сжатии // Вестник ТГАСУ. 2016. №5 (58).
2. **Плевков, В.С.** Прочность и трещино-стойкость изгибаемых фибробетонных элементов с преднапряженной стеклокомпозитной арматурой при статическом и кратковременном динамическом нагружении: монография / В.С. Плевков, А.Г. Тамразян, К.Л. Кудяков. –Томск: Изд-во Том. гос. архит.-строит. ун-та, 2021. – 204 с.
3. **Степанова, В.Ф.** Арматура композитная полимерная / В.Ф. Степанова, А.Ю. Степанов, Е.П. Жирков. – М. : АСВ, 2013. – 200 с.
4. **Степанова В.Ф., Бучкин А.В., Кудяков К.Л., Степанов А.Ю.** Арматура композитная полимерная и компо зитные полимерные изделия. Москва; 2023.
5. **Мамин А.Н., Хлебников С.К**. Использование композитной полимерной арматуры в бетонных конструкциях, подверженных динамическим воздействиям // Железобетонные конструкции. 2025. Т. 9. № 1. С. 26–34.
6. **Юрин Е.Ю., Бучкин А.В., Кудяков К.Л.** Влияние щелочных сред бетона на стеклокомпозитную арматуру при длительном действии нагрузки // Результаты научных и диссертационных исследований : Сборник тезисов докладов отчетной научно-технической сессии, Москва, 01–31 октября 2024 года. – Москва: Научно-исследовательский центр "Строительство", 2024. – С. 20-21.
7. **Rossini M., Saqan E., Nanni A.** Prediction of the creep rupture strength of GFRP bars // Construction and Building Materials, 227, 116620(1-11), 2019. DOI : 10.1016/j.conbuildmat.2019.08.001.
8. **Benmokrane B., Brown V., Khaled M., Nanni A., Rossini M., Shield C.** Creep-Rupture Limit for GFRP Bars Subjected to Sustained Loads // Journal of Composites for

Construction, 2019. 23. 06019001. 10.1061/(ASCE)CC.1943-5614.0000971.
9. **Tanks J., Naito K., Ueda H.** Characterization of the Static, Creep, and Fatigue Tensile Behavior of Basalt Fiber Polypropylene Composite Rods for Passive Concrete Reinforcement // Polymers, 13, 3136, 2021. https://doi.org/10.3390/ polym13183136.
10. **Ray, B.C., Rathorea D. A** review on mechanical behavior of FRP composites at different loading speeds // Critical reviews in solid state and materials sciences. – 2015. – V. 40. – Pp. 119–135. DOI: 10.1080/10408436.2014.940443.
11. **Ocholaa R.O., Marcusa K., Nurickb G.N., Franzc T.** Mechanical behavior of glass and carbon fiber reinforced composites at varying strain rates // Composite Structures. – 2004. – V. 63. – Pp. 455–467.
12. **Тарек М.Ф.Э.** Прочность преднапряженных изгибаемых балочных элементов, армированных стеклопластиковой арматурой, при действии кратковременных динамических нагрузок [диссертация]. Москва; 1992.
13. **Tu J., Hua X., Kui G.** Prediction of the Long-Term Performance and Durability of GFRP Bars under the Combined Effect of a Sustained Load and Severe Environments // Materials, 13, 2020. DOI: 10.3390/ma13102341.
14. **Kornev O., Kakusha V., Zhidkov Y., Lapshinov A., Mikhaldykin E.** Durability and structural evaluation of bridge girders prestressed with gfrp ties after 41 years of maintenance // 11th International Conference on Fiber-Reinforced Polymer (FRP) Composites in Civil Engineering (CICE 24-26 July 2023). https://doi.org/10.5281/zenodo.8161100.
15. ГОСТ 32492-2024 «Арматура композитная полимерная для армирования бетонных конструкций. Методы определения физико-механических характеристик», 2025.
16. ASTM D7337/D7337M-12. Standard Test Method for Tensile Creep Rupture of Fiber Reinforced Polymer Matrix Composite Bars, 2019.
17. ACI 440.3R. Guide Test Methods for Fiber-Reinforced Polymer (FRP) Composites for Reinforcing or Strengthening Concrete and Masonry Structures, 2012.
18. CAN/CSA S806-12 (R2017). Design and construction of building structures with fiber-reinforced polymers, 2017.
19. FIB Bulletin 40: FRP reinforcement in RC structures, 2007.

Evgeny Yurievich Yurin – Post graduate student, Senior Researcher, NIIZHB named after A.A. Gvozdev, JSC Research Center of Construction, 6, bld. 5, 2nd Institutskaya str., Moscow, 109428, Russia, max199107@bk.ru.

Sergey Konstantinovich Khlebnikov – Junior Researcher, NIIZHB named after A.A. Gvozdev, JSC Research Center of Construction, 6, bld. 5, 2nd Institutskaya str., Moscow, 109428, Russia; Post graduate student, National Research Moscow State University of Civil Engineering, 26, Yaroslavskoe Shosse, Moscow, 129337, Russia, s.xlebnikov@mail.ru.

Евгений Юрьевич Юрин – аспирант, старший научный сотрудник, Научно-исследовательский, проектно-конструкторский и технологический институт бетона и железобетона (НИИЖБ) им. А.А. Гвоздева АО «НИЦ «Строительство», д. 6, корп. 5, 2-я Институтская ул., г. Москва, 109428, Россия, max199107@bk.ru.

Сергей Константинович Хлебников – младший научный сотрудник, Научно-исследовательский, проектно-конструкторский и технологический институт бетона и железобетона (НИИЖБ) им. А.А. Гвоздева АО «НИЦ «Строительство», д. 6, корп. 5, 2-я Институтская ул., г. Москва, 109428, Россия; аспирант кафедры железобетонных и каменных конструкций. ФГБОУ ВО «Национальный исследовательский Московский государственный строительный университет» (НИУ МГСУ), д. 26, Ярославское шоссе, г. Москва, 129337, Россия, s.xlebnikov@mail.ru

Ulana Vladimirovna Kudyakova – Post graduate student, Structural Engineer, NIIZHB named after A.A. Gvozdev, JSC Research Center of Construction, 6, bld. 5, 2nd Institutskaya str., Moscow, 109428, Russia, ulyana.pankratyeva@mail.ru.

Ульяна Владимировна Кудякова – аспирант, инженер-конструктор, Научно-исследовательский, проектно-конструкторский и технологический институт бетона и железобетона (НИИЖБ) им. А.А. Гвоздева АО «НИЦ «Строительство», д. 6, корп. 5, 2-я Институтская ул., г. Москва, 109428, Россия, ulyana.pankratyeva@mail.ru.

Konstantin Lvovich Kudyakov – Candidate in Technical Sciences, Head of Department, NIIZHB named after A.A. Gvozdev, JSC Research Center of Construction, 6, bld. 5, 2nd Institutskaya str., Moscow, 109428, Russia; Associate Professor, National Research Moscow State University of Civil Engineering, 26, Yaroslavskoe Shosse, Moscow, 129337, Russia, konst_k@mail.ru.

Константин Львович Кудяков – кандидат технических наук, начальник отдела, Научно-исследовательский, проектно-конструкторский и технологический институт бетона и железобетона (НИИЖБ) им. А.А. Гвоздева АО «НИЦ «Строительство», д. 6, корп. 5, 2-я Институтская ул., г. Москва, 109428, Россия; доцент кафедры железобетонных и каменных конструкций. ФГБОУ ВО «Национальный исследовательский Московский государственный строительный университет» (НИУ МГСУ), д. 26, Ярославское шоссе, г. Москва, 129337, Россия, konst_k@mail.ru

Andrey Viktorovich Buchkin – Candidate of Technical Sciences, Deputy Director, NIIZHB named after A.A. Gvozdev, JSC Research Center of Construction, 6, bld. 5, 2nd Institutskaya str., Moscow, 109428, Russia, andibuch@inbox.ru.

Андрей Викторович Бучкин – кандидат технических наук, заместитель директора, Научно-исследовательский, проектно-конструкторский и технологический институт бетона и железобетона (НИИЖБ) им. А.А. Гвоздева АО «НИЦ «Строительство», д. 6, корп. 5, 2-я Институтская ул., г. Москва, 109428, Россия, andibuch@inbox.ru.

International Journal for Computational Civil and Structural Engineering, 21(4) 102–113 (2025)

DOI:10.22337/2587-9618-2025-21-4-102-113

NEW ALTERNATIVE APPROACH FOR THE ALGERIAN SEISMIC DESIGN CODE (RPA) OF RC BUILDING WITH SOFT FIRST STORY

Hamou Kada, Kheir Eddine Ramdane, Mabrouk Hamane

University of Science and Technology of Oran, Oran, ALGERIA

Abstract - Soft first story buildings, including Reinforced concrete frameworks, are particularly vulnerable during severe earthquakes, making them a critical concern in densely populated cities where such buildings are necessary. The Boumerdes earthquake stands out as one of Algeria's most devastating natural disasters in recent history due to the significant loss of buildings and lives. A notable observation from this earthquake was the collapse of many homes that had open retail spaces or parking areas on their first floors. Several factors contributed to the collapse of these soft first story buildings:

1. Insufficient Transversal Reinforcement: There was a lack of adequate transverse reinforcement in terms considering both of quantity and detailing.
2. More Flexible or Weaker First Story: The first story of these buildings was often more flexible or weaker compared to upper stories.
3. Absence of Shear Walls: The absence of shear walls compromised the lateral load resistance of buildings, especially those with open spaces on the first floor.

Due to the vulnerabilities highlighted by the Boumerdes earthquake, it is imperative to revise and strengthen the Algerian Earthquake-Resistant Design Code (RPA) It is vital to implement stricter guidelines, particularly regarding the construction of soft first-story buildings. These revisions should focus on improving the structural integrity and seismic resilience of such buildings to reduce future risks during earthquakes. By updating the seismic code with rigorous standards for the construction of soft first-story buildings, Algeria can enhance building safety and reduce the potential for catastrophic damage and loss of life in future seismic events.

The objective of this analytical study is to propose amendments to the Algerian seismic code to mitigate the collapse of soft first-story buildings during earthquakes. The study uses the energy constant law as its analytical framework.

In this research, the buildings of interest were modeled using the SAP2000 software. The Pushover analysis method was employed to analyze the seismic behavior of these structures.

Keywords: Soft story collapse, Algerian seismic design code (RPA), stiffness, story shear, drift, displacement, shear wall, natural time period, Pushover Analysis

НОВЫЙ АЛЬТЕРНАТИВНЫЙ ПОДХОД К ПРОЕКТИРОВАНИЮ СЕЙСМОСТОЙКИХ ЖЕЛЕЗОБЕТОННЫХ ЗДАНИЙ С ГИБКИМ ПЕРВЫМ ЭТАЖОМ ДЛЯ СТРОИТЕЛЬНЫХ НОРМ АЛЖИРА (RPA)

Хаму Када, Хейр Эддин Рамдан, Мабрук Хаман

Университет науки и технологии Орана, г. Оран, АЛЖИР

Аннотация. Здания с гибким первым этажом, включая выполненные в железобетонном каркасе, уязвимы при сильных землетрясениях. Обеспечение их сейсмостойкости является критически важной проблемой в густонаселенных городах, где в таких зданиях существует необходимость. Землетрясение в Бумерде является одним из самых разрушительных стихийных бедствий в новейшей истории Алжира из-за значительных разрушений зданий и числа пострадавших. В результате этого землетрясения было отмечено обрушение многих домов, на первых этажах которых находились открытые торговые площади

или парковочные зоны. Обрушению зданий с гибким первым этажом способствовали несколько факторов:
1. Недостаточное поперечное армирование: как с точки зрения расчетных, так и конструктивных требований было недостаточное количество поперечной арматуры.
2. Более гибкий или более слабый первый этаж: первый этаж этих зданий часто был более гибким или более слабым по сравнению с верхними этажами.
3. Отсутствие диафрагм жесткости: отсутствие диафрагм жесткости снижало сопротивление зданий горизонтальным нагрузкам, особенно для зданий с открытыми пространствами на первом этаже.
В связи с уязвимостями, выявленными в результате землетрясения в Бумерде, необходимо пересмотреть и усилить алжирский кодекс сейсмостойкого проектирования (RPA). Крайне важно внедрить более строгие правила, особенно в отношении строительства зданий с гибким первым этажом. Эти изменения должны быть направлены на улучшение структурной целостности и сейсмостойкости таких зданий, чтобы снизить риски в случае землетрясений в будущем. Обновление кодекса сейсмостойкого строительства, включение в него строгих требований для строительства зданий с гибким первым этажом, позволить повысить безопасность зданий и снизить вероятность катастрофических повреждений и гибели людей в случае землетрясений в Алжире в будущем.
Целью данного аналитического исследования является разработка предложений по актуализации положений алжирского кодекса сейсмостойкого строительства с целью предотвращения обрушения зданий с гибким первым этажом во время землетрясений. Аналитическое исследование базируется на использовании закона сохранения энергии.
В данном исследовании рассматриваемые здания были смоделированы с помощью программного обеспечения SAP2000. Для анализа сейсмостойкости конструкций был использован нелинейный статический расчет (Pushover-анализ).

Ключевые слова: обрушение гибких этажей, алжирский кодекс сейсмостойкого строительства (RPA), жесткость, сдвиг этажа, смещение, перемещение, диафрагма жесткости, период собственных колебаний, Pushover-анализ

1. INTRODUCTION

On May 21, 2003, a magnitude 6.8 earthquake hit the Zemmouri region, located approximately 70 kilometers east of Algiers. With a focal depth of roughly 10 km, it was the strongest earthquake in Algeria since 1980, causing widespread destruction. Over 2,200 people lost their lives and more than 11,000 were injured, largely due to the collapse of residential and public buildings. This disaster revealed critical shortcomings in seismic design and highlighted the need to update and enforce Algeria's building codes.

The main structural issues observed in reinforced concrete (RC) buildings are summarized below:

1. Soft First Story Effects: This occurs when the ground floor is less stiff compared to the upper floors, making it more susceptible to collapse during an earthquake.
2. Short Column Effects: Short columns experience higher shear forces, which can lead to failure if not properly designed.
3. Use of Weak and Slender Columns Poorly Reinforced (Generally Unconfined): Columns that are not adequately reinforced or are too slender can buckle and fail under load.
4. Poor Detailing of Structural Joints: Improperly designed connections between beams and columns can weaken the overall structure.
5. Inadequate Transverse Reinforcing Steel Detailing (Tie Spacing and 90-Degree Hook): Insufficient detailing of ties (spacing and hooks) can lead to poor confinement and shear resistance.
6. Poor Material Quality and Unsound Construction Practices: The use of substandard materials and inadequate construction methods can significantly compromise the strength and durability of a structure.
7. Neglect of Lateral Loads in Design: Failure to account for lateral forces, including seismic and wind actions, may result in inadequate structural performance and potential collapse under dynamic loading.

8. Inappropriate Anchoring of eam and Slab Reinforcement: Improper anchoring can lead to weak connections and potential failure points.
9. Use of Irregular uilding Configurations with Discontinuities in Mass, Strength, Stiffness and Ductility: Irregularities in the building s design can create stress concentrations and weak points.
10. Use of Weak Materials for Facades: Weak facade materials can fail and contribute to overall structural failure.
11. Use of Stiff Spandrel Masonry Walls Resulted in Short Captive Columns that Increased the Shear Demand eyond the Shear Capacity Supplied: Stiff walls can create captive columns that are subjected to higher shear forces than they can handle, leading to failure.

These issues highlight the importance of proper design, detailing, material selection, and construction practices to ensure structural safety and resilience of RC buildings.

The field investigation revealed that the collapse of soft first-story buildings was notably prevalent during the oumerdes earthquake, as illustrated in Figure 1.

This category of damage was even more severe during the 1995 obe Earthquake is shown in figure 2 and table 1. Therefore, the, the Japanese Seismic Design Guidelines recommended a design procedure to prevent the column side-sway mechanism, or soft first-story collapse 1, 2-3 .

Such structural deficiencies primarily result from sudden variations in stiffness, strength, or ductility, combined with the lack of shear walls in the lower stories. Their detrimental impact is amplified by poor mass distribution within the structure.

Consequently, multistory reinforced concrete commercial and residential buildings with insufficient or absent lateral resistance at the first story represent one of the most vulnerable structural types.

his study introduces a procedure for determining the failure modes of buildings exhibiting a soft first story, derived from the failure mechanisms of columns and walls at that level. Subsequently, a strength amplification factor, denoted as α, is formulated according to the energy conservation principle to represent the additional capacity required at the soft story for its ductility factor to be equivalent to that of a total collapse mechanism 6, 8 9 .



Figure 1. Soft first story collapses during Boumerdes Earthquake, Algeria 2003. [1-4]



Figure 2. Chuo-ku, Kumamoto city, Japan [5]

Table 1. Damage observation in chuo-ku Earthquake [5]

Damage Type	Soft story Failure	Shear damage to columns	Ground deformation	Moderate to severe damage	minor to moderate damage	Total
Number of buildings	8	4	3	4	3	22

2. METHODS

Following the damage caused by the presence of flexible floors in buildings during the 1995 obe earthquake, Japanese researchers

l e e ee o m o e se sm es o es o ess s e ome o

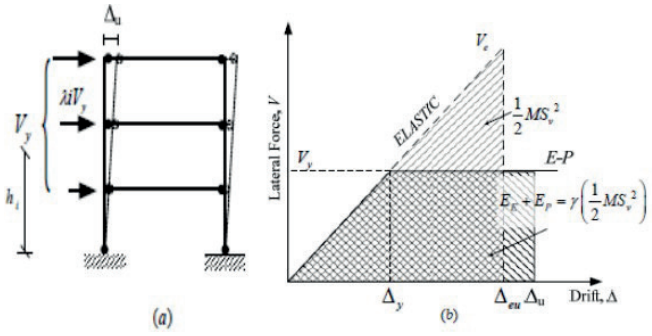


Figure 3. Energy method concept

u e llus es e e l e lo e o m o e o o e s s em e o e e el o s o s s s em e o mul e s

e $\gamma \frac{1}{2}.M.S_v^2) \frac{1}{2}\gamma \frac{T}{2\pi}$ 2 1

e l s e e o l s e e o seu o elo seu o ele o e o e e e u o e e s ollo s

$$\frac{1}{2}\left(\frac{W}{g}\right)\left(\frac{T}{2.\pi}.\frac{V_y}{W}.g\right)^2 V_y\left(\sum_{i=1}^{N}\lambda_i.h_i\right)\theta_p \frac{1}{2}\gamma\left(\frac{W}{g}\right)\left(\frac{T}{2\pi}.S_a.g\right)^2 \quad 2$$

u e 4 llus es e el o s e ee s e e o m o o s le e ee o ee om s s em

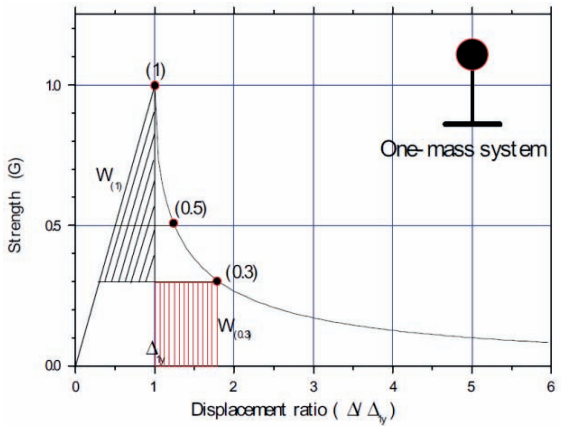


Figure 4. Energy constant law [2][8]

Figure 4 illustrates the idealized indices DS′ s so s o e oll se e ssum el s o l s mo el e l se s ess o o u l s, e o DS′/DS satisfying μ = μ′ is given by Equ o

α s /Ds

e o l s ess o e oll se s s em s o s e e eu l o o e so s o u l , s s o u e e el o s s e e u o 4

$$\frac{\theta_y'}{\theta_y} = \frac{D_s'}{D_s} \quad 4$$

e u l s u e es o e e mo ele us e 2000 so e, e us o e l s s me o s l e e s u u es e e su e e o eme l lo s u e lo e e , e esul el s lo s l eme u e s o e o oll o s l eme o e s u u e, s llus e u e 5 10 1

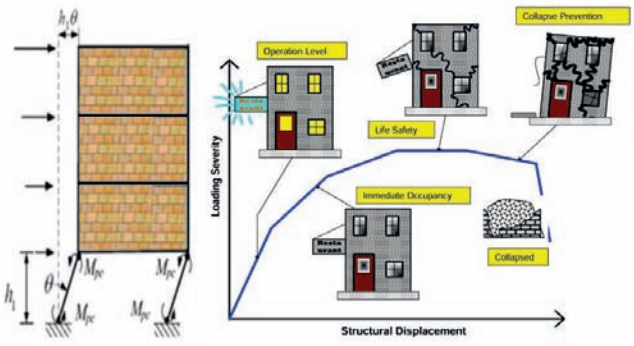


Figure 5. Different loading steps structural response levels [14][15]

C

ee e o e o ee u l s 5 se 1 , se 2 , 12 se s s o e s e l e o ssess e m o e so s o o u o o e s u u es o l e se sm es o se

D

The dimensions and reinforcement of the structural elements (beams, columns, etc.) used in our case study are presented in Figure 6.

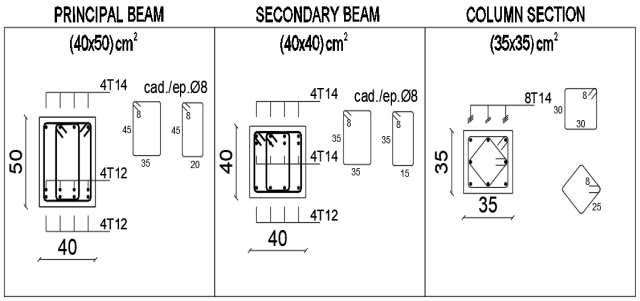


Figure . eams and column reinforcement

D

The loads are distributed in a triangular form, expressed by the following equation:

$$Q_i \quad {}_h.W_i.h_i^2/\sum w_i.h_i^2 \qquad (5)$$

a le 2. oad cases

Name	Dead	Live	Eqx	Eqy	PSHx	PSHy
Type	Linear static	Linear static	Linear static	Linear static	Lateral Load	Lateral Load

Model Analysis:

The numerical model developed using the software is shown in Figure 7.

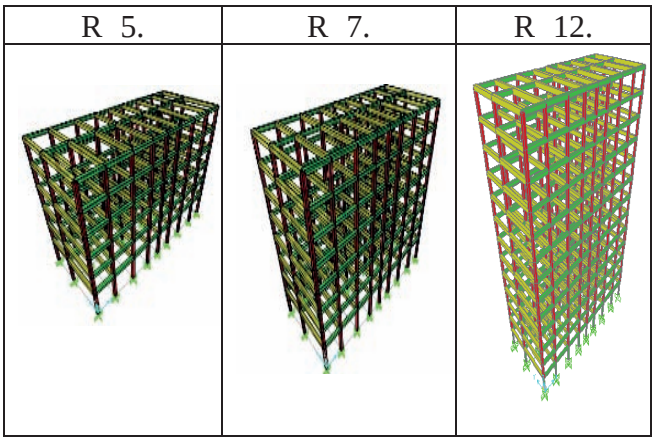


Figure . uilding model in 2 [11 12]

The fragility curve was obtained from the analysis of the numerical model, as illustrated in Figure 8.

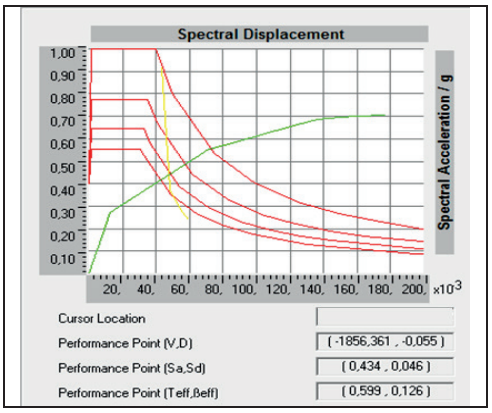
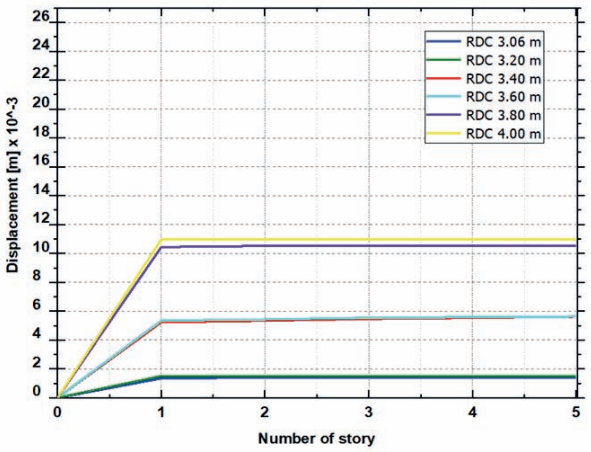


Figure 8. ushover curve for 5 uilding

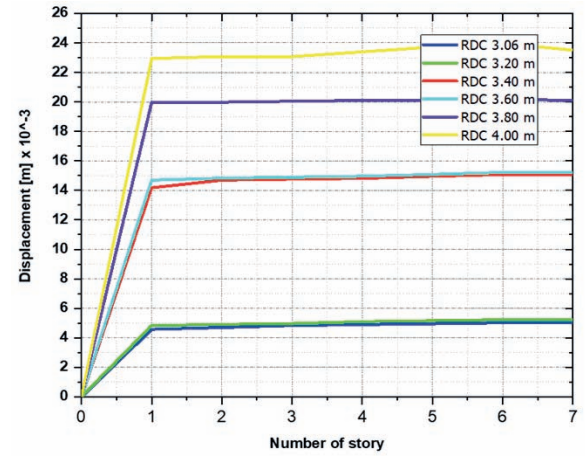
The performance point is defined by the structure s capacity to respond to applied forces and sustain stability under those forces, identified at the intersection of the base shear and displacement. 13 14 15 16 .

The R 7 building with a 4 m ground-floor height exhibits more significant damage, demonstrating that the severity of damage is directly affected by the first-story height: the taller the first story, the greater the damage.

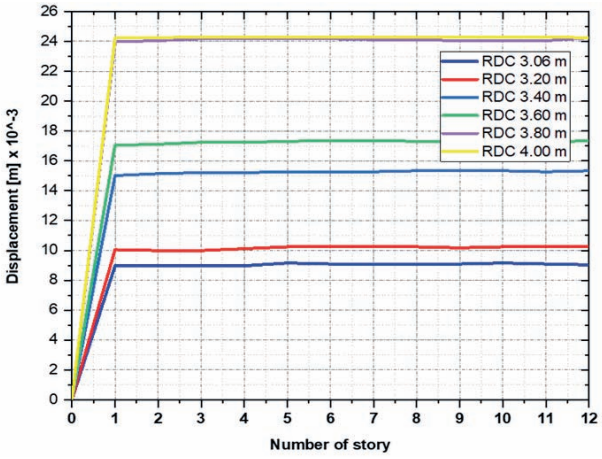
It is reported that the damage plastic hinges are concentrated at the first story (ground floor), highlighting the structural weakness of this level in all three models.



Ground Floor 5



ou loo



ou loo 12

Figure 9. Inter-story displacement

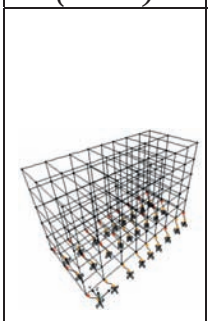
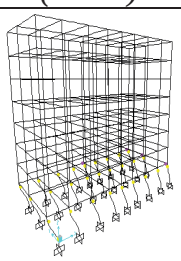
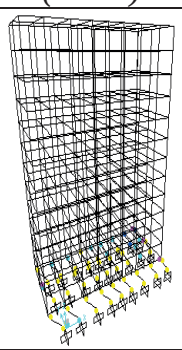
GF+5. (h=4m)	*GF+7. (h=4m)*	*GF+12. (h=4m)*
		

Figure 10. Development of plastic hinges

e e e e o s l eme em e ee s u u es ou so s o e ses o o 4 u e lo se sm , 12 u e mo e e se sm , u o 2 u e se sm

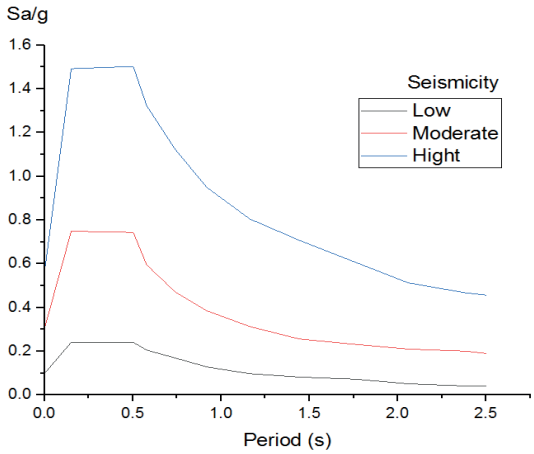


Figure11. Seismicity level

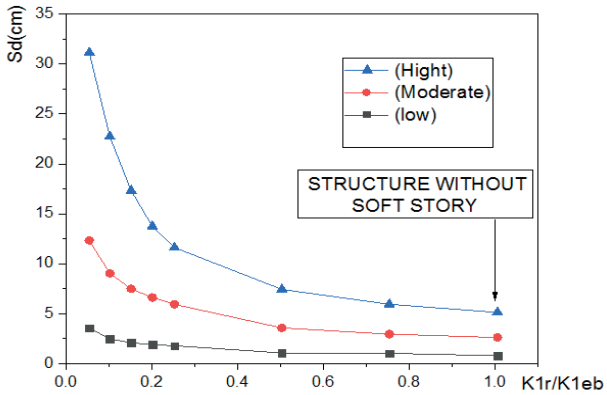


Figure 12. Lateral stiffness displacement in the story

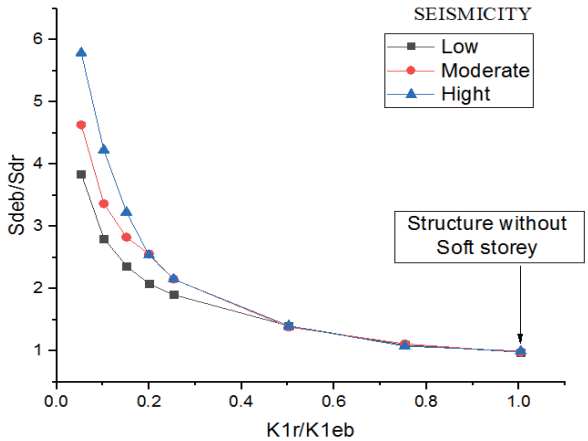


Figure 13. Lateral stiffness by increment request in the story

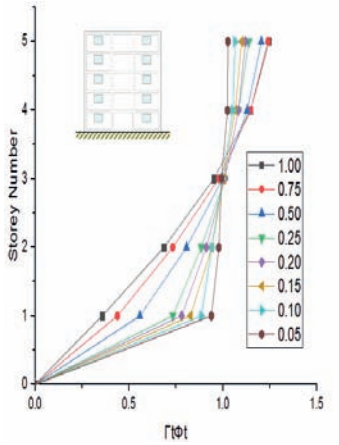


Figure 14. ateral stiffness of regular stories

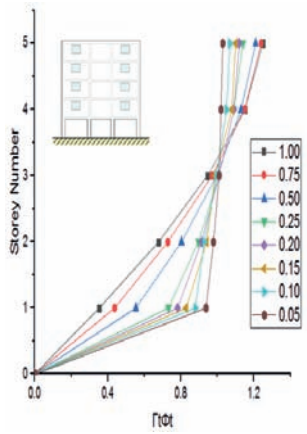


Figure 15. ateral stiffness in the irregular story

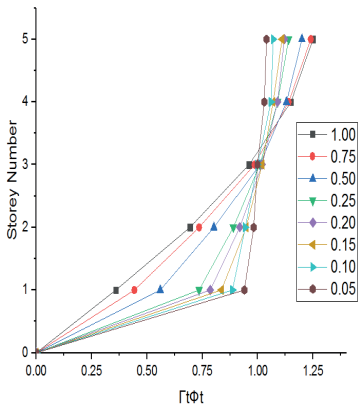


Figure 1 . ateral stiffness soft unsoft story uilding

At the soft-story level, displacement can reach up to 25 of the building's total roof drift. However, in structures characterized by a pronounced soft-story mechanism, the first-story displacement may rise dramatically, reaching 80 90 of the total top displacement. For an equivalent seismic demand, the displacement at the first story of a soft-story building can increase by a factor of two to three compared to a regular structure. This demonstrates the considerable sensitivity of soft-story configurations to lateral deformations.

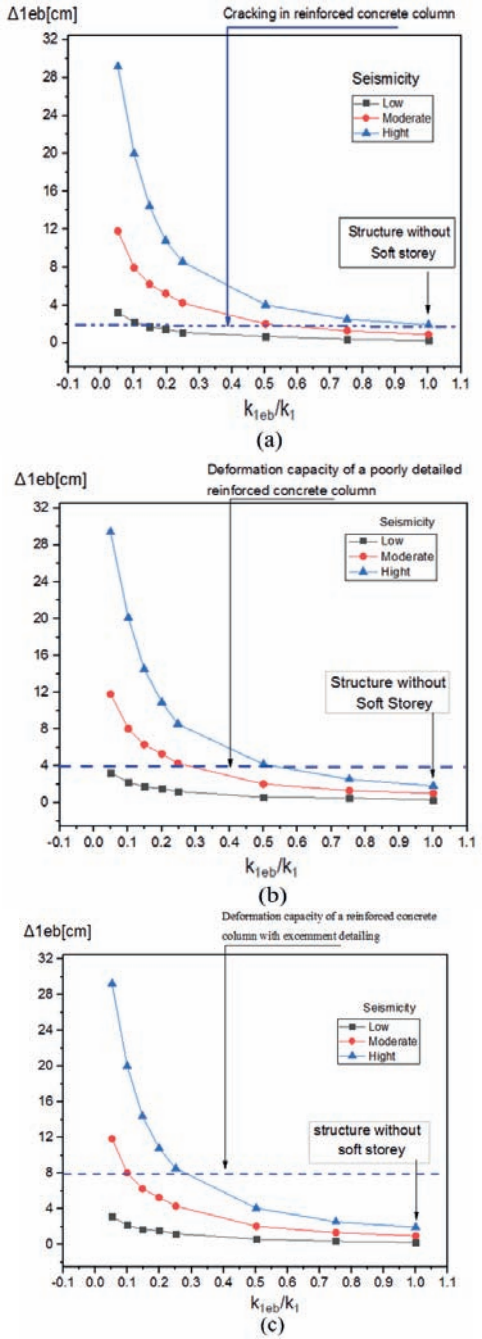


Figure 1 . ateral stiffness with reinforced concrete column

e e ance value of a crack (Δ1e
e o e o e e olum , s o lue, s
lo e o e ul u l s ou so
s o om e o o e ul so s o
u l
om e o se o o e e e e
s l eme e l e ee le le loo
u l o e ul o le le loo
u l e ul

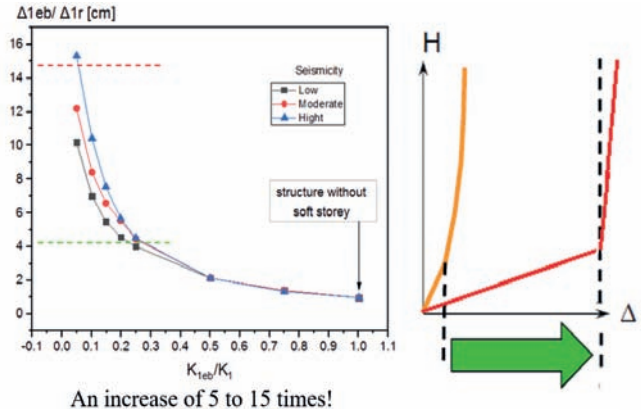
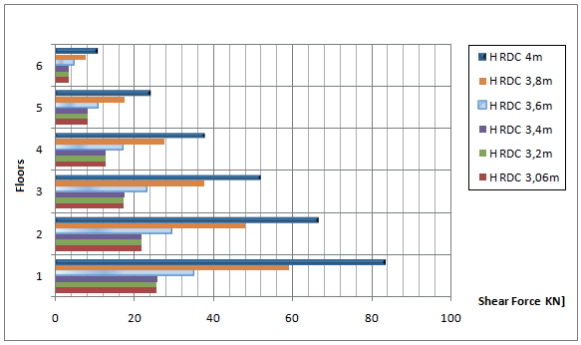
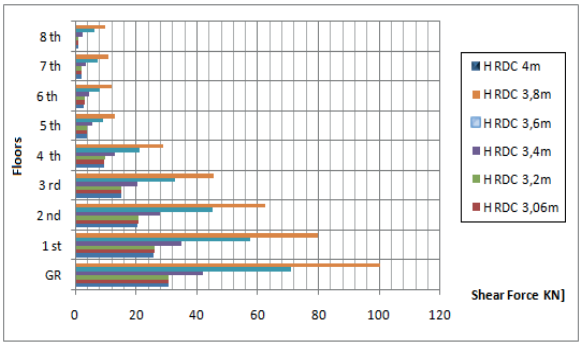


Figure 1 . First floor lateral displacement demand

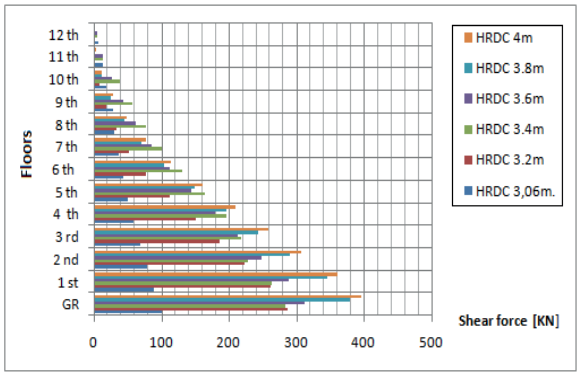
ese e s e e e m e o u
s u es o l s s om so s esse l
o u el u s ssue
u e 1 llus es e o o s e
o es oss e e le els s u o o
e ou loo e
e o e em s o ou s o olum s
e mu e u l s s so
s o e
The characteristic factor Ds′ te s o se s
u l e e ses o e s u u e,
e e e e s o oss ous
se sm o es s ou 5



5 s o



s o



12 s o

Figure 19. omparison of base shear for +5 +7 and +12 storied buildings for different height Ground Floor

able 3. Structural characteristic factor Ds

Code	R+5	R+7	R+12
Japanese	0 5	0 55	0 5
Euro	0 55	0 5	0
RPA	0	0	0 5 0

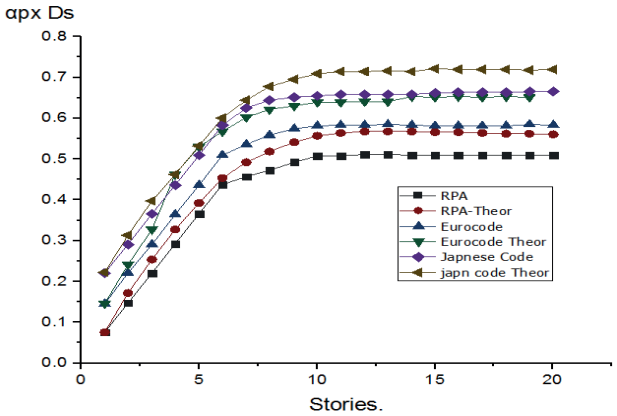


Figure 1 . tructural characteristic factor for uildings with 5 and 12 stories

. CONC U ION

The May 2003 oumerd s earthquake caused significant damage, much of which experts found could have been prevented. This prompted authorities to devise comprehensive prevention plans, especially in major cities like Algiers, Oran, and Constantine, where earthquake risks are high. The adage prevention is better than cure highlights this need.

- Minor damages were observed in the structural elements, particularly on the first soft story. This is attributed to the discontinuity of the frame s mass, as well as its strength, stiffness, and ductility.
- Nonlinear analyses revealed a required lateral load factor (αp×Ds) of 0.50 for 6-story buildings, increasing to 0.55 for 10 stories and 0.60 for 14 or more, according to the Japanese code. For the Eurocode, the factors are 0.60, 0.65, and 0.70 for the RPA code, they are 0.65, 0.70, and 0.75, respectively.
- The nonlinear analysis yields a required lateral load factor of 0.50 for 6-story buildings, increasing to 0.55 for 10 stories and 0.60 for 14 or more. In comparison, the Eurocode specifies 0.60, 0.65, and 0.70, while the RPA code specifies 0.65, 0.70, and 0.75.
- Eurocode 8 and the Japanese code permit larger relative drift displacements than the RPA 99 code (2003 version), due to the higher local ductility levels specified in these codes.
- The RPA code specifies a behavior coefficient RRR that indicates the capacity of dissipative structural systems to endure seismic actions in the inelastic domain (see Table 4.3, Chapter I , p. 39). This coefficient requires that lateral rigidity does not exceed 70 of the rigidity of the story above (Appendix 1, p. 111). However, the code lacks details on how to obtain this coefficient or its applicability to existing buildings versus new designs with a soft first story.
- Calculating earthquake forces for reinforced concrete (RC) buildings with an open ground floor often underestimates the design forces and moments for ground floor columns. Analyses show that base shear can exceed twice the amount predicted by the equivalent force method, whether or not infill is present. Since the response spectrum method is rarely used in practice, it is advisable to double the design shear and moment from the static method to ensure ground floor column safety.
- uildings with open ground floors are particularly vulnerable to seismic actions, especially in developing countries where this construction type is common. The results of this study demonstrate that such buildings should not be treated as conventional reinforced concrete (RC) structures. The sway analysis reveals that columns at the open ground floor level require approximately 75 greater drift capacity than that estimated by the equivalent static method. To accommodate these high ductility demands, special reinforcement detailing designed in accordance with moment-resisting frame principles is essential.

A deeper understanding of this phenomenon is crucial, as it should be identified as a localized issue before it progresses into a broader structural problem.

AC E E E

e u os e ull o le e esu o
o e u es e lu le u e
e ou eme o e e
su e so o su e so ou ou s
ese e e o o e m us

RE ERE CE

1 e o o e oume es u e, ese e o ss e e m e m e e e e m s o , ss e o es e e e e o e s o o e l e u e o e 21s 200 I , , 10 , o e 2004
2 Ra dane e r edd ne e a , m es use oume es u e e omme o s o e sm o l e , I e o l m os um o e sm s e u o , 2 2 l 200 , u es , om
a rou a ane and e r Edd ne Ra dane e a , m e use e oume es u e e omme o s o e u e sm s , o l m os um, ole e le s, s, ul 4 , 200
4 or A C , 200 m ss o e o , m o e , oume es e u e, u e , 200
5 n o os da, u e o l 1 , 201 um mo o, , o l se o o el um e smolo me unsu e an , u e es s es o e o e o e e u l s, ou l o e o e e e olo Vol 2, o 1, 24, e u 2004
J. Prakashvel, C. UmaRani, K. Muthumani, N. Gopalakrishnan u e es o se o e o e o e e me e ou o , o I e o l ou l o I us l ee eme e e, Vol 2, o 4, e em e 2012
e r Edd ne RA A E e a u l e s e es o , 1 ume l s mul o s o s u o e s e es o , 2 e u l ee o e e u l I s u e o , o , e em e 200
e r **Eddine RAMDANE et al.** o l e ume l l ses o m o e e se sm es me o o so s s o u l , 1 V ou e , , u us 2004
10 **Kim, S. and D'Amore, E.** 1 us o e l ss o e u e e u e e ee e , 15 41 4 4
11 11 AP2 o m e e u u l l o o m om u e s u u e I I , l o ,
12 **Hamou Kada, Ramdane Kheir Eddine**, e l , ul 4 , 200 , I e s u u l e lls, us e e o , o l m os um 200 , ole e le s
1 **Hamou Kada, Ramdane Kheir Eddine**, e l , ul 4 , 200 , s l s e l u e s e us e e o , o l m os um 200 , ole e le s
14 A C, 1 e sm lu o e o o o e e u l s, Volume 1, 40 e o , l e e olo ou l, e oo , l o
15 E A, 1 u el es o e e sm e l o o u l s e elo e e u l e sm e ou l e olo ou l, o e e e l me e eme e e o o 2 , s o ,
1 o m u l o e u u l ee es o s o , Volume 2 I e o l o e e e o u l ls, 1
1 l e s sm o e e s o 2024 , ese o l e e l e s sm e us m, s , o e u ,

Earthquake Engineering for Tall uildings, August 2021.

СПИСОК ЛИТЕРАТУРЫ

1. Report on the oumerdes Earthquake, Japanese Reconnaissance Team Edited by Ramdane heir eddine and Hamada Masanori, assigned to investigate the effect of the catastrophic Northern Algeria Earthquake of the 21st May 2003 by JICA, Japan, pp.107, October 2004.
2. **R** , Damages Caused by oumerdes Earthquake and Recommendations for Seismic Mitigation in Algeria , International Symposium on Seismic Risk Reduction, 26-27 April 2007, ucharest, Romania.
3. **R** ., Damage Caused by the oumerdes Earthquake and Recommendations for Reducing Seismic Risk, 7th National AFPS Symposium, Ecole Centrale Paris, Paris, July 4-6, 2007.
4. **D IDO ICI**, AFPS 2003 mission report, Dynamic concept, oumerdes earthquake, June 8, 2003.
5. , Earthquake of April 16, 2016- umamoto, Japan, Royal Observatory of elgium-Seismology-Gravimetry.
6. **O** , Earthquake Resistant Design of Reinforced Concrete uildings, Journal of Advanced Concrete Technology ol. 2, No. 1, 3-24, February 2004.
7. **J. Prakashvel, C. UmaRani, K. Muthumani, N. Gopalakrishnan** Earthquake Response of Reinforced Concrete Frame with Open Ground Story , onfring International Journal of Industrial Engineering and Management Science, ol. 2, No. 4, December 2012.
8. **R D N** . Outline and strength increasing factor , Part 1 and Numerical simulations to study on the strength increasing factor , Part 2. The Annual Meeting of the Architectural Institute of Japan, Nagoya, September 2003.
9. **Eddine RAMDANE et al.** Non-linear numerical analyses to improve the seismic design method for soft first story RC uilding , 13WCEE in ancouver, Canada, August 2004.
10. **Kim, S. and D'Amore, E.** (1999). Pushover analysis procedure in earthquake engineering. Spectra, 15:417-434.
11. Program-Extended Structural Application Program Computer and structure Inc (CSI), California, USA.
12. **Hamou Kada, Ramdane Kheir Eddine**, Chatenay Malabry, July 4-6, 2007, Increasing Structural Capacity by Adding Shear Walls, Push-Over Method, 7th National AFPS Symposium 2007, Ecole Centrale Paris.
13. **Hamou Kada, R** , Chatenay Malabry, July 4-6, 2007, Establishing the Fragility Curve Using the Push-Over Method, 7th National AFPS Symposium 2007, Ecole Centrale Paris.
14. **TC**, 1996 Seismic Evaluation and Retrofit of Concrete uildings, olume 1, ATC-40 Report, Applied Technology Council, Redwood City, California.
15. , 1997 NEHRP Guidelines for the Seismic Rehabilitation of uildings Developed by the uilding Seismic Safety Council Technology Council, for the Federal Emergency Management Agency (Report No. FEMA273), Washington, D.C.
16. Uniform uilding Code U C 97Structural Engineering Design Provision, olume 2. International Conference of uilding Officials, USA 1997.
17. Algerian parasismic code (RPA version 2024), research national Center Applied in Parasismic Genius. Dr. Fawad A. Najam, Pakistan, Prof. Dr. Pennung Warnitchai, Earthquake Engineering for Tall uildings, August 2021.

Hamou Kada , e l, e me l ee , ul o e u e l ee , e s o e es e olo o , l ou , 1505, l 1000, , l e m l mou m l om

Kheir Eddine Ramdane o esso , ul o e u e l ee , e s o e es e olo o , l ou , 1505, l 1000, , l e m l e e oo

Mabrouk Hamane o esso , ul o e u e l ee , e s o e es e olo o , l ou , 1505, l 1000, , l e m l me ou m e u us o

Хаму Када кандидат технических наук, факультета архитектуры и гражданского строительства, Университет науки и технологии Орана, Эль Мнауар, 1505, Бир эль Джир, 1000, Оран, Алжир. m l mou m l om

Хейр Эддин Рамдан профессор, факультета архитектуры и гражданского строительства, Университет науки и технологии Орана, Эль Мнауар, 1505, Бир эль Джир, 1000, Оран, Алжир. m l e e oo

Мабрук Хаман профессор, факультета архитектуры и гражданского строительства, Университет науки и технологии Орана, Эль Мнауар, 1505, Бир эль Джир, 1000, Оран, Алжир. m l me ou m e u us o

DOI:10.22337/2587-9618-2025-21-4-114-129

PREDICTION OF GROUND SUBSIDENCE BY MODELING TUNNEL BORING MACHINE TECHNOLOGY

Armen Z. Ter-Martirosyan [1], Ilya O. Isaev [2], Evgenii N. Kriuchkov [1], Maksim N. Shlapak [1]

[1] National Research Moscow State Civil Engineering University, Moscow, RUSSIA
[2] Institute Mosinzhproekt Limited Liability Company, Moscow, RUSSIA

Abstract: Tunneling using tunnel boring machines (TBMs) induces ground settlement, leading to deformations in buildings and structures located within the zone of influence of the planned construction. Settlement prediction based on volume loss is one of the established practices in Russia; however, this method relies on construction experience and does not directly account for the primary technological parameters affecting soil settlement. In some cases, to obtain accurate deformation predictions using this method, it is necessary to perform a back-calculation of volume loss, considering the tunnel section already excavated. This study examines the modeling of all technological factors involved in TBM tunneling for forecasting settlement resulting from metro tunnel construction. A division of the TBM excavation process into sequential phases is introduced for finite element analysis. Two calculation schemes were formulated for different sections of the Rublyovo–Arkhangelskaya line of the Moscow Metro, in two variants: (1) using volume loss, and (2) accounting for all technological factors. In the latter variant, parameters such as shield face pressure, grout injection pressure, TBM weight, structural stiffness of the TBM, shield tail gap, and others were incorporated. Displacement plots for adjacent buildings were generated from the resulting calculations and compared with measured displacements. A comparative analysis between the volume loss method and the alternative comprehensive technological-factor method was conducted. The comprehensive method demonstrated a high degree of quantitative and qualitative agreement with measured values and allows assessment of the soil's mechanical behavior over time during TBM excavation.

Keywords: TBM, volume loss, face pressure, grouting pressure, subsidence, FEA, tunneling, Plaxis 3D

ПРОГНОЗ ОСАДКИ ЗЕМНОЙ ПОВЕРХНОСТИ ПРИ МОДЕЛИРОВАНИИ ТЕХНОЛОГИИ ПРОХОДКИ ТОННЕЛЯ МЕХАНИЗИРОВАННЫМ КОМПЛЕКСОМ

А.З. Тер-Мартиросян [1], И.О. Исаев [2], Е.Н. Крючков [1], М.Н. Шлапак [1]

[1] Национальный исследовательский Московский государственный строительный университет, г. Москва, РОССИЯ
[2] Институт Мосинжпроект, г. Москва, РОССИЯ

Аннотация: Проходка тоннелей при помощи тоннелепроходческих механизированных комплексов (ТПМК) вызывает осадку поверхности, что приводит к деформациям зданий и сооружений, находящихся в зоне влияния проектируемого строительства. Прогноз осадок с использованием коэффициента перебора является одним из устоявшихся в российской практике, однако этот метод основан на опыте строительства и не учитывает напрямую основные технологические параметры, влияющие на осадку грунта. В ряде случаев для получения корректных деформаций этим методом необходимо делать обратный пересчет коэффициента перебора с учетом уже пройденного участка трассы. В представленном исследовании рассматривается моделирование всех технологических факторов проходки ТПМК для прогноза осадки от строительства тоннелей метрополитена. Предложено разбиение на этапы проходки ТПМК для моделирования МКЭ. Разработаны 2 расчетные схемы разных участков Рублево-Архангельской линии Московского метрополитена в двух вариантах: с использованием коэффициента перебора, с учетом всех технологических факторов. При моделировании альтернативным методом учитывались такие технологические параметры как: давление пригруза, давление нагнетания, вес ТПМК, жесткость конструкций ТПМК, кольцевой зазор и др. В результате расчета построены графики перемещений зданий окружающей застройки. Произведен анализ полученных результатов и их

сравнение со значениями фактических перемещений. Проведено сравнение расчета с использованием коэффициента перебора и альтернативного метода расчета. Предложенный альтернативный метод расчета показывает высокую количественную и качественную сходимость с фактическими значениями, а также позволяет оценить механику поведения грунта при проходке ТПМК во времени.

Ключевые слова: ТПМК, коэффициент перебора, давление пригруза, давление нагнетания, осадка, МКЭ, тоннелирование, Plaxis 3D

1. INTRODUCTION

Tunnel boring machine (TBM) is a high-technology equipment used for the construction of underground tunnels. It was first employed in 1825 during the excavation of the Thames Tunnel in London, marking a major milestone in the history of tunneling. Today, TBMs are widely used for the construction of metro lines, road tunnels, water supply conduits, and other underground structures, especially in densely populated urban areas where usual excavation methods may be impractical. In international practice, TBMs with active face support have been successfully applied in challenging geological conditions for tunnel construction [1–2].

Despite their advantages, tunnel excavation using TBMs involves certain risks and adverse consequences. One of these consequences is the movement of the ground mass [1], which depends not only on the geotechnical conditions of the excavation site but also on the operational parameters of the shield-driven excavation [3]. These settlements can lead to deformations and damage of buildings, structures, and infrastructure located above or adjacent to the tunnel [4–6]. This factor necessitates rigorous monitoring to minimize environmental impact and ensure safety. Surface settlements induced by tunnel excavation has been investigated by numerous foreign researchers, including R. B. Peck [7], N. Loganathan [8], M. O'Reilly and B. New [9], P. B. Attewell [10], and many others. Among domestic scholars, notable contributions have been made by Protosenya A.G. [11], Tupikov M.M. [12], Mazein S.V. [13], and others.

To minimize these risks and ensure construction safety, monitoring of ground surface settlement is employed. This method involves observing soil movements and deformations of buildings within the TBM tunneling influence zone. Geotechnical monitoring encompasses visual and instrumental inspections as well as automated systems that collect real-time data. Monitoring enables timely detection of critical changes such as cracks, tilts, or excess settlement and the implementation of corrective measures to prevent emergency situations [14–16].

To assess potential displacements of the soil mass and surface structures within the projected construction influence zone geotechnical calculations are used.

In practice, ground surface settlement due to TBM excavation is calculated using the volume loss, defined as the ratio of the excavation cross-section to the designed lining cross-section according to SP 249.1325800.2016 "Underground utilities. Design and construction by closed and cut-and-cover methods". It should be noted that this standard applies to trenchless installation of utilities by microtunnel boring machine (MTBM) and horizontal directional drilling (HDD) machine and does not directly cover metro tunneling with TBMs, it is used in the absence of more specific regulations. This approach represents an established practice in Russia and has been described by domestic authors such as Ter-Martirosyan A.Z., Isaev I.O., et al. [17–20], Isaev O.N., Sharafutdinov R.F. [21], and others. Despite its widespread use, the volume loss is grounded in construction experience rather than the physical processes driving soil settlement [1]. It permits determination of settlement on the moment of tunnel completion, and finite-element modeling based on this ratio is further complicated by the lack of a regulated methodology for defining the boundaries of the calculation model – parameter that can significantly affect the accuracy of results [22].

Ground settlement induced by TBM-driven excavation is caused by factors such as shield

tail gap, taper of shield, and backfill shrinkage [23]. In addition, parameters influencing settlement include excavation gradient, tunnel overburden depth, face pressure and grouting pressure [24]. In the study by H. Liu, J. Shi, J. Li, and C. Liu [25], a method was presented for calculating surface settlement that accounts for various technological parameters: face pressure, grouting pressure, shield dimensions, shield tail gap, changes in shield alignment, and hardening of the cement slurry in the annular space behind lining.

The aim of the present work is to establish an optimal methodology for predicting surface settlement induced by TBM excavation, as well as to evaluate an alternative calculation approach that omits the volume loss while incorporating all technological factors affecting settlement, or to refine the existing limits of the volume loss for given excavation conditions.

2. MATERIALS AND METHODS

The article models several TBM tunneling cases along different sections of the Rublyovo-Arkhangelskaya line of the Moscow Metro: from *Bulvar Karbysheva* station to *Zhivopisnaya* station, and from *Zvenigorodskaya* station to *Karamyshevskaya* station.

For the alignment section considered in the first case, the geological structure is as follows: anthropogenic soils (tQIV); alluvial deposits of the 3rd (Khodynka) terrace above the floodplain of the Moscow River (aQIII); fluvioglacial deposits of the Oka-Dnieper horizon (fQII O-D). Beneath these lie Carboniferous rocks of the upper part of the Kasimovian stage: Upper Carboniferous deposits of the Voskresensk subformation (C3vs), and Upper Carboniferous deposits of the Suvorovo subformation (C3sv), represented by fractured limestones degraded to boulders, gravel, and rubble, as well as stiff clays.

For the alignment section in the second case, the geological profile is as follows: anthropogenic soils (t–QIV), alluvial deposits of the 3rd terrace above the floodplain of the Moscow River (a–QIII), moraine deposits of the Dnieper glaciation (g-QIId), fluvioglacial deposits of the Oka–Dnieper horizon (f–QIIo-d), Oxfordian deposits of the upper part of the Jurassic system (J3ox), Bathonian–Callovian deposits of the upper and middle parts of the Jurassic system (J2+3bt–k), Voskresensk subformation (C3vs), and Suvorovo subformation (C3sv) of the upper Carboniferous system.

Geological profiles along the proposed tunnel alignments are shown in Fig. 1 and Fig. 2.

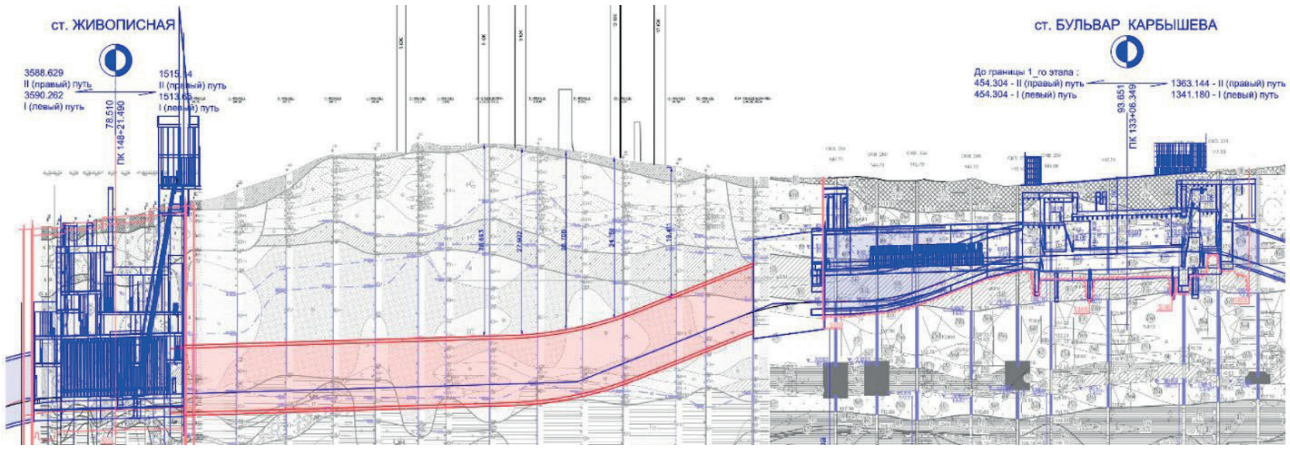


Figure 1. Longitudinal profile of the section from Bulvar Karbysheva station to Zhivopisnaya station

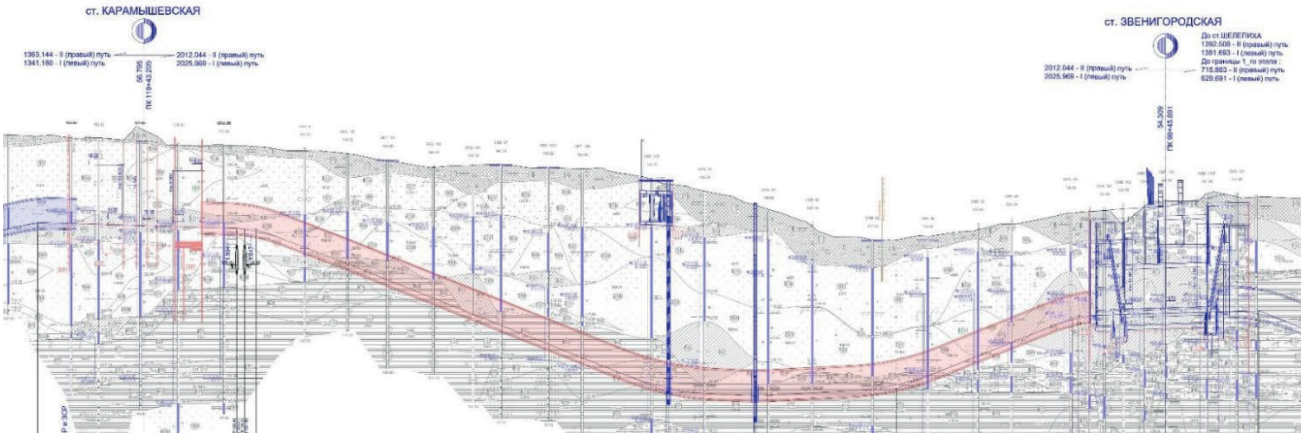


Figure 2. Longitudinal profile of the section from Zvenigorodskaya station to Karamyshevskaya station

Finite Element Model

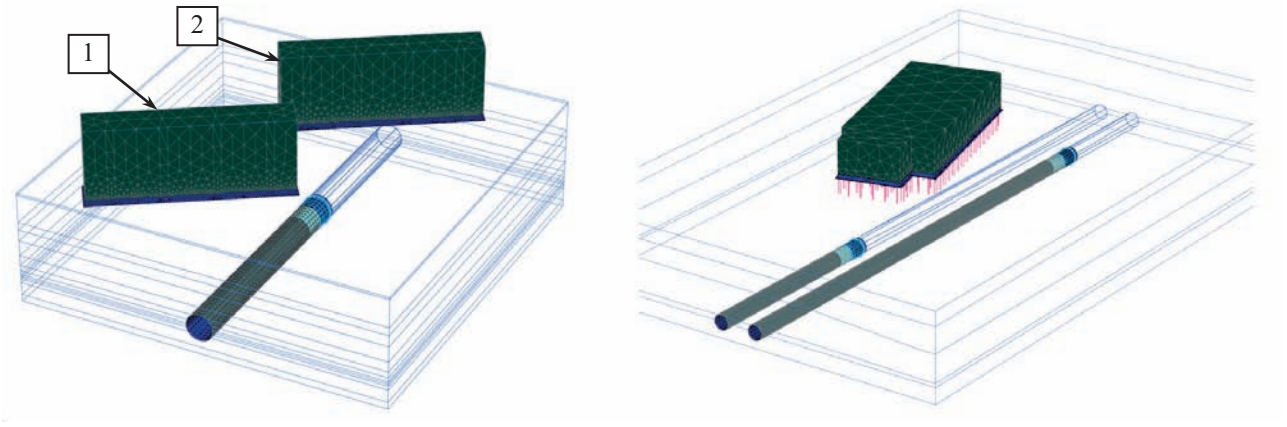
The first model represents a section measuring 145 × 151.2 m with a depth of 45.4 m; tunneling is carried out at a depth of 40 m. Within the calculation scheme, the total tunneling length is 151.2 m, with the excavation length per phase equal to the ring width – 1.8 m.

The calculation scheme for this section is shown in Fig. 3a.

The model includes two buildings (Fig. 3a) located at: Moscow, Marshala Tukhachevskogo Street, 56 bldg. 3 (1) and Moscow, Parshina Street, 21 bldg. 2 (2), both at a distance of 0 m from the tunnel axis.

The second model has dimensions of 163.9 × 248 × 35.4 m. In the model, tunneling is carried out at a depth of 32.4 m, and its length within the calculation scheme is 248 m for both the right and left tunnels. The excavation length per phase is equal to the installed ring width – 1.2 m.

The calculation scheme for this section is shown in Fig. 3b.



a) b)

Figure 3. Calculation schemes:
a) section from Bulvar Karbysheva station to Zhivopisnaya station,
b) section from Zvenigorodskaya station to Karamyshevskaya station

On the ground surface above the model, there is a building located at 2nd Silikatny Passage, 9 bldg. 2, at a distance of 0 m from the tunnel axis.

For settlement calculations using volume loss, a value of **0.78%** was adopted in accordance with [17] for the section from *Bulvar Karbysheva* to *Zhivopisnaya* station, and a value of **1.14%** in accordance with [20] for the section from *Zvenigorodskaya* to *Karamyshevskaya* station.

In developing an alternative calculation method, the approach proposed by H. Liu, J. Shi, J. Li, and C. Liu [25] was used as the basis. In their work, the authors accounted for face support pressure, grouting pressure, TBM shield stiffness, tunnel lining stiffness, the shield tail gap, and grout hardening. In the present study, in addition to these parameters, the TBM shield weight was considered; stiffening ribs were added inside the shield to ensure TBM rigidity; tail grouting pressure in the over-lining space was modeled as hydrostatic pressure instead of a surface-applied load to account for soil pressure and uniform compression of the lining; a sealed TBM brush element was included, enabling simulation of tunnel lining installation under shield protection; and stiffness values for certain materials were corrected.

The tunneling from *Bulvar Karbysheva* to *Zhivopisnaya* station is carried out using an Earth Pressure Balance (EPB) TBM with a diameter D = 10.87 m, length 9.38 m, and weight of about 1,000 t. The external lining diameter is d = 10.5 m, ring width is 1.8 m, and lining thickness is 0.45 m. The face support pressure is set according to the actual pressure during excavation of each ring.

In the area near the buildings, the face support pressure is 2.8 atm, and the tail grouting pressure is 4 atm.

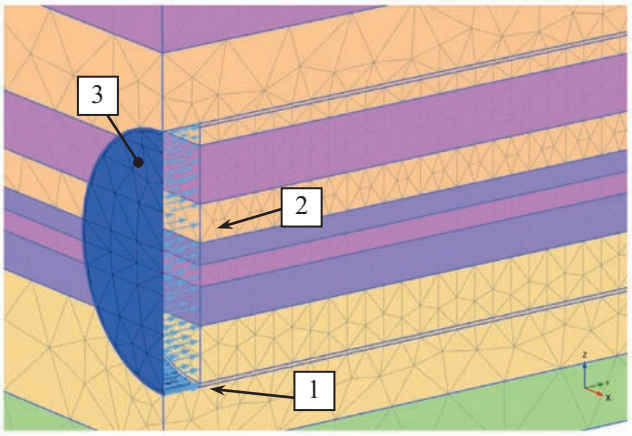
The tunnel section from *Zvenigorodskaya* to *Karamyshevskaya* station of the Rublyovo–Arkhangelskaya line was constructed using two different imported EPB TBMs. The technical characteristics of both shields are similar: diameter – 6.56 m, length – 9.45 m, weight – about 225 t, external tunnel lining diameter – 6.3 m, ring width – 1.2 m, and lining thickness – 0.3 m. The face support pressure was set at 3 atm, and the tail grouting pressure at 4 atm.

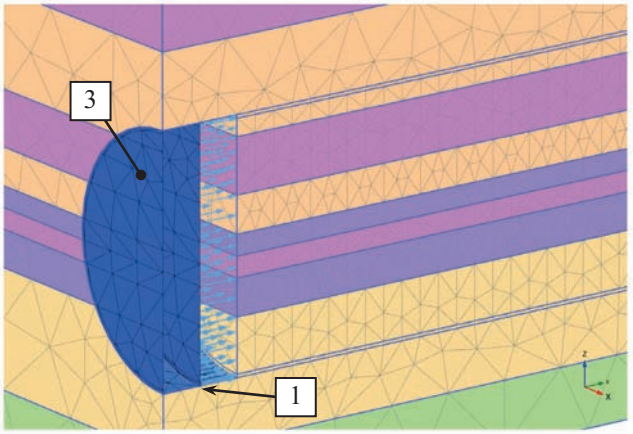
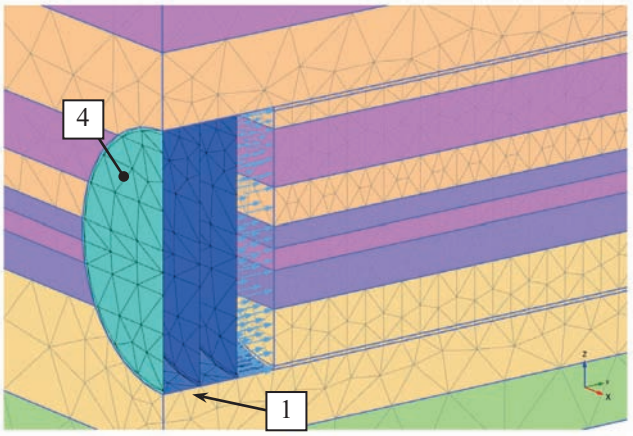
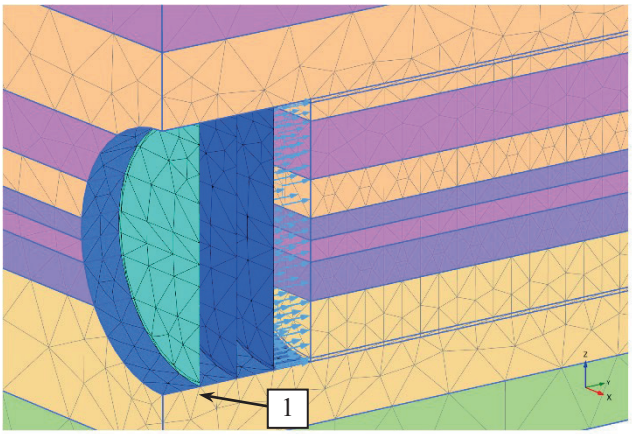
Tunneling sequence

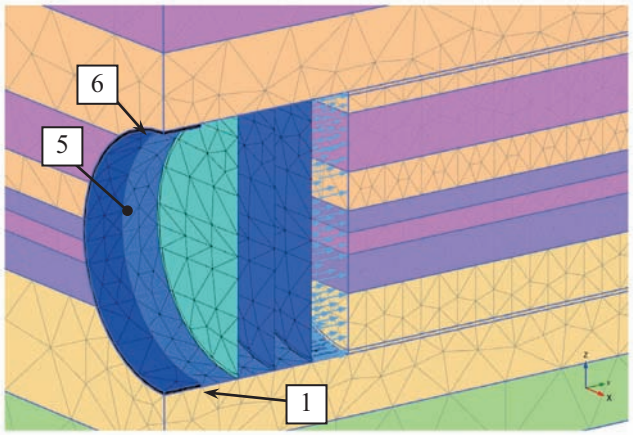
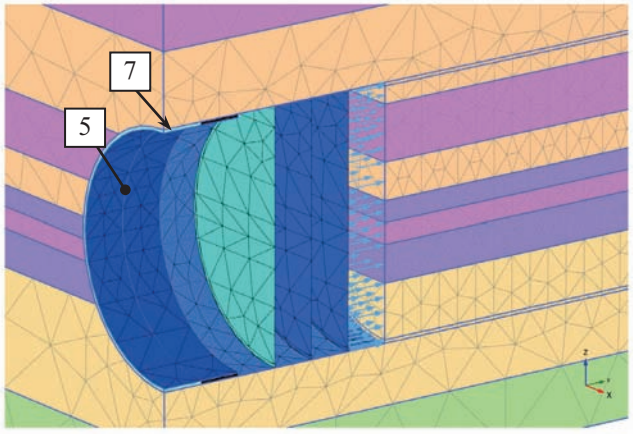
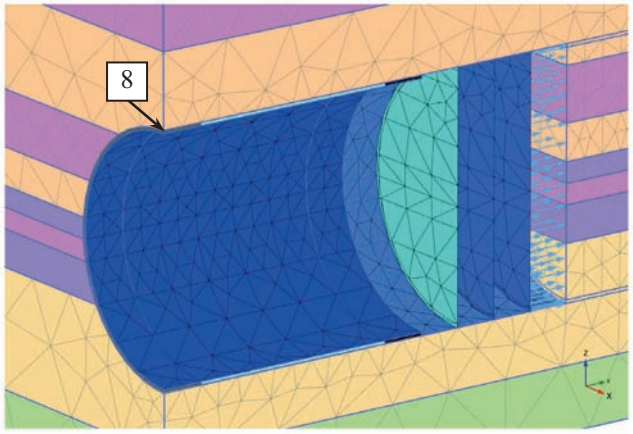
The tunneling on the section from *Bulvar Karbysheva* to *Zhivopisnaya* station is modeled according to the scheme presented in Table 1.

A similar tunneling simulation is performed in the calculation model for the section from *Zvenigorodskaya* to *Karamyshevskaya* station, taking into account the ring width and the shield length used during the construction of that section.

Table 1. Staged modeling of excavation using the alternative method

Tunneling phase No.	Changes at the stage	Model
1	The first shield shell segment (1) is activated; face support pressure (2) is applied at the front plane; at the rear plane of the first section, a bulkhead (3) is activated.	

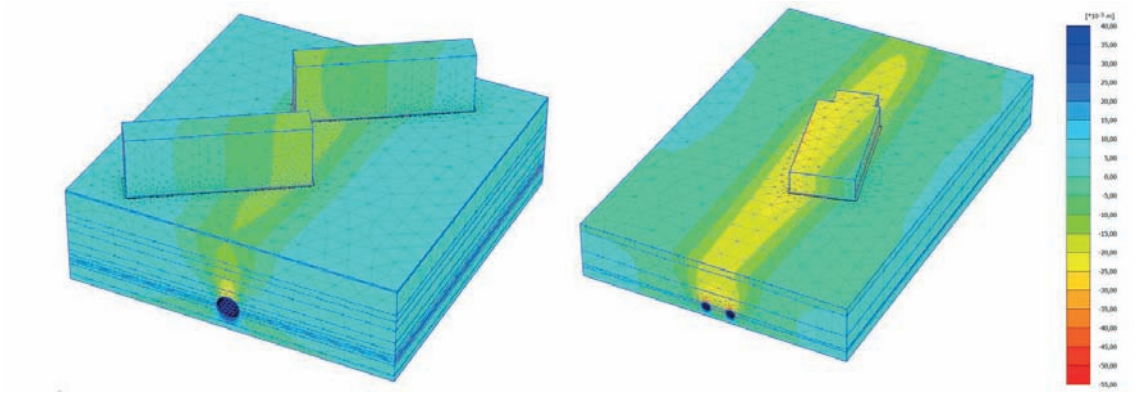
Tunneling phase No.	Changes at the stage	Model
2	The shield shell segment (1) is activated, and a bulkhead element (3) is activated at the rear plane of the section.	
3	The shield shell segment (1) is activated, and a bracing frame (4) is activated at the rear plane of the section.	
4	The shield shell segment (1) is activated.	

Tunneling phase No.	Changes at the stage	Model
5	The shield shell segment (1) and the tunnel lining (5) are activated; within the space between the shield shell (1) and the tunnel lining (5), the TBM tail brush-seal element (6) is activated, and interface elements are assigned at the shell–brush and lining–brush boundaries.	
6-10	The tunnel lining (5) is activated; the void between the cutting diameter and the lining diameter is represented by a grout material (7) with low stiffness, and its hydrostatic pressure is set equal to the grout-injection pressure.	
11	The cement slurry is replaced by hardened backfill grout (8) characterized by increased stiffness parameters.	

Properties of the modeled elements are provided in Tables 2 and 3, and the geological boreholes used in the models are listed in Table 4

3. RESULTS

Contours of vertical displacements for the first and second models are shown in Fig. 4. The results of the numerical models are presented as graphs of vertical deformation in Figs. 5 and 6.



a) b)

Figure 4. Contours of vertical displacements:
a) section from Bulvar Karbysheva station to Zhivopisnaya station,
b) section from Zvenigorodskaya station to Karamyshevskaya station

Table 2. Properties of soils and auxiliary ground elements (1st model)

Soil elements modeled using Linear Elastic и Mohr-Coulomb					
Soil element	*γ / kN/m³*	*E / MPa*	*v*	*c / kPa*	*φ' (phi)*
Anthropogenic layer (1-40)	16	12	0,3	1	29
Medium sands (10-5-3-2)	17	27	0,3	2	34
Loams with grus and crushed stone (24-3-3)	21,4	19	0,35	54	27
Silty sands (25-5-5-1)	18,2	25	0,3	7	33
Fine sands (25-5-4-1)	18,7	40	0,3	5	35
Medium sands (25-5-3-1)	18	44	3	3	37
Clays with sand pockets (41-2-2)	17,8	22	0,35	120	18
Clays with faunal remains (43-2-2)	19,4	29	0,3	85	18
Materials modeled using Linear Elastic и Mohr-Coulomb					
Tail brush-seal	0,1	100	0,3	-	-
Backfill grout material	0,1	1	0,4	-	-
Hardened backfill grout	24,8	700	0,3	43,2	28
Materials modeled using Plate elements					
Material name	*γ / kN/m³*	*E / MPa*	*v*	*G / MPa*	*d / m*
Tunnel lining	15	34000	0,2	14380	0,45
Shield shell	400	360000	0,3	138500	0,075
Bracing frame	0,1	210000	0,3	80770	0,3
Bulkhead	34,8	210000	0,3	80770	0,05

Table 3. Properties of soils and auxiliary ground elements (2nd model)

Soil elements modeled using Linear Elastic и Mohr-Coulomb					
Soil element	*γ / kN/m³*	*E / MPa*	*v*	*c / kPa*	*φ' (phi)*
Anthropogenic layer (1-40)	17,8	14	0,3	2	32
Fine sands (15-5-4-2)	17,9	27	0,3	2	32
Fine sands (25-5-4-1)	20,1	34	0,3	3	36
Limestones (51-16-3)	22,7	50	0,25	-	-
Clays (52-2-2)	19,8	26	0,2	61	21
Materials modeled using Linear Elastic и Mohr-Coulomb					
Tail brush-seal	0,1	100	0,3	-	-
Backfill grout material	0,1	1	0,4	-	-
Tail brush-seal	24,1	700	0,3	43,2	28
Materials modeled using Plate elements					
Material name	*γ / kN/m³*	*E / MPa*	*v*	*G / MPa*	*d / m*
Tunnel lining	25	34000	0,2	14380	0,3
Shield shell	7,35	360000	0,3	138500	0,04
Bracing frame	0,1	210000	0,3	80770	0,3
Bulkhead	355,2	210000	0,3	80770	0,05

Table 4. Geological boreholes used in the models

1st model borehole		2nd model borehole	
Soil elements	*h / m*	Soil elements	*h / m*
Anthropogenic layer (1-40)	0,8	Anthropogenic layer (1-40)	6,0
Medium sands (10-5-3-2)	11,3	Fine sands (15-5-4-2)	10,6
Loams with grus and crushed stone (24-3-3)	3,2	Fine sands (25-5-4-1)	11,0
Fine sands (25-5-4-1)	4,5	Limestones (51-16-3)	1,4
Silty sands (25-5-5-1)	6,2	Clays (52-2-2)	6,6
Fine sands (25-5-4-1)	4,1		
Silty sands (25-5-5-1)	2,4		
Fine sands (25-5-4-1)	1,6		
Medium sands (25-5-3-1)	0,9		
Silty sands (25-5-5-1)	0,9		
Medium sands (25-5-3-1)	1,6		
Clays with sand pockets (41-2-2)	5,1		
Clays with faunal remains (43-2-2)	2,8		

For the first computational scheme, the plot in Fig. 5 is given for the building at Parshina Street, 21 bldg. 2. The plot includes the measured ground-surface displacements. To generate the first plot, the timing of the actual installation of the tunnel lining rings was aligned with the corresponding installation phases in the numerical model, which enabled a proper comparison of the observed building deformations with the calculated time histories.

4. DISCUSSING

The plot in Fig. 5 shows that the alternative method provides sufficient agreement in determining the maximum displacement: the difference is about 0.27 mm, or 2.5% (throughout the article, comparisons are made relative to the maximum observed ground-surface displacement; for this plot it is 10.9 mm). At the same time, the maximum deviation at individual points is 1.4 mm, or 12.8%, at point 6.4, which corresponds to the permissible error of in-situ measurements of vertical displacements of 2 mm for Class II accuracy in accordance with [26], as well as to external factors that may affect the absolute measurement values, including temperature, vibration, etc. In addition, the plot shows that the values obtained from the calculation using the volume loss method are higher than the observed values at every monitoring point, with a maximum difference of 5.0 mm, or 45.9%, at point 6.7, which may lead to an incorrect assessment of the geotechnical situation and to unnecessary additional compensation measures. The difference between the maxima is 2.6 mm, or 23.9%. It should be noted that the calculation using the volume loss coefficient is much simpler and less computationally intensive and gives results with sufficient agreement for a preliminary analysis. However, the volume-loss approach does not explain the physical mechanisms that cause ground-surface settlement. Similar results were obtained in [1].
However, different patterns are observed for the plot in Fig. .6 The alternative calculation likewise agrees with the measured displacements, with a difference between the maxima of 3.1 mm (13.6%), and a maximum pointwise deviation of 4.3 mm (18.9%) at point 15.3. By contrast, the results obtained using the volume-loss approach are substantially lower than the observations: the difference between the maxima is 5.5 mm (24.1%), and the maximum pointwise deviation reaches 12.3 mm (53.9%) at point 15.3. To reconcile the measured displacements with those predicted by the volume-loss method in this case, the volume-loss coefficient must be increased to 2.85% (obtained by back-analysis). The discrepancy between the adopted coefficient and the back-calculated value may indicate the

influence of additional unaccounted factors on the effective volume loss relative to the design assumption. It should be noted that an inaccurate assessment of the geotechnical conditions in such circumstances may lead to operational incidents during tunneling and necessitate complex and costly remedial measures.

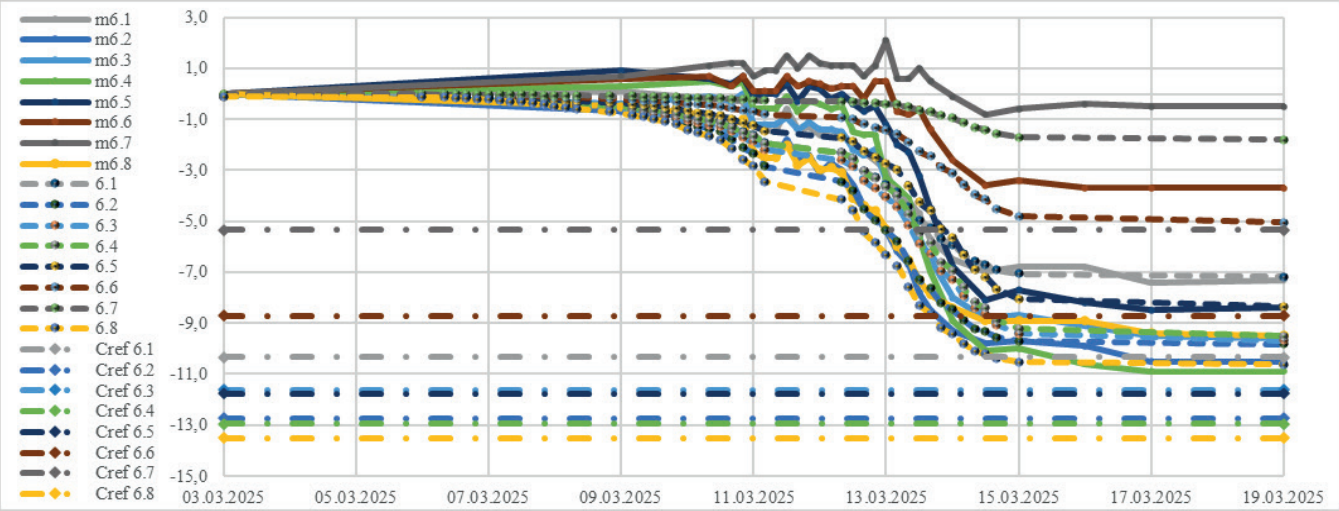


Figure 5. Displacement plot for the building shown in Fig. 3a
m6.1–6.8 — monitoring results
6.1-6.8 – staged modeling of all tunneling processes
Cref 6.1-6.8 – calculation using the volume-loss coefficient

Furthermore, comprehensive stage-by-stage modeling may reveal uplift of surface structures at certain points, caused by the structural stiffness of the buildings – as reported in [3, 5] – or to incorrectly specified face-support pressure or tail-void grouting pressure. This deformation mechanism is not reflected in calculations based on the volume loss coefficient.

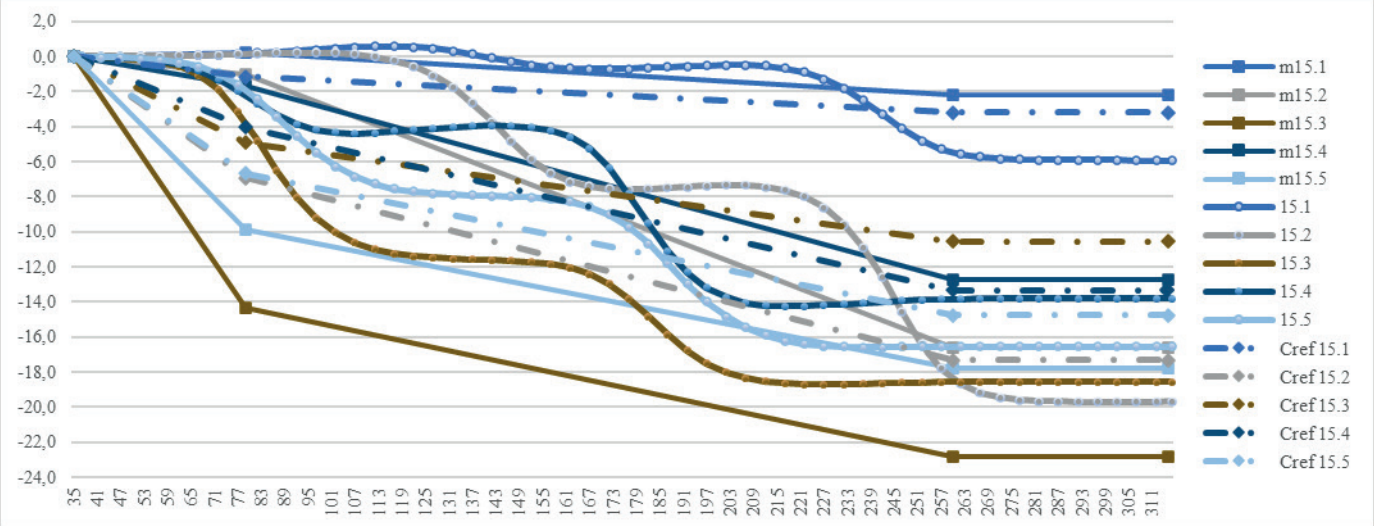


Figure 6. Displacement plot for the building shown in Fig. 3b
m15.1-15.5 – monitoring results
15.1-15.5 – staged modeling of all tunneling processes
Cref 15.1-15.5 – calculation using the volume-loss coefficient

5. CONCLUSIONS

The proposed method exhibits a high degree of qualitative agreement with the monitoring results. Discrepancies in quantitative agreement may be attributable to measurement error in field observations, inaccuracies in the input data for the analysis, and other external factors. A more rigorous treatment of input parameters – such as geological conditions – together with proper modeling of structural behavior and higher-accuracy geotechnical monitoring, would enable closer quantitative agreement.

Consistent with Liu H., Shi J., Li J., and Liu C. [25], the calculation shows uplift of the ground surface as the shield passes the monitoring point and significant settlement after the shield has passed, which corresponds to the actual behavior of the ground during tunneling. The uplift effect may be caused by the stiffness of the building, as well as by improperly specified face support pressure when the TBM operates close to the surface. The volume-loss coefficient does not describe the mechanics of ground behavior during TBM excavation.

If additional, unaccounted factors influence the selected design value of volume loss, calculations based on that coefficient can differ substantially from the results of the alternative method presented in article.

It can also be observed (Fig. 5 – plots Cref 6.1–6.8; Fig. 6 – Cref 15.1–15.5) that the volume-loss approach allows the building-wide maximum displacement to be estimated with reasonable accuracy, whereas displacements at individual points may be entirely inconsistent with their measured values; by contrast, the alternative calculation yields closer agreement with the measured displacements at individual points on the structure.

Note that in [17–21], calculations using a prescribed volume-loss coefficient in accordance with the regulatory standards do not allow surface settlement to be predicted accurately. Accordingly, the only way to obtain an actual volume-loss coefficient is to adjust it by back-analysis using the already constructed section of the alignment.

Results obtained with the volume-loss coefficient differ from monitored values for the structural elements by 24.1%, which suggests that the coefficient is suitable for preliminary, approximate calculations.

For refinement under complex geotechnical conditions, it is recommended to verify results using the method presented in present article, which models all stages of the tunneling process.

Further research is required to refine the calculation methodology and to ensure the necessary accuracy in predicting ground-surface settlement and the response of adjacent structures.

REFERENCES

1. **Festa D., Broere W., Bosch J.W.** (2013) Tunnelling in soft soil: on the correlations between the kinematics of a Tunnel Boring Machine and the observed soil displacements. Underground. The Way to the Future. pp. 2364-2371;
2. **Fedunets B.I., Boiko F.A.** (2008) Stroitel'stvo peregonnyh tonnelej sovremennymi TPMK pri prohodke v slozhnyh gidrogeologicheskih usloviyah uchastkov Mitinsko-Stroginskoj linii Moskovskogo metropolitena [Construction of tunnels by modern TBMs during the tunneling of Mitinsko-Stroginskaya line of the Moscow Metro in difficult hydrogeological conditions]. Mining informational and analytical bulletin. no. 7. pp. 21-27. (in Russian);
3. **Mazein S.V.** (2011) Prognoz stadijnosti podvizhek grunta v prodol'noj mul'de poverhnosti nad tonnelem po kontroliruemym parametram shchitovoj prohodki [Prediction of the stages of soil movement in the longitudinal subsidence

trough of the surface above the tunnel according to the controlled parameters of the TBM tunneling]. Mining informational and analytical bulletin. no. 3. pp. 288–293. (in Russian);

4. **Fu, J., Yang, J., Zhang, X., Klapperich, H., & Abbas, S. M.** (2014) Response of the ground and adjacent buildings due to tunnelling in completely weathered granitic soil. Tunnelling and Underground Space Technology. Vol. 43. pp. 377–388. DOI: 10.1016/j.tust.2014.05.022;
5. **Leca E., New B.** (2007) Settlements induced by tunneling in Soft Ground. Tunnelling and Underground Space Technology. Vol. 22(2). pp. 119-149. DOI: 10.1016/j.tust.2006.11.001;
6. **Comodromos, E.M., Papadopoulou, M.C., & Konstantinidis, G.K.** (2014) Numerical Assessment of Subsidence and Adjacent Building Movements Induced by TBM-EPB Tunneling. Journal of Geotechnical and Geoenvironmental Engineering. Vol. 140(11), 04014061. DOI: 10.1061/(ASCE)GT.1943-5606.0001166;
7. **Peck, R.B.** (1969) Deep Excavation and Tunneling in Soft Ground. State-of-the-Art Report. Proceedings of the 7th International Conference on Soil Mechanics and Foundation Engineering, Mexico. pp. 225–290;
8. **Loganathan N.** (2001) Prediction of tunnelling-induced ground movements: assessment and evaluation / N. Loganathan, R.F. Flanagan. Proceedings of the Underground, Singapore;
9. **O'Reilly M.P., New B.M.** (1982) Settlements above tunnels in the United Kingdom – Their magnitude and prediction / M.P. O'Reilly, B.M. New. Tunnelling. pp. 173–181;
10. **Attewell, P.B., Yeates J., Selby A.R.** (1986) Soil movements induced by tunnelling and their effects on pipelines and structures. Blackie, Glasgow;
11. **Protosenya A.G., Belyakov N.A., Do Ngoc Thai.** (2015) Razrabotka metoda prognoza davleniya prigruza zaboya i osadok zemnoj poverhnosti pri stroitel'stve tonnelej mekhanizirovannymi prohodcheskimi kompleksami [The development of prediction method of earth-pressure balance and earth surface settlement during tunneling with mechanized tunnel boring machines]. Journal of Mining Institute. Vol. 211. St. Petersburg. pp. 53-63. (in Russian);
12. **Tupikov M.M.** (2010) Osobennosti deformirovaniya gruntovogo massiva i sooruzhenij pri stroitel'stve melkozaglublennyh kommunikacionnyh tonnelej v gorodskih usloviyah [Peculiarities of the ground massif and structures deformation during the construction of shallow communication tunnels in urban conditions]. Dissertation. Abstract Ph. D. thesis. Moscow. pp. 184. (in Russian);
13. **Mazein S.V.** (2009) Razrabotka matematicheskih modelej dlya prognoznyh osadok dnevnoj poverhnosti po dannym kontrolya grunta i tekhnologicheskih pokazatelej TPMK [Development of mathematical models for predictive settlement of the day surface according to soil control data and technological indicators of TPMK]. Mining informational and analytical bulletin. no. 2. pp. 98-109. (in Russian);
14. **Shashkin A.G.** (2013) Osnovy geotekhnicheskogo monitoringa [The basics of geotechnical monitoring]. Engineering survey. no. 10-11. pp. 18-21; (in Russian)
15. **Shashkin A.G.** (2011) Osnovy rascheta podzemnyh sooruzhenij v usloviyah gorodskoj zastrojki na slabyh glinistyh gruntah [Principles of Design of Underground Structures UnderConditions of Urban Development on Soft Clay Soils]. Housing Construction. № 6. pp. 39-46. (in Russian);

16. **Ivanova A.V., Solovieva T.A., Bugakova T.Yu.** (2019) Geotekhnicheskij monitoring - osnova zhiznennogo cikla zdanij i sooruzhenij [Geotechnical monitoring of buildings and structures for the control and construction safety]. Interekspo Geo-Sibir'. Vol. 6. no. 1. pp. 214-220. DOI: 10.33764/2618-981X-2019-6-1-214-220. (in Russian);
17. **Ter-Martirosian A.Z., Kivliuk V.P., Isaev I.O., Shishkina V.V.** (2021) Opredelenie fakticheskogo koefficienta perebora (uchastok «Kosino» – «Yugo-Vostochnaya») [Determination of the actual excess excavation ratio (section "Kosino" – "Yugo-Vostochnaya")]. Construction and Geotechnics. Vol. 12. no. 2. pp. 5–14. DOI: 10.15593/2224-9826/2021.2.01. (in Russian);
18. **Ter-Martirosian A.Z., Isaev I.O., Almakaeva A.S.** (2020) Opredelenie fakticheskogo koefficienta perebora (uchastok «Stahanovskaya ulica» — «Nizhegorodskaya ulica») [Identification of the actual excess excavation ratio (Stakhanovskaya street – Nizhegorodskaya street site)]. Vestnik MGSU. Vol. 15, no. 12, pp. 1644–1653, DOI: 10.22227/1997-0935.2020.12.1644-1653. (in Russian);
19. **Ter-Martirosian A.Z., Cherkesov R.H., Isaev I.O., Rud V.V.** (2023) Fakticheskoe znachenie koefficienta perebora dlya tonnelej v dispersnyh i skal'nyh gruntah [The actual volume loss of soil coefficient for tunnels in cohesive and rock soils]. Housing Construction. no. 9. pp. 61–73. DOI: 10.31659/0044-4472-2023-9-61-73. (in Russian);
20. **Ter-Martirosian A.Z., Kivliuk V.P., Isaev I.O., Shishkina V.V.** (2021) Opredelenie fakticheskogo koefficienta perebora v skal'nyh gruntah [Determination of the actual outbreak ratio in rocky soils]. Housing Construction. no. 9. pp. 3–9. DOI: 10.31659/0044-4472-2021-9-3-9. (in Russian);
21. **Isaev O.N., Sharafutdinov R.F.** (2012) Perebor grunta pri stroitel'stve kommunikacionnyh tonnelej shchitovym sposobom [Ground loss during construction of the engineering communications with shield tunnel]. Mechanization of Construction. no. 6. pp. 2–7. (in Russian);
22. **Ter-Martirosian A.Z., Cherkesov R.H., Isaev I.O., Rud V.V., Ambrushkevich M.I.** (2023) Opredelenie parametrov granic raschetnoj modeli pri ocenke vliyaniya na okruzhayushchuyu zastrojku ot tonneleprohodcheskih rabot [Determination of parameters of the boundaries of the computational model for assessing the impact on the surrounding development from tunneling]. International Journal for Computational Civil and Structural Engineering. Vol. 19(2), pp. 95-108. DOI: 10.22337/2587-9618-2023-19-2-95-108;
23. **Bernat, S., & Cambou, B.** (1998) Soil-structure interaction in shield tunnelling in soft soil. Computers and Geotechnics. Vol. 22(3-4). pp. 221–242. DOI: 10.1016/s0266-352x(98)00007-x;
24. **Mazein S.V.**, **Pavlenko A.M.** (2007) Vliyanie tekushchih parametrov shchitovoj prohodki na osadku poverhnosti [Influence of the current parameters of the TBM tunneling on the surface settlement]. Mining informational and analytical bulletin. no. 5. pp. 133–138. (in Russian);
25. **Liu H., Shi J., Li J., and Liu C.** (2021) Investigation on the influence caused by shield tunneling: WSN monitoring and numerical simulation. Advances in Civil Engineering. Vol. 2021(1), pp. 1–11. DOI: 10.1155/2021/6620706;
26. GOST 24846-2019 Grunty. Metody izmereniya deformacij osnovanij zdanij i sooruzhenij [Soils. Measuring methods of strains of structures and building bases]. Interstate Council For Standardization,

Metrology And Certification (ISC). pp. 17.

СПИСОК ЛИТЕРАТУРЫ

1. **Festa D., Broere W., Bosch J.W.** Tunnelling in soft soil: on the correlations between the kinematics of a Tunnel Boring Machine and the observed soil displacements // Underground. The Way to the Future. 2013. с. 2364-2371;
2. **Федунец Б.И., Бойко Ф.А**. Строительство перегонных тоннелей современными ТПМК при проходке в сложных гидрогеологических условиях участков Митинско-Строгинской линии Московского метрополитена // Горный информационно-аналитический бюллетень. 2008. №7. с. 21-27;
3. **Мазеин С.В.** Прогноз стадийности подвижек грунта в продольной мульде поверхности над тоннелем по контролируемым параметрам щитовой проходки // Горный информационно-аналитический бюллетень. 2011. № 3. с. 288–293;
4. **Fu, J., Yang, J., Zhang, X., Klapperich, H., & Abbas, S. M.** Response of the ground and adjacent buildings due to tunnelling in completely weathered granitic soil // Tunnelling and Underground Space Technology. 2014. Vol. 43. с. 377–388. DOI: 10.1016/j.tust.2014.05.022;
5. **Leca E., New B.** Settlements induced by tunneling in Soft Ground // Tunnelling and Underground Space Technology. 2007 Vol. 22(2), с. 119-149. DOI:10.1016/j.tust.2006.11.001;
6. **Comodromos, E.M., Papadopoulou, M.C., & Konstantinidis, G.K.** Numerical Assessment of Subsidence and Adjacent Building Movements Induced by TBM-EPB Tunneling // Journal of Geotechnical and Geoenvironmental Engineering. 2014. Vol. 140(11), 04014061 DOI: 10.1061/(ASCE)GT.1943-5606.0001166;
7. **Peck, R.B.** Deep Excavation and Tunneling in Soft Ground // State-of-the-Art Report. Proceedings of the 7th International Conference on Soil Mechanics and Foundation Engineering, Mexico. 1969. с. 225–290;
8. **Loganathan N.** Prediction of tunnelling-induced ground movements: assessment and evaluation / N. Loganathan, R.F. Flanagan // Proceedings of the Underground, Singapore. 2001;
9. **O'Reilly M.P., New B.M.** Settlements above tunnels in the United Kingdom – Their magnitude and prediction / M.P. O'Reilly, B.M. New // Tunnelling. 1982. с. 173–181;
10. **Attewell, P.B., Yeates J., Selby A.R.** Soil movements induced by tunnelling and their effects on pipelines and structures. 1986. Blackie, Glasgow;
11. **Протосеня А.Г., Беляков Н.А., До Нгок Тхай.** Разработка метода прогноза давления пригруза забоя и осадок земной поверхности при строительстве тоннелей механизированными проходческими комплексами // Записки горного института. 2015 Том 211. Санкт-Петербург. с. 53-63;
12. **Тупиков М.М.** Особенности деформирования грунтового массива и сооружений при строительстве мелко-заглубленных коммуникационных тоннелей в городских условиях // Диссертация на соискание ученой степени кандидата технических наук. ГОУ ВПО РУТ «МИИТ», Москва. 2010. с. 184;
13. **Мазеин С.В**. Разработка математических моделей для прогнозных осадок дневной поверхности по данным контроля грунта и технологических показателей ТПМК // Горный информационно-

аналитический бюллетень. 2009. № 2. с. 98-109;
14. **Шашкин А.Г.** Основы геотехнического мониторинга // Журнал «Инженерные изыскания». 2013. №10-11. с. 18-21;
15. **Шашкин А.Г.** Основы расчета подземных сооружений в условиях городской застройки на слабых глинистых грунтах // Жилищное строительство. 2011. № 6. с. 39-46;
16. **Иванова А.В., Соловьева Т.А., Бугакова Т.Ю.** Геотехнический мониторинг - основа жизненного цикла зданий и сооружений // Интерэкспо Гео-Сибирь. Магистерская научная сессия «Первые шаги в науке». 2019. Том6. № 1. с. 214-220. DOI: 10.33764/2618-981X-2019-6-1-214-220;
17. **Тер-Мартиросян А.З., Кивлюк В.П., Исаев И.О., Шишкина В.В.** Определение фактического коэффициента перебора (участок «Косино» – «Юго-Восточная») // Construction and Geotechnics. 2021. Т. 12. № 2. с. 5–14. DOI: 10.15593/2224-9826/2021.2.01;
18. **Тер-Мартиросян А.З., Исаев И.О., Алмакаева А.С.** Определение фактического коэффициента перебора (участок «Стахановская улица» — «Нижегородская улица») // Вестник МГСУ. 2020. Том 15, № 12, с. 1644–1653, DOI: 10.22227/1997-0935.2020.12.1644-1653;
19. **Тер-Мартиросян А.З., Черкесов Р.Х., Исаев И.О., Рудь В.В.** Фактическое значение коэффициента перебора для тоннелей в дисперсных и скальных грунтах // Жилищное строительство. 2023. № 9. с. 61–73. DOI: 10.31659/0044-4472-2023-9-61-73;
20. **Тер-Мартиросян А.З., Кивлюк В.П., Исаев И.О., Шишкина В.В.** Определение фактического коэффициента перебора в скальных грунтах // Жилищное строительство. 2021. № 9. с. 3–9. DOI: 10.31659/0044-4472-2021-9-3-9;
21. **Исаев О.Н., Шарафутдинов Р.Ф.** Перебор грунта при строительстве коммуникационных тоннелей щитовым способом // Механизация строительства. 2012. № 6. с. 2–7;
22. **Тер-Мартиросян, А.З., Черкесов, Р.Х., Исаев, И.О., Рудь, В.В., Амбрушкевич, М.И.** Определение параметров границ расчетной модели при оценке влияния на окружающую застройку от тоннеле-проходческих работ // International Journal for Computational Civil and Structural Engineering. 2023. Vol. 19(2), с. 95-108. DOI: 10.22337/2587-9618-2023-19-2-95-108;
23. **Bernat, S., & Cambou, B.** Soil-structure interaction in shield tunnelling in soft soil // Computers and Geotechnics. 1998. Vol. 22 (3-4). с. 221–242. DOI: 10.1016/s0266-352x(98)00007-x;
24. **Мазеин С.В., Павленко А.М.** Влияние текущих параметров щитовой проходки на осадку поверхности // Горный информационно-аналитический бюллетень. 2007. № 5. с. 133–138;
25. **Liu H., Shi J., Li J., and Liu C.** Investigation on the influence caused by shield tunneling: WSN monitoring and numerical simulation // Advances in Civil Engineering. 2021. Vol. 2021(1), с. 1–11. DOI: 10.1155/2021/6620706;
26. ГОСТ 24846-2019 Грунты. Методы измерения деформаций оснований зданий и сооружений. с. 17.

Armen Z. Ter-Martirosyan, Vice-Rector, Doctor of Science, Professor; National Research Moscow State Civil Engineering University, 26, Yaroslavskoye Shosse, 129337 Moscow, Russia; E-mail: gic-mgsu@mail.ru

Ter-Martirosyan Armen Zavenovich, проректор, доктор технических наук, профессор кафедры механики грунтов, оснований и фундаментов; Национальный исследовательский Московский государственный строительный университет (НИУ МГСУ), 129337, Россия, г. Москва, Ярославское шоссе, д. 26; E-mail: gic-mgsu@mail.ru.

Ilya O. Isaev, Director of Scientific and Technical Activities; Institute Mosinzhproekt Limited Liability Company, 4/1, Sverchkov Ln, 101000 Moscow, Russia; E-mail: IsaevIO@mipi.ru.

Исаев Илья Олегович, директор по научно-технической деятельности; ООО Институт Мосинжпроект, 101000, Россия, г. Москва, Сверчков переулок, д. 4/1, стр.1; E-mail: IsaevIO@mosinzhproekt.ru.

Evgenii N. Kriuchkov, Ph.D. student, National Research Moscow State Civil Engineering University, 26, Yaroslavskoye Shosse, 129337 Moscow, Russia; E-mail: Kriuchkov.EN@mipi.ru.

Крючков Евгений Николаевич, аспирант; Национальный исследовательский Московский государственный строительный университет (НИУ МГСУ), 129337, Россия, г. Москва, Ярославское шоссе, д. 26; E-mail: Kriuchkov.EN@mipi.ru.

Maksim N. Shlapak, Ph.D. student, National Research Moscow State Civil Engineering University, 26, Yaroslavskoye Shosse, 129337 Moscow, Russia; E-mail: Shlapak.MN@mipi.ru.

Шлапак Максим Николаевич, аспирант; Национальный исследовательский Московский государственный строительный университет (НИУ МГСУ), 129337, Россия, г. Москва, Ярославское шоссе, д. 26; E-mail: Shlapak.MN@mipi.ru.

International Journal for Computational Civil and Structural Engineering, 21(4) 130–145 (2025)

DOI:10.22337/2587-9618-2025-21-4-130-145

NUMERICAL MODELING OF CAST-IN-PLACE REINFORCED CONCRETE BUBBLE DECK FLOOR SLABS UTILIZED IN EARTHQUAKE-PRONE REGIONS. PART TWO

Alexander M. Belostotsky [1,2]***, Alexander I. Nagibovich*** [1,2]***, Sergey V. Scherbina*** [1,2]***, Tatiana N. Vasileva*** [1,2]

[1] National Research Moscow State University of Civil Engineering, Moscow, RUSSIA
[2] Research & Development Centre StaDyO, Moscow, RUSSIA

Abstract: This article presents developed techniques for numerical modelling of lightweight cast-in-place reinforced concrete bubble deck floor slabs and a comparative analysis of different approaches to numerical modelling of buildings and structures with such lightweight floors, that are constructed in earthquake-prone regions.

Keywords: finite element method, modal analysis, earthquake excitation, mechanical safety, void formers, lightweight cast-in-place reinforced concrete floor slabs

ЧИСЛЕННОЕ МОДЕЛИРОВАНИЕ МОНОЛИТНЫХ ЖЕЛЕЗОБЕТОННЫХ ПЕРЕКРЫТИЙ С ПУСТОТООБРАЗОВАТЕЛЯМИ, ПРИМЕНЯЕМЫХ В СЕЙСМИЧЕСКИ АКТИВНЫХ РАЙОНАХ. ЧАСТЬ 2

А.М. Белостоцкий [1,2]***, А.И. Нагибович*** [1,2]***, С.В. Щербина*** [1,2]***, Т.Н. Васильева*** [1,2]

[1] Национальный исследовательский Московский государственный строительный университет, г. Москва, РОССИЯ
[2] АО «Научно-исследовательский центр СтаДиО», г. Москва, РОССИЯ

Аннотация: В настоящей статье представлены разработанные авторами методики численного моделирования облегченных монолитных железобетонных перекрытий с пустотообразователями и сравнительный анализ различных подходов к численному моделированию зданий и сооружений, строящихся в сейсмически активных районах и имеющих в своём составе подобные облегчённые плиты перекрытий.

Ключевые слова: метод конечных элементов, модальный анализ, сейсмическое воздействие, механическая безопасность, пустотообразователи, облегченные монолитные железобетонные перекрытия.

1. INTRODUCTION

A reinforced concrete bubble deck floor slab solution is widely used as a building design solution in earthquake-prone regions. Utilization of void formers is one of the ways to decrease the dead weight of concrete structures, that leads to reduced seismic loads and loads on vertical load-bearing structures and foundation.

The finite element method is widely used to solve structural mechanics problems, eigenvalue problems, and to perform a response spectrum analysis. The best way to extract eigenmodes and eigenfrequencies of a system with structural elements having complex cross-sections, to determine its stress-strain state is spatial discretization of such a system with solid elements. However, such a technique is computationally ineffective. Therefore, a common practice is to use structural finite elements, shell and beam ones, to spatially discretize a structural mechanics problem.

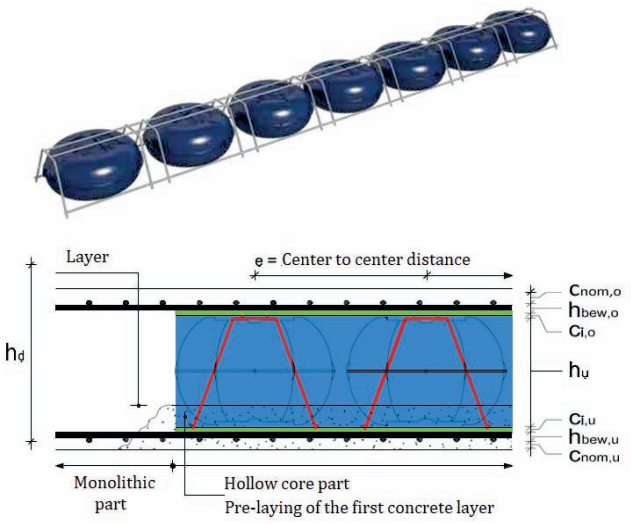


Figure 1. An example of void formers used in reinforced concrete floor slabs, and their geometrical parameters

The first part of the present research [1] has considered a single floor cell of a reinforced concrete frame building (see Fig. 2). The chosen part of the floor slab has dimensions of 5.6×5.6 meters and comprises 16 void former cells in each direction. The floor slab has the following values of its geometrical parameters: the floor slab thickness h_d = 250mm; the void former height h_u = 140mm; the concrete cover at the upper slab face $c_{nom,o}$ = 20mm; the concrete cover at the lower slab face $c_{nom,u}$ = 20mm; the distance between bubbles centers e = 350mm; the void former diameter d = 315mm. A cross-section of the single void former cell is shown in Fig. 3.

Properties of the considered bubble deck floor slab material are given in Table 1.

The verified ANSYS software [2] has been used for all simulations (a static loading analysis and a modal analysis). A reference finite element model of the simulated part of the floor slab has been assembled using solid finite elements of the type SOLID185 for spatial discretization of the problem. Corresponding mesh within the void former cell is illustrated in Fig. 4. Because only elastic part of the problem has been considered, utilization of the numerical solution obtained using the FE model meshed with solid elements is appropriate, since high accuracy of finite element simulations within the theory of elasticity has been verified multiple times (see, for instance, [2]).

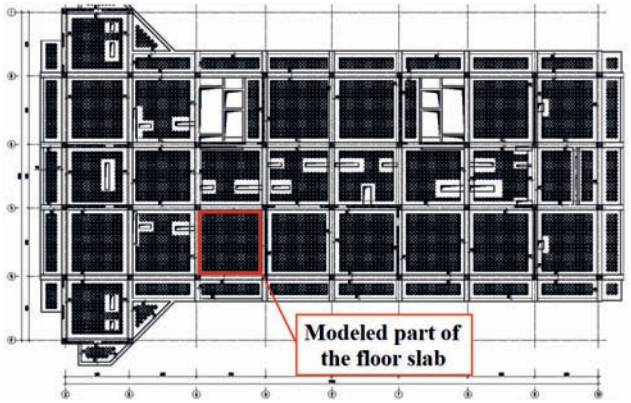


Figure 2. The drawing of a bubble deck floor slab in the reinforced concrete frame building (a part of the slab chosen for a comparative analysis of various numerical modelling techniques is outlined in red)

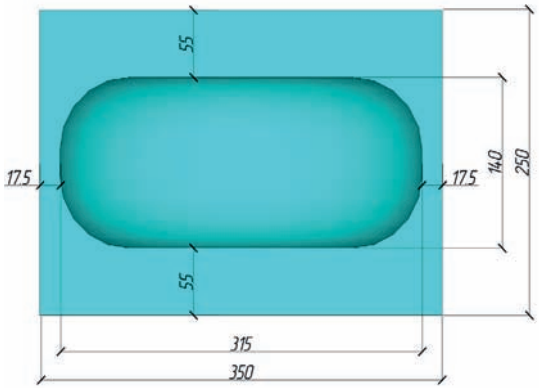


Figure 3. The cross-section of a void former cell used in the considered bubble deck floor slab

Table 1. Bubble deck floor slab material properties

Material	Elastic Modulus E, GPa	Poisson's ratio ν	Density ρ, kg/m^3
Concrete B25	30	0.2	2500

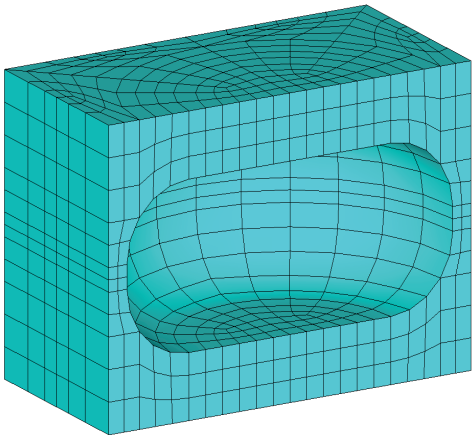


Figure 4. Mesh within the void former cell used in the reference model of the considered cast-in-place reinforced concrete bubble deck floor slab

According to the results of the first part of the present research [1], within which the modal analysis and static analysis have been performed for the models of the considered bubble deck floor slab meshed with either solid finite elements (the reference model) or structural finite elements, the closest agreement to the results calculated with the reference finite element model has been obtained for the following two cases. In the first case, the slab has been simulated as two horizontal layers of shell finite elements of the type SHELL181, in which the Reissner-Mindlin plate theory is implemented, with effective density (increased by a factor of k_ρ = 1.1484 to match the mass of the model to that of the reference model) connected together with a honey-comb structure also meshed with shell finite elements of the type SHELL181 with effective density (increased by the same factor of k_ρ = 1.1484) and effective elastic modulus (iteratively changed to match the results of the modal analysis with the reference ones) (see Table 2). In the second case, the slab has been modeled with one layer of shell finite elements of the type SHELL181 with effective density (decreased by a factor of k_ρ = 1.4376) and effective elastic modulus (see Table 3).

In the present paper, various approaches to numerical simulation of structural assembly comprised reinforced concrete bubble deck floor slab and reinforced concrete vertical load-bearing structural elements, in particular a column and wall with an embedded column, are considered.

Table 2. Parameters of the double-layer engineering finite element model

#	Element	E, GPa	ν	ρ, kg/m^3	t, mm
1	Horizontal plate of the floor slab	30	0.2	2871.1	55
2	Vertical rib of the floor slab	87	0.2	2871.1	35

Note: parameters different from the reference ones are colored in blue

Table 3. Parameters of the single-layer engineering finite element model

#	Element	E, GPa	ν	ρ, kg/m^3	t, mm
1	Floor slab	24	0.2	1739.1	250

Note: parameters different from the reference ones are colored in blue

2. PROBLEM ONE. INTERACTION OF THE BUBBLE DECK PART AND THE SOLID PART OF THE FLOOR SLAB

The reinforced concrete bubble deck floor slab, as illustrated in Fig. 5, has two distinct areas. The central part of the slab contains void formers, while the perimeter of the slab is solid to provide mechanical safety of the structural element.

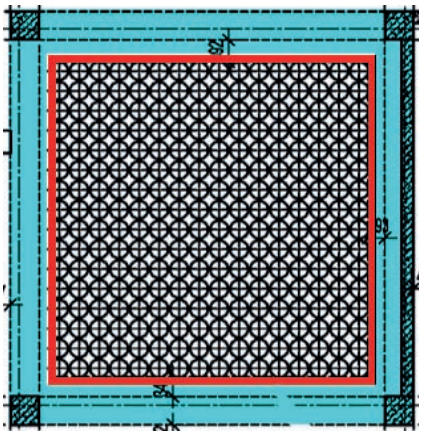


Figure 5. The simulated part of the bubble deck floor slab (the part of the slab with void formers is outlined in red, the solid area of the slab is colored in blue)

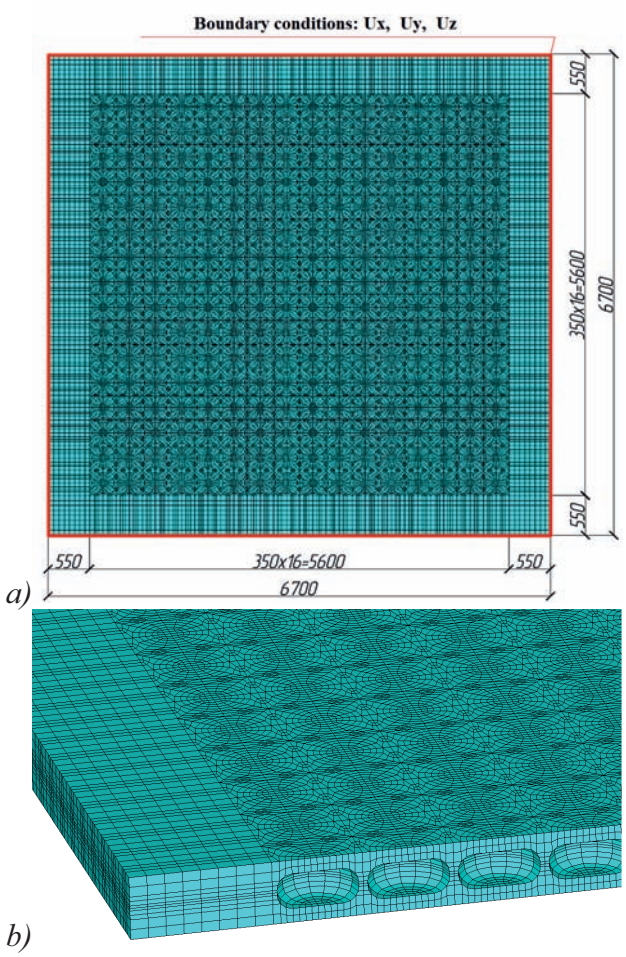


Figure 6. The numerical model meshed with solid finite elements: a) geometrical parameters and boundary conditions, b) cross-section view

To simulate various structural assemblies including bubble deck floor slab, it is necessary to accurately model transition between the part of the slab with void formers and the solid one.

A finite element model of the whole floor slab utilized for reference simulations is shown in Fig. 6. All DOFs (Ux, Uy, Uz) of the nodes located at the slab boundaries are restrained.

Two different techniques to simulate the bubble deck floor slab, including its solid part, using structural finite elements are considered.

Within the first technique, the void former cell of the slab is modelled as a honeycomb structure with top and bottom cover plates, which are all discretized through shell finite elements, while the solid part of the slab is discretized via a single layer of shell finite elements located at the middle surface (see Fig. 7).

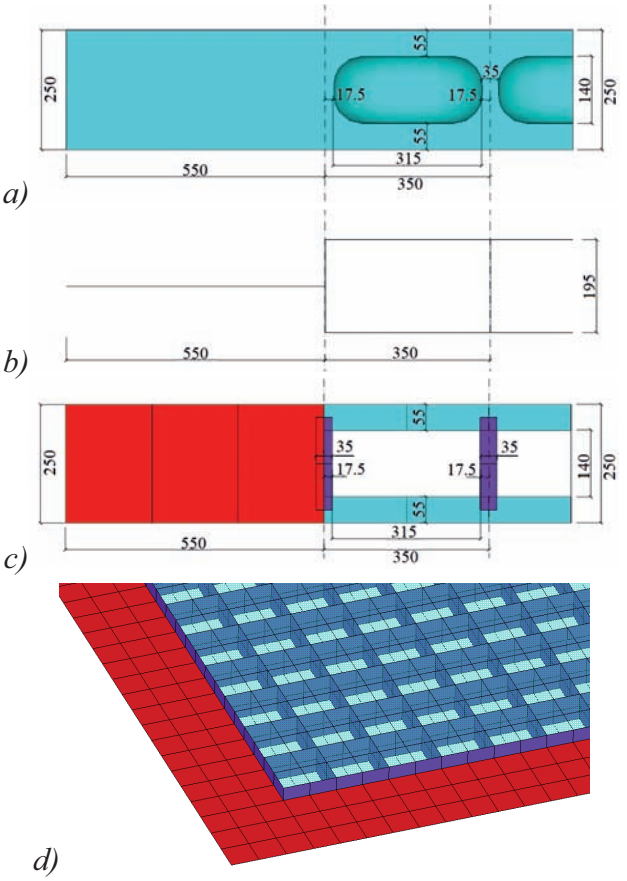


Figure 7. Finite element model for the first simulation technique: a) cross-section of the actual structure; b) computational model of the structure; c) computational model of the structure with displayed element thickness; d) orthogonal view (red – solid floor slab; light blue – cover plates of the bubble deck part of the floor slab; purple – vertical ribs of the bubble deck part of the floor slab)

With the first engineering technique (Model 1), two different sets of material properties have been adopted (see Tables 4, 5).

In the first parameter set, 1A, vertical ribs between the solid and the bubble deck parts of the floor slab have effective properties (density, elastic modulus) similar to those of other vertical ribs for parameter set 1A.

Table 4. The parameters set 1A

#	Element	E, GPa	ν	ρ, kg/m^3	t, mm
1	Horizontal plate of the bubble deck part of the floor slab	30	0.2	2871.1	55
2	Vertical rib of the bubble deck part of the floor slab	87	0.2	2871.1	35
3	Solid part of the floor slab	30	0.2	2500	250

Note: parameters different from the reference ones are colored in blue

The parameter set 1B is based onto the parameter set 1A. In the parameter set 1B, the elastic modulus of the vertical ribs between the solid part and the bubble deck parts of the floor slab elastic modulus has been significantly increased for the simulation results to match eigenfrequencies, eigenmodes, and static response of the reference model.

Table 5. The parameters set 1B

#	Element	E, GPa	ν	ρ, kg/m^3	t, mm
1	Horizontal plate of the bubble deck part of the floor slab	30	0.2	2871.1	55
2	Vertical rib of the bubble deck part of the floor slab	87	0.2	2871.1	35
3	Solid part of the floor slab	30	0.2	2500	250
4	Vertical rib at the perimeter of the bubble deck part of the floor slab	400	0.2	2871.1	35

Note: parameters different from the parameters set 1A are colored in yellow

Within the second engineering technique (Model 2), both the solid part and the bubble deck part of the floor slab are discretized through one layer of shell finite elements. To match mass, stiffness, and dynamic response characteristics of the actual structure, effective values of material properties – a parameters set 2A – have been used (see Table 6).

Table 6. The parameters set 2A

#	Element	E, GPa	ν	ρ, kg/m^3	t, mm
1	Bubble deck part of the floor slab	24	0.2	1739.1	250
2	Solid part of the floor slab	30	0.2	2500	250

Note: parameters different from the reference ones are colored in blue

In the finite element models utilized within both considered techniques, all DOFs (Ux, Uy, Uz, Rotx, Roty, Rotz) of the nodes located at the slab boundaries are restrained.
Results of the modal analyses performed using different numerical models are given in Table 7. Results of the static response analyses performed using different numerical models are presented in Tables 8, 9, and Fig. 8.

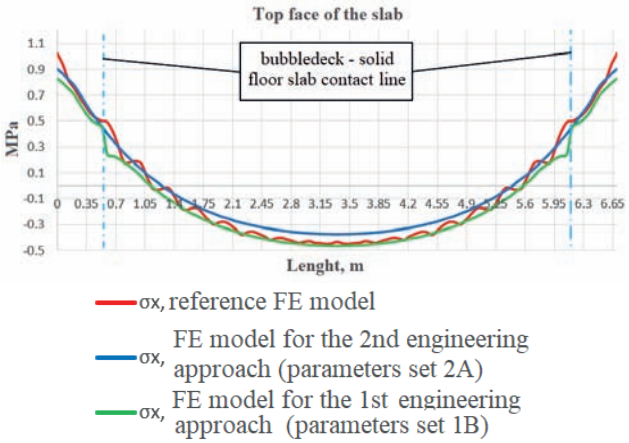


Figure 8. Normal stress along X-axis at the top face of the slab in the central cross-section due to the slab dead weight

The finite element model created within the first engineering technique using the values of the parameters given in the set 1B and the finite element model created within the second engineering approach using the values of the parameters given in the set 2A have yielded the closest agreement with the results of the modal analysis and the static response analysis obtained using the reference finite element model. The finite element model implementing the first engineering approach with the parameters set 1B has been chosen for further research.

Table 7. Results of the modal analyses (In brackets given are the discrepancy, in percent, from the results obtained with the reference finite element model)

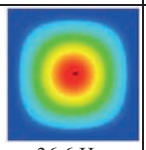
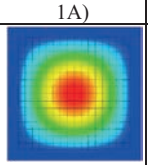
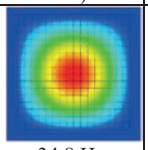
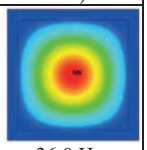
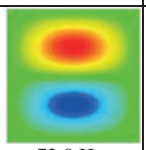
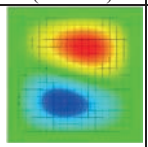
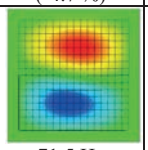
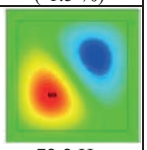
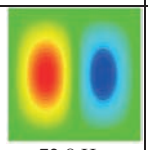
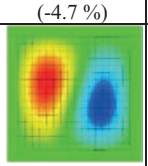
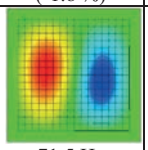
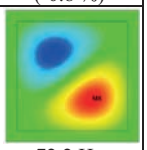
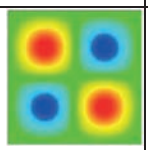
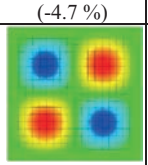
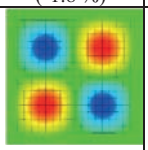
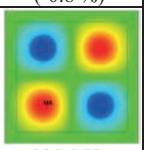
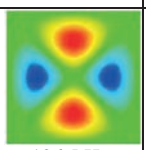
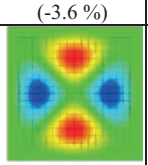
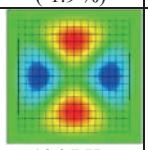
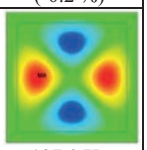
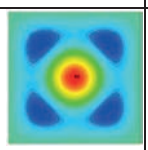
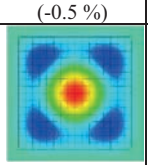
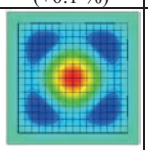
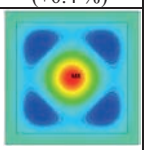
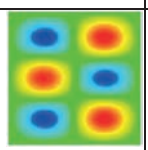
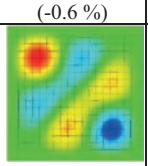
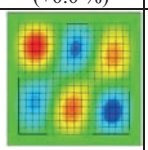
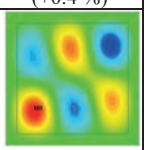
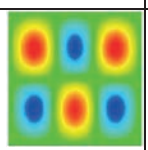
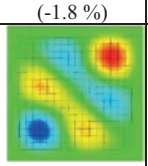
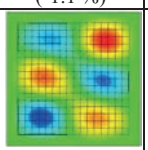
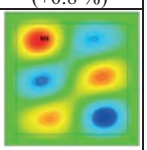
#	Reference model	Model 1 (parameters set 1A)	Model 1 (parameters set 1B)	Model 2 (parameters set 2A)
1	 36.6 Hz	 32.1 Hz (-12.1 %)	 34.8 Hz (-4.7 %)	 36.0 Hz (-1.5 %)
2	 72.8 Hz	 69.4 Hz (-4.7 %)	 71.5 Hz (-1.8 %)	 72.2 Hz (-0.8 %)
3	 72.8 Hz	 69.4 Hz (-4.7 %)	 71.5 Hz (-1.8 %)	 72.2 Hz (-0.8 %)
4	 105.3 Hz	 101.5 Hz (-3.6 %)	 103.3 Hz (-1.9 %)	 105.1 Hz (-0.2 %)
5	 126.5 Hz	 125.9 Hz (-0.5 %)	 126.7 Hz (+0.1 %)	 127.0 Hz (+0.4 %)
6	 127.2 Hz	 126.4 Hz (-0.6 %)	 127.2 Hz (+0.0 %)	 127.7 Hz (+0.4 %)
7	 156.2 Hz	 153.4 Hz (-1.8 %)	 154.5 Hz (-1.1 %)	 157.4 Hz (+0.8 %)
8	 156.2 Hz	 153.4 Hz (-1.8 %)	 154.5 Hz (-1.1 %)	 157.4 Hz (+0.8 %)

Table 8. Comparison of the vertical displacements due to the slab dead weight (In brackets given are the discrepancy, in percent, from the results obtained with the reference finite element model)

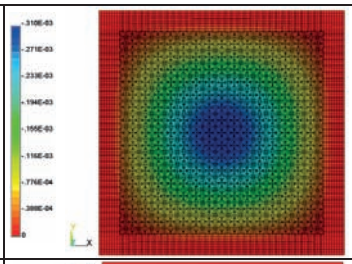
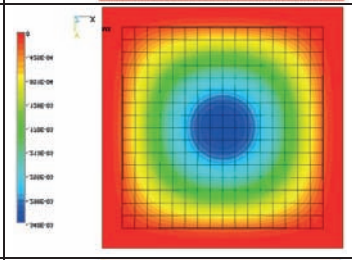
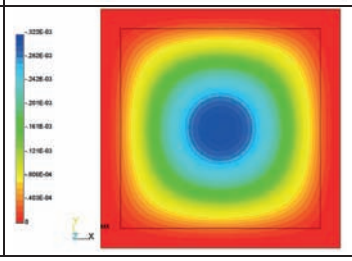
Reference model		Uz_{max} = -0.31 mm
Model 1 (parameters set 1B)		Uz_{max} = -0.34 mm (-9.7%)
Model 2 (parameters set 2A)		Uz_{max} = -0.32 mm (-3.2%)

Table 9. Comparison of the normal stress along X-axis at the top face of the slab in the central cross-section due to the slab dead weight (see also Fig. 8)

Finite element model	Min σ_x, Pa	Δ, %	Max σ_x, Pa	Δ, %
Reference model	-448349	-	1025472	-
Model 1 (parameters set 1B)	-466473	-4	831076	-19
Model 2 (parameters set 2A)	-376800	+16	901916.2	-12

3. PROBLEM TWO. A STRUCTURAL ASSEMBLY COMPRISING A BUBBLE DECK FLOOR SLAB AND A COLUMN

The second formulated problem deals with simulation of a structural assembly comprising a

bubble deck floor slab and a column using shell and beam finite elements for its spatial discretization. To determine the most accurate and efficient engineering technique for this problem, several models based on shell finite elements have been assembled and tested. Accuracy and efficiency of the particular engineering technique has been evaluated through comparison of the results of modal analysis with those obtained using a reference finite element model. As in the first case considered in the present work, as well as in the first part of the research [1], the reference model is the one constructed using solid finite elements. The reference finite element model is shown in Fig. 9.

According to the solution of the first problem describe in the previous section, the constructed engineering models are all based onto representation of the bubble deck part of the floor slab as a honey-comb structure covered with top and bottom plates, and discretization of the solid part of the floor slab with one layer of shell finite elements located at its middle surface. A total of three engineering models have been constructed, which use the same mesh (shown in Fig. 10) and differ from each other only in their parameter values.

The first parameters set, 1A, (see Table 10) is based onto the parameters set 1A from the previous section (see Table 4) with an extension to include column parameters.

In the second parameters set, 1B, (see Table 11) which is based onto the parameters set 1A, an area of the floor slab within the projection of the column cross-section (see Fig. 11) has the Young's modulus several orders of magnitude greater than that for the rest of the slab to more precisely simulate a column-slab intersection which response within the considered problem is close the rigid body one.

In the third parameters set, 1C, (see Table 12) the Young's modulus of the vertical ribs at the perimeter of the bubble deck part of the floor slab (see Fig. 11) has been increased by several times, like in the parameters set 1B of the previous section (see Table 5).

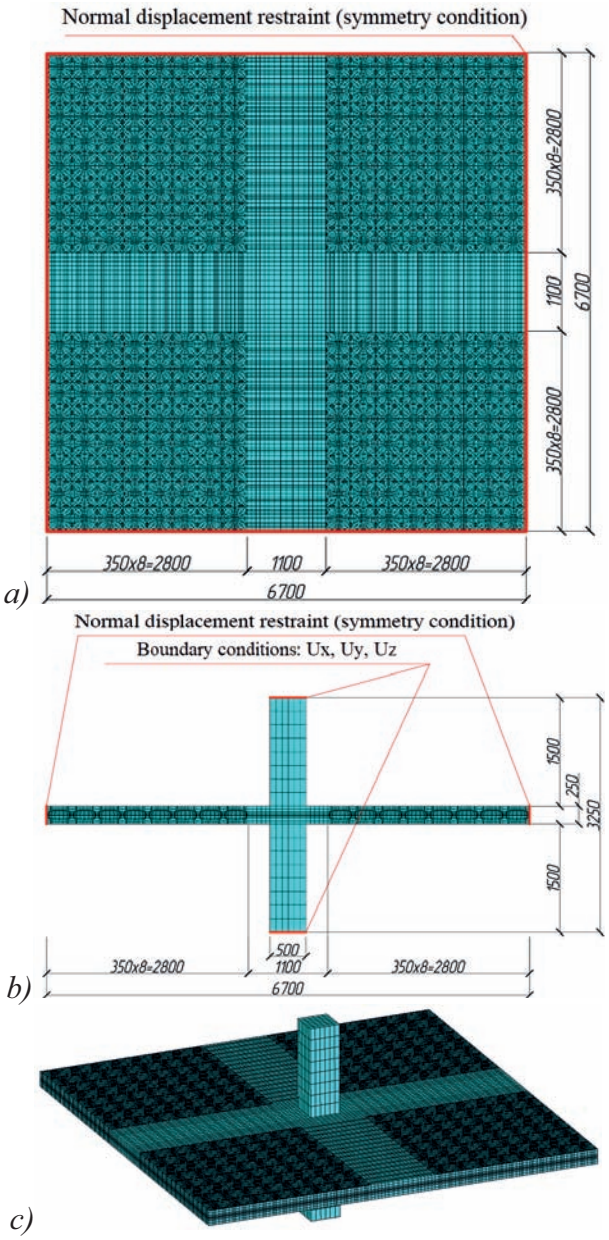


Figure 9. Geometrical parameters and boundary conditions (red lined) of the reference model of the structural assembly comprising the bubble deck floor slab and the column: a) top view; b) side view; c) orthogonal view

All DOFs (Ux, Uy, Uz, Rotx, Roty, Rotz for the models constructed using shell and beam finite elements and Ux, Uy, Uz for the reference model discretized with solid finite elements) of the nodes located at the column top and bottom are restrained. Boundary conditions at the simulated slab perimeter take into account symmetry of the problem, in particu-

lar horizontal displacements in the normal direction to a corresponding edge are restrained.

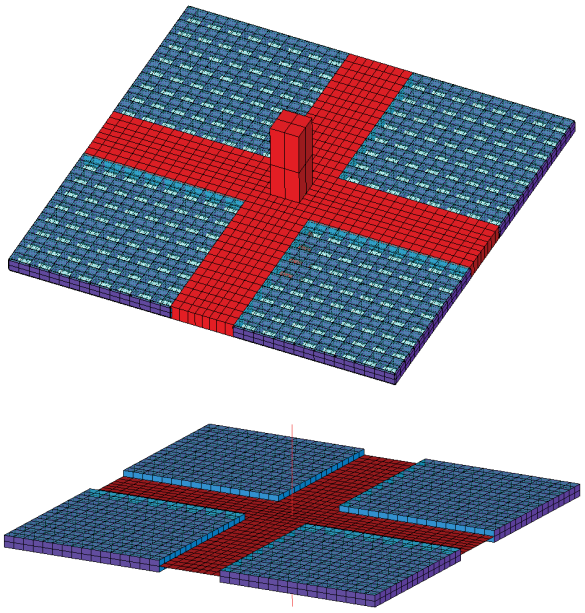


Figure 10. Finite element mesh used to simulate the structural assembly comprising the bubble deck floor slab and the column: a) element thickness displayed; b) element thickness is not displayed

Table 10. The parameters set 1A

#	Element	E, GPa	ν	ρ, kg/m^3	t, mm
1	Horizontal plate of the bubble deck part of the floor slab	30	0.2	2871.1	55
2	Vertical rib of the bubble deck part of the floor slab	87	0.2	2871.1	35
3	Solid part of the floor slab	30	0.2	2500	250
4	Column	30	0.2	2500	500×500

Note: parameters different from the reference ones are colored in blue

The results of the modal analysis of the structural assembly comprising the bubble deck floor slab and the column are given in Table 13. The engineering finite element model used in conjunction with the parameters set 1C (see in Table 11) has yielded the closest agreement with the eigenproblem solution obtained using the reference finite element model discretized with solid finite elements. The largest discrepancy amounts to 5%.

Table 11. The parameters set 1B

#	Element	E, GPa	ν	ρ, kg/m^3	t, mm
1	Horizontal plate of the bubble deck part of the floor slab	30	0.2	2871.1	55
2	Vertical rib of the bubble deck part of the floor slab	87	0.2	2871.1	35
3	Solid part of the floor slab	30	0.2	2500	250
4	Column	30	0.2	2500	500×500
5	Floor slab within the projection of the column cross-section	3e06	0.2	0	250

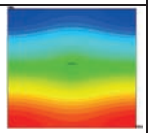
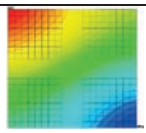
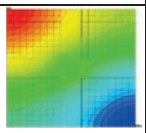
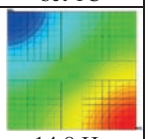
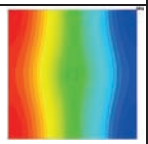
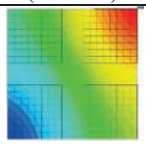
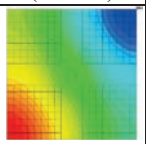
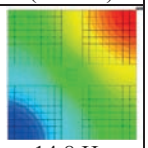
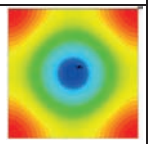
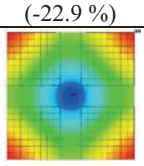
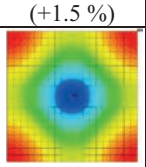
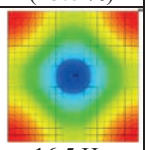
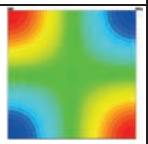
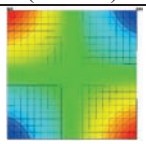
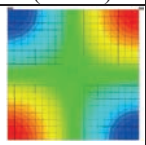
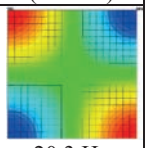
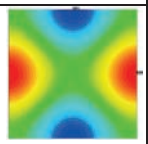
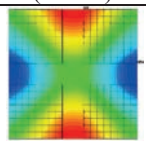
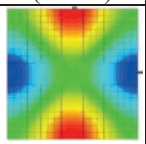
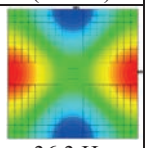
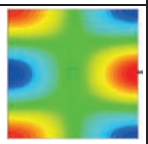
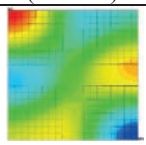
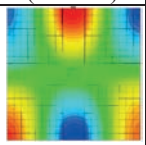
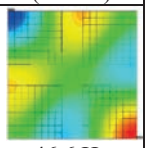
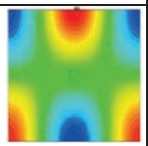
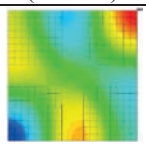
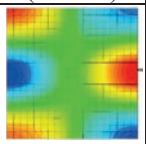
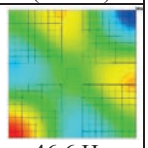
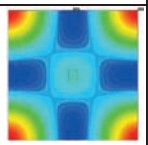
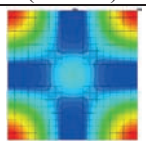
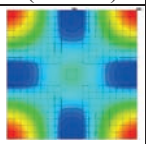
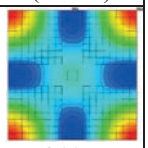
Note: parameters different from the parameters set 1A are colored in yellow

Table 12. The parameters set 1C

#	Element	E, GPa	ν	ρ, kg/m^3	t, mm
1	Horizontal plate of the floor slab	30	0.2	2871.1	55
2	Vertical rib of the floor slab	87	0.2	2871.1	35
3	Solid part of the floor slab	30	0.2	2500	250
4	Column	30	0.2	2500	500×500
5	Floor slab within the projection of the column cross-section	3e06	0.2	0	250
6	Vertical rib at the perimeter of the bubble deck part of the floor slab	400	0.2	2871.1	35

Note: parameters different from the parameters set 1B are colored in yellow

Table 13. Results of the modal analysis (In brackets given are the discrepancy, in percent, from the results obtained with the reference finite element model)

#	Reference model	Parameter set 1A	Parameter set 1B	Parameter set 1C
1	 14.3 Hz	 11.0 Hz (-22.9 %)	 14.5 Hz (+1.5 %)	 14.8 Hz (+3.6 %)
2	 14.3 Hz	 11.0 Hz (-22.9 %)	 14.5 Hz (+1.5 %)	 14.8 Hz (+3.6 %)
3	 16.3 Hz	 13.9 Hz (-15.1 %)	 15.4 Hz (-5.4 %)	 16.5 Hz (+1.3 %)
4	 20.5 Hz	 19.6 Hz (-4.1 %)	 20.1 Hz (-1.7 %)	 20.3 Hz (-0.7 %)
5	 37.4 Hz	 31.9 Hz (-14.7 %)	 32.7 Hz (-12.6 %)	 36.3 Hz (-3.1 %)
6	 49.1 Hz	 41.6 Hz (-15.2 %)	 43.2 Hz (-12.0 %)	 46.6 Hz (-5.0 %)
7	 49.1 Hz	 41.6 Hz (-15.2 %)	 43.2 Hz (-12.0 %)	 46.6 Hz (-5.0 %)
8	 58.6 Hz	 50.0 Hz (-14.7 %)	 52.7 Hz (-10.1 %)	 56.11 Hz (-4.3 %)
…	…	…	…	…

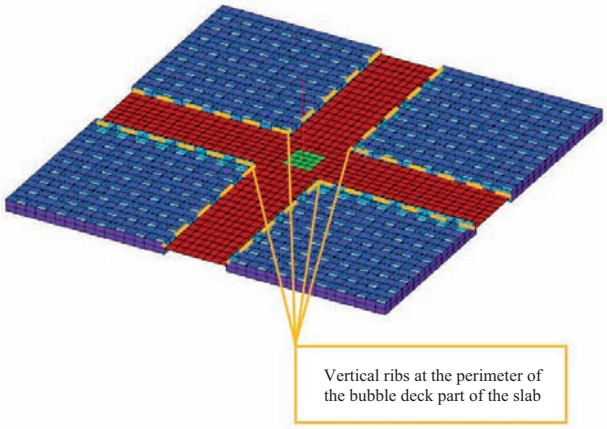


Figure 11. The finite element model used in conjunction with the parameters set 1C (finite elements within the projection of the column cross-section are colored in green)

4. PROBLEM THREE. A STRUCTURAL ASSEMBLY COMPRISING A BUBBLE DECK FLOOR SLAB AND A WALL WITH AN EMBEDDED COLUMN

Another problem considered in the present paper deals with simulation of a structural assembly comprising a bubble deck floor slab and a wall with an embedded column using shell and beam finite elements for its spatial discretization. Three engineering approaches have been tested to determine the most accurate and efficient one. Accuracy and efficiency of the particular engineering technique has been evaluated through comparison of the results of modal analysis with those obtained using a reference finite element model. As in the first two cases considered in the present work, as well as in the first part of the research [1], the reference model is the one constructed using solid finite elements. Geometrical parameters and spatial discretization of the reference finite element model are given in Fig. 12.

All DOFs (Ux, Uy, Uz, Rotx, Roty, Rotz for the models constructed using shell and beam finite elements and Ux, Uy, Uz for the reference model discretized with solid finite elements) of the nodes located at the column top and bottom are restrained. Boundary conditions at the simulated slab perimeter take into account symmetry of

the problem, in particular horizontal displacements in the normal direction to a corresponding edge are restrained.

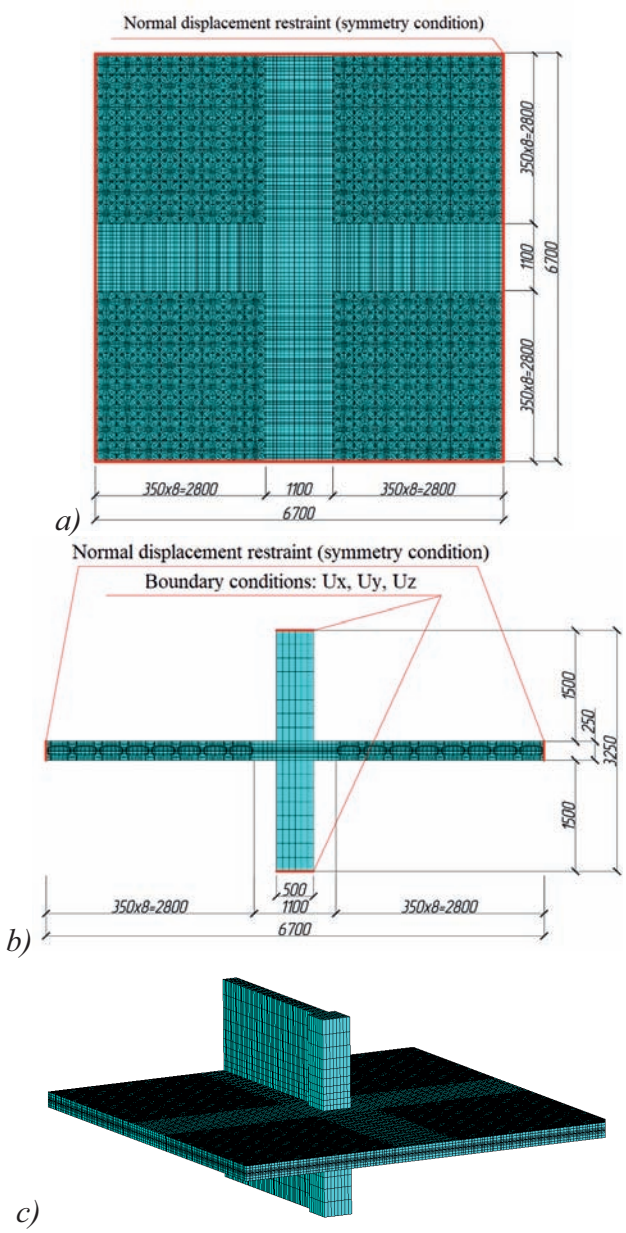


Figure 12. Geometrical parameters and boundary conditions (red lined) of the reference model of the structural assembly comprising the bubble deck floor slab and the wall with the embedded column: a) top view; b) side view; c) orthogonal view

The engineering finite element model used to solve the considered problem is based onto the model constructed in the previous section with the only difference that the wall has been added (see Fig. 13). As in the previous case, a difference between the three tested engineering techniques concerns values of the parameters defined in each case (see Tables 14–16).

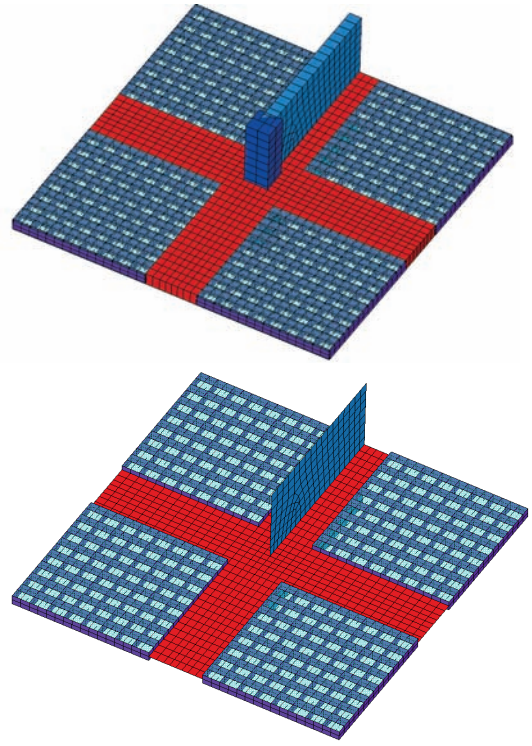


Figure 13. Finite element mesh used to simulate the structural assembly comprising the bubble deck floor slab and the wall with the embedded column: a) element thickness displayed; b) element thickness is not displayed

Table 14. The parameters set 1A

#	Element	E, GPa	ν	ρ, kg/m^3	t, mm
1	Horizontal plate of the bubble deck part of the floor slab	30	0.2	2871.1	55
2	Vertical rib of the bubble deck part of the floor slab	87	0.2	2871.1	35
3	Solid part of the floor slab	30	0.2	2500	250
4	Column	30	0.2	2500	500×500
5	Wall	30	0.2	2500	250

Note: parameters different from the reference ones are colored in blue

Table 15. The parameters set 1B

#	Element	E, GPa	ν	ρ, kg/m^3	t, mm
1	Horizontal plate of the bubble deck part of the floor slab	30	0.2	2871.1	55
2	Vertical rib of the bubble deck part of the floor slab	87	0.2	2871.1	35
3	Solid part of the floor slab	30	0.2	2500	250
4	Column	30	0.2	2500	500×500
5	Wall	30	0.2	2500	250
6	Floor slab within the projection of the column cross-section	3e06	0.2	0	250

Note: parameters different from the parameters set 1A are colored in yellow

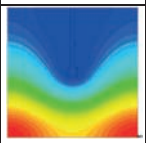
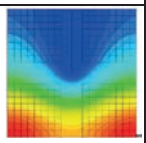
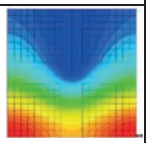
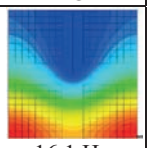
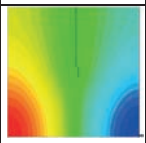
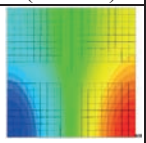
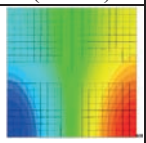
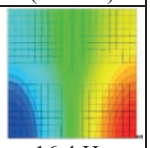
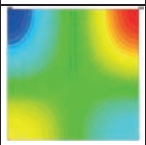
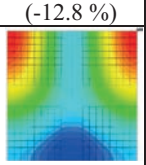
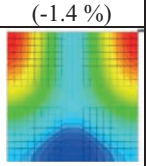
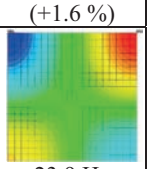
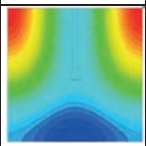
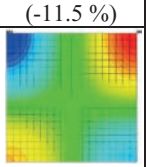
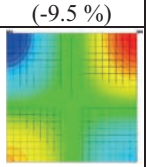
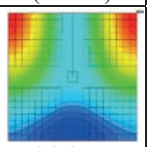
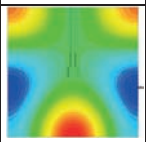
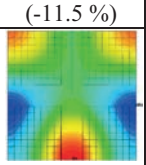
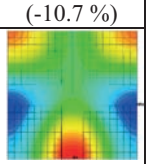
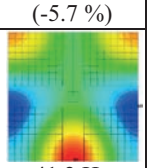
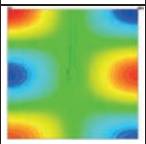
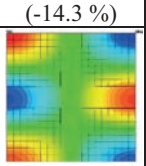
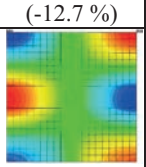
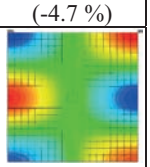
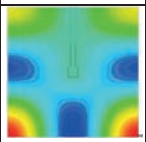
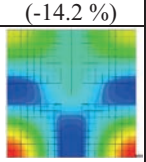
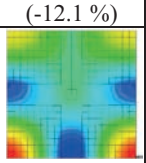
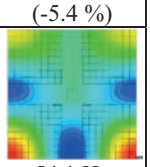
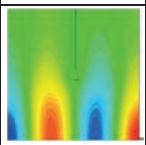
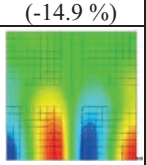
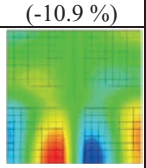
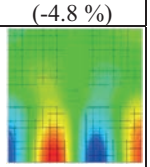
Table 16. The parameters set 1C

#	Element	E, GPa	ν	ρ, kg/m^3	t, mm
1	Horizontal plate of the bubble deck part of the floor slab	30	0.2	2871.1	55
2	Vertical rib of the bubble deck part of the floor slab	87	0.2	2871.1	35
3	Solid part of the floor slab	30	0.2	2500	250
4	Column	30	0.2	2500	500×500
5	Wall	30	0.2	2500	250
6	Floor slab within the projection of the column cross-section	3e06	0.2	0	250
7	Vertical rib at the perimeter of the bubble deck part of the floor slab	400	0.2	2871.1	35

Note: parameters different from the parameters set 1B are colored in yellow

The results of the modal analysis of the structural assembly comprising the bubble deck floor slab and the wall with the embedded column are given in Table 17. The engineering model used in conjunction with the parameters set 1C (see in Table 16) has yielded the closest agreement with the solution obtained using the reference finite element model discretized with solid finite elements. The largest discrepancy amounts to 5.7%.

Table 17. Results of the modal analysis (In brackets given are the discrepancy, in percent, from the results obtained with the reference finite element model)

#	Reference model	Parameter set 1A	Parameter set 1B	Parameter set 1C
1	 15.8 Hz	 13.1 Hz (-17.0 %)	 15.3 Hz (-2.9 %)	 16.1 Hz (+2.2 %)
2	 16.1 Hz	 14.1 Hz (-12.8 %)	 15.9 Hz (-1.4 %)	 16.4 Hz (+1.6 %)
3	 24.9 Hz	 22.0 Hz (-11.5 %)	 22.6 Hz (-9.5 %)	 23.9 Hz (-4.0 %)
4	 25.9 Hz	 22.9 Hz (-11.5 %)	 23.1 Hz (-10.7 %)	 24.4 Hz (-5.7 %)
5	 43.2 Hz	 37.1 Hz (-14.3 %)	 37.7 Hz (-12.7 %)	 41.2 Hz (-4.7 %)
6	 50.3 Hz	 43.1 Hz (-14.2 %)	 44.2 Hz (-12.1 %)	 47.6 Hz (-5.4 %)
7	 56.8 Hz	 48.4 Hz (-14.9 %)	 50.6 Hz (-10.9 %)	 54.1 Hz (-4.8 %)
8	 93.5 Hz	 81.7 Hz (-12.6 %)	 84.3 Hz (-9.8 %)	 91.8 Hz (-1.8 %)

CONCLUSION

The following conclusions can be made based on the first part of the research [1], the present paper, and their comparison:

1. Three types of finite element models have been constructed to perform static response analysis and modal analysis of a reinforced concrete bubble deck floor slab as a separate unit or as a part of a structural assembly comprising the slab and a column or the slab and a wall with an embedded column:

– Models of the first type have been spatially discretized with solid finite elements, that has allowed one to precisely repeat the bubble deck floor slab geometry. Numerical results obtained with such models have been considered as reference ones.

– Models of the second type have been spatially discretized with shell and beam finite elements. In these models the void former cell of the slab is modelled as a honey-comb structure with top and bottom cover plates.

– Models of the third type have also been spatially discretized with shell and beam finite elements, but in these models the part of the floor slab with void formers is modelled through one layer of shell finite elements located at the slab middle surface and been assigned effective mass and stiffness properties.

2. Numerical models based on solid finite elements allow one to accurately simulate static and dynamic responses of structural elements with a complex cross-section, like the considered bubble deck floor slab. Yet, application of such an approach to a building arises enormous difficulties during model construction and is very time consuming at the analysis stage. Moreover, common tools to design reinforcement are not applicable within such an approach.
3. The engineering approach, within which the void former cell of the slab is modelled as a honeycomb structure with top and bottom cover plates, all discretized with shell finite elements, significantly reduces human and computational resources necessary to construct and analyze the model of a building, in which the considered lightweight structural solution is adopted. It provides sufficient accuracy and allows one to use standard design tools, in particular to determine the required amount of reinforcement. This developed technique is recommended to be utilized for simulation of building with similar lightweight structural elements solutions, in particular located in earthquake-prone regions.
4. The engineering approach, in which the reinforced concrete bubble deck floor slab is modelled with one layer of shell finite elements located at the slab middle surface and been assigned effective mass and stiffness properties, provides relatively low accuracy with respect to both static and dynamic responses of such structural elements and assemblies comprising them, and, given the more accurate alternative exists, should not be utilized for simulation of buildings with bubble deck floor slabs exposed to seismic loads.

ACKNOWLEDGEMENTS

The research was conducted as part of the development programme for 2025-2036 of Moscow State University of Civil Engineering under the framework of strategic academic leadership programme “Priority 2030”.

REFERENCES

1. **Belostotsky A., Nagibovich A., Scherbina S., Vasileva T.** Numerical modeling of cast-in-place reinforced concrete bubble deck floor slabs utilized in earthquake-prone region // Int. J. Comput. Civil Struct. Eng. – 2025. – Vol. 21. – No. 2. – Pp. 187-199.
2. **Dzhamuev B.K.** The effect of non-removable void generators on the strength of monolithic reinforced concrete floor slabs clamped along the contour // Building and Reconstruction. – 2024. – Vol. 2. Pp. 3-15. (In Russian)

3. **Tiwari N., Zafar S.** Structural behavior of bubble deck slabs and its application: Main paper // Int. J. Sci. Res. Dev. – 2016. – Vol. 4. – Iss. 02. – Pp. 433-437.
4. **Ibrahim A.M., Ali N.K., Salman W.D.** Flexural capacities of reinforced concrete two-way bubble deck slabs of plastic spherical voids // J. Print. Iraq. – 2013. – Vol. 06. – No. 02. – Pp: 9-20.
5. **Valivonis J., Skuturna T, Daugeviius M., Šneideris A.** Punching shear strength of reinforced concrete slabs with plastic void formers // Constr. Build. Mater. – 2017. – Vol.145. – Pp. 518-527.
6. **Saifulla M., Azeem M.A.** Comparative seismic performance of a conventional slab and flat slab over a bubble deck slab // Int. J. Emerg. Technol. Adv. Eng. – 2017. – Vol. 7. – Iss. 11. – Pp. 137-143.
7. **Teja P.P., Kumar P.V, Mounika C.H., Saha P.** Structural behavior of bubble deck slab / In: Proceedings of the IEEE-International Conference on Advances in Engineering, Science and Management, Nagapattinam, Tamil Nadu, India, 2012. – Pp: 383-388.
8. **Lakshmikanth L., Poluraju P.** Performance of structural behaviour of bubble deck slab // Int. J. Recent Technol. Eng. – 2019. – Vol.7. – Iss. 6C2. – Pp. 865-870.
9. **Varghese J.P, George M.** Parametric investigation on the seismic response of voided and solid flat slab systems // Int. J. Innov. Sci. Eng. Technol. – 2018. – Vol. 5. – Iss. 3. – Pp 256-258.
10. **Nagashree B, Shariff S., Kumar M.** Experimental studies on comparison of conventional slab and bubble deck slab based on strength // Int. J. Sci. Res. Dev. – 2017. – Vol. 5. – Iss. 3. – Pp: 1160-1162.
11. **Orlova M.D., Mnushkin M.A., Evtushenko I.S., Vinogradova K.I., Egarmin K.A.** Analysis of the use of hollow formers from recycled polypropylene in the creation of lightweight monolithic floors. Research of various directions of modern science: Collection of materials of the XXI International Scientific and practical Conference. Part 1. Moscow. 2017. Pp. 562-567. (In Russian)
12. **Filimonova E.S**. Analysis of the stress-strain state of a monolithic floor slab with void generators according to the Cobiax system based on various computational models // Young Scientist. – 2022. – No. 20 (415). – Pp. 107-109. (In Russian)
13. STO 35546020.001-2016 «Fixed formwork (voids and couplings) Sibforma ®. General information about the technology, product range. Recommendations for the calculation and design of monolithic girderless floor slabs with non-removable formwork Sibform ® in accordance with Code of Practice 63.13330.2012». (In Russian)
14. STO 38311046-001-2019 «Monolithic reinforced concrete lightweight slabs with Simkar void formers. Rules of design and construction». (In Russian)
15. Recommendations for the calculation of monolithic beamless floor slabs with Simkar void-forming slabs (without prestressing) / National Research Moscow State University of Civil Engineering, 2014. – 119 p.
16. **Белостоцкий А.М., Дубинский С.И., Аул А.А., Нагибович А.И., Афанасьева И.Н., Козырев О.А., Павлов А.С.** Verification report ANSYS Mechanical software (4 volume). – M.: National Research Moscow State University of Civil Engineering, Research & Development Centre StaDyO, 2009, 2024.
17. Code of Practice 63.13330.2018 “Concrete and reinforced concrete structures. General provisions”.
18. Structural Analysis Guide, Documentation for ANSYS, Release 21R2. 2021.
19. **Belostotsky A., Nagibovich A., Novikov P., Vershinin V.** Earthquake of buildings and structures: regulatory “must-do” or scientifically substantiated results // Int. J. Comput. Civil Struct. Eng. – 2024. – Vol. 20. – No. 4. – Pp. 241-252.

20. **Dmitriev D., Novikov P., Petryashev S., Nagibovich A.** Consideration of the seismic impact's wave nature in the design justification of high-rise buildings seismic resistance // Int. J. Comput. Civil Struct. Eng. – 2024. – Vol. 20. – No. 3. – Pp. 198-205.
21. **Belostotsky A., Nagibovich A., Pavlov A.** Numerical simulation of the stress-strain state of a large-span structure with joints with gap under the seismic loads in a transient dynamic // Int. J. Comput. Civil Struct. Eng. – 2023. – Vol. 19. – No. 3. – Pp. 165-172.
22. **Malahova A.N**. Pustotnye kessonnye plity perekrytij monolitnyh mnogoetazhnyh zdanij [Hollow coffered floor slabs of monolithic multi-storey buildings] // Vestnik MGSU. – 2016. – No. 6. – Pp. 15-24. (In Russian)

СПИСОК ЛИТЕРАТУРЫ

1. **Belostotsky A., Nagibovich A., Scherbina S., Vasileva T.** Numerical modeling of cast-in-place reinforced concrete bubble deck floor slabs utilized in earthquake-prone region // Int. J. Comput. Civil Struct. Eng. – 2025. – Vol. 21. – No. 2. – P. 187-199.
2. **Джамуев Б.К.** Влияния несъемных пустотообразователей на прочность защемленных по контуру монолитных железобетонных плит перекрытия // Строительство и реконструкция. –2024. – Т. 2. – С. 3-15.
3. **Tiwari N., Zafar S.** Structural behavior of bubble deck slabs and its application: Main paper // Int. J. Sci. Res. Dev. – 2016. – Vol. 4. – Iss. 02. – Pp. 433-437.
4. **Ibrahim A.M., Ali N.K., Salman W.D.** Flexural capacities of reinforced concrete two-way bubble deck slabs of plastic spherical voids // J. Print. Iraq. – 2013. – Vol. 06. – No. 02. – Pp: 9-20.
5. **Valivonis J., Skuturna T, Daugeviius M., Šneideris A.** Punching shear strength of reinforced concrete slabs with plastic void formers // Constr. Build. Mater. – 2017. – Vol.145. – Pp. 518-527.
6. **Saifulla M., Azeem M.A.** Comparative seismic performance of a conventional slab and flat slab over a bubble deck slab // Int. J. Emerg. Technol. Adv. Eng. – 2017. – Vol. 7. – Iss. 11. – Pp. 137-143.
7. **Teja P.P., Kumar P.V, Mounika C.H., Saha P.** Structural behavior of bubble deck slab / In: Proceedings of the IEEE-International Conference on Advances in Engineering, Science and Management, Nagapattinam, Tamil Nadu, India, 2012. – Pp: 383-388.
8. **Lakshmikanth L., Poluraju P.** Performance of structural behaviour of bubble deck slab // Int. J. Recent Technol. Eng. – 2019. – Vol.7. – Iss. 6C2. – Pp. 865-870.
9. **Varghese J.P, George M.** Parametric investigation on the seismic response of voided and solid flat slab systems // Int. J. Innov. Sci. Eng. Technol. – 2018. – Vol. 5. – Iss. 3. – Pp 256-258.
10. **Nagashree B, Shariff S., Kumar M.** Experimental studies on comparison of conventional slab and bubble deck slab based on strength // Int. J. Sci. Res. Dev. – 2017. – Vol. 5. – Iss. 3. – Pp: 1160-1162.
11. **Орлова М.Д., Мнушкин М.А., Евтушенко И.С., Виноградова К.И., Егармин К.А.** Анализ применения пустотообразователей из рециклированного полипропилена при создании облегченных монолитных перекрытий. Исследование различных направлений современной науки: Сборник материалов XXI Международной научнопрактической конференции. Ч.1. Москва. 2017. С. 562-567.
12. **Филимонова Е.С.** Анализ напряженно-деформированного состояния монолитной плиты перекрытия с пустотообразователями по системе Cobiax на основании различных расчетных моделей // Молодой ученый. – 2022. – № 20 (415). – С. 107-109.

13. СТО 35546020.001-2016 «Несъемная опалубка (пустотообразователи и соединительные муфты) Сибформа®. Общие сведения о технологии, номенклатура изделий. Рекомендации по расчету и конструированию монолитных безбалочных плит перекрытий с несъемной опалубкой Сибформа® в соответствии с СП 63.13330.2012».
14. СТО 38311046-001-2019 «Монолитные железобетонные облегченные плиты с пустотообразователями Simkar. Правила проектирования и возведения».
15. Рекомендации по расчету монолитных безбалочных плит перекрытий с пустотообразователями «Симкар» (без предварительного напряжения) / ФБГОУ ВПО «МГСУ». – М.: МГСУ, 2014. –119 с.
16. **Белостоцкий А.М., Дубинский С.И., Аул А.А., Нагибович А.И., Афанасьева И.Н., Козырев О.А., Павлов А.С.** Верификационный отчет по программному комплексу ANSYS Mechanical (4 тома). – М.: ЗАО НИЦ СтаДиО, НОЦ КМ МГСУ, 2009, 2024.
17. СП 63.13330.2018. Бетонные и железобетонные конструкции. М., Минстрой, 2018.
18. Structural Analysis Guide, Documentation for ANSYS, Release 21R2. 2021.
19. **Belostotsky A., Nagibovich A., Novikov P., Vershinin V.** Earthquake of buildings and structures: regulatory “must-do” or scientifically substantiated results // Int. J. Comput. Civil Struct. Eng. – 2024. – Vol. 20. – No. 4. – Pp. 241-252.
20. **Dmitriev D., Novikov P., Petryashev S., Nagibovich A.** Consideration of the seismic impact’s wave nature in the design justification of high-rise buildings seismic resistance // Int. J. Comput. Civil Struct. Eng. – 2024. – Vol. 20. – No. 3. – Pp. 198-205.
21. **Belostotsky A., Nagibovich A., Pavlov A.** Numerical simulation of the stress-strain state of a large-span structure with joints with gap under the seismic loads in a transient dynamic // Int. J. Comput. Civil Struct. Eng. – 2023. – Vol. 19. – No. 3. – Pp. 165-172.
22. **Малахова А.Н.** Пустотные кессонные плиты перекрытий монолитных многоэтажных зданий // Вестник МГСУ. – 2016. – № 6. – С. 15-24

Alexander M. Belostotsky – DSc, Professor, Full Member of the Russian Academy of Architecture and Construction Sciences, Scientific adviser at Zolotov Research and Educational Center for Computational Modelling of the National Research Moscow State University of Civil Engineering; 129337, Russia, Moscow, Yaroslavskoe shosse, 26. E-mail: amb@stadyo.ru

Белостоцкий Александр Михайлович – д.т.н., профессор, академик РААСН, научный руководитель НОЦ КМ им. А.Б. Золотова Национального исследовательского Московского государственного строительного университета; 129337, Россия, г. Москва, Ярославское шоссе, д. 26. E-mail: amb@stadyo.ru

Alexander I. Nagibovich – engineer at Zolotov Research and Educational Center for Computational Modelling of the National Research Moscow State University of Civil Engineering; 129337, Russia, Moscow, Yaroslavskoe shosse, 26. Leading calculation engineer at the Scientific and Research Center StaDyO; 18, The 3rd Yamskogo Polya st., Moscow, 125040, Russia. E-mail: nagibovich@yandew.ru

Нагибович Александр Игоревич – к.т.н., старший научный сотрудник НОЦ КМ им. А.Б. Золотова Национального исследовательского Московского государственного строительного университета; 129337, Россия, г. Москва, Ярославское шоссе, д. 26. Ведущий инженер-расчетчик АО НИЦ СтаДиО; E-mail: nagibovich@yandex.ru

Sergey V. Scherbina – engineer at Zolotov Research and Educational Center for Computational Modelling of the National Research Moscow State University of Civil Engineering; 129337, Russia, Moscow, Yaroslavskoe shosse, 26. Calculation engineer at the Scientific and Research Center StaDyO; 18, The 3rd Yamskogo Polya st., Moscow, 125040, Russia. E-mail: scherbine@mail.ru

Щербина Сергей Викторович – инженер НОЦ КМ им. А.Б. Золотова Национального исследовательского Московского государственного строительного университета; 129337, Россия, г. Москва, Ярославское шоссе, д. 26. Инженер-расчетчик АО НИЦ СтаДиО; E-mail: scherbine@mail.ru

Tatiana N. Vasileva – engineer at Zolotov Research and Educational Center for Computational Modelling of the National Research Moscow State University of Civil Engineering; 129337, Russia, Moscow, Yaroslavskoe shosse, 26. Calculation engineer at the Scientific and Research Center StaDyO; 18, The 3rd Yamskogo Polya st., Moscow, 125040, Russia. E-mail: rabitfew@gmail.com

Васильева Татьяна Николаевна – инженер НОЦ КМ им. А.Б. Золотова Национального исследовательского Московского государственного строительного университета; 129337, Россия, г. Москва, Ярославское шоссе, д. 26. Инженер-расчетчик АО НИЦ СтаДиО; E-mail: rabitfew@gmail.com

International Journal for Computational Civil and Structural Engineering, 21(4) 146–161 (2025)

DOI:10.22337/2587-9618-2025-21-4-146-161

PROBABILISTIC DYNAMIC ANALYSIS OF A SINGLE-MASS VIBRATION ISOLATION SYSTEM

Vladimir A. Smirnov, Marina V. Shitikova

Moscow State University of Civil Engineering. Moscow, RUSSIA

Abstract: The article considers the problem of probabilistic calculation of a single-mass oscillatory system intended for solving problems of force or kinematic vibration isolation. The solution of three problems for the mode of free and forced oscillations is considered depending on the element, the probabilistic characteristics of which are determined. The first problem includes the case of a known probabilistic distribution of the load and constant system parameters. The second problem includes the case of a known probabilistic distribution of the system parameters under a constant external influence. The third problem will combine known probabilistic characteristics for both the external influence and the system parameters. The purpose of solving these problems is to obtain the distribution of the system response under the specified types of influences, as well as to test the methodology for their numerical solution using the Monte Carlo method.

Keywords: vibration isolation, probabilistic calculations, randomness, force vibration protection, kinematic vibration protection, single-mass system

ВЕРОЯТНОСТНЫЙ РАСЧЁТ ОДНОМАССОВОЙ ВИБРОЗАЩИТНОЙ СИСТЕМЫ

В.А. Смирнов, М.В. Шитикова

Национальный исследовательский Московский государственный строительный университет, г. Москва, РОССИЯ

Аннотация: В статье рассматривается задача вероятностного расчёта одномассовой колебательной системы, предназначенной для решения задач силовой или кинематической виброизоляции. Рассматривается решение трёх задач для режима свободных и вынужденных колебаний в зависимости от элемента, вероятностные характеристики которого определены. К первой задаче относим случай известного вероятностного распределения нагрузки и постоянными параметрами системы. Ко второй – случай известного вероятностного распределения параметров системы при постоянном внешнем воздействии. Третья задача будет объединять известные вероятностные характеристики как для внешнего воздействия, так и для параметров системы. Целью решения данных задач является получение распределения отклика системы при указанных видах воздействий, а также апробация методики численного их решения, используя метод Монте-Карло.

Ключевые слова: виброизоляция, вероятностные расчёты, случайность, силовая виброзащита, кинематическая виброзащита, одномассовая система

1. INTRODUCTION

The single-degree-of-freedom (SDOF) mechanical model is widely used as the simplest model for analyzing oscillations and vibration isolation of various objects. The equation of motion of such a linear system is written as [1]

$$m\ddot{u}(t) + c\dot{u}(t) + ku(t) = F_1(t), \qquad (1)$$

where m is the mass of the object, kg; c is the coefficient of viscous damping, Ns/m; k is the dynamic stiffness of the elastic element, N/m; and $F_1(t)$ is the external force, N.

The natural frequency of the system could be determined as $\omega_0 = \sqrt{k/m}$, while the relative damping coefficient is defined as $\zeta = \dfrac{c}{2\sqrt{km}}$.

The deterministic approach to vibration isolation calculation assumes that the system parameters (m, c, k) and the external loading $f(t)$ are precisely known and constant. However, in real conditions, both factors could vary significantly, being random in nature due to manufacturing tolerances, changes in material properties and unpredictability of external loads [2, 3]. Ignoring this random variability leads either to unreasonably high safety margins (and an increase in the mass and cost of vibration isolation system) or to reduced reliability if the actual deviations exceed the calculated tolerances [3, 4]. Considering the probabilistic characteristics of both the load and system parameters allows for a more realistic assessment of the dynamic response of the vibration-isolated object and the reliability of vibration protection [1]. Modern design standards for structures and machines are increasingly based on the concepts of reliability and the probabilistic approach, especially for critical structures under severe dynamic loads (seismicity, explosion, road disturbances, etc.) [3].

For vibration isolation systems, the statistical approach means determining the probability distribution of the response (displacements, and/or| accelerations) instead of a single deterministic value. In this way, it is possible to estimate the probability with which critical vibration levels will be exceeded and to select the system parameters that ensure a given level of reliability under random impacts [3]. In practice there are problems in which the external impact on the system could be represented as a random variable (or random process) with known distribution parameters. A large body of work is devoted to the study of this issue, including the monographs by Bolotin [5], Biderman [6], Mondrus [7], Raiser [8], etc. Such types of random loads include wind loads [9, 10], transport loads [11, 12], pedestrian loads [13, 14], microseismic activity [15, 16], and many others. There is also a class of problems in which the system parameters (bearing capacity, deformation characteristics) could be expressed as random variables with known distribution parameters [18 – 20].

This article is aimed at the assessment of the response probabilistic characteristics for a simple SDOF system subjected to an external load, provided that either the load is a random variable with a known distribution, or the system parameters have known probabilistic characteristics. Since the materials used in vibration isolation systems for buildings, structures, and various units have a certain manufacturing error: either geometric dimensions or mechanical parameters, this problem is of high interest. In addition, the forces acting on vibration isolation system often vary greatly over time, which leads to the need to use probabilistic approaches in their calculation justification.

In connection with the above, we consider problems of three types:

1. Random characteristics of system parameters.
2. Random load with a known distribution.
3. Combination of tasks of types 1 and 2.

2. MODEL

We consider the SDOF model for the vibration isolation system shown in Figure 1, in which the isolated body of mass m rests on the Kelvin-Voigt element, which has an elastic element of stiffness k and a viscous element c. The body m is subject to either an external load of the type $F_1(x,t)$ (to simplify the problem, we will assume that its value does not depend on the displacement x of mass m), or a kinematic disturbance of the base of the type $F_2(t) = z(t)$ is applied.

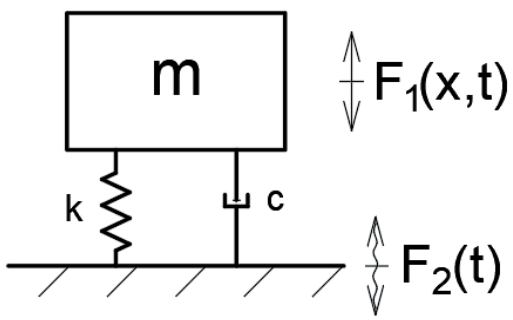


Figure 1. Calculation scheme of a single-mass oscillatory system

The equation for an oscillating mass m under the action of an external load $F_1(t)$ is described by equation (1) subjected to the initial conditions

$$x(0) = x_{00}, \qquad \dot{x}(0) = x_{10}\,. \tag{2}$$

In the case of an external motion of the base $\ddot{z}(t)$, equation (1) is reduced to the form:

$$m\ddot{x} + c\dot{x} + kx = -m\ddot{z}\,. \tag{3}$$

The quality of the vibration isolation is assessed by the value of the transfer function:

$$\Delta L = 20\log\sqrt{\frac{1+\eta^2\left(\frac{f}{f_0}\right)^2}{\left(1-\left(\frac{f}{f_0}\right)^2\right)^2+\eta^2\left(\frac{f}{f_0}\right)^2}}\,, \tag{4}$$

where f is the external load frequency, Hz; f_0 is the natural frequency of the system, Hz, $\omega_0 = 2\pi f_0$; and $\eta = 2\zeta$ is the loss coefficient of the system.

To account for the spread of parameters in calculations of single-mass systems, both numerical Monte Carlo methods and analytical approaches are used [21, 22]. The direct Monte Carlo method involves multiple modeling of the system response with different realizations of random load parameters or stiffness/damping (generated according to a known distribution law) and subsequent statistical analysis of the response (assessment of the amplitude distribution, probability of exceeding threshold values, etc.). This approach is universal and is easily implemented for the SDOF model [23]. However, it does not provide an explicit analytical understanding of the influence of parameter uncertainty and may require large computational costs when it is necessary to estimate small failure probabilities. Therefore, analytical methods have been developed in the literature that make it possible to obtain response characteristics without directly enumerating a set of realizations. One of the classical results is the so-called "damping effect" in stochastic oscillators: it was shown that random fluctuations of the natural frequency ω_0 lead to a decrease in the average resonant response as if the system had more damping, smoothing out the resonance [24]. Adhikari and Pascual [1] considered a linear oscillator with a given distribution of the natural frequency (uncertainty in k for fixed m, c) and obtained an analytical expression for the mean square response in the vicinity of resonance. In particular, for the case of ω_0 uniform distribution, a closed formula for the equivalent damping coefficient was derived, explaining the decrease in the amplitude of the average response compared to a deterministic system [24]. In addition, they developed a hybrid analytical-numerical method (the Laplace method) for calculating not only the average, but also the variance of the response function (frequency characteristic) of the SDOF system for various specified parameter distributions (normal, lognormal, gamma distribution, etc.) [25, 26]. The obtained approximate formulas were successfully verified by comparison with direct simulation using the Monte Carlo method [27]. An important conclusion was that standard small parameter methods (series expansion in small parameter variance) or polynomial chaos could give large errors near resonance [28]. This is due to the nonlinear dependence of the forced vibration amplitude on the natural frequency near the resonant point. Thus, special approaches that take the stochastic nature of resonance into account are required for a reliable estimate of the maximum response. Since for the vibration isolation system its operational range is usually far from resonance, the Monte Carlo method was used for the calculations in further analysis.

2.1. Problem I

In real vibration isolators, the system parameters – primarily the elastic element

stiffness (k) and the damping coefficient (c) – are not strictly constant values, but have a spread due to such technological features as material degradation over time, variations in temperature and humidity conditions, and so on [29]. This leads to the fact that the resonant frequency ω_0 and the quality factor of the system also become random variables. If the external influence (e.g., harmonic force or acceleration of the foundation) is fixed and defined, then the system response (oscillation amplitudes, transmitted forces) will be random due to the uncertainty in k, c (or m) [29]. Such a scatter in properties is incidental for elastomeric vibration isolators and rubber mounts: the actual elastic moduli and damping properties may differ from sample to sample. In addition to the discrepancies between the nominal and actual parameters due to manufacturing tolerances, additional changes occur during operation (e.g., rubber aging leads to changes in stiffness and damping). The spread of stiffness and loss factor values is usually described by statistical distributions determined based on experiments. There are various hypotheses about the distribution law of such parameters in literature. In the absence of sufficient experimental data, some researchers assume a uniform spread of ±5% from the nominal value or use a normal distribution with a variation coefficient of about 10–25% [30]. However, recent studies indicate that actual distributions could differ significantly from the normal one. For example, for rubber-metal building supports (seismic isolators), it was shown that the distributions of horizontal and vertical stiffness are better described by a lognormal law or a generalized extreme distribution, whereas the assumption of a "normal" distribution yields large systematic discrepancies [31, 32]. In Wu et al. [2], the characteristics of 224 rubber bearings were measured and statistical processing of different distributions was performed. Thus, based on the goodness-of-fit criteria, it was found that the lognormal and generalized extreme distributions (type I) provide the best fit to the experimental stiffness histograms, while the normal distribution deviates significantly [33, 34]. At the same time, the stiffness variation coefficients obtained in these tests lie in the range of ~1–5%, which reflects the relative homogeneity of serial isolators during controlled production [35, 36]. Nevertheless, even such a spread significantly affects the dynamic properties of the system. Vibration isolation systems often use vibration damping mats laid along the base of the foundation of the protected building, structure or machine. Let us assume a design situation in which a vibration damping mat with plan dimensions a x b and thickness t is laid along the base of the protected mass m. In this case, the system parameters have statistical characteristics presented in Table 1.

In the case of using vibration damping mats, their dynamic rigidity k_{dyn} could be determined by the formula:

$$k_{dyn} = \frac{E_{dyn} \cdot A_{surf}}{t}, \tag{5}$$

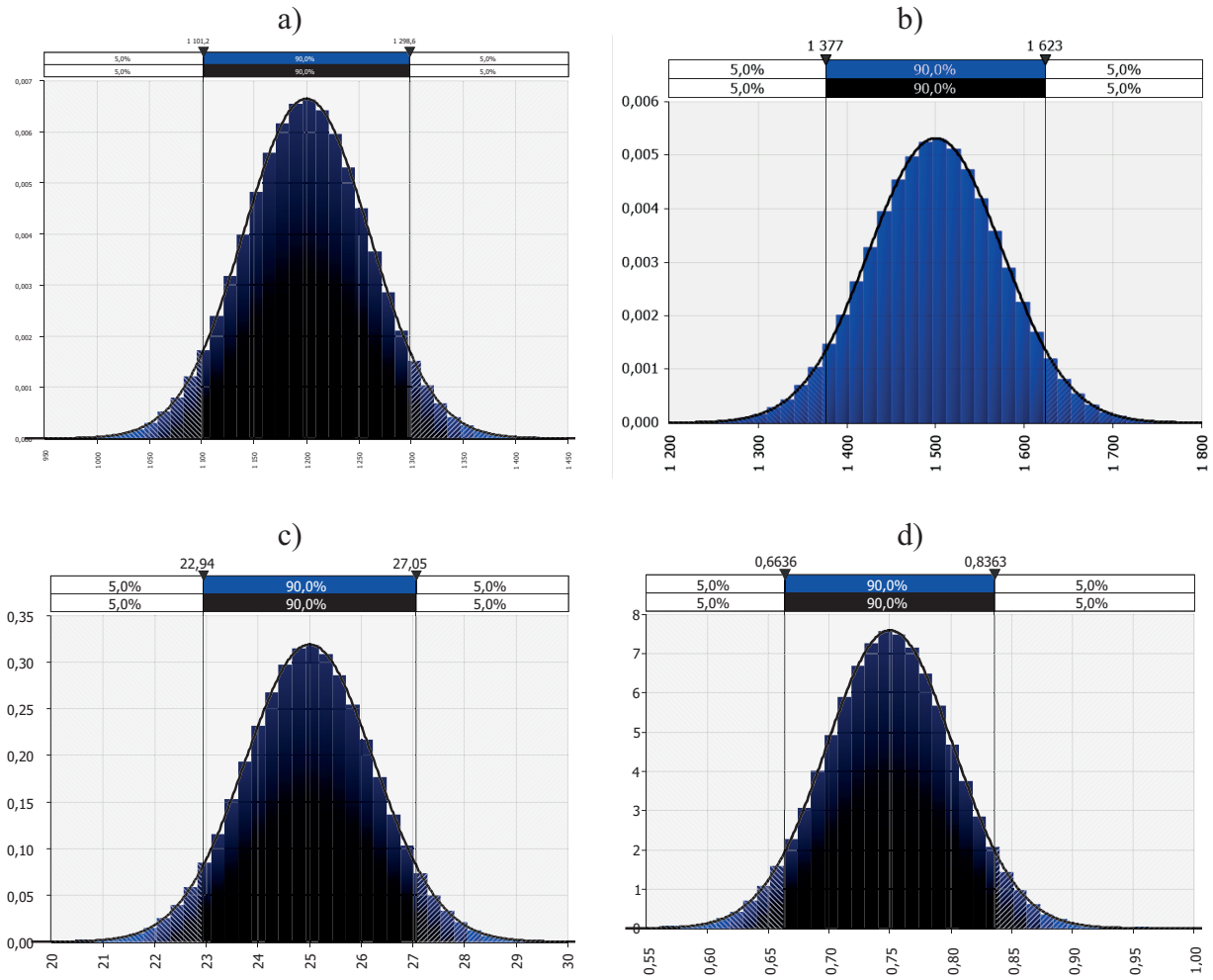
where E_{dyn} is the value of the dynamic modulus of elasticity corresponding to the specified load on the sample, the frequency of load application and its shape factor, N/m^2; A_{surf} is the area of the loaded sample, m^2; and t is the thickness of the loaded sample, m.

Assuming that the specified parameters have a normal distribution, it is possible to evaluate the quality of the specified vibration protection system and to estimate the sensitivity to a set of factors.

Figures 2 a – f show the normal distribution curves of the parameters used in the calculations. The curves were obtained by the Monte Carlo method (at least 100,000 tests) taking into account the distribution parameters according to Table 1.

Table 1. Statistical characteristics of vibration protection system elements

Parameter	Mean value	Dimension	Variance	Notes
Geometric dimensions of vibration damping mats				
a	1200	mm	5%	ISO3302-1:1999 (Class L3)
b	1500	mm	5%	
t	25	mm	5%	
Physical and mechanical characteristics of mats				
E_{dyn}	0.75	N/mm^2	7%	Author data
η	0.13	-	7%	
Isolated mass				
m	10500	kg	10%	Considering safety factors + errors in dimensions + errors in material density



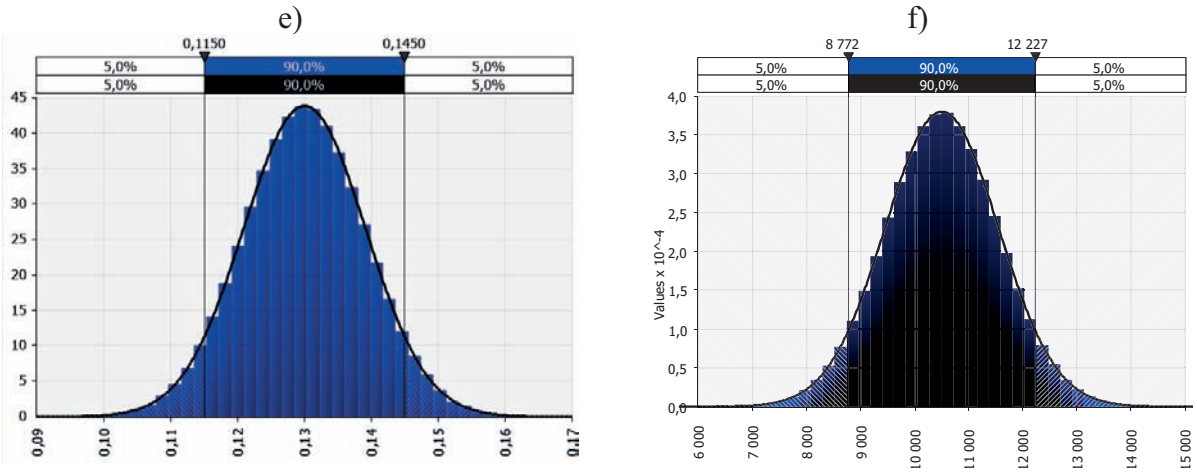


Figure 2. Distribution of design parameters according to Table 1: a) length; b) width; c) thickness; d) Edyn; e) η; f) m.

By setting the parameters in formulas (4) and (5) in the form of random variables having a normal distribution with the characteristics given in Table 1, it is possible to estimate the distribution of the calculation results, namely: the natural oscillation frequency of the vibration protection system, as well as the efficiency of vibration isolation in the frequency range from 1 to 100 Hz (a 1/3-octave spectrum was selected for calculation).

The distribution of the natural oscillation frequency of the vibration protection system is shown in Figure 3.

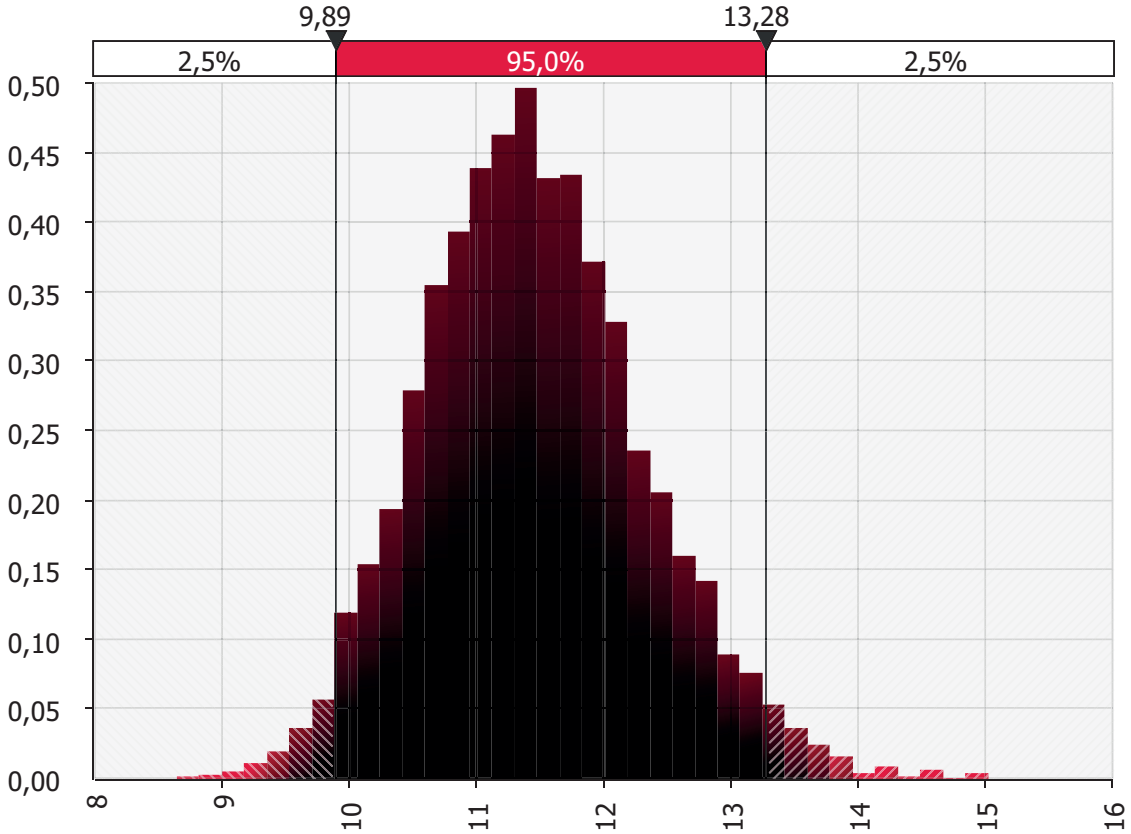


Figure 3. Probability density of the natural oscillation frequency of the vibration protection system

The calculation results show that the 95% confidence interval includes f_0 values from 9.89 to 13.28 Hz with the median value being 11.42 Hz. The standard deviation for f_0 is 0.86 Hz. The graph in Figure 3 illustrates a slight asymmetry relative to the median value, the asymmetry coefficient is 0.34 (i.e. the right tail of the distribution is larger than the left). When performing a deterministic calculation, f_0 = 11.41 Hz, which coincides with the median value.

To assess the efficiency of the vibration protection system, we will estimate the distribution of the transfer function (4). The results are presented in the form of a Whisker diagram in Figure 4.

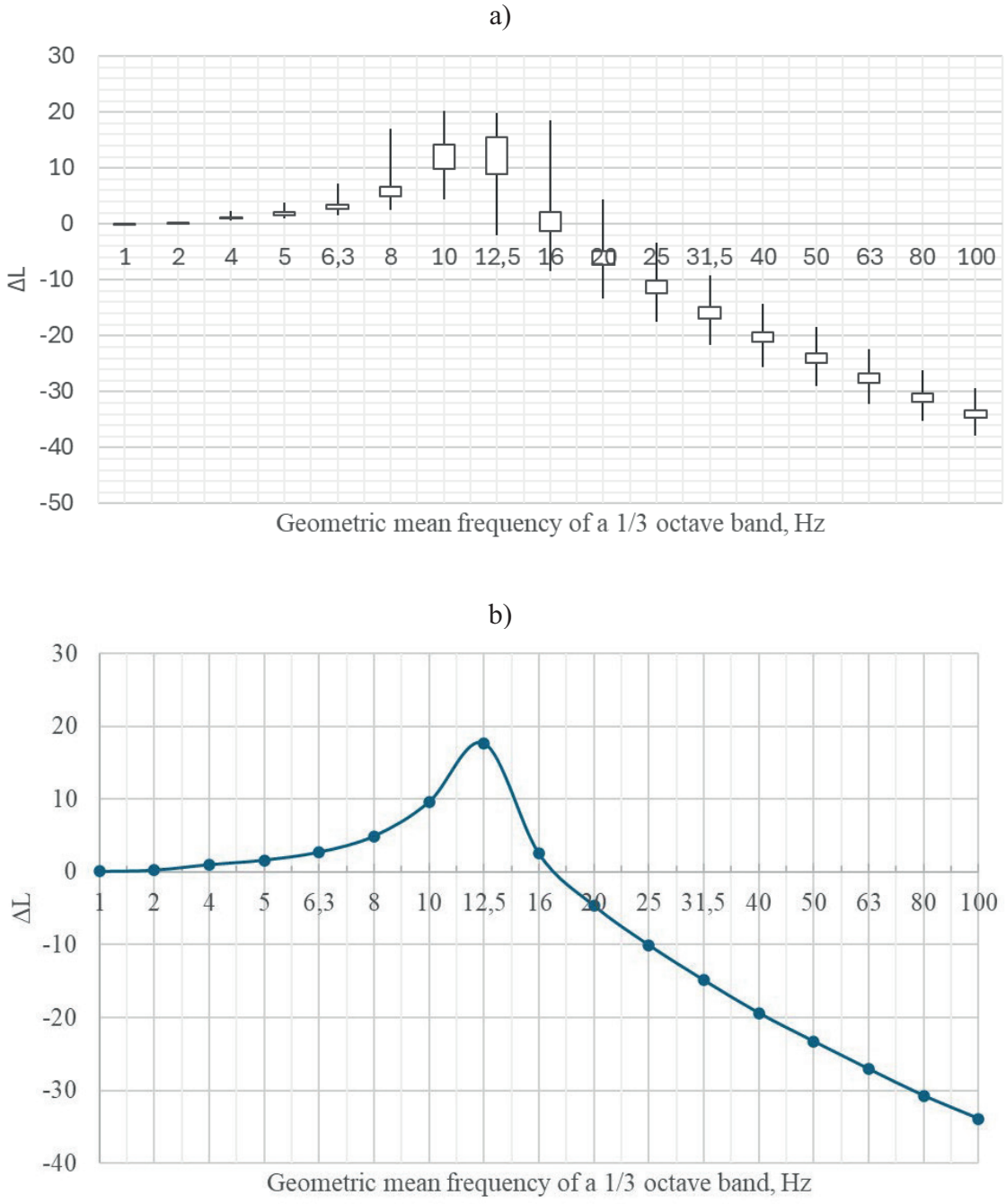


Figure 4. Distribution of calculation results for the ΔL function: a) with due account for the probability distribution; b) deterministic case

According to the graph in Figure 4a, it can be noted that, in contrast to the deterministic graph of the frequency response of the system (Figure 4b), the account for the statistical distribution of the parameters of the vibration isolation system leads to an expansion of the resonance zone (which corresponds to an increase in the spread of the natural oscillation frequency according to Figure 3 - from 9.89 to 13.28 Hz). The median value shown in Figure 4a repeats the graph in Figure 4b. But at the same time, the spread of the maximum and minimum values (end points of straight lines) in the resonance region has the greatest significance. In this case, the vibration isolation system is extremely sensitive to the reliability of the specified values. It could be emphasized that the pre-resonance mode has a distribution of results shown in Figure 5a - with a predominance of the right tail. i.e. the asymmetrical coefficient has positive values increasing to the resonance mode.

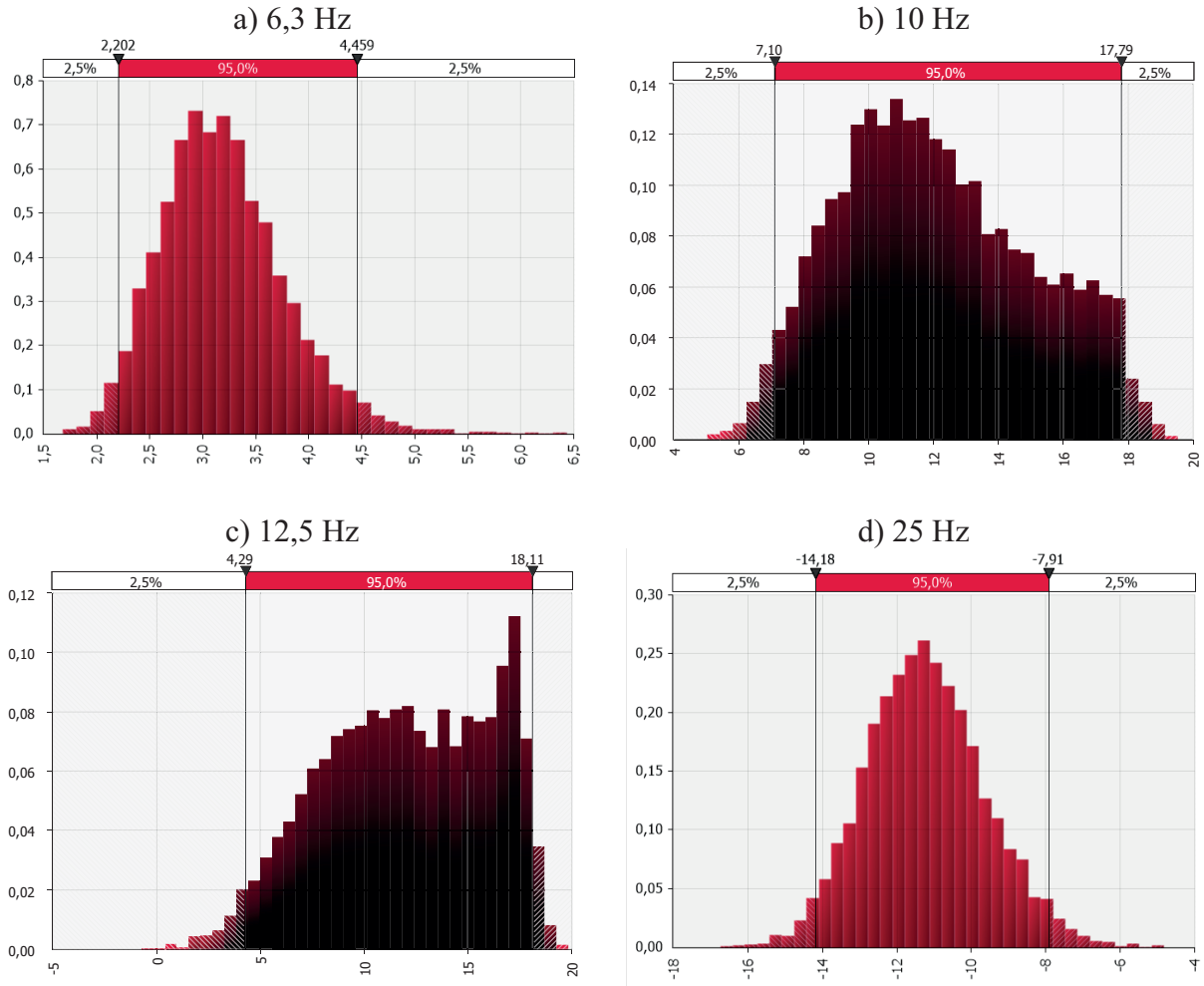


Figure 5. Distribution of the ΔL function depending on the geometric mean frequency of the 1/3-octave band.

In the resonance mode in the 1/3-octave band with the geometric mean frequency of 12.5 Hz, the asymmetry coefficient has negative values, as does the value of the standard deviation. The spread of the value of the resonance increase of oscillations has significant values from 2.5 to 4 dB.

2.2. Problem II

Another fundamental source of uncertainty in vibration protection problems is the random

nature of the external dynamic impact. Many disturbing forces and impacts are random processes by their nature: for example, seismic shocks, turbulent wind gusts, uneven road surfaces under a car, technological vibrations from equipment with a chaotic operating mode, etc. Even if the system parameters (*m, c, k*) could be considered as constant and known, the time implementation of the load *f*(*t*) continuously changes and is not exactly predictable, although it could have statistical regularities (spectral density, probability distribution of amplitudes, etc.). For the second type of problem, we consider the solution of equation (1) for an external load with a known distribution [23] shown in Figure 6. Many studies have shown that logistic distribution allows the most reliable assessment of the dynamic impact created, for example, by the movement of rail trains [11, 37].

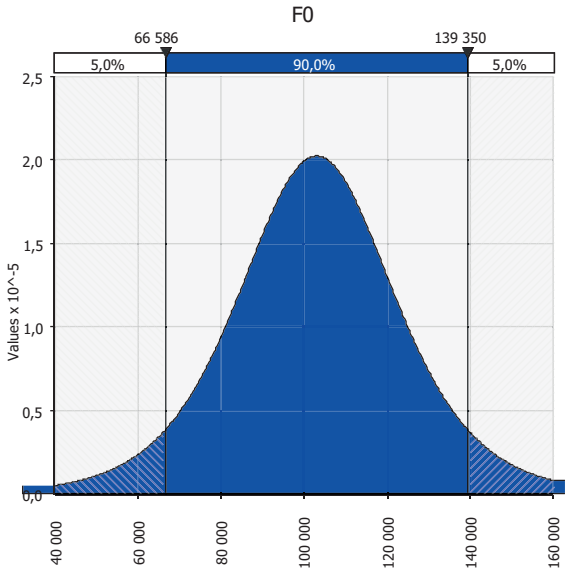


Figure 6. External load probability density

The solution for the response of the system (spectral displacement of the vibration-isolated mass) under the action of a known external force is

$$X = \frac{F_0}{\sqrt{\left(k - m\omega^2\right)^2 - \left(c\omega\right)^2}}. \qquad (6)$$

By using the numerical Monte Carlo method, it is possible to consider various variants of distributions for the F_0 load, obtained, among other things, from the results of field tests. In particular, according to the results of the studies in [11], it is shown that in different octave bands, the form of the distribution function differs significantly (which is associated with different mechanisms of generating the specified vibration). Since the parameters of the system in the problem of the second type are deterministic, the distribution function will be a single curve, and not a family of realizations. In this case, of particular interest is the assessment of the spectral distribution for the mass displacement (6), which is shown in Figure 7 as a Whisker plot.

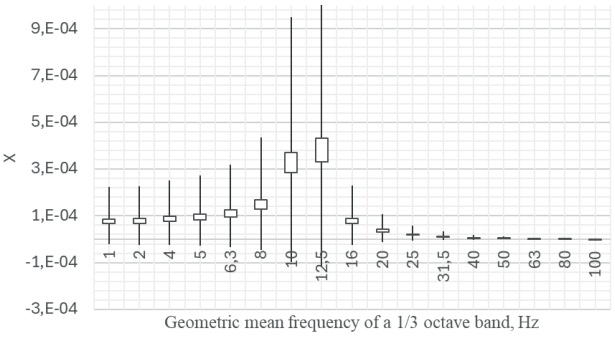


Figure 7. Response spectrum of the vibration protection system in the 2d type problem

The nature of the graph shown in Figure 7 (at least its median values) corresponds to the theoretical deterministic frequency response curve of a single-mass system, but differs in the magnitude of the spread. A significant spread is observed (between the maximum and minimum recorded values) in the pre-resonance region - one-third octave bands with a geometric mean frequency of 1 – 8 Hz. In this case, the largest values of the spread of the calculation results occur at resonance - one-third octave bands with geometric mean frequencies of 10 and 12.5 Hz. In the post-resonance region, the spread is reduced, thus, in one-third octave bands with geometric mean frequencies above 25 Hz it becomes of little influence. The 25% and 75% percentile, which are the extreme shelves of the boxes on the graph of

Figure 7, behaves similarly, however, the spread between these values is approximately an order of magnitude smaller than the spread between the maximum values.

2.3. Problem III

The most complex, but also the most realistic situation is when uncertainty is present both in the parameters of the vibration-isolated system and in the external dynamic impact. In this case, to adequately assess the response, it is necessary to conduct a joint probabilistic analysis that considers two sources of variability [5]. The problem is complicated by the fact that the response distribution is determined by the convolution (combination) of the distributions of random parameters and a random input process. A rigorous analytical approach is often impossible, and one must resort to either rough estimates (for example, assuming that the total effect of randomness is equivalent to some effective uncertainty) or large-scale numerical experiments. The Monte Carlo method was used in the problem precisely for this purpose. In the direct approach, a pair was generated: a random realization of a set of system parameters (*m, c, k*) and a random realization of the loading process *f*(*t*), after which the response was calculated using formula (6). Having repeated this process tens of thousands (or millions) times, the response distribution was empirically constructed. The calculation result is shown in Figure 8.

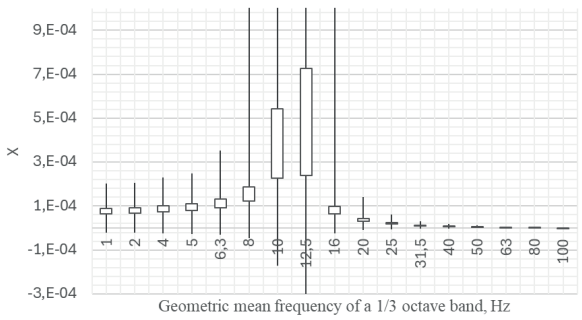


Figure 8. Response spectrum of the vibration protection system in the 3d type problem

The system response in the 3d type problem is characterized by the same principles as in the 2d type problem - repetition of the frequency response curve of a single-mass system. Comparison of the calculation results shown in Figures 7 and 8 reveals that the spread both in maximum values and in percentiles of 25% and 75% in the case of the 3d type problem is much higher. This is especially observed in the resonance region, where for the 3d type problem not only the external load contributes to the spread of values, but also the system parameters themselves (in this case, the natural frequency) fluctuate in a wide range of values (similar to the 1s type problem). Figures 9 a and b present comparative graphs of the mathematical expectation and the root mean square deviation (RMS), respectively.

The mathematical expectation (Figure 9a) in the problem of the 3d type, as predicted, is higher than in the problem of the 2d type by in average of 1–7% (larger values correspond to one-third octave bands near the resonance band), but at resonance this difference increases to 6.4 times. A similar observation could be made based on the results of the standard deviation analysis shown in Figure 9b. On average, the standard deviation in problems of the 3d type is higher than in problems of the 2d type by 14–79%, but at resonance this difference increases to 2000 times.

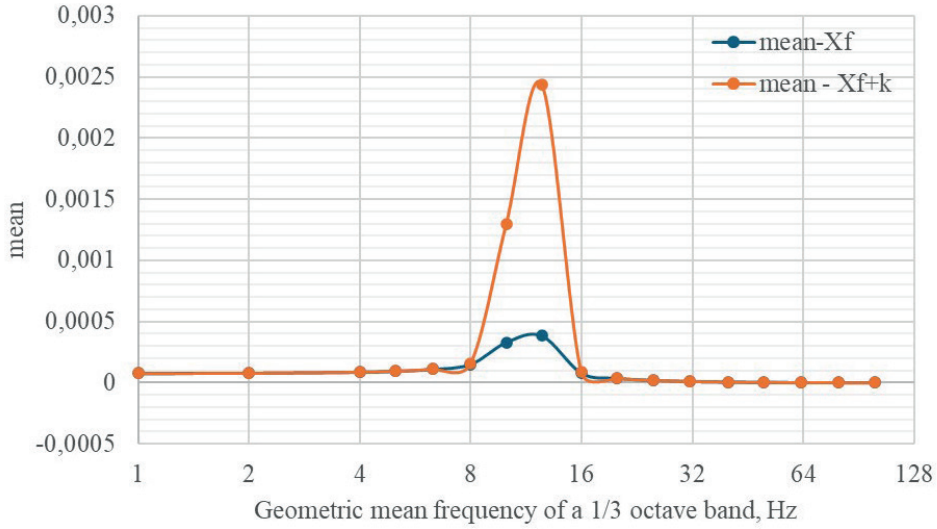
In this work, a comparison of the probability density of the response in characteristic one-third octave bands corresponding to the pre-resonance, resonant, and post-resonant operating modes was performed. The distribution curve for a problem of the 2d type is shown in red on the graphs in Figures 10a–c, and in blue – for a problem of the 3d type. The nature of the distribution density graph in the pre-resonance mode (in the one-third octave band with a geometric mean frequency of 6.3 Hz) for the problem of the 3d type partly repeats the nature of the frequency response distribution shown in Figure 5a with the predominance of the right tail of the distribution: the asymmetry coefficient is 0.63 versus 0.0088 for the problem of the 2d type. For the post-resonance region shown in Figure 10c, the behavior is identical to the pre-resonance one.

The largest and most significant difference between the calculation results is observed at resonance, as is seen in Figure 10b. For ease of

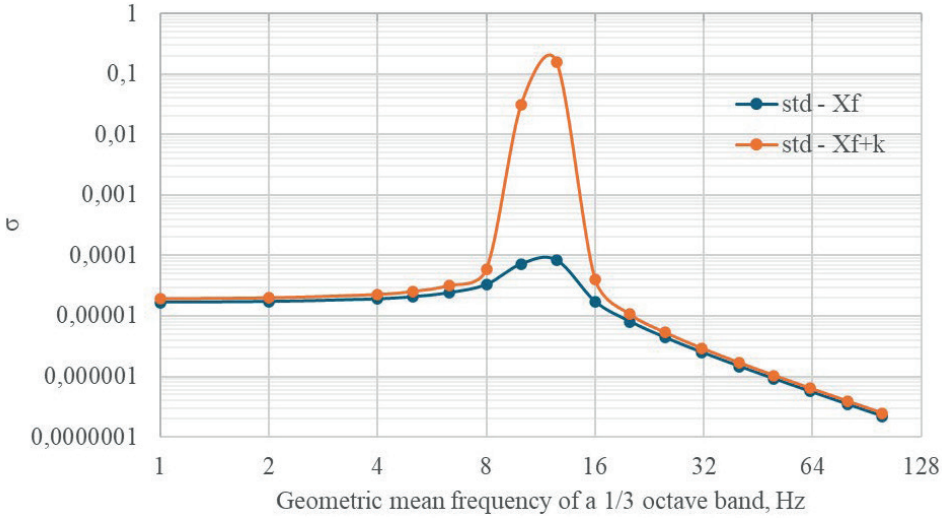
display, the calculation results for problems of the 2d and 3d types are presented as a distribution function.

The resonance mode (Figure 10b) is characterized by a significant scatter in the measurement results, only 81.1% of the values for the problem of the 3d type fall within the displacement range from 0.0001 to 0.001 m, with 99.8% for the problem of the 2d type. The distribution for the 3d type problem has a large right tail – the asymmetry coefficient is 211 versus 0.01 for the 2d type problem, what indicates a higher probability of high displacement values of the vibration-isolated mass and a higher probability of exceeding the established criterion of the threshold displacement value. The influence of the model parameters on the calculation results is shown in Figure 11 for the resonance vibration mode.

Considering the results shown in Figure 11, it could be stated that the control of the dynamic state of objects depends significantly on their mass, namely, the accuracy with which this parameter is determined. In second place is the accuracy of determining the geometric dimensions of vibration damping materials and the spread of dynamic load values. Under the current restrictions shown in Table 1, in third place are the dynamic characteristics of vibration damping materials used in a specific vibration isolation system.



a)



b)

Figure 9. Spectra of mathematical expectation (a) and root mean square value (b) for problems of the 2d and 3d types

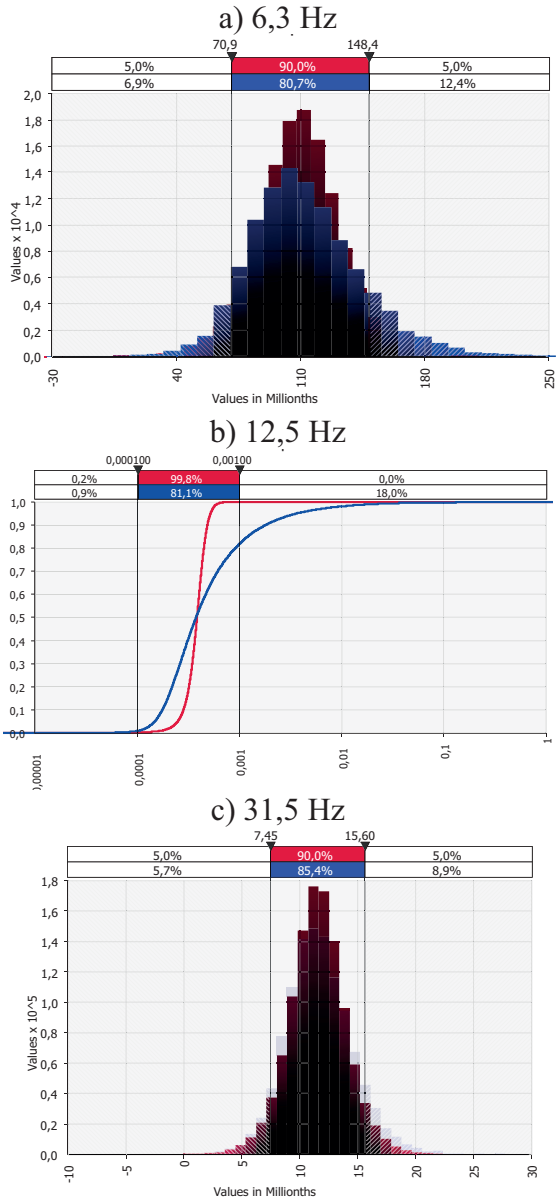


Figure 10. Comparative graphs of the probability density distribution of the system response

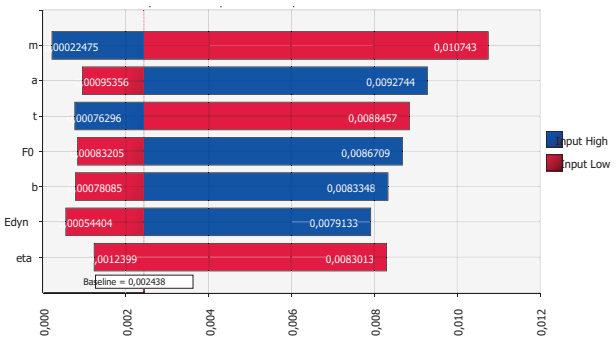


Figure 11. Influence of model parameters on calculation results for the 3d type problem

3. CONCLUSION

The conducted calculations of SDOF systems and their analysis demonstrate that accounting for random factors significantly alters the assessment of dynamic behavior in such systems. When system parameters are stochastic, distributions of resonant frequencies and amplitude-frequency characteristics (for example, within each band of a one-third octave spectrum) can be predicted to estimate the probabilistic range of vibration isolation efficiency. For random external excitations, advanced spectral and statistical analysis tools provide mean and extreme estimates of response considering actual load characteristics.

Consideration of both types of uncertainties simultaneously is more complex and currently addressed by combining analytical and numerical methods, including Monte Carlo simulations. The approach developed in this work enables determination of probabilities of exceeding threshold values established for the isolated object using experimental results, while remaining within the linear operating region of vibration isolator components. Additionally, the Monte Carlo method numerically evaluates how element-to-element variability contributes to probabilistic response characteristics, allowing variation of these parameters as needed to increase accuracy.

These approaches enable engineers to make more informed decisions when selecting vibration isolator parameters, balancing mass-stiffness trade-offs with required probability levels for reducing vibrations below safe thresholds. As reliability and durability requirements grow for machinery and structures, the probabilistic approach to vibration isolation transitions from scientific research into practical engineering calculation tools, ensuring safety and economic efficiency in vibration protection projects.

ACKNOWLEDGEMENTS

The research was funded by the National Research Moscow State University of Civil Engineering (grant for fundamental and applied research, Project No. 03-661/130).

REFERENCES

1. **Adhikari S., Pascual B.** The 'damping effect' in the dynamic response of stochastic oscillators // Probabilistic Engineering Mechanics, 2016, vol. 44, pp. 2–1
2. **Wu D., Li C., Yang Z., Liu Y., Xiong Y., Jiang G**. Probability distribution characteristics of horizontal and vertical mechanical properties of rubber bearings // Materials, 2022, vol. 15, PaperID 8031.
3. **Navarro-Quiles A.** et al. Effect of uncertain damping coefficient on the response of a SDOF system // Probabilistic Engineering Mechanics, 2022, vol. 68, PaperID 103238.
4. **Shen L., Ostoja-Starzewski M., Porcu E.** Harmonic oscillator driven by random processes having fractal and Hurst effects // Acta Mechanica, 2015, vol. 226, pp. 3653–3665.
5. **Bolotin V.V.** Methods of the theory of probability and theory of safety in structural analysis (in Russian). Moscow: Stroyizdat Publisher, 1982. 351 p.
6. **Biderman V.I.** Elements of the theory of probability (in Russian). Khabarovsk: Tikho-okeanskiy Univeristy Publisher, 2017. 232 p.
7. **Smirnov V.A., Mondrus V.L.** Probability analysis of precision equipment vibration isolation system // Applied Mechanics and Materials, 2014, vol. 467, pp. 410-415.
8. **Raizer V.D.** Probabilistic methods in the analysis of safety of structures (in Russian). Moscow: ASV Publisher, 2018. 396 c.
9. **Khusainov D.M., Shmelev G.N., Kozlov M.V.** Determination of probabilistic chatacteristics of wind loading in Kazan' city (in Russian) // Izvestiya KazGASU, 2010, No.2, pp. 121-125.
10. **Krasnoschekov Y.V., Zapoleva M.Y.** Расчетные Designed values of wind loads with the given probability (in Russian) // Vestnik SibADI, 2015, No.2, pp. 68-73.
11. **Smirnov V., Cherkasova D., Lebedev A., Smolyakov M.** Vibration data probability analysis inside residential premises adjacent to underground train lines // IOP Conference Series: Materials Science and Engineering, 2020, vol. 753.
12. **Levin A.I., Vinokurov G.G.** Influence of statistical characteristics of road's profile on vibrations of Siberian automobiles' bearing (in Russian) // Vestnik SVFU, 2018, No.5, Pp. 54-64.
13. **Li J., Chen Y., Ling X., Wen T.** Research on comfort analysis method and optimization design of pedestrian bridge // Applied and Computational Engineering, 2023, vol. 25, pp. 150-158.
14. **Schweizer M., Fina M., Wagner W., Kasic S., Freitag S.** Uncertain pedestrian load modeling for structural vibration assessment in footbridge design // Engineering Structures, 2024, vol. 311, PaperID 118070.
15. **Bayat A., Gordon C.G.** A discussion of vibration issues in microelectronics fabrication – Past, present and future // Proceedings of the ICCCS 14th Int. Symp. on Contamination Control, Institute of Environmental Sciences and Technology (IEST), 1998. pp. 139-143.
16. **Miller A.** Vibration criterion curves -Part 1: Evolution and interpretation // Proceedings of Acoustics 2024, pp. 1-10.
17. **Deminov P.D.** Estimation of probabilistic parameters of deflections and internal forces in a reinforced beam with random characteristics, resting on statistically inhomogeneous half-plane (in Russian) // Inzhenernui Vestnik Dona, 2023, No.1 (97), pp. 2003-2023.
18. **Angulo S.C., Silva N.V., Lange D.A., Tavares L.M.** Probability distributions of mechanical properties of natural aggregates using a simple method // Construction and Building Materials, 2020, vol. 233, PaperID 117269.
19. **Steele C.** (2014) The probability distribution of the elastic properties of pure metals // Applied Mathematics 2014, vol. 5, pp. 898-903.
20. **Ignatov V.I., Rabotnov N.A.** Probability characteristics of the shear modulus of

glass-reinforced plastics // Polymer Mechanics, 1973, vol. 9, pp. 144–146.
21. **Manapov A.Z.** Algorithms of Monte-Carlo method for modelling building structures work and resource (in Russian) // Izvestiya KazGASU, 2010, No.1 (13), pp. 141-146.
22. **Maystrenko I.Yu., Manapov A.Z.** Statistical modeling of work of building structures by the method of Monte-Carlo. Work with numerical sets (in Russian) // Izvestiya KazGASU, 2012, №2 (20), pp. 84-93.
23. **Chen L., Zhu H., Sun J.Q.** Novel method for random vibration analysis of single-degree-of-freedom vibroimpact systems with bilateral barriers // Applied Mathematics and Mechanics, 2019, vol. 40, pp. 1759–1776.
24. **Tsuchida T., Uehara D., Kimura K.** Response distribution of a SDOF linear system under non-Gaussian random excitation // Transactions of JSME, 2017, vol. 83, pp. 317–318.
25. **Conceição R.S., Evangelista F.** Wind-induced dynamic critical response in buildings using machine learning techniques // ASCE-ASME Journal of Risk and Uncertainty in Engineering Systems, 2023, vol. 9(1), PaperID 04090205.
26. **Choi S.** et al. Reliability-based design optimization of uncertain linear systems subjected to random vibrations // ASME Letters in Dynamic Systems and Control, 2023, vol. 4(1), PaperID 011005.
27. **Koyluoglu H.U., Nielsen S.R.K., Cakmak A.S.** Linear dynamic analysis of SDOF systems with random properties subject to random seismic loading. In: Structural Dynamics & Earthquake Engineering, WIT Press, 1993, pp. 775–784.
28. **Sana V., Rokos O., Maca J.** The response of a SDOF system driven by a periodic random force // Proc. of XX Advanced Materials Research, 2017, 1144, pp. 153–158.
29. **Wu L.-C., Zeng M.-L., Yan K.-Z.** Point estimation-based dynamic reliability analysis of beam bridges under seismic excitation considering uncertain parameters // Buildings, 2024, vol. 14(7), paperID 2003.
30. **Sebeshev V.G., Gerber Yu.A.** Structural analysis of random parameters under harmonic load (in Russian) // Vestnik TGASU, 2014, No. 4, pp. 93-105.
31. **Singh R., Lee C.** Frequency response of linear systems with parameter uncertainties // Journal of Sound and Vibration, 1993, vol. 168(1), pp. 71–83.
32. **Sepahvand K.** et al. Stochastic finite element method for random harmonic analysis of composite plates with uncertain modal damping parameters // Journal of Sound and Vibration, 2017, vol. 400, pp. 1–16.
33. **Tiliouine B.** et al. On the sensitivity of dynamic response of structures with random damping // Probabilistic Engineering Mechanics, 2018, vol. 55, pp. 20–29.
34. **Hart G.C., Jain A.** Random damping in buildings // Journal of Wind Engineering & Industrial Aerodynamics, 1996, vol. 59, pp. 233–242.
35. **Fang Y., Chen X.** Random damping in buildings and its AR model // Journal of Wind Engineering and Industrial Aerodynamics, 1998, vol. 79, pp. 159–175.
36. **Behnia D., Hendry M.T., Abdulrazagh P.H., Wahba A.** Railway dynamic load factors developed from instrumented wheelset measurements // Journal of Transportation Engineering, Part A: Systems, vol. 148, Issue 7, PaperID 04022042.

СПИСОК ЛИТЕРАТУРЫ

1. **Adhikari S., Pascual B.** The 'damping effect' in the dynamic response of stochastic oscillators // Probabilistic Engineering Mechanics, 2016, vol. 44, pp. 2–1
2. **Wu D., Li C., Yang Z., Liu Y., Xiong Y., Jiang G**. Probability distribution characteristics of horizontal and vertical mechanical properties of rubber bearings // Materials, 2022, vol. 15, PaperID 8031.

3. **Navarro-Quiles A.** et al. Effect of uncertain damping coefficient on the response of a SDOF system // Probabilistic Engineering Mechanics, 2022, vol. 68, PaperID 103238.
4. **Shen L., Ostoja-Starzewski M., Porcu E.** Harmonic oscillator driven by random processes having fractal and Hurst effects // Acta Mechanica, 2015, vol. 226, pp. 3653–3665.
5. **Болотин В.В.** Методы теории вероятностей и теории надежности в расчетах сооружений. М.: Стройиздат, 1982. 351 с.
6. **Бидерман В.И.** Элементы теории вероятностей. Хабаровск: Изд-во Тихоокеан. гос. ун-та, 2017. 232 с.
7. **Smirnov V.A., Mondrus V.L.** Probability analysis of precision equipment vibration isolation system // Applied Mechanics and Materials, 2014, vol. 467, pp. 410-415.
8. **Райзер В.Д.** Вероятностные методы в анализе надежности и живучести сооружений. М.: Издательство Ассоциации строительных вузов (АСВ), 2018. 396 с.
9. **Хусаинов Д.М., Шмелев Г.Н., Козлов М.В.** Определение вероятностных характеристик ветровой нагрузки в г. Казани // Известия КазГАСУ, 2010. №2 (14). С. 121-125.
10. **Краснощеков Ю.В., Заполева М.Ю.** Расчетные значения ветровой нагрузки с заданной обеспеченностью // Вестник СибАДИ, 2015, №2 (42). С. 68-73.
11. **Smirnov V., Cherkasova D., Lebedev A., Smolyakov M.** Vibration data probability analysis inside residential premises adjacent to underground train lines // IOP Conference Series: Materials Science and Engineering, 2020, vol. 753.
12. **Левин А.И., Винокуров Г.Г.** Влияние статистических характеристик профиля дороги на колебания подвески автомобильной техники Севера // Вестник СВФУ, 2018, №5 (67). С. 54-64.
13. **Li J., Chen Y., Ling X., Wen T.** Research on comfort analysis method and optimization design of pedestrian bridge // Applied and Computational Engineering, 2023, vol. 25, pp. 150-158.
14. **Schweizer M., Fina M., Wagner W., Kasic S., Freitag S.** Uncertain pedestrian load modeling for structural vibration assessment in footbridge design // Engineering Structures, 2024, vol. 311, PaperID 118070.
15. **Bayat A., Gordon C.G.** A discussion of vibration issues in microelectronics fabrication – Past, present and future // Proceedings of the ICCCS 14th Int. Symp. on Contamination Control, Institute of Environmental Sciences and Technology (IEST), 1998. pp. 139-143.
16. **Miller A.** Vibration criterion curves -Part 1: Evolution and interpretation // Proceedings of Acoustics 2024, pp.1-10.
17. **Деминов П.Д.** Оценка вероятностных параметров прогибов и усилий в железобетонной балке со случайными характеристиками, лежащей на статистически неоднородной полуплоскости // Инженерный вестник Дона, 2023, №1 (97)б С. 2003-2023.
18. **Angulo S.C., Silva N.V., Lange D.A., Tavares L.M.** Probability distributions of mechanical properties of natural aggregates using a simple method // Construction and Building Materials, 2020, vol. 233, PaperID 117269.
19. **Steele C.** (2014) The probability distribution of the elastic properties of pure metals // Applied Mathematics 2014, vol. 5, pp. 898-903.
20. **Игнатов В.И., Работнов Н.А.** Вероятностные характеристики модуля сдвига стеклоармированных пластиков // Механика полимеров, 1973, том 9, С. 160–162.
21. **Манапов А.З.** Алгоритмы метода Монте-Карло для моделирования работы и ресурса строительных конструкций // Известия КазГАСУ, 2010, №1 (13). С. 141-146.
22. **Майстренко И.Ю., Манапов А.З.** Статистическое моделирование работы строительных конструкций методом Монте-Карло. Работа с числовыми

множествами // Известия КазГАСУ, 2012, №2 (20). С. 84-93.
23. **Chen L., Zhu H., Sun J.Q.** Novel method for random vibration analysis of single-degree-of-freedom vibroimpact systems with bilateral barriers // Applied Mathematics and Mechanics, 2019, vol. 40, pp. 1759–1776.
24. **Tsuchida T., Uehara D., Kimura K.** Response distribution of a SDOF linear system under non-Gaussian random excitation // Transactions of JSME, 2017, vol. 83, pp. 317–318.
25. **Conceição R.S., Evangelista F.** Wind-induced dynamic critical response in buildings using machine learning techniques // ASCE-ASME Journal of Risk and Uncertainty in Engineering Systems, 2023, vol. 9(1), PaperID 04090205.
26. **Choi S.** et al. Reliability-based design optimization of uncertain linear systems subjected to random vibrations // ASME Letters in Dynamic Systems and Control, 2023, vol. 4(1), PaperID 011005.
27. **Koyluoglu H.U., Nielsen S.R.K., Cakmak A.S.** Linear dynamic analysis of SDOF systems with random properties subject to random seismic loading. In: Structural Dynamics & Earthquake Engineering, WIT Press, 1993, pp. 775–784.
28. **Sana V., Rokos O., Maca J.** The response of a SDOF system driven by a periodic random force // Proc. of XX Advanced Materials Research, 2017, 1144, pp. 153–158.
29. **Wu L.-C., Zeng M.-L., Yan K.-Z.** Point estimation-based dynamic reliability analysis of beam bridges under seismic excitation considering uncertain parameters // Buildings, 2024, vol. 14(7), paperID 2003.
30. **Себешев В.Г., Гербер Ю.А.** Анализ влияния стохастической изменчивости параметров конструкций с динамическими гасителями колебаний на надежность при гармонических нагрузках // Вестник ТГАСУ, 2014, №4 (45). С. 93-105.
31. **Singh R., Lee C.** Frequency response of linear systems with parameter uncertainties // Journal of Sound and Vibration, 1993, vol. 168(1), pp. 71–83.
32. **Sepahvand K.** et al. Stochastic finite element method for random harmonic analysis of composite plates with uncertain modal damping parameters // Journal of Sound and Vibration, 2017, vol. 400, pp. 1–16.
33. **Tiliouine B.** et al. On the sensitivity of dynamic response of structures with random damping // Probabilistic Engineering Mechanics, 2018, vol. 55, pp. 20–29.
34. **Hart G.C., Jain A.** Random damping in buildings // Journal of Wind Engineering & Industrial Aerodynamics, 1996, vol. 59, pp. 233–242.
35. **Fang Y., Chen X.** Random damping in buildings and its AR model // Journal of Wind Engineering and Industrial Aerodynamics, 1998, vol. 79, pp. 159–175.
36. **Behnia D., Hendry M.T., Abdulrazagh P.H., Wahba A.** Railway dynamic load factors developed from instrumented wheelset measurements // Journal of Transportation Engineering, Part A: Systems, vol. 148, Issue 7, PaperID 04022042.

Vladimir A. Smirnov, PhD (Eng.), Associate Professor of the Department of Structural and Theoretical Mechanics, National Research Moscow State University of Civil Engineering; 129337, Russia, Moscow, Yaroslavskoe shosse, 26, E-mail: VASmirnov@mgsu.ru; ORCID: 0000-0001-5679-9542

Marina V. Shitikova, Prof., Dr.Sc., Head of the Department of High Mathematics, National Research Moscow State University of Civil Engineering; Yaroslavskoe shosse 26, Moscow, 129337, Russia; E-mail: mvs@cchgeu.ru; ORCID: 0000-0003-2186-1881.

Смирнов Владимир Александрович, канд. техн. наук, доцент кафедры Строительной и теоретической механики, Научный исследовательский Московский государственный строительный университет; 129337, Россия, г. Москва, Ярославское шоссе, д. 26, E-mail: VASmirnov@mgsu.ru; ORCID: 0000-0001-5679-9542

Шитикова Марина Вячеславовна, профессор, доктор физико-математических наук; заведующая кафедрой Высшей математики, Научный исследовательский Московский государственный строительный университет; 129337, Россия, г. Москва, Ярославское шоссе, д. 26, E-mail: ShitikovaMV@mgsu.ru; ORCID: 0000-0003-2186-1881.

DOI:10.22337/2587-9618-2025-21-4-162-176

STRESS-STRAIN STATE OF SLIP-CRITICAL CONNECTIONS IN METAL STRUCTURES, WITH REGARD TO THE SPECIFICS OF BOLT TENSION CONTROL

Andrey A. Vasilkin, Georgiy V. Zubkov

National Research University Moscow State University of Civil Engineering, Moscow, RUSSIA

Abstract: The load-bearing capacity of a slip-critical connection depends on two factors: the bolt tension force and the friction coefficient between the coupled surfaces. Reliably achieving the specified tension force is necessary to guarantee the design performance of the connection. A number of methods for accomplishing this task are known, but only one of them is sufficiently well regulated and used in practice – the torque method.

This article analyzes the requirements and guidelines of foreign and domestic regulatory documents, research conducted in this area in the construction industry and adjacent fields, and identifies the most reasonable methods for further study of bolt tension control.

An analytical model of the stress-strain state of a slip-critical connection is proposed, and the relationship between the bolt tension force and the nut rotation angle is determined. The results obtained are compared with the recommendations of foreign regulations.

An experimental study of the tensioning process for high-strength bolt sets of various diameters – M16, M20, and M24 – has been carried out. The relationships between the nut rotation angle, torque, and tension in the bolt body were described and analyzed. The obtained data were compared with the proposed calculation model. The nut rotation angles that allow the design bolt tension force to be achieved were established.

Keywords: slip-critical connection, bolted joint, bolt pretensioning, high-strength bolts

НАПРЯЖЕННО-ДЕФОРМИРОВАННОЕ СОСТОЯНИЕ ФРИКЦИОННЫХ СОЕДИНЕНИЙ МЕТАЛЛИЧЕСКИХ КОНСТРУКЦИЙ С УЧЕТОМ ОСОБЕННОСТЕЙ КОНТРОЛЯ НАТЯЖЕНИЯ БОЛТОВ

А.А. Василькин, Г.В. Зубков

Национальный исследовательский Московский государственный строительный университет, г. Москва, РОССИЯ

Аннотация: Несущая способность сдвигоустойчивого соединения зависит от двух величин: усилия натяжения болта и коэффициента трения между соединяемыми поверхностями. Надежное обеспечение заданного усилия натяжения необходимо для того, чтобы гарантировать проектную работу соединения. Известно несколько способов решения этой задачи, однако в настоящее время достаточно полно регламентирован и используется на практике только один – по моменту закручивания.

В данной статье проанализированы требования и указания зарубежной и отечественной нормативной документации, исследования, проведенные в этой области в строительной сфере и в смежных областях, выделены наиболее рациональные для дальнейшего изучения методы контроля натяжения болтов.

Предложена аналитическая модель напряженно-деформированного состояния болтового фрикционного соединения, определена зависимость усилия натяжения болта от угла поворота гайки. Полученные результаты сопоставлены с рекомендациями зарубежных норм.

Выполнено экспериментальное исследование процесса натяжения высокопрочных болтокомплектов различных диаметров – М16, М20 и М24. Описаны и проанализированы зависимости между углом поворота гайки, крутящим моментом и усилием в теле болта. Проведено сравнение полученных данных с предложенной расчетной моделью. Установлены углы поворота гайки, позволяющие достичь расчетного усилия натяжения болта.

Ключевые слова: фрикционное соединение, болтовое соединение, преднапряжение болтов, высокопрочные болты

INTRODUCTION

Slip-critical connections with pretensioned bolts are widely used in construction. The specific features of this type of connection, which involve the transfer of forces by means of friction, ensure reliability and high fatigue resistance of the connection under various types of loads and stresses, including seismic, dynamic, and vibrational. Currently, research is being conducted in the domestic scientific community and abroad to study various factors affecting the load-bearing capacity of joints [1...8].

One of the main conditions for achieving the design load capacity of a slip-critical connection is to ensure sufficient bolt pretension. Currently, two methods of pretension control are described in the normative documentation applicable: by tightening torque and by nut rotation angle. The method of controlling the pretension force by moment of tightening has been sufficiently researched and is widely used in practice. In turn, the method of controlling the pretension force by nut rotation angle has not been fully researched, and there are no guidelines for its use for a wide range of bolt diameters. It ensures that the design tension force is achieved in the fasteners used to execute the connection with a higher degree of reliability, and eliminates the influence of the tightening coefficient on tension force, which allows increasing the load-bearing capacity of the connection [10, 15, 16].

The purpose of this study is, firstly, to analyze the methods of pretension control used in international construction practice and related industries, the application of which can improve the reliability of controlled-tension bolted connections, increase labor productivity in the assembly of metal structures, and reduce the cost of their installation.

Secondly, the aim is to describe the stress-strain state of a friction connection during bolt tensioning. Research into this process has been undertaken previously, for example in [12], but most of the relationships proposed were empirical. An analytical description of the performance of different connection elements during bolt tensioning will allow for experimental and numerical studies of the method of controlling bolt tension by angle of rotation and for the development of recommendations for its use, thereby increasing the load-bearing capacity of friction connections in metal building structures.

Thirdly, to confirm the hypotheses adopted in the formation of the calculation model of the stress-strain state of the connection, it is necessary to conduct an experimental study, describe and analyze the dependencies between the nut rotation angle, torque, and tension in the bolt body, compare them with the proposed calculation model and with the values obtained by other researchers and recommended in foreign and domestic documentation. The result of the work should be recommendations that allow the use of various methods of controlling bolt tension and identified directions for further research.

METHODS

The article analyzes the requirements of domestic and foreign regulatory documents regarding methods for controlling bolt pretension, domestic and foreign research on this topic, and identifies the most promising methods for further study of controlling the pretension of bolts in shear-resistant connections.

Stress-strain state mathematical models of shear-resistant joints proposed in previous studies are analyzed. Research experience and calculation methods in related disciplines, such as mechanical engineering, are examined and applied to analyze joints used in construction. The theoretical values of the nut rotation angle required to achieve the design bolt tension in the joint are calculated, and methods for determining the initial reference point of the nut rotation angle are analyzed.

During the experiment, 15 bolt sets with diameters of M24, M20, and M16 ′5 samples of each diameter) of strength class 10.9 according to GOST R 52644-2006 were tensioned. The thickness of the package formed by the testing

setup described below was 110 mm for all bolt set diameters.

The bolt tensioning setup is shown in Figure 1. It consists of a 260x260 mm, 30 mm thick support plate made of C345 steel, which is attached to a solid fixed base with four M20 bolts of strength class 10.9 according to GOST R 52644 -2006 through steel spacers made of C245 steel, which provide the necessary distance from the bottom of the support plate to the base surface for the bolt head to be placed. Three plates with different central hole diameters were manufactured for the experiment, which made it possible to test bolts of three different diameters. For testing M24 bolts, the hole diameter is 26 mm, for testing M20 bolts – 22 mm, and for M16 bolts – 18 mm. The drawing of the support plate for the M24 bolt is shown in Figure 2.

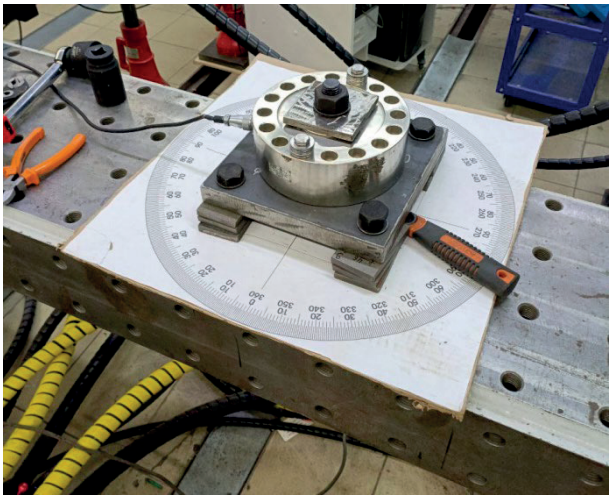


Figure 1. Testing setup

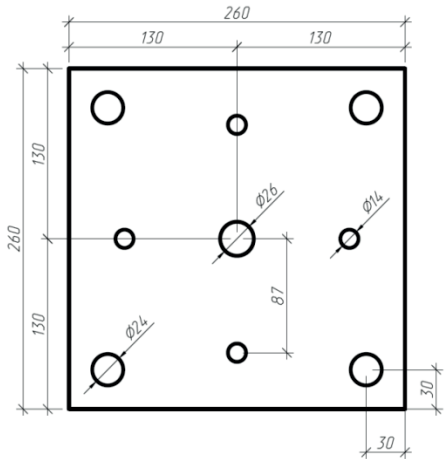


Figure 2. Support plate for the M24 bolt

A calibrated load cell capable of measuring forces in the range from 0 to 500 kN is attached to the base plate with two M12 bolts. A 95x95 mm distribution plate with a thickness of 10 mm, made of C245 steel, is installed on the upper surface of the load cell. Three distribution washers with different central hole diameters were manufactured for the experiment. The hole diameter is 26 mm for testing M24 bolts, 22 mm for testing M20 bolts, and 18 mm for testing M16 bolts. The drawing of the distribution washer for the M24 bolt is shown in Figure 3.

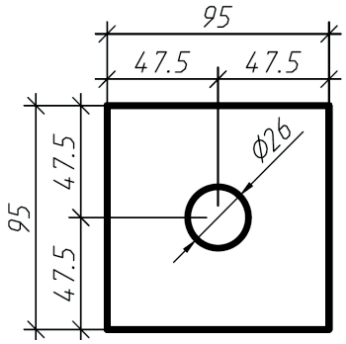


Figure 3. Distribution washer for the M24 bolt

Preparation for the bolt pretensioning procedure was carried out in accordance with the instructions of SP 70.13330.2012. Bolts, nuts, and washers were deconserved by washing them in a mixture consisting of 70-75% unleaded gasoline and 30-25% mineral oil. After deconservation, the threads of the bolts and nuts were lubricated with mineral oil in accordance with GOST R 51634.

The bolt set was installed in the assembled unit. Washers of the appropriate diameter were placed under the bolt head and nut. The bolt head was secured against movement.

The first step in testing the bolt set was to tighten the nut by hand, without using tools. The nut was screwed onto the bolt thread with the fingers, applying as much force as possible.

Two torque wrenches were used to tighten the bolt. The first, with a handle length of 0.5 m, was used to tighten the bolt to a torque of up to 400 N*m. The second, with a handle length of 2 m, was used to tighten the bolt to a torque of more than 400 N*m. Before the experiment, the

wrenches were calibrated in accordance with the procedure described in GOST 33530-2015. Further tightening of the bolt was carried out in accordance with the following algorithm:

1. Setting the required torque value on the torque wrench;
2. Fixing the initial angle between the wrench handle and the reference point on a specially designed dial;

In the first tensioning step, the initial angle value was fixed as the force in the bolt increased from a starting value of 0.6–0.9 kN to 1–2 kN. In the steps following the first, the initial angle was taken to be equal to the previous final one if the tensioning was performed without repositioning the wrench handle. If the wrench handle was repositioned between steps, a force equal to that applied in the previous step was applied to the wrench handle to measure the initial angle, and the initial angle was measured with the wrench in the "tensioned" position;

3. Tensioning the bolt to the torque setting on the wrench. Tensioning was performed smoothly, without sudden movements;
4. Measuring the final angle between the wrench handle and the angle measuring axis. The final angle was recorded when the wrench was in the "tension" position, with a force applied to the wrench handle corresponding to the required torque;
5. Measuring the force in the bolt after tightening to the torque set on the wrench.

In this way, the bolt tightening process was broken down into steps, each of which recorded the torque applied to the nut, its angle of rotation relative to the starting position, and the force in the bolt. The torque increase step was selected so that the calculated torque, determined in accordance with the instructions of SP 70.13330.2012 at a tightening coefficient of 0.17, was achieved in 10 steps. The calculated forces for bolt sets were determined in accordance with the instructions of SP 16.13330.2017.

The design force for M24 bolt sets of strength class 10.9 is 257.0 kN, for M20 bolt sets – 178.4 kN, for M16 bolt sets – 114.3 kN. The design torque for M24 bolt sets is 1048.5 N*m, for M20 bolt sets – 606.4 N*m, and for M16 bolt sets – 310.8 N*m.

The tested bolt set specimens are shown in Figure 4.



Figure 4. Bolt set specimens

RESULTS AND DISCUSSION

The test results shown below were compared with the values specified in the standards of the Russian Federation (SP 70.13330.2012 Load-bearing and enclosing structures), the United States (RCSC Specification for Structural Joints Using High-Strength Bolts 2020), the European Union (BS EN 1090-2:2018 – Execution of steel structures and aluminum structures) and Canada (CSA S16-09 – Design of steel).

The reference point for the nut rotation angle when using the single-stage rotation angle control method is not clearly defined in foreign standards, however, SP 70.13330.2012 specifies the torque at which the angle measurement can be started – 176.4...240.1 N*m, with an average of 207.0 N*m. This value is 207.0/1148.5 = 0.18

of the design torque value at a tightening coefficient of 0.17. There are no recommendations for determining the initial torque for bolt sets of other diameters in the normative documentation, so we will assign the torque at which the nut rotation angle is counted to be proportional to the calculated torque with a tightening coefficient of 0.17. Then, for bolt sets with a diameter of M20, it will be equal to 606.4*0.18 = 109.15 N*m, and for bolt sets with a diameter of M16, it will be equal to 310.8*0.18 = 55.9 N*m. Due to the characteristics of the experimental setup, we will round the values to 200, 100, and 60 N*m, respectively.

The standard values for nut rotation angles are given in Table 1.

Table 1. Standard values for nut rotation angles

d	Grip thickness	RCSC 2020	CSA S16-24
M16	t<4d	120+60	120±30
	4d<t<8d	180+60	180±30
	t>8d	240+60	240±30
M20	t<4d	120+60	120±30
	4d<t<8d	180+60	180±30
	t>8d	240+60	240±30
M24	t<4d	120+60	120±30
	4d<t<8d	180+60	180±30
	t>8d	240+60	240±30

Table 1(cont.). Standard values for nut rotation angles, SP 70.13330.2012

d	Grip thickness	SP 70.13330.2012
M16	-	-
	-	-
	-	-
M20	-	-
	-	-
	-	-
M24	40…140 (1,7…5.8d)	180±30

A comparison was also made with the combined method described in BS EN 1090-2:2018. When using this method, in the first stage of pre-tensioning, the bolt set is tightened to a torque equal to 0.75 of the design torque. In the second stage, the nut of the bolt set is turned to a specific angle.

The torque of the first stage for a bolt set with a diameter of M24 is 557 N*m, for a bolt set with a diameter of M20 – 322 N*m, and for a bolt set with a diameter of M16 – 165 N*m. We shall round these figures to 600, 300, and 150 N*m.

The rotation angles recommended by the combined method described in BS EN 1090-2:2018 are shown in Table 2.

Table 2. Standard values for nut rotation angles for combined method, EN 1090-2:2018

d	Grip thickness	EN 1090-2:2018
M16	t<2d	60
	2d<t<6d	90
	t>6d	120
M20	t<2d	60
	2d<t<6d	90
	t>6d	120
M24	t<2d	60
	2d<t<6d	90
	t>6d	120

It should be noted that the approach used in conducting the experiment made it possible to compare the values obtained as a result of tensioning the same sample with the values regulated by various methods.

The analytical model of the connection was formulated based on the following hypotheses:

- the joint components fit tightly together, their geometry is close to ideal;
- A certain angle of rotation of the nut corresponds to a certain displacement, depending on the thread pitch;
- By determining the nut rotation angles corresponding to the deformations of various parts of the connection, it is possible to determine the total angle required to achieve the specified force.

The angle of rotation of the nut and the displacement caused by this rotation are related by the following relationship:

$$\frac{\Delta l}{s} = \frac{\varphi}{360°} \qquad (1)$$

The following values were identified as components of the total nut rotation angle:

$$\varphi = \varphi_б + \varphi_р + \varphi_{гб} + \varphi_д, \qquad (2)$$

where: φ – nut rotation angle required to create the design bolt tension;
$\varphi_б$ – nut rotation angle corresponding to the displacement caused by the elongation of the bolt;
$\varphi_р$ – nut rotation angle corresponding to the displacement caused by thread deformation;
$\varphi_{гб}$ – nut rotation angle corresponding to the displacement caused by deformation of the bolt head;
$\varphi_д$ – nut rotation angle corresponding to the displacement caused by the flexibility of the joint components.
The design force in a bolted connection, in accordance with the requirements of the normative documentation, is taken to be equal to:

$$P = 0{,}7A_{bn}R_{bun},$$

Then the nut rotation angle corresponding to the displacement caused by the bolt elongation, if the deformable part of the bolt is equal to the grip thickness:

$$\varphi_б = 360\frac{t \cdot 0{,}7R_{bun}}{E \cdot s}, \qquad (3)$$

However, the research [9] has shown that the strained part of the bolt, where axial stresses occur, includes several threads inside the nut in addition to the thickness of the package. In Figure 5, it is marked asL_e.

$$L_e \approx t + 3 \cdot s;$$

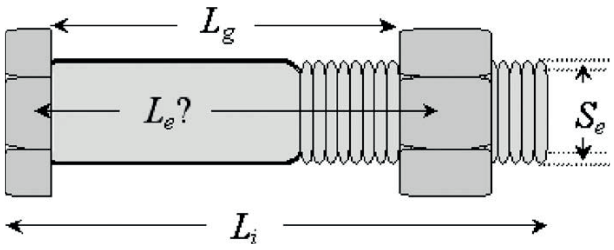


Figure 5. Scheme of bolt assembly under preload, according to [9]

Therefore:

$$\varphi_{б2} = 360\frac{(t + 3 \cdot s) \cdot 0{,}7R_{bun}}{E \cdot s}, \qquad (4)$$

The results of the.$\varphi_б$ calculation are shown in Figure 6.

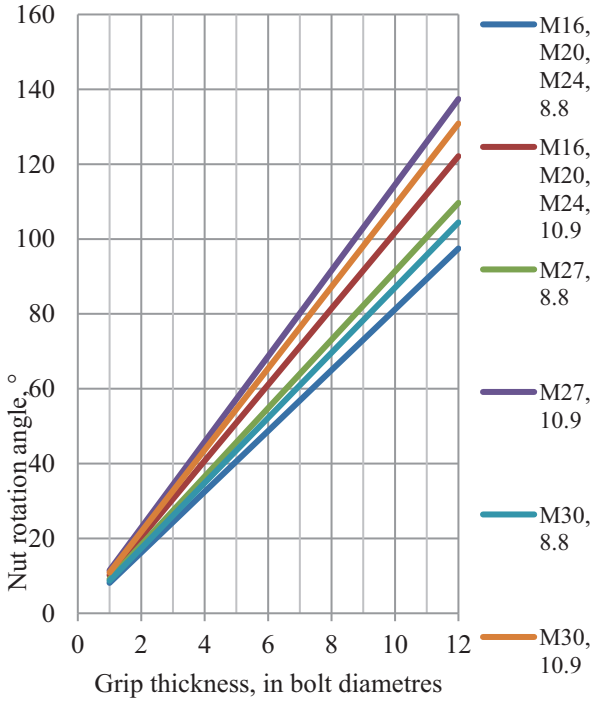


Figure 6. Nut rotation angle corresponding to the displacement caused by the elongation of the bolt

In [12], required rotation angles were calculated assuming that the bolt head and thread are not flexible; however, this approach cannot be considered entirely correct. In mechanical

engineering [11, 13, 14], relationships have been established for determining the deformations of these parts of the connection during tightening.
In [13], a relationship is proposed for determining the flexibility of the thread during bolt tightening. By deriving the angle of rotation of the nut corresponding to the displacement caused by thread deformation, we receive:

$$\varphi_{\text{р1}} = \frac{0{,}49 \cdot 360 \cdot 0{,}7 A_{bn} R_{bun}}{d_2 Es} \cdot \sqrt{1{,}44 + 9{,}28\frac{s}{d}}, \quad (5)$$

where d_2 – average thread diameter
The same source suggests an alternative method for determining thread flexibility: when calculating bolt flexibility, increase its tensile strength by 1/3 to 1/2 of the nut height.

$$\varphi_{\text{р2}} = 360\frac{0{,}28d \cdot 0{,}7R_{bun}}{\text{E}s}; \quad (6)$$

However, experimental studies have shown that these equations significantly overestimate thread stiffness, which doesn't match up with experimental data. In [14], an alternative equation for thread flexibility was proposed, allowing for a more accurate determination. When using this relationship, the nut rotation angle is:

$$\varphi_{\text{р3}} = \frac{360 \cdot 0{,}7 A_{bn} R_{bun} \cdot (0{,}8 - 12{,}04d) \cdot 10}{s} \quad (7)$$

The results of the calculations utilizing equation 7, which more closely matches the experimental data, are presented in Table 3.
In addition to thread deformation, bolt head deformation must also be taken into account. To account for its flexibility, it is possible to assume that the bolt head only experiences shear deformation. In this case, the nut rotation angle corresponding to the displacement caused by bolt head deformation will be:

$$\varphi_{\text{гб}} = \frac{0{,}15 \cdot 360 \cdot 0{,}7 A_{bn} R_{bun}}{Ehs} \quad (8)$$

Table 3. Nut rotation angle corresponding to the displacement caused by thread deformation

8.8		10.9	
Bolt diameter	$\varphi_{\text{р3}}$, °	Bolt diameter	$\varphi_{\text{р3}}$, °
M16	9,97	M16	12,50
M20	11,46	M20	14,36
M24	12,58	M24	15,76
M27	15,20	M27	19,04
M30	14,71	M30	18,43

The results of the calculation are shown in Table 4.

Table 4.Nut rotation angle corresponding to the displacement caused by deformation of the bolt head

8.8		10.9	
Bolt diameter	$\varphi_{\text{гб}}$, °	Bolt diameter	$\varphi_{\text{гб}}$, °
M16	1,20	M16	1,50
M20	1,19	M20	1,50
M24	1,19	M24	1,50
M27	1,37	M27	1,72
M30	1,31	M30	1,64

Finally, a significant portion of the deformations in the joint occur in the components of the joint itself. The main issue in calculating these deformations is determining the area of the compressed part of the component. For small joint thicknesses, it can be assumed that this area can be taken as equal to the cross-sectional area of a cylinder with a circular cutout, the outer diameter of which is equal to the size of the bolt under the

wrench S, and the diameter of the cutout is equal to the diameter of the bolt hole. Assuming the diameter of the bolt hole $d_0 = d + 2$, we obtain:

$$\varphi_{д1} = \frac{4 \cdot 360 \cdot t \cdot 0{,}7A_{bn}R_{bun}}{s \cdot E_д \cdot \pi \cdot (S^2 - (d+2)^2)}; \qquad (8)$$

However, such a linear relationship between the thickness of the joint and its deformations is not entirely accurate. Thus, [13] describes another calculation hypothesis that is much more consistent with the results of bolt joint tests. It is assumed that the stresses are evenly distributed across the cross-section of the part in the form of a cone starting from the bearing surface of the bolt and nut. The angle of inclination of its sides α is about 22...25 degrees to the vertical. The connection performance diagram according to this hypothesis is shown in Figure 7.

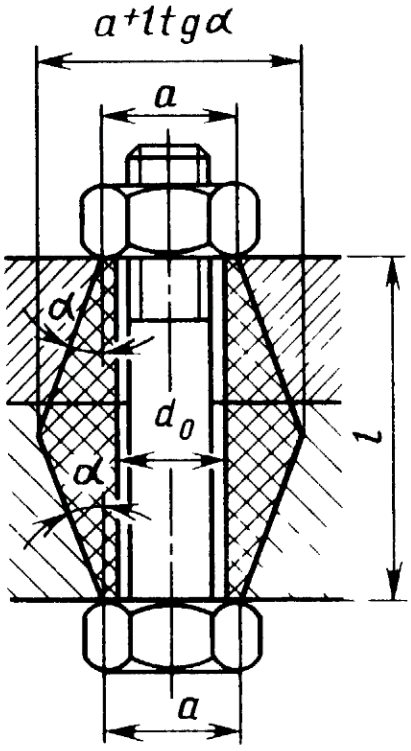


Figure 7. Stress distribution diagram in compressed parts of the assembly, [13]

Nut rotation angle corresponding to the displacement caused by the flexibility of the joint components, with the assumption of a compressed part of the component limited by pressure cones:

$$\varphi_{д2} = \frac{360 \cdot 0{,}7A_{bn}R_{bun}}{s} \cdot \frac{2}{E_д \cdot \pi \cdot d_0 \cdot tg\alpha} * \ln \frac{(a + d_0)(a + l\,tg\alpha - d_0)}{(a - d_0)(a + l\,tg\alpha + d_0)} \qquad (9)$$

The results of the $\varphi_{д2}$ calculation are shown in Figure 8. The final total theoretical nut rotation angle required to achieve the design bolt tension in a shear-resistant connection is shown in Figure 9.

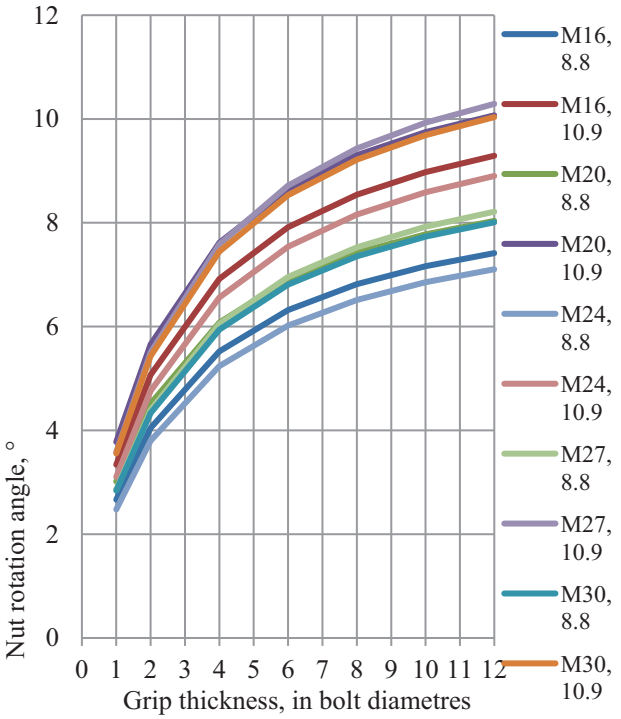


Figure 8. Nut rotation angle corresponding to the displacement caused by the flexibility of the joint components

The relationships between tensile force in the bolt and torque are shown in Figures 10–12, while the relationships between tensile force in the bolt and nut rotation angle are shown in Figures 13–15.

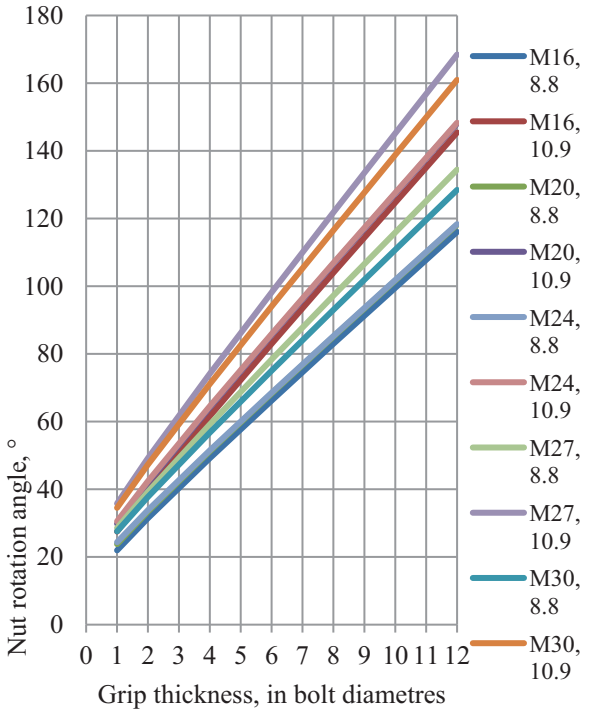


Figure 9. Nut rotation angle required to achieve the design bolt tension

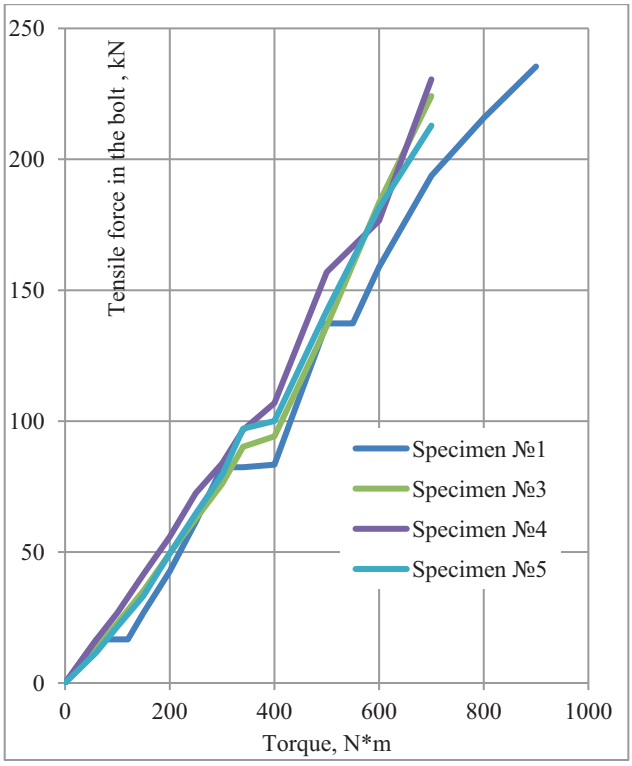


Figure 11. Force vs. torque relationship, M20, 10.9

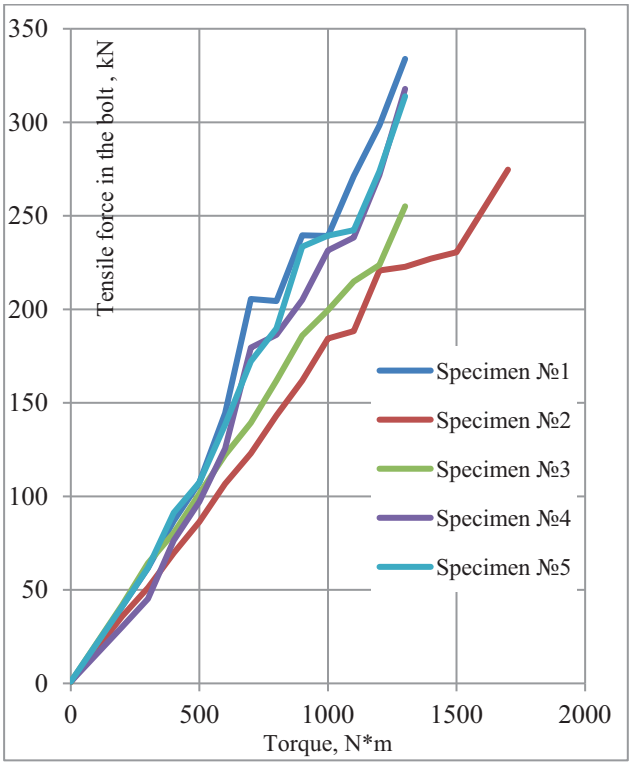


Figure 10. Force vs. torque relationship, M24, 10.9

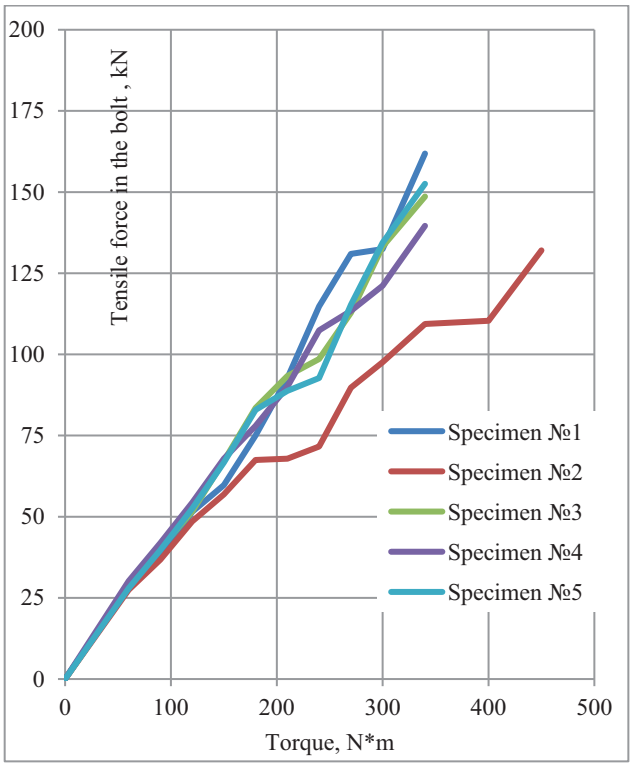


Figure 12. Force vs. torque relationship, M16, 10.9

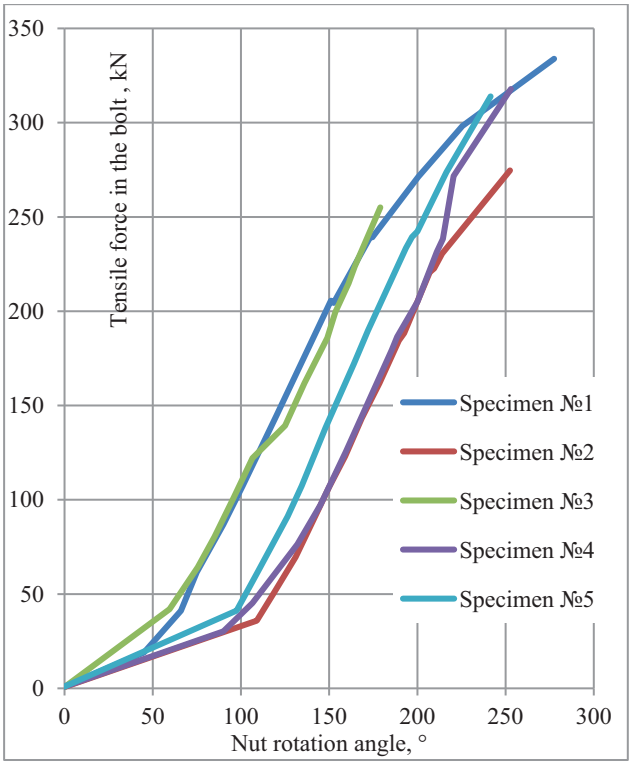


Figure 13. Force vs. nut rotation angle relationship, M24, 10.9

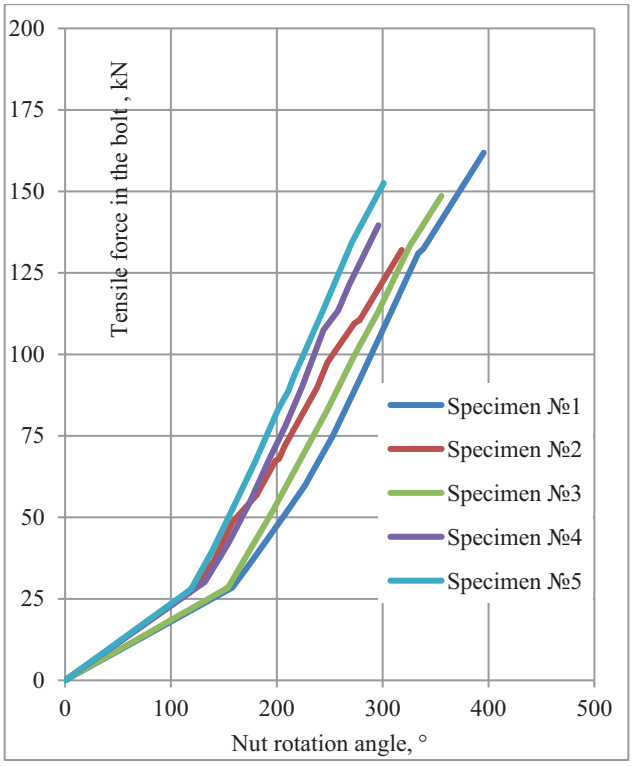


Figure 15. Force vs. nut rotation angle relationship, M16, 10.9

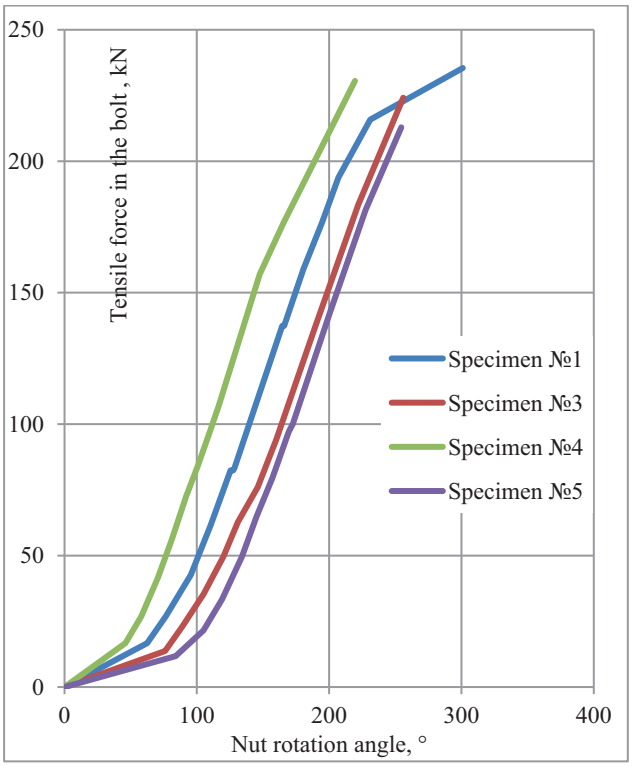


Figure 14. Force vs. nut rotation angle relationship, M20, 10.9

Now we will describe the relationship between the preload force in the bolt and the angle of rotation of the nut. From the point of view of this relationship, the bolt tightening process can be divided into four stages.

The first stage, not shown in the graphs, will be the free rotation of the nut onto the bolt, occurring until the nut comes into contact with the washer. At this stage, no force is generated in the bolt and is equal to zero.

The second stage involves tightening the connection and compressing the washers and other elements. A significant part of the displacement caused by the rotation of the nut is "consumed" not by creating preload in the bolt, but by elastic and plastic deformation of the connection elements, bringing them into contact. The dependence of the force in the bolt on the angle of rotation at this stage is nonlinear.

The third stage is characterized by a linear relationship between the angle of rotation (displacement) and the force in the bolt. It can be assumed that after all the elements of the

connection have been brought into contact, its complete "compression", elastic deformations occur in the connection. Elements such as the thread in the nut and bolt, the plates that make up the connection, the bolt head, and the bolt body itself are deformed. The elastic nature of the deformations occurring in the connection results in a linear relationship between the angle of rotation (displacement) of the nut and the force in the bolt.

The fourth stage is presumably characterized by the onset of plastic deformation in the connection elements. Not all samples reached this state during the experiment; it can be observed in specimen №1 with a diameter of M24. At this stage, the linear dependence of the prestressing force again becomes nonlinear.

We shall compare the test results with the recommendations of various normative documents.

Table 5 shows the rotation angles at which the bolt assemblies achieved the design force, interpreting the process as tightening by nut rotation angle. The rotation angle was determined taking into account the starting reference points defined above (200 N*m, 100 N*m, and 60 N*m, respectively).

Table 6 shows the rotation angles at which bolt assemblies achieved the design force, when interpreting the process as tightening using a combined method. The rotation angle was determined taking into account the reference points defined above (600 N*m, 300 N*m, and 150 N*m, respectively). Determining the angles from these reference points also allows the experimental results to be compared with the values obtained from the calculation.

Table 5. Comparison of experimental results with recommended RCSC and CSA values

Bolt diameter	Specimen	Nut rotation angle	Achieved force, kN	Mean nut rotation angle	RCSC 2020	CSA S16-24
M24	1	134,5	271,25	129,4	180+60	180±30
	2	143,5	274,68			
	3	119,5	255,06			
	4	130,5	271,74			
	5	119,0	273,70			
M20	1	132,0	176,58	123,75		
	3	133,0	183,45			
	4	107,5	176,58			
	5	122,5	181,49			
M16	1	152,5	114,78	141,0		
	2	158,0	110,36			
	3	141,5	112,82			
	4	126,0	113,40			
	5	127,0	115,27			

Table 6. Comparison of experimental results with recommended EN values and values obtained from calculations

Bolt diameter	Specimen	Nut rotation angle	Achieved force, kN	Mean nut rotation angle	EN 1090-2:2018	Calculated nut rotation angle
M24	1	80,5	271,25	77,0	90	74,6
	2	102,5	274,68			
	3	72,5	255,06			
	4	61,0	271,74			
	5	68,5	273,70			
M20	1	69,0	176,58	70,1		84,1
	3	76,0	183,45			
	4	65,0	176,58			
	5	70,5	181,49			
M16	1	152,5	114,78	77,2	120	96,0
	2	158,0	110,36			
	3	141,5	112,82			
	4	126,0	113,40			
	5	127,0	115,27			

CONCLUSION

As shown by foreign experience and domestic and foreign research, the method of controlling bolt tension by nut rotation angle is more accurate than by tightening torque, eliminating the need for time-consuming calibration of torque wrenches and experimental determination of bolt tightening coefficients. It seems relevant to expand the scope of application of this method, which is currently very limited by the guidelines of SP 70.13330.2012.

As a result of developing the proposed calculation model and conducting the experiment, it was possible to obtain the values of the angles of rotation required to achieve the calculated force. The initial hypotheses of the calculation model make its application somewhat limited, but when these hypotheses are satisfied, the values obtained by means of the model correspond to the experimental values.

The nut rotation angles obtained as a result of the experiment are slightly lower than those given in the literature, which may be due to both the large margins included in the standard values and the differences between the experimental setup and the actual operating conditions of bolt assemblies. To study the operation of connection elements at large rotation angles, it is necessary to slightly modify the experimental procedure, bringing the samples to significant plastic deformation. To confirm the obtained data, it is also necessary to conduct a study on a statistically significant sample.

REFERENCES

1. **Andrey Vasilkin, Roman Akhmetzyanov, Georgiy Zubkov and Ilya Vasilkin**. Experimental determination of the tightening coefficient of bolts according to the din standard. E3S Web of Conferences 389, 01080 (2023).
2. **Vasilkin A.A., Zubkov G.V., Prokaev S.A., Vasilkin I.A.** Razmer ploshchadki treniya frikcionnogo boltovogo soedineniya [Friction area of a slip-critical bolt

connection]// Stroitel'stvo: nauka i obrazovanie [Construction: science and education]. 2024. Vol. 14. Issue. 1. p. 4. URL: http://nso-journal.ru. DOI: 10.22227/2305-5502.2024.1.4.

3. **Vasilkin A.A., Zubkov G.V.** Metody kontrolya usiliya natyazheniya boltov sdvigoustojchivyh soedinenij [Methods for controlling the tension force of bolts in slip-critical connections]// Aktual'nye problemy stroitel'noj otrasli i obrazovaniya — 2023: sbornik dokladov IV Nacional'noj nauchnoj konferencii (g. Moskva, 15 dekabrya 2023 g.). Moskva : Izdatel'stvo MISI – MGSU [Current Issues in Construction and Education — 2023: Proceedings of the IV National Scientific Conference (Moscow, December 15, 2023). Moscow: Moscow State University of Civil Engineering Publishing House], 2024.
4. **Василькин А.А., Зубков Г.В.** Deformaciya elementov sdvigoustojchivyh soedinenij pri predvaritel'nom natyazhenii bolta [Deformation of slip-critical connection elements during pretensioning of the bolt].// Aktual'nye problemy stroitel'noj otrasli i obrazovaniya — 2024: sbornik dokladov V Nacional'noj nauchnoj konferencii (g. Moskva, 16 dekabrya 2024 g.). Moskva : Izdatel'stvo MISI – MGSU [Current Issues in Construction and Education — 2024: Proceedings of the V National Scientific Conference (Moscow, December 16, 2023). Moscow: Moscow State University of Civil Engineering Publishing House], 2025.
5. **Martynov G.V., Monastyreva D.E., Makarov A.I., Morina E.A.** Napryazhenno-deformirovannoye sostoyaniye friktsionnykh soyedineniy s lazernoy obrabotkoy kontaktnykh poverkhnostey [Stress-strain state of friction joints with laser treatment of contact surfaces]. Vestnik MGSU [Proceedings of the Moscow State University of Civil Engineering]. 2019. vol. 14. issue. 1. pp. 72–82. DOI: 10.22227/1997-0935.2019.1.72-82. (In Russian)
6. **Kovalenko A.I., Konin D.V., Nakhval′nov P.V., Solov′yev D.V.** Eksperimental′noye issledovaniye koeffitsiyenta treniya friktsionnykh boltovykh soyedineniy [Experimental studyof the friction coefficient of friction bolted joints]. Stroitel′naya mekhanika i raschet sooruzheniy [Construction mechanics and calculation of structures]. 2022. № 4 (303), pp. 61-67. (In Russian)
7. **Vedyakov I.I., Konin D.V., Nakhval′nov P.V.** Eksperimental′noye issledovaniye friktsionnykh boltovykh soyedineniy iz vysokoprochnykh staley [Experimental study of friction bolted joints made of high-strength steels]. Promyshlennoye i grazhdanskoye stroitel′stvo [Industrial and civil construction]. 2022. № 7. pp. 24-33. (In Russian)
8. **Monville J-M:** Optimal tightening process of bolted joints. Int. J. Simul. Multisci. Des. Optim., 2016, 7, A4.
9. **Chaki, Salim & Corneloup, G. & Lillamand, Ivan & Walaszek, Henri.** (2007). Combination of Longitudinal and Transverse Ultrasonic Waves for In Situ Control of the Tightening of Bolts. Journal of Pressure Vessel Technology-transactions of The Asme - J PRESSURE VESSEL TECHNOL. 129. 10.1115/1.2748821.
10. **Jacques Berenbak** Evaluation tightening preloaded bolt assemblies according to EN 1090-2 “Technical requirements for steel structures” for 95% reliability EN 1990 // Delft University of Technology. 2012.
11. **Iosiflevich G.B., Stroganov G.B., Sharlovskij G.B.** Zatyazhka i stoporenie rez'bovyh soedinenij [Tightening and locking threaded connections] 2nd edition, revised and expanded // M.: Mashinostroenie, 1985.
12. **Chesnokov A.S., Knyazhev A.F.** Sdvigoustojchivye soedineniya na vysokoprochnyh boltah [slip-critical

connections using high-strength bolts]// M.: Strojizdat, 1974.
13. **Birger I.A., Iosiflevich G.B.** Rez'bovye i flancevye soedineniya [Threaded and flanged connections]// M.: Mashinostroenie, 1990. – 368 pp.
14. **V.D. Prodan, G.V. Bozhko, A.V. Vasil'ev, M.S.** Fokina Utochnenie koefficienta osevoj podatlivosti rez'bovogo elementa raz"emnogo soedineniya [Specifying the axial ductility coefficient of a threaded element in a detachable connection]// TSTU Bulletin. 2016. Vol 22. № 4. pp. 674-678. DOI: 10.17277/vestnik.2016.04. pp. 674-678.
15. **Kulak G.L.** High Strength Bolting for Canadian Engineers // Canadian Institute Of Steel Construction. 2005.
16. **Bickford, J.H.** (2007). Introduction to the Design and Behavior of Bolted Joints: Non-Gasketed Joints (4th ed.). CRC Press.

СПИСОК ЛИТЕРАТУРЫ

1. **Andrey Vasilkin, Roman Akhmetzyanov, Georgiy Zubkov and Ilya Vasilkin.** Experimental determination of the tightening coefficient of bolts according to the din standard. E3S Web of Conferences 389, 01080 (2023).
2. **Василькин А.А., Зубков Г.В., Прокаев С.А., Василькин И.А.** Размер площадки трения фрикционного болтового соединения // Строительство: наука и образование. 2024. Т. 14. Вып. 1. Ст. 4. URL: http://nso-journal.ru. DOI: 10.22227/2305-5502.2024.1.4.
3. **Василькин А.А., Зубков Г.В.** Методы контроля усилия натяжения болтов сдвигоустойчивых соединений // Актуальные проблемы строительной отрасли и образования — 2023: сборник докладов IV Национальной научной конференции (г. Москва, 15 декабря 2023 г.). Москва : Издательство МИСИ – МГСУ, 2024.
4. **Василькин А.А., Зубков Г.В.** Деформация элементов сдвигоустойчивых соединений при предварительном натяжении болта.// Актуальные проблемы строительной отрасли и образования — 2024: сборник докладов V Национальной научной конференции (г. Москва, 16 декабря 2024 г.). Москва : Издательство МИСИ – МГСУ, 2025.
5. **Мартынов Г.В., Монастырева Д.Е., Макаров А.И., Морина Е.А.** Напряженно-деформированное состояние фрикционных соединений с лазерной обработкой контактных поверхностей // Вестник МГСУ. 2019. Т. 14. Вып. 1. С. 72–82. DOI: 10.22227/1997-0935.2019.1.72-82.
6. **Коваленко А.И., Конин Д.В., Нахвальнов П.В., Соловьев Д.В.** Экспериментальное исследование коэффициента трения фрикционных болтовых соединений // Строительная механика и расчет сооружений. 2022. № 4 (303), С. 61-67.
7. **Ведяков И.И., Конин Д.В., Нахвальнов П.В.** Экспериментальное исследование фрикционных болтовых соединений из высокопрочных сталей // Промышленное и гражданское строительство. 2022. № 7. С. 24-33.
8. **Monville J-M:** Optimal tightening process of bolted joints. Int. J. Simul. Multisci. Des. Optim., 2016, 7, A4.
9. **Chaki, Salim & Corneloup, G. & Lillamand, Ivan & Walaszek, Henri.** (2007). Combination of Longitudinal and Transverse Ultrasonic Waves for In Situ Control of the Tightening of Bolts. Journal of Pressure Vessel Technology-transactions of The Asme - J PRESSURE VESSEL TECHNOL. 129. 10.1115/1.2748821.
10. **Jacques Berenbak** Evaluation tightening preloaded bolt assemblies according to EN 1090-2 “Technical requirements for steel structures” for 95% reliability EN 1990 // Delft University of Technology. 2012.

11. **Иосифлевич Г.Б., Строганов Г.Б., Шарловский Г.Б.** Затяжка и стопорение резьбовых соединений -2-е изд., перераб. и доп. // М.: Машиностроение, 1985.
12. **Чесноков А.С., Княжев А.Ф.** Сдвигоустойчивые соединения на высокопрочных болтах // М.: Стройиздат, 1974.
13. **Биргер И.А., Иосифлевич Г.Б.** Резьбовые и фланцевые соединения // М.: Машиностроение, 1990. – 368 с.
14. **В.Д. Продан, Г.В. Божко, А.В. Васильев, М.С. Фокина.** Уточнение коэффициента осевой податливости резьбового элемента разъемного соединения // Вестник ТГТУ. 2016. Том 22. № 4. С. 674-678. DOI: 10.17277/vestnik.2016.04.pp.674-678.
15. **Kulak G.L.** High Strength Bolting for Canadian Engineers // Canadian Institute Of Steel Construction. 2005.
16. **Bickford, J.H.** (2007). Introduction to the Design and Behavior of Bolted Joints: Non-Gasketed Joints (4th ed.). CRC Press.

Andrey A. Vasilkin – Candidate of Technical Sciences, Associate Professor of the Department of Metal and Wooden Structures; National Research "Moscow State University of Civil Engineering" (NRU MGSU), 129337, Moscow, Yaroslavskoe sh., 26; vasilkinaa@mgsu.ru

Georgiy V. Zubkov – graduate student, Industrial and Civil Engineering Institute; National Research "Moscow State University of Civil Engineering" (NRU MGSU), 129337, Moscow, Yaroslavskoe sh., 26; gronar363@gmail.com

Андрей Александрович Василькин – кандидат технических наук, доцент кафедры металлических и деревянных конструкций; Национальный исследовательский «Московский государственный строительный университет» (НИУ МГСУ), 129337, г. Москва, Ярославское ш., 26; vasilkinaa@mgsu.ru

Георгий Владиславович Зубков – аспирант 4 курса Института промышленного и гражданского строительсва Национальный исследовательский Московский государственный строительный университет (НИУ МГСУ), 129337, г. Москва, Ярославское шоссе, 26, адрес электронной почты: gronar363@gmail.com

International Journal for Computational Civil and Structural Engineering, 21(4) 177–184 (2025)

DOI:10.22337/2587-9618-2025-21-4-177-184

DRAWING THE NOMOGRAM FOR OVERHUMIDIFICATION OF THE BUILDING ENVELOPE

Kirill P. Zubarev, Yulia A. Sapronova, Vladimir D. Fedoseev

National Research Moscow State University of Civil Engineering, Moscow, RUSSIA

Abstract: In the current paper, a new method of protecting building envelopes from waterlogging based on the construction of specialized nomograms has been developed. During the analysis of the Russian climate, it was determined that for the entire territory of the country the period of moisture accumulation does not exceed 8 months. It was found that the criterion of waterlogging of the building envelopes depends on three main parameters: temperature and relative humidity of the outside air during the period with negative average monthly temperatures, and the duration of the period of moisture accumulation. Based on the critical value of criterion l, a nomogram of waterlogging of the enclosing structure was constructed, according to which a decision on the construction of the designed building can be taken. An algorithm of constructing and applying a nomogram of waterlogging of a building envelope has been presented. The effectiveness of the proposed method is shown in comparison with the classical approach by calculating protection against waterlogging in such cities as Blagoveshchensk and Yerofey Pavlovich.

Keywords: protection against waterlogging, operating conditions, temperature, relative humidity, duration of moisture accumulation

ПОСТРОЕНИЕ НОМОГРАММЫ ПЕРЕУВЛАЖНЕНИЯ ОГРАЖДАЮЩЕЙ КОНСТРУКЦИИ ЗДАНИЯ

К.П. Зубарев, Ю.А. Сапронова, В.Д. Федосеев

Национальный исследовательский Московский государственный строительный университет, г. Москва, РОССИЯ

Аннотация: В статье разработан новый метод защиты от переувлажнения ограждающих конструкций зданий, основанный на построении специализированных номограмм. В ходе анализа климата России было определено, что для всей территории страны период влагонакопления не превышает 8 месяцев. Получено, что критерий переувлажнения ограждающей конструкции зависит от трех основных параметров: температура и относительная влажность наружного воздуха за период с отрицательными среднемесячными температурами и продолжительность периода влагонакопления. На основании критического значения критерия *l,* была построена номограмма переувлажнения ограждающей конструкции, по которой можно принять решение о строительстве проектируемой стены здания. Приведен алгоритм построения и применения номограммы переувлажнения ограждающей конструкции. Показана эффективность предложенного метода в сравнении с классическим подходом путем расчета защиты от переувлажнения в городах Благовещенск и Ерофей Павлович.

Ключевые слова: защита от переувлажнения, условия эксплуатации, температура, относительная влажность, продолжительность влагонакопления

INTRODUCTION

When designing buildings and structures [1], engineers face various tasks: calculating the strength of reinforced concrete and metal structures, calculating the thickness of shells, determining the temperature influences on the building [2-7].

When calculating the protection of the building envelope against waterlogging, the Russian regulatory document Set of Rules 50.13330.2012 “Thermal protection of buildings” is used. The method of protection against waterlogging presented in the regulatory document appears to be quite effective, but at the same it is complicated for

engineering use. Therefore, the research on the development of a new simplified method of protecting the building envelope from waterlogging is currently relevant [8].

In calculating building structures, it is important to take into account the physical characteristics of building materials: humidity, density, vapor permeability, etc. However, the choice of thermal conductivity value depends on the humidity conditions in residential premises and the humidity zone in which the building structure is placed. Therefore, there are 2 operating conditions: A and B.

Thermal conductivity values for some building materials have been given (Table 1).

Table 1. Thermal conductivity values for some building materials

Material	Thermal conductivity, $W / m\,^{\circ}C$	
	A	B
Mineral wool slabs made of stone fiber	0.045	0.048
Gravel expanded clay	0.13	0.145
Gas and foam concrete on cement binder	0.38	0.43
Reinforced concrete	1.92	2.04
Cement-sand mortar	0.76	0.93
Plywood	0.15	0.18

To simplify calculations of protection against waterlogging, the waterlogging criterion found using the following formula was introduced:

$$l = \frac{\mathrm{R}_n^{req}}{\mathrm{R}_n}. \qquad (1)$$

where R_n – vapor permeation resistance, $m^2 \cdot s \cdot Pa / kg$; R_{n1}^{req}, R_{n2}^{req} – required vapor permeation resistances, $m^2 \cdot s \cdot Pa / kg$.

Using the waterlogging criterion, it is possible determine whether the structure will be waterlogged. However, the criterion is calculated for each city taking into account climatic conditions, which complicates the method of protection against waterlogging. In this regard, there is a need to develop alternative methods of studying the balance of moisture transfer in more simplified ways. This article develops a method of assessing the construction of a building envelope using a waterlogging nomogram.

1. THE PROBLEM

To develop a method of calculating protection against waterlogging of external building envelopes using a waterlogging nomogram.

2. MATERIALS AND METHODS

2.1. Studying the value of the waterlogging criterion at different duration of the moisture accumulation period

Analyzing the obtained values of the criterion of waterlogging of the building envelope in different cities in Russia, it was found that the criterion l depends on climatic parameters. It was determined that the period of moisture accumulation does not exceed 8 months. Graphs of the dependence of the waterlogging criterion on the values of the average monthly negative outdoor air temperature at different durations of the period of moisture accumulation were obtained (Figure 1, Figure 2).

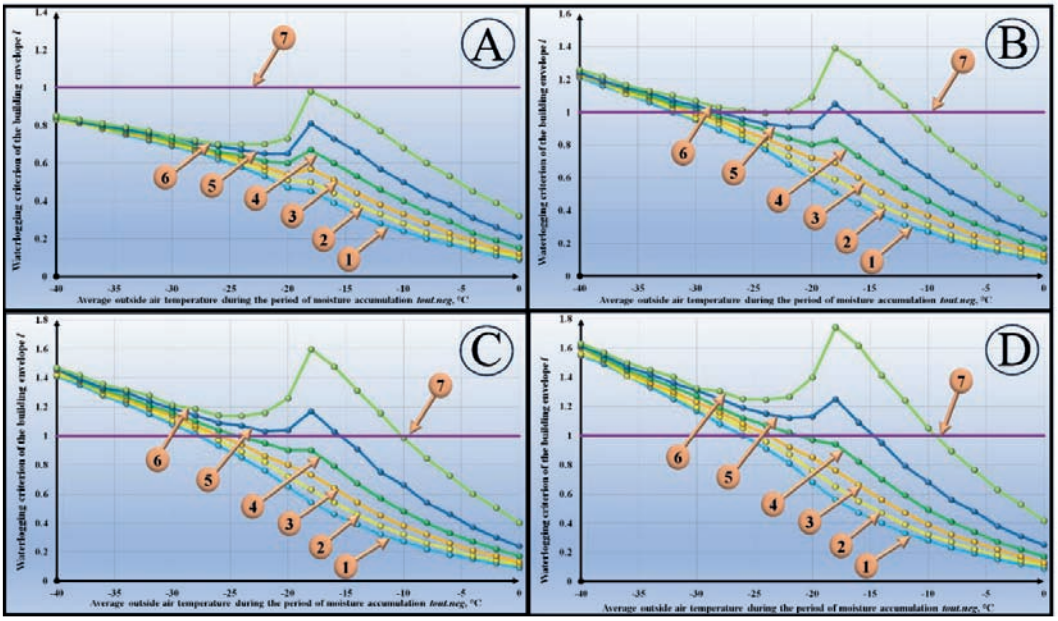


Figure 1. Dependence of the waterlogging criterion on the outside air temperature and the duration of the moisture accumulation period for 1, 2, 3 and 4 months of moisture accumulation (A – 1 month; B – 2 months; C – 3 months; D – 4 months; the relative humidity of the outside air during the period with negative average monthly temperatures: 1 – $\varphi_{out.neg} = 70$ %; 2 – $\varphi_{out.neg} = 75$ %; 3 – $\varphi_{out.neg} = 80$ %; 4 – $\varphi_{out.neg} = 85$ %; 5 – $\varphi_{out.neg} = 90$ %; 6 – $\varphi_{out.neg} = 95$ %; 7 – $I = 1$)

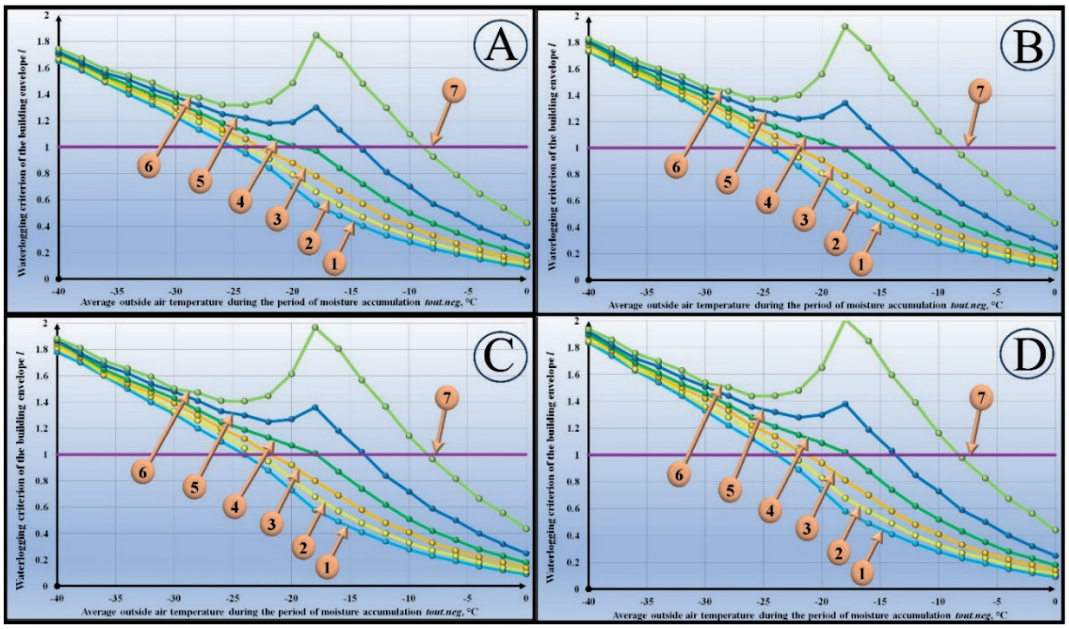


Figure 2. Dependence of the waterlogging criterion on the outside air temperature and the duration of the moisture accumulation period for 5, 6, 7 and 8 months of moisture accumulation (A – 5 months; B – 6 months; C – 7 months; D – 8 months; the relative humidity of the outside air during the period with negative average monthly temperatures: 1 – $\varphi_{out.neg} = 70$ %; 2 – $\varphi_{out.neg} = 75$ %; 3 – $\varphi_{out.neg} = 80$ %; 4 – $\varphi_{out.neg} = 85$ %; 5 – $\varphi_{out.neg} = 90$ %; 6 – $\varphi_{out.neg} = 95$ %; 7 – $I = 1$)

2.2. Construction of a nomogram of waterlogging of the building envelope

While analyzing the obtained graphical dependencies (Figure 1, Figure 2), it was found that waterlogging is influenced by 3 main factors: the temperature of the outside air during the period of moisture accumulation, the relative humidity of the outside air during the period with negative average monthly temperatures, and the duration of the period of moisture accumulation. By varying the values of the main factors, it is possible to construct a dependence graph when the criterion of waterlogging of the building envelope is equal to one. The values of the outside air temperature are plotted on the abscissa axis, the relative air humidity values are marked on the ordinate axis, and dependence lines that depend on the duration of the period of moisture accumulation are obtained. Due to the fact that there are operating conditions A and B, two waterlogging nomograms are obtained (Figure 3, Figure 4).

2.3. Algorithm for constructing and using a nomogram of waterlogging of building envelopes

To construct a nomogram of waterlogging of a building envelope based on the method of protection against waterlogging the following measures are taken:

1. The required design is selected;
2. The operating conditions of the building envelope are determined;
3. The value of the relative humidity of the outside air is set in increments of 5% and the duration of moisture accumulation;
4. The range of outdoor air temperature values during the period of moisture accumulation varies in increments of 1 °C;
5. The criterion of waterlogging of the building envelope is calculated;
6. The criterion values l=1 are selected, and the corresponding values of the outside air temperature, relative humidity of the outside air and the period of moisture accumulation are recorded;

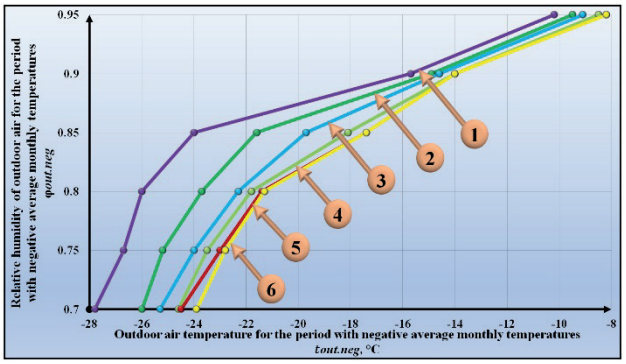


Figure 3. Nomogram of waterlogging of the building envelope for operating conditions A (duration of moisture accumulation period: 1 – three months; 2 – four months; 3 – five months; 4 – six months; 5 – seven months; 6 – eight months)

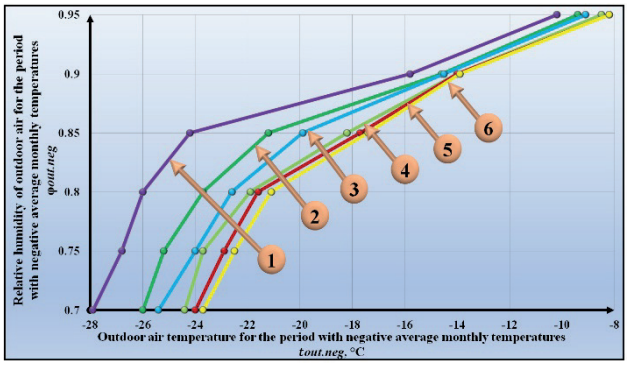


Figure 4. Nomogram of waterlogging of the building envelope for operating conditions B (duration of moisture accumulation period: 1 – three months; 2 – four months; 3 – five months; 4 – six months; 5 – seven months; 6 – eight months)

7. After finding all the points at which l=1, the values of the average outdoor air temperature for the period of moisture accumulation at the corresponding relative humidity and the period of moisture accumulation are reduced to a waterlogging nomogram, which enables us to arrive at decision on the possibility of the building envelope construction.

For structures under different operating conditions, different waterlogging nomograms are constructed.

To calculate the protection of the building envelope from waterlogging using the

waterlogging nomogram, the following steps are taken:

1. A nomogram that corresponds to the calculated building envelope taking into account operating conditions is selected.
2. The abscissa axis marks the outside air temperature for the period of moisture accumulation in accordance with the city in which the calculation is performed.
3. A vertical straight line is drawn from the found outside air temperature point until it intersects with the line of the desired moisture accumulation period.
4. A horizontal line is drawn from the found point until it intersects with the ordinate axis, thereby determining the critical value of the relative humidity of the outside air.
5. The value of the relative humidity of the outside air is determined from the ratio of the average partial pressure of water vapor of the outside air during the period with negative average monthly temperatures to the pressure of saturated water vapor in the plane of greatest moisture for the period of moisture accumulation, and then a horizontal straight line is drawn.
6. If the horizontal straight line of the critical humidity value is higher than the horizontal line of the relative humidity of the outside air, the structure has passed the waterlogging protection test successfully.
7. If the horizontal line of the critical humidity value is lower than the horizontal line of the relative humidity of the outside air, the structure fails to pass protection test against waterlogging.

3. RESULTS AND DISCUSSION

A calculation of protection of the building envelopes from waterlogging located in Blagoveshchensk and Yerofey Pavlovich has been conducted.

For a structure designed in Blagoveshchensk, the criterion of waterlogging of the building envelope is calculated using formula (1):

$$l = \frac{\mathrm{R}_n^{req}}{\mathrm{R}_n} = \frac{0.96}{1.655} = 0.58.$$

The value of the waterlogging criterion according to the calculation is less than one, therefore, the building structure in Blagoveshchensk has passed the test against waterlogging successfully.

Let us carry out calculations of protection of the building structure against waterlogging using the waterlogging nomogram. In Blagoveshchensk, the structure is operated under conditions B, and the main climatic parameters are: outside air temperature during the period with negative average monthly temperatures is -15.3 °C, the duration of moisture accumulation is 5 months. Relative humidity is determined by the formula:

$$\varphi_{out.neg} = \frac{e_{out.neg}}{E_0}. \quad (2)$$

where $e_{out.neg}$ – average partial pressure of water vapor of the outside air during periods with negative average monthly temperatures, Pa; E_0 – pressure of saturated water vapor in the plane of greatest moisture for the period of moisture accumulation, Pa.

Taking into account formula (2) we obtain:

$$\varphi_{out.neg} = \frac{e_{out.neg}}{E_0} = \frac{148}{192} = 0.77 .$$

We plot the obtained values of the outdoor air temperature for the period with negative temperatures per month and the relative humidity of the outdoor air on the nomogram (Figure 5).

The critical humidity horizontal line is higher than the horizontal line of relative humidity of the outside air, so the structure passes the test against waterlogging successfully.

Let us calculate the value of the waterlogging criterion for a building structure in such city as Yerofey Pavlovich using formula (1):

$$l = \frac{R_n^{req}}{R_n} = \frac{2.8}{1.655} = 1.69.$$

It was found that the waterlogging criterion was greater than one, therefore, the building envelope Yerofey Pavlovich fails the waterlogging test.

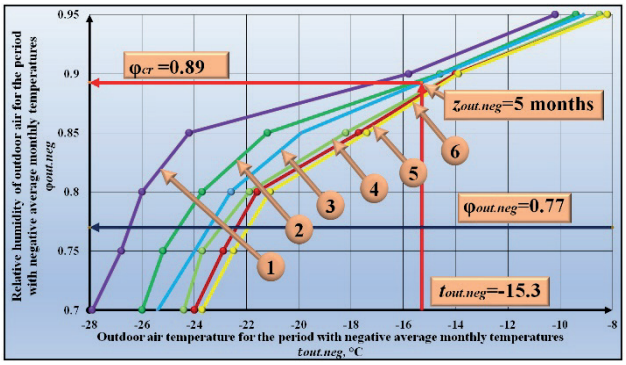


Figure 5. Nomogram of critical ratios of temperature and relative humidity of outdoor air and the duration of the period of moisture accumulation, used to make a decision on the construction of the enclosing structure of a building wall in Blagoveshchensk (duration of the period of moisture accumulation: 1 – three months; 2 – four months; 3 – five months; 4 – six months; 5 – seven months; 6 – eight months)

Let us consider a possibility to construct a building structure in Yerofey Pavlovich using a new method such as the waterlogging nomogram. The enclosing structure is located in the second humidity zone (normal), which corresponds to operating conditions B. Basic climatic parameters: outside air temperature is -17.4, the duration of moisture accumulation is 7 months. Relative air humidity is calculated using formula (2):

$$\varphi_{out.neg} = \frac{e_{out.neg}}{E_0} = \frac{173}{183} = 0.945$$

The values of outside air temperature and relative humidity are plotted on the waterlogging nomogram (Figure 6).

The horizontal line of critical humidity is lower than the horizontal line with the value of relative air humidity, therefore, it is impossible to design a building envelope in such city as Yerofey Pavlovich, since it fails the test against waterlogging.

The proposed method, namely, a nomogram of waterlogging of the enclosing structure has a number of advantages compared to the classical method of protection against waterlogging. The main advantage compared to the classical approach is that no calculations are required.

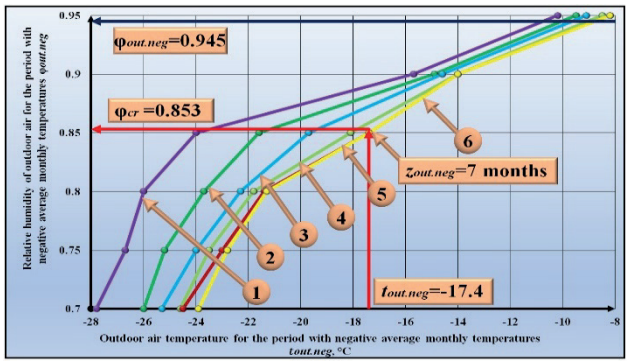


Figure 6. Nomogram of critical ratios of temperature and relative humidity of outdoor air and the duration of the period of moisture accumulation, used to make a decision on the construction of the enclosing structure of the building wall in Yerofey Pavlovich (duration of the period of moisture accumulation: 1 – three months; 2 – four months; 3 – five months; 4 – six months; 5 – seven months; 6 – eight months)

Also, this method can be applied by manufacturers of building materials who develop facade solutions. For each solution, the manufacturer can develop a series of waterlogging nomograms, with the help of which engineers can decide on the construction of the chosen building structure. This method will accelerate the process of designing buildings and structures and will facilitate decisions about constructing in a more convenient and visual form.

4. CONCLUSIONS

In the current work, a new effective method of determining the protection of a building envelope

from waterlogging has been developed as a waterlogging nomogram constructed using the following main climatic characteristics: temperature and relative humidity of the outside air, and the period of moisture accumulation. An algorithm of constructing and using a nomogram of waterlogging of a building envelope for various operating conditions has been presented. Classic method of protection against waterlogging and a new method of determining waterlogging of a building structure using a nomogram have been compared. The new method may be used by engineers when calculating and assessing the protection of a building envelope against waterlogging.

5. FUNDING

The research was funded by a grant from the Russian Science Foundation, project number 25-79-00205, https://rscf.ru/en/project/25-79-00205/.

REFERENCES

1. **Kotlyarova E.** Improving the methodology for assessing the level of environmental safety of urban areas as the basis of their life cycle // E3S Web of Conferences, 2023, Vol. 389, No. 09062.
2. **Zaborova D., Musorina T.** Environmental and Energy-Efficiency Considerations for Selecting Building Envelopes // Sustainability, 2022, Vol. 14(10), No. 5914.
3. **Chakin E., Gamayunova O.** Materials for facade glazing // Lecture Notes in Civil Engineering, 2021, Vol. 141, pp. 182–189
4. **Beskopylny A.N., Stel'makh S.A., Shcherban' E.M., Dolgov V., Beskopylny N., Elshaeva D., Chernil'nik A., Panfilov I., Razveeva I.** Defects Identification and Crack Depth Determination in Porous Media on the Brick Masonry Example Using Ultrasonic Methods: Numerical Analysis and Machine Learning // Journal of Composites Science, 2025, Vol.9, No. 267.
5. **Klyuev S.V., Ayubov N.A., Fomina E.V., Ageeva M.S., Klyuev A.V., Nedoseko I.V.** Influence of carbon black additives and finely ground waste from stone wool production on characteristics of cement systems // Construction Materials and Products, 2025, Vol. 8 (4), No. 8.
6. **Akimov P.A., Mozgaleva M.L., Kaytukov T.B.** Numerical Solution of the Problem of Isotropic Plate Analysis with the Use of B-Spline Discrete-Continual Finite Element Method. // International Journal for Computational Civil and Structural Engineering, 2020, Vol. 16, No. 4, pp. 14-28.
7. **Sidorov V.N., Primkulov, A.M.** Coupled heat and mass transfer problem with dependent heat conductivity properties and its semi-analytical solution // International Journal for Computational Civil and Structural Engineering, 2023, Vol. 19, No. 3, pp. 69–82.
8. **Gagarin V.G., Akhmetov V.K., Zubarev K.P.** Unsteady-state moisture behavior calculation for multilayer enclosing structure made of capillary-porous materials // IOP Conference Series: Earth and Environmental Science, 2019, Vol. 177(1), pp. 925-932.

СПИСОК ЛИТЕРАТУРЫ

1. **Kotlyarova E.** Improving the methodology for assessing the level of environmental safety of urban areas as the basis of their life cycle // E3S Web of Conferences, 2023, Vol. 389, No. 09062.
2. **Zaborova D., Musorina T.** Environmental and Energy-Efficiency Considerations for Selecting Building Envelopes // Sustainability, 2022, Vol. 14(10), No. 5914.
3. **Chakin E., Gamayunova O.** Materials for facade glazing // Lecture Notes in Civil Engineering, 2021, Vol. 141, pp. 182–189

4. **Beskopylny A.N., Stel'makh S.A., Shcherban' E.M., Dolgov V., Beskopylny N., Elshaeva D., Chernil'nik A., Panfilov I., Razveeva I.** Defects Identification and Crack Depth Determination in Porous Media on the Brick Masonry Example Using Ultrasonic Methods: Numerical Analysis and Machine Learning // Journal of Composites Science, 2025, Vol.9, No. 267.
5. **Klyuev S.V., Ayubov N.A., Fomina E.V., Ageeva M.S., Klyuev A.V., Nedoseko I.V.** Influence of carbon black additives and finely ground waste from stone wool production on characteristics of cement systems // Construction Materials and Products, 2025, Vol. 8 (4), No. 8.
6. **Akimov P.A., Mozgaleva M.L., Kaytukov T.B.** Numerical Solution of the Problem of Isotropic Plate Analysis with the Use of B-Spline Discrete-Continual Finite Element Method. // International Journal for Computational Civil and Structural Engineering, 2020, Vol. 16, No. 4, pp. 14-28.
7. **Sidorov V.N., Primkulov, A.M.** Coupled heat and mass transfer problem with dependent heat conductivity properties and its semi-analytical solution // International Journal for Computational Civil and Structural Engineering, 2023, Vol. 19, No. 3, pp. 69–82.
8. **Gagarin V.G., Akhmetov V.K., Zubarev K.P.** Unsteady-state moisture behavior calculation for multilayer enclosing structure made of capillary-porous materials // IOP Conference Series: Earth and Environmental Science, 2019, Vol. 177(1), pp. 925-932.

Zubarev Kirill Pavlovich, Ph.D. (Candidate of Engineering Sciences), Associate Professor, Associate Professor of the Department of Computer Science and Applied Mathematics of the Moscow State University of Civil Engineering, 129337, Moscow, Yaroslavskoe shosse, 26. e-mail.: zubarevkirill93@mail.ru

Sapronova Yulia Aleksandrovna, laboratory research assistant of the A.B. Zolotov Research and Education Center of Computer Modelling of the National Research Moscow State University of Civil Engineering; 129337, Moscow, Yaroslavskoe shosse, 26; e-mail: ho5metown@gmail.com

Fedoseev Vladimir Dmitrievich, laboratory research assistant of the A.B. Zolotov Research and Education Center of Computer Modelling of the National Research Moscow State University of Civil Engineering; 129337, Moscow, Yaroslavskoe shosse, 26; e-mail: fedosseev.vs@gmail.com

Зубарев Кирилл Павлович, кандидат технических наук, доцент, доцент кафедры информатики и прикладной математики Национального исследовательского Московского государственного строительного университета 129337, г. Москва, Ярославское шоссе, 26. e-mail.: zubarevkirill93@mail.ru

Сапронова Юлия Александровна, лаборант-исследователь научно-образовательного центра компьютерного моделирования уникальных зданий, сооружений и комплексов им. А. Б. Золотова» (НОЦ КМ) Национального исследовательского Московского государственного строительного университета; 129337, г. Москва, Ярославское шоссе, 26; e-mail: ho5metown@gmail.com

Федосеев Владимир Дмитриевич, лаборант-исследователь научно-образовательного центра компьютерного моделирования уникальных зданий, сооружений и комплексов им. А. Б. Золотова» (НОЦ КМ) Национального исследовательского Московского государственного строительного университета; 129337, г. Москва, Ярославское шоссе, 26; e-mail: fedosseev.vs@gmail.com

International Journal for Computational Civil and Structural Engineering, 21(4) 185–204 (2025)

DOI:10.22337/2587-9618-2025-21-4-185-204

NUMERICAL MODELLING OF WIND LOADS. VERIFICATION AND VALIDATION FOR THE KEMEROVO MUSEUM, THEATRE AND EDUCATION COMPLEX

Alexander M. Belostotsky, Oleg S. Goryachevsky, Sergey G. Saiyan, Alexandra M. Efimova

National Research Moscow State University of Civil Engineering, Moscow, RUSSIA

Abstract: This paper presents the results of numerical modelling of mean and peak pressure coefficients for a unique facility, conducted within the verification procedure of Ansys Fluent in the RAASN system. The applicability of the steady-state (RANS) simulations and three turbulence models (SST k-ω, EARSM, GEKO k-ω) is verified for the wind loads determination. The results are compared against experimental data obtained in the MSUCE wind tunnel. The weak applicability of often recommended methods of grid extrapolation (Richardson extrapolation and approximate error spline) is revealed. It is shown that the GEKO k-ω turbulence model with the separation parameter C_{SEP} = 1.25 provides a better fit to the wind tunnel data than SST k-ω and EARSM.

Keywords: computational fluid dynamics (CFD), wind loads, verification, validation, Richardson extrapolation, Approximate Error Spline

ВЕРИФИКАЦИЯ И ВАЛИДАЦИЯ ЧИСЛЕННОГО МОДЕЛИРОВАНИЯ ВЕТРОВЫХ НАГРУЗОК НА ПРИМЕРЕ МУЗЕЙНОГО И ТЕАТРАЛЬНО-ОБРАЗОВАТЕЛЬНОГО КОМПЛЕКСА В Г. КЕМЕРОВО

А.М. Белостоцкий, О.С. Горячевский, С.Г. Саиян, А.М. Ефимова

Национальный исследовательский Московский государственный строительный университет, г. Москва, РОССИЯ

Аннотация: Для уникального здания представлены результаты численного моделирования аэродинамических коэффициентов средних и пиковых давлений, полученные в рамках процедуры верификации в системе РААСН программного комплекса ANSYS Fluent. Проверяется применимость для определения ветровых нагрузок стационарной постановки (RANS) и трёх моделей турбулентности: SST k-ω, EARSM, GEKO k-ω. Результаты сопоставляются с экспериментальными данными, полученными в аэродинамической трубе НИУ МГСУ. Выявлена слабая применимость часто рекомендуемых методов сеточной экстраполяции: метода Ричардсона и аппроксимации ошибки сплайном. Выявлено, что модель турбулентности GEKO k-ω с параметром C_{SEP} = 1.25 позволяет получить лучшее соответствие данным из аэродинамической трубы, чем SST k-ω и EARSM.

Ключевые слова: вычислительная аэродинамика, ветровая нагрузка, верификация, валидация, экстраполяция Ричардсона, аппроксимация ошибки сплайном

1. INTRODUCTION

Reliable and efficient methods of wind loads determination for buildings and structures is still an urgent task. Mass construction of unique and architecturally outstanding facilities in dense urban areas stimulates the search for new approaches to solving this problem.

Currently, the following methods are used to determine wind loads:

1. Engineering normative and analytical methods (do not meet the needs of modern construction);

2. Physical modelling in wind tunnels (WTs) [1,2];
3. Numerical modelling [3-11];
4. Monitoring and in-situ measurements [12] (suitable for academic research only);
5. Machine learning and neural networks [13] (under study and yet unapplicable to design).

Physical (experimental) modelling in WTs is currently the most used method to determine wind loads. In the middle of the XX century, an appropriate methodology was developed and validated with in-situ measurements that provides a sufficient level of plausibility under a number of limitations. Still, the high costs of construction and maintenance of WTs, poor scalability, significant experimentation time, low information content and other limitations gradually reduce the role of physical modelling in practice.

Numerical modelling (using CFD), on the other hand, appears to be a more prospective direction: it is devoid of the WT limitations and promises potentially faster research. Therefore, it has already been limitedly legitimised in the regulations of technologically advanced countries [14], STO [15], ASCE 7-22.

For the time of transition from physical to numerical modelling, the most reliable approach is a hybrid one, which means a synthesis of numerical and physical modelling [15].

Currently, the best fit to experimental data is shown by utilising the LES turbulence model. However, its high computational costs hamper its application outside of specialised computational clusters.

Therefore, steady-state (RANS-based) approaches [16] remain the most used ones for fast wind loads determination.

In any case, verification and validation (V&V) procedures are required to confirm the reliability of numerical modelling results. The most general definitions of V&V are given in GOST [17] and ASME [18], but they do not regulate specific procedures and features of individual applications, such as structural aerodynamics.

Due to the lack of exact solutions of mathematical models, ***verification*** in applications to structural aerodynamics is reduced to evaluating the errors of the numerical model (iteration, time, grid, etc.) [19-21,15].

To assess the grid convergence, a number of sources [19,22-27] recommend the use of such methods, as Richardson extrapolation and approximate error spline. In the present paper, it is shown that these methods do not provide any advantages to the wind loads determination problem.

The ***validation*** procedure in structural aerodynamics is more straightforward and complies with [17, 18], but it has one peculiarity: in the vast majority of cases, the results of numerical modelling can only be compared with experimental data from WTs.

In the present paper the V&V procedure of the numerical modelling was carried out for a unique facility, the Museum, Theatre and Education Complex (MTEC) in Kemerovo. Three turbulence models were used: SST k-ω, EARSM, GEKO k-ω (with the separation parameter C_{SEP} = 1.25, 1.75, 2.25). Iteration convergence and three mesh variants were investigated.

The results of numerical modelling are compared against experimental data obtained in the MSUCE WT.

The work was carried out within the verification procedure of Ansys Fluent for the problems of "determination of wind and snow actions on buildings and structures on the basis of numerical solutions of the equations of aero-hydrodynamics" in the system of the Russian Academy of Architecture and Construction Sciences (RAASN) [28].

2. OBJECT AND METHODOLOGY

2.1 Object and task description

In the present paper, a unique facility of the Museum, Theatre and Education Complex (MTEC) in Kemerovo (Fig. 1) was investigated.



Figure 1. Renders of the MTEC in Kemerovo

MTEC has a complex deconstructivist shape. Façades combine glass and metal elements. The building has 10 floors with a total area of ~81100 m^2 and an underground car park. The MTEC is planned to house branches of the Mariinsky Theatre and the State Russian Museum, as well as the Kuzbass Arts Centre. The ensemble of the facility is conceived of four parts: a "floating" theatre "cloud", two "crystals" (a museum and an art centre with workshops), and a public foyer.

The paper investigates the mean (c_e) and peak ($c_{e,+}$, $c_{e,-}$) pressure coefficients at control points on the façade and roof of the facility (Fig. 3):

$$c_e = \frac{\Delta\overline{p}}{Q_{ref}}; c_e = \frac{\Delta\overline{p} + \theta_+ \sigma_p}{Q_{ref}}; c_e = \frac{\Delta\overline{p} - \theta_- \sigma_p}{Q_{ref}} \quad (1)$$

where $\Delta\overline{p} = \overline{p} - p_{ref}$ is the pressure drop; Q_{ref}- is the reference wind pressure; σ_p is the standard deviation of pressure; $\theta_{+(-)}$ are the reliability coefficients.

In the experiment, $\theta_{+(-)} = 3$, and σ_p is calculated using a known formula from statistics. In the numerical simulations, these parameters are determined using the methodology for steady-state modelling outlined in [8,16].

The simulations were carried out for the two most typical wind directions (15°, from the surrounding buildings, and 180°, from the unobstructed side, Fig. 2).

Experimental values of pressure coefficients were obtained in the MSUCE WT through physical modelling at a 1:200 scale (Fig. 3).

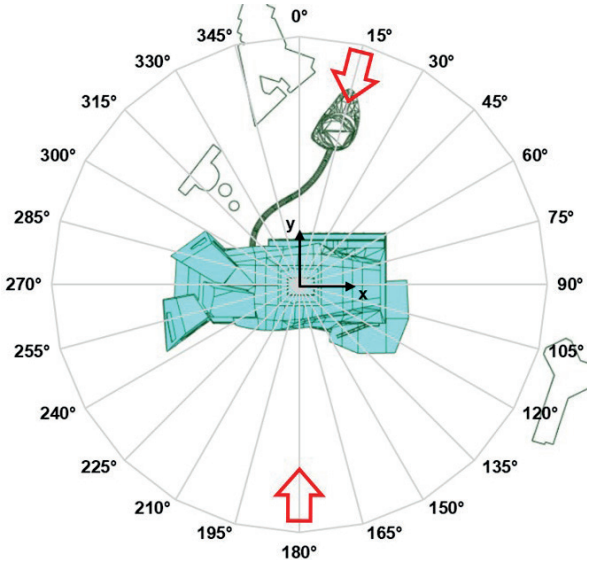
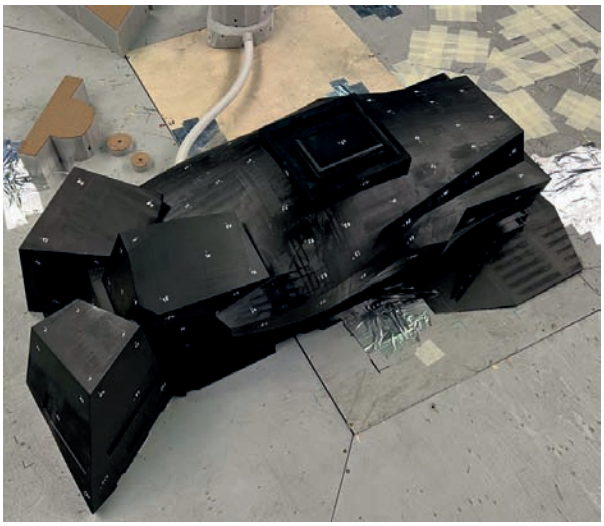


Figure 2. Investigated wind directions



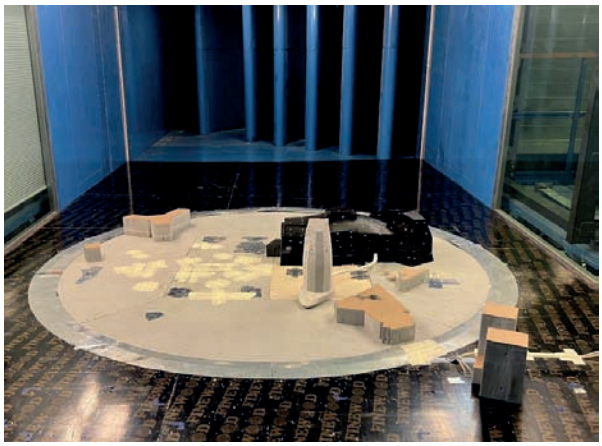


Figure 3. MTEC model in the MSUCE WT (control points are coloured white)

2.2 Mathematical models

In the present paper, the calculation of wind flow and wind actions is reduced to the numerical solution of time-averaged (RANS) three-dimensional nonlinear Navier-Stokes equations. For the determination of wind loads and actions on buildings and structures with practically justified simplification the wind flow is assumed to be incompressible and isothermal, and external mass forces are omitted [10]:

$$\frac{\partial \overline{u}_i \overline{u}_j}{\partial x_j} = -\frac{1}{\rho}\frac{\partial}{\partial x_i}\left(\overline{p} + \frac{2}{3}\rho k\right) + \\ + \frac{\partial}{\partial x_j}\left((\nu + \nu_t)\left(\frac{\partial \overline{u}_i}{\partial x_j} + \frac{\partial \overline{u}_j}{\partial x_i}\right)\right), \quad (2)$$

where $\overline{u}_i$ are the components of the averaged flow velocity, [m/s]; t is the time, [s]; $\overline{p}$ is the averaged pressure, [Pa]; ρ = 1.225 kg/m^3 is the air density; ν = 1.46·10^{-5} m^2/s is the kinematic viscosity of air; ν_t is the turbulent viscosity.

The continuity equation is given as:

$$\frac{\partial \overline{u}_j}{\partial x_j} = 0 \quad (3)$$

The following turbulence models are considered:

– Shear-Stress Transport (SST) k-ω is a widely used two-parameter model that combines the advantages of k-ω and k-ε models for more accurate prediction of turbulent flows. A mixing function [29] is used to transition from the k-ω formulation near the boundaries to the k-ε formulation in the free flow;

– GEKO k-ω (Generalised k-ω) is a two-parameter turbulence model developed by Ansys. It is based on the classic Wilcox k-ω formulation, but rewritten in a "generalised" form: all dimensional and dimensionless constants are replaced by special functions that are controlled through the model parameters to adjust for different types of flow. In this paper, the parameter C_{SEP} (equal to 1.25, 1.75 or 2.25), which governs the

adverse pressure gradients and flow separation [29], is varied.

– Explicit Algebraic Reynolds Stress Model (EARSM) is an extension of the standard two-parameter model derived from the Reynolds stress transport equations to account for the non-linear relationship between the Reynolds stresses, the mean strain rate tensor and the vorticity tensor. WJ-BSL-EARSM extends the BSL model to account for the following effects [29]:

- Anisotropy of Reynolds stresses;
- Secondary flows.

2.3 CFD models

In order to correctly compare the results of numerical and physical modelling, the CFD model reproduces the main parameters of the experiment: the scale, the dimensions of the WT's working area section, and the boundary conditions.

The numerical geometry of the MTEC with the surrounding buildings totally corresponds to the experimental one (Fig.4).

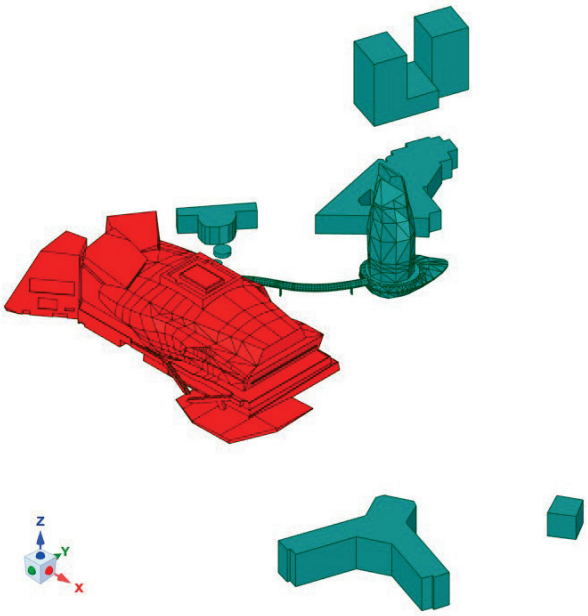
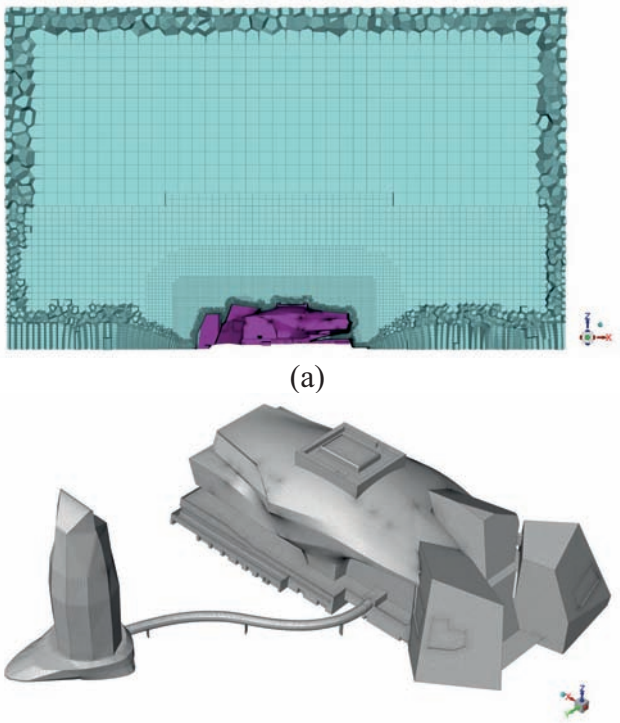


Figure 4. Geometric model of the facility with the surrounding building in Ansys SpaceClaim

Finite-volume meshes were created in Ansys Fluent Meshing using polyhexcore method and combine polygonal, prismatic and cubic finite volumes. Three meshes were developed to analyse the mesh independence of the solution and verify the CFD model: a coarse one (3.1 million cells), a basic one (5.6 million cells, Fig. 6), and a fine one (12.8 million cells). All meshes are similar to each other and differ only in the size of the cells by a factor of 1.5. The number of prismatic layers in the boundary layer is 5 for the coarse mesh, 7 for the basic mesh and 10 for the fine mesh.



(a)

(b)

Figure 5. Finite-volume mesh: a – in the cross-section of the domain; b – on the surface of MTEC and hotel with an elevated bridge

The boundary conditions are shown in Fig. 6:

– at the inlet, a flow velocity profile and turbulent characteristics are set according to the experimental data from the WT (Fig. 7);

– a free outlet with zero additional pressure;

– at the upper, lower, lateral boundaries and surfaces of the facility and surrounding buildings, a no-slip wall condition is set.

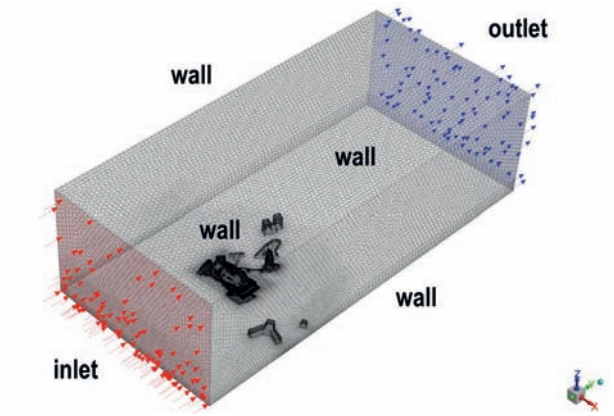


Figure 6. Boundary conditions

A total of 30 3D steady-state simulations (2 angles of attack × 3 finite-volume meshes × 5 turbulence models) were performed using Ansys Fluent (see Section 2.2).

The coupled velocity-pressure scheme and 2nd order schemes were used for the momentum, turbulent transport and pressure equations. The total number of iterations was set to 700, of which the first 200 were calculated with the time scale factor equal to 1.0, while the next 500 were calculated with the said factor reduced to 0.25.

Data sampling for the iteration convergence analysis was performed on the last 100 iterations.

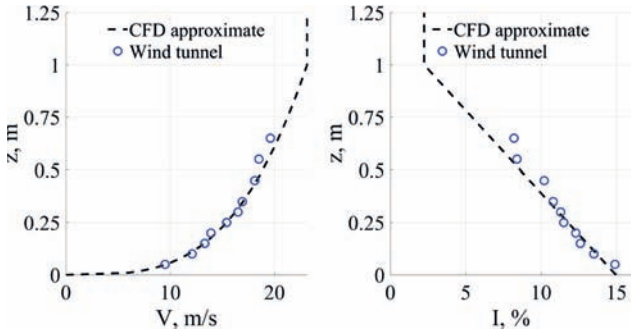


Figure 7. Velocity [m/s] and turbulence intensity [%] profile from WT measurements and CFD approximations

2.4 Verification methods

A combined approach, based on two methods outlined in [21-27], was used to estimate the spatial discretisation error: Richardson Extrapolation (RE) and Approximate Error Spline (AES).

The *Richardson extrapolation* suggests extrapolating the investigated parameter to an infinitesimal grid ($h \to 0$) using the values obtained on a number of finite grids ($h_1 = h$, $h_2 = \alpha_1 h$, $h_3 = \alpha_2 h$). When the coefficient α is equal to both α_1 and α_2 (in this paper, to 1.5), we get:

$$\varepsilon_1 = \phi_{\alpha h} - \phi_h, \quad \varepsilon_2 = \phi_{\alpha^2 h} - \phi_{\alpha h}, \tag{4}$$

$$p = \frac{\left|\ln\left|\varepsilon_2/\varepsilon_1\right|\right|}{\ln(\alpha)} \in [1;2], \tag{5}$$

$$\phi_{ext} = \frac{\alpha^p \phi_h - \phi_{\alpha h}}{\alpha^p - 1} \tag{6}$$

where ϕ_h, $\phi_{\alpha h}$, $\phi_{\alpha^2 h}$ are the values of the sought parameters on the fine, basic and coarse finite-volume grid, respectively; p is the order of the generalised numerical scheme used for extrapolation; ϕ_{ext} is the extrapolated value ($h \to 0$).

Application of this method showed that the parameter p often reaches unrealistic values, resulting in inadequate values of ϕ_{ext}. Therefore, as recommended by the authors, the values of p were restricted in the range of 1.0 to 2.0.

To estimate the range of grid error, Roache [26-27] proposed the Grid Convergence Index (GCI) (formula 7), which characterises the measure of discrepancy between the numerical result on the fine mesh and the asymptotic value, as well as indicates the behaviour of the numerical solution during further refinement of the finite-volume mesh. When the GCI value is small, the solution is within the asymptotic range:

$$GCI = 1.25 \frac{e_A}{\alpha^p - 1}, \tag{7}$$

where $e_A = \left|\frac{\phi_h - \phi_{\alpha h}}{\phi_h}\right|$ is the relative approximation error.

Approximate Error Spline method [25] assumes the proportionality between the error from the solution E_T and the error between the numerical solutions E_A:

$$E_T = \phi - \phi_h, \quad E_A = \phi_h - \phi_{\alpha h}, \tag{8}$$

$$E_T = \beta E_A \tag{9}$$

where ϕ is the unknown exact solution.
According to [25], for $\phi = \phi_{ext}$:

$$\phi_{ext} = \phi_{\alpha^2 h} + \beta\left(\phi_{\alpha^2 h} - \phi_{\alpha h}\right) \tag{10}$$

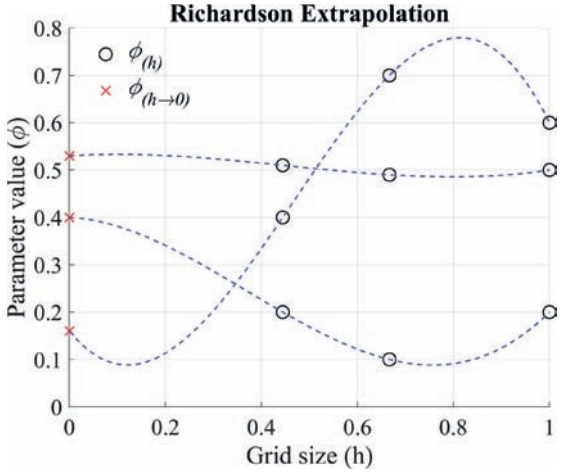
$$\beta = \frac{1}{2}\frac{\phi_{\alpha^2 h} - \phi_h}{\phi_{\alpha^2 h} - 2\phi_{\alpha h} + \phi_h}. \tag{11}$$

The developers of AES [24] do not provide any methods to estimate the error of the obtained extrapolation. Since in the present work the AES method is used only for oscillatory convergence (see below), we propose to use the 3σ rule on the values obtained on three grids:

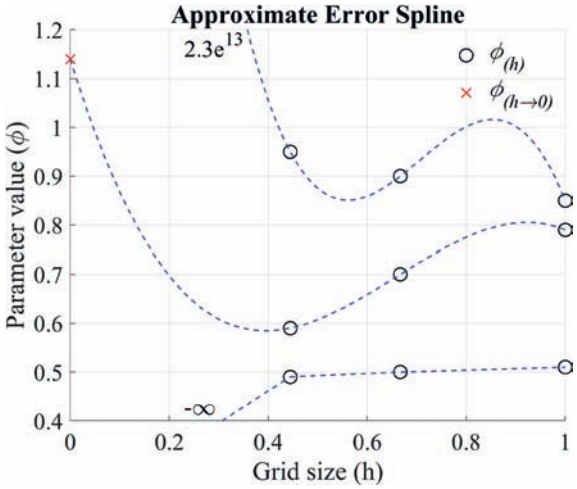
$$\sigma_\phi = \sqrt{\frac{1}{2}\sum_{i=0}^{2}\left(\phi_{\alpha^i h} - \overline{\phi}\right)^2}, \tag{12}$$

where $\overline{\phi} = \frac{1}{3}\sum_{i=0}^{2}\phi_{\alpha^i h}$ is the average value on the three grids.
Fig. 8 demonstrates the behaviour of the RE and AES methods for typical possible situations.
As can be seen from the results, the AES method gives incorrect predictions for monotone convergence and tends to infinity if the values are located on the same line, while the RE method gives inadequate extrapolation for oscillatory convergence. To avoid incorrect extrapolation, it was decided to combine the two approaches and utilise AES for oscillating values and RE for monotone values. Thus, the resulting error is calculated as:

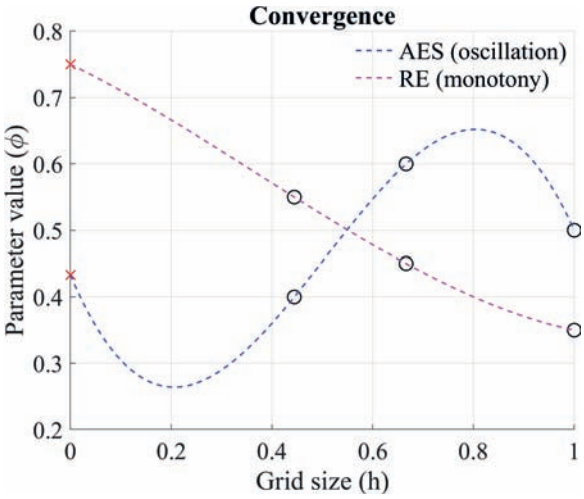
$$E_g = \begin{cases} GCI \cdot \left|\phi_h\right|, (\phi_h - \phi_{\alpha h})(\phi_{\alpha h} - \phi_{\alpha^2 h}) > 0 \\ 3\sigma_\phi, \quad (\phi_h - \phi_{\alpha h})(\phi_{\alpha h} - \phi_{\alpha^2 h}) < 0 \end{cases} \tag{13}$$



(a) demonstration of RE failure for oscillatory convergence $\phi_{\alpha h} < \phi_h, \phi_{\alpha^2 h}$ or $\phi_{\alpha h} > \phi_h, \phi_{\alpha^2 h}$



(b) demonstration of AES failure for monotone convergence of $\phi_h < \phi_{\alpha h} < \phi_{\alpha^2 h}$ or $\phi_h > \phi_{\alpha h} > \phi_{\alpha^2 h}$



(c) correct operation of the methods

Figure 8. Extrapolation examples

To evaluate the iteration convergence, the values sampled at the last 100 iterations were processed:

$$e_{it} = \left| \frac{\max(\phi_k) - \min(\phi_k)}{2\,\mathrm{mean}(\phi_k)} \right|, \qquad (14)$$

where ϕ_k are the values of an investigated variable at the kth iteration (k = 601...700).
For mean(ϕ_k) ≈ 0, the iteration error e_i takes very large values, not characterising convergence. In such cases, formula (14) is not applicable and the corresponding points are discarded.

2.5 Validation methods

When comparing the results of numerical and physical simulations, in addition to qualitative evaluations, the values of the validation metrics proposed in [8] were determined:

$$D_n = \frac{\sum_{j=1}^{N} \left| \phi_j^{efd} - \phi_j^{cfd} \right|}{\sum_{j=1}^{N} \left| \phi_j^{efd} \right|} \cdot 100\%; \qquad (15)$$

$$R_{eq} = \frac{M}{N} \cdot 100\%, \qquad (16)$$

where ϕ_j^{efd}, ϕ_j^{cfd} are the iteratively averaged values of the investigated variables achieved from the physical and numerical modelling in the jth control point, respectively; M is the number of control points with statistically coincident values; N is the total number of control points; D_n is the normalised deviation of the results; and R_{eq} is the fraction of the points that match taking into account the error estimates or have a deviation of no more than 15%.
Metrics (11-12) are not subject to the disadvantage of the often-used R^2 metric, which is insensitive to linear shifts.
In the current work, the following criteria for validation metrics are adopted:
$D_n \leq 15\%$ – good (green);
$15\% < D_n \leq 20\%$ – satisfactory (yellow);
$D_n > 20\%$ – not satisfactory (red);
$R_{eq} \geq 75\%$ – good (green);
$50\% \leq R_{eq} < 75\%$ – satisfactory (yellow);
$R_{eq} < 50\%$ – not satisfactory (red).

3. RESULTS AND DISCUSSION

This section presents the iteration and grid independence analyses results for the numerical solutions, and a comparison of the mean and peak pressure coefficients against the experimental data.

3.1 Iteration errors estimation

Iteration error can contribute significantly to the numerical solution error (Fig. 9).
The analysis shows that SST k-ω has the worst iteration convergence, with e_{it} reaching 38% for some of the control points. The EARSM and GEKO models show significantly better convergence (e_{it} < 15%), and reducing the value of C_{SEP} leads to an even more improved convergence (e_{it} < 5% for C_{SEP} = 1.25).
For the most cases, refining the mesh reduces e_{it}, although this is not a general rule.
For all turbulence models, the influence of the surrounding buildings (180°) worsens the iteration convergence. This effect can be explained by the complexity of the flow structure.

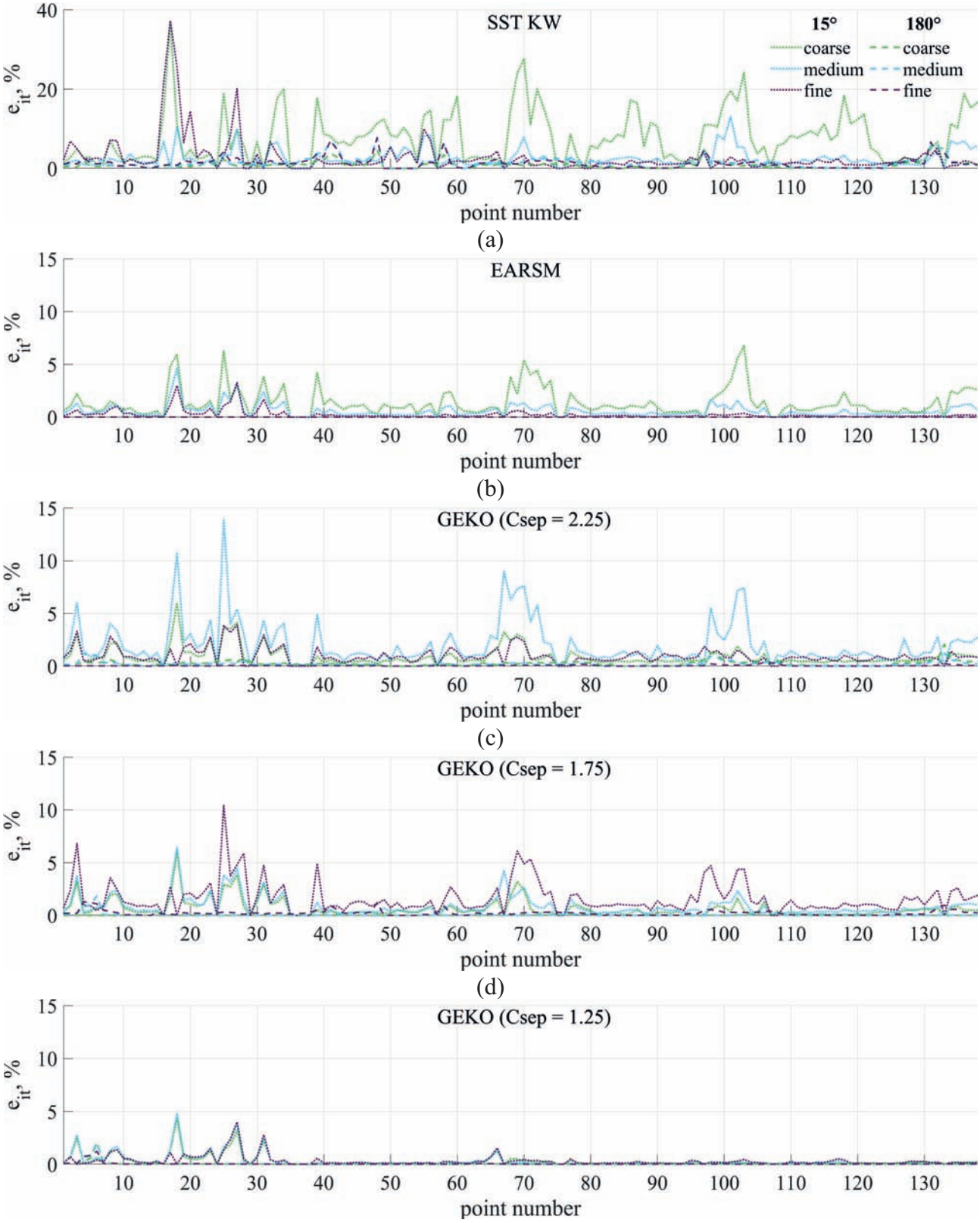


Figure 9. Iteration error e_{it} [%] for different turbulence models

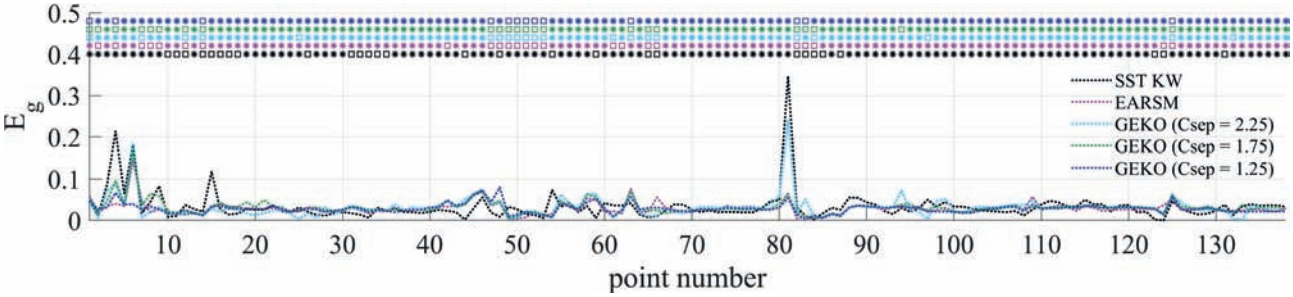
3.2 Grid errors estimation

Grid independence analysis using a combination of RE and AES methods (formula 13) resulted in plots of the absolute values of the errors E_g (Fig. 10).

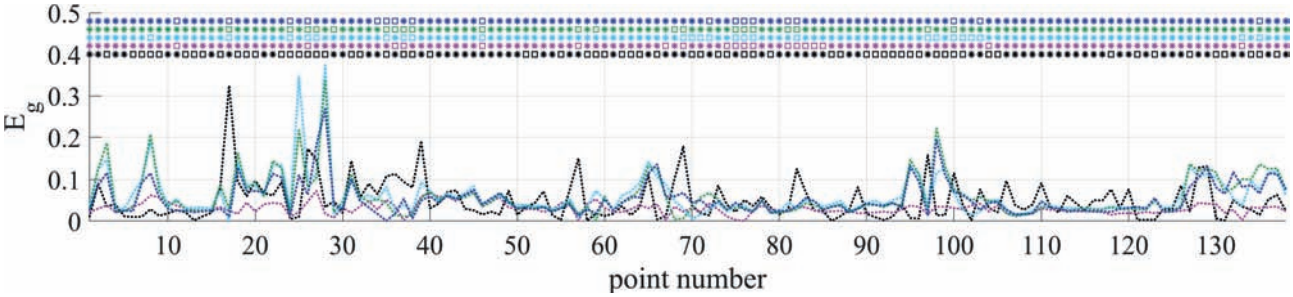
For all turbulence models, the influence of the surrounding buildings (180°) worsens the grid independence as well, which can be explained by the complication of the flow structure, too.

The solution for all turbulence models mostly demonstrates oscillatory behaviour (>80% of points).

The best grid independence was achieved with the EARSM model (E_g < 0.1), followed by GEKO (C_{SEP} = 1.25), while the worst results were obtained with GEKO (C_{SEP} = 2.25) and SST (E_g < 0.4) models.



(a) 180° (not influenced by the surrounding buildings)



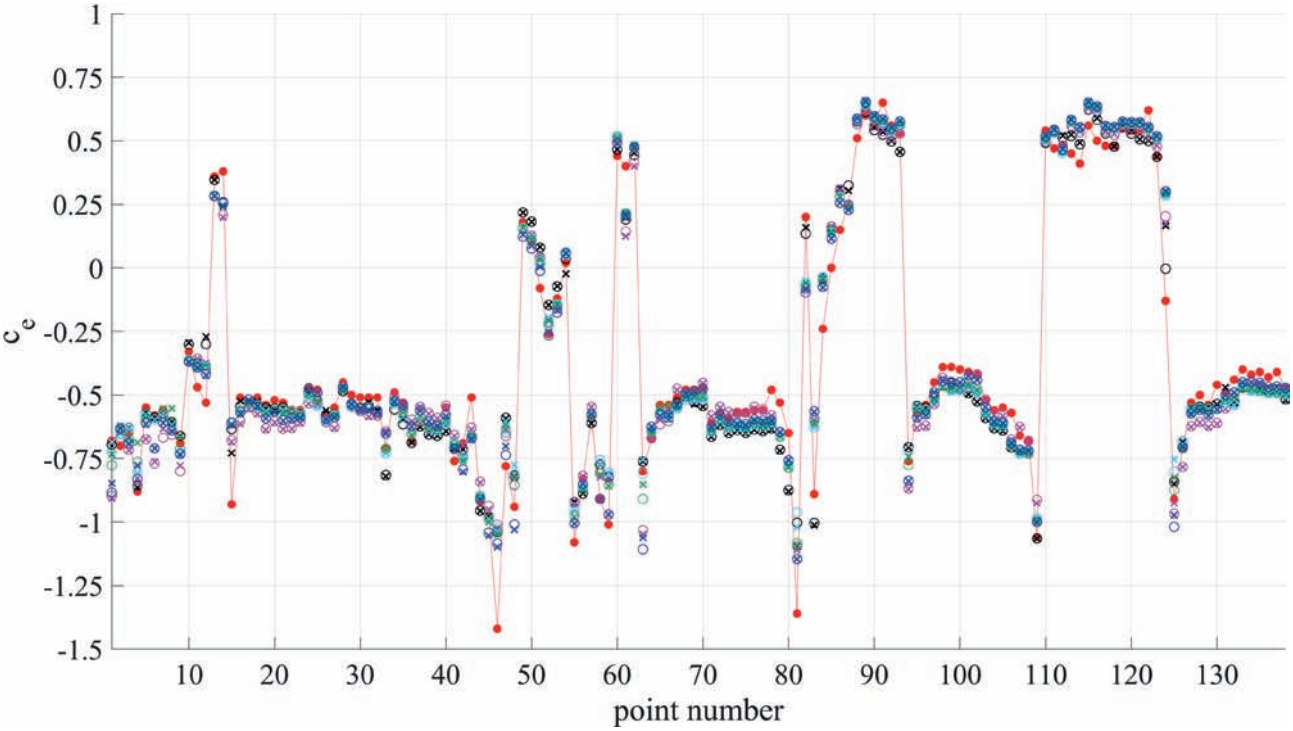
(b) 15° (influenced by the surrounding buildings)

Figure 10. Grid error E_g for different turbulence models; the markers on the horizontal lines indicate the convergence behaviour:
** – oscillatory; □ – monotone*

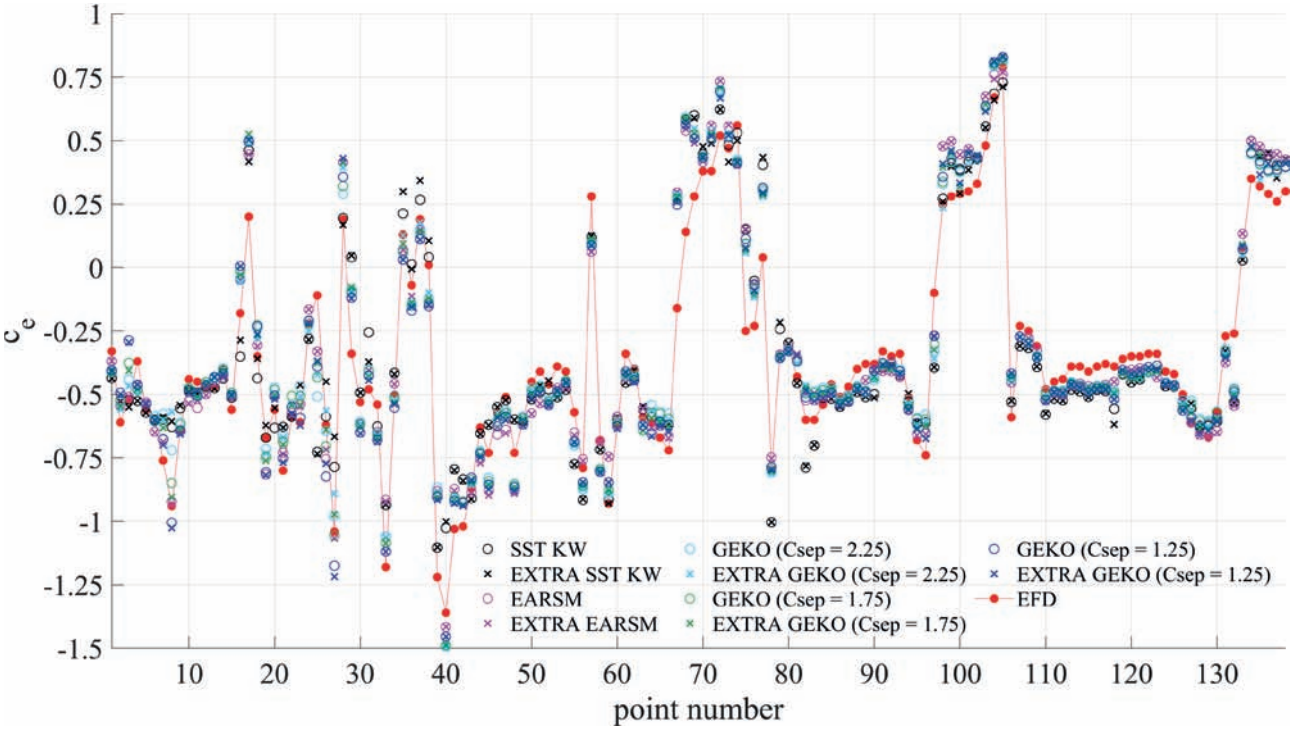
3.3 CFD and EFD results comparison (validation)

Figures 11-13 show the comparison of mean and peak pressure coefficients from the numerical (with different turbulence models) and physical modelling. In the peak coefficient plots, the shaded areas (negative for $c_{e,+}$ and positive for $c_{e,-}$) highlight values that are of no practical interest.

Table 1 summarises the values of the validation metrics (formulae 15-16). In calculating the validation metrics for peak coefficients, points in shaded areas were not considered.

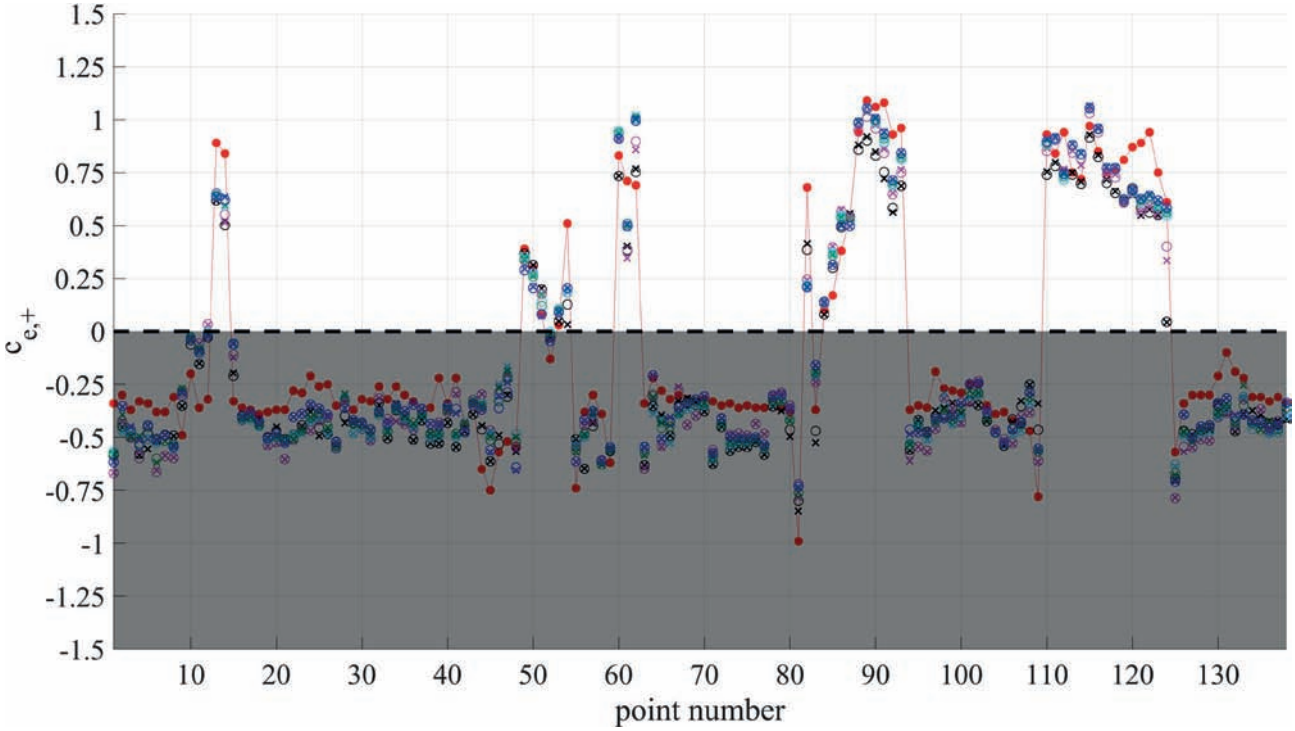


(a) 180° (not influenced by the surrounding buildings)

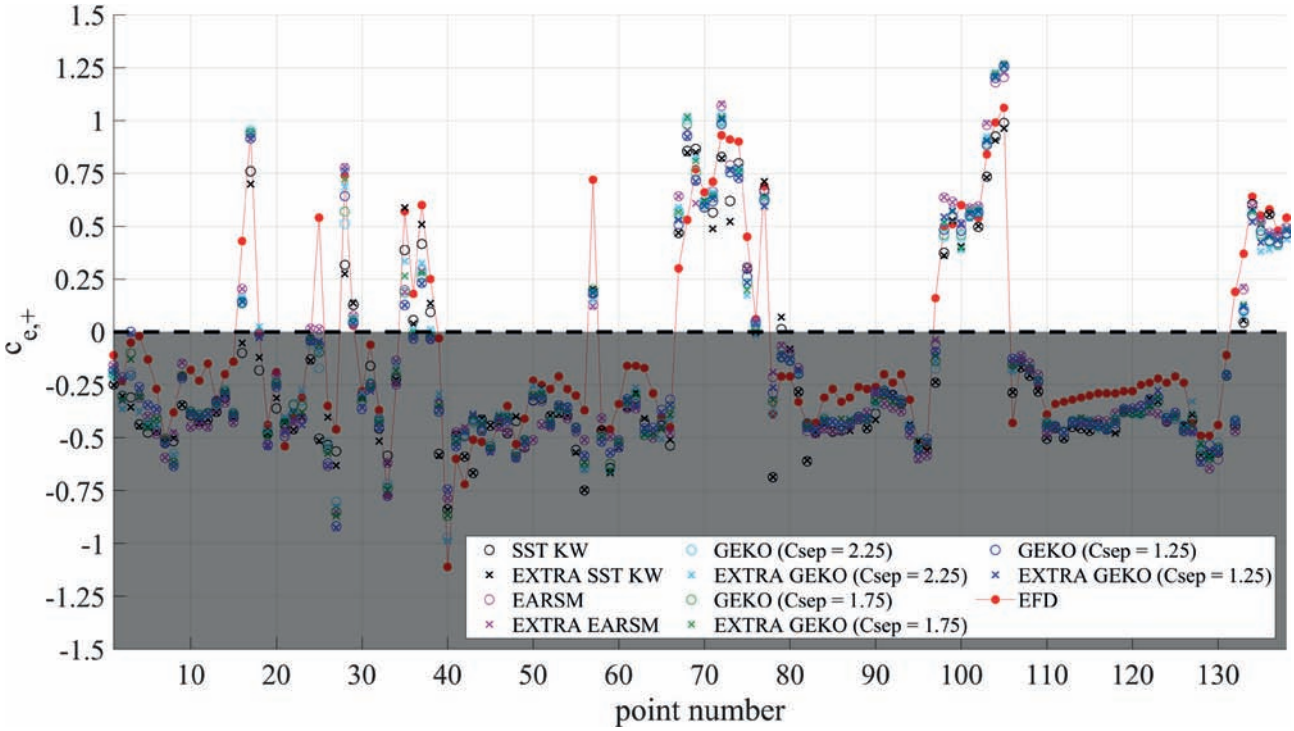


(b) 15° (influenced by the surrounding buildings)

Figure 11. Comparison of mean pressure coefficients c_e for numerical and physical modelling

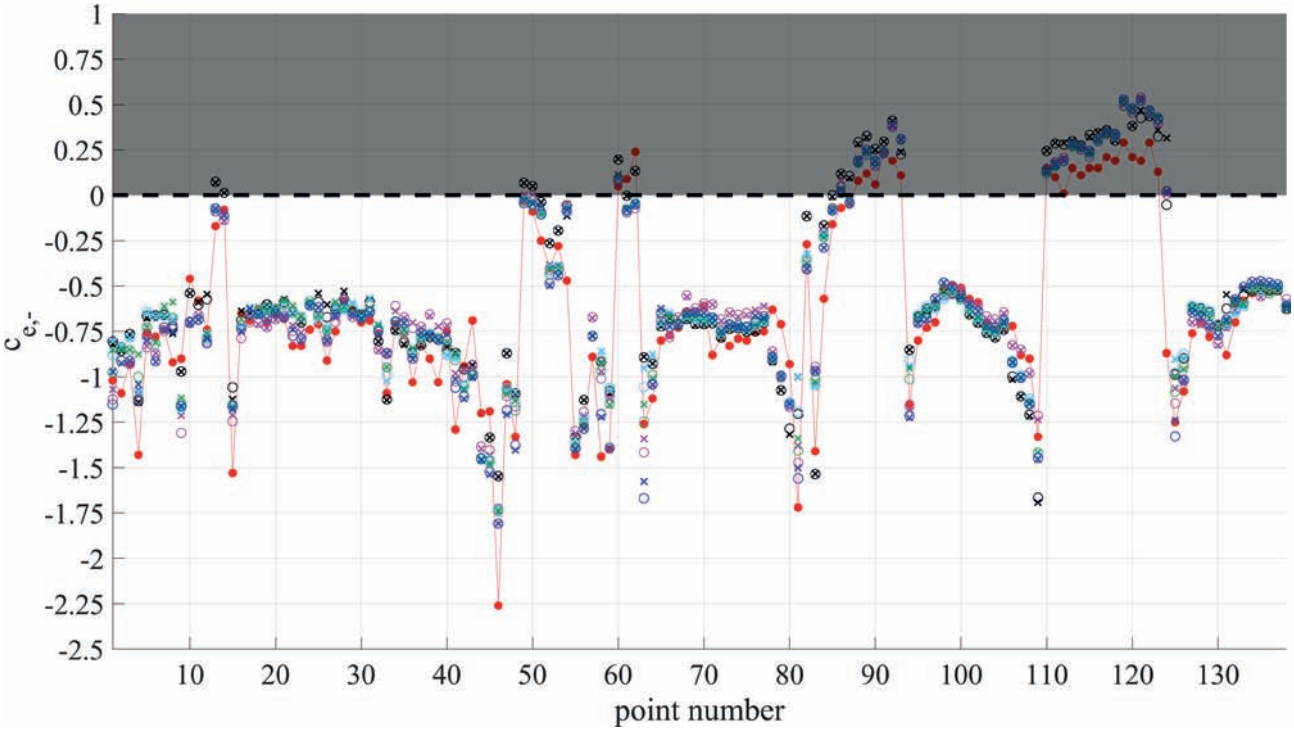


(a) 180° (not influenced by the surrounding buildings)

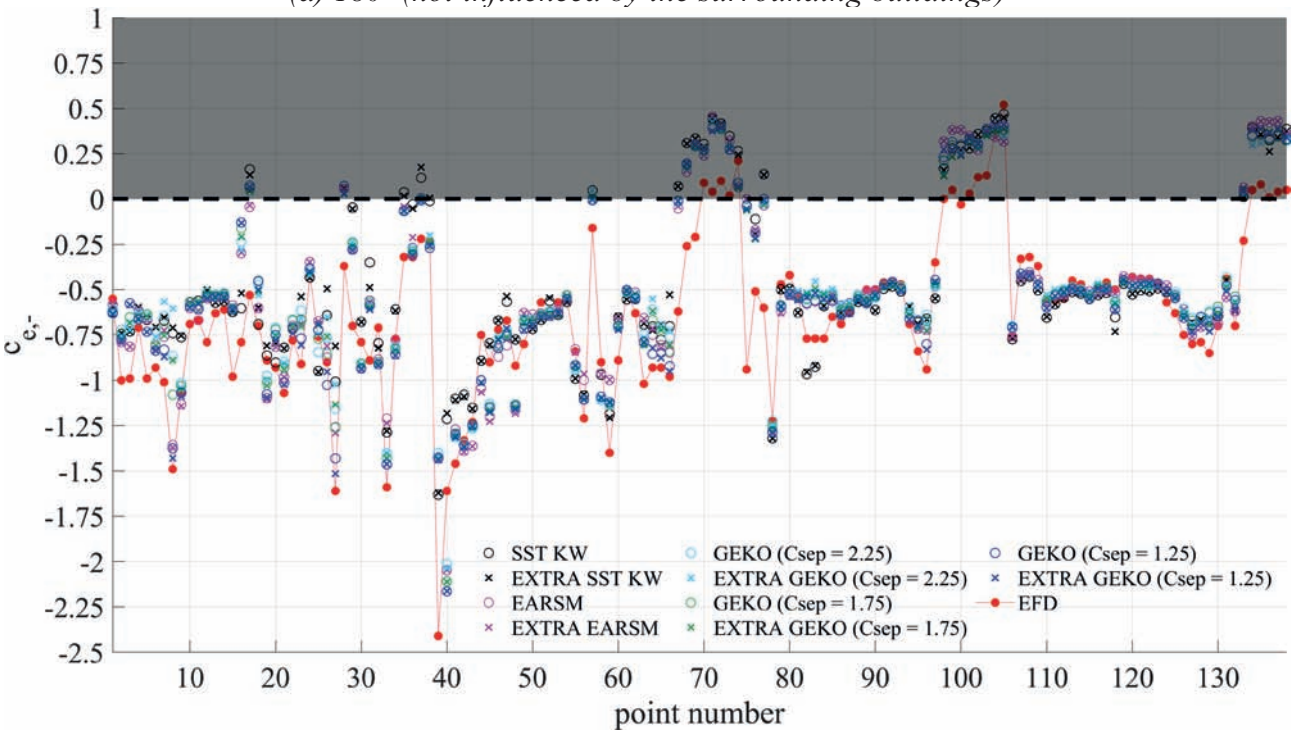


(b) 15° (influenced by the surrounding buildings).

Figure 12. Comparison of positive peak pressure coefficients $c_{e,+}$ for numerical and physical modelling



(a) 180° (not influenced by the surrounding buildings)



(b) 15° (influenced by the surrounding buildings)

Figure 13. Comparison of negative peak pressure coefficients $c_{e,-}$ for numerical and physical modelling

Table 1. Parameters of finite-volume meshes

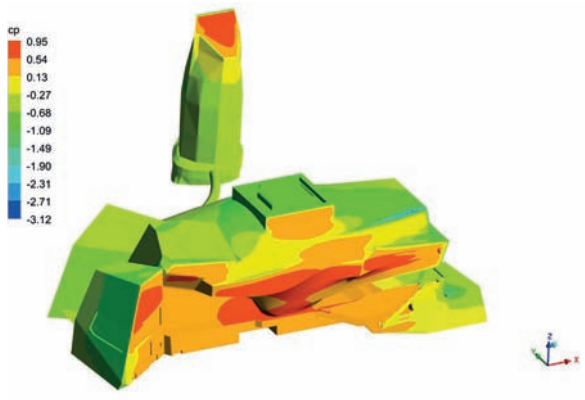
c	Grid	15°		180°	
		D_n,%	R_{eq},%	D_n,%	R_{eq},%
SST k-ω					
c_e	*ext*	22,66	42,75	12,56	65,94
	fine	22,25	40,57	12,33	68,11
	med.	22,62	47,82	14,08	68,84
	coarse	21,65	54,34	13,24	68,84
$c_{e,+}$	*ext*	34,00	48,64	24,37	36,11
	fine	33,79	45,94	24,28	36,11
	med.	36,80	48,64	21,44	38,88
	coarse	30,99	56,75	22,16	38,88
$c_{e,-}$	*ext*	27,48	40,49	20,07	46,08
	fine	26,36	41,32	19,29	46,95
	med.	25,54	48,76	18,48	55,65
	coarse	23,09	61,15	18,78	57,39
EARSM					
c_e	*ext*	20,36	59,42	14,21	75,36
	fine	20,29	64,49	14,16	77,53
	med.	21,80	65,94	15,31	81,88
	coarse	20,88	65,94	14,76	81,88
$c_{e,+}$	*ext*	30,92	56,75	22,43	44,44
	fine	29,72	64,86	22,37	44,44
	med.	30,32	64,86	21,76	47,22
	coarse	29,20	64,86	21,94	47,22
$c_{e,-}$	*ext*	22,86	58,67	16,31	71,30
	fine	22,35	67,76	16,08	73,04
	med.	21,75	70,24	15,48	76,52
	coarse	21,73	70,24	15,26	77,39
GEKO k-ω (C_{SEP} = 2.25)					
c_e	*ext*	19,35	66,66	13,15	83,33
	fine	19,60	70,28	12,90	84,05
	med.	21,11	70,28	14,06	84,05
	coarse	20,37	70,28	12,98	84,05
$c_{e,+}$	*ext*	32,30	64,86	20,75	55,55
	fine	33,09	70,27	20,52	61,11
	med.	31,27	70,27	20,12	61,11
	coarse	30,98	70,27	20,15	61,11
$c_{e,-}$	*ext*	24,80	69,42	18,08	75,65
	fine	24,39	74,38	17,53	82,60
	med.	22,49	74,38	16,61	82,60
	coarse	22,60	74,38	16,42	82,60
GEKO k-ω (C_{SEP} = 1.75)					
c_e	*ext*	19,40	65,21	12,70	81,88
	fine	19,56	70,28	12,34	84,05
	med.	21,59	70,28	13,87	84,05
	coarse	20,69	70,28	12,89	84,05
$c_{e,+}$	*ext*	30,74	62,16	20,24	55,55
	fine	32,04	70,27	19,97	61,11
	med.	30,77	70,27	19,57	61,11
	coarse	30,54	70,27	19,77	61,11
$c_{e,-}$	*ext*	23,28	69,42	16,96	75,65
	fine	23,37	74,38	16,11	82,60
	med.	21,75	74,38	15,25	82,60
	coarse	21,81	74,38	15,10	82,60
GEKO k-ω (C_{SEP} = 1.25)					
c_e	*ext*	19,71	64,49	12,21	81,15
	fine	19,78	69,56	12,03	83,33
	med.	22,75	69,56	13,86	84,05
	coarse	21,79	69,56	13,00	84,05
$c_{e,+}$	*ext*	31,51	62,16	19,18	55,55
	fine	31,22	64,86	19,36	58,33
	med.	30,16	70,27	19,06	61,11
	coarse	31,07	70,27	19,28	61,11
$c_{e,-}$	*ext*	20,84	69,42	14,90	75,65
	fine	21,56	72,72	14,86	79,13
	med.	20,59	74,38	14,74	82,60
	coarse	20,63	74,38	14,90	82,60

The results show that the GEKO k-ω model with C_{SEP} = 1.25 showed the best fit to the experimental data. In contrast, the widely used SST k-ω model showed the worst fit.

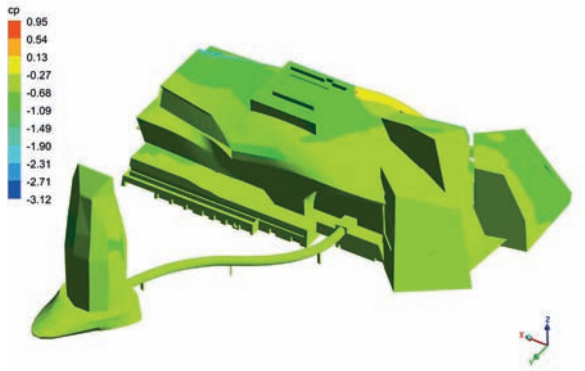
For all the models, the cases without the influence of the surrounding buildings (180°) show significantly better fits to the experimental data than the ones accounting for it (15°).

3.4 Results visualisation

To better understand the flow regimes in the domain, the contours of the mean pressure coefficients and mean flow velocity obtained for the SST k-ω (coarse grid) model are presented.



(a) 180º (windward)



(b) 180º (leeward)

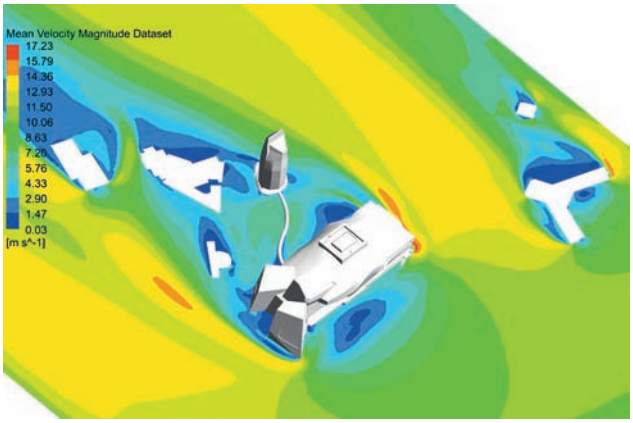


(c) 15º (windward)

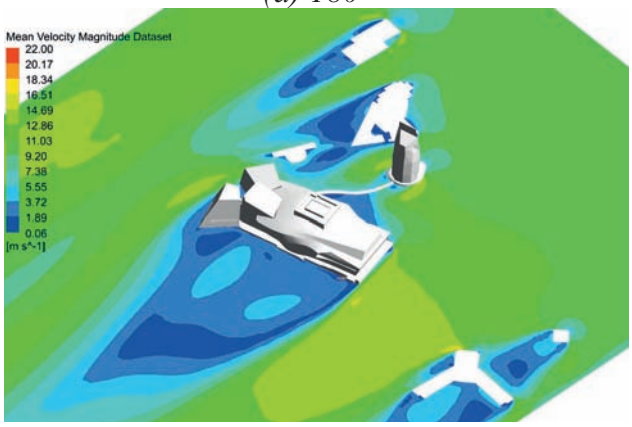


(d) 15º (leeward)

Figure 14. Mean pressure coefficient c_e



(a) 180º



(b) 15º

Figure 15. Mean flow velocity at 0.045 m

4. CONCLUSIONS

The following conclusions are made from the conducted research:

1. Numerical models of a unique facility, the MTEC in Kemerovo, and the surrounding buildings have been developed in Ansys Fluent. A total of 2 wind directions (with and without the influence of the buildings), 3 levels of mesh detailing (3.1, 5.6, 12.8 million cells) and 5 turbulence models (SST k-ω, EARSM, GEKO k-ω (C_{SEP} = 1.25, 1.75, 2.25)) were considered.

2. A thorough **verification** has been carried out to investigate the iteration and grid independence of the solution:

- Iteration and grid error can contribute significantly to the numerical solution results. To minimise this effect, it is necessary to use iterative averaging and improve the mesh quality for the bad areas.

● The often recommended methods for extrapolating the solution to an infinitesimal mesh cannot simply be applied in general. Richardson extrapolation may give inadequate predictions for oscillatory convergence, while the approximate error spline may fail for monotone convergence.
● For all turbulence models, the influence of the surrounding buildings negatively impacts the iteration and grid independence of the solution. This effect can be explained by the complexity of the flow structure.
● The solution for all the turbulence models mostly (>80% of the points) demonstrates oscillatory behaviour on different meshes.
● It has been found that the SST *k*-ω show the worst iteration and grid independence among the studied models.
● The EARSM and GEKO models show significantly better iteration independence (e_{it} < 15%), and decreasing the C_{SEP} further improves it (e_{it} < 5% for C_{SEP} = 1.25).
● The best grid independence is achieved for the EARSM model (E_g < 0.1), followed by GEKO (C_{SEP} = 1.25), and the worst for GEKO (C_{SEP} = 2.25) and SST (E_g < 0.4).
3. A thorough **validation** has been carried out, which is a comparison of the numerical (CFD) and physical (WT) modelling results using the special metrics D_n and R_{eq}.
● The application of RE and AES extrapolation methods did not lead to a systematic improvement of the results (the fit with experiment), so these methods are not recommended the validation of structural aerodynamics problems.
● For all the turbulence models, the influence of the surrounding building negatively impacts the fit to the experiment. This effect can be explained by the complexity of the flow structure.
● The GEKO *k*-ω turbulence model with the parameter C_{SEP} = 1.25 showed a significantly better fit to the experimental data for both mean and peak pressure coefficients' values. This model is recommended for use in wind loads determination for relatively low buildings (meaning their height is less than both their width and length) in steady-state simulations.
4. It is confirmed that Ansys Fluent allows the mean and peak wind loads determination on buildings of complex shape with the accuracy sufficient enough for practical purposes, provided that modern turbulence models and methods set out in the STO [15] are used.

ACKNOWLEDGEMENTS

The research was conducted as part of the development programme for 2025-2036 of Moscow State University of Civil Engineering under the framework of strategic academic leadership programme "Priority 2030".

REFERENCES

1. **Cochran L.** State of the art review of wind tunnels and physical modelling to obtain structural loads and cladding pressures //Architectural Science Review. – 2006. – Vol. 49. – No. 1. – Pp. 7-16.
2. **Cermak J. E.** Wind-tunnel development and trends in applications to civil engineering // J. Wind Eng. Ind. Aerodyn. – 2003. – Vol. 91. – No. 3. – Pp. 355-370.
3. **Li Y., Zhu Y., Chen F. B., Li Q. S.** Aerodynamic loads of tapered tall buildings: Insights from wind tunnel test and CFD // Structures. – 2023. – Vol.56. – PaperID 104975.
4. **Dubinsky S.I.** Numerical modeling of wind impacts on high-rise buildings and complexes: Dissertation for the degree of Candidate of Technical Sciences. Moscow, 2010. – 198 p. (In Russ.)
5. **Doroshenko A.V.** Methodology for numerical modeling of wind speeds and pedestrian comfort in residential areas: Dissertation for the degree of Candidate of Technical Sciences. Moscow, 2013. – 169 p. (In Russ.)

6. **Britikov N.A.** Numerical modeling of snow loads on roofs of large-span buildings and structures: Dissertation for the degree of Candidate of Technical Sciences. Moscow, 2023. – 150 p. (In Russ.)
7. **Afanasyeva I.N.** Adaptive methodology for numerical modeling of three-dimensional dynamic problems of structural aerohydroelasticity: Dissertation for the degree of Candidate of Technical Sciences. Moscow, 2014. – 200 p. (In Russ.)
8. **Goryachevsky O.S.** Dynamic analysis of flexible façade structures under numerically simulated wind loads: Dissertation for the degree of Candidate of Technical Sciences. Moscow, 2024. – 210 p. (In Russ.)
9. **Saiyan S.G., Efimova A.M.** Computational aerodynamic studies of the MIBC "Moscow-City" complex during sequential construction of buildings // Vestnik MSUCE. – 2024. – Vol. 19. – No. 6. – Pp. 906-941. (In Russ.)
10. **Belostotsky A.M., Akimov P.A., Afanas'eva I.N.** Vychislitel'naya aerodinamika v zadachah stroitel'stva, M.: Izdatel'stvo ASV. – 2017. – 720 p. (In Russ.)
11. **Thordal M. S., Bennetsen J. C., Capra S., Koss H. H. H.** Towards a standard CFD setup for wind load assessment of high-rise buildings: Part 1–Benchmark of the CAARC building // J. Wind Eng. Ind. Aerodyn.. – 2020. – Vol.205. – PaperID 104283.
12. **Wang X. J., Li Q. S., Yan B. W.** Full-scale measurements of wind pressures on a low-rise building during typhoons and comparison with wind tunnel test results and aerodynamic database // J. of Struct. Eng. – 2020. – Vol.146. – PaperID 04020196.
13. **Lamberti G., Gorlé C.** A multi-fidelity machine learning framework to predict wind loads on buildings // J. Wind Eng. Ind. Aerodyn.. – 2021. – Vol.214. – PaperID 104647.
14. **Saiyan S.G., Shitikova M.V.** Analysis of wind loads and impacts on high-rise buildings and structures. Review of the current state, challenges, and prospects. Part 1. Wind loads and methods for their determination. News of Higher Educational Institutions. Construction. – 2025. – No. 4. – Pp. 5–19. (In Russ.)
15. STO 02066523-089-1-2024. Numerical modelling of wind and snow actions.
16. **Goryachevsky O.S.** Numerical modelling of wind loads on windows. Validation for a high-rise square plan building // J. Comput. Civ. Struct. Eng. – 2023. – Vol. 19. – No. 3. – Pp. 114–129.
17. GOST R 57188–2016 Numerical modeling of physical processes. Terms and definitions. (In Russ.)
18. ASME V&V 20–2009 Standard for Verification and Validation in Computational Fluid Dynamics and Heat Transfer
19. **Celik I. B., Ghia U., Roache P. J., Freitas C. J.** Procedure for Estimation and Reporting of Uncertainty Due to Discretization in CFD Applications // J. Fluids Eng. – 2008. – Vol. 130. – No.7. – PaperID 078001.
20. **Franke J.** Best practice guideline for the CFD simulation of flows in the urban enviroment // COST Office Brussels. – 2007. – ISBN: 3-00-018312-4.
21. **Tominaga Y., Mochida A., Yoshie R., Kataoka H., Nozu T., Yoshikawa M., et al.** AIJ guidelines for practical applications of CFD to pedestrian wind enviroment around building // J. Wind Eng. Ind. Aerodyn. – 2008. – Vol. 96. – pp. 1749-1761.
22. **Roache P.J.** Verification and Validation in Computational Science and Engineering // Hermosa Publishers,

Albuquerque, New Mexico – 1998. – p. 446.

23. **Freitas C. J.** Journal of fluids engineering editorial policy statement on the control of numerical accuracy // J. Fluids Eng. – 1986. – Pp. 339-340.
24. **Celik I., Karatekin O.** Numerical Experiments on Application of Richardson Extrapolation With Nonuniform Grids // J. Fluids Eng. – 1997. Vol. 119. – No. 3. – Pp. 584-590.
25. **Celik I., Karaismail E., Parsons D. A.** Reliable Error Estimation Technique for CFD Applications // AVT-147 Symposium on Computational Uncertainty in Military Vehicle Design – 2007. – PaperID RTO-MP-AVT-147
26. **Roache P. J.** Perspective: A Method for Uniform Reporting of Grid Refinement Studies // J. Fluids Eng. – 1994. – Vol. 116. – No. 3. – Pp. 405-413.
27. **Roache P. J.** Quantification of uncertainty in computational fluid dynamics // Annu. Rev. Fluid Mech. – 1997. Vol. 29. – No. 1. – Pp. 123-160.
28. Regulation on the verification of software tools used to determine loads and impacts, stress-strain (and other) states, dynamic characteristics, and to assess the strength, stability, and safety of structures, buildings, and facilities / RAASN // Approved by the Presidium of RAASN, Protocol No. 11 of November 25, 2016. – Moscow, 2016. – 28 p. (In Russ.)
29. Ansys Fluent Theory Guide. Release 2024 R1. // Canonsburg: ANSYS Inc. – 2021. – p. 1320.

СПИСОК ЛИТЕРАТУРЫ

1. **Cochran L.** State of the art review of wind tunnels and physical modelling to obtain structural loads and cladding pressures //Architectural Science Review. – 2006. – Vol. 49. – No. 1. – Pp. 7-16.
2. **Cermak J. E.** Wind-tunnel development and trends in applications to civil engineering // J. Wind Eng. Ind. Aerodyn. – 2003. – Vol. 91. – No. 3. – Pp. 355-370.
3. **Li Y., Zhu Y., Chen F. B., Li Q. S.** Aerodynamic loads of tapered tall buildings: Insights from wind tunnel test and CFD // Structures. – 2023. – Vol.56. – PaperID 104975.
4. **Дубинский С.И.** Численное моделирование ветровых воздействий на высотные здания и комплексы: диссертация на соискание ученой степени кандидата технических наук. – Москва, 2010. – 198 с.
5. **Дорошенко А.В.** Методика численного моделирования скоростей ветра и пешеходной комфортности в зонах жилой застройки: диссертация на соискание ученой степени кандидата технических наук. – Москва, 2013. – 169 с.
6. **Бритиков Н.А.** Численное моделирование снеговых нагрузок на покрытия большепролетных зданий и сооружений: диссертация на соискание ученой степени кандидата технических наук. – Москва, 2023. – 150 с.
7. **Афанасьева И.Н.** Адаптивная методика численного моделирования трехмерных динамических задач строительной аэрогидроупругости: диссертация на соискание ученой степени кандидата технических наук. – Москва, 2014. – 200 с.
8. **Горячевский О.С.** Динамический расчет гибких фасадных конструкций на численно моделируемые ветровые воздействия: диссертация на соискание ученой степени кандидата технических наук. – Москва, 2024. – 210 с.
9. **Саиян С.Г., Ефимова А.М.** Расчетные аэродинамические исследования комплекса Московского

международного делового центра «Москва-Сити» при последовательном возведении зданий // Вестник МГСУ. – 2024. – Т. 19, № 6. – С. 906-941.

10. **Белостоцкий А.М., Акимов П.А., Афанасьева И.Н.** Вычислительная аэродинамика в задачах строительства, М.: Издательство АСВ, 2017, 720 с.
11. **Thordal M. S., Bennetsen J. C., Capra S., Koss H. H. H.** Towards a standard CFD setup for wind load assessment of high-rise buildings: Part 1 – Benchmark of the CAARC building // J. Wind Eng. Ind. Aerodyn. – 2020. – Vol.205. – PaperID 104283.
12. **Wang X. J., Li Q. S., Yan B. W.** Full-scale measurements of wind pressures on a low-rise building during typhoons and comparison with wind tunnel test results and aerodynamic database // J. of Struct. Eng. – 2020. – Vol.146. – PaperID 04020196.
13. **Lamberti G., Gorlé C.** A multi-fidelity machine learning framework to predict wind loads on buildings // J. Wind Eng. Ind. Aerodyn. – 2021. – Vol.214. – PaperID 104647.
14. **Саиян С.Г., Шитикова М.В.** Анализ ветровых нагрузок и воздействий на высотные здания и сооружения. Обзор современного состояния, проблемы и перспективы. Часть 1. Ветровые нагрузки и методы их определения // Известия вузов. Строительство. – 2025. – № 4. – С. 5-19.
15. СТО 02066523-089-1-2024. Численное моделирование ветровых и снеговых воздействий.
16. **Горячевский О.С.** Численное моделирование ветровых давлений на окна. Валидация для типового многоэтажного здания квадратной формы // J. Comput. Civ. Struct. Eng. – 2023. – Том. 19. – №. 3. – с. 114–129.
17. ГОСТ Р 57188–2016 Численное моделирование физических процессов. Термины и определения.
18. ASME V&V 20–2009 Standard for Verification and Validation in Computational Fluid Dynamics and Heat Transfer
19. **Celik I. B., Ghia U., Roache P. J., Freitas C. J.** Procedure for Estimation and Reporting of Uncertainty Due to Discretization in CFD Applications // J. Fluids Eng.. – 2008. – Vol. 130. – No.7. – PaperID 078001.
20. **Franke J.** Best practice guideline for the CFD simulation of flows in the urban enviroment // COST Office Brussels. – 2007. – ISBN: 3-00-018312-4.
21. **Tominaga Y., Mochida A., Yoshie R., Kataoka H., Nozu T., Yoshikawa M., et al.** AIJ guidelines for practical applications of CFD to pedestrian wind enviroment around building // J. Wind Eng. Ind. Aerodyn. – 2008. – Vol. 96. – pp. 1749-1761.
22. **Roache P.J.** Verification and Validation in Computational Science and Engineering // Hermosa Publishers, Albuquerque, New Mexico – 1998. – p. 446.
23. **Freitas C. J.** Journal of fluids engineering editorial policy statement on the control of numerical accuracy // J. Fluids Eng. – 1986. – Pp. 339-340.
24. **Celik I., Karatekin O.** Numerical Experiments on Application of Richardson Extrapolation With Nonuniform Grids // J. Fluids Eng. – 1997. Vol. 119. – No. 3. – Pp. 584-590.
25. **Celik I., Karaismail E., Parsons D. A.** Reliable Error Estimation Technique for CFD Applications // AVT-147 Symposium on Computational Uncertainty in Military Vehicle Design – 2007. – PaperID RTO-MP-AVT-147
26. **Roache P. J.** Perspective: A Method for Uniform Reporting of Grid Refinement

Studies // J. Fluids Eng. – 1994. – Vol. 116. – No. 3. – Pp. 405-413.

27. **Roache P. J.** Quantification of uncertainty in computational fluid dynamics // Annu. Rev. Fluid Mech. – 1997. Vol. 29. – No. 1. – Pp. 123-160.
28. Положение о верификации программных средств, применяемых при определении нагрузок и воздействий, напряженно-деформированного (и иного) состояния, динамических характеристик, оценке прочности, устойчивости и безопасности конструкций, зданий и сооружений / РААСН // Утв. президиумом РААСН, протокол №11 от 25 нояб. 2016 г. – М., 2016. – 28 с.
29. Ansys Fluent Theory Guide. Release 2024 R1. // Canonsburg: ANSYS Inc. – 2021. – p. 1320.

Alexander Mikhailovich Belostotsky – DSc, Professor, Full Member of the Russian Academy of Architecture and Construction Sciences, General Director R&D Centre StaDyO; 125040, Russia, Moscow, 3ya Ulitsa Yamskogo Polya, 18. Scientific adviser at A.B. Zolotov REC CM of the National Research Moscow State University of Civil Engineering; 129337, Russia, Moscow, Yaroslavskoe shosse, 26. e-mail: amb@stadyo.ru

Александр Михайлович Белостоцкий – генеральный директор АО НИЦ СтаДиО; 125040, Россия, Москва, 3-я улица Ямского поля, 18. Научный руководитель НОЦ КМ им. А.Б. Золотова Национального исследовательского Московского государственного строительного университета; 129337, Россия, г. Москва, Ярославское шоссе, д. 26.
e-mail: amb@stadyo.ru

Oleg Sergeevich Goryachevsky – CSc, Deputy Director at A.B. Zolotov REC CM of the National Research Moscow State University of Civil Engineering; 129337, Russia, Moscow, Yaroslavskoe shosse, 26. Leading engineer of R&D Centre StaDyO; 125040, Russia, Moscow, 3ya Ulitsa Yamskogo Polya, 18.
e-mail: osg@reccm.ru

Олег Сергеевич Горячевский – к.т.н., заместитель директора НОЦ КМ им. А.Б. Золотова Национального исследовательского Московского государственного строительного университета; 129337, Россия, г. Москва, Ярославское шоссе, д. 26. Ведущий инженер-расчетчик АО НИЦ СтаДиО; 125040, Россия, г. Москва, 3-я улица Ямского поля, 18
e-mail: osg@reccm.ru

Sergey Gurgenovich Saiyan – Researcher at A.B. Zolotov REC CM of the National Research Moscow State University of Civil Engineering; 129337, Russia, Moscow, Yaroslavskoe shosse, 26. e-mail: berformert@gmail.com

Сергей Гургенович Саиян – научный сотрудник НОЦ КМ им. А.Б. Золотова Национального исследовательского Московского государственного строительного университета; 129337, Россия, г. Москва, Ярославское шоссе, д. 26.
e-mail: berformert@gmail.com

Efimova Alexandra Mikhailovna – leading research engineer at LLC «ТМН Advance Technology Center»; 121205, Russia, Moscow, Skolkovo, Nobel str. 7
e-mail: sasha.basket.8@yandex.ru

Ефимова Александра Михайловна – ведущий инженер-исследователь ООО «Центр Перспективных Технологий ТМХ»; 121205, г. Москва, тер. Сколково Инновационного центра, ул. Нобеля, д. 7
e-mail: sasha.basket.8@yandex.ru

International Journal for Computational Civil and Structural Engineering, 21(4) 205–214 (2025)

DOI:10.22337/2587-9618-2025-21-4-205-214

KINETICS OF SOLID-PHASE INTERACTION BETWEEN DISSIMILAR CRYSTALLINE MATERIALS UNDER AN APPLIED LOAD IN A WIDE TEMPERATURE RANGE

Valery V. Abramov, Yulia G. Zheglova, Vera V. Dolgusheva

National Research Moscow State University of Civil Engineering, Moscow, RUSSIA

Abstract: In the paper, a functional dependence of the kinetics of plastic strain and the change in shape of copper microprotrusions under the action of an applied load in a wide temperature range was obtained. The equations obtained in the paper can further find wide practical application for calculating the microstresses of the 2nd kind arising at the interface of a metal - an inorganic material (for example, iron carbide, oxides, nitrides, etc.) during plastic strain, and will also allow estimating the intensity of the processes of the first stage of a solid-phase topochemical reaction between dissimilar crystalline materials with sharply different creep resistance, leading to the formation of a real and physical contact between the surfaces. Synthetic monocrystalline corundum was chosen as such a response material in the paper.

Keywords: kinetics, plastic strain, contact interaction, applied load in a wide temperature range, correlation-regression analysis, microstresses of the 2nd kind, relay transmission of strain

КИНЕТИКА ТВЕРДОФАЗНОГО ВЗАИМОДЕЙСТВИЯ МЕЖДУ РАЗНОРОДНЫМИ КРИСТАЛЛИЧЕСКИМИ МАТЕРИАЛАМИ ПОД ДЕЙСТВИЕМ ПРИЛОЖЕННОЙ НАГРУЗКИ В ШИРОКОМ ДИАПАЗОНЕ ТЕМПЕРАТУР

В.В. Абрамов, Ю.Г. Жеглова, В.В. Долгушева

Национальный исследовательский Московский государственный строительный университет, г. Москва, РОССИЯ

Аннотация: В работе получена функциональная зависимость кинетики пластической деформации и формоизменения микровыступов меди под действием приложенной нагрузки в широком диапазоне температур. Полученные в работе уравнения в дальнейшем могут найти широкое применение на практике для расчета микронапряжений 2-ого рода, возникающих на границе раздела металла - неорганический материал (например, карбид железа, оксиды, нитриды и т.п.) при пластической деформации, а также позволят оценить интенсивность протекания процессов первой стадии твердофазной топохимической реакции между разнородными кристаллическими материалами с резко различной сопротивляемостью ползучести, приводящих к образованию действительного и физического контакта между поверхностями. В качестве такого ответного материала в работе был выбран синтетический монокристаллический корунд.

Ключевые слова: кинетика, пластическая деформация, контактное взаимодействие, приложенная нагрузка в широком диапазоне температур, корреляционно-регрессионный анализ, микронапряжения второго рода, эстафетная передача деформации

INTRODUCTION

Continuing the series of papers devoted to the study of solid-phase interaction under the influence of applied load in a wide range of temperatures, in particular the kinetics of contact formation between dissimilar crystalline materials using copper-corundum as an example, this paper is devoted to obtaining the dependence of the kinetics of plastic strain of microprotrusions at different levels of applied loads in a wide range of

temperatures. A microprotrusion corresponds to the size of one grain of metal.

The need for research

Establishing the kinetics of plastic strain of microprotrusions (a microprotrusion corresponds to the size and structure of one grain) is a very important issue in the process of obtaining a precision detachable or permanent connection - a smoothing process that allows obtaining high-frequency metal surfaces with controlled and adjustable mechanical properties or obtaining a permanent precision connection (welding) when establishing physical contact between the surfaces.

The objective of the paper is to establish the dependence of the formation of plastic strain of copper microprotrusions ε_m, determined in %, on time *t,* determined in seconds, in a wide range of temperatures from room temperature to pre-melting (from 293 K to 973 K) and nominal pressures from 5 to 30 MPa. Of interest is the kinetics of the process of plastic strain of microprotrusions and the influence of temperature and nominal pressure on its course, since in metal under the action of a variable applied load in a wide range of temperatures there is a transition from elastic to elastic-plastic and plastic contact, which must be taken into account in real calculations. In this case, the formulas for calculating strains under elastic mechanical contact cannot be applied. Also, under plastic strain of metal grain, microstresses of the 2nd kind arise, responsible for the relay transmission of strains from soft to hard using the example of copper-corundum or ferrite-cementite Fe_3C contact.

METHODS

Experimental study

The papers [1, 2, 3] describe in detail the experiment and its methodology.

The data considered in the paper were obtained using experimental processing of changes in the roughness indices of the study of contact surfaces of copper grade MB and synthetic single-crystal corundum (sapphire) α-Al_2O_3, 60^O-orientation, carried out using a profilograph-profilometer mod. 201 with a special computer program of the information computing complex (ICC) [4, 5-9].

The experiment was carried out for a wide range of temperatures T from 293 K to 973 K and nominal pressures σ_n from 5 MPa to 30 MPa, the height of the processing microprotrusions R_z was within the range: 3.2 ... 6.3 ... 10 μm and 40-80 μm. The data obtained as a result of the experiment are presented in Table 1.

Table 1. Experimental values of plastic strain ε_m, between copper grade MB and synthetic single-crystal corundum (sapphire) α-Al_2O_3

σ_n, MPa	t, s	ε_m, %							
		T=293, K	T=373, K	T=743, K	T=573, K	T=673, K	T=773, K	T=873, K	T=973, K
5	30	3.9	5.7	11.5	12.3	17.7	15.7	19.7	21.7
	150	7.8	8	15.3	16.4	21.5	23	26.4	28
	330	8	9.5	17.1	17.7	24.2	24.3	28.8	29.9
	570	8.9	9.8	17.3	17.8	25.9	25.4	29.9	31.1
	870					27	25.9	32	32.2
	1170	10.2	10.5	18.7	20.3	28	27.5	32.2	33.4
	1470					28.5	29	33.1	34.2
	2070	10.7	11.5	20.2	22	29.8	30.8	35.1	36.1

σ_n, MPa	t, s	ε_m, %							
		T=293, K	T=373, K	T=743, K	T=573, K	T=673, K	T=773, K	T=873, K	T=973, K
10	30	6.8	8.5	12.7	14.4	17.5	18.3	21.1	22.6
	150	11.5	13	16	17.4	20.9	23.1	26.2	29.8
	330	13.4	14.7	18	19.7	23.9	26.1	29.8	34.2
	570	13.8	15.6	19.2	20.5	25.7	28	30.5	36.7
	870					26	29.3	32	37.9
	1170	15.4	16.7	19.3	21	26.4	29.8	33	39
	1470					27	30.2	33.5	39.4
	2070	17.3	18.3	20.8	22.8	28.2	31.2	34.7	40.3
15	30	9.1	11.5	13.8	14.5	17.7	19	21.6	26.4
	150	12	13.4	16	18.3	21.5	23.7	27	32.2
	330	13.4	15.2	18	20	24.2	27.3	29.6	36.1
	570	14.1	16	19	21	25.9	28.5	30.8	39
	870					27	29	31.9	39.6
	1170	14.8	16.7	19.7	22	28	30.2	32.8	40.2
	1470					28.5	31	33.7	41.2
	2070	16.3	17.7	21.3	23	29.8	33.1	35.9	42.2
20	30	10.30	11.90	14.10	15.60	19.00	20.60	23.70	29.00
	150	12.30	13.80	16.30	18.30	21.90	25.10	28.50	35.50
	330	13.40	15.20	19.00	21.00	25.90	28.50	32.00	39.40
	570	14.10	16.00	20.00	21.60	27.20	30.00	33.80	41.20
	870					27.50	30.50	34.50	41.80
	1170	14.80	16.70	20.30	22.50	28.00	31.00	35.00	
	1470					28.50	31.50	35.50	42.60
	2070	16.30	18.00	21.30	23.70	29.00	32.20	36.00	43.50
30	30	11	13	16	17	19.3	20.7	24.8	31
	150	13	15.6	18.7	20.3	23.3	21.9	31.7	34.2
	330	14.2	16.7	20.6	21.9	26.4	25.6	35	38.3
	570	14.8	17.4	21.9	22.7	28.5	31.3	35.9	41.2
	870					29	32.4	37.1	42.8
	1170	15.2	17.7	22.5	23.7	29.6	33.6	39.6	44.5
	1470					30	35	40.3	46.2
	2070	16	18.7	23	24.2	31.5	37.1	42.2	47.5

RESULTS AND DISCUSSION

Obtaining kinetic equations for plastic strain of copper microprotrusions under the action of an applied load in a wide temperature range

Based on the analysis of the data in Table 1, a one-to-one correspondence was obtained and substantiated using correlation-regression analysis methods, allowing one to obtain a specific value of plastic strain ε_m arising in copper depending on the contact time t.

The analysis carried out in the paper allowed us to establish that the kinetics of plastic strain of copper microprotrusions obeys the logarithmic law

$$\varepsilon_m = a + b\ln(t). \quad (1)$$

In accordance with formulas (2), the coefficients a and b of the equation for determining plastic strain (1) were determined

$$a = \overline{\varepsilon_m} - b\overline{X}\,,\quad b = \frac{\overline{\varepsilon_m X} - \overline{\varepsilon_m}\cdot\overline{X}}{\overline{X^2} - \left(\overline{X}\right)^2}, \qquad (2)$$

where $X = \ln t$; the overline in formulas (2) denotes the average values.

Table 2 presents the obtained equations for calculating the kinetics of plastic strain in copper under the action of variable load in a wide temperature range.

Table 2. Values of the coefficients a and b included in equation (1) for temperatures T from 293 K to 973 K and nominal pressures σ_n = 5, 10, 15, 20 and 30 MPa

σ_n, MPa	5		10		15		20		30	
T, K	*a*	*b*	*a*	*b*	*a*	*b*	*a*	*b*	*a*	*b*
293	-0.9161	1.5599	-0.839	2.3608	3.6918	1.6323	5.5765	1.3541	7.1514	1.1712
373	1.2949	1.3396	1.3314	2.2354	6.3405	1.4879	6.933	1.4182	8.8503	1.3047
473	5.1083	1.9699	6.5898	1.8851	7.6295	1.7592	8.1104	1.768	10.265	1.7332
573	4.998	2.1701	7.9196	1.9367	8.0523	1.9992	9.0525	1.9396	11.472	1.7292
673	7.5722	2.8797	8.8366	2.5327	7.5722	2.8797	10.506	2.493	9.4443	2.8802
773	5.3888	3.2136	7.8274	3.11	8.1487	3.1755	11.493	2.787	3.8381	4.1951
873	8.4701	3.4356	10.406	3.1947	10.91	3.1635	13.833	3.0077	11.546	3.9383
973	11.281	3.1703	8.5363	4.2907	13.63	3.8092	18.143	3.4553	15.521	4.0863

For all obtained equations type (1) of the kinetics of plastic strain of copper with coefficients a and b (Table 2), the coefficient of determination R^2 was calculated in accordance with formula (3), showing the quality of the equations

$$R^2 = 1 - \frac{\sum_{t=1}^{n}\left(\varepsilon_{m_t} - \overset{\pm}{\varepsilon}_{m_t}\right)^2}{\sum_{t=1}^{n}\left(\varepsilon_{m_t} - \overline{\varepsilon_m}\right)^2} \qquad (3)$$

where ε_{m_t} is the value of plastic strain of copper microprotrusions at time *t*, obtained as a result of the experiment (in %), $\overset{\pm}{\varepsilon}_{m_t}$ is the value of plastic strain of copper microprotrusions at time *t*, calculated using formula (1) (in %), $\overline{\varepsilon_m}$ is the average value of plastic strain of copper microprotrusions (in %).

The values of the determination coefficient obtained in accordance with formula (3) are presented in Table 3.

It is evident from Table 3 that all values of the coefficient of determination exceed 0.9, from which it follows that the equations obtained in Table 2 describe the kinetics of plastic strain in copper under the action of variable load in a wide temperature range with an accuracy of more than 90%. This makes it possible to apply these equations in practice for calculating plastic strains occurring in copper in a wide range of temperatures and pressures.

Table 3. Values of the coefficient of determination R^2 for kinetic equations (Table 2) for T from 293 K to 973 K and σ_n = 5, 10, 15, 20, 30 MPa

σ_n, MPa / *T*, K	5	10	15	20	30
293	0.960	0.984	0.990	0.987	0.988
373	0.987	0.987	0.989	0.991	0.979
473	0.984	0.973	0.987	0.961	0.977
573	0.975	0.982	0.989	0.981	0.983
673	0.996	0.985	0.996	0.964	0.989
773	0.962	0.994	0.987	0.980	0.908
873	0.989	0.994	0.990	0.981	0.988
973	0.987	0.988	0.988	0.967	0.966

An example of the application of the obtained formulas in practice

The formulas obtained in the paper will allow modeling the kinetics of plastic strain of copper microprotrusions under the action of variable load in a wide temperature range at each stage of contact formation [2].

The process of contact formation can be conditionally divided into three stages, each of which is characterized by its own physical and mechanical features of the behavior and activity of atoms in the near-contact volume of microprotrusions and is controlled by a certain mechanism of plastic strain at each stage of the kinetic curve [5, 6, 9].

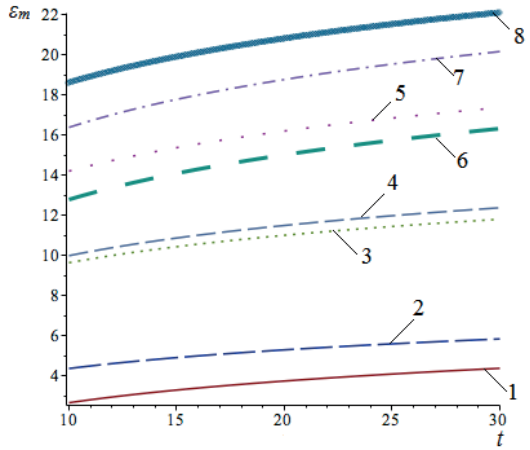
As an example, we will consider the period of active strain or the loading period corresponding to a time *t* from 10 to 30 seconds. Let us construct kinetic curves of plastic strain of copper microprotrusions for the temperature range *T* considered in the paper from 293 K to 973 K and nominal pressures σ_n = 5, 10, 15, 20 and 30 MPa (Figure 1).

In Figure 1 (a-e), the curves are designated by numbers: 1 – T=293 K, 2 – T=373 K, 3 – T=473 K, 4 – T=573 K, 5 – T=673 K, 6 – T=773 K, 7 – T=873 K, 8 – T=973 K.

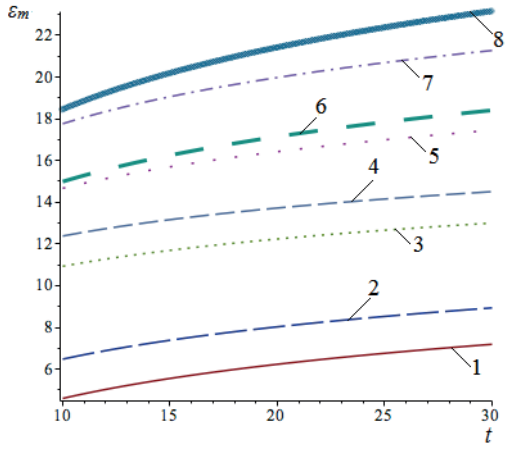
Using the graphs in Figure 1, it is possible to determine the value of plastic strain in copper with an accuracy of 90% during the period of active strain for a specific *t* from 10 to 30 s. Taking into account the formulas obtained in the paper (Table 2), it is possible to determine plastic strain at any other stage (formation of contact of transient and steady creep) with the stated accuracy.

The modeling results obtained in the paper can be confirmed by studies of copper microhardness H_μ (Figure 2).

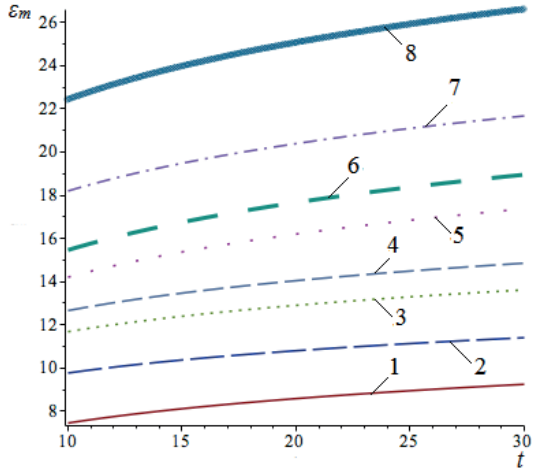
The greatest hardening of copper corresponds to the period of active strain (corresponding to a time *t* from 10 to 30 seconds) and the stage of unsteady creep (6-8 minutes). After completion, the process of changing hardness stabilizes, i.e. corresponds to the stage of steady creep.



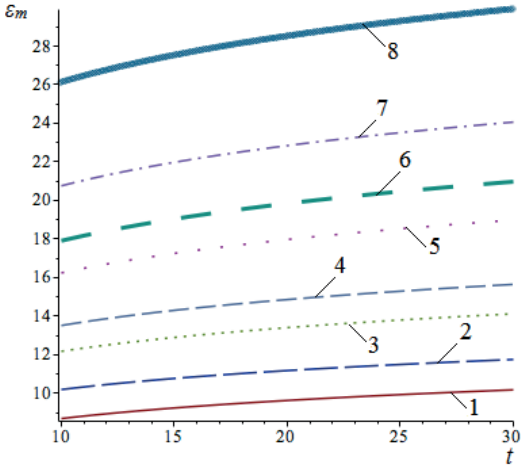
(a) σ_n *= 5 MPa*



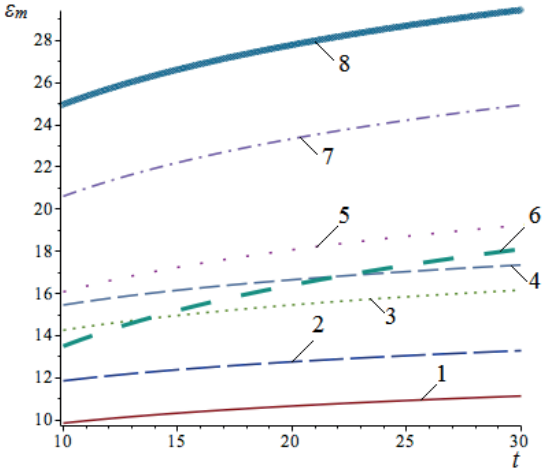
(b) σ_n *= 10 MPa*



(c) σ_n *= 15 MPa*

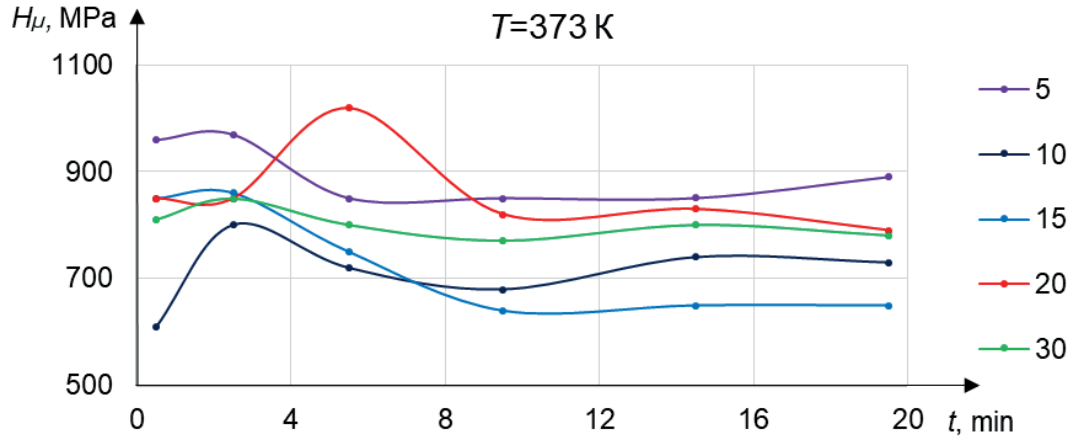


(d) σ_n *= 20 MPa*

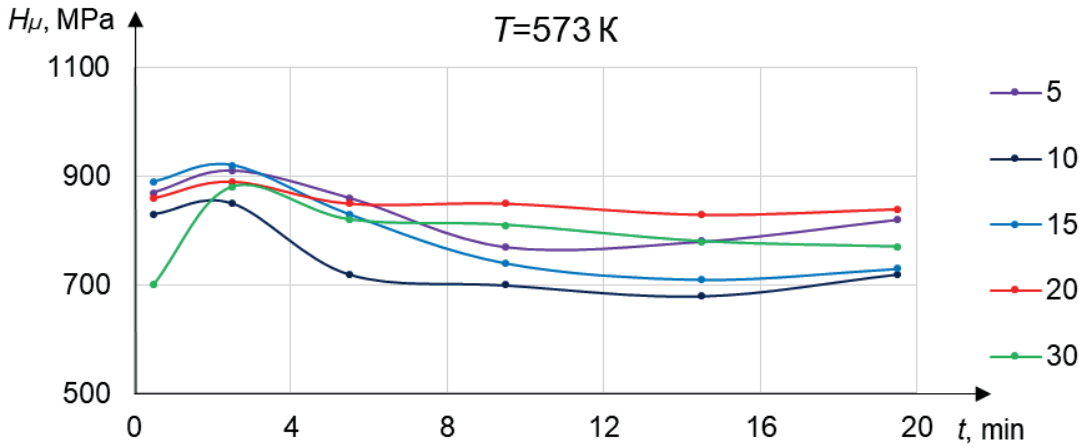


(e) σ_n *= 30 MPa*

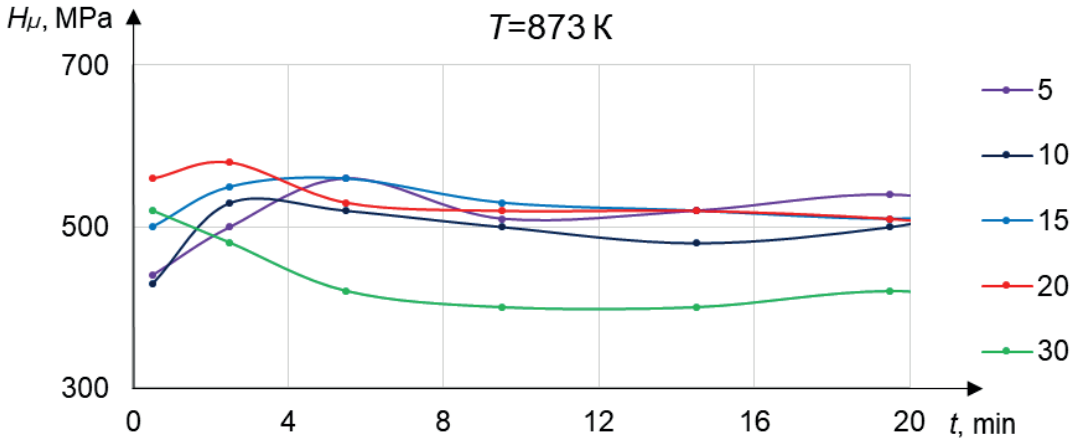
Figure 1. Kinetics of plastic strain of copper microprotrusions, t=10-30 s, T=293, 373, 473, 573, 673, 773, 873, 973 K: (a) σ_n *= 5 MPa, (b).* σ_n *= 10 MPa, (c)* σ_n *= 15 MPa, (d)* σ_n *= 20 MPa, (e)* σ_n *= 30 MPa*



(a)



(b)



(c)

Figure 2. Effect of pressure (σ_n = 5…30 MPa) and temperature (a): T =373 K, (b) T = 573 K, (c) T =873 K on the magnitude and nature of the change in hardness (H_μ) on the surface of the contact pads of copper microprotrusions

CONCLUSION

The paper presents kinetic equations that can be used to determine plastic strains of copper microprotrusions under the influence of applied load in a wide range of temperatures, starting with the period of active strain and ending with the stage of steady-state creep.

Knowledge of the patterns of contact formation due to plastic strain of microprotrusions and their shape change at each stage of the solid-phase topochemical reaction in the contact volumes of the metal allows for a more complete justification of the technological process for obtaining a precision detachable or permanent connection, to manage it and actively control its flow. In addition, the established patterns allow for the calculation of the level of acting normal and tangential microstresses of the 2nd kind in the contact volume of the metal and to explain the mechanism of relay transmission of strains from a soft metal to a harder material and activate its contact surfaces (e.g., semiconductors, inorganic dielectrics, etc. materials) or the destruction of inclusions in steels (carbides, oxides, nitrides) and the subsequent sudden catastrophic destruction of welded metal structures [3]. The established mechanism of relay transmission of strain under the action of microstresses of the 2nd kind combines macroscopic concepts of the mechanics of deformation of solids with microscopic ones, considered from the standpoint of dislocation theory [7, 10]. Knowing these features, it is possible to control the process of obtaining high-purity metal surfaces necessary for high-tech industries such as aviation and radio electronics, nuclear power engineering, as well as the theory of sudden brittle failure of welded metal structures [5, 6, 11].

REFERENCES

1. **Abramov V.V.** (2025) Otsenka formoizmeneniya mikrovystupov i razvitiya kontakta mezhdu raznorodnymi kristallicheskimi materialami pri termodeformatsionnom vozdeystvii [Evaluation of the change in the shape of microprotrusions and the development of contact between dissimilar crystalline materials under thermal deformation action]. *Izvestiya TulGU*, no 2. pp. 502-517. doi: 10.24412/2071-6168-2025-2-502-503
2. **Abramov V.V.** (2024) Kinetika sovmeshchennykh protsessov vyglazhivaniya i svarki davleniyem s nagrevom raznorodnykh kristallicheskikh materialov s sil'no razlichayushcheysya soprotivlyayemost'yu plasticheskoy deformatsii [Kinetics of combined processes of smoothing and pressure welding with heating of dissimilar crystalline materials with greatly differing resistance to plastic strain]. *Physics and chemistry of materials treatment*, no 2, pp. 65-76. doi: 10.30791/0015-3214-2024-2-65-77
3. **Abramov V.V., Rakunov Yu.P., Zheglova Yu.G.** (2025) Rol' mikronapryazheniy vtorogo roda v mekhano-fiziko-khimicheskikh protsessakh skhvatyvaniya raznorodnykh kristallicheskikh materialov pri termodeformatsionnom vozdeystvii [The role of microstresses of the second kind in the mechanical-physical-chemical processes of seizure of dissimilar crystalline materials under thermal deformation action]. *Handbook. An Engineering Jpurnal*, no 5, pp. 63-78. doi: 10.14489/hb.2025.04.pp.063-078
4. **Bobylev A. V.** (1980) *Mekhanicheskiye i tekhnologicheskiye svoystva metallov. Spravochnik* [Mechanical and technological properties of metals. Handbook]. Moskow: Metallurgiya. (in Russian)
5. **Dorn J. E. (eds.), Shanley F.R., Gilman J. J., Fisher J. J., Schoeck G.** (1961) *Mechanical behavior of materials at elevated temperatures*, New York: McGraw-Hill book company, Inc.

6. **Rosenberg V.M.** (1967) *Polzuchest' metallov* [Creep of metals]. Moscow: Metallurgiya. (in Russian).
7. **Cottrell A.** (1964) T*heory of crystal dislocations*, .New York: Gordon and Breach.
8. **Edited by M.V.** Klassen-Neklyudova and H.S. Bagdasarov (1974) *Rubin i sapphir* [Ruby and Sapphire], Moscow: Naula.
9. **Kramer I.R.** (1964) *Trans. Met. Sec. AIME*, vol. 230, no 5, pp. 991-1000.
10. **Panin V.E., Grinyaev Yu.V.** (2003) Fizicheskaya mezomekhanika – novaya paradigma na styke fiziki i mekhaniki deformiruyemogo tverdogo tela [Physical mesomechanics – a new paradigm at the junction of physics and mechanics of deformable solids]. *Physical Mesomechanics*, vol. 6, no 4, pp. 9-36.
11. **Kulikov A.D., Petrov P.A., Demetrashvili I.S., Burlakov I.A., Khanh Toan Nguyen** (2024) Evolyutsiya mikrostruktury medi M1 pri plasticheskoy deformatsii [Evolution of the microstructure of copper M1 during plastic strain]// *Technology of light alloys*, no 4. doi: 10.24412/0321-4664-2024-4-38-44

СПИСОК ЛИТЕРАТУРЫ

1. **Абрамов В.В.** (2025) Оценка формоизменения микровыступов и развития контакта между разнородными кристаллическими материалами при термодеформационном воздействии. *Изв. ТулГУ*, № 2. с. 502-517. doi: 10.24412/2071-6168-2025-2-502-503
2. **Абрамов В.В.** (2024) Кинетика совмещенных процессов выглаживания и сварки давлением с нагревом разнородных кристаллических материалов с сильно различающейся сопротивляемостью пластической деформации. *ФИЗХОМ, АН РФ*, № 2, с. 65-76. doi: 10.30791/0015-3214-2024-2-65-77
3. **3. Абрамов В.В., Ракунов Ю.П., Жеглова Ю.Г.** (2025) Роль микронапряжений второго рода в механо-физико-химических процессах схватывания разнородных кристаллических материалов при термодеформационном воздействии. *Инженерный журнал. Справочник*, № 5, с. 63-78. doi: 10.14489/hb.2025.04.pp.063-078
4. **Бобылев А.В.** (1980) *Механические и технологические свойства металлов* Москва: Металлургия, 295 с.
5. **Dorn J.E. (eds.), Shanley F.R., Gilman J.J., Fisher J.J., Schoeck G.** (1961) *Mechanical behavior of materials at elevated temperatures*, New York: McGraw-Hill book company, Inc.
6. **Розенберг В.М.** (1967) *Ползучесть металлов*. Москва: Металлургия, 276 с.
7. **Cottrell A.** (1964) Theory of crystal dislocations, New York: Gordon and Breach.
8. Рубин и сапфир (1974). **Под ред. М.В. Классен-Неклюдовой и Х.С. Багдасарова**. М.: Наука, 236 с.
9. **Kramer I.R.** (1964) *Trans. Met. Sec*. AIME, vol. 230, no 5, pp. 991-1000.
10. **Панин В.Е., Гриняев Ю.В.** (2003) Физическая мезомеханика – новая парадигма на стыке физики и механики деформируемого твердого тела. *Физ. Мезомеханика*, т.6. №4. с. 9-36.
11. **Куликов А.Д., Петров П.А., Деметрашвили И.С., Бурлаков И.А., Хань Тоан Нгуен** (2024) Эволюция микроструктуры меди М1 при пластической деформации. *Технология легких сплавов*, №4. doi: 10.24412/0321-4664-2024-4-38-44

Abramov Valery Vasilyevich — D.Sc. (Eng.), professor, professor of the Department of Mechanization, Automation and Robotics in Construction of the National Research Moscow State University of Civil Engineering; 129337, Russia, Moscow, Yaroslavskoe shosse, 26. E-mail: valabramov@rambler.ru

Zheglova Yulia Germanovna — Ph.D. (Eng.), associate professor, associate professor of the Department of Information Systems, Technologies and Automation in Construction of the National Research Moscow State University of Civil Engineering; 129337, Russia, Moscow, Yaroslavskoe shosse, 26. E-mail: Jeglovayug@mgsu.ru

Dolgusheva Vera Vitalievna - senior lecturer of the Department of Metal and Wooden Structures of the National Research Moscow State University of Civil Engineering; 129337, Russia, Moscow, Yaroslavskoe shosse, 26. E-mail: DolgushrvaVV@mgsu.ru

Абрамов Валерий Васильевич — д.т.н., профессор, профессор кафедры механизации, автоматизации и роботизации строительства Национального исследовательского Московского государственного строительного университета; 129337, Россия, г. Москва, Ярославское шоссе, д. 26. E-mail: valabramov@rambler.ru

Жеглова Юлия Германовна — к.т.н., доцент, доцент кафедры Информационных систем, технологий и автоматизации в строительстве Национального исследовательского Московского государственного строительного университета; 129337, Россия, г. Москва, Ярославское шоссе, д. 26. E-mail: Jeglovayug@mgsu.ru

Долгушева Вера Витальевна -старший преподаватель кафедры металлических и деревянных конструкций Национального исследовательского Московского государственного строительного университета; 129337, Россия, г. Москва, Ярославское шоссе, д. 26. E-mail: DolgushrvaVV@mgsu.ru

International Journal for Computational Civil and Structural Engineering, 21(4) 215–228 (2025)

DOI:10.22337/2587-9618-2025-21-4-215-228

ABOUT DEVELOPMENT OF COMPUTATIONAL SCHEMES OF GROUP TARGETED KINEMATIC DEVICES FOR SOME ELASTIC SYSTEMS

Leonid S. Lyakhovich [1], Pavel A. Akimov [2], Zaur R. Galyautdinov [1], Andrey S. Plyaskin [1]

[1] Tomsk State University of Architecture and Civil Engineering, Tomsk, RUSSIA
[2] National Research Moscow State University of Civil Engineering, Moscow, RUSSIA

Abstract: For some elastic systems with a finite number of degrees of freedom of mass, in which the directions of mass movement are parallel, methods have been developed for creating additional kinematic devices, the introduction of each of which targetly reduces the value of only one natural frequency to a given value, while not changing any of the other natural frequencies and not one of the forms of natural oscillations. If it is necessary to precisely reduce the values of several natural frequencies, then this requirement can be realized by creating an appropriate number of separate targeted kinematic devices. The computational scheme of each of the individual targeted devices should include racks installed at the mass application nodes and directed along the trajectory of their movement. In some cases, separate targeted constraints can be independently installed in the source system. In most cases, on the basis of individual targeted kinematic devices, a computational scheme of a single group targeted device is formed, which reduces all the intended frequencies to the set values without changing any of the other natural frequencies and not one of the forms of natural oscillations. The distinctive paper is devoted to the method for forming a matrix of coefficients of additional inertial forces, which corresponds to a group targeted kinematic device. An algorithm for the creation of group targeted kinematic devices is proposed. Algorithm is tested with the use of "SCAD" and "Lira" software products.

Keywords: natural oscillation frequency, natural oscillation shape, natural modes, separate targeted kinematic device, group targeted kinematic device, coefficients of additional inertial forces

О ФОРМИРОВАНИИ РАСЧЕТНЫХ СХЕМ ГРУППОВЫХ ПРИЦЕЛЬНЫХ КИНЕМАТИЧЕСКИХ УСТРОЙСТВ ДЛЯ НЕКОТОРЫХ УПРУГИХ СИСТЕМ

Л.С. Ляхович [1], П.А. Акимов [2], З.Р. Галяутдинов [1], А.С. Пляскин [1]

[1] Томский государственный архитектурно-строительный университет, г. Томск, РОССИЯ
[2] Национальный исследовательский Московский государственный строительный университет, г. Москва, РОССИЯ

Аннотация: Для некоторых упругих систем с конечным числом степеней свободы масс, у которых направления движения масс параллельны, разработаны методы создания дополнительных кинематических устройств, введение каждого из которых прицельно уменьшает величину только одной собственной частоты до заданного значения, не изменяет при этом ни одну из остальных собственных частот и ни одну из форм собственных колебаний. Если необходимо прицельно уменьшить величины нескольких собственных частот, то это требование можно реализовать созданием соответствующего количества отдельных прицельных кинематических устройств. Расчётная схема каждого из отдельных прицельных устройств должна включать стойки, установленные в узлах приложения масс и направленные по траектории их движения. В некоторых случаях отдельные прицельные связи могут автономно устанавливаться в исходной системе. В большинстве случаев на основе отдельных прицельных кинематических устройств формируется расчётная схема единого группового прицельного устройства, которое уменьшает все намеченные частоты до заданных значений,

не изменяя при этом ни одну из остальных собственных частот и ни одну из форм собственных колебаний. В данной статье рассмотрен способ формирования матрицы коэффициентов дополнительных инерционных сил, которой соответствует групповое прицельное кинематическое устройство. Предложен алгоритм формирования групповых прицельных кинематических устройств. Первичная пробация (тестирование) алгоритма была реализована с использованием программных продуктов “SCAD” и «Лира».

Ключевые слова: частота собственных колебаний, форма собственных колебаний, отдельная прицельное кинематическое устройство, групповое прицельное кинематическое устройство, коэффициенты дополнительных инерционных сил

1. INTRODUCTION

For some elastic systems with a finite number of degrees of freedom of the masses, in which the directions of motion of the masses are parallel, methods have been developed for creating additional kinematic devices, which introduction specifically reduces the magnitude of only one natural frequency to a given value, without changing any of the other natural frequencies or any of the natural oscillation modes [2, 7, 10-13]. If it is necessary to specifically reduce the values of several natural frequencies, this requirement can be realized by creating an appropriate number of separate targeted kinematic devices [1]. The computational scheme [3, 4] for each of the separate targeted devices must include posts installed in the nodes of mass application and directed along the trajectory of their motion. In some cases, individual targeted constraints can be independently installed in the original system. In most cases, a computational scheme for a single group targeted device [8] is formed on the basis of individual targeted kinematic devices, which reduces all the intended frequencies to given values, without changing any of the other natural frequencies or any of the natural oscillation modes. The distinctive paper is devoted to the method of forming of matrix of additional inertial force coefficients corresponding to a group kinematic targeted device. An algorithm [9, 16-21] for forming group kinematic targeted devices is proposed. Initial testing of the algorithm was carried out with the use of “SCAD” and “Lira” software products [18].

2. ALGORITHM FOR CREATION OF COMPUTATIONAL SCHEME OF A GROUP TARGETED KINEMATIC DEVICE

The following algorithm for creation of computational scheme for a group targeted kinematic device is used:

1) Individual targeted kinematic devices are generated; each of them reduces one of the intended natural frequencies to a specified value;
2) All individual targeted kinematic devices are placed at the nodes of the original system;
3) In areas where several posts are aligned, only one is left;
4) Hinges are introduced at the intersections of the rods.

During the first step of the algorithm, the natural frequency spectrum of the original system with n degrees of freedom is considered

$$\omega[1],\ \omega[2],\ ...,\ \omega[q],\ ..,\ \omega[q+j],\ \omega[q+(j+1)],\ ...,\ \omega[n].$$

It is necessary to specifically clear the frequency interval $\omega[q],\ ..,\ \omega[q+j]$ from j frequencies, reducing their values to values $\omega[s],\ ..,\omega[s+j-1]$.

3. NUMERICAL EXAMPLE OF IMPLEMENTING OF ALGORITHM OF CREATION OF COMPUTATIONAL SCHEME OF GROUP TARGETED KINEMATIC DEVICE

Let us demonstrate the implementation of the algorithm described in the previous paragraph using the example of a system with five degrees of freedom from [2]. The beam section is a composite I-beam (Figure 1). The modulus of elasticity of the system material is $E = 206000$ MPa. The mass values are equal to

$$m[1] = m[5] = 400 \text{ kg};$$
$$m[2] = m[4] = 800 \text{ kg}; \; m[3] = 1200 \text{ kg}.$$

The frequencies and modes of the natural oscillations of the original system are determined by the displacement method, in which the unknowns are the displacements in the direction of mass motion. The basic system of the displacement method is shown in Figure 2.

The coefficients of the displacement method equations and the values of the nodal masses form matrices

$$A = \|a[i, k]\|; \quad M = \|m[i]\|. \tag{1}$$

The roots of the equation

$$|A - \omega^2 M| = 0 \tag{2}$$

define the frequency spectrum of the system's natural oscillations. The frequencies and modes of natural oscillations of the original system are presented in Table 1.

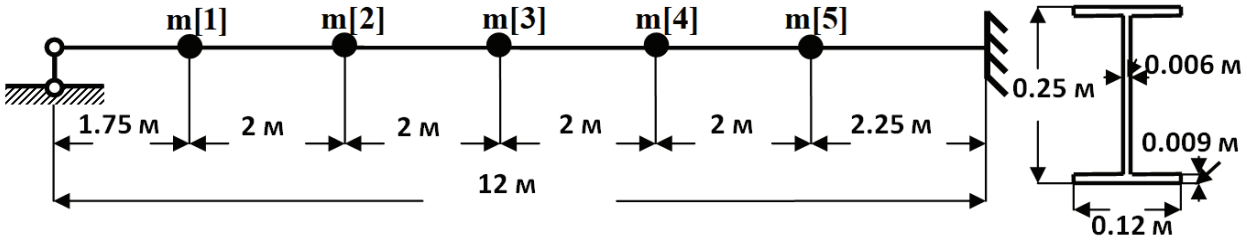


Figure 1. Considering structure (numerical example)

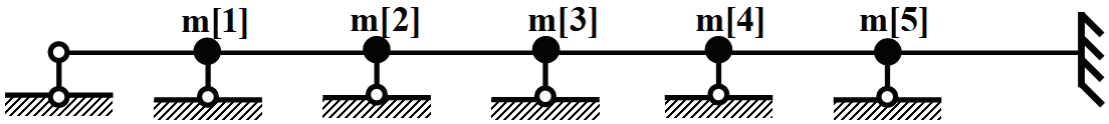


Figure 2. The basic system of the displacement method (numerical example)

Table 1. Frequencies and modes of natural oscillations of the original system

Number k	Формы собственных колебаний					$m[k]$
	for frequency 14.07953	for frequency 53.0752	for frequency 109.5337	for frequency 195.0757	for frequency 226.8870	
0	0.0000	0.0000	0.0000	0.0000	0.0000	0
1	-0.315087	-0.502865	-0.594382	-0.73793	-0.369613	400
2	-0.565080	-0.520103	-0.174580	0.370387	-0.264938	800
3	-0.606213	0.103822	0.432120	-0.086169	0.212601	1200
4	-0.432097	0.574986	-0.359747	-0.137055	-0.383591	800
5	-0.164932	0.367738	-0.547801	0.540420	0.775147	400
6	0.0000	0.0000	0.0000	0.0000	0.0000	0

In order to form individual targeted kinematic devices, it is necessary to determine the forces that should appear in the device's posts [2, 5-7, 10-15]

$$R_0[i,\ k] = m[i]v[i,\ k], \qquad (3)$$

where i, k are the numbers of the components of the k-th mode of natural oscillations, respectively.

If in the considering example it is required to reduce the value of the first natural oscillation frequency from 14.0715 sec^{-1} to 10 sec^{-1}, and the second natural oscillation frequency from 53.0769 sec^{-1} to 11 sec^{-1}, then

$$R_0[i,\ 1] = m[i]v[i,\ 1]; \quad R_0[i,\ 2] = m[i]v[i,\ 2].$$

The values are given in Table 2.

Table 2. Values of $R_0[i,\ k]$

i	1	2	3	4	5
$R_0[i,\ 1]$	63.04	226.24	364.32	173.28	33.08
$R_0[i,\ 2]$	-101.52	-210	62.88	232.16	74.24

Table 3. Frequencies and modes of natural oscillations of the modified system

Number k	Формы собственных колебаний					$m[k]$
	for frequency 10.0095	for frequency 53.0752	for frequency 109.5337	for frequency 195.0757	for frequency 226.8870	
0	0.0000	0.0000	0.0000	0.0000	0.0000	0
1	0.315087	-0.502865	-0.594382	-0.73793	-0.369613	400
2	0.565080	-0.520103	-0.174580	0.370387	-0.264938	800
3	0.606213	0.103822	0.432120	-0.086169	0.212601	1200
4	0.432097	0.574986	-0.359747	-0.137055	-0.383591	800
5	0.164932	0.367738	-0.547801	0.540420	0.775147	400
6	0.0000	0.0000	0.0000	0.0000	0.0000	0

In order to construct a computational model for a kinematic targeted device that reduces $\omega[q]$ to $\omega[s]$, a matrix of additional inertial forces is formed:

$$M_0 = M_{m0}M_m; \qquad (4)$$

$$M_m = \left\| m_0[i,k] \right\|_{i,k=1}^{n}; \qquad (5)$$

$m_0[i,\ k] = m[i]m[k]v_\omega[i,\ q]v_\omega[k,\ q]$ or

$$m_0[i,\ k] = R_0[i,\ q]R_0[k,\ q]; \qquad (6)$$

$$M_{m0} = \frac{\sum_{i=1}^{n}\sum_{k=1}^{n}(a[i,\ k] - (\omega[s])^2 m[i,\ k])v_\omega[i,\ q]v_\omega[k,\ q]}{\sum_{i=1}^{n}\sum_{k=1}^{n}(\omega[s])^2 m_0[i,\ k]v_\omega[i,\ q]v_\omega[k,\ q]}. \qquad (7)$$

After forming the matrix, the following equation is solved:

$$\left| A - \omega^2 (M + M_{m0}M_m) \right| = 0. \qquad (8)$$

The solution results determine the frequency spectrum and natural oscillation modes of the modified system.

For systems in which the directions of mass motion during natural oscillations lie in the same plane, the method of creation of computational model is based on the properties of a rope polygon constructed from the forces $R_0[i,\ k]$. For the initial system considered in the distinctive paper, such an approach is given, for example, in [2]. There we have $R_0[i,\ 1] = m[i]v[i,\ 1]$ and corresponding kinematic targeted device is formed,

that reduces the first natural oscillation frequency from 14.0715 sec^{-1} to 10 sec^{-1}. The frequencies and forms of natural oscillations of the modified system are presented in Table 3.

The general view of this kinematic targeted device is shown in Figure 3. We have the following lengths of posts:

$$l_p[1] = 2.6934\,\text{m}; \quad l_p[2] = 0.9406\,\text{m};$$
$$l_p[3] = 0.2000\,\text{m}; \quad l_p[4] = 1.0879\,\text{m};$$
$$l_p[5] = 2.7498\,\text{m}.$$

The magnitude of the additional mass is determined by the relationship (see, for example, [2])

$$M_{add} = M_{mo}(N[j])^2, \qquad (9)$$

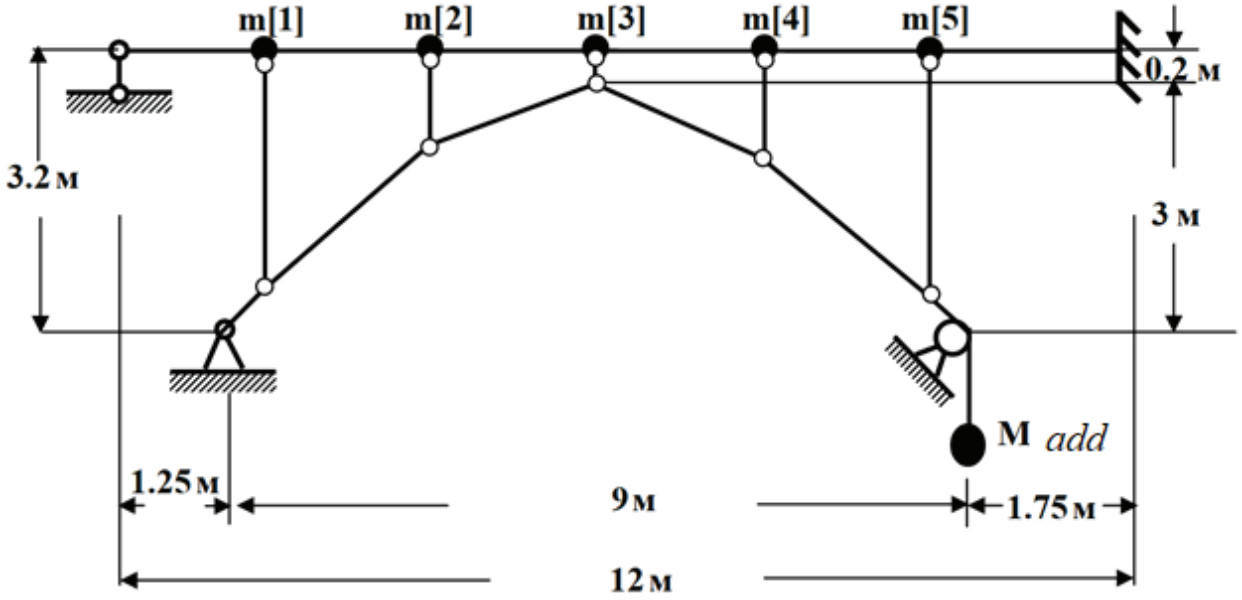


Figure 3. The general view of computational scheme of targeted kinematic device

Table 4. Coordinates of the belt nodes

Number of	0 node	1	2	3	4	5	6
Coordinate of node	4.0557	2.9725	1.6217	6.4406	9.4115	5.5631	4.0557

Table 5. Frequencies and modes of natural oscillations of the modified system

Number k	Формы собственных колебаний					$m[k]$
	for frequency 11.0062	for frequency 14.07953	for frequency 109.5337	for frequency 195.0757	for frequency 226.8870	
0	0.0000	0.0000	0.0000	0.0000	0.0000	0
1	-0.502865	-0.315087	-0.594382	-0.73793	-0.369613	400
2	-0.520103	-0.565080	-0.174580	0.370387	-0.264938	800
3	0.103822	-0.606213	0.432120	-0.086169	0.212601	1200
4	0.574986	-0.432097	-0.359747	-0.137055	-0.383591	800
5	0.367738	-0.164932	-0.547801	0.540420	0.775147	400
6	0.0000	0.0000	0.0000	0.0000	0.0000	0

where $N[j]$ is the force in the outermost post of the device's belt, to which the additional mass is attached.

The additional mass for the formed device is equal to $M_{add} = 1586.5229\,\text{kg}$. The cross-sectional areas of the kinematic device rods are identical; their values can be chosen arbitrarily. A cable runs from the lower hinge of fifth post through the block to the ground.

Similarly we have $R_0[i,\ 2] = m[i]v[i,\ 2]$ and a matrix of additional inertial forces is formed based on the forces, reducing the second natural frequency from 53.0769 sec^{-1} to 11 sec^{-1}, and a corresponding computational model for the targeted kinematic device is created. A general view of the computational model for this targeted kinematic device is shown in Figure 4.

The additional mass is equal to

$$M_{add} = 6301.7206915414\,\text{kg}.$$

The frequencies and modes of natural vibrations of this modified system are presented in Table 5.

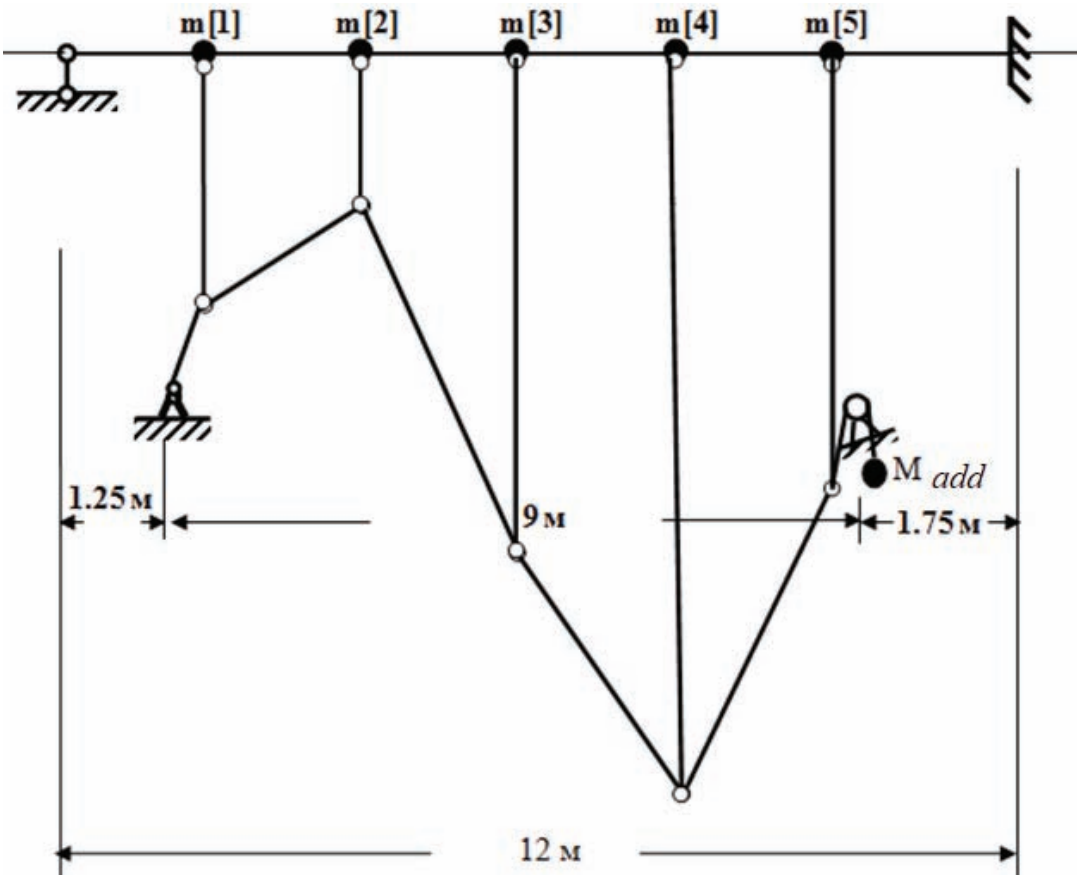


Figure 4. The general view of computational scheme of targeted kinematic device

Table 6. Coordinates of the belt nodes

Number f o node 0	1	2	3	4	5	6
Node coordinate (upper chord)	3.2000	2.6934	0.9406	0.2000	1.0879	2.7498	3.2000
Node coordinate (lower chord)	4.0557	2.9725	1.6217	6.4406	9.4115	5.5631	4.0557

After creation of individual kinematic targeted devices necessary for solving the problem, a group matrix of additional inertial force coefficients can be formed. In order to do this it is required simply sum the coefficients of the additional inertial force matrices of the individual kinematic devices.

By implementing the second step of the algorithm described above, we form a group targeted kinematic device. In order to do this, the generated computational schemes for the individual targeted kinematic devices are placed at the nodes of the original system. The general view of this device is shown in Figure 5.

We have the following additional masses:

$$M_{add1} = 1586.5229\,\text{kg}, \quad M_{add2} = 6301.72069\,\text{kg}.$$

In this version of the group targeted kinematic device, both additional masses are attached to the rightmost links of the individual kinematic devices' belts.

In some cases, it may be necessary to attach additional masses to different sides of the group targeted kinematic device. Implementing this requirement does not complicate the procedure of creation of the group targeted device. In this case, in the individual kinematic devices used, the corresponding numbers j of the outermost belt links are selected when determining the values (9).

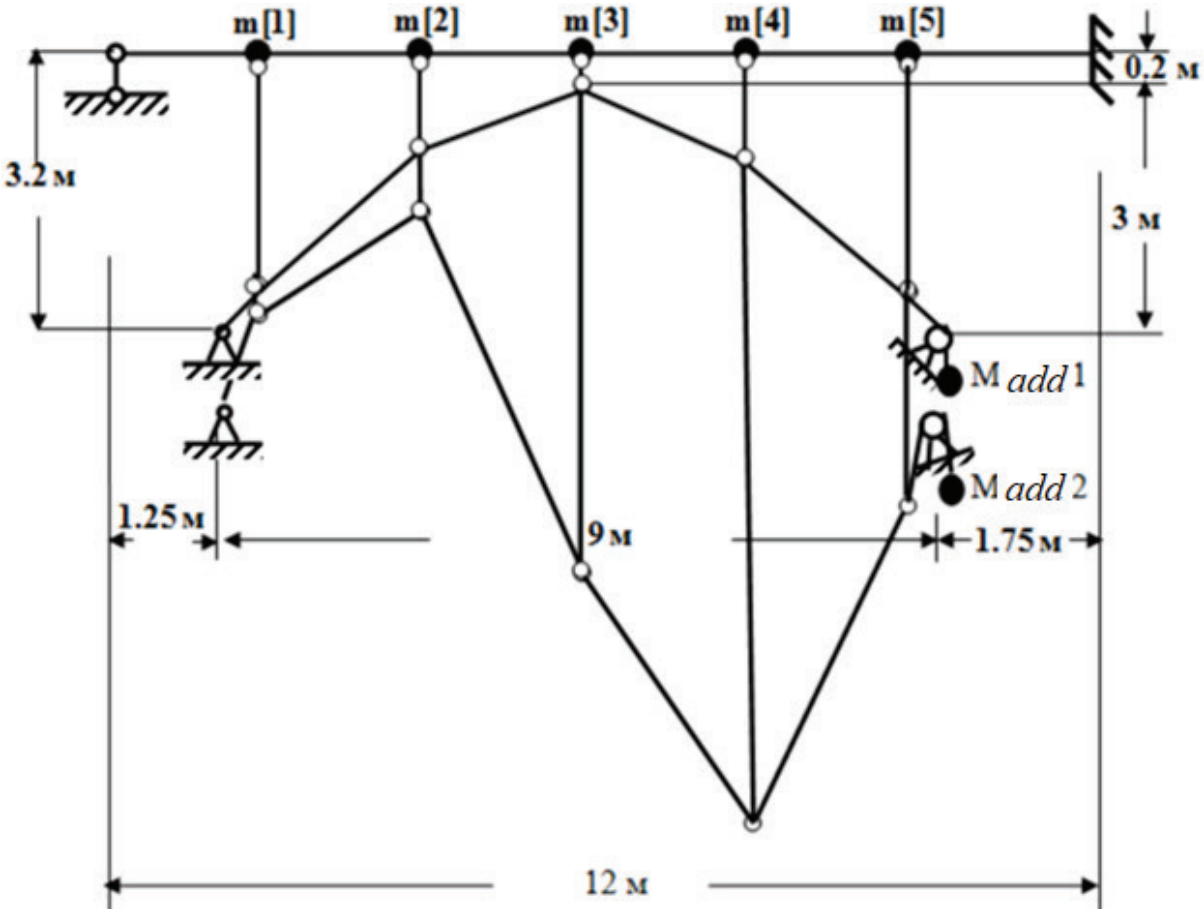


Figure 5. The general view of the device

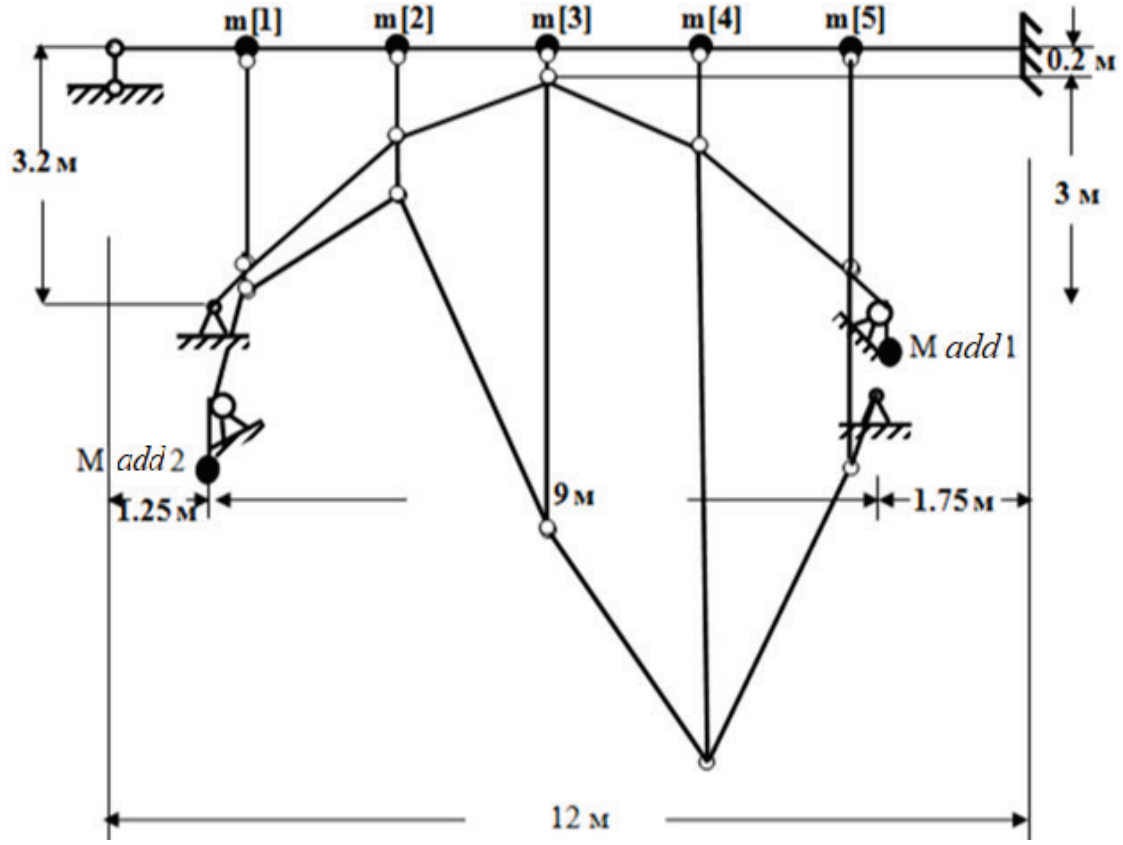


Figure 6. The variant of group targeted kinematic device.

Table 7. Frequencies and modes of oscillation of both variants of the group targeted kinematic device

Number k	Формы собственных колебаний					$m[k]$
	for frequency 11.0062	for frequency 14.07953	for frequency 109.5337	for frequency 195.0757	for frequency 226.8870	
0	0.0000	0.0000	0.0000	0.0000	0.0000	0
1	-0.502865	-0.315087	-0.594382	-0.73793	-0.369613	400
2	-0.520103	-0.565080	-0.174580	0.370387	-0.264938	800
3	0.103822	-0.606213	0.432120	-0.086169	0.212601	1200
4	0.574986	-0.432097	-0.359747	-0.137055	-0.383591	800
5	0.367738	-0.164932	-0.547801	0.540420	0.775147	400
6	0.0000	0.0000	0.0000	0.0000	0.0000	0

Table 8. Comparison of the natural frequencies of the original system with the results of testing using the "SCAD" and "LIRA" software products

	$\omega[1]$	$\omega[2]$	$\omega[3]$	$\omega[4]$	$\omega[5]$
Proposed pproach	14.0715	53.0769	109.5339	195.0757	226.8873
"SCAD" and "LIRA" software packages	14,0820	53,4030	111,5070	201,4150	237,1590

A version of the group sighting kinematic device in which the additional masses are attached to different sides is shown in Figure 6.

The frequencies and modes of natural oscillations of both variants of the group targeted kinematic device are identical and are presented in Table 7.

The posts of the individual targeted kinematic devices, mounted at the mass application nodes and directed along their trajectory, are aligned. Forces $R_0[i,\ k] = m[i]v[i,\ k]$ arise in the aligned posts, each of which determines one of the individual targeted kinematic devices.

The absence of mutual influence between the forces determining the various individual kinematic devices is justified by the properties of the forces $R_0[i,\ k]$. The forces $R_0[i,\ k_1]$ determining the targeted device, which reduces the natural frequency $\omega[k_1]$, do not perform work on the displacements of the natural oscillation mode of any other natural frequency, that is,

$$\text{if } k_1 \neq k_2 \text{ we get } \sum_{i=1}^{n} R_0[i,\ k_1]v[i,\ k_2] = 0. \quad (10)$$

Relationship (10) determines the absence of mutual influence between the forces $R_0[i,\ k]$ arising in the posts of the group targeted device.

The results presented in Table 7 confirm that the introduction of the group targeted kinematic device reduces only the first two selected natural oscillation frequencies to the intended values and does not lead to a change in the natural modes and values of the remaining frequencies. The results presented in Tables 1, 2, 3, 5, 7 were obtained by the finite element method (FEM) [18] by dividing (discretizing) the length of the original beam into 24 sections. A comparison of the natural vibration frequencies of the original system with the test results of the "SCAD" and "LIRA" software products is presented in Table 8. Considering the difference in the calculation method for Tables 1, 2, 3, 5, 7 between the "SCAD" and "LIRA" software products, the agreement between the results can be considered fairly close, confirming the reliability of the original data.

Table 9. Testing the group targeted kinematic device

	$\omega[1]$	$\omega[2]$	$\omega[3]$	$\omega[4]$	$\omega[5]$
Initial	14,0820	53,4030	111,5070	201,4150	237,1590
Group	10,8000	11,1400	111,5200	201,4200	237,1600

We will now test the group targeted kinematic device using the "SCAD" and "LIRA" software products. The results are presented in Table 9.

The data presented in Table 9 prove that the testing performed convincingly demonstrates a reduction exclusively in those frequencies targeted by the group kinematic device, while the other natural oscillation frequencies remained unchanged.

In summary, the distinctive paper proposes an algorithm of creation of group targeted kinematic devices. Besides, a method of creation of a matrix of additional inertial forces corresponding to a group kinematic targeted device is considered. We provide a rationale for the absence of mutual interference between the forces $R_0[i,\ k]$ arising in the group kinematic device posts, and tests the proposed algorithm using the "SCAD" and "LIRA" software products.

REFERENCES

1. **Akimov P.A, Lyahovich L.S.** Pricel'noe regulirovanie spektra chastot sobstvennyh kolebanij uprugih plastin s konechnym chislom stepenej svobody mass putem vvedenija dopolnitel'nyh obobshhennyh svjazej i obobshhennyh kinematicheskih ustrojstv [Precision control for eigen-frequency of elastic

plates with finite number of mass degrees of freedom by using additional generalized connections and kinematic devices]. // Vestnik Tomskogo gosudarstvennogo arkhitekturno-stroitel'nogo universiteta. Journal of Construction and Architecture, 2021, Vol. 23, No. 4, pp. 57-67 (In Russian).

2. **Lyahovich L.S.** Osobye svojstva optimal'nyh sistem i osnovnye napravlenija ih realizacii v metodah rascheta sooruzhenij [Special properties of optimal systems and the main directions of their implementation in the methods of structural analysis]. Tomsk, TGASU, 2009. – 372 pages (In Russian).
3. **Lyakhovich L.S., Akimov P.A.** About Development of Computational Schemes of Some Additional Constraints for Elastic Systems. Part 1: Theoretical Foundations [O formirovanii raschetnyh shem nekotoryh dopolnitel'nyh svjazej dlja uprugih sistem. Chast' 1: Teoreticheskie osnovy podhoda]. // Promyshlennoe i Grazhdanskoe Stroitelstvo, 2022, No. 9, pp. 4-10 (in Russian).
4. **Lyakhovich L.S., Akimov P.A., Mescheulov N.V.** About Development of Computational Schemes of Some Additional Constraints for Elastic Systems. Part 2: Samples of Analysis [O formirovanii raschetnyh shem nekotoryh dopolnitel'nyh svjazej dlja uprugih sistem. Chast' 2: Primery raschetov]. // Promyshlennoe i Grazhdanskoe Stroitelstvo, 2022, No. 9, pp. 4-10 (in Russian).
5. **Lyakhovich L.S., Akimov P.A., Galyautdinov Z.R., Plyaskin A.S.** About Development of Computational Schemes of Generalized Kinematic Devices, Which Precisely Regulate the Frequency Spectrum of Natural Oscillations of Elastic Systems with a Finite Number of Degrees of Mass Freedom, the Directions of Movement of Which are Parallel, but do not Lie in the Same Plane. Part 1: Theoretical Foundations [O sozdanii raschetnyh shem obobshhennyh kinematicheskih ustrojstv, pricel'no regulirujushhih spektr chastot sobstvennyh kolebanij uprugih sistem s konechnym chislom stepenej svobody mass, u kotoryh napravlenija dvizhenija parallel'ny, no ne lezhat v odnoj ploskosti. Chast' 1. Teoreticheskie osnovy podhoda]. Fundamental exploratory and applied research of the Russian Academy of Architecture and Construction Sciences (RAASN) on scientific support for the development of architecture, urban planning, and the construction industry of the Russian Federation in 2022–2023: Scientific works of the RAACS: In 2 volumes: Volume 2. Moscow: RAACS, 2024, pp. 265-274 (in Russian).
6. **Lyakhovich L.S., Akimov P.A., Galyautdinov Z.R., Plyaskin A.S.** About Development of Computational Schemes of Generalized Kinematic Devices, Which Precisely Regulate the Frequency Spectrum of Natural Oscillations of Elastic Systems with a Finite Number of Degrees of Mass Freedom, the Directions of Movement of Which are Parallel, but do not Lie in the Same Plane. Part 2: Samples of Analysis [O sozdanii raschetnyh shem obobshhennyh kinematicheskih ustrojstv, pricel'no regulirujushhih spektr chastot sobstvennyh kolebanij uprugih sistem s konechnym chislom stepenej svobody mass, u kotoryh napravlenija dvizhenija parallel'ny, no ne lezhat v odnoj ploskosti. Chast' 2. Primery raschetov]. Fundamental exploratory and applied research of the Russian Academy of Architecture and Construction Sciences (RAASN) on scientific support for the development of architecture, urban planning, and the construction industry of the Russian Federation in 2022–2023: Scientific works of the RAACS: In 2 volumes: Volume 2. Moscow: RAACS, 2024, pp. 275-285 (in Russian).
7. **Lyahovich L.S., Maletkin O.Ju.** O pricel'nom regulirovanii sobstvennyh chastot uprugih system [On targeted control of natural frequencies of elastic systems]. // Izvestija vuzov. Stroitel'stvo i arhitektura, 1990, No. 1, pp. 113-117 (In Russian).
8. **Faizullin I.E., Lyakhovich L.S., Akimov P.A., Galautdinov Z.R., Plyaskin A.S.** Development of computational schemes of group targeted connections for some elastic

systems [Formirovanie raschetnyh shem gruppovyh pricel'nyh svjazej dlja nekotoryh uprugih system]. // Vestnik MGSU, 2025, Volume 20, Issue 1, pp. 60-72 (in Russian).
9. **Do B., Ohsaki M.** A random search for discrete robust design optimization of linear-elastic steel frames under interval parametric uncertainty. // Computers & Structures, 2021, Volume 249, 106506.
10. **Lyakhovich L.S., Akimov P.A.** Aimed control of the frequency spectrum of eigenvibrations of elastic plates with a finite number of degrees of freedom of masses by superimposing additional constraints. // International Journal for Computational Civil and Structural Engineering, 2021, Volume 17, Issue 2, pp. 76-82.
11. **Lyakhovich L.S., Akimov P.A.** Aimed control of the frequency spectrum of eigenvibrations of elastic plates with a finite number of degrees of freedom by introducing additional generalized kinematic devices. // International Journal for Computational Civil and Structural Engineering, 2021, Volume 17, Issue 3, pp. 14-20.
12. **Lyakhovich L.S., Akimov P.A.** Formation of Computational Schemes of Additional Targeted Constraints That Regulate The Frequency Spectrum of Natural Oscillations of Elastic Systems With a Finite Number of Degrees of Mass Freedom, the Directions of Movement of Which are Parallel, But Do Not Lie in the Same Plane. Part 1: Theoretical Foundations. // International Journal for Computational Civil and Structural Engineering, 2022, Volume 18, Issue 2, pp. 183-193.
13. **Lyakhovich L.S., Akimov P.A.** Formation of Computational Schemes of Additional Targeted Constraints That Regulate The Frequency Spectrum of Natural Oscillations of Elastic Systems With a Finite Number of Degrees of Mass Freedom, the Directions of Movement of Which are Parallel, But Do Not Lie in the Same Plane. Part 2: The First Sample of Analysis. // International Journal for Computational Civil and Structural Engineering, 2022, Volume 18, Issue 3, pp. 137-146.
14. **Lyakhovich L.S., Akimov P.A., Galyautdinov Z.R., Plyaskin A.S.** Development of computational schemes of generalized kinematic devices that precisely regulate the natural frequency spectrum of elastic systems with a finite number of degrees of mass freedom, in which the directions of motion are parallel, but do not lie in the same plane. Part 1: Theoretical foundations. // International Journal for Computational Civil and Structural Engineering, 2023, Volume 19, Issue 3, pp. 173-183.
15. **Lyakhovich L.S., Akimov P.A., Galyautdinov Z.R., Plyaskin A.S**. Development of computational schemes of generalized kinematic devices that precisely regulate the natural frequency spectrum of elastic systems with a finite number of degrees of mass freedom, in which the directions of motion are parallel, but do not lie in the same plane. Part 2. Samples of analysis. // International Journal for Computational Civil and Structural Engineering, 2023, Volume 19, Issue 4, pp. 155-165.
16. **Mittal G., Gibi A.K.** A modified steepest descent method for solving non-smooth inverse problems. // Journal for Computational and Applied Mathematics, 2023, Volume 424, 114997.
17. **Mittal G., Gibi A.K.** Convergence analysis of an optimally accurate frozen multi-level projected steepest descent iteration for solving inverse problems. // Journal of Complexity, 2023, Volume 75, 101711.
18. **Mozgaleva M.L., Akimov P.A.** Deep Beam Analysis with the Use of Discrete-Continual Finite Element Method in the Presence of a Vertical Crack. // International Journal for Computational Civil and Structural Engineering, Volume 21, Issue 2, 2025, pp. 177-186.
19. **Oztas G.Z., Erdem S.** Random search with adaptive boundaries algorithm for obtaining better initial solutions. // Advances in Engineering Software, 2022, Volume 169, 103141.
20. **Ren Q.** Seismic acoustic full waveform inversion based on the steepest descent method

and simple linear regression analysis. // Journal of Applied Geophysics, 2022, Volume 203, 104686.
21. **Wosniack M.E., Raposo E.P., Viswanathan G.M., da Luz M.G.E.** A parallel algorithm for ran- dom searches. // Computer Physics Communications, 2015, Volume 196, pp. 390-397.

СПИСОК ЛИТЕРАТУРЫ

1. **Акимов П.А., Ляхович Л.С.** Прицельное регулирование спектра частот собственных колебаний упругих пластин с конечным числом степеней свободы масс путем введения дополнительных обобщенных связей и обобщенных кинематических устройств. // Вестник Томского государственного архитектурно-строительного университета, 2021, том 23, № 4, с. 57-67.
2. **Ляхович Л.С.** Особые свойства оптимальных систем и основные направления их реализации в методах расчета сооружений. Монография. – Томск: Издательство ТГАСУ, 2009. – 372 с.
3. **Ляхович Л.С., Акимов П.А.** О формировании расчетных схем некоторых дополнительных связей для упругих систем. Часть 1. Теоретические основы подхода. // Промышленное и гражданское строительство, 202, №9, с. 4-10.
4. **Ляхович Л.С., Акимов П.А., Мешеулов Н.В.** О формировании расчетных схем некоторых дополнительных связей для упругих систем. Часть 2. Примеры расчёта. // Промышленное и гражданское строительство, 2022, №9, с. 11-19.
5. **Ляхович Л.С., Акимов П.А., Галяутдинов З.Р., Пляскин А.С.** О создании расчетных схем обобщенных кинематических устройств, прицельно регулирующих спектр частот собственных колебаний упругих систем с конечным числом степеней свободы масс, у которых направления движения параллельны, но не лежат в одной плоскости. Часть 1. Теоретические основы подхода. Фундаментальные поисковые и прикладные исследования РААСН по научному обеспечению развития архитектуры, градостроительства и строительной отрасли Российской Федерации в 2022-2023 годы: Научные труды РААСН: В 2-х томах: Том 2. – Москва: РААСН, 2024, с. 265-274.
6. **Ляхович Л.С., Акимов П.А., Галяутдинов З.Р., Пляскин А.С.** О создании расчетных схем обобщенных кинематических устройств, прицельно регулирующих спектр частот собственных колебаний упругих систем с конечным числом степеней свободы масс, у которых направления движения параллельны, но не лежат в одной плоскости. Часть 2. Примеры расчетов. Фундаментальные поисковые и прикладные исследования РААСН по научному обеспечению развития архитектуры, градостроительства и строительной отрасли Российской Федерации в 2022-2023 годы: Научные труды РААСН: В 2-х томах: Том 2. – Москва: РААСН, 2024, с. 275-285.
7. **Ляхович Л.С., Малеткин О.Ю.** О прицельном регулировании собственных частот упругих систем. // Известия вузов. Строительство и архитектура, 1990, № 1, с. 113-117.
8. **Файзуллин И.Э., Ляхович Л.С., Акимов П.А., Галяутдинов З.Р., Пляскин А.С.** Формирование расчетных схем групповых прицельных связей для некоторых упругих систем. // Вестник МГСУ, 2025, Том 20, Выпуск 1, с. 60-72.
9. **Do B., Ohsaki M.** A random search for discrete robust design optimization of linear-elastic steel frames under interval parametric uncertainty. // Computers & Structures, 2021, Volume 249, 106506.
10. **Lyakhovich L.S., Akimov P.A.** Aimed control of the frequency spectrum of eigenvibrations of elastic plates with a finite number of degrees of freedom of masses by superimposing additional constraints. // International

Journal for Computational Civil and Structural Engineering, 2021, Volume 17, Issue 2, pp. 76-82.

11. **Lyakhovich L.S., Akimov P.A.** Aimed control of the frequency spectrum of eigenvibrations of elastic plates with a finite number of degrees of freedom by introducing additional generalized kinematic devices. // International Journal for Computational Civil and Structural Engineering, 2021, Volume 17, Issue 3, pp. 14-20.
12. **Lyakhovich L.S., Akimov P.A.** Formation of Computational Schemes of Additional Targeted Constraints That Regulate The Frequency Spectrum of Natural Oscillations of Elastic Systems With a Finite Number of Degrees of Mass Freedom, the Directions of Movement of Which are Parallel, But Do Not Lie in the Same Plane. Part 1: Theoretical Foundations. // International Journal for Computational Civil and Structural Engineering, 2022, Volume 18, Issue 2, pp. 183-193.
13. **Lyakhovich L.S., Akimov P.A.** Formation of Computational Schemes of Additional Targeted Constraints That Regulate The Frequency Spectrum of Natural Oscillations of Elastic Systems With a Finite Number of Degrees of Mass Freedom, the Directions of Movement of Which are Parallel, But Do Not Lie in the Same Plane. Part 2: The First Sample of Analysis. // International Journal for Computational Civil and Structural Engineering, 2022, Volume 18, Issue 3, pp. 137-146.
14. **Lyakhovich L.S., Akimov P.A., Galyautdinov Z.R., Plyaskin A.S.** Development of computational schemes of generalized kinematic devices that precisely regulate the natural frequency spectrum of elastic systems with a finite number of degrees of mass freedom, in which the directions of motion are parallel, but do not lie in the same plane. Part 1: Theoretical foundations. // International Journal for Computational Civil and Structural Engineering, 2023, Volume 19, Issue 3, pp. 173-183.
15. **Lyakhovich L.S., Akimov P.A., Galyautdinov Z.R., Plyaskin A.S**. Development of computational schemes of generalized kinematic devices that precisely regulate the natural frequency spectrum of elastic systems with a finite number of degrees of mass freedom, in which the directions of motion are parallel, but do not lie in the same plane. Part 2. Samples of analysis. // International Journal for Computational Civil and Structural Engineering, 2023, Volume 19, Issue 4, pp. 155-165.
16. **Mittal G., Gibi A.K.** A modified steepest descent method for solving non-smooth inverse problems. // Journal for Computational and Applied Mathematics, 2023, Volume 424, 114997.
17. **Mittal G., Gibi A.K.** Convergence analysis of an optimally accurate frozen multi-level projected steepest descent iteration for solving inverse problems. // Journal of Complexity, 2023, Volume 75, 101711.
18. **Mozgaleva M.L., Akimov P.A.** Deep Beam Analysis with the Use of Discrete-Continual Finite Element Method in the Presence of a Vertical Crack. // International Journal for Computational Civil and Structural Engineering, Volume 21, Issue 2, 2025, pp. 177-186.
19. **Oztas G.Z., Erdem S.** Random search with adaptive boundaries algorithm for obtaining better initial solutions. // Advances in Engineering Software, 2022, Volume 169, 103141.
20. **Ren Q.** Seismic acoustic full waveform inversion based on the steepest descent method and simple linear regression analysis. // Journal of Applied Geophysics, 2022, Volume 203, 104686.
21. **Wosniack M.E., Raposo E.P., Viswanathan G.M., da Luz M.G.E.** A parallel algorithm for ran- dom searches. // Computer Physics Communications, 2015, Volume 196, pp. 390-397.

Leonid S. Lyakhovich, Full Member of the Russian Academy of Architecture and Construction Sciences, Professor, DSc, Professor of Department of Structural Mechanics, Tomsk State University of Architecture and Building; 2, Solyanaya St., 2, Tomsk, 634003, Russia; E-mail: lls@tsuab.ru

Pavel A. Akimov, Full Member of the Russian Academy of Architecture and Construction Sciences, Professor, Dr.Sc.; Rector, Professor of Department of Applied Mathematics and Computer Science of National Research Moscow State University of Civil Engineering; 26, Yaroslavskoe Shosse, Moscow, 129337, Russia; E-mail: AkimovPA@mgsu.ru, rector@mgsu.ru, pavel.akimov@gmail.com

Zaur R. Galyautdinov, Associate Professor, DSc, Professor of Department of Reinforced Concrete and Stone Structures, Tomsk State University of Architecture and Building; 2, Solyanaya St., 2, Tomsk, 634003, Russia; E-mail: gazr@yandex.ru

Andrey S. Plyaskin, Associate Professor, Ph.D., Head of Department of Metal and Wooden Structures, Tomsk State University of Architecture and Building; 2, Solyanaya St., 2, Tomsk, 634003, Russia; E-mail: plyaskinandrei@mail.ru

Ляхович Леонид Семенович, академик РААСН, профессор, доктор технических наук, профессор кафедры строительной механики, Томский государственный архитектурно-строительный университет; 634003, Россия, г. Томск, Соляная пл. 2; E-mail: lls@tsuab.ru

Акимов Павел Алексеевич, академик РААСН, профессор, доктор технических наук; ректор, профессор кафедры информатики и прикладной математики Национального исследовательского Московского государственного строительного университета; 129337, Россия, г. Москва, Ярославское шоссе, дом 26; Email: AkimovPA@mgsu.ru, rector@mgsu.ru, pavel.akimov@gmail.com

Галяутдинов Заур Рашидович, доцент, доктор технических наук, доцент кафедры железобетонных и каменных конструкций, Томский государственный архитектурно-строительный университет; 634003, Россия, г. Томск, Соляная пл. 2; E-mail: gazr@yandex.ru

Пляскин Андрей Сергеевич, доцент, кандидат технических наук, заведующий кафедрой металлических и деревянных конструкций, Томский государственный архитектурно-строительный университет; 634003, Россия, г. Томск, Соляная пл. 2; E-mail: plyaskinandrei@mail.ru

DOI:10.22337/2587-9618-2025-21-4-229-239

TITLE EMERGENCY CALCULATION OF THE INDUSTRIAL BUILDING STRUCTURE

Valeriy I. Telichenko [1], Vladimir I. Rimshin [1], Ekaterina S. Ketsko [2]

[1] Moscow State University of Civil Engineering, Moscow, RUSSIA

[2] Research Institute for Building Physics of Russian Academy of the Architecture and Construction Sciences, Moscow, RUSSIA

Abstract: Emergency situations calculation for the industrial buildings structures is an important element in ensuring their reliability and safety in conditions that contribute to the emergence of significant social, environmental and economic consequences. This calculation is mandatory for objects of a high responsibility level (class KS-3), and can be carried out on a voluntary basis for objects of class KS-2, where a large number of people are expected to be present. The article presents the calculation of the industrial building structures with a high responsibility level and analyzes its results. The calculation was performed in accordance with paragraph 5.1 in SP 56.13330.2011 «Industrial buildings» for resistance to progressive collapse as an emergency situation result. A secondary model was created based on the primary calculation model. An emergency failure case of the middle load-bearing column in the frame along the 18/H axis was selected having analyzed the space-planning and design solutions for this building. It was established that the required beams and the roof slab reinforcement obtained as a calculation result of the secondary model does not exceed that obtained as a primary model calculation result based on the calculations performed results. Also, based on the calculation results of the ozone-sorption block building secondary model (fast filter section) for an emergency situation, it was determined that when such a situation occurs - when one of the columns is turned off - the remaining load-bearing elements take on additional forces without losing strength and stability, that is, resistance to the structure progressive collapse will be ensured.

Keywords: emergency situation, industrial structure, progressive collapse, load combinations, load-bearing elements

РАСЧЁТ АВАРИЙНОЙ СИТУАЦИИ КОНСТРУКЦИИ ПРОИЗВОДСТВЕННОГО ЗДАНИЯ

В.И. Теличенко [1], В.И. Римшин [1], Е.С. Кецко [2]

[1] Национальный исследовательский Московский государственный строительный университет», г. Москва, РОССИЯ

[2] Научно–исследовательский институт строительной физики Российской академии архитектуры и строительных наук, г. Москва, РОССИЯ

Аннотация: Расчёт на аварийные ситуации для конструкций производственных зданий является важным элементом обеспечения их надежности и безопасности в условиях, способствующих возникновению значительных последствий социального, экологического и экономического характера. Этот расчёт является обязательным для объектов повышенного уровня ответственности, а именно класса КС-3, и может быть проведен на добровольной основе для объектов класса КС-2, где предполагается массовое пребывание людей. В статье приведён расчёт конструкций производственного здания повышенного уровня ответственности и проанализированы его результаты. Расчёт был выполнен согласно пункту 5.1 СП 56.13330.2011 «Производственные здания» на устойчивость к прогрессирующему обрушению в результате аварийной ситуации. На основании первичной расчётной модели выполнена вторичная модель. Проанализировав объемно–планировочные и конструктивные решения данного здания, был выбран аварийный случай выхода из строя средней несущей колонны каркаса по оси 18/Н. По результатам выполненных расчётов установлено, что требуемое армирование балок и плиты покрытия, полученное в результате расчёта вторичной модели не превышает полученного в результате расчёта первичной модели. Также по результатам выполненного расчёта вторичной модели здания озоно–сорбционного блока (отделение быстрых фильтров) на аварийную ситуацию было определено, что при возникновении такой ситуации – выключении одной из колонн из работы – остальные несущие элементы сооружения воспринимают на себя дополнительные усилия, не теряя при этом прочность и устойчивость, то есть устойчивость к прогрессирующему обрушению сооружения будет обеспечена.

Ключевые слова: аварийная ситуация, производственное сооружение, прогрессирующее обрушение, сочетания нагрузок, несущие элементы

INTRODUCTION

Emergency situations calculation for the industrial buildings structures is an important element in ensuring their reliability and safety in conditions that contribute to the emergence of significant social, environmental and economic consequences. This calculation is mandatory for objects of a high level of responsibility (class KS-3), and can also be carried out on a voluntary basis for class KS-2 objects, where a large number of people are expected in accordance with GOST 27751-2014 «Reliability of building structures and foundations». Such measures are aimed at increasing the safety and reliability level in construction projects, which is especially important in the conditions of modern construction and buildings operation [1-10].

The structure considered in this article, the ozone-sorption unit, is a structure of a high responsibility level KS-3, accordingly, this calculation is mandatory in its design.

The purpose calculation for the emergency situations occurrence is to check and ensure the safety and reliability of the adopted design solutions, and to determine the methods for protecting the industrial building supporting structures from progressive collapse in emergency situations.

METHODS

The following methods are used to assess the structures resistance to emergency situations:

- A model describing possible emergency scenarios creation. For each scenario, external and internal impacts combinations are taken into account.
- The load-bearing elements determination, the failure of which can lead to the progressive collapse of the entire system.
- The possible failures and their impact on the overall structure stability research.
- The correlation analysis between the structure elements. Possible sequential reactions that occur when one or more elements fail are considered [11-18].

Calculation for the occurrence of an emergency situation. The calculation of the ozone-sorption block model in axes 4 - 19 m/o K - R (fast filter section) was performed in accordance with paragraph 5.1 in SP 56.13330.2011 «Industrial buildings» for resistance to progressive collapse as an emergency situation result. A secondary model was created based on the primary calculation model.

A secondary model was created based on the primary calculation model (Figure 1).

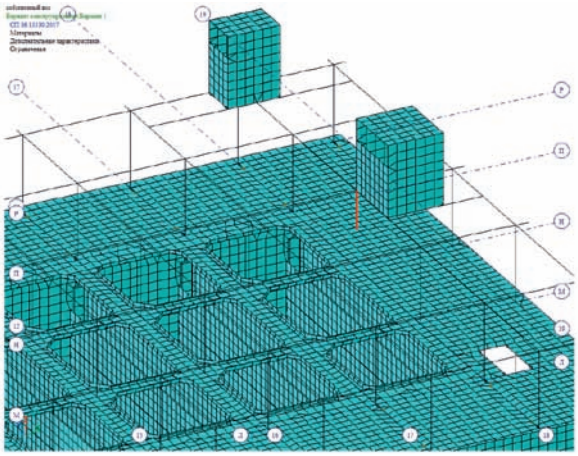


Figure 1. Calculation model

An emergency failure case of the middle load-bearing column in the frame along the 18/H axis was selected having analyzed the space-planning and design solutions for this building (marked in red in Figure 1).

The lower part of the column, 2.15 m high, was removed to simulate the failure (the covering is not shown). The calculation for progressive collapse in the emergency was performed with a special combination of standard load values, including the failure of one of the load-bearing structure elements.

The calculation is performed according to the criterion of extreme stress values at characteristic element sections points based on the rules established by regulatory documents SP 20.13330.2011 «Loads and Impacts», SP

22.13330.2011 «Foundations of Buildings and Structures», SP 63.13330.2012 «Concrete and Reinforced Concrete Structures», SP 385.1325800.2018 «Protection of Buildings from Progressive Collapse», SP 296.1325800.2017 «Buildings and Structures. Special Impacts» [19-25].

RESULTS AND DISCUSSION

The spatial static calculation was performed using the finite element method using the LIRA-SAPR software package. The walls and floor slabs and roofs were modeled using the finite elements of a universal shell in the calculation model, all rod elements were modeled using a universal spatial rod finite element [26-30].

The roof slab vertical displacements isofields is shown in Figure 2. Longitudinal forces N in the frame supporting elements after an emergency situation fragment is shown in Figure 3.

The maximum value of N occurred in columns 17/M, 18/M, 18/P, 19/N as a result of the forces redistribution.

The results of calculating the maximum force M_y in the frame supporting elements after an emergency situation is shown in Figure 4. The roof beams vertical displacements mosaic is shown in Figure 5.

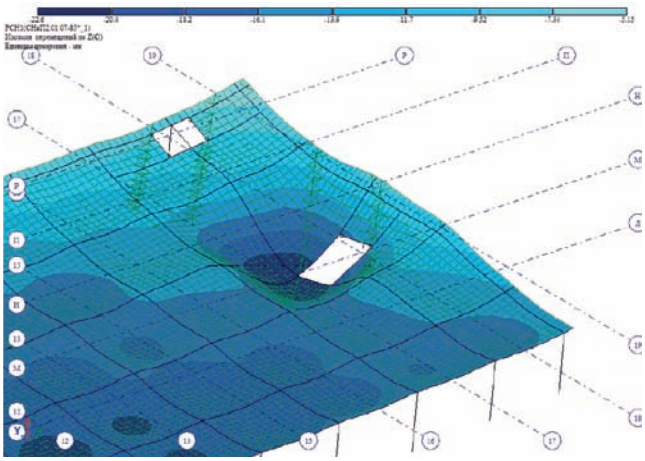


Figure 2. The roof slab vertical displacements isofields (fragment)

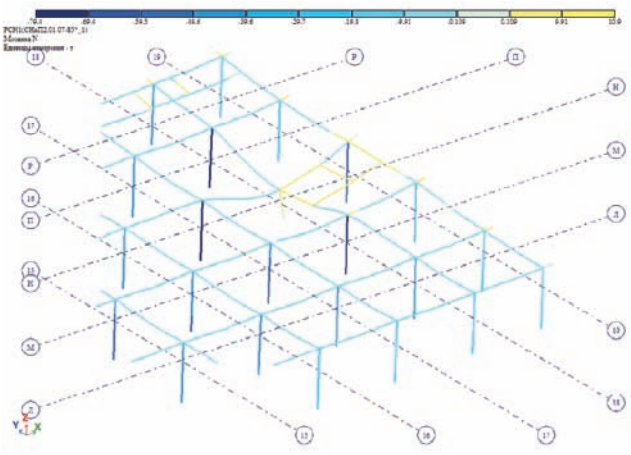


Figure 3. Longitudinal forces N in the frame supporting elements after an emergency situation (fragment)

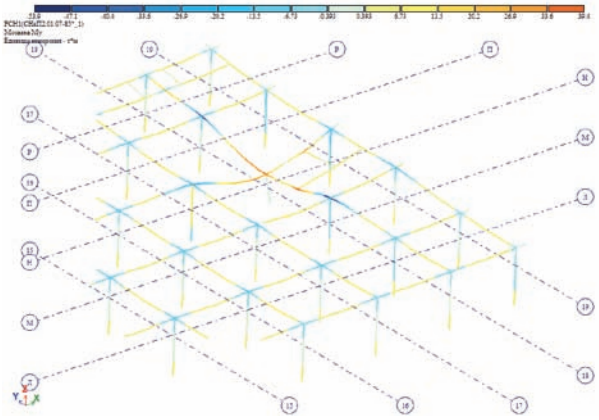


Figure 4. Maximum forces M_y in the frame supporting elements after an emergency situation (fragment)

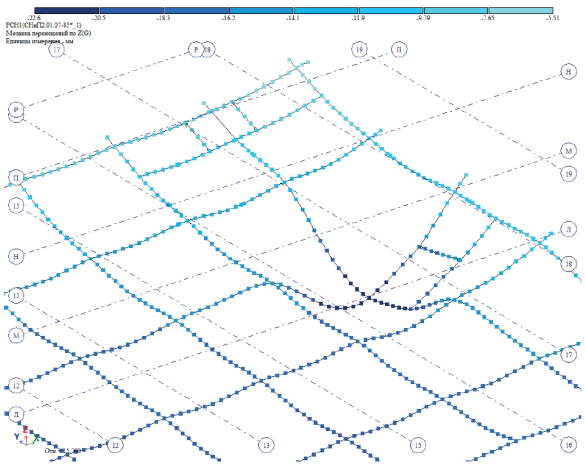


Figure 5. The roof beams vertical displacements mosaic (fragment)

The results of calculating the required reinforcement in beams with a cross-section of 40x80 cm and the reinforcement calculation diagram are shown in Figures 6, 7 and 8. The results of calculating the required reinforcement in columns are shown in Figure 9.

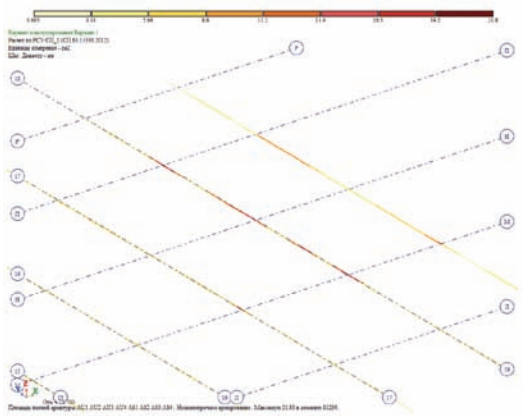


Figure 6. Required reinforcement in beams 40x80 mm (fragment)

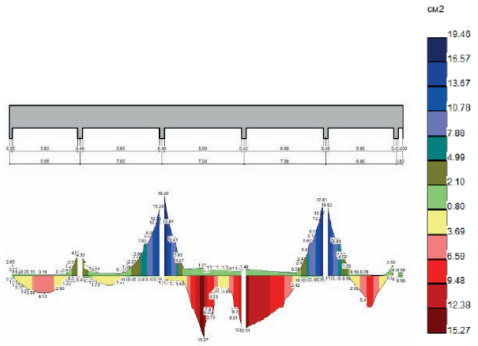


Figure 7. Required reinforcement in beams 40x80 mm (diagram)

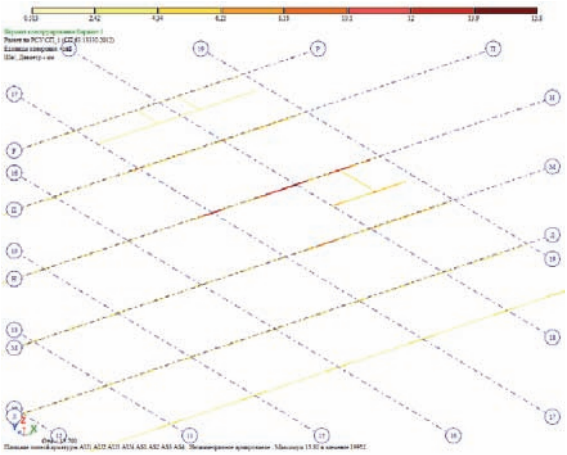


Figure 8. Required reinforcement in beams 40x80 mm (fragment)

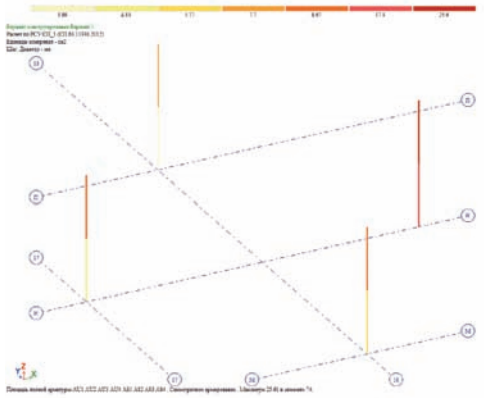


Figure 9. Required reinforcement in columns (fragment)

The authors proposed a reinforcement variant for the considered column KmK74, shown in Figure 10. The KmK74column specification and the steel specifications are given in Tables 1 and 2, respectively.

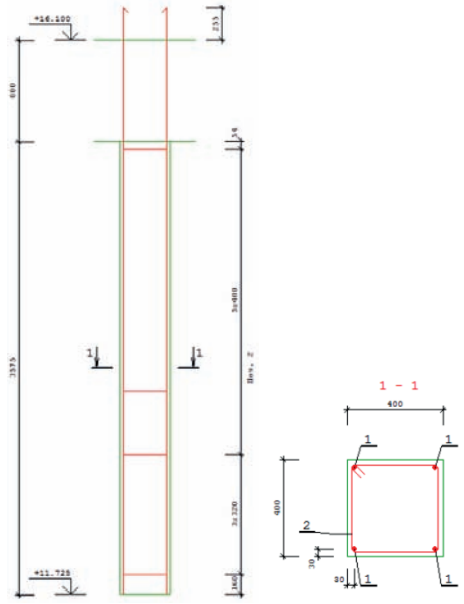


Figure 10. Column reinforcement option

Table 1. The column specification KmK74

Position	Name	Quantity	Weight, kg	Notes
	Specifications			
1	Ø32 A500 l=4630 mm	4	29.2	
2	Ø8 A240 l=1540 mm	9	0.6	
	Materials			
	Concrete class B25			0.6 m^2

Table 2. Steel consumption statement

Unit	Reinforcement products				
	Reinforcement class				Total, kg
	A240		A500		
	GOST 5781-82		GOST 5781-82		
	Ø8	Total	Ø32	Total	
KmK74	5	5	117	117	122

The forces in the roof slab Mx and My, Nx and Ny (fragments) are shown in Figures 11-14, respectively.

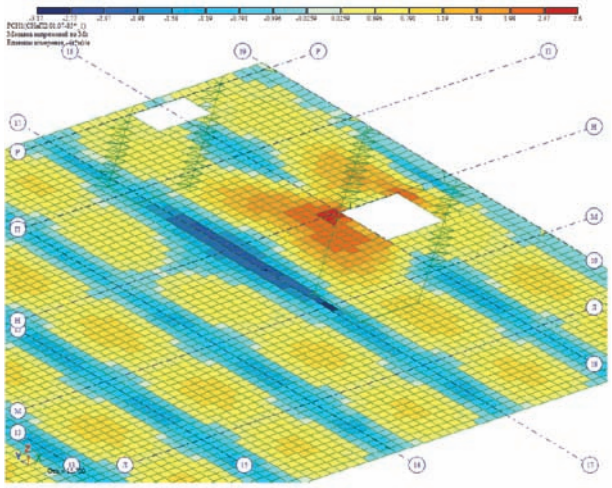


Figure 11. Forces in the roof slab M_x (fragment)

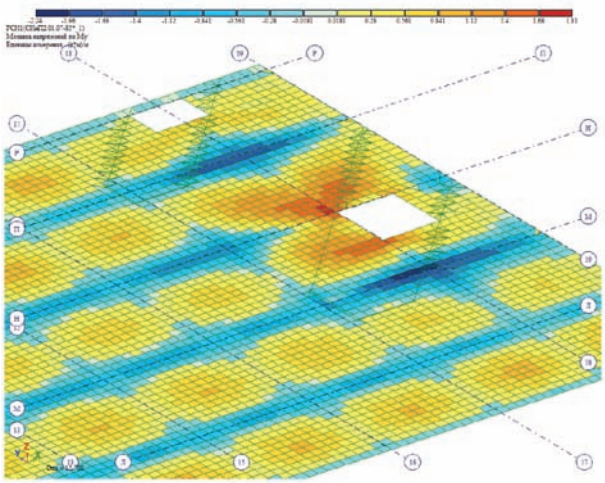


Figure 12. Forces in the roof slab M_y (fragment)

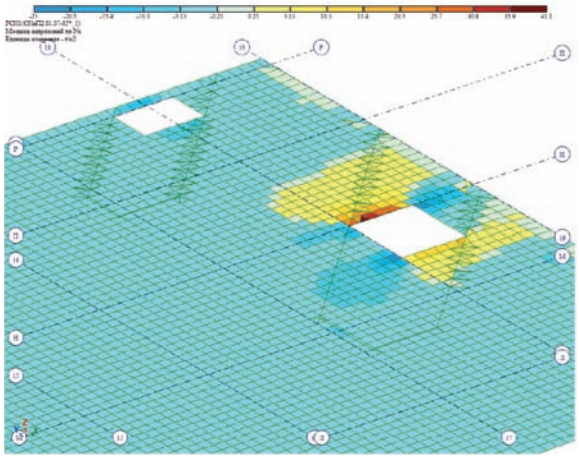


Figure 13. Forces in the roof slab Nx (fragment)

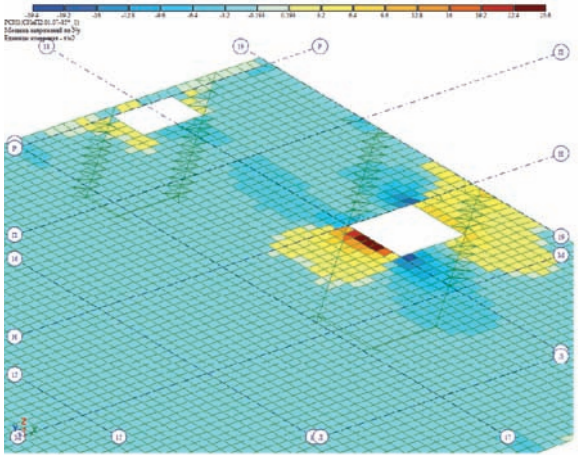


Figure 14. Forces in the roof slab Ny (fragment)

The calculation results for the required reinforcement in the roof slabs are shown in Figures 15-18, respectively.

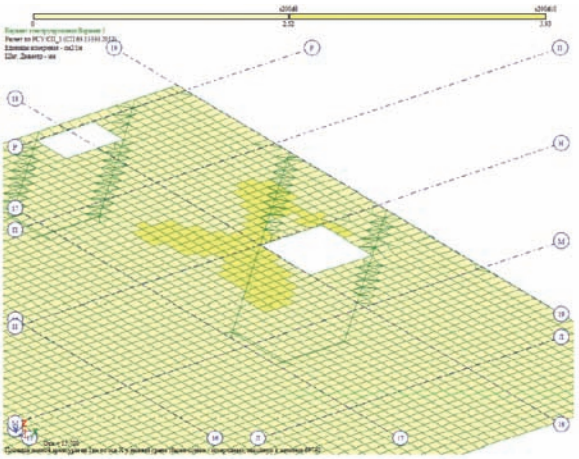


Figure 15. Required reinforcement in the roof slab. Lower along the X axis (fragment)

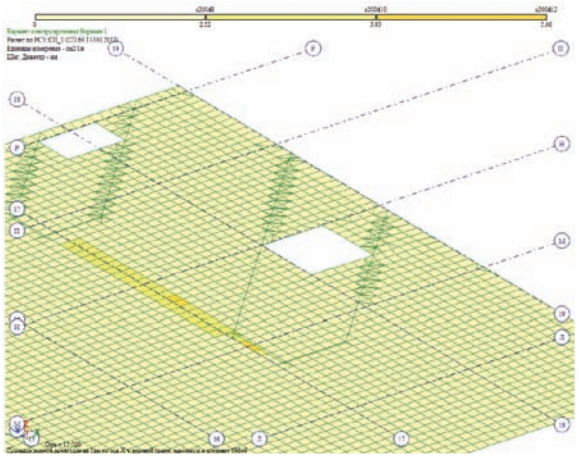


Figure 16. Required reinforcement in the roof slab. Upper along the X axis (fragment)

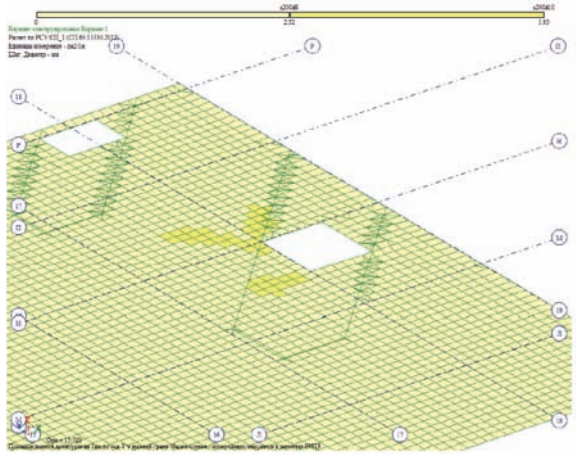


Figure 17. Required reinforcement in the roof slab. Bottom along the Y axis (fragment)

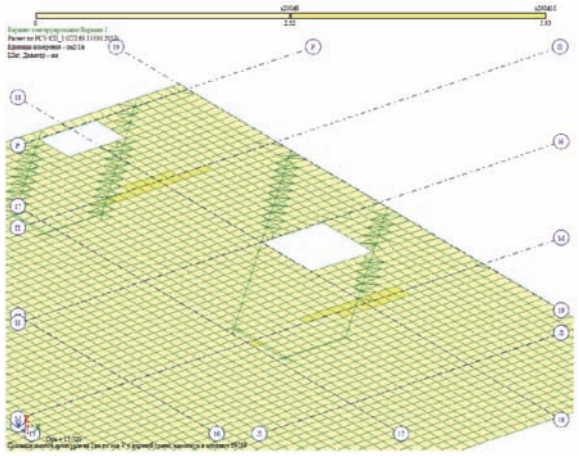


Figure 18. Required reinforcement in the roof slab. Upper along the Y axis (fragment)

CONCLUSION

The maximum displacement along the Z axis of a 7 m long roof beam is 22.6 mm. The required column reinforcement (25.6 cm^2) does not exceed that obtained as a primary model calculation result (28.2 cm^2).

The required beams and roof slabs reinforcement obtained as a result of calculating the secondary model does not exceed that obtained as a result of calculating the primary model.

was established that when such a situation occurs – when one of the columns is switched off from operation – the remaining load-bearing elements take on additional forces without losing strength and stability, i.e., resistance to progressive collapse is ensured based on the calculation results of the ozone-sorption block building secondary model in axes 4–19 m/o K–R (fast filter section) for an emergency situation.

REFERENCES

1. **Onoprienko A.R., Solovyov A.K., Rimshin V.I.,** The use of solar energy for heating premises in the southern regions of the Russian federation in the spring-autumn period. Light & Engineering, **32(1)**, pp. 18-22 (2024) DOI: 10.33383/2023-067
2. **Mihail V. Lukin, Svetlana I. Roshchina, Anastasia V. Lukina, Rimshin V.I.,** Computer modeling of energy-efficient joints of wood composite panels. International Journal for Computational Civil and Structural Engineering, **20(1)**, pp. 68-80 (2024) DOI: 10.22337/2587-9618-2024-20-1-68-80
3. **Valeriy Telichenko, Vladimir Rimshin and Ekaterina Ketsko,** Promising directions for the artificial intelligence development in the housing and utilities sector. E3S Web of Conferences, **533**, 05001 (2024) DOI: https://doi.org/10.1051/e3sconf/202453505001
4. **Telichenko V., Rimshin V., Ketsko E.,** Digital robotic systems for non-destructive reinforced concrete structures testing. E3S

Web of Conferences, **533**, 02045 (2024) DOI: 10.1051/e3sconf/202453302045

5. **Rimshin V.I., Roshchina S.I., Lesovik R.V., Lukin M.V., Lukina A.V.**, Prolongation of the life cycle of wooden structures due to the use of joints on aluminum connectors. Eurasian Chemical Communications, **6**, p. 122 (2024) DOI:10.48309/jmpcr.2024.183586
6. **Monastyrev P.V., Elchishcheva T.F., Makarchuk M.V.1, Erofeev V.T., Rimshin V.I., Erofeeva I.V.,** The effect of montmorillonite on the rheological and physico-mechanical properties of a thermosetting polymer composite. International Journal for Computational Civil and Structural Engineering, **20(2)**, pp. 109-117 (2024) DOI: 10.22337/2587-9618-2024-20-2-109-117
7. **Rimshin V., Ketsko E.,** Justification of strengthening of reinforced concrete structures of an industrial building with composite materials. Lecture Notes in Civil Engineering, **372**, pp. 129 (2024) https://doi.org/10.1007/978-3-031-36723-6_14
8. **Rimshin V., Khamrakulov R., Alikabulov Sh., Radjabov Y., Abdurakhmonov A., Mirazimova G., Jamolova M.,** Study on the possibilities of increasing the effectiveness of thermal insulation of enclosing structures in window openings using low-emission coatings and films. E3S Web of Conferences, **563**, 02024 (2024) DOI:10.1051/e3sconf/202456302024
9. **Semenov V.A., Morozov S.V., Arishin S.V., Kuzina O.N., Rimshin V.I., Makisha E.V.,** Formal specification and verification of requirements in architecture and construction using the express modeling language Programming and Computer Software, **50 (5)**, pp. 376-391 (2024) https://doi.org/10.1134/S036176882470018X
10. **Svetlana Roshchina, Mikhail Lukin, Ekaterina Ketsko,** Scientific Basis of Studying the Pile Foundations Bearing Capacity During Building Reconstruction. Lecture Notes in Civil Engineering, **576**, pp. 283-294 (2024) https://doi.org/10.1007/978-3-031-81635-2_28
11. **Svetlana Roshchina, Anatoly Krishan, Ekaterina Ketsko,** Tube-Concrete Structures Stress-Strain State Theory. Lecture Notes in Civil Engineering, **576**, pp. 295-301 (2024) https://doi.org/10.1007/978-3-031-81635-2_29
12. **Shafranovsky T., Rimshin V., Varlamov A., Merkulov S.,** Comparison of the durability of buildings in a group. IOP Conference Series: Materials Science and Engineering, **1079 (6)**, 062004 (2021) DOI:10.1088/1757-899X/1079/6/062004
13. **Rimshin V.I., Kurbatov V.L., Erofeev V.T., Ketsko E.S.,** Comprehensive survey of the silt reservoir structures technical condition. IOP Conference Series: Materials Science and Engineering, **1079 (4)**, 042077 (2021) DOI:10.1088/1757-899X/1079/4/042077
14. **Kostyuchenko Ya.B., Varlamov A.A., Rimshin V.I., Bykov G.S., Roschina S.,** Bearing capacity of steel-polystyrene concrete slab. IOP Conference Series: Materials Science and Engineering, **1079 (6)**, 062003(2021) DOI:10.1088/1757-899X/1079/6/062003
15. **Varlamov A.A., Rimshin V.I., Davydov A., Minnatov A.R., Kurbatov A.M.,** Research of the degradation process of reinforced concrete structures. IOP Conference Series: Materials Science and Engineering, **1079 (6)**, 062005 (2021) DOI:10.1088/1757-899X/1079/6/062005
16. **Telichenko Valery, Rimshin Vladimir, Ketsko Ekaterina,** Design and Calculation Solutions for Designing Biological Treatment Facilities on The Pumping Station Example. AIP Conference Proceedings, **2497**, 020009 (2023) https://doi.org/10.1063/5.0103519
17. **P. A. Amelin , V. I. Rimshin , A. A. Kryuchkov , D. V. Obernikhin,** Finite Element Modeling of the Work of Bent Reinforced Concrete Elements of Rectangular Section in the Abaqus Software Environment. Lecture Notes in Civil

Engineering, **307**, pp. 268-275 (2022) https://doi.org/10.1007/978-3-031-20459-3_34

18. **Rimshin V.I., Truntov P.S.,** Technical inspection stages of the textile industry building. Izvestiya Visshih Uchebnih Zavedenii, Seriya Tehnologiya Tekstilnoi Promishlennosti, **1 (403)**, pp. 153-158 (2023) DOI 10.47367/0021-3497_2023_1_153
19. **Krishan A.L., Astafeva M.A., Chernyshova E.P.,** Numerical and Experimental Investigation of Axially Loaded Columns with Spiral Reinforcement. Materials Science Forum, **1087**, pp. 163-168 (2023) DOI: 10.4028/p-7841oa
20. **Alexey Bulgakov, Jens Otto Wen-der Yu, Vladimir Rimshin and Alexey Shleenko,** Structural organization of robotic building and mounting complexes. Journal of Robotics and Mechatronics, Proceedings of the 40th ISARC, Chennai, India, ISBN 978-0-6458322-0-4, ISSN 2413-58442023, pp. 208-213 (2023) DOI:10.22260/ISARC2023/0030
21. **V. Telichenko, V. Rimshin, E. Ketsko,** Engineering structures stability against progressive collapse. E3S Web of Conferences, 02037 (EDP Sciences, 2023) https://doi.org/10.1051/e3sconf/202341002037 FORM-2023
22. **Vladimir Rimshin, Anatoly Krishan, Elena Korol, Svetlana Roshchina, and Igor Shubin,** Square-Section Tube-Concrete Structures Studying Under Axial Compression Both with Spiral Reinforcement of the Concrete Core and Without Reinforcement. Proceedings of MPCPE 2022, Lecture Notes in Civil Engineering, **335**, pp. 165-181 (2023) https://doi.org/10.1007/978-3-031-30570-2_15
23. **Artem Strekalkin, Mikhail Sergeev, Dmitry Reva , and Vladimir Rimshin,** Strength and Deformability of Butt Joints Made of Wood with Local Modification. Proceedings of MPCPE 2022, Lecture Notes in Civil Engineering, **335**, pp. 191-199 (2023) https://doi.org/10.1007/978-3-031-30570-2_17
24. **Mikhail Lukin, Roschina Svetlana, and Vladimir Rimshin,** Mechanical Properties of Polymer Composition Based on Dimethacrylic Polyester with Nanostructured Filler for Wood Modification. Proceedings of MPCPE 2022, Lecture Notes in Civil Engineering, **335**, pp. 277-287 (2023) https://doi.org/10.1007/978-3-031-30570-2_25 18
25. **Martinov V., Lukin M., Rimshin V., Rusak K., Ivaniuk A.,** Influence of Different Types of Aggregates on the Structural Properties of Fiber-Reinforced Concrete. Lecture Notes in Networks and Systems, **403 LNNS**, pp. 1467–1476 (2022) DOI: 10.1007/978-3-030-96383-5_164
26. **Neverov A.N., Truntov, P.S., Ketsko E.S., Rimshin, V.I.,** Calculating the Strengthening of Construction Structures Before the Reconstruction of the Building. Lecture Notes in Civil Engineering, **182**, pp. 173–179 (2022) DOI: https://doi.org/10.1007/978-3-030-85236-8_14
27. **Lukin M., Martynov V., Rimshin V., Aleksiievets I.,** Reinforced Concrete Vertical Structures Under a Gently Sloping Shell of Double Curvature Under the Influence of Progressive Collapse. Lecture Notes in Civil Engineering, **182**, pp. 577–587 (2022) DOI: 10.1007/978-3-030-85236-8_50
28. **A.L. Krishan, V.I. Rimshin, I.L. Shubin, M.A. Astafeva, A.A. Stupak,** Compressed Reinforced Concrete Elements Bearing Capacity of Various Flexibility. Lecture Notes in Civil Engineering, **182**, pp. 283–291 (2022) DOI: 10.1007/978-3-030-85236-8_26
29. **Rimshin V.I., Roshchina S.I., Ketsko E.S.,Truntov P.S., Kuzina I.S.,** Engineering Calculations of Acidifier Retaining Walls During Water Treatment Facilities Designing. Lecture Notes in Civil Engineering, **182**, pp. 55–73 (2022) DOI: 10.1007/978-3-030-85236-8_5

30. **Tho V.D., Korol E.A., Rimshin V.I., Anh P.T.,** Model of stress-strain state of three-layered reinforced concrete structure by the finite element methods. International Journal for Computational Civil and Structural Engineering, **18(2)**, pp. 62–73(2022) DOI: 10.22337/2587-9618-2022-18-2-62-73

СПИСОК ЛИТЕРАТУРЫ

1. **Onoprienko A.R., Solovyov A.K., Rimshin V.I.,** The use of solar energy for heating premises in the southern regions of the Russian federation in the spring-autumn period. Light & Engineering, **32(1)**, pp. 18-22 (2024) DOI: 10.33383/2023-067
2. **Mihail V. Lukin, Svetlana I. Roshchina, Anastasia V. Lukina, Rimshin V.I.,** Computer modeling of energy-efficient joints of wood composite panels. International Journal for Computational Civil and Structural Engineering, **20(1)**, pp. 68-80 (2024) DOI: 10.22337/2587-9618-2024-20-1-68-80
3. **Valeriy Telichenko, Vladimir Rimshin and Ekaterina Ketsko,** Promising directions for the artificial intelligence development in the housing and utilities sector. E3S Web of Conferences, **533**, 05001 (2024) DOI: https://doi.org/10.1051/e3sconf/202453505001
4. **Telichenko V., Rimshin V., Ketsko E.,** Digital robotic systems for non-destructive reinforced concrete structures testing. E3S Web of Conferences, **533**, 02045 (2024) DOI: 10.1051/e3sconf/202453302045
5. **Rimshin V.I., Roshchina S.I., Lesovik R.V., Lukin M.V., Lukina A.V.**, Prolongation of the life cycle of wooden structures due to the use of joints on aluminum connectors. Eurasian Chemical Communications, **6**, p. 122 (2024) DOI:10.48309/jmpcr.2024.183586
6. **Monastyrev P.V., Elchishcheva T.F., Makarchuk M.V.1, Erofeev V.T., Rimshin V.I., Erofeeva I.V.,** The effect of montmorillonite on the rheological and physico-mechanical properties of a thermosetting polymer composite. International Journal for Computational Civil and Structural Engineering, **20(2)**, pp. 109-117 (2024) DOI: 10.22337/2587-9618-2024-20-2-109-117
7. **Rimshin V., Ketsko E.,** Justification of strengthening of reinforced concrete structures of an industrial building with composite materials. Lecture Notes in Civil Engineering, **372**, pp. 129 (2024) https://doi.org/10.1007/978-3-031-36723-6_14
8. **Rimshin V., Khamrakulov R., Alikabulov Sh., Radjabov Y., Abdurakhmonov A., Mirazimova G., Jamolova M.,** Study on the possibilities of increasing the effectiveness of thermal insulation of enclosing structures in window openings using low-emission coatings and films. E3S Web of Conferences, **563**, 02024 (2024) DOI:10.1051/e3sconf/202456302024
9. **Semenov V.A., Morozov S.V., Arishin S.V., Kuzina O.N., Rimshin V.I., Makisha E.V.,** Formal specification and verification of requirements in architecture and construction using the express modeling language Programming and Computer Software, **50 (5)**, pp. 376-391 (2024) https://doi.org/10.1134/S036176882470018X
10. **Svetlana Roshchina, Mikhail Lukin, Ekaterina Ketsko,** Scientific Basis of Studying the Pile Foundations Bearing Capacity During Building Reconstruction. Lecture Notes in Civil Engineering, **576**, pp. 283-294 (2024) https://doi.org/10.1007/978-3-031-81635-2_28
11. **Svetlana Roshchina, Anatoly Krishan, Ekaterina Ketsko,** Tube-Concrete Structures Stress-Strain State Theory. Lecture Notes in Civil Engineering, **576**, pp. 295-301 (2024) https://doi.org/10.1007/978-3-031-81635-2_29
12. **Shafranovsky T., Rimshin V., Varlamov A., Merkulov S.,** Comparison of the durability of buildings in a group. IOP Conference Series: Materials Science and Engineering, **1079 (6)**, 062004 (2021) DOI:10.1088/1757-899X/1079/6/062004

13. **Rimshin V.I., Kurbatov V.L., Erofeev V.T., Ketsko E.S.,** Comprehensive survey of the silt reservoir structures technical condition. IOP Conference Series: Materials Science and Engineering, **1079 (4)**, 042077 (2021) DOI:10.1088/1757-899X/1079/4/042077
14. **Kostyuchenko Ya.B., Varlamov A.A., Rimshin V.I., Bykov G.S., Roschina S.,** Bearing capacity of steel-polystyrene concrete slab. IOP Conference Series: Materials Science and Engineering, **1079 (6)**, 062003(2021) DOI:10.1088/1757-899X/1079/6/062003
15. **Varlamov A.A., Rimshin V.I., Davydov A., Minnatov A.R., Kurbatov A.M.,** Research of the degradation process of reinforced concrete structures. IOP Conference Series: Materials Science and Engineering, **1079 (6)**, 062005 (2021) DOI:10.1088/1757-899X/1079/6/062005
16. **Telichenko Valery, Rimshin Vladimir, Ketsko Ekaterina,** Design and Calculation Solutions for Designing Biological Treatment Facilities on The Pumping Station Example. AIP Conference Proceedings, **2497**, 020009 (2023) https://doi.org/10.1063/5.0103519
17. **P.A. Amelin, V.I. Rimshin, A.A. Kryuchkov, D.V. Obernikhin,** Finite Element Modeling of the Work of Bent Reinforced Concrete Elements of Rectangular Section in the Abaqus Software Environment. Lecture Notes in Civil Engineering, **307**, pp. 268-275 (2022) https://doi.org/10.1007/978-3-031-20459-3_34
18. **Rimshin V.I., Truntov P.S.,** Technical inspection stages of the textile industry building. Izvestiya Visshih Uchebnih Zavedenii, Seriya Tehnologiya Tekstilnoi Promishlennosti, **1 (403)**, pp. 153-158 (2023) DOI 10.47367/0021-3497_2023_1_153
19. **Krishan A.L., Astafeva M.A., Chernyshova E.P.,** Numerical and Experimental Investigation of Axially Loaded Columns with Spiral Reinforcement. Materials Science Forum, **1087**, pp. 163-168 (2023) DOI: 10.4028/p-7841oa
20. **Alexey Bulgakov, Jens Otto Wen-der Yu, Vladimir Rimshin and Alexey Shleenko,** Structural organization of robotic building and mounting complexes. Journal of Robotics and Mechatronics, Proceedings of the 40th ISARC, Chennai, India, ISBN 978-0-6458322-0-4, ISSN 2413-58442023, pp. 208-213 (2023) DOI:10.22260/ISARC2023/0030
21. **V. Telichenko, V. Rimshin, E. Ketsko,** Engineering structures stability against progressive collapse. E3S Web of Conferences, 02037 (EDP Sciences, 2023) https://doi.org/10.1051/e3sconf/202341002037 FORM-2023
22. **Vladimir Rimshin, Anatoly Krishan, Elena Korol, Svetlana Roshchina, and Igor Shubin,** Square-Section Tube-Concrete Structures Studying Under Axial Compression Both with Spiral Reinforcement of the Concrete Core and Without Reinforcement. Proceedings of MPCPE 2022, Lecture Notes in Civil Engineering, **335**, pp. 165-181 (2023) https://doi.org/10.1007/978-3-031-30570-2_15
23. **Artem Strekalkin, Mikhail Sergeev, Dmitry Reva , and Vladimir Rimshin,** Strength and Deformability of Butt Joints Made of Wood with Local Modification. Proceedings of MPCPE 2022, Lecture Notes in Civil Engineering, **335**, pp. 191-199 (2023) https://doi.org/10.1007/978-3-031-30570-2_17
24. **Mikhail Lukin, Roschina Svetlana, and Vladimir Rimshin,** Mechanical Properties of Polymer Composition Based on Dimethacrylic Polyester with Nanostructured Filler for Wood Modification. Proceedings of MPCPE 2022, Lecture Notes in Civil Engineering, **335**, pp. 277-287 (2023) https://doi.org/10.1007/978-3-031-30570-2_25 18
25. **Martinov V., Lukin M., Rimshin V., Rusak K., Ivaniuk A.,** Influence of Different Types of Aggregates on the Structural Properties of Fiber-Reinforced Concrete. Lecture Notes in Networks and

Systems, **403 LNNS**, pp. 1467–1476 (2022) DOI: 10.1007/978-3-030-96383-5_164
26. **Neverov A.N., Truntov, P.S., Ketsko E.S., Rimshin, V.I.,** Calculating the Strengthening of Construction Structures Before the Reconstruction of the Building. Lecture Notes in Civil Engineering, **182**, pp. 173–179 (2022) DOI: https://doi.org/10.1007/978-3-030-85236-8_14
27. **Lukin M., Martynov V., Rimshin V., Aleksiievets I.,** Reinforced Concrete Vertical Structures Under a Gently Sloping Shell of Double Curvature Under the Influence of Progressive Collapse. Lecture Notes in Civil Engineering, **182**, pp. 577–587 (2022) DOI: 10.1007/978-3-030-85236-8_50
28. **A.L. Krishan, V.I. Rimshin, I.L. Shubin, M.A. Astafeva, A.A. Stupak,** Compressed Reinforced Concrete Elements Bearing Capacity of Various Flexibility. Lecture Notes in Civil Engineering, **182**, pp. 283–291 (2022) DOI: 10.1007/978-3-030-85236-8_26
29. **Rimshin V.I., Roshchina S.I., Ketsko E.S., Truntov P.S., Kuzina I.S.,** Engineering Calculations of Acidifier Retaining Walls During Water Treatment Facilities Designing. Lecture Notes in Civil Engineering, **182**, pp. 55–73 (2022) DOI: 10.1007/978-3-030-85236-8_5
30. **Tho V.D., Korol E.A., Rimshin V.I., Anh P.T.,** Model of stress-strain state of three-layered reinforced concrete structure by the finite element methods. International Journal for Computational Civil and Structural Engineering, **18(2)**, pp. 62–73(2022) DOI: 10.22337/2587-9618-2022-18-2-62-73

Telichenko Valeriy Ivanovich, the President of MGSU, Doctor of Technical Sciences, Professor, Honored Scientist of the Russian Federation, the Academician of the Russian Academy of Architecture and Construction Sciences (RAACS), Professor of the Department of Construction of Thermal and Atomic Power Stations, Moscow State University of Civil Engineering, 129337, Moscow, Yaroslavskoe shosse, 26, Russia, president@mgsu.ru

Теличенко Валерий Иванович, Президент ФГБОУ ВО «Национальный исследовательский Московский государственный строительный университет», Доктор технических наук, профессор, Заслуженный деятель науки Российской Федерации, академик Российской академии архитектуры и строительных наук (РААСН), профессор кафедры Строительства объектов тепловой и атомной энергетики МГСУ, Федеральное государственное бюджетное образовательное учреждение высшего образования «Национальный исследовательский Московский государственный строительный университет» (НИУ МГСУ), 129337, Центральный федеральный округ, г. Москва, Ярославское шоссе, д. 26, president@mgsu.ru

Rimshin Vladimir Ivanovich, Doctor of Technical Sciences, Professor, Corresponding Member of the Russian Academy of Architecture and Construction Sciences (RAACS), Honored Builder of the Russian Federation, Professor of the Department of Housing and Utilities Sector Moscow State University of Civil Engineering, 129337, Moscow, Yaroslavskoe shosse, 26, Russia, v.rimshin@niisf.ru

Римшин Владимир Иванович, Доктор технических наук, профессор, член-корреспондент РААСН, Заслуженный строитель РФ, профессор кафедры Жилищно-коммунального комплекса, Федеральное государственное бюджетное образовательное учреждение высшего образования «Национальный исследовательский Московский государственный строительный университет» (НИУ МГСУ), 129337, Центральный федеральный округ, г. Москва, Ярославское шоссе, д. 26, v.rimshin@niisf.ru

Ketsko Ekaterina Sergeevna, postgraduate student, Research Institute for Building Physics of Russian Academy of the Architecture and Construction Sciences, 129238, Moscow, Lokomotivny p., 21, Russia, kkuzzina@mail.ru

Кецко Екатерина Сергеевна, аспирант, Научно–исследовательский институт строительной физики Российской академии архитектуры и строительных наук (ФГБУ «НИИСФ РААСН»), 127238, г. Москва, Локомотивный проезд, д. 21, kkuzzina@mail.ru

DOI:10.22337/2587-9618-2025-21-4-240-257

ABOUT DEVELOPMENT OF COMPUTATIONAL SCHEMES OF ADDITIONAL DEVICE ON A STRUCTURE, THAT ALLOWS FOR TARGETED CHANGES OF NATURAL FREQUENCIES TO PRESET VALUES

Leonid S. Lyakhovich [1], Pavel A. Akimov [2], Zaur R. Galyautdinov [1], Andrey S. Plyaskin [1]

[1] Tomsk State University of Architecture and Civil Engineering, Tomsk, RUSSIA
[2] National Research Moscow State University of Civil Engineering, Moscow, RUSSIA

Abstract: For some elastic systems with a finite number of degrees of freedom of masses, in which the directions of mass movement are parallel, methods have been developed for creating additional constraints, the introduction of each of which specifically increases the value of only one natural frequency to a given value, without changing any of the other natural frequencies and any of the forms of natural vibrations. Methods have also been developed for creating additional kinematic devices, the introduction of each of which specifically reduces the value of only one natural frequency to a given value, without changing any of the other natural frequencies or any of the forms of natural vibrations. If it is necessary to aim at increasing the values of some natural frequencies and reducing the values of some others, then these requirements can be implemented by creating appropriate separate targeted constraints and separate targeted kinematic devices. If the operating conditions of the facility allow, then these individual targeted devices can be independently installed in the source system. The distinctive paper proposes a method for development of integrated (complex, unified) group targeted device that increases some intended natural frequencies to preset values and reduces other intended frequencies to preset values, without changing any of the other natural frequencies and any of the forms of natural vibrations. An algorithm for the creation of such a single targeted group device is proposed. It is shown that the group targeted device created in this way can be used in special cases both as a group targeted kinematic device and as a group targeted constraint. The initial probation (testing) of the algorithm was implemented with the use of the software products “SCAD” and “Lira”. Some special cases of development of computational schemes of such devices are considered.

Keywords: natural oscillation frequency, natural oscillation shape, separate aiming kinematic device, coefficients of additional inertial forces, separate aiming coupling, coefficients of additional stiffness, aiming control of the natural oscillation frequency spectrum, group aiming device, building structures, elastic systems

О ФОРМИРОВАНИИ РАСЧЕТНОЙ СХЕМЫ ДОПОЛНИТЕЛЬНОГО УСТРОЙСТВА НА СООРУЖЕНИИ, ПОЗВОЛЯЮЩЕГО ПРИЦЕЛЬНО ИЗМЕНЯТЬ ДО ЗАДАННЫХ ЗНАЧЕНИЙ ЧАСТОТЫ СОБСТВЕННЫХ КОЛЕБАНИЙ

Л.С. Ляхович [1], П.А. Акимов [2], З.Р. Галяутдинов [1], А.С. Пляскин [1]

[1] Томский государственный архитектурно-строительный университет, г. Томск, РОССИЯ
[2] Национальный исследовательский Московский государственный строительный университет, г. Москва, РОССИЯ

Аннотация: Для некоторых упругих систем с конечным числом степеней свободы масс, у которых направления движения масс параллельны, разработаны методы создания дополнительных связей, введение каждой из которых прицельно увеличивает величину только одной собственной частоты до заданного значения, не изменяя при этом ни одну из остальных собственных частот и ни одну из форм собственных колебаний. Также разработаны методы создания дополнительных кинематических устройств, введение каждой из которых прицельно уменьшает величину только одной собственной частоты до заданного значения, не

изменяя при этом ни одну из остальных собственных частот и ни одну из форм собственных колебаний. Если необходимо прицельно увеличить величины некоторых собственных частот и уменьшить величины некоторых других, то эти требования можно реализовать созданием соответствующих отдельных прицельных связей и отдельных прицельных кинематических устройств. Если условия эксплуатации сооружения позволяют, то эти отдельные прицельные устройства могут автономно устанавливаться в исходной системе. В данной статье предлагается способ формирования комплексного (единого) группового прицельного устройства, которое увеличивает одни намеченные собственные частоты до заданных значений и уменьшает до заданных значений другие намеченные частоты, не изменяя при этом ни одну из остальных собственных частот и ни одну из форм собственных колебаний. Предложен алгоритм формирования такого комплексного единого прицельного группового устройства. Показано, что сформированное таким образом комплексное групповое прицельное устройство в частных случаях может использоваться и как групповое прицельное кинематическое устройство и как групповая прицельная связь. Первичная пробация (тестирование) алгоритма была реализована с использованием программных продуктов “SCAD” и «Лира». Рассмотрены некоторые частные случаи формирования расчётных схем таких устройств.

Ключевые слова: частота собственных колебаний, форма собственных колебаний, отдельное прицельное кинематическое устройство, коэффициенты дополнительных инерционных сил, отдельная прицельная связь, коэффициенты дополнительных жесткостей, прицельное регулирование спектра частот собственных колебаний, групповое прицельное устройство, строительные конструкции, упругие системы

1. INTRODUCTION

In [1-7, 16-22], theoretical approaches were formulated and methods for development of computational schemes for targeted constraints and targeted kinematic devices were proposed for elastic systems with a finite number of degrees of freedom of the masses, in which the directions of mass motion are parallel. Each targeted constraint increases, and each targeted kinematic device decreases, the value of only one natural frequency of oscillations to a specified value, without changing any of the other natural frequencies or any of the natural oscillation modes. If it is necessary to specifically increase the values of some natural frequencies and decrease the values of others, then these requirements can be achieved by creating appropriate individual targeted constraints and individual targeted kinematic devices and autonomously placing them on the original system. In [8], a method for development of computational scheme for a single group targeted constraint based on individual targeted constraints is considered, which increases all the intended frequencies to specified values.

The distinctive paper is devote to continuation of research works, presented in papers [1-8, 16-22]. It is devoted to method for development of integrated (complex, unified) group targeted device that increases some intended natural frequencies to specified values and decreases other intended frequencies to specified values, without changing any of the remaining natural frequencies or any of the natural oscillation modes. In specific cases, the integrated group targeted device created in this manner can be used both as a group kinematic targeted device and as a group targeted constraint.

2. ALGORITHM FOR CREATION OF COMPUTATIONAL SCHEME OF A GROUP TARGETED CONSTRAINT

The following algorithm for creation of computational scheme for a group targeted constraint is used:

1) In accordance with the considering particular case individual targeted devices (individual targeted constraints, individual targeted kinematic devices) are formed, each of which changes only one of the intended natural frequencies to a given value, while all actions are performed [2], in which the lengths of all the main posts will be of the same sign.

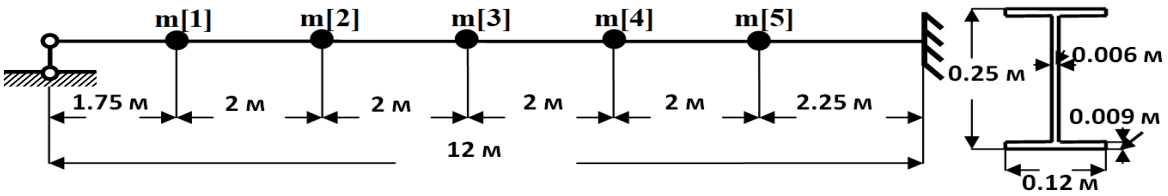


Figure 1. Considering structure (numerical example)

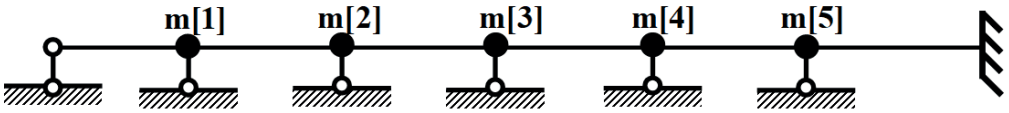


Figure 2. The basic system of the displacement method (numerical example)

2) All individual targeted devices are placed in the nodes of the structure;
3) In areas where several posts are combined, only one is left.
4) Hinges are introduced at the intersections of the rods.
When implementing the first step of the algorithm, the frequency spectrum of the natural oscillations of the original system with n degrees of freedom is considered,

$$\omega[1],\ \omega[2],\ ...,\ \omega[q],\ ..,$$
$$\omega[q+j],\ \omega[q+(j+1)],\ ...,\ \omega[n].$$

It is necessary to specifically free the frequency interval $\omega[q],\ ..,\ \omega[q+j]$ from j frequencies, reducing some of them to values smaller than $\omega[q]$ and increasing the remaining frequencies from this interval to values greater than $\omega[q+j]$.

3. NUMERICAL EXAMPLE OF IMPLEMENTING OF ALGORITHM OF CREATION OF COMPUTATIONAL SCHEME OF GROUP TARGETED KINEMATIC DEVICE

Let us demonstrate the implementation of the algorithm described in the previous paragraph using the example of a system with five degrees of freedom from [2]. The beam section is a composite I-beam (Figure 1). The modulus of elasticity of the system material is $E = 206000$ MPa. The mass values are equal to

$$m[1] = m[5] = 400 \text{ kg};$$
$$m[2] = m[4] = 800 \text{ kg};\ m[3] = 1200 \text{ kg}.$$

The frequencies and modes of the natural oscillations of the original system are determined by the displacement method, in which the unknowns are the displacements in the direction of mass motion. The basic system of the displacement method is shown in Figure 2.
The coefficients of the displacement method equations and the values of the nodal masses form matrices

$$A = \|a[i,\ k]\|;\quad M = \|m[i]\|. \tag{1}$$

The roots of the equation

$$\left|A - \omega^2 M\right| = 0 \tag{2}$$

define the frequency spectrum of the system's natural oscillations. The frequencies and modes of natural oscillations of the original system are presented in Table 1.
In order to form individual targeted kinematic devices, it is necessary to determine the forces that should appear in the device's posts [1-8, 16-22]

$$R_0[i,\ j] = m[i]v[i,\ j], \tag{3}$$

where i, j are the numbers of the components of the j-th mode of natural oscillations, respectively.

Table 1. Frequencies and modes of natural oscillations of the original system

Number k	Natural vibration modes					$m[k]$
	for frequency 14.07953	for frequency 53.0752	for frequency 109.5337	for frequency 195.0757	for frequency 226.8870	
0	0.0000	0.0000	0.0000	0.0000	0.0000	0
1	-0.315087	-0.502865	-0.594382	-0.73793	-0.369613	400
2	-0.565080	-0.520103	-0.174580	0.370387	-0.264938	800
3	-0.606213	0.103822	0.432120	-0.086169	0.212601	1200
4	-0.432097	0.574986	-0.359747	-0.137055	-0.383591	800
5	-0.164932	0.367738	-0.547801	0.540420	0.775147	400
6	0.0000	0.0000	0.0000	0.0000	0.0000	0

Table 2. Values of $R_0[i,\ k]$

i	1	2	3	4	5
$R_0[i,\ 1]$	63.04	226.24	364.32	173.28	33.08
$R_0[i,\ 2]$	-101.52	-210	62.88	232.16	74.24

If in the considering example it is required to reduce the value of the first natural oscillation frequency from 14.0715 sec^{-1} to 10 sec^{-1}, and the second natural oscillation frequency from 53.0769 sec^{-1} to 11 sec^{-1}, then

$$R_0[i,\ 1] = m[i]v[i,\ 1];\quad R_0[i,\ 2] = m[i]v[i,\ 2].$$

The values $R_0[i,\ k]$ are given in Table 2.

In order to construct a computational model for a kinematic targeted device that reduces $\omega[q]$ to $\omega[s]$, a matrix of additional inertial forces is formed:

$$M_0 = M_{m0}M_m; \quad (4)$$

$$M_m = \left\| m_0[i,k] \right\|_{i,k=1}^{n}; \quad (5)$$

$m_0[i,\ k] = m[i]m[k]v_\omega[i,\ q]v_\omega[k,\ q]$ or

$$m_0[i,\ k] = R_0[i,\ q]R_0[k,\ q]; \quad (6)$$

$$M_{m0} = \frac{\sum_{i=1}^{n}\sum_{k=1}^{n}(a[i,\ k] - (\omega[s])^2 m[i,\ k])v_\omega[i,\ q]v_\omega[k,\ q]}{\sum_{i=1}^{n}\sum_{k=1}^{n}(\omega[s])^2 m_0[i,\ k]v_\omega[i,\ q]v_\omega[k,\ q]}. \quad (7)$$

After forming the matrix, the following equation is solved:

$$\left| A - \omega^2 (M + M_{m0}M_m) \right| = 0. \quad (8)$$

The solution results determine the frequency spectrum and natural oscillation modes of the modified system.

For systems in which the directions of mass motion during natural oscillations lie in the same plane, the method of creation of computational model is based on the properties of a rope polygon constructed from the forces $R_0[i,\ k]$. For the initial system considered in the distinctive paper, such an approach is given, for example, in [2]. There we have $R_0[i,\ 1] = m[i]v[i,\ 1]$ and corresponding kinematic targeted device is formed, that reduces the first natural oscillation frequency from 14.0715 sec^{-1} to 10 sec^{-1}.

Table 3. Frequencies and modes of natural oscillations of the modified system

Number k	Natural vibration modes					$m[k]$
	for frequency 10.0095	for frequency 53.0752	for frequency 109.5337	for frequency 195.0757	for frequency 226.8870	
0	0.0000	0.0000	0.0000	0.0000	0.0000	0
1	0.315087	-0.502865	-0.594382	-0.73793	-0.369613	400
2	0.565080	-0.520103	-0.174580	0.370387	-0.264938	800
3	0.606213	0.103822	0.432120	-0.086169	0.212601	1200
4	0.432097	0.574986	-0.359747	-0.137055	-0.383591	800
5	0.164932	0.367738	-0.547801	0.540420	0.775147	400
6	0.0000	0.0000	0.0000	0.0000	0.0000	0

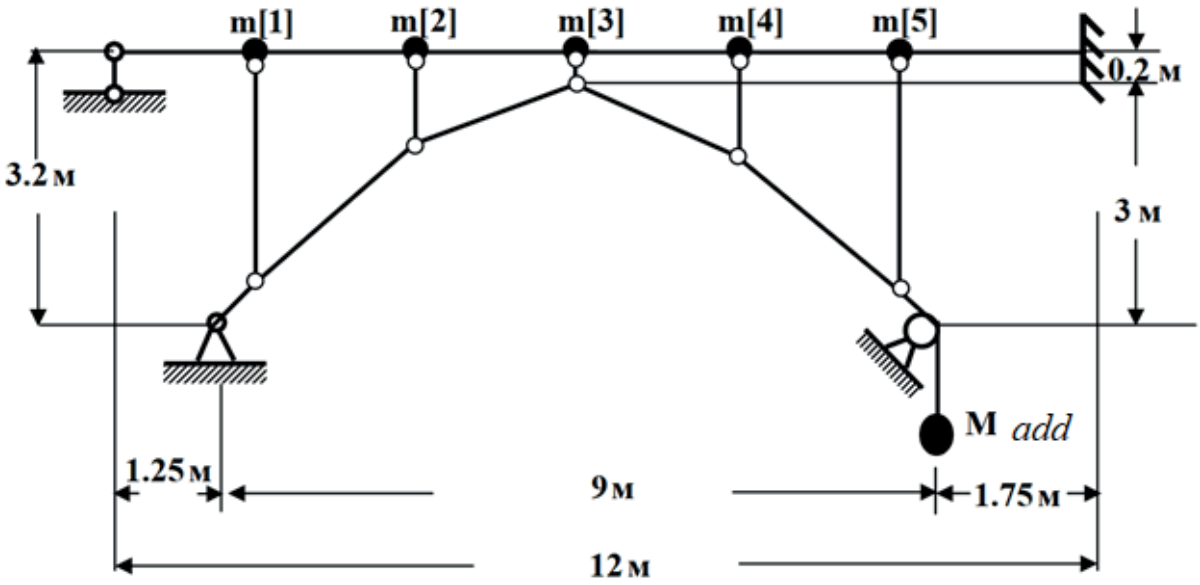


Figure 3. The general view of computational scheme of targeted kinematic device

The frequencies and forms of natural oscillations of the modified system are presented in Table 3. The general view of this kinematic targeted device is shown in Figure 3. We have the following lengths of posts:

$$l_p[1] = 2.6934\,\text{m}; \quad l_p[2] = 0.9406\,\text{m};$$
$$l_p[3] = 0.2000\,\text{m}; \quad l_p[4] = 1.0879\,\text{m};$$
$$l_p[5] = 2.7498\,\text{m}.$$

The magnitude of the additional mass is determined by the relationship (see, for example, [2])

$$M_{add} = M_{mo}(N[n])^2, \qquad (9)$$

where $N[n]$ is the force in the outermost post of the device's belt, to which the additional mass is attached.

The additional mass for the formed device is equal to $M_{add} = 1586.5229\,\text{kg}$. The cross-sectional areas of the kinematic device rods are identical; their values can be chosen arbitrarily. A cable runs from the lower hinge of fifth post through the block to the ground.

In [3, 4, 18, 19, 22] it is shown that changing the lengths of all the targeted device posts by the

same amount does not affect the spectrum of natural frequencies and vibration modes.

Figure 4 shows a kinematic device formed from the one shown in Figure 3, by lengthening all the posts by 2 m.

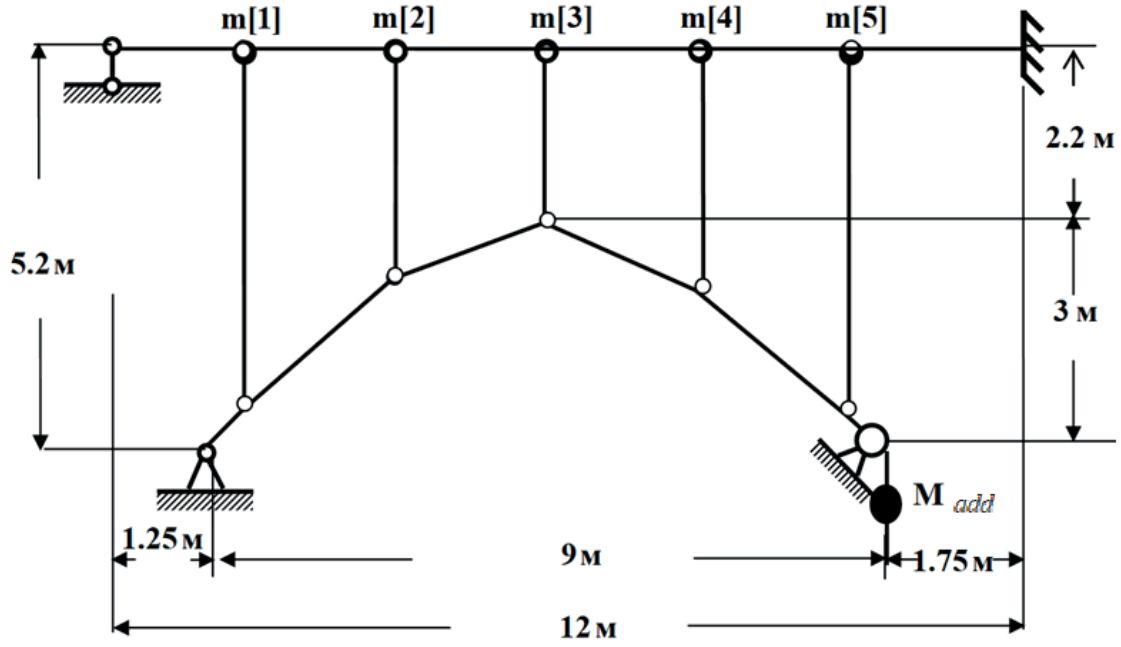


Figure 4. The general view of computational scheme of targeted kinematic device

Table 4. Coordinates of the belt nodes

Number of node	0	1	2	3	4	5	6
Coordinate of node	4.0557	2.9725	1.6217	6.4406	9.4115	5.5631	4.0557

Table 5. Frequencies and modes of natural oscillations of the modified system

Number k	Natural vibration modes					$m[k]$
	for frequency 11.0062	for frequency 14.07953	for frequency 109.5337	for frequency 195.0757	for frequency 226.8870	
0	0.0000	0.0000	0.0000	0.0000	0.0000	0
1	-0.502865	-0.315087	-0.594382	-0.73793	-0.369613	400
2	-0.520103	-0.565080	-0.174580	0.370387	-0.264938	800
3	0.103822	-0.606213	0.432120	-0.086169	0.212601	1200
4	0.574986	-0.432097	-0.359747	-0.137055	-0.383591	800
5	0.367738	-0.164932	-0.547801	0.540420	0.775147	400
6	0.0000	0.0000	0.0000	0.0000	0.0000	0

Similarly we have $R_0[i, 2] = m[i]v[i, 2]$ and a matrix of additional inertial forces is formed based on the forces, reducing the second natural frequency from 53.0769 sec^{-1} to 11 sec^{-1}, and a corresponding computational model for the targeted kinematic device is created. A general view of the computational model for this targeted kinematic device is shown in Figure 4.

The additional mass is equal to

$$M_{add} = 6301.7206915414\,\text{kg}.$$

The frequencies and modes of natural vibrations of this modified system are presented in Table 5.

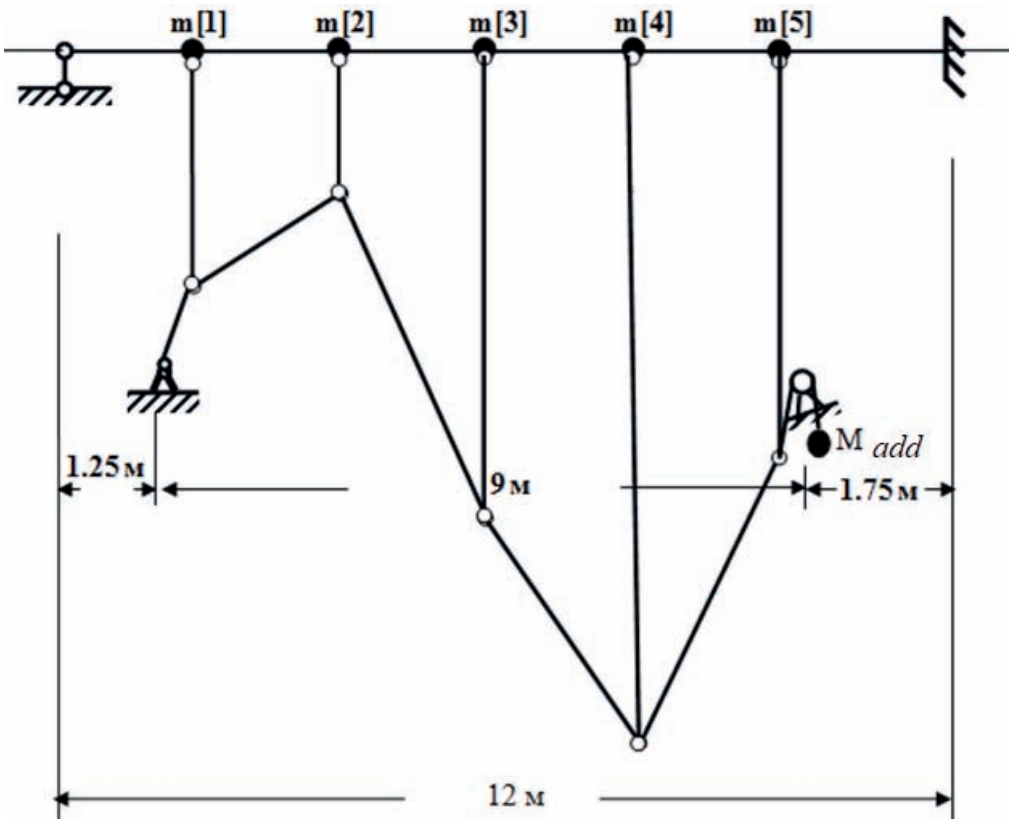


Figure 5. The general view of computational scheme of targeted kinematic device

Table 6. Coordinates of the belt nodes.

Number of node	0	1	2	3	4	5	6
Node coordinate (upper chord)	3.2000	2.6934	0.9406	0.2000	1.0879	2.7498	3.2000
Node coordinate (lower chord)	4.0557	2.9725	1.6217	6.4406	9.4115	5.5631	4.0557

After creation of individual kinematic targeted devices necessary for solving the problem, a group matrix of additional inertial force coefficients can be formed. In order to do this it is required simply sum the coefficients of the additional inertial force matrices of the individual kinematic devices.

By implementing the second step of the algorithm described above, we form a group targeted kinematic device. In order to do this, the generated computational schemes for the individual targeted kinematic devices are placed at the nodes of the original system. The general view of this device is shown in Figure 6.

We have the following additional masses:

$$M_{add1} = 1586.5229\,\text{kg}, \quad M_{add2} = 6301.72069\,\text{kg}.$$

In this version of the group targeted kinematic device, both additional masses are attached to the rightmost links of the individual kinematic devices' belts.

In some cases, it may be necessary to attach additional masses to different sides of the group targeted kinematic device. Implementing this requirement does not complicate the procedure of creation of the group targeted device. In this case, in the individual kinematic devices used, the corresponding numbers j of the outermost belt links are selected when determining the values (9).

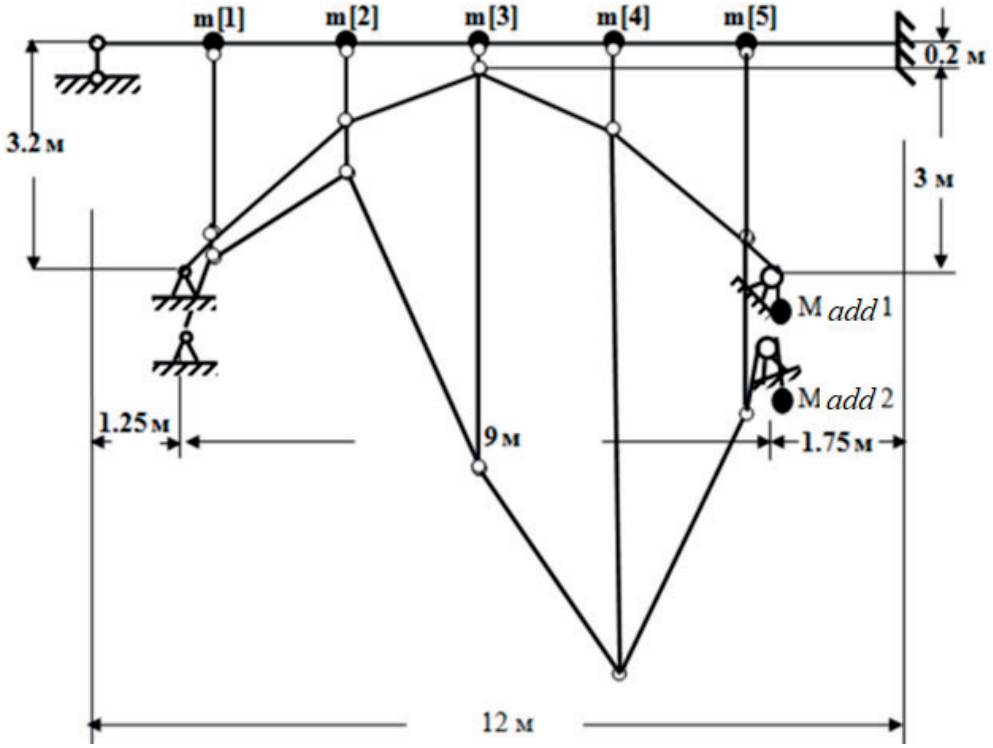


Figure 6. The general view of the device

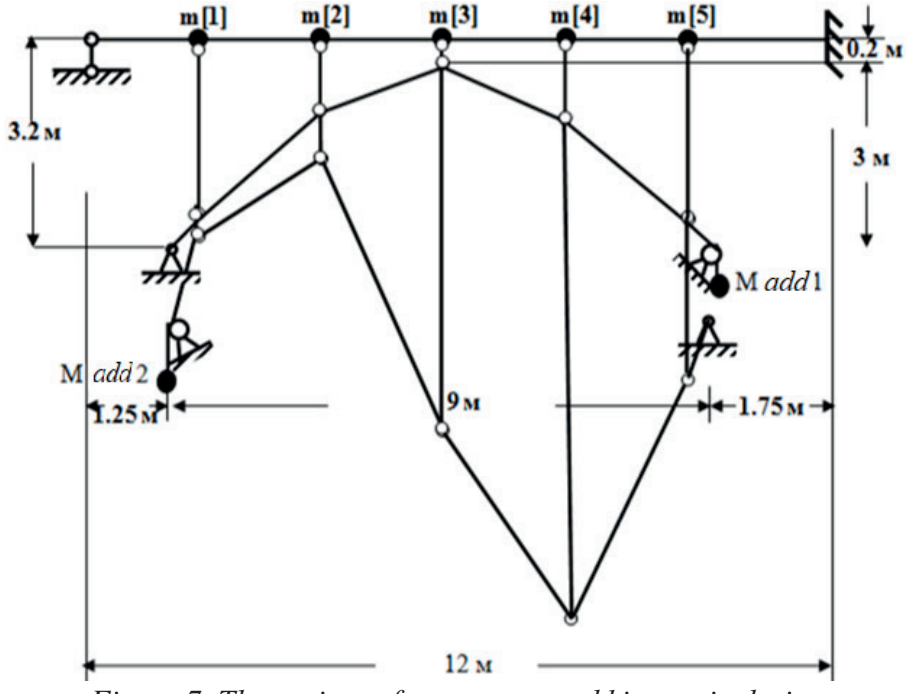


Figure 7. The variant of group targeted kinematic device

Table 7. Frequencies and modes of oscillation of both variants of the group targeted kinematic device

Number k	Natural vibration modes					$m[k]$
	for frequency 11.0062	for frequency 14.07953	for frequency 109.5337	for frequency 195.0757	for frequency 226.8870	
0	0.0000	0.0000	0.0000	0.0000	0.0000	0
1	-0.502865	-0.315087	-0.594382	-0.73793	-0.369613	400
2	-0.520103	-0.565080	-0.174580	0.370387	-0.264938	800
3	0.103822	-0.606213	0.432120	-0.086169	0.212601	1200
4	0.574986	-0.432097	-0.359747	-0.137055	-0.383591	800
5	0.367738	-0.164932	-0.547801	0.540420	0.775147	400
6	0.0000	0.0000	0.0000	0.0000	0.0000	0

Table 8. Comparison of the natural frequencies of the original system with the results of testing using the "SCAD" and "LIRA" software products

	$\omega[1]$	$\omega[2]$	$\omega[3]$	$\omega[4]$	$\omega[5]$
Proposed pproach	14.0715	53.0769	109.5339	195.0757	226.8873
"SCAD" and "LIRA" software packages	14,0820	53,4030	111,5070	201,4150	237,1590

A version of the group sighting kinematic device in which the additional masses are attached to different sides is shown in Figure 7.

The frequencies and modes of natural oscillations of both variants of the group targeted kinematic device are identical and are presented in Table 7.

The posts of the individual targeted kinematic devices, mounted at the mass application nodes and directed along their trajectory, are aligned. Forces $R_0[i,\ k] = m[i]v[i,\ k]$ arise in the aligned posts, each of which determines one of the individual targeted kinematic devices.

The absence of mutual influence between the forces determining the various individual kinematic devices is justified by the properties of the forces $R_0[i,\ k]$. The forces $R_0[i,\ k_1]$ determining the targeted device, which reduces the natural frequency $\omega[k_1]$, do not perform work on the displacements of the natural oscillation mode of any other natural frequency, that is,

$$\text{if } k_1 \neq k_2 \text{ we get } \sum_{i=1}^{n} R_0[i,\ k_1]v[i,\ k_2] = 0\,. \quad (10)$$

Relationship (10) determines the absence of mutual influence between the forces $R_0[i,\ k]$ arising in the posts of the group targeted device.

The results presented in Table 7 confirm that the introduction of the group targeted kinematic device reduces only the first two selected natural oscillation frequencies to the intended values and does not lead to a change in the natural modes and values of the remaining frequencies. The results presented in Tables 1, 2, 3, 5, 7 were obtained by the finite element method (FEM) [18] by dividing (discretizing) the length of the original beam into 24 sections. A comparison of the natural vibration frequencies of the original system with the test results of the "SCAD" and "LIRA" software products [9-15] is presented in Table 8. Considering the difference in the calculation method for Tables 1, 2, 3, 5, 7 between the "SCAD" and "LIRA" software products, the agreement between the results can be considered fairly close, confirming the reliability of the original data.

We will now test the group targeted kinematic device using the "SCAD" and "LIRA" software products. The results are presented in Table 9.

Table 9. Testing the group targeted kinematic device

	$\omega[1]$	$\omega[2]$	$\omega[3]$	$\omega[4]$	$\omega[5]$
Initial	14,0820	53,4030	111,5070	201,4150	237,1590
Group	10,8000	11,1400	111,5200	201,4200	237,1600

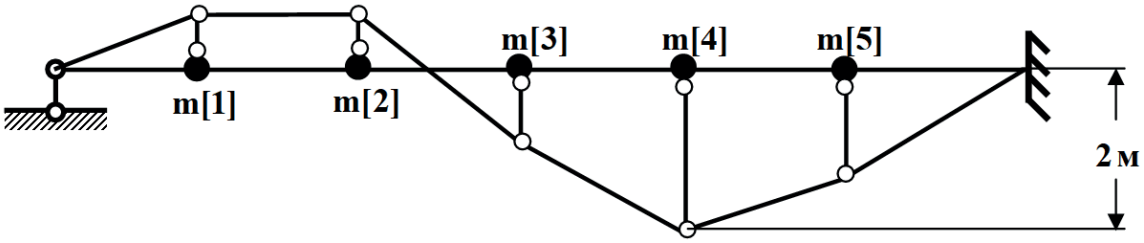


Figure 8. The general view of the device

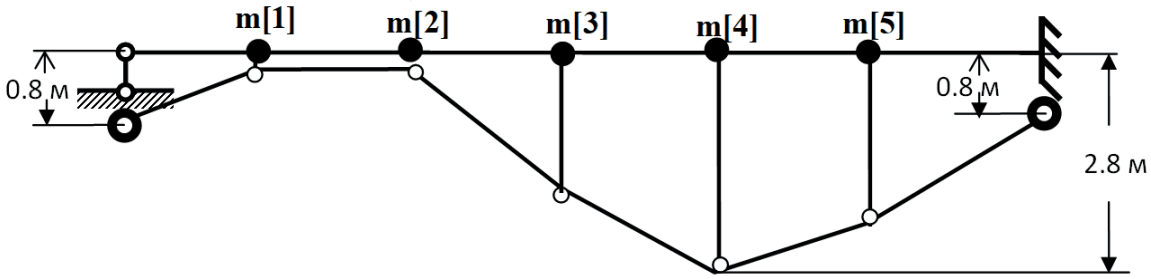


Figure 9. The general view of the modified device

The data presented in Table 9 prove that the testing performed convincingly demonstrates a reduction exclusively in those frequencies targeted by the group kinematic device, while the other natural oscillation frequencies remained unchanged.

If for the initial system (Figure 1) it is required to reduce the value of the first natural frequency from 14.0820 sec^{-1} to 10 sec^{-1} and to increase the value of the second frequency from 53.4030 sec^{-1} to $\omega_{S2} = 110\ sec^{-1}$, then one of the separate targeted kinematic devices shown in Figure 3 and Figure 4 can be used to reduce the first frequency. In order to increase the value of the second frequency, a separate targeted constraint, created in [58], can be used.

For this purpose, a matrix of additional stiffness coefficients is formed based on the forces

$$A_0 = A_{S0} A_S; \qquad (11)$$

$$A_S = \left\| a_0[i,k] \right\|_{i,k=1}^{n}; \qquad (12)$$

$$a_0[i,\ k] = R_0[i] R_0[k]; \qquad (13)$$

$$A_{SO} = \frac{-\sum_{i=1}^{n}\sum_{k=1}^{n}(a[i,\ k] - \omega_{S2}^2 m[i,\ k]) v_\omega[i,2] v_\omega[k,2]}{\sum_{i=1}^{n}\sum_{k=1}^{n} a_0[i,k] v_\omega[i,2] v_\omega[k,2]}. \qquad (14)$$

In accordance with [2], a separate targeted constraint is formed. The general appearance of this device is shown in Figure 8.

The lengths of the posts of this device are of different signs. To avoid the complications associated with this circumstance, we will increase the lengths of all legs by 0.8 m.

The general appearance of this modified device is shown in Figure 9.

We have the following lengths of posts:

$$l_p[1] = 0.1264\ \text{m}; \quad l_p[2] = 0.1212\ \text{m};$$

Table 10. Frequencies and modes of oscillation of the separate targeted constraint

Number k	Natural vibration modes					$m[k]$
	for frequency 14.07953	for frequency 109.5337	for frequency 109.9983	for frequency 195.0757	for frequency 226.8870	
0	0.0000	0.0000	0.0000	0.0000	0.0000	0
1	-0.315087	-0.594382	-0.502865	-0.73793	-0.369613	400
2	-0.565080	-0.174580	-0.520103	0.370387	-0.264938	800
3	-0.606213	0.432120	0.103822	-0.086169	0.212601	1200
4	-0.432097	-0.359747	0.574986	-0.137055	-0.383591	800
5	-0.164932	-0.547801	0.367738	0.540420	0.775147	400
6	0.0000	0.0000	0.0000	0.0000	0.0000	0

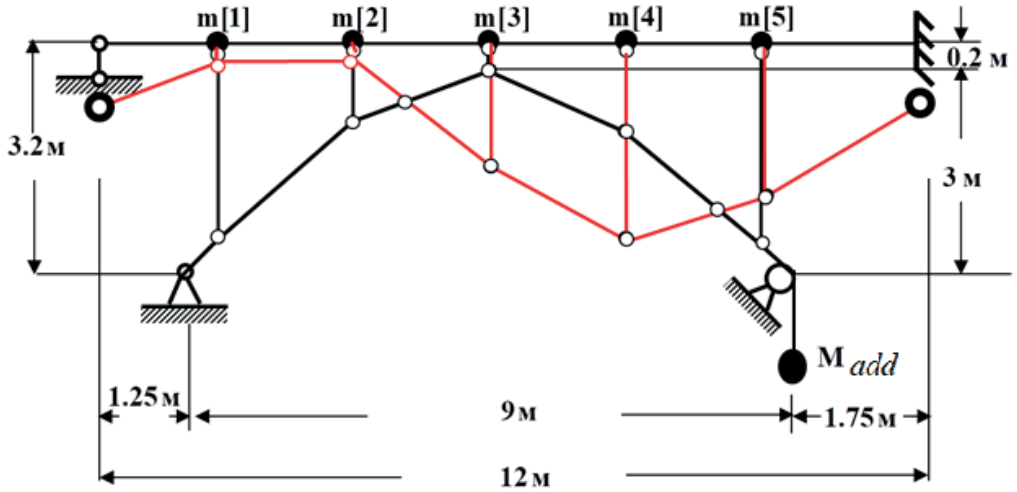


Figure 10. The general view of the considering variant of integrated group targeted device

$$l_p[3] = 1.6981\,\text{m}; \quad l_p[4] = 2.8000\,\text{m};$$
$$l_p[5] = 2.1555\,\text{m}.$$

The cross-sectional areas of the belt rods and the posts are, respectively, equal to:

$$F_b = 0.0003538\,\text{m}^2; \quad F_p = 0.0007075\,\text{m}^2.$$

The diameters of the belt rods and the posts are, respectively, equal to:

$$D_b = 0.02122\,\text{m}; \quad D_p = 0.0007075\,\text{m}.$$

The frequencies and modes of natural vibrations of this individual targeted constraint are presented in Table 10. They are determined by the roots of the equation

$$\left|(A + A_{SO}A_S) - \omega^2 M\right| = 0. \qquad (15)$$

By implementing the second step of the above algorithm, we create an integrated group targeted device. Let us first consider the variant in which the integrated targeted device is created based on the individual targeted constraint shown in Figure 9 and the individual targeted kinematic device shown in Figure 3.

In order to achieve this, the selected computational schemes for individual targeted devices are placed within the nodes of the original system.

The general view of this version of the integrated group targeted device is shown in Figure 10.

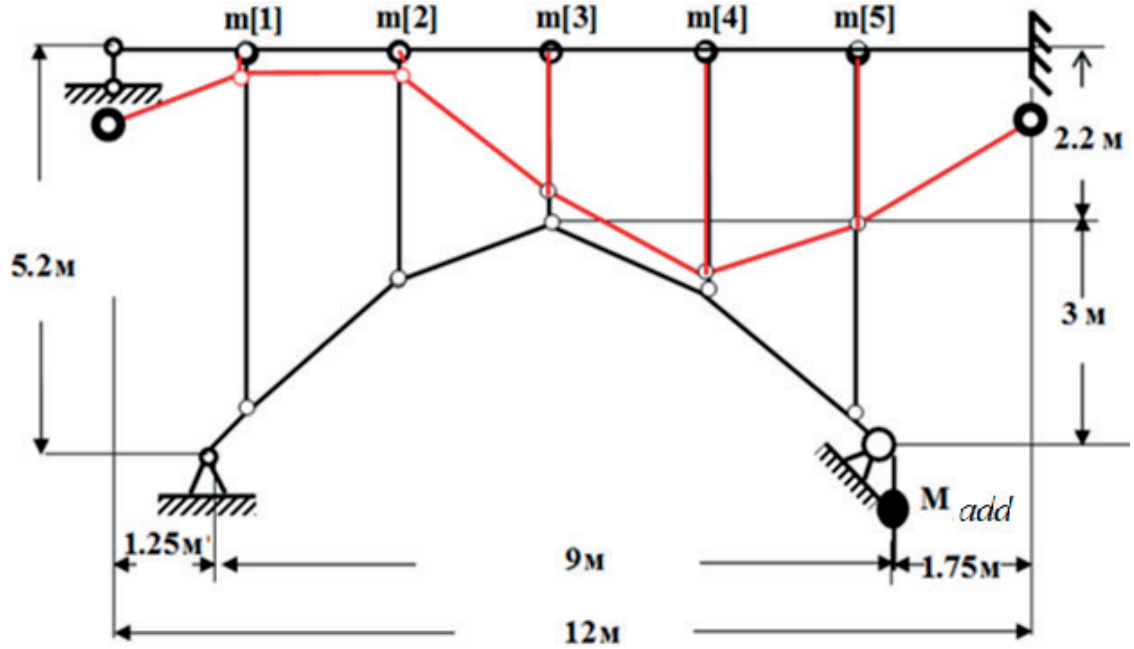


Figure 10. The general view of the considering variant of integrated group targeted device

It should be clarified that the symbol ⊙ denotes a fixed flat hinge, with a cable running from the fifth post to the block and down.
The additional mass is equal to

$$M_{add} = 1586.5229125936\,\text{kg}.$$

The cross-sectional areas of the red belt rods are equal to

$$F_b = 0.0003538\,\text{m}^2.$$

The cross-sectional areas of the red posts are equal to

$$F_p = 0.0007075\,\text{m}^2.$$

The diameter of the belt rods is equal to

$$D_b = 0.02122\,\text{m}.$$

The diameter of the belt rods is equal to

$$D_b = 0.03001\,\text{m}.$$

The cross-sections of the black rods are the same. Where posts overlap, the cross-sections are not doubled.
In the considered computational scheme for the integrated group targeted device, the belt of separate targeted constraint and belt of separate targeted kinematic device intersect.
Let us now consider a variant in which the integrated targeted device is created based on the separate targeted constraint shown in Figure 9 and the separate targeted kinematic device shown in Figure 4.
The general view of this variant of the integrated group targeted device is shown in Figure 11. In this computational scheme, the belt of separate targeted constraint and belt of separate targeted kinematic device do not intersect.
The posts of the separate targeted devices are superimposed. Forces

$$R_0[i,\ k] = m[i]v[i,\ k]$$

arise in the combined posts, each of which determines one of the individual targeted devices.

Table 12. Frequencies and modes of oscillation of both variants of computational schemes

Number k	Natural vibration modes					$m[k]$
	for frequency 10.07953	for frequency 109.5337	for frequency 109.9983	for frequency 195.0757	for frequency 226.8870	
0	0.0000	0.0000	0.0000	0.0000	0.0000	0
1	-0.502865	-0.315087	-0.594382	-0.73793	-0.369613	400
2	-0.520103	-0.565080	-0.174580	0.370387	-0.264938	800
3	0.103822	-0.606213	0.432120	-0.086169	0.212601	1200
4	0.574986	-0.432097	-0.359747	-0.137055	-0.383591	800
5	0.367738	-0.164932	-0.547801	0.540420	0.775147	400
6	0.0000	0.0000	0.0000	0.0000	0.0000	0

Table 13. Test of group targeted device

	$\omega[1]$	$\omega[2]$	$\omega[3]$	$\omega[4]$	$\omega[5]$
Table 12	10.0095	11.0062	109.5337	195.0757	226.8870
Test	10,8000	11.1400	111.5200	201.4200	237.1600

The absence of mutual influence between the forces determining the different individual targeted devices is explained by the properties of the forces $R_0[i,\ k]$, which are represented by the relationship (10).

The frequencies and modes of natural vibrations of both variants of the computational schemes are the same. They are determined by the roots of the equation

$$\left|(A + A_{SO}A_S) - \omega^2\left(M + M_{m0}M_m\right)\right| = 0\,. \quad (16)$$

Equation (16) is formed from equation (2) by adding the matrix of additional stiffness coefficients (11), (12) to matrix A (1) and the matrix of additional inertial forces (4) to matrix (1).

The frequencies and coordinates of the natural oscillation modes presented in Table 12 were obtained as the roots of Equation (16) before the computational model of the integrated group sighting device was created.

Table 2.3.12 shows that the intended changes in the natural oscillation frequencies occurred with sufficient accuracy. Only the first natural oscillation frequency decreased, and only the second increased. The remaining frequencies and all natural oscillation modes remained unchanged.

We will now test the group targeted device with the use of "SCAD" and "LIRA" software products [9-15]. The results are presented in Table 13.

The data presented in Table 13 demonstrate that the testing of the computational model convincingly demonstrates the closeness of the test results to the roots of equation (16) and confirms the change in only those frequencies targeted by the integrated group targeted device, while the remaining natural oscillation frequencies remained unchanged.

Thus, the distinctive paper proposes an algorithm for generating an integrated group targeted device that increases some targeted natural frequencies to specified values and decreases other targeted frequencies to specified values, without changing any of the remaining natural frequencies or any of the natural oscillation modes. A method for generating a matrix defining an equation whose roots determine the frequencies and natural oscillation modes of the integrated group targeted device is considered. A justification is provided for the absence of mutual influence between the forces $R_0[i,\ k]$ arising in the posts of the integrated group targeted device. The proposed algorithm was tested with the use of "SCAD" and "LIRA" software products [9-15].

REFERENCES

1. **Akimov P.A, Lyahovich L.S.** Pricel'noe regulirovanie spektra chastot sobstvennyh kolebanij uprugih plastin s konechnym chislom stepenej svobody mass putem vvedenija dopolnitel'nyh obobshhennyh svjazej i obobshhennyh kinematicheskih ustrojstv [Precision control for eigen-frequency of elastic plates with finite number of mass degrees of freedom by using additional generalized connections and kinematic devices]. // Vestnik Tomskogo gosudarstvennogo arkhitekturno-stroitel'nogo universiteta. Journal of Construction and Architecture, 2021, Vol. 23, No. 4, pp. 57-67 (In Russian).
2. **Lyahovich L.S.** Osobye svojstva optimal'nyh sistem i osnovnye napravlenija ih realizacii v metodah rascheta sooruzhenij [Special properties of optimal systems and the main directions of their implementation in the methods of structural analysis]. Tomsk, TGASU, 2009. – 372 pages (In Russian).
3. **Lyakhovich L.S., Akimov P.A.** About Development of Computational Schemes of Some Additional Constraints for Elastic Systems. Part 1: Theoretical Foundations [O formirovanii raschetnyh shem nekotoryh dopolnitel'nyh svjazej dlja uprugih sistem. Chast' 1: Teoreticheskie osnovy podhoda]. // Promyshlennoe i Grazhdanskoe Stroitelstvo, 2022, No. 9, pp. 4-10 (in Russian).
4. **Lyakhovich L.S., Akimov P.A., Mescheulov N.V.** About Development of Computational Schemes of Some Additional Constraints for Elastic Systems. Part 2: Samples of Analysis [O formirovanii raschetnyh shem nekotoryh dopolnitel'nyh svjazej dlja uprugih sistem. Chast' 2: Primery raschetov]. // Promyshlennoe i Grazhdanskoe Stroitelstvo, 2022, No. 9, pp. 4-10 (in Russian).
5. **Lyakhovich L.S., Akimov P.A., Galyautdinov Z.R., Plyaskin A.S.** About Development of Computational Schemes of Generalized Kinematic Devices, Which Precisely Regulate the Frequency Spectrum of Natural Oscillations of Elastic Systems with a Finite Number of Degrees of Mass Freedom, the Directions of Movement of Which are Parallel, but do not Lie in the Same Plane. Part 1: Theoretical Foundations [O sozdanii raschetnyh shem obobshhennyh kinematicheskih ustrojstv, pricel'no regulirujushhih spektr chastot sobstvennyh kolebanij uprugih sistem s konechnym chislom stepenej svobody mass, u kotoryh napravlenija dvizhenija parallel'ny, no ne lezhat v odnoj ploskosti. Chast' 1. Teoreticheskie osnovy podhoda]. Fundamental exploratory and applied research of the Russian Academy of Architecture and Construction Sciences (RAASN) on scientific support for the development of architecture, urban planning, and the construction industry of the Russian Federation in 2022–2023: Scientific works of the RAACS: In 2 volumes: Volume 2. Moscow: RAACS, 2024, pp. 265-274 (in Russian).
6. **Lyakhovich L.S., Akimov P.A., Galyautdinov Z.R., Plyaskin A.S.** About Development of Computational Schemes of Generalized Kinematic Devices, Which Precisely Regulate the Frequency Spectrum of Natural Oscillations of Elastic Systems with a Finite Number of Degrees of Mass Freedom, the Directions of Movement of Which are Parallel, but do not Lie in the Same Plane. Part 2: Samples of Analysis [O sozdanii raschetnyh shem obobshhennyh kinematicheskih ustrojstv, pricel'no regulirujushhih spektr chastot sobstvennyh kolebanij uprugih sistem s konechnym chislom stepenej svobody mass, u kotoryh napravlenija dvizhenija parallel'ny, no ne lezhat v odnoj ploskosti. Chast' 2. Primery raschetov]. Fundamental exploratory and applied research of the Russian Academy of Architecture and Construction Sciences (RAASN) on scientific support for the development of architecture, urban planning, and the construction industry of the Russian Federation in 2022–2023: Scientific works of the RAACS: In 2 volumes: Volume 2. Moscow: RAACS, 2024, pp. 275-285 (in Russian).
7. **Lyahovich L.S., Maletkin O.Ju.** O pricel'nom regulirovanii sobstvennyh chastot

uprugih system [On targeted control of natural frequencies of elastic systems]. // Izvestija vuzov. Stroitel'stvo i arhitektura, 1990, No. 1, pp. 113-117 (In Russian).
8. **Faizullin I.E., Lyakhovich L.S., Akimov P.A., Galautdinov Z.R., Plyaskin A.S.** Development of computational schemes of group targeted connections for some elastic systems [Formirovanie raschetnyh shem gruppovyh pricel'nyh svjazej dlja nekotoryh uprugih system]. // Vestnik MGSU, 2025, Volume 20, Issue 1, pp. 60-72 (in Russian).
9. **Fialko S.** Nonlinear dynamic analysis of the progressive collapse on multi-core computers. // Selected problems of solid mechanics and solving methods / Advanced Structured Materials, 2024, Number 204, Cham, Springer, pp.167-183.
10. **Fialko S.** Parallel finite element solver for multi-core computers with shared memory. // Computers & Mathematics with Applications, 2021, Volume 94, pp. 1-14.
11. **Fialko S.** Parallel finite element solver PARFES for the structural analysis in NUMA architecture. // Advances in Engineering Software, 2022, Volume 174, 103290 pp. 1-12.
12. **Fialko S.** Time history analysis of buildings and structures design models in SCAD software on multicore computers. // ECMS 2024: proceedings of the 38th ECMS International Conference on Modelling and Simulation, June 4th-June 7th, 2024 Cracow, Poland / Communications of the ECMS, 2024, Volume 38, Number 1, Caserta, ECMS, pp.187-193.
13. **Fialko S.Yu.** Block Subspace Iteration Method for Structural Analysis on Multicore Computers. // Proceedings of the of the 17th Conference on Computer Science and Intelligence Systems, 2022, Volume 30, pp. 457-465.
14. **Fialko S.Yu., Kabantsev O.V., Perelmuter A.V.** Elasto-plastic progressive collapse analysis based on the integration of the equations of motion. // Magazine of Civil Engineering, 2021, Number 102 (2), pp. 1-10.
15. **Karpilovskyi V.S.** Finite Elements for the Analysis of Reissner-Mindlin Plates With Joint Interpolation of Displacements and Rotations (JIDP). // International Journal for Computational Civil and Structural Engineering, 2021, Volume 17, Issue 3, pp. 49-63.
16. **Lyakhovich L.S., Akimov P.A.** Aimed control of the frequency spectrum of eigenvibrations of elastic plates with a finite number of degrees of freedom of masses by superimposing additional constraints. // International Journal for Computational Civil and Structural Engineering, 2021, Volume 17, Issue 2, pp. 76-82.
17. **Lyakhovich L.S., Akimov P.A.** Aimed control of the frequency spectrum of eigenvibrations of elastic plates with a finite number of degrees of freedom by introducing additional generalized kinematic devices. // International Journal for Computational Civil and Structural Engineering, 2021, Volume 17, Issue 3, pp. 14-20.
18. **Lyakhovich L.S., Akimov P.A.** Formation of Computational Schemes of Additional Targeted Constraints That Regulate The Frequency Spectrum of Natural Oscillations of Elastic Systems With a Finite Number of Degrees of Mass Freedom, the Directions of Movement of Which are Parallel, But Do Not Lie in the Same Plane. Part 1: Theoretical Foundations. // International Journal for Computational Civil and Structural Engineering, 2022, Volume 18, Issue 2, pp. 183-193.
19. **Lyakhovich L.S., Akimov P.A.** Formation of Computational Schemes of Additional Targeted Constraints That Regulate The Frequency Spectrum of Natural Oscillations of Elastic Systems With a Finite Number of Degrees of Mass Freedom, the Directions of Movement of Which are Parallel, But Do Not Lie in the Same Plane. Part 2: The First Sample of Analysis. // International Journal for Computational Civil and Structural Engineering, 2022, Volume 18, Issue 3, pp. 137-146.
20. **Lyakhovich L.S., Akimov P.A., Galyautdinov Z.R., Plyaskin A.S.** Develop-

ment of computational schemes of generalized kinematic devices that precisely regulate the natural frequency spectrum of elastic systems with a finite number of degrees of mass freedom, in which the directions of motion are parallel, but do not lie in the same plane. Part 1: Theoretical foundations. // International Journal for Computational Civil and Structural Engineering, 2023, Volume 19, Issue 3, pp. 173-183.

21. **Lyakhovich L.S., Akimov P.A., Galyautdinov Z.R., Plyaskin A.S**. Development of computational schemes of generalized kinematic devices that precisely regulate the natural frequency spectrum of elastic systems with a finite number of degrees of mass freedom, in which the directions of motion are parallel, but do not lie in the same plane. Part 2. Samples of analysis. // International Journal for Computational Civil and Structural Engineering, 2023, Volume 19, Issue 4, pp. 155-165.
22. **Lyakhovich L.S., Akimov P.A., Meccheulov N.V.** Formation of computational schemes of additional targeted constraints that regulate the frequency spectrum of natural oscillations of elastic systems with a finite number of degrees of mass freedom, the directions of movement of which are parallel, but do not lie in the same plane. Part 3. The second sample of analysis and conclusion. // International Journal for Computational Civil and Structural Engineering, 2022, Volume 18, Issue 4, pp. 71-81.

СПИСОК ЛИТЕРАТУРЫ

1. **Акимов П.А., Ляхович Л.С.** Прицельное регулирование спектра частот собственных колебаний упругих пластин с конечным числом степеней свободы масс путем введения дополнительных обобщенных связей и обобщенных кинематических устройств. // Вестник Томского государственного архитектурно-строительного университета, 2021, том 23, № 4, с. 57-67.
2. **Ляхович Л.С.** Особые свойства оптимальных систем и основные направления их реализации в методах расчета сооружений. Монография. – Томск: Издательство ТГАСУ, 2009. – 372 с.
3. **Ляхович Л.С., Акимов П.А.** О формировании расчетных схем некоторых дополнительных связей для упругих систем. Часть 1. Теоретические основы подхода. // Промышленное и гражданское строительство, 202, №9, с. 4-10.
4. **Ляхович Л.С., Акимов П.А., Мешеулов Н.В.** О формировании расчетных схем некоторых дополнительных связей для упругих систем. Часть 2. Примеры расчёта. // Промышленное и гражданское строительство, 2022, №9, с. 11-19.
5. **Ляхович Л.С., Акимов П.А., Галяутдинов З.Р., Пляскин А.С.** О создании расчетных схем обобщенных кинематических устройств, прицельно регулирующих спектр частот собственных колебаний упругих систем с конечным числом степеней свободы масс, у которых направления движения параллельны, но не лежат в одной плоскости. Часть 1. Теоретические основы подхода. Фундаментальные поисковые и прикладные исследования РААСН по научному обеспечению развития архитектуры, градостроительства и строительной отрасли Российской Федерации в 2022-2023 годы: Научные труды РААСН: В 2-х томах: Том 2. – Москва: РААСН, 2024, с. 265-274.
6. **Ляхович Л.С., Акимов П.А., Галяутдинов З.Р., Пляскин А.С.** О создании расчетных схем обобщенных кинематических устройств, прицельно регулирующих спектр частот собственных колебаний упругих систем с конечным числом степеней свободы масс, у которых направления движения параллельны, но не лежат в одной плоскости. Часть 2. Примеры расчетов. Фундаментальные поисковые и прикладные исследования РААСН по научному обеспечению развития архитектуры, градостроительства и

строительной отрасли Российской Федерации в 2022-2023 годы: Научные труды РААСН: В 2-х томах: Том 2. – Москва: РААСН, 2024, с. 275-285.

7. **Ляхович Л.С., Малеткин О.Ю.** О прицельном регулировании собственных частот упругих систем. // Известия вузов. Строительство и архитектура, 1990, № 1, с. 113-117.
8. **Файзуллин И.Э., Ляхович Л.С., Акимов П.А., Галяутдинов З.Р., Пляскин А.С.** Формирование расчетных схем групповых прицельных связей для некоторых упругих систем. // Вестник МГСУ, 2025, Том 20, Выпуск 1, с. 60-72.
9. **Fialko S.** Nonlinear dynamic analysis of the progressive collapse on multi-core computers. // Selected problems of solid mechanics and solving methods / Advanced Structured Materials, 2024, Number 204, Cham, Springer, pp.167-183.
10. **Fialko S.** Parallel finite element solver for multi-core computers with shared memory. // Computers & Mathematics with Applications, 2021, Volume 94, pp. 1-14.
11. **Fialko S.** Parallel finite element solver PARFES for the structural analysis in NUMA architecture. // Advances in Engineering Software, 2022, Volume 174, 103290 pp. 1-12.
12. **Fialko S.** Time history analysis of buildings and structures design models in SCAD software on multicore computers. // ECMS 2024: proceedings of the 38th ECMS International Conference on Modelling and Simulation, June 4th-June 7th, 2024 Cracow, Poland / Communications of the ECMS, 2024, Volume 38, Number 1, Caserta, ECMS, pp.187-193.
13. **Fialko S.Yu.** Block Subspace Iteration Method for Structural Analysis on Multicore Computers. // Proceedings of the of the 17th Conference on Computer Science and Intelligence Systems, 2022, Volume 30, pp. 457-465.
14. **Fialko S.Yu., Kabantsev O.V., Perelmuter A.V.** Elasto-plastic progressive collapse analysis based on the integration of the equations of motion. // Magazine of Civil Engineering, 2021, Number 102 (2), pp. 1-10.
15. **Karpilovskyi V.S.** Finite Elements for the Analysis of Reissner-Mindlin Plates With Joint Interpolation of Displacements and Rotations (JIDP). // International Journal for Computational Civil and Structural Engineering, 2021, Volume 17, Issue 3, pp. 49-63.
16. **Lyakhovich L.S., Akimov P.A.** Aimed control of the frequency spectrum of eigenvibrations of elastic plates with a finite number of degrees of freedom of masses by superimposing additional constraints. // International Journal for Computational Civil and Structural Engineering, 2021, Volume 17, Issue 2, pp. 76-82.
17. **Lyakhovich L.S., Akimov P.A.** Aimed control of the frequency spectrum of eigenvibrations of elastic plates with a finite number of degrees of freedom by introducing additional generalized kinematic devices. // International Journal for Computational Civil and Structural Engineering, 2021, Volume 17, Issue 3, pp. 14-20.
18. **Lyakhovich L.S., Akimov P.A.** Formation of Computational Schemes of Additional Targeted Constraints That Regulate The Frequency Spectrum of Natural Oscillations of Elastic Systems With a Finite Number of Degrees of Mass Freedom, the Directions of Movement of Which are Parallel, But Do Not Lie in the Same Plane. Part 1: Theoretical Foundations. // International Journal for Computational Civil and Structural Engineering, 2022, Volume 18, Issue 2, pp. 183-193.
19. **Lyakhovich L.S., Akimov P.A.** Formation of Computational Schemes of Additional Targeted Constraints That Regulate The Frequency Spectrum of Natural Oscillations of Elastic Systems With a Finite Number of Degrees of Mass Freedom, the Directions of Movement of Which are Parallel, But Do Not Lie in the Same Plane. Part 2: The First Sample of Analysis. // International Journal for

Computational Civil and Structural Engineering, 2022, Volume 18, Issue 3, pp. 137-146.

20. **Lyakhovich L.S., Akimov P.A., Galyautdinov Z.R., Plyaskin A.S.** Development of computational schemes of generalized kinematic devices that precisely regulate the natural frequency spectrum of elastic systems with a finite number of degrees of mass freedom, in which the directions of motion are parallel, but do not lie in the same plane. Part 1: Theoretical foundations. // International Journal for Computational Civil and Structural Engineering, 2023, Volume 19, Issue 3, pp. 173-183.
21. **Lyakhovich L.S., Akimov P.A., Galyautdinov Z.R., Plyaskin A.S**. Development of computational schemes of generalized kinematic devices that precisely regulate the natural frequency spectrum of elastic systems with a finite number of degrees of mass freedom, in which the directions of motion are parallel, but do not lie in the same plane. Part 2. Samples of analysis. // International Journal for Computational Civil and Structural Engineering, 2023, Volume 19, Issue 4, pp. 155-165.
22. **Lyakhovich L.S., Akimov P.A., Meccheulov N.V.** Formation of computational schemes of additional targeted constraints that regulate the frequency spectrum of natural oscillations of elastic systems with a finite number of degrees of mass freedom, the directions of movement of which are parallel, but do not lie in the same plane. Part 3. The second sample of analysis and conclusion. // International Journal for Computational Civil and Structural Engineering, 2022, Volume 18, Issue 4, pp. 71-81.

Leonid S. Lyakhovich, Full Member of the Russian Academy of Architecture and Construction Sciences, Professor, DSc, Professor of Department of Structural Mechanics, Tomsk State University of Architecture and Building; 2, Solyanaya St., 2, Tomsk, 634003, Russia; E-mail: lls@tsuab.ru.

Ляхович Леонид Семенович, академик РААСН, профессор, доктор технических наук, профессор кафедры строительной механики, Томский государственный архитектурно-строительный университет; 634003, Россия, г. Томск, Соляная пл. 2; E-mail: lls@tsuab.ru.

Pavel A. Akimov, Full Member of the Russian Academy of Architecture and Construction Sciences, Professor, Dr.Sc.; Rector, Professor of Department of Applied Mathematics and Computer Science of National Research Moscow State University of Civil Engineering; 26, Yaroslavskoe Shosse, Moscow, 129337, Russia; E-mail: AkimovPA@mgsu.ru, rector@mgsu.ru, pavel.akimov@gmail.com.

Акимов Павел Алексеевич, академик РААСН, профессор, доктор технических наук; ректор, профессор кафедры информатики и прикладной математики Национального исследовательского Московского государственного строительного университета; 129337, Россия, г. Москва, Ярославское шоссе, дом 26; Email: AkimovPA@mgsu.ru, rector@mgsu.ru, pavel.akimov@gmail.com.

Zaur R. Galyautdinov, Associate Professor, DSc, Professor of Department of Reinforced Concrete and Stone Structures, Tomsk State University of Architecture and Building; 2, Solyanaya St., 2, Tomsk, 634003, Russia; E-mail: gazr@yandex.ru.

Галяутдинов Заур Рашидович, доцент, доктор технических наук, доцент кафедры железобетонных и каменных конструкций, Томский государственный архитектурно-строительный университет; 634003, Россия, г. Томск, Соляная пл. 2; E-mail: gazr@yandex.ru.

Andrey S. Plyaskin, Associate Professor, Ph.D., Head of Department of Metal and Wooden Structures, Tomsk State University of Architecture and Building; 2, Solyanaya St., 2, Tomsk, 634003, Russia; E-mail: plyaskinandrei@mail.ru.

Пляскин Андрей Сергеевич, доцент, кандидат технических наук, заведующий кафедрой металлических и деревянных конструкций, Томский государственный архитектурно-строительный университет; 634003, Россия, г. Томск, Соляная пл. 2; E-mail: plyaskinandrei@mail.ru.